



Doctoral Program in Health Sciences D420

**Isolation and design of diterpenoids
from *Plectranthus* species**

Doctoral Thesis presented by:

Epole Ngolle Ntungwe

Universidad Alcala de Henares

2021



En virtud del acuerdo de colaboración con la *Universidade Lusófona de Humanidade e Tecnologias*

Programa de Doctorado en Ciencias de la Salud
Programa de Doutorado em Ciências da Saúde

**AISLAMIENTO Y DISEÑO DE DERIVADOS DE DITERPENOS
DE *PLECTRANTHUS SPP.***

*ISOLAMENTO E DESIGN DE DITERPENÓIDES DE
PLECTRANTHUS SPP.*

Tesis Doctoral Presentada Por:
Epole Ngolle Ntungwe

Directores:

Dra. Patrícia Dias Mendonça Rijo

Dra. Ana Maria Díaz-Lanza

Universidad Alcala de Henares, 2021

This work is dedicated to my parents who have unconditionally supported me.

“All outstanding work, in art as well as in science, results from immense zeal applied to a great idea.”

Santiago Ramón

ACKNOWLEDGMENTS

This thesis was made possible through collaboration with different Universities and research centers. Most especially it is a product of the partnership between Research Center for Biosciences & Health Technologies (CBIOS) of Universidade Lusófona de Humanidades e Tecnologias and Department of Biomedical Sciences, Faculty of Pharmacy, University of Alcalá, Alcalá de Henares, Spain under the supervision of Professor Doctor Patrícia Dias de Mendonça Rijo, Ph.D, and co-supervision of Professor Ana Díaz-Lanza.

My PhD journey would not have been complete without the support and encouragement of many people and institutions. I am grateful to the PADDIC 2019 – 2021 (ALIES-COFAC) as part of the PhD Program in Health Sciences from Universidad de Alcalá and Universidade Lusófona de Humanidades e Tecnologias. Also, to the Fundação para a Ciência e Tecnologia (FCT) for the financial support under the reference UID/DTP/04567/2016, UID/MULTI/04378/2013 and the project (3599-PPCDT) PTDC/DTP-FTO/1981/2014 – POCI-01-0145-FEDER-016581.

Firstly, I would like to thank Prof. Dr. Luís Monteiro Rodrigues (Director - CBIOS) for your expertise, leadership, generosity, and your drive towards excellence.

Special words to my supervisors, Professor Doctor Patrícia Dias de Mendonça Rijo, Ph.D. for giving me a research direction and for all the help, ideas, comments, and constant encouragement throughout this work. You were the first professor I met at CBIOS, through the CBIOS fellowship program which lasted for in the Phytochemistry Lab. I will never forget how welcome you made me feel from the outset. I'll forever be grateful for the opportunity we had to work together. Thanks for your keen guidance, through the skills you taught me and the subtleties of scientific writing. I also thank my co-supervisors Professor Doctor Ana Díaz-Lanza. Thank you both for your important contributions, valuable opinions, discussions, ideas, and availability with immediate responses when necessary.

I am grateful to the entire teaching and research CBIOS staff that have taken some time to discuss and enrich my work. Particularly valuable were the CBIOS science sessions that have provided me with a very stimulating environment in what concerns

the extraordinary quality of its academic staff, and that experience will leave marks beyond this thesis. Special thanks to Prof. Amílcar Roberto for *Artemia salina* general toxicity model teaching, Prof. Maria João Cebola, and Prof. Paula Pereira for guidance through the *A. salina* model review.

I also like to acknowledge the help of the master students Catarina Teodósio, Carolina Oliveira, Cláudia Oliveira which aided in specific points of the work. Thanks for your help and friendship. To my colleagues Catarina Garcia, Vera Isca, Eva María Domínguez-Martín, Gabrielle Bangay, thanks for providing intellectual support, sincerity, and encouragement from day one, for all the fun times and hangout, you made it worth going to the lab every day.

For external collaborations, I would like to thank Prof. Dr. Noélia Duarte (FFUL, Portugal) for the LC-MS analysis and your scientific advice. To Prof. Attila Hunyadi (University of Szeged, Hungary) who have greatly contributed to this thesis. Thank you for accepting me to your lab during the COST ACTION – STSM and for your enormous support throughout my stay at your lab. This greatly contributed to accomplishing the goals of this thesis.

I also want to appreciate the support of Prof. Milica Pesic (University of Belgrade, Serbia) and Prof. Natalia Armas Capote (Centro Atlántico del Medicamento, Tenerife, Spain) for the cytotoxicity studies and your assistance with the interpretation of the anticancer assay results. To Eleonora Colombo and Prof. Daniele Passarella of Università Degli Studi di Milano, Italy. Thank you both for providing the squalene linker and the scientific advice for the self-assemble nanoparticles.

Words cannot express how grateful I am for the support and words of encouragement that my family has showered me with. I dedicate this thesis to my mother and father. Thank you, Mum, and thank you Dad, for your understanding and unwavering faith in me. Your love and guidance are with me wherever I go. You thought me how to employ my inner strength and never to give up and this has always kept me going. Words cannot express my gratitude to you. To my little princess Reema Mesame, you have been a source of my strength. To my siblings and Kelechi Wisdom, thank you for your positive and caring nature. What would I have done without all your encouraging words and prayers? Finally, to all my friends who help me in one way or the other, I say a big thank you.

General Table of Contents

| | |
|--|------|
| ACKNOWLEDGMENTS | i |
| List of Figures..... | vi |
| List of Tables | viii |
| List of Schemes | ix |
| ABSTRACT AND RESUMEN..... | x |
| ABSTRACTS | xi |
| RESUMEN..... | xiii |
| BACKGROUND, HYPOTHESIS AND OBJECTIVES | 1 |
| BACKGROUND | 2 |
| HYPOTHESIS..... | 3 |
| OBJECTIVES..... | 4 |
| References..... | 5 |
| CHAPTER I | 7 |
| Article I..... | 8 |
| <i>Artemia</i> species: An Important Tool to Screen General Toxicity Samples..... | 8 |
| CHAPTER II | 26 |
| Using <i>Artemia salina</i> model as a screening method for general toxicity | 27 |
| Introduction..... | 28 |
| Methodology of <i>A. salina</i> Bioassay employed in the papers below. | 29 |
| References..... | 32 |

| | |
|---|----|
| CHAPTER III | 34 |
| Article 2..... | 35 |
| Preliminary Biological Activity Screening of <i>Plectranthus</i> spp. Extracts for the Search of Anticancer Lead Molecules | 35 |
| CHAPTER IV..... | 48 |
| Article 3..... | 49 |
| One new C ₂₀ -nor-abietane and three abietane-type diterpenoids from <i>Plectranthus mutabilis</i> Codd. leaves as modulators of P-glycoprotein activity | 49 |
| Abstract | 50 |
| Introduction..... | 51 |
| Material and methods..... | 53 |
| General experimental procedures..... | 53 |
| Plant material..... | 53 |
| Extraction, bioguided fractionation and isolation | 54 |
| NMR analysis..... | 55 |
| UHPLC-MS/MS Analysis | 55 |
| HPLC-DAD Analysis..... | 56 |
| Computational Studies..... | 56 |
| Cytotoxicity study | 57 |
| Results and Discussion | 59 |
| HPLC–DAD Profiling of <i>P. mutabilis</i> acetonic extract..... | 64 |
| Biosynthetic relation between 2-4..... | 65 |
| Interaction with P-gp activity..... | 70 |
| Effects on P-gp expression..... | 72 |
| Reversal of DOX resistance | 73 |
| Conclusion:..... | 75 |
| References..... | 77 |

| | |
|---|-----|
| Supplementary information S. | 83 |
| CHAPTER V..... | 95 |
| Article 4..... | 96 |
| Self-Assembly Nanoparticles of Natural Bioactive Abietane Diterpenes..... | 96 |
| CONCLUSIONS | 114 |
| ANNEX A | 117 |
| ANNEX B..... | 126 |
| ANNEX C..... | 140 |
| ANNEX D | 157 |
| ANNEX E..... | 170 |
| ANNEX F..... | 184 |
| ANNEX G | 202 |
| ANNEX H | 215 |
| ANNEX I..... | 260 |
| ANNEX J | 271 |
| ANNEX K..... | 283 |
| ANNEX L..... | 301 |

List of Figures

| | |
|--|----|
| Figure IV.1. Structures of compounds 1–4 from <i>P. mutabilis</i> | 60 |
| Figure IV.2. Key ^1H – ^1H COSY (bold lines) and HMBC (blue arrows) correlations of compound 1..... | 61 |
| Figure IV.3. Electrophilic (f_k^-), nucleophilic (f_k^+) and radical (f_k^0) Fukui functions of 2-4. The higher condensed Fukui indexes are indicated as green circles, red triangles, and blue arrows, respectively representing the sites in the molecules that are most susceptible for a radical attack, most nucleophilic, and most electrophilic. | 66 |
| Figure IV.4. Electrophilic Fukui functions (f_k^-) and Gibbs energy for the formation of anions derived from deprotonation of Coleon U (4) at hydroxyl positions on C11 a) and C14 b)..... | 67 |
| Figure IV.5. Effects of compounds and extract on the ABCB1 expression. Mean fluorescence of untreated NCI-H460/R cells was set to 100 and used for the comparison of other mean fluorescence (untreated NCI-H460 cells and treated NCI-H460/R cells) in GraphPad Prism 6 software (unpaired t-test). Mean fluorescence was calculated from three independent experiments. Significant difference to untreated NCI-H460/R cells was considered if $p < 0.05$ (*), $p < 0.001$ (***). | 73 |
| Figure S.IV.1: Key ^1H – ^1H COSY (bold lines), HMBC (blue arrows) and NOESY (red arrows) correlations of 2, 3 and 4..... | 83 |
| Figure S.IV.2: Screening of the <i>P. mutabilis</i> column fractions for general toxicity at a concentration of 10 ppm using the <i>Artemia salina</i> test | 84 |
| Figure S.IV.3. Calibration curves for the HPLC quantification of diterpenoids from the acetonic extract of <i>P. mutabilis</i> . UV detection at 270 nm. Mutabilol (1), Coleon U quinone (2), $8\alpha,9\alpha$ -Epoxycoleon U quinone, (3), Coleon U (4) | 85 |
| Figure S.IV.4: 1D and 2D- NMR data..... | 86 |
| Figure S.IV.5: HMBC– compound 1 | 87 |
| Figure S.IV.6: HSQC– compound 1 | 87 |
| Figure S.IV.7: ^{13}C –NMR compound 1..... | 88 |

| | |
|---|----|
| Figure S.IV.8: ESI- Comparison of chromatographic profiles of isolated compounds with <i>P. mutabilis</i> leaves extract..... | 88 |
| Figure S.IV.12: MS/MS spectrum Mutabilol, 1 (ESI-)..... | 89 |
| Figure S.IV.9: MS/MS spectrum of Coleon U quinone, 2 (ESI+). | 89 |
| Figure S.IV.10: MS/MS spectrum of 8 α ,9 α -epoxycoleon U quinone, 3 (ESI-)..... | 90 |
| Figure S.IV.11: MS/MS spectrum of Coleon U, 4 (ESI-) | 90 |
| Figure S.IV.13: MS/MS spectrum of acetoxy derivative of an abietane diterpenoid, 5 (ESI+)..... | 90 |
| Figure S.IV.14. Reversal of DOX resistance in NCI-H460/R cells in subsequent treatment with compounds 2, 3, and 4. Left panel: Cell growth inhibition induced by combined treatments of compounds 2, 3, and 4 with DOX. Right panel: IC50 values obtained by non-linear regression in GraphPad Prism 6 software. Dunnett's multiple comparisons test in Two-way ANOVA was used to determine the significant differences among treatment strategies ($p \leq 0.01^{***}$). Results were obtained from three independent experiments ($n=3$). | 91 |
| Figure S.IV.15. Single treatment with compounds 2, 3, and 4 in NCI-H460/R cells assessed by MTT after 144 h (control treatments of combined effect with DOX). A: Cell growth inhibition induced by single treatments of compounds 2, 3, and 4 with DOX. B: Non-linear regression used to calculate the IC50 values of compounds 2, 3, and 4. IC50 values obtained by non-linear regression in GraphPad Prism 6 software. Results were obtained from three independent experiments ($n=3$). The results confirmed that 1 μ M, 2 μ M, and 5 μ M used in combination with DOX (Annex 6) did not affect the cell viability after 144 h. Only 10 μ M and 20 μ M inhibited the cell growth of NCI-H460/R but these concentrations were not used in combination studies..... | 92 |

List of Tables

| | |
|---|----|
| Table IV.1. NMR data of compound 1 (CD ₃ OD, ¹ H 500 MHz, ¹³ C 126 MHz; δ in ppm, J in Hz)..... | 62 |
| Table IV.2. Abietane Diterpenoids compositions of the extract from <i>P. mutabilis</i> by HPLC–DAD..... | 65 |
| Table IV.3. Hydrogen Bond Dissociation Energies (BDEs; kcal/mol) of O-H bonds in 4. | 66 |
| Table IV.4. Inhibition of cell viability assayed by MTT in non-small cell lung cancer cells (NCI-H460 and NCI-H460/R) and embryonic pulmonary fibroblasts (MRC-5)..... | 69 |
| Table IV.5. Rho123 accumulation assay, 30 min simultaneous treatment with tested compounds, shows direct interaction with P-gp and interference with its activity (inhibition or stimulation) | 70 |
| Table IV.6. Rho123 accumulation assay, 30 min load after 72 h treatment with tested compounds and extract, shows the indirect effect on P-gp activity (inhibition or stimulation)..... | 72 |
| Table IV.7. Reversal of DOX resistance in NCI-H460/R cells pre-treated with 1, 2, and 3, assayed by MTT | 74 |
| Table S.IV.3. ¹³ C-NMR data of compounds 2-4 δ, (1, 3, 4-126 MHz, 2- 75 MHz) | 84 |
| Table S.IV.4. Atomic coordinates for all the optimized species (PBE1PBE/6-31G**) | 93 |

List of Schemes

Scheme IV.1 68

ABSTRACT AND RESUMEN

ABSTRACTS

Despite the great development in human medicine, cancer is still a serious threat to public health. It is a well-known leading cause of morbidity and mortality worldwide, consequently, research on new anticancer agents ought to be continued. Natural products from medicinal plants represent a major resource of novel therapeutic substances for combating serious diseases including cancer. The *Plectranthus* genus (Family: Lamiaceae) represents a large and widespread group of species with a diversity of traditional uses for the treatment of several ailments. Cytotoxicity screenings have identified *Plectranthus* plants as potential sources of antitumor lead compounds. They are rich in diterpenoids which are reported to be responsible for various pharmacological activities such as cytotoxic activity.

In this project, sixteen plants from the *Plectranthus* genus were studied. The acetonic extracts were prepared by the ultrasound-assisted extraction method (10 % (w/v)). The prepared extracts were screened for their antimicrobial, antioxidant, general toxicity, and cytotoxicity. The antimicrobial activity of each extract was screened against yeasts, Gram-positive and Gram-negative bacteria. *P. hadiensis* and *P. mutabilis* extracts were the most active using the well diffusion method. Their MIC and MBC (microdilution method) were determined, and they possessed significant activity against *Staphylococcus aureus* and *Candida albicans* with MIC values ranging from 3.91 µg/mL to 125 µg/mL and MBC from 62.5 to 250 µg/mL.

The antioxidant activity of the extracts was quantitatively determined using the DPPH (2,2-diphenyl-1-picrylhydrazyl) scavenging radical assay. *P. hadiensis* and *P. mutabilis* extracts having the highest scavenging activities of 46.14% and 36.24% respectively. The general toxicity of all the extracts was determined using the Brine Shrimp Lethality assay (BSLA) and the cytotoxicity of the most toxic extract was determined. *P. hadiensis* and *P. mutabilis* we found to be the most bioactive and the compounds responsible for their bioactivity identified. The HPLC analysis of *P. hadiensis* leaves showed that the known abietane diterpene, 7 α -acetoxy-6 β -hydroxyroyleanone (Roy) was the major compound in this extract. Roy was isolated using preparative TLC and tested against the aggressive type triple-negative breast cancer (MDA-MB-231S). *P. hadiensis* extract and 7 α -acetoxy-6 β -hydroxyroyleanone reduced the viability of MDA-MB-231S cancer cell line cells,

showing an IC₅₀ value of 25.6 µg/mL and 5.5 µM (2.15 µg/mL) respectively, suggesting that this lead molecule could be responsible for the bioactivity of this extract.

The phytochemistry of the second bioactive extract (*P. mutabilis*) was done. Bio-guided fractionation of ultrasound-assisted acetonetic extract of *P. mutabilis* leaves resulted in the isolation of a new nor-abietane diterpene, (+)-(5*S*,10*R*)-10,11,12-trihydroxy-6,7-dioxo-20-*nor*-abieta-8,11,13-triene (**1**) alongside three known abietane-type diterpenoids Coleon-U-quinone (**2**), 8α,9α-epoxycoleon-U-quinone (**3**), and Coleon U (**4**). From the ESI+ MS/MS fragmentation patterns analysis, compound (**5**) was tentatively identified as acetoxy derivative of an abietane diterpenoid. HPLC analysis revealed Coleon U (96 ± 0.048 µg/mg) to be the major compound of the *P. mutabilis* extract in the wavelengths analyzed. Computational data indicates a biosynthetic relation between **2**, **3**, and **4**. These results suggest that both the quinone (**2**) and the epoxyquinone (**3**) are formed directly from Coleon U (**4**).

Coleon U, coleon U quinone, and 8α,9α-Epoxycoleon U quinone were found to be selective towards the cancer cell lines and their anticancer effect was not compromised by P-gp activity in NCI-H460/R cells. Importantly, **2**, **3**, and **4** were able to inhibit P-gp activity in NCI-H460/R cells at longer exposure of 72 h and consequently revert doxorubicin (DOX) resistance in subsequent combined treatment. Compound **1** was inactive against all three cell lines in the range of concentrations (2 to 50 µM) tested. All compounds did not influence the ABCB1 expression in NCI-H460/R cells, while the extract significantly increased it. This work identified *P. hadiensis* leaves and *P. mutabilis* extracts as a potential source of bioactive compounds to fight MDR. Cytotoxic 7α-acetoxy-6β-hydroxyroyleanone previously isolated from *P. hadiensis*, its hemisynthetic derivative 7α-acetoxy-6β-benzoyloxyroyleanone (12BzRoy) and 6,7-dehydroroyleanone (DHR) isolated from the essential oil of *P. madagascariensis* were employed in the present work as lead molecules for the synthesis of self-assembled nanoparticles. Roy-OA, DHR-sq, and 12BzRoy-sq conjugates were successfully synthesized and their nanoassemblies characterized. Roy-OA NPs were most promising and was characterized based on size (509.33 nm), Pdl (0.249), zeta potential (-46.2mV), and morphology. The release profile of Roy was determined from Roy-OA NPs at physiological pH 7.4. The biological activity of DHR.sq and, Roy-OA NPs were evaluated, and both were found to have less bioactivity when compared with DHR and Roy respectively. These results

suggested that these nanoassemblies act as prodrugs for the release of cytotoxic lead molecules.

RESUMEN

A pesar del gran desarrollo de la medicina, el cáncer continúa siendo una amenaza para la salud pública. Esta enfermedad es una de las principales causas de morbilidad y mortalidad a nivel mundial, y es por ello por lo que la investigación de nuevos agentes antitumorales debe continuar. Los productos naturales aislados de plantas medicinales representan la mayor fuente de nuevos compuestos bioactivos para combatir graves enfermedades como el cáncer. El género *Plectranthus* (Familia: Lamiaceae) comprende numerosas especies ampliamente distribuidas, empleadas tradicionalmente para el tratamiento de distintas enfermedades. Los cribados de citotoxicidad han identificado cuáles de las especies de *Plectranthus* pueden proporcionar posibles nuevos fármacos antitumorales, ya que son ricas en diterpenos los cuáles son responsables de varias actividades farmacológicas como la citotóxica.

En este proyecto, dieciséis plantas del género *Plectranthus* fueron estudiadas. Se prepararon extractos acetónicos mediante el método de extracción asistido por ultrasonidos (10% m/v). A continuación, se ensayó la actividad antimicrobiana, antioxidante, la toxicidad general y la citotoxicidad de los extractos previamente preparados. La actividad antimicrobiana de cada extracto fue estudiada frente a levaduras, bacterias Gram-positivas y Gram-negativas. De los extractos estudiados, los de *P. hadiensis* y *P. mutabilis* fueron los más activos en el Método de Difusión por Pozos (*Well Diffusion Method*). Empleando el método de microdilución, fueron determinados los valores de MIC (*Minimal Inhibitory Concentration* - Concentración Mínima Inhibitoria) y MBC (*Minimal Bactericidal Concentration* - Concentración Mínima Bactericida) de los extractos. Estos mostraron una actividad significativa frente a *Staphylococcus aureus* y *Candida albicans* con valores de MIC entre los 3.91 µg/mL y los 125 µg/mL y de MBC entre 62.5 µg/mL y 250 µg/mL.

La actividad antioxidante de los extractos fue determinada cuantitativamente usando el ensayo del difenilpicrilhidrazilo (DPPH). Los extractos de *P. hadiensis* y *P. mutabilis*

mostraron las mayores actividades antioxidantes con unos valores de 46.14% y 36.24% respectivamente. La toxicidad general de todos los extractos fue determinada mediante el ensayo de letalidad con *Artemia salina*, y a continuación, la citotoxicidad del extracto más tóxico fue determinado, mostrando en ambos casos la mayor actividad los extractos de *P. hadiensis* y *P. mutabilis*. El análisis por cromatografía líquida de alta resolución (HPLC, *High Liquid Column Chromatography*) del extracto de hojas de *P. hadiensis* reveló que el conocido diterpeno abietano, 7 α -acetoxi-6 β -hidroxirooleanona (Roy) fue el compuesto mayoritario de este extracto. Roy fue aislada empleando Cromatografía en Capa Fina Preparativa y su actividad fue testada frente a la agresiva línea de cáncer de mama triple negativo MDA-MB-231S. Tanto el extracto de *P. hadiensis* como Roy redujeron la viabilidad de las líneas celulares de cáncer MDA-MB-231S, mostrando un valor de IC₅₀ de 25.6 μ g/mL y de 5.5 μ M (2.15 μ L/mL), sugiriendo que esta molécula principal podía ser la responsable de la bioactividad del extracto.

Por otro lado, fue realizado el estudio fitoquímico del segundo extracto bioactivo (*P. mutabilis*). El fraccionamiento biodirigido del extracto acetónico previamente preparado mediante ultrasonidos resultó en el aislamiento de un nuevo nor-abietano diterpeno, (+)-(5S,10R)-10,11,12-trihidroxy-6,7-dioxo-20-nor-abieta-8,11,13-trieno (**1**), junto con otros tres diterpenoides de tipo abietano previamente conocidos Coleon-U-quinona (**2**), 8 α ,9 α -epoxicoleon-U-quinona (**3**) y Coleon U (**4**). De los patrones de fragmentación del análisis por ESI+ MS/MS, el compuesto (**5**) fue identificado en principio como un derivado acetoxi de un diterpeno abietano. El análisis por HPLC manifestó que Coleon U (96 \pm 0.048 μ g/mg) era el compuesto mayoritario del extracto de *P. mutabilis* entre las longitudes de onda analizadas y comparadas. Los datos *in silico* de estos compuestos indicaron una relación biosintética entre los compuestos **2**, **3** y **4**. Estos resultados sugieren que tanto la quinona (**2**) como la epoxiquinona (**3**) se biosintetizaron directamente desde Coleon U (**4**). Coleon-U-quinona (**2**), 8 α ,9 α -epoxicoleon-U-quinona (**3**) y Coleon U (**4**) fueron selectivos frente a las líneas celulares de cáncer y su efecto antitumoral no estuvo comprometido por la actividad P-gp en líneas celulares NCI-H460/R. Cabe destacar que **2**, **3** y **4** fueron capaces de inhibir la actividad P-gp en células NCI-H460/R en una exposición larga de 72h, consiguiendo revertir consecuentemente la resistencia a Doxorubicina (DOX) al emplear el tratamiento combinado compuesto

aislado + DOX. El compuesto 1 fue inactivo frente a las tres líneas celulares ensayadas en un rango de concentración de 2 a 50 μM . Ninguno de los compuestos aislados tuvo influencia en la expresión de ABCB1 en la línea celular NCI-H460/R, mientras que el extracto la incrementó significativamente. Este trabajo identificó los extractos de hojas de *P. hadiensis* y el extracto de *P. mutabilis* como fuentes potenciales para la obtención de nuevos compuestos bioactivos frente a la resistencia a múltiples fármacos (MDR, *MultiDrug-Resistance*) para el tratamiento del cáncer. El compuesto citotóxico previamente aislado de *P. hadiensis* 7 α -acetoxi-6 β -hidroxiroileanona, su derivado hemisintético 7 α -acetoxi-6 β -benzoiloxiroileanona (12BzRoy) y el compuesto 6,7-dehidroroileanona (DHR) aislado del aceite esencial de *P. madagascariensis* fueron empleados en este trabajo como los compuestos principales para la síntesis de nanopartículas de autoensamblaje. Los conjugados Roy-OA (OA, Oleic Acido- Ácido Oleico), DHR-sq (sq, Squalene- Escualeno) y 12BzRoy-sq fueron sintetizados con éxito y su nanoensamblaje fue caracterizado. Las nanopartículas (NPs) Roy-OA fueron las más prometedoras y fueron caracterizada en base a su tamaño (509.33 nm), Pdl (0.249), potencial zeta (-46.2 mV) y morfología. El perfil de liberación de Roy fue determinado de las nanopartículas de Roy-OA a pH fisiológico de 7.4. La actividad biológica de las nanopartículas de DHR-sq y Roy-OA fue evaluada, y ambas tenían menor actividad que los compuestos de partida DHR y Roy respectivamente. Estos resultados ponen de manifiesto que los nanoensamblajes actúan como profármacos en la liberación de molécula citotóxicas.

BACKGROUND, HYPOTHESIS AND OBJECTIVES

BACKGROUND

Cancer is one of the most important causes of mortality and morbidity worldwide. It is the second leading cause of death globally with about 1 in 6 deaths resulting from cancer ("World Health Organization (WHO), fact sheet on Cancer," 2018). Despite improvements in diagnosis and therapies, cancer remains a major concern in public health [2]. Different types of therapies are available to treat cancer, however, these have limitations such as non-specificity at a single target causing side effects [3,4]. More so, Multidrug resistance (MDR) is a challenge in cancer therapy and is associated with the overexpression of P-glycoprotein (P-gp), resulting in the increased efflux of chemotherapeutics from cancer cells [5].

Natural products from medicinal plants have been used for thousands of years, as traditional medicines for the treatment of many ailments [6–8]. Their vast ethnomedicinal and ethnopharmacological applications have inspired current research in drug discovery [9]. According to the estimation by the World Health Organization, about 80% of people on the globe are still dependent on traditional herb-based medications due to their low cost, easy accessibility, and likely negligible side effects in comparison to allopathic medicines [10]. As reported in the literature, plants are the first medical treatment used by humankind [11].

Natural products and their derivatives have been and continue to be rich sources for lead compounds. They play a valuable role in the drug discovery process, particularly in the areas of cancer and infectious diseases [12]. Natural products continue to provide greater structural diversity than standard combinatorial chemistry and so they offer major opportunities for finding novel low molecular weight lead structures that are active against a wide range of assayed targets [13]. This has led to the exploration and exploitation of new plant sources for their medicinal properties. It has been estimated that over 60% of all commercial anticancer agents originate from natural sources [14]. By so doing, a substantial number of anticancer agents used in the clinic are either natural or derived from natural products [15,16], for example, Vincristine, irinotecan, etoposide, and paclitaxel are classic examples of plant-derived compounds [17]. Thus, plants have an important role in pharmacological research and drug development.

The Lamiaceae members of plant species belonging to commercially important genera, such as *Plectranthus*, *Salvia*, *Ocimum*, and *Mentha*, are attributed with a rich diversity of ethnobotanical benefits [18]. *Plectranthus* is an economically important genus due to its horticultural, floricultural, and ethnomedicinal uses [19]. In addition, over 85% of the literature, documentation of *Plectranthus* is on the therapeutic values of this genus attributed to its aromatic nature and essential oil-producing capability [20]. Corroborating the empirical medicinal uses, extracts, and isolated compounds from *Plectranthus* that have shown anti-inflammatory, antioxidant, antimicrobial, diuretic, and antitumoral activities [21]. The species of *Plectranthus* are known as producers of flavonoids, phenolic constituents, and essential oils [22]. They are a source of abietane-type diterpenoids as common secondary metabolites with reported cytotoxic activities [18]. The more frequently found diterpenes are abietane and labdane type, in addition to some kaurane, pimarane, halimane, and beyranes [19]. From the abundant diterpenes from this genus, royleanones are the most occurrence, widely recognized for their antifungal, antimycobacterial, cytotoxic, and antitumor potentials [23].

This work describes the screening of sixteen *Plectranthus* species for their antioxidant, antimicrobial, general toxicity, and cytotoxicity. The phytochemistry of the two most bioactive extracts was done to identify the compounds that may be responsible for their biological activity. In addition, the cytotoxic 7α -acetoxy- 6β -hydroxyroyleanone (Roy) from the most active extract (*P. hadiensis*) and its derivative with improved cytotoxicity 7α -acetoxy- 6β -benzoyloxyroyleanone (12BzRoy) were used to prepare self-assembling nanoparticles to improve the solubility of these two bioactive molecules.

HYPOTHESIS

The Lamiaceae members of plant species belonging to commercially important genera, such as *Plectranthus* are attributed with a rich diversity of ethnobotanical benefits. In this work, we established the following hypothesis:

- Would the sixteen selected *Plectranthus* (Lamiaceae) spp. be a source of bioactive extracts?
- Will the selected *Plectranthus* extracts result in potential bioactive compounds?
- Will there be an advantage in using new self-assembly nanoparticles with royleanones?

OBJECTIVES

Taking into account the set hypothesis, the following objectives were stipulated:

Objective I: *Artemia*, commonly known as brine shrimp is highly valued for its application in general toxicity detection. Thus, this chapter is a Review on “*Artemia*: An Important Tool to Screen General Toxicity Samples”

Objective II: *Artemia salina* commonly known as brine shrimp is one of the *Artemia* species employed in natural product chemistry and it helps to determine the general toxicity of a broad number of samples. In this chapter several examples reinforce the use of this screening model for general toxicity study.

Objective III: The biological activity screening of sixteen *Plectranthus* acetonc extracts prepared by ultrasound-assisted extraction method. Evaluate their antioxidant, antimicrobial, general toxicity, and cytotoxic activities. Identify the bioactive compound(s) from the most bioactive extract and compare the cytotoxic effects between the crude extract and the isolated compound.

Objective IV: Phytochemical study of *P. mutabilis* Codd. acetonc extract to identify, characterise, and evaluate the cytotoxicity of its isolated compounds that may be responsible for its cytotoxic activity. Studies for the modulation of P-gp activity by both the *P. mutabilis* acetonc extract and its isolated compounds.

Objective V: The optimization of royleanone conjugates for self-assembly nanoparticles in order to obtain a pro-drug nanosystem with improved aqueous solubility.

References

- [1] World Health Organization (WHO), fact sheet on Cancer [homepage on the Internet]. n.d.
- [2] Muniyandi K, George E, Mudili V, Kalagatur NK, Anthuvan AJ, Krishna K, et al. Antioxidant and anticancer activities of *Plectranthus stocksii* Hook. f. leaf and stem extracts 2017.
- [3] Girotti MR, Salatino M, Dalotto-Moreno T, Rabinovich GA, Rabinovich GA. Sweetening the hallmarks of cancer: Galectins as multifunctional mediators of tumor progression 2020; 217: 1–14.
- [4] Schirmmayer V. From chemotherapy to biological therapy: A review of novel concepts to reduce the side effects of systemic cancer treatment (Review) 2019; 54: 407–19.
- [5] Waghray D, Zhang Q. Inhibit or Evade Multidrug Resistance P-Glycoprotein in Cancer Treatment 2018; 61: 5108–21.
- [6] Yuan H, Ma Q, Ye L, Piao G. The traditional medicine and modern medicine from natural products 2016; 21.
- [7] Benarba B, Pandiella A. Medicinal Plants as Sources of Active Molecules Against COVID-19 2020; 11: 1–16.
- [8] Maher T, Raus RA, Daddiouaissa D, Ahmad F, Adzhar NS, Latif ES, et al. Medicinal plants with anti-leukemic effects: A review 2021; 26.
- [9] Petran M, Dragos D, Gilca M. Historical ethnobotanical review of medicinal plants used to treat children diseases in Romania (1860s-1970s) 2020; 16.
- [10] Swamy MK, Sinniah UR. A comprehensive review on the phytochemical constituents and pharmacological activities of *Pogostemon cablin* Benth.: An aromatic medicinal plant of industrial importance 2015; 20: 8521–47.
- [11] Petrovska BB. Historical review of medicinal plants' usage 2012; 6: 1–5.
- [12] Demain AL, Vaishnav P. Natural products for cancer chemotherapy 2011; 4: 687–99.
- [13] Harvey A. Strategies for discovering drugs from previously unexplored natural products 2000; 5: 294–300.
- [14] Taïbi K, Abderrahim LA, Ferhat K, Betta S, Taïbi F, Bouraada F, et al. Ethnopharmacological study of natural products used for traditional cancer therapy in Algeria 2020; 28: 1451–65.
- [15] Cragg GM, Pezzuto JM. Natural Products as a Vital Source for the Discovery of Cancer Chemotherapeutic and Chemopreventive Agents 2016; 25: 41–59.
- [16] Khalifa SAM, Elias N, Farag MA, Chen L, Saeed A, Hegazy MEF, et al. Marine natural products: A source of novel anticancer drugs 2019; 17.

- [17] Lichota A, Gwozdziński K. Anticancer activity of natural compounds from plant and marine environment 2018; 19.
- [18] Garcia C, Teodósio C, Oliveira C, Oliveira C, Díaz-Lanza A, Reis C, et al. Naturally Occurring *Plectranthus*-derived Diterpenes with Antitumoral Activities 2019; 24: 4207–36.
- [19] Matias DHC. Isolation, modeling, and phytosome forms of antimicrobial and antiproliferative compounds from *plectranthus* spp. 2016: 235.
- [20] Arumugam G, Swamy MK, Sinniah UR. *Plectranthus amboinicus* (Lour.) Spreng: Botanical, Phytochemical, Pharmacological and Nutritional Significance 2016; 21.
- [21] Mesquita LSF, Matos TS, Do Nascimento Ávila F, Da Silva Batista A, Moura AF, De Moraes MO, et al. Diterpenoids from Leaves of Cultivated *Plectranthus ornatus* 2020.
- [22] Al Musayeb NM, Amina M, Al-Hamoud GA, Mohamed GA, Ibrahim SRM, Shabana S. *Plectrabarbene*, a new abietane diterpene from *plectranthus barbatus* aerial parts 2020; 25: 1–11.
- [23] Santos-Rebelo A, Garcia C, Eleutério C, Bastos A, Coelho SC, Coelho MAN, et al. Development of parvifloron D-loaded smart nanoparticles to target pancreatic cancer 2018; 10: 1–15.

CHAPTER I

Article 1

***Artemia* species: An Important Tool to Screen General Toxicity Samples**

Epole Ntungwe N^{a, b}, Eva M Domínguez-Martín^{a, b}, Amilcar Roberto^a, Joana Tavares^a, Vera M S Isca^{a, c}, Paula Pereira^{a, d}, Maria-João Cebola^{a, d}, Patrícia Rijo^{a, c*}

^a CBIOS - Center for Research in Biosciences & Health Technologies, Universidade Lusófona de Humanidades e Tecnologias, Campo Grande 376, 1749-024 Lisbon, Portugal

^b Department of Biomedical Sciences, Faculty of Pharmacy, University of Alcalá, Ctra. A2 Km 33.600 - Campus Universitario, 28871 Alcalá de Henares, Spain

^c Instituto de Investigação do Medicamento (iMed.Ulisboa), Faculdade de Farmácia da Universidade de Lisboa, Lisbon, Portugal

^d CERENA - Centre for Natural Resources and the Environment, Instituto Superior Técnico, Universidade de Lisboa, Av. Rovisco Pais, 1049-001 Lisbon, Portugal

* Corresponding author: patricia.rijo@ulusofona.pt

Universidade Lusófona de Humanidades e Tecnologias, Campo Grande 376, 1749-024 Lisboa

Curr Pharm Des. 2020;26(24):2892-2908.

Doi: 10.2174/1381612826666200406083035.

Artemia species: An Important Tool to Screen General Toxicity Samples

Epole Ntungwe N^{1,2}, Eva M. Domínguez-Martín^{1,2}, Amílcar Roberto¹, Joana Tavares¹, Vera M. S. Isca^{1,3}, Paula Pereira^{1,4}, Maria-João Cebola^{1,4} and Patrícia Rijo^{*1,3}

¹CBIOS - Center for Research in Biosciences & Health Technologies, Universidade Lusófona de Humanidades e Tecnologias, Campo Grande 376, 1749-024 Lisbon, Portugal; ²Department of Biomedical Sciences, Faculty of Pharmacy, University of Alcalá, Ctra. A2, Km 33.600 - Campus Universitario, 28871 Alcalá de Henares, Spain; ³Instituto de Investigação do Medicamento (iMed.U LISBOA), Faculdade de Farmácia da Universidade de Lisboa, Lisbon, Portugal; ⁴CERENA - Centre for Natural Resources and the Environment, Instituto Superior Técnico, Universidade de Lisboa, Av. Rovisco Pais, 1049-001 Lisbon, Portugal

ARTICLE HISTORY

Received: December 13, 2019
Accepted: March 9, 2020

DOI:
10.2174/138161282666200406083035

Abstract: Medicinal plants are a good source of novel therapeutic drugs, due to the phytochemicals present. *Artemia*, commonly known as brine shrimp, is a tiny halophilic invertebrate belonging to class *Crustacean*, which plays an important role in saline aquatic and marine eco-systems. Besides its usage in aquaculture, it is also highly valued for its application in toxicity detection and it is used in areas such as Ecology, Physiology, Ecotoxicology, Aquaculture and Genetics. Furthermore, *Artemia* based lethality assay (brine shrimp lethality assay, BSLA) is rapid, convenient and low cost. Presently, brine shrimp lethality assays are enormously employed in research and applied toxicology. It has been used in the study of natural products as a preliminary toxicity assay to screen a large number of extracts and compounds for drug discovery in medicinal plants. The aim of this review paper is to collect, organize, select and discuss the existing knowledge about the different uses of *Artemia salina* as a bench-top bioassay for the discovery and purification of bioactive natural products.

Keywords: *Artemia*, brine shrimp, general toxicity, natural products, correlation, alternative model, screening.

1. INTRODUCTION

Natural products contain hundreds to thousands of interrelated chemical compounds that show different biological and therapeutic effects [1, 2]. There is an increasing interest in the use of natural products from plants, animals or microorganisms for the development of new therapies for the treatment of cancer [3]. However, the management and treatment of cancer are often ineffective due to adverse reactions, drug resistance or inadequate target specificity of the anti-cancer agents [4].

About 12.5% of the 422,000 species of higher plants are known to possess medicinal properties and constitute a principal source of bioactive molecules. These figures may expect to increase as many of them have not yet been screened for their biological properties. In modern times, more than a quarter of all commercialized drugs are obtained from compounds isolated from plant extracts and many others are synthetic analogues [5].

Natural products can be a valuable source for the development of new medicines due to their varied range of biological and pharmacological activities. Nevertheless, their potential toxicity should be considered to avoid adverse side effects which are usually common. In this regard, toxicity studies should be done in parallel with pharmacological activity to ensure their safe use as potential drugs. Traditional methods of drug discovery through the assessment of the biological activities (*In-vitro* cancer cell lines, small mammals like mice) of a large number of compounds have proven to be financially costly, time-consuming and, above all, the probability of the evaluated compounds to finally succeed is low [6, 7]. The use of mammalian models in drug discovery has increased over the past decades as they provide meaningful human-like predictions and

information on the mechanistic, effectiveness and toxicity of the plants studied. However, actions from non-governmental organizations (NGOs) towards protecting and preserving animals are still frequently causing restrictions on the use of animals in science mainly due to religious, social and ethical dilemmas [8]. For these reasons, other organisms have started to be used as laboratory model organisms in the search of novel bioactive compounds [9]. The best study models with minimal ethical requirements are invertebrate animal models. They may be highly imperfect, but they are quite useful in research studies and can be inferred to vertebrates. In addition, a preliminary screening in *in vitro* assays serves to prioritize only the best chemicals for further screening of vertebrates [10].

Brine shrimps, *Artemia* also commonly known as sea monkeys, are the most suitable and advantageous way to examine the biological activities of different plant extracts [11]. *Artemia* spp are broadly used in lethality studies and they are also a convenient starting point for cytotoxicity assessment, when screening for the toxicity of natural products, and is based on their ability to kill a laboratory nauplii [12].

Among other animal model assays, the brine shrimp lethality test is the most user-friendly and efficient [13, 14]. This method is habitually used as a safe approach when studying the cytotoxicity and antitumor activity of natural or synthetic compounds derived from plant extracts screening in traditional drug discovery [15]. Although there may be a decrease in the solubility of some chemical substances in the saline medium producing false positives due to the toxicity of the solvent itself, this method is cost-effective, simple, rapid, reliable, comprehensive and can be used to detect the general toxicity in a broad spectrum of natural products. The wide use of *Artemia* as a test organism is mostly because it is easy to culture and well-studied [16-24]. This review intends to evaluate and summarize the use of the *Artemia* lethality bioassay also known as brine shrimp for the general toxicity study of natural products.

*Address correspondence to this author at the CBIOS - Center for Research in Biosciences & Health Technologies, Universidade Lusófona de Humanidades e Tecnologias, Campo Grande 376, 1749-024 Lisbon, Portugal; E-mail: patricia.rijo@ulusofona.pt

1.1. General Features of the Genus *Artemia*

Brine shrimp belongs to the *Artemia* genus (family Artemiidae, order Anostraca, subphylum Crustacea), a primitive aquatic arthropod present in salt lakes [25]. It was first reported from Urmia Lake in 982 AC by an unknown Iranian geographer, and then in 1756, Schlösser pictured both sexes clearly. Linnaeus (1758) described brine shrimp as *Cancer salinus* but 61 years later, Leach (1819) transferred it to *Artemia salina* [26].

Generally speaking, genus *Artemia* contains six bisexual species namely, *A. franciscana*, *A. salina*, *A. sinica*, *A. urmiana*, *A. persimili* and *A. tibetiana* and many other parthenogenetic *Artemia* populations which are distributed all over the world [27]. *Artemia salina*, *Artemia franciscana* and *Artemia urmiana* are the most commonly used species for biological activity study. Nonetheless, *A. salina* is the most extensively studied of the *Artemia* species; estimated to represent over 90% of the studies in which *Artemia* is used as an experimental test organism [7]. They are very important for aquaculture because of their high nutritional value.

The brine shrimp *Artemia* is a primitive arthropod with thin chitin coated segmented body. It grows to an adult size of about 8-12mm long [28]. They are vital in the flow of energy in the aquatic food chain [29, 30] due to the fact that, they feed on microalgae and, in turn, constitute the zooplankton that is used to feed larval fishes [27, 31]. Various authors have demonstrated that the cysts and nauplii biometry and the nutritional properties of *Artemia* may largely differ from one batch to another. Also, contrasting biological, chemical and physiological features can be observed depending on the geographical regions of origin [32]. The *Artemia* nauplii provide better growth and survival rate to fish and thus, they have economic and ecological importance.

Brine shrimps have a short life cycle which makes them suitable as laboratory animal. They have a high fecundity rate, and they

can be obtained from cysts hatching (Fig. 1) [33]. Commonly, they can be found living and breeding in the sea and brackish water. *Artemia* are common in isolated environments with high salinity and relatively warm temperatures, like salt lakes, lagoons and salt mines. The prevalent attribute of all *Artemia* habitats lies in their great ability to reside in highly elevated saline conditions and in maintaining osmotic homeostasis in those conditions [29, 34]. Its habitat ranges in salinity from 5-250 gL⁻¹ and in temperatures from 6 to 35°C. There are three main features that lead to their ability to survive in these hostile environments. The first is the capability to synthesize pigments that help them manage the low oxygen levels of high salinity mediums; the second is their ability to form dormant cysts when conditions become unfavourable [35, 36]; and the third is the presence of the Na⁺/K⁺-ATPase in specialized organs that expel salt from the isosmotic internal hemolymph to the external medium [37]. Their ability to survive in hypertonic environments is a unique mechanism used by them for defense against predators.

2. USE OF ARTEMIA IN BIOLOGICAL ACTIVITY STUDY

2.1. Methodology for the Brine Shrimp Lethality Bioassay

There is an increasing need to evaluate the pharmacological activity and toxicity potential of novel molecules using animal models. The choice of an adequate animal model should take into account global aspects of biology, adaptability to laboratory conditions, ecological relevance, systematic use, and life cycle [38]. However, there is a current tendency towards limiting the use of laboratory animals in toxicological tests. Due to the fact that larvae of the crustacean *Artemia* are sensitive to a variety of substances, the brine shrimp bioassay has been used as a quick and simple test for predicting the toxicity of natural product extracts, as well as compounds with biological activity [20]. Brine shrimp cysts are hatched in artificial seawater (3.5% NaCl solution) for approxi-

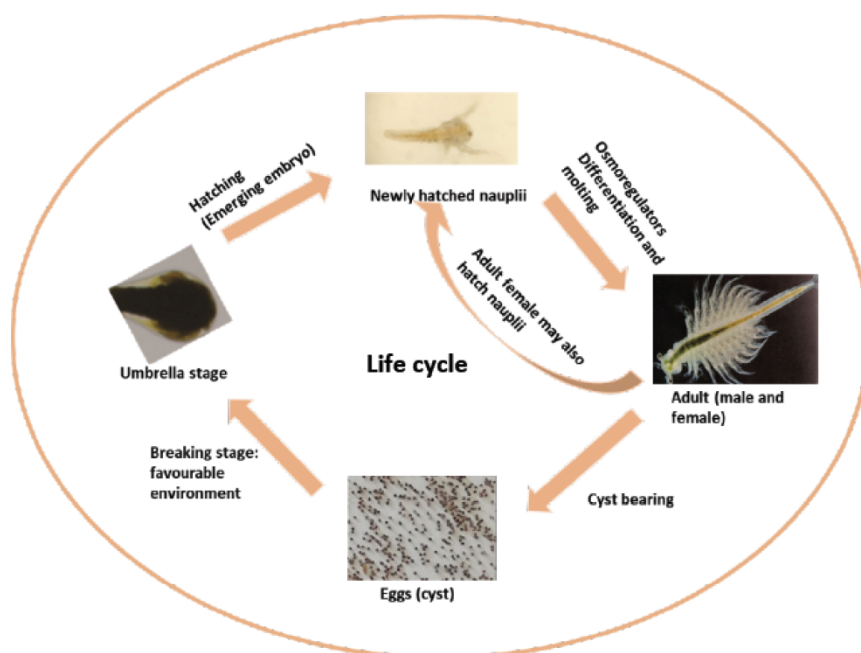


Fig. (1). Different stages of *Artemia* life cycle. (A higher resolution / colour version of this figure is available in the electronic copy of the article).

mately 48h under conditions of aeration, continuous illumination and temperatures of 22-29°C. Nauplii are separated from the eggs by attracting the organisms to one side of the vessel with a light source. After hatching, the active nauplii are collected with a plastic pipette for study. Next, ten to fifteen brine shrimp larvae (nauplii), which have developed for 48 hours, are transferred to each well. The test samples added, and plates are incubated at 22-29°C for 24 hours. The test sample is dissolved in DMSO (dimethyl sulfoxide) at 2% maximum to prevent possible toxicity due to this solvent [13, 39]. The plates are then examined under a binocular microscope (12.5×). After, the nauplii are killed with methanol and the number of deaths (non-mobile nauplii) in each well is counted. The percentage of death calculated and half of the lethal concentration (LC₅₀) is determined using the equation below [7, 40]. All tests should be done in triplicates.

$$(\%Deaths) = \frac{\text{Test-Control}}{\text{Control}} \times 100$$

The positive controls used in this assay are potassium dichromate, thymol, glacial acetic acid, berberine chloride and pure DMSO [16, 41-45]. According to Meyer *et al.*, crude extracts and pure substances with LC₅₀ value < 1000 µg/ml are toxic and the mortality rate of brine shrimp is proportional to the concentration of the test samples.

2.2. *Artemia* as a Model Organism

Small animals are often used as a toxicological model for humans' systems in biological, medical and environmental research. Invertebrates possess a unique advantage as model organisms for biological study. Due to their simple anatomy, brief life cycle and small size, a huge number of invertebrates can be studied in a single experiment. Besides, these organisms combine genetic amenability, low cost compatible with large-scale screens. Despite these characteristics, invertebrates have a primitive organ system and do not have an adaptive immune system, giving rise to some limitations for their use in human diseases [46, 47]. On the downside, protein divergence between invertebrates and humans causes a high rate of false negatives. Regardless of these important limitations, they are still a necessary tool to close the gap between traditional *in vitro* and preclinical animal assays. Their cost of housing is less compared to animals. There is also the possibility of extrapolating research studies to vertebrates [39, 40].

Aquatic animals used to assess the toxicity of chemicals include zebrafish (*Danio rerio*), different species of *Daphnia* (*D. magna*, *D. pulex*), *Thamnocephalus platyurus* and *Artemia* spp. Although brine shrimp was considered to be the least sensitive organism among a group, it is better due to the simplicity of procedures and lower volumes of toxicant required to develop the test [38].

The acute fish test for example has long been used in initial toxicity testing; for this reason, a lot of information has been accumulated for existing chemicals. A closer inspection of existing acute fish LC₅₀ data, however, reveals differences in orders of magnitude not only between the species, but also for the same species between laboratories. Single species LC₅₀ data may thus raise doubts on the accuracy, reproducibility and, in more general terms, regarding toxicological relevance. In addition, sincere ethical concern has evolved, considering the fact that there are doubts that fish exposed to acutely toxic concentrations of chemicals suffer serious distress and pain, which is certainly not compatible with current animal welfare legislation [49].

In an attempt to solve these issues, in 2001, a working group convened by the German Standardisation Organisation (*Deutsches Institut für Normung*, DIN) came up with a protocol for an alternative assay based on zebrafish embryos as a replacement for the acute fish test in routine whole-effluent testing. In this assay, the toxicological endpoints for assessment are coagulation, failure to develop somites, lack of tail detachment from the yolk as well as

lack of heartbeat after 48h of exposure after fertilization. Zebrafish only hatch after approximately 72-96h, thus this alternative method does not represent an animal test in legal terms [50]. On the contrary, several studies have shown consistent distinct patterns of toxicity among different brine shrimp strains and even geographical origin of the cyst lot. Studies have also proven genetic similarities between *Artemia* and humans e.g. the highly conserved Heat shock proteins 70 (Hsp70) family. The Hsp70 family is a group of stress response proteins that have been studied extensively in prokaryotic and eukaryotic organisms due to their potential role in pathology, e.g., cancer and apoptosis. The number of Hsp70 family members expressed depends on the species. Heat shock proteins (HSPs) are a family of highly conserved proteins which respond to environmental stressors, such as high temperature, ultraviolet light, inflammation, infection and toxins [51]. Several Hsp70 gene family members (conserved Hsp70 domains: heat shock cognate 70 (HSC70); heat shock 70kDa cognate 5, HSC70-5; heat shock 70 kDa cognate 3 (HSC70-3)/BIP/Grp78 and hypoxia up-regulated protein 1, HYOU1) have been identified in *Artemia* species as a result of its representation of the vertebrates in toxicity testing. On the other hand, Hsp70 genes existing in the human genome are also involved in the response to environmental changes in the human organism [52]. As both organisms present the same kind of genes that could be expressed in the same conditions (e.g. the presence of toxins or drugs), this may favour the further establishment of the link between humans and *Artemia* spp. genomes that could make it possible to extrapolate the toxicity of the test samples.

As was stated before, *Artemia* spp. is a crustacean with the ability to survive under tough conditions, living mostly in hypersaline habitats. In the evolution tree, they are closely linked to zooplankton such as copepods and *Daphnia* [53]. *Artemia salina* and *Artemia franciscana* are the two brine shrimps species often used in the biological activity study. They are used as test organisms in ecotoxicology, having applications in various fields as research models [48, 59] mainly due to the abundance of their cysts, availability for purchase, easy transformation from hatching into the larvae cycle and the ease to maintain in a laboratory environment as compared to other brine shrimps. In most situations, they are employed as laboratory test organisms in ecotoxicological studies to estimate short-term acute (STA) [54] and long-term chronic (LTC) toxicities [24]. This is because the molecular, cellular, and physiological levels of *Artemia* spp. are drastically altered when in contact with even slight levels of contamination [34, 43].

Artemia acute toxicity tests are known to show low sensitivity; however, prolonged exposure assays are more sensitive but require quite complex procedures that discourages their use [23]. In STA toxicity, the death rate and behavioral parameters are used to study the impact of compounds on the *Artemia* nauplii. The swimming speed, the length and the rate of death after 5-30 seconds of no visible appendage movement are monitored [56]. Furthermore, STA toxicity is highly exploited to study the consequence of biocides on *Artemia* and their aquatic environment that could endanger the survival of other aquatic organisms. Some of these biocides include acetylcholinesterase, organochlorine, organophosphate, carbamate, pyrethroid. It also has applications in the measurement of oxidative stress parameters (glutathione-peroxidase, glutathione reductase, glutathione-S-transferases) and lipid peroxidation [57, 58]. Conversely, in LTC, the *Artemia* is observed based on its evolutionary phases from the larval phase to adulthood evaluating features such as growth, reproduction and survival after 7-28 days exposure using low concentrations of the test samples (µg/L) [11].

The bioassay methods have the advantage of being able to detect global toxicity, i.e., they detect any toxic compound to which the bioindicator would be sensitive and not only a specific target toxin [59]. These bioassays also allow toxin identification and quantification using dose-response curves when pure toxin stan-

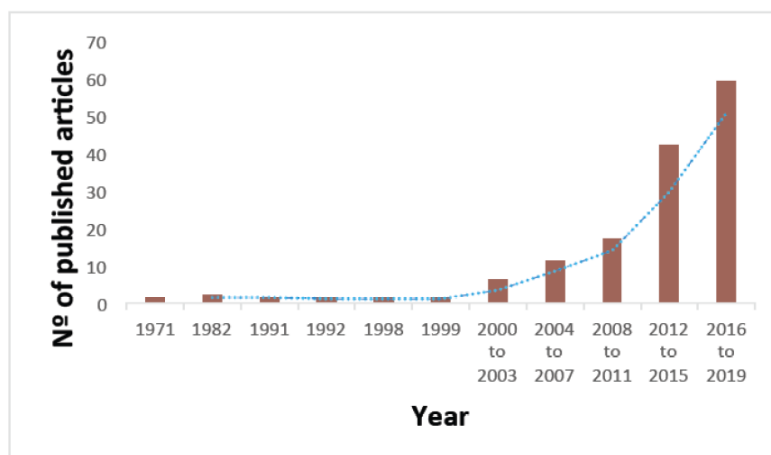


Fig. (2). Publications in which Brine shrimp is used as a screening method for general toxicity in plants from 1971 to 2019. (A higher resolution / colour version of this figure is available in the electronic copy of the article).

dards are available. They are an economic alternative and suitable for small laboratories with limited resources [16-23].

For all these reasons, *Artemia* assay has been used for several years around the world as a laboratory organism. It is used to study the cytotoxicity of medicinal plant extracts most likely toxic to shrimp larvae [16, 60-62]. It is also used to help choose the plant fraction with more potential of containing active components or to detect the possible toxicity of their constituents [63-65]. *Artemia* appear to have the capability to be suitable model species to investigate the general toxicity of medicinal plants and their possible use in drug lead compound search through laboratory experiments [66].

2.3. *Artemia* in Natural Product Chemistry

Natural products could be a good source of novel anti-multidrug resistant agents thanks to their several biological activities and wide structural divergence [67]. However, there is a great need to carry out several and diverse studies, including both pharmacological and toxicity studies, in order to make these plant-based treatments harmless. The toxic effects of plants can originate from several sources. They can come from several kinds of contaminants or the actual components of the mixture. Plants may be useful either in their crude state, advance forms or pure forms providing a source for therapeutic agents. *Artemia salina*, *Artemia franciscana*, *Artemia urmiana* and *Thamnocephalus platyurus* can serve as triage for toxic compounds *i.e.*, used for the initial screening of toxicity [16, 68]. Over the past few years, BSLA has been a useful tool for toxicity studies of different types of plant products (Fig. 2 and Table 1) [16].

BSLA is used for the preliminary study of the general toxicity of natural products [7, 60, 119-133], compounds [155-162], heavy metals [134, 135] metal ions [136], cyanobacteria [137-139] algae [63], dental materials [55], nanoparticles [140] and to screen marine natural products. It is an indicator of potential antitumor, insecticidal, and fungicidal activity [141]. It evaluates toxicity after 24h [17, 45, 100, 144, 147, 151, 153, 160, 169] and after 48h of exposure [150]. Rodrigues *et al.* used the *Artemia salina* to determine the percentage (%) of viability of *Limonium algarvense* Erben and *Camellia sinensis* (L.) Kuntze (green tea) extracts after 48hrs of exposure. The results are expressed as the mean of three independent experiments, each with internal triplicates (n = 9) [150].

The use of *Artemia* spp to determine the general toxicity of natural products has been reported in several papers. They report

using mainly *Artemia salina* [18, 44, 45, 63, 100, 118, 127, 141-167] and *Artemia franciscana* [24, 42, 43, 168].

Akhalwaya *et al.* used *Artemia franciscana* to establish the toxic concentrations for leaves, stems and essential oils of *Cissampelos torulosa* E.Mey. ex Harv. & Sond., *Clausena anisate* (Willd.) Hook.f. ex Benth., *Croton gratissimus* Burch., *Warburgia salutaris* (G.Bertol.) Chiov., *Tarconanthus camphoratus* L. and *Tetradenia riparia* (Hochst.) Codd plants traditionally used for the treatment of oral diseases. The plant extracts and essential oils were selected if they exhibited noteworthy (>1mg/mL) Minimum Inhibitory Concentration (MIC) values against any of the oral pathogens investigated in this study. In this study, BSLA revealed that the leaves, stems and essential oils are considered highly toxic with LC₅₀ values of 132 µg/mL, 126 µg/mL and 194 µg/mL, respectively. The toxicity was determined both after 24h and 48h using glacial acetic acid as a positive control [44].

Lechen plants are often sited as a source of several bioactive natural compounds. Jha *et al.* studied the effect of 84 of these plant extracts on brine shrimp live nauplii mortality after 24 h of treatment. The activity was categorized into four groups-strong (80% to 100% death of nauplii), moderate (50% to 80% death of nauplii), weak (less than 50% death of nauplii) and inactive (no death at all). Berberine chloride was used as positive control and seawater was used as negative control and these samples were toxic against the *Artemia* nauplii [45].

Noé *et al.* used *Artemia franciscana* Kellogg nauplii to study the general toxicity of the *Syzygium australe* (H.L. Wnddl. ex. Link) B. Hyland, *Syzygium luehmianii* (F. Muell.) L.A.S. Johnson, *Syzygium jambos* L. (Alston), *Terminalia ferdinandiana* Exell. and *Tasmannia lanceolata* (Poir.) A.C.Sm. used traditionally for the treatment of a variety of pathogenic diseases. The toxicity of extracts and toxins was determined after 24h of exposure. Concisely, 400 µL of artificial seawater containing 40-60 live *A. franciscana* nauplii, was added to each well of a 48 well micro-titre plate. Individual 400 µL volumes of the test samples were added to the wells and incubated at 25°C. Negative controls (32 g/L artificial seawater: Sigma Australia) and positive controls (1 mg/mL potassium dichromate (K₂Cr₂O₇) (AR grade, Chem-Supply, Australia) were included in all plates. The LD₅₀ value was determined as the concentration of a test substance necessary to have a lethal effect on 50% of the *A. franciscana* nauplii. The results are expressed as the

Table 1. Published studies on which Brine shrimp is used as a screening method for general toxicity in plants.

| Plant | Part | Endpoint of the <i>Artemia</i> Assay | Published Year | Refs. |
|---|-----------------|--------------------------------------|----------------|-------|
| <i>Acacia senegal</i> (L.) Willd. | Fruits | 24h % mortality | 2014 | [69] |
| <i>Ambrosia maritima</i> L. | Leaves | | | |
| <i>Ammi visnaga</i> (L.) Lam. | Fruits | | | |
| <i>Foeniculum vulgare</i> Mill. | Fruits | | | |
| <i>Nigella sativa</i> L. | Seeds | | | |
| <i>Sesamum indicum</i> L. | Seeds | 24h % mortality | 2012 | [70] |
| <i>Trigonella foenum-graecum</i> L. | Seeds | | | |
| <i>Glycine max</i> (L.) Merr. | Seeds | | | |
| <i>Sesamum indicum</i> L. | Seeds | 24h % mortality | 2011 | [71] |
| <i>Tamarindus indica</i> L. | Stem bark | | | |
| <i>Amphipteryngium adstringens</i> (Schltdl.) Standl. | Stem bark | 24h % mortality | 2007 | [72] |
| <i>Arracacia toluensis</i> var. <i>multifida</i> (Kunth) Hemsl. | Aerial parts | | | |
| <i>Brickellia veronicaefolia</i> (Kunth) A.Gray | Aerial parts | | | |
| <i>Exostema caribaeum</i> (Jacq.) Schult. | Stem bark | | | |
| <i>Gnaphalium</i> spp. | Inflorescences | | | |
| <i>Haematoxylon brasiletto</i> H.Karst. | Stem bark | | | |
| <i>Hintonia latiflora</i> (Sessé & Moc. ex DC.) Bullock | Stem bark | | | |
| <i>Hintonia standleyana</i> Bullock | Stem bark | | | |
| <i>Hippocratea excelsa</i> Kunth | Roots | | | |
| <i>Iostephane heterophylla</i> (Cav.) Benth. | Roots | | | |
| <i>Ligusticum porteri</i> J.M.Coult. & Rose | Roots | | | |
| <i>Piper sanctum</i> (Miq.) Schltdl. ex C.DC. | Leaves | | | |
| <i>Poliomintha longiflora</i> A.Gray | Aerial parts | | | |
| <i>Scaphyglottis livida</i> (Lindl.) Schltr. | Whole plant | | | |
| <i>Valeriana procera</i> Kunth | Roots, rhizomes | | | |
| <i>Quercus infectoria</i> G.Olivier | Galls | 24h and 48h % mortality | 2009 | [73] |
| <i>Kaempferia galanga</i> L. | Rhizomes | | | |
| <i>Coptis chinensis</i> Franch. | Roots | | | |
| <i>Glycyrrhiza uralensis</i> Fisch. | Roots | | | |
| <i>Callistemon citrinus</i> (Curtis) Skeels | Fruits | 24h % mortality | 2011 | [74] |
| <i>Rubus fruticosus</i> L. ex Dierb. | Fruits | 24h % mortality | 2013 | [75] |
| <i>Coriandrum sativum</i> L. | Essential oil | 24h and 48h % mortality | 2015 | [76] |
| <i>Thymus vulgaris</i> L. | Essential oil | | | |
| <i>Indigofera gerardiana</i> Baker | Whole plant | 24h % mortality | 2009 | [77] |
| <i>Peltophorum pterocarpum</i> (DC.) K. Heyne | Root | 24h % mortality | 2011 | [78] |

(Table 1) Contd....

| Plant | Part | Endpoint of the Artemia Assay | Published Year | Refs. | | | | |
|--|--------------|-------------------------------|----------------|-------|--------|-----------------|------|------|
| <i>Passiflora glandulosa</i> Cav. | Fruit | 24h % mortality | 2018 | [79] | | | | |
| <i>Persicaria orientalis</i> (L.) Spach | Leaves | 24h % mortality | 2016 | [80] | | | | |
| <i>Jurinea dolomiaea</i> Boiss. | Roots | 24h % mortality | 2014 | [81] | | | | |
| <i>Asparagus gracilis</i> Salisb. | Aerial parts | | | | | | | |
| <i>Sida cordata</i> (Burm.f.) Borss. Waalk. | Whole plant | | | | | | | |
| <i>Stellaria media</i> (L.) Vill. | Whole plant | | | | | | | |
| <i>Chukrasia tabularis</i> A.Juss. | Bark, leaves | | | | | | | |
| <i>Turraea vogelii</i> Hook.f. | Leaves | 24h % mortality | 2016 | [82] | | | | |
| <i>Psophocarpus tetragonolobus</i> (L.) DC. | Pods | 24h % mortality | 2006 | [83] | | | | |
| <i>Vanda tessellata</i> (Roxb.) Hook. ex G.Don | Leaves | 24h % mortality | 2014 | [84] | | | | |
| <i>Heritiera fomes</i> Buch.-Ham. | Bark | 24h % mortality | 2009 | [85] | | | | |
| <i>Acalypha hispida</i> Blume | Stem barks | 24h % mortality | 2018 | [86] | | | | |
| <i>Baccaurea lanceolata</i> (Miq.) Müll. Arg | | | | | | | | |
| <i>Bischofia javanica</i> Blume | | | | | | | | |
| <i>Codiaeum variegatum</i> (L.) Rumph. ex A.Juss. | | | | | | | | |
| <i>Croton paniculatus</i> Lam | | | | | | | | |
| <i>Euphorbia antiquorum</i> L. | | | | | | | | |
| <i>Euphorbia hirta</i> L. | | | | | | | | |
| <i>Jatropha podagrica</i> Hook. | | | | | | | | |
| <i>Glochidion arborescens</i> Blume | | | | | | | | |
| <i>Macaranga tanarius</i> (L.) Müll.Arg | | | | | | | | |
| <i>Sapium baccatum</i> Roxb. | | | | | | | | |
| <i>Parabaena sagittata</i> Miers | | | | | Leaves | 24h % mortality | 2013 | [87] |
| <i>Adenia rumicifolia</i> Engl. & Hamms. | | | | | Leaves | 24h % mortality | 2001 | [88] |
| <i>Caesalpinia bonduc</i> (L.) Roxb. | | | | | Roots | | | |
| <i>Cassia occidentalis</i> L. | Roots | | | | | | | |
| <i>Citrus aurantifolia</i> (Christm.) Swingle | Leaves | | | | | | | |
| <i>Cleistopholis patens</i> (Benth.) Engl. & Diels | Leaves | | | | | | | |
| <i>Cnestis ferruginea</i> Vahl ex DC. | Roots | | | | | | | |
| <i>Momordica cissoides</i> Planch. ex Benth. | Whole plant | | | | | | | |
| <i>Morinda morindoides</i> (Baker) Milne-Redh. | Roots | | | | | | | |
| <i>Oncoba spinosa</i> Forssk. | Seed | | | | | | | |
| <i>Pleiocarpa mutica</i> Benth. | Roots | | | | | | | |
| <i>Rothmannia longiflora</i> Salisb. | Stem bark | | | | | | | |
| <i>Turraea heterophylla</i> Sm. | Leafy twigs | | | | | | | |
| <i>Uvaria chamae</i> P.Beauv. | Roots | | | | | | | |
| <i>Vernonia colorata</i> (Willd.) Drake | Stem bark | | | | | | | |

(Table 1) Contd....

| Plant | Part | Endpoint of the <i>Artemia</i> Assay | Published Year | Refs. |
|--|------------------------|--------------------------------------|----------------|-------|
| <i>Carissa edulis</i> (Forssk.) Vahl | Roots | 24h % mortality | 2006 | [89] |
| <i>Neoboutonia macrocalyx</i> Pax | Stem bark | | | |
| <i>Acacia nilótica</i> (L.) Delile | Stem bark | | | |
| <i>Strychnos henningsii</i> Gilg | Stem bark | | | |
| <i>Azadirachta indica</i> A.Juss. | Leaves | | | |
| <i>Myrica salicifolia</i> Hochst. ex A. Rich. | Stem bark | | | |
| <i>Fagaropsis angolensis</i> (Engl.) H.M.Gardner | Stem bark | | | |
| <i>Zanthoxylum usambarense</i> (Engl.) Kokwaro | Stem bark | | | |
| <i>Harrisonia abyssinica</i> Oliv. | Stem bark | | | |
| <i>Withania somnifera</i> (L.) Dunal | Stem bark | | | |
| <i>Cola cordifolia</i> (Cav.) R.Br. | Bark, leaves | 24h % mortality | 2012 | [90] |
| <i>Acalypha hispida</i> (Burm.) F | Flower (essential oil) | 24h % mortality | 2011 | [91] |
| <i>Mimosa pudica</i> L. | Stems | 24h % mortality | 2008 | [92] |
| <i>Mimosa rubicaulis</i> Lam. | Stems | | | |
| <i>Centaurea persica</i> Boiss. | Aerial parts | 24h % mortality | 2012 | [93] |
| <i>Grewia trichocarpa</i> Hochst. ex A. Rich. | Roots | 24h % mortality | 2014 | [94] |
| <i>Dichrostachys cinerea</i> (L.) Wight et Arn. | Roots | | | |
| <i>Tamarindus indica</i> L. | Stem bark | | | |
| <i>Azadirachta indica</i> (L.) Burn. | Root bark | | | |
| <i>Acacia seyal</i> Del. | Roots | | | |
| <i>Azadirachta indica</i> (L.) Burn | Root bark | | | |
| <i>Dichrostachys cinerea</i> (L.) Wight et Arn | Roots | 24h % mortality | 2013 | [95] |
| <i>Tamarindus indica</i> L. | Stem bark | | | |
| <i>Acacia seyal</i> Del. | Roots | | | |
| <i>Grewia trichocarpa</i> Hochst ex A.Rich. | Roots | | | |
| <i>Albizia gummifera</i> (J.F. Gmel.) C.A. Sm. | Leaves, roots | | | |
| <i>Cyathula cylindrica</i> Moq. | Leaves, roots | 24h % mortality | 2004 | [96] |
| <i>Cyathula polycephala</i> Bak. | Leaves, roots | | | |
| <i>Pentas longiflora</i> Oliv. | Leaves, roots | | | |
| <i>Pittosporum lanatum</i> Hutch. & E.A. Bruce | Leaves, roots | | | |
| <i>Croton argyrophyloides</i> Müll. Arg. | Aerial parts | | | |
| <i>Maranta arundinacea</i> Linn. | Leaves | 24h % mortality | 2015 | [98] |
| <i>Maytenus obtusifolia</i> Mart. | Leaves | 24h % mortality | 2008 | [99] |
| <i>Ocimum suave</i> Willd. | Leaves | 24h % mortality | 2015 | [100] |
| <i>Plectranthus barbatus</i> Andrews | Root barks | | | |
| <i>Zanthoxylum chalybeum</i> Engl. | Roots barks | | | |

(Table 1) Contd....

| Plant | Part | Endpoint of the Artemia Assay | Published Year | Refs. |
|--|---------------|-------------------------------|----------------|-------|
| <i>Morus alba</i> L. | Leaves | 24h % mortality | 2015 | [101] |
| <i>Lonchocarpus montanus</i> A.M.G. Azevedo | Roots | 24h % mortality | 2007 | [102] |
| <i>Acacia caven</i> (Molina) Molina | Seeds | 24h % mortality | 1992 | [103] |
| <i>Acaena argentea</i> Ruiz & Pav. | Aerial parts | | | |
| <i>Apium australe</i> Thouars | Aerial parts | | | |
| <i>Aristolelia chilensis</i> (Molina) Stuntz | Leaves | | | |
| <i>Baccharis linearis</i> (Ruiz & Pav.) Pers. | Aerial parts | | | |
| <i>Baccharis rhomboidalis</i> J.Rémy | Aerial parts | | | |
| <i>Buddleja globosa</i> Hope | Leaves, stem | | | |
| <i>Centaurium cachenlahuen</i> (Molina) B.L.Rob. | Whole plant | | | |
| <i>Cestrum parqui</i> (Lam.) L'Hér. | Aerial parts | | | |
| <i>Cryptocarya alba</i> (Molina) Looser | Leaves, bark | | | |
| <i>Equisetum bogotense</i> Kunth | Whole plant | | | |
| <i>Escallonia illinita</i> C.Presl | Leaves, Stem | | | |
| <i>Fabiana imbricata</i> Ruiz & Pav. | Aerial parts | | | |
| <i>Fuchsia magellanica</i> Lam. | Aerial parts | | | |
| <i>Geranium core-core</i> Steud. | Aerial parts | | | |
| <i>Gunnera tinctoria</i> (Molina) Mirb. | Aerial parts | | | |
| <i>Lapageria rosea</i> Ruiz & Pav. | Aerial parts | | | |
| <i>Laurelia sempervirens</i> Tul. | Leaves | | | |
| <i>Loasa tricolor</i> Ker Gawl. | Aerial parts | | | |
| <i>Lomatia ferruginea</i> R. Br. | Aerial parts | | | |
| <i>Luzuriaga radicans</i> Ruiz & Pav. | Aerial parts | | | |
| <i>Modiola caroliniana</i> (L.) G.Don | Aerial parts | | | |
| <i>Muehlenbeckia hastulata</i> (Sm.) I.M.Johnst. | Whole plant | | | |
| <i>Nertera granadensis</i> (Mutis ex L.f.) Druce | Aerial parts | | | |
| <i>Oxalis rosea</i> Jacq. | Whole plant | | | |
| <i>Plantago major</i> L. | Aerial parts | | | |
| <i>Relbunium hypocarpium</i> (L.) Hemsl. | Whole plant | | | |
| <i>Rumex crispus</i> L. | Whole plant | | | |
| <i>Schinus latifolius</i> (Gillies ex Lindl.) Engl. | Bark | | | |
| <i>Tristerix tetrandrus</i> (Ruiz & Pav.) Mart. | Leaves, seeds | | | |
| <i>Borago officinalis</i> L. | Leaves | 24h % mortality | 2011 | [104] |
| <i>Lawsonia inermis</i> L. | Leaves | 24h % mortality | 2014 | [105] |
| <i>Carissa edulis</i> (Forssk.) Vahl | Stem bark | 24h % mortality | 2009 | [106] |
| <i>Periploca linearifolia</i> Quart. (Dill & A.Rich) | Stem bark | | | |
| <i>Kigelia africana</i> (Lam.) Benth. | Leaves | | | |

(Table 1) Contd....

| Plant | Part | Endpoint of the Artemia Assay | Published Year | Refs. | | | | |
|---|-------------------------|-------------------------------|----------------|-------|-------------|-----------------|------|-------|
| <i>Maytenus heterophylla</i> (Eckl. & Zeyh.) N. Robson | Root bark | - | - | - | | | | |
| <i>Microglossa pyrifolia</i> (Lam.) Kuntze | Leaves | | | | | | | |
| <i>Strychnos usambarensis</i> Gilg ex Engl. | Root bark | | | | | | | |
| <i>Strychnos henningstii</i> Gilg | Root bark | | | | | | | |
| <i>Lippia javanica</i> (Burm f.) Gaertn. | Roots | | | | | | | |
| <i>Ocimum gratissimum</i> L. | Seeds, leaves and stems | 24h % mortality | 2014 | [107] | | | | |
| <i>Acrostichum heterophyllum</i> L. | Leaves | 24h % mortality | 2016 | [108] | | | | |
| <i>Buddleja thyrsoides</i> Lam. | Leaves | 24h % mortality | 2012 | [109] | | | | |
| <i>Vernonia kotschyana</i> Sch. Bip. ex Walp. | Roots | 24h % mortality | 2012 | [90] | | | | |
| <i>Adenantha pavonina</i> L. | Leaves | 24h % mortality | 2016 | [110] | | | | |
| <i>Acacia mearsii</i> De Wild. | Bark | 24h % mortality | 2012 | [111] | | | | |
| <i>Ritchiea capparoides</i> (Andr.) Britten var. <i>longipedicellata</i> (Glig) De Wolf | Leaves, stem bark | 24h % mortality | 1998 | [112] | | | | |
| <i>Boerhavia elegans</i> Choisy | Whole plants | 24h % mortality | 2010 | [113] | | | | |
| <i>Solanum surattense</i> Burm. f. | | | | | | | | |
| <i>Solanum alatum</i> Dunal | | | | | | | | |
| <i>Prosopis juliflora</i> (Sw.) DC. | | | | | | | | |
| <i>Ficus benghalensis</i> L. | | | | | | | | |
| <i>Ficus carica</i> L. | | | | | | | | |
| <i>Citrus limon</i> (L.) Osbeck | | | | | | | | |
| <i>Morus alba</i> L. | | | | | | | | |
| <i>Acacia farnesiana</i> (L.) Willd. | | | | | | | | |
| <i>Citrus aurantifolia</i> (Christm.) Swingle | | | | | | | | |
| <i>Acanthospermum hispidum</i> DC. | | | | | Aerial part | 24h % mortality | 2011 | [114] |
| <i>Argemone mexicana</i> L. | | | | | Whole plant | | | |
| <i>Byrsocarpus coccineus</i> Schumach. & Thonn. | Roots | | | | | | | |
| <i>Croton lobatus</i> L. | Aerial part | | | | | | | |
| <i>Canthium setosum</i> Hiem | Aerial part | | | | | | | |
| <i>Dichapetalum guineense</i> (DC.) Keay | Leaves | | | | | | | |
| <i>Nauclea latifolia</i> Sm. | Roots | | | | | | | |
| <i>Pterocarpus erinaceus</i> Poir. | Aerial part | | | | | | | |
| <i>Schrankia leptocarpa</i> DC. | Whole plant | | | | | | | |
| <i>Secamone afzelii</i> (Roem. & Schult.) K. Schum. | Aerial part | | | | | | | |
| <i>Gynotroches axillaris</i> Blume | Leaves | 24h % mortality | 2013 | [115] | | | | |
| <i>Ocimum gratissimum</i> L. | Leaves | 24h % mortality | 2017 | [116] | | | | |
| <i>Iris germanica</i> L. | Rhizomes | 24h % mortality | 2003 | [117] | | | | |
| <i>Coffea arabica</i> L. | Cherries | 24h % viability | 2016 | [118] | | | | |
| <i>Coffea canephora</i> Pierre ex A. Froehner | | | | | | | | |

mean of three independent experiments, each with internal triplicates (n = 9) [42].

3. CORRELATION OF ARTEMIA SALINA ASSAY TO OTHER TOXICITY ASSAYS

Many studies have established a positive correlation between the brine shrimp assay and mice acute oral toxicity [16, 139, 151, 169-171]. Parra *et al.* studied the acute oral toxicity of 20 Cuban plant extracts which have important pharmacological properties and are used widely by the local population using “*in vivo*” and “*in vitro*” methods. Their results showed a positive correlation ($r = 0.85$ $p < 0.05$), suggesting that BSLA is a useful alternative model for toxicological studies and predicting the general toxicity of plant extracts. Also, in the work of Hossain *et al.*, the *Cassia reniger* ethanolic extracts had more activity in both the *Artemia salina* assay and mice acute toxicity study in both the 500 mg/Kg and 1000 mg/kg body weight dose indicating a positive correlation between the two assays [172].

Araújo *et al.* studied the general toxicity and *in vivo* antitumor activity against Sarcoma-180 of *Crataeva tapia* Bark Lectin (CrataBL). In this study, CrataBL exhibited *A. salina* mortality with an LC_{50} of 71.73 $\mu\text{g/ml}$ and as proposed by Meyer *et al.*, crude extracts and pure substances with LC_{50} value $< 1000 \mu\text{g/ml}$ are toxic. In the same light, the treatment of albino Swiss mice with CrataBL (20 mg/kg) significantly ($p < 0.05$) reduced the Sarcoma 180 volume as compared to the tumor volume of the control group; for which the antitumor activity of lectin has already been described. Hence, this reinforced a good correlation between these two assays [173]. Moshi *et al.* evaluated the toxicity of *Crassocephalum vitellinum* (Benth.) S. Moore extracts in mice and BSLA having similar results. In both assays, the extract exhibited low brine shrimp toxicity and no toxicity to mice and all the animals survived to the 28 days of observation period [174]. Ali *et al.* also showed that *Rubus fruticosus* G.N.Jones used in tribal medicine had moderate toxicity in both acute mice toxicity assay and the BSLA [75]. Other studies showed equivalent results between brine shrimp-mice models [12,13], however there is a need for adequate interlaboratory validation of these methods in toxicity testing.

Cytotoxicity using cell lines requires special facilities and technical skills that are not usually available in most field-monitoring laboratories. Therefore, a convenient and reliable method as BSLA for routine screening of natural product toxicity is needed. The National Cancer Institute (NCI) revealed there is a symbolic correlation amidst the *Artemia salina* assay and the *in vitro* inhibitory growth of human tumor cell lines [175, 176]. Potent anticancer activity against human cancer cell lines using the 3-(4,5-dimethylthiazol-2-yl)-2,5-diphenyltetrazolium bromide (MTT) and Brine shrimp assays was also proven to be in agreement and consistent [177-179].

Rajabi *et al.* assessed the cytotoxicity of 16 natural products using two methods: the brine shrimp lethality assay and the MTT assay in L929 cells. According to the results, the correlation between the LC_{50} and IC_{50} values is significant ($R^2 = 0.72$, $P = 0.000$). This means that 72% variability noted in MTT method could be accounted for the BSLA and 28% is unaccounted for due to measurement error. There was no statistically significant difference between the two assays when the results were compared with paired t-test ($P = 0.402$). Also, the comparison between LC_{50} and IC_{50} mean values was statistically analysed by the Chi-square test and the result showed that there are no differences between the two assay methods ($P = 0.235$). Thus, the results obtained by BSLA are comparable with MTT results [121].

Zengin *et al.* confirmed good biocompatibility between the general toxicity using the *A. salina* model and MTT method. They studied the toxicity of *Rubus sanctus* Schreb. and *Rubus ibericus* Juz. collected from Turkey using the BSLA. This revealed LC_{50} values in the range of 2.52-5.12 mg/mL. Due to LC_{50} values ob-

tained, a concentration of 500 $\mu\text{g/mL}$ was selected, and the cytotoxicity was evaluated on human colon cancer derived HCT 116 cell using the MTT test. The tested extracts (10-500 $\mu\text{g/mL}$) confirmed good biocompatibility, as revealed by the null effect on cell line viability in the range (10-100 $\mu\text{g/mL}$) [167].

While in the search for new molecules that exhibit selectivity for a tumor cell but not a normal cell, the work of Natalija *et al.* proved similar results. They tested compounds against the K562 leukemia cells and in the brine shrimp test. The results of the brine shrimp test were in good correlation with cytotoxicity. The five steroid dimers that exhibited the highest cytotoxic actions against tested malignant cell lines were also active in the *A. salina* model with an IC_{50} in the range of 0.026-0.068 mg per disc [180].

The series of studies conducted by Mondal *et al.* on the methanolic extract from the leaves of *Colocasia affinis* Schott demonstrated a correlation between the brine shrimp assay and *in vitro* growth inhibition of human solid tumor cell lines demonstrated by the NCI [181]. More so, in 2019, Olivares-Bañuelos *et al.* studied the Hexane (Hx) and Chloroform (Chl) extracts of Brown Seaweed *Egrecia menziesii* (Turner) Areschoug in both the *A. salina* assay and the MTT assay using the glioma cancer cell lines from mouse, rat and human. Their results showed that the extracts are effective by diminishing the viability of glioma cell lines. Similar results were observed in the BSLA as the Hx and Chl extracts inhibited up to 100% of *A. salina*'s growing, and therefore, they must be considered as cytotoxic agents. This further affirms the possibility of extrapolating the results of BSLA to the cytotoxicity of cell lines [162]. It should be however noted that the toxic doses for *Artemia salina* are in the range of 10-100 times higher in comparison to cell culture methods [55].

In the study of Matthews, the *Artemia salina* was used as a laboratory organism to investigate the capacity of compounds to prevent superoxide-mediated toxicity. In this study, it was established that *Artemia salina* are remarkably active against the menadione bisulfite. The toxicity of this compound is believed to be seemingly mediated by intracellular superoxide generation. Hence, for this reason, this cheap, useful, user-friendly assay requiring little skills could be a good tool to evaluate and search for compounds with the ability to prevent harmful effects by superoxide or other active oxygen species [182].

In the past, the cytotoxicity of cyanobacteria could be determined using only the brine shrimp bioassay. However, contrary to the above works, Hisem *et al.* suggested that it is not enough to determine the cytotoxicity of cyanobacteria only with the brine shrimp bioassay because cytotoxicity is more a distinctive attribute in cyanobacteria in comparison with toxicity to *A. salina*. In the work reported, the murine lymphoblastic cell line Sp/2 and brine shrimp (*A. salina*) were used to screen the general toxicity of heterocystous cyanobacteria from different habitats to determine the danger presented by cyanobacteria in order to contrast these two laboratory models. It was found that just 8.6% of the tested strains were exceedingly toxic to both *A. salina* and the Sp/2 cell line, and only two of the tested strains were toxic to *A. salina* and not to the murine cell line. The authors concluded that *A. salina* toxicity test should not be used to determine the possibility of the health risk posed by cyanobacteria to humans, proposing instead that *in vitro* mammal cells be used to assess the risk of cyanobacteria [137].

The BSLA shows the general toxicity and is not peculiar to any pharmacological activity. Therefore, toxicity from this test should be treated with caution and more specific toxicology assays should be performed. This is because in a study done by Movahhedini *et al.*, regardless of the slight toxicity demonstrated by the methanolic extracts of *Caulerpa peltata* J.V.Lamouroux against the *Artemia nauplii*, this extract was almost inactive against the L5178Y mouse lymphoma cells. Thus, cytotoxic molecules with activity in the BSLA may not all be anti-cancerous [183].

4. SENSITIVITY OF ARTEMIA SALINA ASSAY

For the past decades, *Artemia* nauplii has been used as a tool to analyse the general toxicity in teratology screens, ecotoxicology and natural products. It has been found to have a good relationship with other model laboratory assays to detect antitumoral compounds in natural products. BSLA can be done using hatched nauplii (lethality test) based on the inhibition of hatching of the cyst (hatchability test), different age specimens and the disruptions on enzyme properties [136]. However, most researchers have made use of the lethality test. Carballo *et al.* demonstrated that natural products could be tested for their biological activity using both the BSLA and the hatchability assays with the lethality test being more sensitive [184].

Artemia salina assay is reported for a high natural death rate up to 83% as a consequence of the lack of food [11,55]. Dose-response experiments indicate that the sensitivity of *A. salina* to algae extracts and commercially available Decadienal is strongly dependent upon an increase in dose, exposure period and the particular assay chosen [185]. Comparing the relationship between an increase in concentration and lethality of the nauplii, the degree of mortality increased in a concentration-dependent manner which peaked at 1 mg/mL [186].

High death rates occur within 24h of exposure compared with the control with a significant difference of $p < 0.01$. Death may be due to abnormalities observed which included improper development of mandibles and under developed endopod, endite, and the swimming setae of the second pair antenna, which resulted in an imbalanced and irregular swimming pattern [187]. According to Unuofin *et al.*, maximum sensitivity of nauplii is achieved at the second and third instar stage and it is interpreted to be after 48 hours of incubation [186].

CONCLUSION

The use of alternative models for toxicity screening has been well accepted by the scientific community worldwide. Microcrustacean used in research are easily managed organisms and feasibly cultured in large populations using laboratory methods. One of these microcrustaceans is the *Artemia*, which has been used as a method to test the biological activity and general toxicity of different drugs, and of medicinal plant extracts. The use of *Artemia* for toxicity studies is being debated by many researchers. As previously discussed, some studies did not find a good correlation between the brine shrimp assay and other cytotoxic assays and stated that there is no significant correlation between the toxicity in cell lines and *Artemia*. On the contrary, others are of the opinion that although brine shrimp test does not provide specific information regarding drugs mechanism of action, it has a good correlation with other mammalian models. It is used to detect cytotoxicity which can be extrapolated to the cell lines, making it a good method to study new cancer treatments. Hence the use of *Artemia* as a test model should be critical as its toxicity appears to depend on the mechanism of action of the test sample. It seems that samples whose toxic effect targets various basal metabolic pathways present in the eukaryotic cell, rather than being a specific mechanism against a complex multi-cellular organism may not be active in the brine shrimp assay. Thus, it is important to note that, when using *Artemia* as a test organism, further and more specific bioassays are necessary in order to confirm these presumptions.

LIST OF ABBREVIATIONS

| | | |
|---------|---|------------------------------------|
| AC | = | After Christ |
| BSLA | = | Brine Shrimp Lethality Assay |
| BSLT | = | Brine Shrimp Lethality Test |
| Chl | = | Chloroform |
| CrataBL | = | <i>Crataeva tapia</i> Bark Lecitin |

| | | |
|---|---|---|
| DIN | = | German Standardisation Organisation (<i>Deutsches Institut für Normung</i>) |
| DMSO | = | Dimethyl sulfoxide |
| Hx | = | Hexane |
| IC ₅₀ | = | Medium Inhibitory Concentration |
| K ₂ Cr ₂ O ₇ | = | Potassium Dichromate |
| LC ₅₀ | = | Medium Lethal Concentration |
| LD ₅₀ | = | Medium Lethal Dose |
| LTC | = | Long-Term Chronic |
| MIC | = | Minimum Inhibitory Concentration |
| MTT | = | 3-(4,5-dimethylthiazol-2-yl)-2,5-diphenyltetrazolium bromide |
| N | = | Number (of samples, etc.) |
| NCI | = | National Cancer Institute |
| P | = | Probability |
| R | = | Ratio |
| Ref. | = | Reference(s) |
| R & D | = | Research & Development |
| STA | = | Short-Term Acute |

CONSENT FOR PUBLICATION

Not applicable.

FUNDING

This research and APC were funded by Fundação para a Ciência e Tecnologia (FCT) grant number UID/DTP/04567/2016, UID/QUI/50006/2019 and UID/DTP/04567/2019.

CONFLICT OF INTEREST

The authors declare no conflict of interest, financial or otherwise.

ACKNOWLEDGEMENTS

This work was supported by PADDIC 2019 (ALIES-COFAC) as part of the PhD Program in Health Sciences from Universidad de Alcalá and Universidade Lusófona de Humanidades e Tecnologias.

REFERENCES

- [1] Campos KC, Rivera JH, Gutierrez JR, *et al.* Biological screening of select puerto rican plants for cytotoxic and antitumor activities. *P R Health Sci J* 2015; 34(1): 25-30.
- [2] Fatima I, Kanwal S, Mahmood T. Evaluation of biological potential of selected species of family *Poaceae* from Bahawalpur. *BMC Complement Altern Med* 2018; 18(1): 27. <http://dx.doi.org/10.1186/s12906-018-2092-1>
- [3] Cragg GM, Newman DJ. Natural products: A continuing source of novel drug leads. *Biochim Biophys Acta* 2013; 1830(6): 3670-95. <http://dx.doi.org/10.1016/j.bbagen.2013.02.008>
- [4] Conniot J, Silva JM, Fernandes JG, *et al.* Cancer immunotherapy: Nanodelivery approaches for immune cell targeting and tracking. *Front Chem* 2014; 2: 105. <http://dx.doi.org/10.3389/fchem.2014.00105>
- [5] Ramawat KG, Goyal S. Natural Products in cancer chemoprevention and chemotherapy. *Herbal drugs: Ethnomedicine to Modern Medicine* Heidelberg. Springer 2008; 153-71.
- [6] Onguéné PA, Simoben CV, Fotso GW, *et al.* *In silico* toxicity profiling of natural product compound libraries from African flora with anti-malarial and anti-HIV properties. *Comput Biol Chem* 2018; 72: 136-49. <http://dx.doi.org/10.1016/j.compbiolchem.2017.12.002>
- [7] Meyer BN, Ferrigni NR, Putnam JE, Jacobsen LB, Nichols DE, McLaughlin JL. Brine shrimp: A convenient general bioassay for active plant constituents. *Planta Med* 2007; 45(5): 31-4. <http://dx.doi.org/10.1055/s-2007-971236>

- [8] Freires IA, Sardi J de CO, de Castro RD, Rosalen PL. Alternative animal and non-animal models for drug discovery and development: Bonus or burden? *Pharm Res* 2017; 34(4): 681-6. <http://dx.doi.org/10.1007/s11095-016-2069-z>
- [9] Monteiro JA, Ferreira Júnior JM, Oliveira IR, et al. Bioactivity and toxicity of *Senna cana* and *Senna pendula* extracts. *Biochem Res Int* 2018; 2018: 8074306. <http://dx.doi.org/10.1155/2018/8074306>
- [10] Mandrell D, Truong L, Jephson C, et al. Automated zebrafish chorion removal and single embryo placement: Optimizing Throughput of zebrafish developmental toxicity screens. *J Lab Autom* 2012; 17(1): 66-74. <http://dx.doi.org/10.1177/2211068211432197>
- [11] Libralato G, Prato E, Migliore L, Cicero AM, Manfra L. A review of toxicity testing protocols and endpoints with *Artemia* spp. *Ecol Indic* 2016; 69: 35-49. <http://dx.doi.org/10.1016/j.ecolind.2016.04.017>
- [12] Dominguez-Villegas V, Dominguez-Villegas V, Garcia ML, Calpena A, Clares-Naveros B, Garduño-Ramírez ML. Anti-inflammatory, antioxidant and cytotoxicity activities of methanolic extract and prenylated flavanones isolated from leaves of *Eysehardia platycarpa*. *Nat Prod Commun* 2013; 8(2): 177-80. <http://dx.doi.org/10.1177/1934578X1300800211>
- [13] Baravalia Y, Vaghiasya Y, Chanda S. Brine shrimp cytotoxicity, anti-inflammatory and analgesic properties of *Woodfordia fruticosa* Kurz flowers. *Iran J Pharm Res* 2012; 11(3): 851-61.
- [14] Khodaie L, Delazar A, Nazemiyeh H. Biological activities and phytochemical study of *Pedicularis wilhelmsiana* Fisch Ex. from Iran. *Iran J Pharm Res* 2019; 18(1): 339-47.
- [15] Islam S. *In vitro* pharmacological investigations of dichloromethane fraction of *Opuntia elatior* submitted by Silvia Islam department of pharmacy, Medicine (Baltimore) 2010; 1: 70-049.
- [16] Hamidi M, Jovanova B, Panovska T. Toxicological evaluation of the plant products using Brine Shrimp (*Artemia salina* L.) model Macedonian pharmaceutical bulletin 2014; 60(1): 9-18.
- [17] Ntungwe NE, Marçalo J, Garcia C, et al. Biological activity screening of seven *Plectranthus* species. *Biomed Biopharm Res* 2017; 1(4): 95-108. <http://dx.doi.org/10.19277/BBR.14.1.153>
- [18] Alanis-Garza BA, González-González GM, Salazar-Aranda R, Waksman de Torres N, Rivas-Galindo VM. Screening of antifungal activity of plants from the northeast of Mexico. *J Ethnopharmacol* 2007; 114(3): 468-71. <http://dx.doi.org/10.1016/j.jep.2007.08.026>
- [19] Rimpiläinen T, Andrade J, Nunes A, et al. Aminobenzylated 4-nitrophenols as antibacterial agents obtained from 5-nitrosalicylaldehyde through a petasis borono-mannich reaction. *ACS Omega* 2018; 3(11): 16191-202. <http://dx.doi.org/10.1021/acsomega.8b02381>
- [20] Melo LF de A, Camara CAG da, Oliveira LLD da SS de, Modesto JCDA, Pérez CD. Toxicity against *Artemia salina* of the zoanthid *Palythoa caribaeorum* (Cnidaria: Anthozoa) used in folk medicine on the coast of Pernambuco. *Biotemas* 2012; 25(3): 145-51. <http://dx.doi.org/10.5007/2175-7925.2012v25n3p145>
- [21] Rekulapally R, Murthy Chavali LN, Idris MM, Singh S. Toxicity of TiO₂, SiO₂, ZnO, CuO, Au and Ag engineered nanoparticles on hatching and early nauplii of *Artemia* spp. *Peer J* 2019; 6: e6138. <http://dx.doi.org/10.7717/peerj.6138>
- [22] Lu Y, Yu J, Lu Y. *Artemia* spp. model - a well-established method for rapidly assessing the toxicity on an environmental perspective. *Med Res Arch* 2018; 6(2): 1-15.
- [23] Rotini A, Manfra L, Canepa S, Tornambè A, Migliore L. Can *Artemia* hatching assay be a (Sensitive) alternative tool to acute toxicity test? *Bull Environ Contam Toxicol* 2015; 95(6): 745-51. <http://dx.doi.org/10.1007/s00128-015-1626-1>
- [24] Manfra L, Savorelli F, Pisapia M, Magaletti E, Cicero AM. Long-term lethal toxicity test with the crustacean *Artemia franciscana*. *J Vis Exp* 2012; (62): 3790. <http://dx.doi.org/10.3791/3790>
- [25] Dumitrascu M. *Artemia salina*. *Balneo-Research J* 2011; 2(4): 119-22. <http://dx.doi.org/10.12680/balneo.2011.1022>
- [26] Asem A, Rastegar-Pouyani N, De P, Ríos-Escalante L. The genus *Artemia* Leach, 1819 (Crustacea: Branchiopoda). I. true and false taxonomical descriptions. *Lat Am J Aquat Res* 2010; 38(3): 501-6.
- [27] El-Magsodi MO, El-Ghebli HM, Enbaya MA, Hamza M, Drebika UA, Sorgeloos P. Reproductive and lifespan characteristics of *Artemia* from Lybian Abu Kammash Sabha. *Libian Journal of Marine Science* 2005; 10: 1-8.
- [28] Ogello EO, Kembanya E, Githukia CM, Betty M, Munguti JM. The occurrence of the brine shrimp, *Artemia franciscana* (Kellogg 1906) in Kenya and the potential economic impacts among Kenyan coastal communities. *Int J Fisheries Aquatic Studies* 2014; 1(5): 151-6.
- [29] Arulvasu C, Jennifer SM, Prabhu D, Chandhirasekar D. Toxicity effect of silver nanoparticles in brine shrimp *Artemia*. *Scientific-WorldJournal* 2014; 2014: 256919. <http://dx.doi.org/10.1155/2014/256919>
- [30] Carrasco NK, Perissinotto R. Development of a halotolerant community in the St. Lucia Estuary (South Africa) during a hypersaline phase. *PLoS One* 2012; 7(1): e29927. <http://dx.doi.org/10.1371/journal.pone.0029927>
- [31] Abatzopoulos TJ, Agh N, Van Stappen G, Razavi Rouhani SM, Sorgeloos P. *Artemia* sites in Iran. *J Mar Biol Assoc U K* 2006; 86: 299-307. <http://dx.doi.org/10.1017/S0025315406013154>
- [32] Ben Naceur H, Jenhani ABR, El Cafsi M, Romdhane MS. Determination of biological characteristics of *Artemia salina* (Crustacea: Anostraca) population from Sabkhet Sijoumi (NE Tunisia). *Transit Waters Bull* 2008; 2(3): 65-74.
- [33] Oliveira TMN, Vaz C. Bioassays: Advanced methods and applications. Amsterdam, The Netherlands: Elsevier 2018.
- [34] John C, Marian P, Abatzopoulos T. Characterization of a new parthenogenetic *Artemia* population from Thamaraiikulam, India. *J Biol Res (Thessalon)* 2004; 2: 63-74.
- [35] Camargo WN, Durán GC, Rada OC, et al. Determination of biological and physicochemical parameters of *Artemia franciscana* strains in hypersaline environments for aquaculture in the Colombian Caribbean. *Saline Syst* 2005; 1(9): 9. <http://dx.doi.org/10.1186/1746-1448-1-9>
- [36] Amarouayache M, Kara MH. Aspects of life history of *Artemia salina* (Crustacea, Branchiopoda) from Algeria reared in different conditions of salinity. *Vie Milieu* 2017; 67(1): 15-20.
- [37] Sáez AG, Escalante R, Sastre L. High DNA sequence variability at the α 1 Na/K-ATPase locus of *Artemia franciscana* (brine shrimp): Polymorphism in a gene for salt-resistance in a salt-resistant organism. *Mol Biol Evol* 2000; 17(2): 235-50. <http://dx.doi.org/10.1093/oxfordjournals.molbev.a026303>
- [38] Nunes BS, Carvalho FD, Guilhermino LM, Van Stappen G. Use of the genus *Artemia* in ecotoxicity testing. *Environ Pollut* 2006; 144(2): 453-62. <http://dx.doi.org/10.1016/j.envpol.2005.12.037>
- [39] Thong O, Chiew S, Geetha S, Thavamany P. Interference from ordinarily used solvents in the outcomes of *Artemia salina* lethality test. *J Adv Pharm Technol Res* 2013; 4(4): 179. <http://dx.doi.org/10.4103/2231-4040.121411>
- [40] Rahman A, Choudhary MI, Thomson WJ. Bioassay techniques for drug development. San Diego, USA: Harwood Academic Publishers 2005.
- [41] Braguini WL, Alves BB, Pires NV. Toxicity assessment of *Lavandula officinalis* extracts in Brine Shrimp (*Artemia salina*). *Toxicol Mech Methods* 2019; 29(6): 411-2. <http://dx.doi.org/10.1080/15376516.2019.1567892>
- [42] Noé W, Murhekar S, White A, Davis C, Cock IE. Inhibition of the growth of human dermatophytic pathogens by selected Australian and Asian plants traditionally used to treat fungal infections. *J Mycol Med* 2019; 29(4): 331-44. <http://dx.doi.org/10.1016/j.mycmed.2019.05.003>
- [43] Mandeville A, Edwin I. *Terminalia chebula* Retz. Fruit extracts inhibit bacterial triggers of some autoimmune diseases and potentiate the activity of tetracycline. *Indian J Microbiol* 2018; 58: 496-50. <http://dx.doi.org/10.1007/s12088-018-0754-9>
- [44] Akhalwaya S, van Vuuren S, Patel M. An *in vitro* investigation of indigenous South African medicinal plants used to treat oral infections. *J Ethnopharmacol* 2018; 210: 359-71. <http://dx.doi.org/10.1016/j.jep.2017.09.002>

- [45] Jha BN, Shrestha M, Pandey DP, Bhattarai T, Bhattarai HD, Paudel B. Investigation of antioxidant, antimicrobial and toxicity activities of lichens from high altitude regions of Nepal. *BMC Complement Altern Med* 2017; 17(1): 2.
<http://dx.doi.org/10.1186/s12906-017-1797-x>
- [46] Doke SK, Dhawale SC. Alternatives to animal testing: A review. *Saudi Pharm J* 2015; 23(3): 223-9.
<http://dx.doi.org/10.1016/j.jsps.2013.11.002>
- [47] Adamski Z, Bufo SA, Chowański S, et al. Beetles as model organisms in physiological, biomedical and environmental studies - A review. *Front Physiol* 2019; 10: 319.
<http://dx.doi.org/10.3389/fphys.2019.00319>
- [48] Ségalat L. Invertebrate animal models of diseases as screening tools in drug discovery. *ACS Chem Biol* 2007; 2(4): 231-6.
<http://dx.doi.org/10.1021/cb700009m>
- [49] Castano A. Applying the three Rs in acute ecotoxicity. *ALTEX* 2005; 22(2): 298-303.
- [50] Braunbeck T, Boettcher M, Hollert H, et al. Towards an alternative for the acute multi-species - an update the fish embryo toxicity test goes fish LC50 test in chemical assessment. *ALTEX* 2005; 22(2): 87-102.
- [51] Junprung W, Norouzitallab P, De Vos S, et al. Sequence and expression analysis of HSP70 family genes in *Artemia franciscana*. *Sci Rep* 2019; 9(8391): 1-13.
<http://dx.doi.org/10.1038/s41598-019-44884-y>
- [52] Brocchieri L, Conway De Macario E, Macario AJL. Hsp70 genes in the human genome: Conservation and differentiation patterns predict a wide array of overlapping and specialized functions. *BMC Evol Biol* 2008; 8: 1-20.
<http://dx.doi.org/10.1186/1471-2148-8-19>
- [53] Grubišić MR, Dulić ZP, Stanković MB, et al. Importance of zooplankton as live feed for carp larvae Proceedings of 6th Central European Congress on Food - CEFood Congress. 1553-57.
- [54] Meyer BN, Ferrigni NR, Putnam JE, Jacobsen LB, Nichols DE, McLaughlin JL. Brine shrimp: A convenient general bioassay for active plant constituents. *Planta Med* 1982; 45(5): 31-4.
<http://dx.doi.org/10.1055/s-2007-971236>
- [55] Pelka M, Danzl C, Distler W, Petschelt A. A new screening test for toxicity testing of dental materials. *J Dent* 2000; 28(5): 341-5.
[http://dx.doi.org/10.1016/S0300-5712\(00\)00007-5](http://dx.doi.org/10.1016/S0300-5712(00)00007-5)
- [56] Manfra L, Canepa S, Piazza V, Faimali M. Lethal and sublethal endpoints observed for *Artemia* exposed to two reference toxicants and an ecotoxicological concern organic compound. *Ecotoxicol Environ Saf* 2016; 123: 60-4.
<http://dx.doi.org/10.1016/j.ecoenv.2015.08.017>
- [57] Baek I, Choi HJ, Rhee JS. Inhibitory effects of biocides on hatching and acetylcholinesterase activity in the brine shrimp *Artemia salina*. *Toxicol Environ Health Sci* 2015; 7: 303-8.
<http://dx.doi.org/10.1007/s13530-015-0253-x>
- [58] Nunes B, Carvalho F, Guilhermino L. Effects of widely used pharmaceuticals and a detergent on oxidative stress biomarkers of the crustacean *Artemia parthenogenetica*. *Chemosphere* 2006; 62(4): 581-9.
<http://dx.doi.org/10.1016/j.chemosphere.2005.06.013>
- [59] Libralato G. The case of *Artemia* spp. in nanoecotoxicology. *Mar Environ Res* 2014; 101: 38-.
<http://dx.doi.org/10.1016/j.marenvres.2014.08.002>
- [60] Kummara S, Patil MB, Uriah T. Synthesis, characterization, biocompatible and anticancer activity of green and chemically synthesized silver nanoparticles - A comparative study. *Biomed Pharmacother* 2016; 84: 10-21.
<http://dx.doi.org/10.1016/j.biopha.2016.09.003>
- [61] Amado PA, Ferraz V, da Silva DB, Carollo CA, Castro AHF, Alves Rodrigues dos Santos Lima L. Chemical composition, antioxidant and cytotoxic activities of extracts from the leaves of *Smilax brasiliensis* Sprengel (*Smilacaceae*). *Nat Prod Res* 2018; 32(5): 610-5.
<http://dx.doi.org/10.1080/14786419.2017.1327861>
- [62] Silva FRG, Matias TMS, Souza LJO, et al. Phytochemical screening and *in vitro* antibacterial, antifungal, antioxidant and antitumor activities of the red propolis Alagoas. *Braz J Biol* 2019; 79(3): 452-959.
<http://dx.doi.org/10.1590/1519-6984.182959>
- [63] Mayorga P, Pérez KR, Cruz SM, Cáceres A. Comparison of bioassays using the anostracan crustaceans *Artemia salina* and *Thamnocephalus platyurus* for plant extract toxicity screening. *Rev Bras Farmacogn* 2010; 20(6): 897-90.
<http://dx.doi.org/10.1590/S0102-695X2010005000029>
- [64] Ohikhen A, Wintola OA, Afolayan AJ. Toxicity assessment of different solvent extracts of the medicinal plant, *Phragmanthera capitata* (sprengel) balle on brine shrimp (*Artemia salina*). *Int J Pharmacol* 2016; 12(7): 701-10.
<http://dx.doi.org/10.3923/ijp.2016.701.710>
- [65] Khalighi-Sigaroodi F, Ahvazi M, Yazdani D, Kashefi M. Cytotoxicity and antioxidant activity of five plant species of *solanaceae* family from Iran. *Fashnamah-i Giyahan-i Daruyi* 2012; 11(43): 41-53.
- [66] Mirzaei M, Mirzaei A. Comparison of the *Artemia salina* and *Artemia uramiana* bioassays for toxicity of 4 Iranian medicinal plants. *Int Res J Biol Sci* 2013; 8(1): 11-6.
- [67] Atanasov AG, Waltenberger B, Pferschy-Wenzig EM, et al. Discovery and resupply of pharmacologically active plant-derived natural products: A review. *Biotechnol Adv* 2015; 33(8): 1582-614.
<http://dx.doi.org/10.1016/j.biotechadv.2015.08.001>
- [68] Khatun A, Rahman M, Haque T. Cytotoxicity potentials of eleven Bangladeshi medicinal plants. *Scientific World J* 2014; 2014: 913127.
<http://dx.doi.org/10.1155/2014/913127>
- [69] Hilmi Y, Abushama MF, Abdalgadir H, Khalid A, Khalid H. A study of antioxidant activity, enzymatic inhibition and *in vitro* toxicity of selected traditional Sudanese plants with anti-diabetic potential. *BMC Complement Altern Med* 2014; 14: 149.
<http://dx.doi.org/10.1186/1472-6882-14-149>
- [70] Shariffar F, Moshafi MH, Shafazand E, Koohpayeh A. Acetyl cholinesterase inhibitory, antioxidant and cytotoxic activity of three dietary medicinal plants. *Food Chem* 2012; 130(1): 20-3.
<http://dx.doi.org/10.1016/j.foodchem.2011.06.034>
- [71] Nwodo UU, Ngene AA, Anaga AO, Chigor VN, Henrietta II, Okoh AI. Acute toxicity and hepatotoxicokinetic studies of *Tamarindus indica* extract. *Molecules* 2011; 16(9): 7415-27.
<http://dx.doi.org/10.3390/molecules16097415>
- [72] Deciga-Campos M, Rivero-Cruz I, Arriaga-Alba M, et al. Acute toxicity and mutagenic activity of Mexican plants used in traditional medicine. *J Ethnopharmacol* 2007; 110(2): 334-42.
<http://dx.doi.org/10.1016/j.jep.2006.10.001>
- [73] Wathanachaiyingcharoen R, Kamkaen N, Phanwichien K, Pradernmwong A. Acute toxicity test of medicinal plants and herbal remedies of aphthous ulcer. *J Health Res* 2009; 23(4): 169-74.
- [74] Ali N, Ahmed G, Shah SW, Shah I, Ghias M, Khan I. Acute toxicity, brine shrimp cytotoxicity and relaxant activity of fruits of *Calistemon citrinus* Curtis. *BMC Complement Altern Med* 2011; 11: 99.
<http://dx.doi.org/10.1186/1472-6882-11-99>
- [75] Ali N, Aleem U, Shah SWA, et al. Acute toxicity, brine shrimp cytotoxicity, anthelmintic and relaxant potentials of fruits of *Rubus fruticosus* Agg. *BMC Complement Altern Med* 2013; 13: 138.
<http://dx.doi.org/10.1186/1472-6882-13-138>
- [76] Bogavac M, Karaman M, Janjusevic L, et al. Alternative treatment of vaginal infections - *in vitro* antimicrobial and toxic effects of *Coriandrum sativum* L. and *Thymus vulgaris* L. essential oils. *J Appl Microbiol* 2015; 119(3): 697-710.
<http://dx.doi.org/10.1111/jam.12883>
- [77] Nisar M, Tariq SA, Marwat IK, Shah MR, Khan IA. Antibacterial, antifungal, insecticidal, cytotoxicity and phytotoxicity studies on *Indigofera gerardiana*. *J Enzyme Inhib Med Chem* 2009; 24(1): 224-9.
<http://dx.doi.org/10.1080/14756360802051313>
- [78] Islam MS, Ali S, Rahman M, et al. Antidiabetic, cytotoxic activities and phytochemical screening of *Peltophorum pterocarpum* (DC.) K. Heyne root. *J Med Plants Res* 2011; 5(16): 3745-50.
- [79] Queiroz EAM, Paim RTT, Lira SM, et al. Antihyperglycemic effect of *Passiflora glandulosa* cav. fruit rinds flour in streptozotocin-induced diabetic mice. *Asian Pac J Trop Med* 2018; 11(9): 510-1.
<http://dx.doi.org/10.4103/1995-7645.242308>
- [80] Ansari P, Uddin MJ, Rahman MM, et al. Anti-inflammatory, anti-diarrheal, thrombolytic and cytotoxic activities of an ornamental medicinal plant: *Persicaria orientalis*. *J Basic Clin Physiol Pharmacol* 2017; 28(1): 51-8.
<http://dx.doi.org/10.1515/jbcp-2016-0023>

- [81] Shah NA, Khan MR, Nadhman A. Antileishmanial, toxicity, and phytochemical evaluation of medicinal plants collected from Pakistan. *BioMed Res Int* 2014; 2014384204
<http://dx.doi.org/10.1155/2014/384204>
- [82] Ogbole OO, Saka YA, Fasinu PS, Fadare AA, Ajaiyeoba EO. Antimalarial and cytotoxic properties of *Chukrasia tabularis* A. Juss and *Turraea vogelii* Hook F. *Ex Benth Parasitol Res* 2016; 115(4): 1667-74.
<http://dx.doi.org/10.1007/s00436-016-4906-8>
- [83] Latha LY, Sasidharan S, Zuraini Z, et al. Antimicrobial activities and toxicity of crude extract of the *Psophocarpus tetragonolobus* pods. *Afr J Tradit Complement Altern Med* 2006; 4(1): 59-63.
- [84] Chowdhury MA, Rahman MM, Chowdhury MR, Uddin MJ, Sayeed MA, Hossain MA. Antinociceptive and cytotoxic activities of an epiphytic medicinal orchid: *Vanda tessellata* Roxb. *BMC Complement Altern Med* 2014; 14: 464.
<http://dx.doi.org/10.1186/1472-6882-14-464>
- [85] Wangenstein H, Dang HC, Uddin SJ, Alamgir M, Malterud KE. Antioxidant and antimicrobial effects of the mangrove tree *Heritiera fomes*. *Nat Prod Commun* 2009; 4(3): 371-6.
<http://dx.doi.org/10.1177/1934578X0900400311>
- [86] Saefudin S, Basri E, Sukito A. Antioxidant activity and toxicity effect of eleven types of bark extracts acquired from *Euphorbiaceae*. *Indones J For Res* 2018; 5(2): 133-46.
<http://dx.doi.org/10.20886/ijfr.2018.5.2.133-146>
- [87] Quadery TM, Islam F, Ahsan M, Hasan CM. Antioxidant and cytotoxic activities of *Parabaena sagittata* Miers. *Bangladesh J Bot* 2012; 41(2): 155-8.
<http://dx.doi.org/10.3329/bjb.v41i2.13441>
- [88] Addae-Kyereme J, Croft SL, Kendrick H, Wright CW. Antiplasmodial activities of some Ghanaian plants traditionally used for fever/malaria treatment and of some alkaloids isolated from *Pleiocarpa mutica*; *in vivo* antimalarial activity of pleiocarpine. *J Ethnopharmacol* 2001; 76(1): 99-103.
[http://dx.doi.org/10.1016/S0378-8741\(01\)00212-4](http://dx.doi.org/10.1016/S0378-8741(01)00212-4)
- [89] Kirira PG, Rukunga GM, Wanyonyi AW, et al. Anti-plasmodial activity and toxicity of extracts of plants used in traditional malaria therapy in Meru and Kilifi Districts of Kenya. *J Ethnopharmacol* 2006; 106(3): 403-7.
<http://dx.doi.org/10.1016/j.jep.2006.01.017>
- [90] Austerheim I, Nergard CS, Sanogo R, Diallo D, Paulsen BS. Inulin-rich fractions from *Vernonia kotschyana* roots have anti-ulcer activity. *J Ethnopharmacol* 2012; 144(1): 82.
<http://dx.doi.org/10.1016/j.jep.2012.08.031>
- [91] Onocha PA, Oloyede GK, Afolabi QO. Chemical Composition, cytotoxicity and antioxidant activity of essential oils of *Achypha hispida* flowers. *Int J Pharmacol* 2011; 7(1): 144-8.
<http://dx.doi.org/10.3923/ijp.2011.144.148>
- [92] Genest S, Kerr C, Shah A, Rahman M, et al. Comparative bioactivity studies on two *Mimosa* species. *BLACPMA* 2008; 7(1): 38-43.
- [93] Sarker SD, Nahar L, Gujja S, Begum S, Celik S. Bioactivity of *Centaurea persica* Boiss. (*Asteraceae*). *Arch Biol Sci* 2012; 64(2): 517-23.
<http://dx.doi.org/10.2298/ABS1202517S>
- [94] Mwangi GG, Wagacha JM, Nguta JM, Mbaria JM. Brine shrimp cytotoxicity and antimalarial activity of plants traditionally used in treatment of malaria in Msambweni district. *Pharm Biol* 2015; 53(4): 588-93.
<http://dx.doi.org/10.3109/13880209.2014.935861>
- [95] Nguta JM, Mbaria JM. Brine shrimp toxicity and antimalarial activity of some plants traditionally used in treatment of malaria in Msambweni district of Kenya. *J Ethnopharmacol* 2013; 148(3): 988-92.
<http://dx.doi.org/10.1016/j.jep.2013.05.053>
- [96] Wanyoike GN, Chhabra SC, Lang'at-Thoruwa CC, Omar SA. Brine shrimp toxicity and antiplasmodial activity of five Kenyan medicinal plants. *J Ethnopharmacol* 2004; 90(1): 129-33.
<http://dx.doi.org/10.1016/j.jep.2003.09.047>
- [97] de França-Neto A, Cardoso-Teixeira AC, Medeiros TC, et al. Essential oil of croton argyrophyllloides: toxicological aspects and vasorelaxant activity in rats. *Nat Prod Commun* 2012; 7(10): 1397-400.
<http://dx.doi.org/10.1177/1934578X1200701040>
- [98] Rahman MK, Chowdhury MA, Islam MT, Chowdhury MA, Uddin ME, Sumi CD. Evaluation of anti-diarrheal activity of methanolic extract of *Maranta arundinacea* Linn. leaves. *Advances in Pharmacol Pharm Sci* 2015; 2015: 257057.
- [99] Mota KSL, Pita J, Estevam EC, et al. Evaluation of the toxicity and antiulcerogenic activity of the ethanol extract of *Maytenus obtusifolia* Mart. leaves. *Br J Pharmacol* 2008; 18(3): 441-6.
<http://dx.doi.org/10.1590/S0102-695X2008000300019>
- [100] Kiraithe MN, Nguta JM, Mbaria JM, Kiama SG. Evaluation of the use of *Ocimum suave* Willd. (*Lamiaceae*), *Plectranthus barbatus* Andrews (*Lamiaceae*) and *Zanthoxylum chalybeum* Engl. (*Rutaceae*) as antimalarial remedies in Kenyan folk medicine. *J Ethnopharmacol* 2016; 178(266): 7-71.
- [101] de Oliveira AM, Mda SM, da Silva GC, et al. Evaluation of toxicity and antimicrobial activity of an ethanolic extract from leaves of *Morus alba* L. (*Moraceae*). *Evid Based Complement Alternat Med* 2015; 2015: 513978.
<http://dx.doi.org/10.1155/2015/513978>
- [102] Magalhaes AF, Tozzi AM, Magalhaes EG, Sannomiya M, Mdel PS, Perez MA. Flavonoids of *Lonchocarpus montanus* A.M.G. Azevedo and biological activity. *Annals of the Brazilian Academy of Science* 2007; 79(3): 351-67.
<http://dx.doi.org/10.1590/S0001-37652007000300001>
- [103] Schmeda-Hirschmann G, Loyola JI, Sierra J, Retamal R, Rodriguez J. Hypotensive effect and enzyme inhibition activity of mapuche medicinal plant extracts. *Phytother Res* 1992; 6(4): 184-8.
<http://dx.doi.org/10.1002/ptr.2650060404>
- [104] Leos-Rivas C, Verde-Star MJ, Torres LO, et al. *In vitro* Amoebicidal activity of Borage (*Borago officinalis*) extract on *Entamoeba histolytica*. *J Med Food* 2011; 14(7-8): 866-9.
<http://dx.doi.org/10.1089/jmf.2010.0164>
- [105] Ojwunmi OO, Oshodi T, Ogundele OI, Micah C, Adenekan S. *In vitro* Antioxidant, antihyperglycaemic and antihyperlipidaemic activities of ethanol extract of *Lawsonia inermis* leaves. *Br J Pharm Res* 2014; 4(3): 301.
<http://dx.doi.org/10.9734/BJPR/2014/6359>
- [106] Ayuko TA, Njau RN, Cornelius W, Leah N, Ndiege IO. *In vitro* antiplasmodial activity and toxicity assessment of plant extracts used in traditional malaria therapy in the Lake Victoria Region. *Mem Inst Oswaldo Cruz* 2009; 104(5): 689-94.
<http://dx.doi.org/10.1590/S0074-02762009000500004>
- [107] Kpoviessi BGK, Kpoviessi SD, Ladekan EY, et al. *In vitro* antitrypanosomal and antiplasmodial activities of crude extracts and essential oils of *Ocimum gratissimum* Linn. from Benin and influence of vegetative stage. *J Ethnopharmacol* 2014; 155(3): 1417-2.
<http://dx.doi.org/10.1016/j.jep.2014.07.014>
- [108] George M, Josekumar VS. *In vitro* cytotoxicity screening, phytochemical profile and heavy metal analysis of different extracts of *Acrostichum heterophyllum* L. *Indian J Nat Prod Resour* 2016; 7(1): 19-2.
- [109] Mahlke JD, Boligon AA, Machado MM, Athayde ML. *In vitro* toxicity, antiplatelet and acetylcholinesterase inhibition of *Buddleja thyrsoides* Lam. leaves. *Nat Prod Res* 2012; 26(23): 2223-6.
<http://dx.doi.org/10.1080/14786419.2011.643884>
- [110] Wickramaratne MN, Punchihewa JC, Wickramaratne DB. *In-vitro* alpha amylase inhibitory activity of the leaf extracts of *Adenanthera pavonina*. *BMC Complement Altern Med* 2016; 16(1): 466.
<http://dx.doi.org/10.1186/s12906-016-1452-y>
- [111] Olajuyigbe OO, Afolayan AJ. Pharmacological assessment of the medicinal potential of *Acacia meamsii* De Wild.: antimicrobial and toxicity activities. *Int J Mol Sci* 2012; 13(4): 4255-67.
<http://dx.doi.org/10.3390/ijms13044255>
- [112] Ajaiyeoba EO, Rahman AU, Choudhary IM. Preliminary antifungal and cytotoxicity studies of extracts of *Ritchiea capparoides* var. longipedicellata. *J Ethnopharmacol* 1998; 62(3): 243-6.
[http://dx.doi.org/10.1016/S0378-8741\(98\)00010-5](http://dx.doi.org/10.1016/S0378-8741(98)00010-5)
- [113] Ramazani A, Zakeri S, Sardari S, Khodakarim N, Djadid ND. *In vitro* and *in vivo* anti-malarial activity of *Boerhavia elegans* and *Solanum surattense*. *Malar J* 2010; 9: 124.
<http://dx.doi.org/10.1186/1475-2875-9-124>
- [114] Lagnika L, Anago E, Sanni A. Screening for antibacterial, antioxidant activity and toxicity of some medicinal plants used in Benin folkloric medicine. *J Med Plants Res* 2011; 5(5): 773-7.

- [115] Abed SA, Sirat HM, Taher M. Total phenolic, antioxidant, antimicrobial activities and toxicity study of *Gynotroches axillaris* blume (*Rhizophoraceae*). *EXCLI J* 2013; 12: 404-12.
- [116] Ajayi AM, Umukoro S, Ben-Azu B, Adzu B, Ademowo OG. Toxicity and protective effect of phenolic-enriched ethylacetate fraction of *Ocimum gratissimum* (Linn.) leaf against acute inflammation and oxidative stress in rats. *Drug Dev Res* 2017; 78(3-4): 135-45. <http://dx.doi.org/10.1002/ddr.21384>
- [117] Orhan I, Nasim S, Sener B, *et al.* Two isoflavones and bioactivity spectrum of the crude extracts of *Iris germanica* rhizomes. *Phytother Res* 2003; 17(5): 575-7. <http://dx.doi.org/10.1002/ptr.1169>
- [118] Wagemaker TAL, Campos PMBGM, *et al.* Unsaponifiable matter from oil of green coffee beans: cosmetic properties and safety evaluation. *Drug Dev Ind Pharm* 2016; 42(10): 1695-9. <http://dx.doi.org/10.3109/03639045.2016.1165692>
- [119] Satish L, Santhakumari S, Gowrishankar S. Rapid biosynthesized AgNPs from *Gelidiella acerosa* aqueous extract mitigates quorum sensing mediated biofilm formation of *Vibrio* species - an *in vitro* and *in vivo* approach. *Environ Sci Pollut Res Int* 2017; 24(35): 27254-68. <http://dx.doi.org/10.1007/s11356-017-0296-4>
- [120] Silva CO, Rijo P, Molpeceres J, *et al.* Polymeric nanoparticles modified with fatty acids encapsulating betamethasone for anti-inflammatory treatment. *Int J Pharm* 2015; 493(1-2): 271-84. <http://dx.doi.org/10.1016/j.ijpharm.2015.07.044>
- [121] Rajabi S, Ramazani A, Hamidi M, Naji T. *Artemia salina* as a model organism in toxicity assessment of nanoparticles. *Daru* 2015; 23(1): 20. <http://dx.doi.org/10.1186/s40199-015-0105-x>
- [122] Zhu S, Xue MY, Luo F, Chen WC, Zhu B, Wang GX. Developmental toxicity of Fe₃O₄ nanoparticles on cysts and three larval stages of *Artemia salina*. *Environ Pollut* 2017; 230: 683-91. <http://dx.doi.org/10.1016/j.envpol.2017.06.065>
- [123] Freire PLL, Albuquerque AJR, Farias IAP, *et al.* Antimicrobial and cytotoxicity evaluation of colloidal chitosan - silver nanoparticles - fluoride nanocomposites. *Int J Biol Macromol* 2016; 93(Pt A): 896-903.
- [124] Abbasi BA, Iqbal J, Mahmood T, Qyyum A, Kanwal S. Biofabrication of iron oxide nanoparticles by leaf extract of *Rhamnus virgata*: characterization and evaluation of cytotoxic, antimicrobial and antioxidant potentials. *Appl Organomet Chem* 2019; 33(7): e4947. <http://dx.doi.org/10.1002/aoc.4947>
- [125] Khalil AT, Ovais M, Ullah I, *et al.* *Sageretia thea* (Osbeck.) mediated synthesis of zinc oxide nanoparticles and its biological applications. *Nanomedicine (Lond)* 2017; 12(15): 1767-89. <http://dx.doi.org/10.2217/nmm-2017-0124>
- [126] Latha LY, Sasidharan S, Zuraini Z, *et al.* Antimicrobial activities and toxicity of crude extract of the *Psophocarpus tetragonolobus* Pods. *Afr J Tradit Complement Altern Med* 2007; 4(1): 59-63. <http://dx.doi.org/10.4314/ajtcam.v4i1.31195>
- [127] Balalakshmi C, Gopinath K, Govindarajan M, *et al.* Green synthesis of gold nanoparticles using a cheap *Sphaeranthus indicus* extract: Impact on plant cells and the aquatic crustacean *Artemia nauplii*. *J Photochem Photobiol B* 2017; 173: 598-6. <http://dx.doi.org/10.1016/j.jphotobiol.2017.06.040>
- [128] dos Santos Ramos MA, Da Silva PB, De Toledo LG, *et al.* Intravaginal delivery of *Syngonanthus nitens* (Bong.) Ruhland fraction based on a nanoemulsion system applied to vulvovaginal candidiasis treatment. *J Biomed Nanotechnol* 2019; 15(5): 1072-89. <http://dx.doi.org/10.1166/jbn.2019.2750>
- [129] Iqbal J, Abbasi BA, Mahmood T, Hameed S, Munir A, Kanwal S. Green synthesis and characterizations of Nickel oxide nanoparticles using leaf extract of *Rhamnus virgata* and their potential biological applications. *Appl Organomet Chem* 2019; 33(8): e4950. <http://dx.doi.org/10.1002/aoc.4950>
- [130] Anand K, Tiloke C, Phulukdaree A, *et al.* Biosynthesis of palladium nanoparticles by using *Moringa oleifera* flower extract and their catalytic and biological properties. *J Photochem Photobiol B* 2016; 165: 87-95. <http://dx.doi.org/10.1016/j.jphotobiol.2016.09.039>
- [131] Phull A-R, Abbas Q, Ali A, Raza H. Antioxidant, cytotoxic and antimicrobial activities of green synthesized silver nanoparticles from crude extract of *Bergenia ciliata*. *Future J Pharm Sci* 2016; 2(1): 31-6. <http://dx.doi.org/10.1016/j.fjps.2016.03.001>
- [132] Kumara swamy M, Pokharen N, Dahal S, Anuradha M. Phytochemical and antimicrobial studies of leaf extract of *Euphorbia nerifolia*. *J Med Plant Res* 2011; 5(24): 5785-88.8.
- [133] Ravichandran A, Subramanian P, Manoharan V, *et al.* Phyto-mediated synthesis of silver nanoparticles using fucoidan isolated from *Spatoglossum asperum* and assessment of antibacterial activities. *J Photochem Photobiol B* 2018; 185: 117-25. <http://dx.doi.org/10.1016/j.jphotobiol.2018.05.031>
- [134] Contreras-Cortés AG, Almandariz-Tapia FJ, Gómez-Álvarez A, *et al.* Toxicological assessment of cross-linked beads of chitosan-alginate and *Aspergillus australensis* biomass, with efficiency as biosorbent for copper removal. *Polymers (Basel)* 2019; 11(2): E222. <http://dx.doi.org/10.3390/polym11020222>
- [135] Nemati T, Sarkheil M, Johari SA. Trophic transfer of CuO nanoparticles from brine shrimp (*Artemia salina*) nauplii to convict cichlid (*Amatitlania nigrofasciata*) larvae: uptake, accumulation and elimination. *Environ Sci Pollut Res Int* 2019; 26(10): 9610-8. <http://dx.doi.org/10.1007/s11356-019-04263-6>
- [136] Kokkali V, Katramados I, Newman JD. Monitoring the effect of metal ions on the mobility of *Artemia salina* Nauplii. *Biosensors (Basel)* 2011; 1(2): 36-45. <http://dx.doi.org/10.3390/bios1020036>
- [137] Hisem D, Hrouzek P, Tomek P, Tomšičková J, *et al.* Cyanobacterial cytotoxicity versus toxicity to brine shrimp *Artemia salina*. *Toxicol* 2011; 57(1): 76-83. <http://dx.doi.org/10.1016/j.toxicol.2010.10.002>
- [138] Kiviranta J, Sivonen K, Niemelä SI, Huovinen K. Detection of toxicity of cyanobacteria by *Artemia salina* bioassay. *Environ Toxicol Water Qual* 1991; 6(4): 423-36. <http://dx.doi.org/10.1002/tox.2530060407>
- [139] Lee T-H, Chen Y-M, Chou H-N. Toxicity assay of cyanobacterial strains using *Artemia salina* in comparison with the mouse bioassay. *Acta Zool Taiwanica* 1999; 10(1): 1-8.
- [140] Maurer-Jones MA, Love SA, Meierhofer S, Marquis BJ, Liu Z, Haynes CL. Toxicity of nanoparticles to brine shrimp: An introduction to nanotoxicity and interdisciplinary science. *J Chem Educ* 2013; 90(4): 475-8. <http://dx.doi.org/10.1021/ed3005424>
- [141] Karchesy YM, Kelsey RG, Constantine G, Karchesy JJ. Biological screening of selected Pacific Northwest forest plants using the brine shrimp (*Artemia salina*) toxicity bioassay. *Springerplus* 2016; 5: 510. <http://dx.doi.org/10.1186/s40064-016-2145-1>
- [142] Chichiricó G, Ferrante C, Menghini L, *et al.* *Crocus sativus* by-products as sources of bioactive extracts: Pharmacological and toxicological focus on anthers. *Food Chem Toxicol* 2019; 126: 7-14. <http://dx.doi.org/10.1016/j.fct.2019.01.040>
- [143] Ferrante C, Recinella L, Maurizio R, *et al.* Multiple pharmacognostic characterization on hemp commercial cultivars: Focus on inflorescence water extract activity. *Food Chem Toxicol* 2019; 125: 452-61.
- [144] Taviano MF, Rashed K, Filocamo A, *et al.* Phenolic profile and biological properties of the leaves of *Ficus vasta* Forssk. (Moraceae) growing in Egypt. *BMC Complement Altern Med* 2018; 18(1): 161. <http://dx.doi.org/10.1186/s12906-018-2210-0>
- [145] Barth EF, Pinto LS, Dileli P, *et al.* Biological screening of extracts from leaf and stem bark of *Croton floribundus* Spreng. (Euphorbiaceae). *Braz J Biol* 2018; 78(4): 601-8. <http://dx.doi.org/10.1590/1519-6984.166522>
- [146] Naz R, Ayub H, Nawaz S, *et al.* Antimicrobial activity, toxicity and anti-inflammatory potential of methanolic extracts of four ethnomedicinal plant species from Punjab, Pakistan. *BMC Complement Altern Med* 2017; 17(1): 302. <http://dx.doi.org/10.1186/s12906-017-1815-z>
- [147] Olivas-Quintero S, López-Angulo G, Montes-Avila J, *et al.* Chemical composition and biological activities of *Helicteres vegae* and *Helipopsis sinaloensis*. *Pharm Biol* 2017; 55(1): 1473-82. <http://dx.doi.org/10.1080/13880209.2017.1306712>

- [148] Castanho S, Califano G, Soares F, *et al.* The effect of live feeds bathed with the red seaweed *Asparagopsis armata* on the survival, growth and physiology status of *Sparus aurata* larvae. *Fish Physiol Biochem* 2017; 43(4): 1043-54. <http://dx.doi.org/10.1007/s10695-017-0351-6>
- [149] Nguyen TL, Rusten A, Bugge MS, *et al.* Flavonoids, gallotannins and ellagitannins in *Syzygium guineense* and the traditional use among Malian healers. *J Ethnopharmacol* 2016; 192: 450-8. <http://dx.doi.org/10.1016/j.jep.2016.09.035>
- [150] Rodrigues MJ, Neves V, Martins A, *et al.* *In vitro* antioxidant and anti-inflammatory properties of *Limonium algarvense* flowers' infusions and decoctions: A comparison with green tea (*Camellia sinensis*). *Food Chem* 2016; 200: 322-9. <http://dx.doi.org/10.1016/j.foodchem.2016.01.048>
- [151] Olaru OT, Venables L, Van De Venter M, *et al.* Anticancer potential of selected *Fallopia* Adans species. *Oncol Lett* 2015; 10(3): 1323-32. <http://dx.doi.org/10.3892/ol.2015.3453>
- [152] Arcanjo D, Albuquerque A, Melo-Neto B, Santana L, Medeiros M, Citó A. Bioactivity evaluation against *Artemia salina* Leach of medicinal plants used in Brazilian Northeastern folk medicine. *Braz J Biol* 2012; 72(3): 505-9. <http://dx.doi.org/10.1590/S1519-69842012000300013>
- [153] Lawi Y, Saria J, Kidukuli AW. Brine shrimp cytotoxicity, phytochemical screening and larvicidal activities of *Plectranthus barbatus* extracts. *Res Rev Insights* 2018; 2(1): 2-4.
- [154] Biological activity screening of seven *Plectranthus* species *Pesquisa de actividade biológica de sete espécies de Plectranthus*. *Biomedical Biopharmaceutical Research* 2017; 14: 95-108. <http://dx.doi.org/10.19277/BBR.14.1.153>
- [155] Garcia C, Teodósio C, Oliveira C, *et al.* Naturally occurring *Plectranthus*-derived diterpenes with antitumoral activities. *Curr Pharm Des* 2018; 24(36): 4207-36. <http://dx.doi.org/10.2174/1381612825666190115144241>
- [156] Prakash S, Ramasubburayan R, Ramkumar VS, Kannapiran E, Palavesam A, Immanuel G. *In vitro*-Scientific evaluation on antimicrobial, antioxidant, cytotoxic properties and phytochemical constituents of traditional coastal medicinal plants. *Biomed Pharmacother* 2016; 83: 648-57.
- [157] Seremet OC, Olaru OT, Gutu CM, *et al.* Toxicity of plant extracts containing pyrrolizidine alkaloids using alternative invertebrate models. *Mol Med Rep* 2018; 17(6): 7757-63.
- [158] Ogbole OO, Segun PA, Adeniji AJ. *In vitro* cytotoxic activity of medicinal plants from Nigeria ethnomedicine on Rhabdomyosarcoma cancer cell line and HPLC analysis of active extracts. *BMC Complement Altern Med* 2017; 17(1): 494. <http://dx.doi.org/10.1186/s12906-017-2005-8>
- [159] Regueiras A, Pereira S, Costa MS, Vasconcelos V. Differential toxicity of cyanobacteria isolated from marine sponges towards echinoderms and crustaceans. *Toxins (Basel)* 2018; 10(7): E297. <http://dx.doi.org/10.3390/toxins10070297>
- [160] Ferraz-Filha ZS, Lombardi JA, Guzzo LS, Saúde-Guimarães DA. Brine shrimp (*Artemia salina* Leach) bioassay of extracts from *Lychnophoriopsis candelabrum* and different *Lychnophora* species. *Rev Bras Pl Med* 2012; 14(2): 358-61. <http://dx.doi.org/10.1590/S1516-05722012000200016>
- [161] Mendonça de Assis P, Cypriano Dutra R, Amarante CBD, *et al.* *Plinia cauliflora* (Mart.) Kausel: toxicological assays, biological activities, and elemental analysis of organic compounds. *Nat Prod Res* 2019; 2019: 1-5. <http://dx.doi.org/10.1080/14786419.2019.1633642>
- [162] Olivares-Bañuelos T, Gutiérrez-Rodríguez AG, Méndez-Bellido R, *et al.* Brown seaweed *Egregia menziesii*'s cytotoxic activity against brain cancer cell lines. *Molecules* 2019; 24(2): 260. <http://dx.doi.org/10.3390/molecules24020260>
- [163] Arslanyoulu M, Erdemgil FZ. Evaluation of the antibacterial activity and toxicity of isolated arctiin from the seeds of *Centaurea sclerolepis*. *J Fac Pharm, Ankara* 2006; 35(2): 103-9.
- [164] Nguta JM, Mbaria JM. Brine shrimp toxicity and antimalarial activity of some plants traditionally used in treatment of malaria in Msambweni district of Kenya. *J Ethnopharmacology* 2013; 148: 988-2.
- [165] Bhatt D, Jethva K, Zaveri M. Cytotoxicity screening of the commonly used indigenous medicinal plants using brine shrimp lethality bio-assay. *Int J Pharm Sci Rev Res* 2016; 37(2): 147-50.
- [166] Tlili H, Marino A, Ginestra G, *et al.* Polyphenolic profile, antibacterial activity and brine shrimp toxicity of leaf extracts from six Tunisian spontaneous species. *Nat Prod Res* 2019; 1-7. Online ahead or print. <http://dx.doi.org/10.1080/14786419.2019.1616725>
- [167] Zengin G, Ferrante C, Senkardes I, *et al.* Multidirectional biological investigation and phytochemical profile of *Rubus sanctus* and *Rubus iberticus*. *Food Chem Toxicol* 2019; 127: 237-50. <http://dx.doi.org/10.1016/j.fct.2019.03.041>
- [168] Winnett V, Sirdaarta J, White A, Clarke FM, Cock IE. Inhibition of *Klebsiella pneumoniae* growth by selected Australian plants: natural approaches for the prevention and management of ankylosing spondylitis. *Inflammopharmacology* 2017; 25(2): 223-35. <http://dx.doi.org/10.1007/s10787-017-0328-1>
- [169] Parra A, Silva R, Guerra SI, Iglesias BL. Comparative study of the assay of *Artemia salina* L. and the estimate of the medium lethal dose (LD₅₀ value) in mice, to determine oral acute toxicity of plant extracts. *Phytomedicine* 2001; 8(5): 395-400. <http://dx.doi.org/10.1078/0944-7113-00044>
- [170] Naidu JR, Ismail R, Sasidharan S. Acute oral toxicity and brine shrimp lethality of methanol extract of *Mentha spicata* L.(Lamiaceae). *Trop J Pharm Res* 2014; 13(1): 101-7. <http://dx.doi.org/10.4314/tjpr.v13i1.15>
- [171] Sasidharan S, Mordi MN, Ismail S, Mansor S, Sahgal G, Ramathan S. Brine shrimp lethality and acute oral toxicity studies on *Swietenia mahagoni* (Linn.) Jacq. seed methanolic extract 2010; *Pharmacognosy Res* 2010; 2(4): 215-0.
- [172] Hossain MM, Mondal M, Morad RU, *et al.* Evaluation of bioactivities of methanol and petroleum ether extracts of *Cassia renigera* seed. *Clinical Phytoscience* 2018; 4: 33. <http://dx.doi.org/10.1186/s40816-018-0091-x>
- [173] Araújo RMS, Vaz AFM, Aguiar JS, *et al.* Lectin from *Crataeva tapia* bark exerts antitumor, anti-inflammatory and analgesic activities. *Nat Prod Bioprospect* 2011; 1(2): 97-100. <http://dx.doi.org/10.1007/s13659-011-0014-8>
- [174] Moshi MJ, Nondo RSO, Haule EE, Mahunnah RLA, Kidukuli AW. Antimicrobial activity, acute toxicity and cytoprotective effect of *Crassocephalum vitellinum* (Benth.) S. Moore extract in a rat ethanol-HCl gastric ulcer model. *BMC Research Notes* 2014; 7: 91-7.
- [175] Hamimed S, Boulebdia N, Laouer H, Belkhirri A. Bioactivity-guided isolation of alkaloids from a cytotoxic fraction of the ethyl acetate extract of *Anacyclus pyrethrum* (L.) DC. Roots. *Curr Issues Pharm Med Sci* 2018; 31(4): 18. <http://dx.doi.org/10.1515/cipms-2018-0033>
- [176] Silva TMS, Nascimento RJB, Batista MM, Agra MF, Camara CA. Brine shrimp bioassay of some species of *Solanum* from Northeastern Brazil. *Rev Bras Farmacogn* 2007; 17(1): 35-8. <http://dx.doi.org/10.1590/S0102-695X2007000100008>
- [177] Martins RL, Simões RC, De Menezes Rabelo E, *et al.* Chemical composition, an antioxidant, cytotoxic and microbiological activity of the essential oil from the leaves of *Aeollanthus suaveolens* mart. ex Spreng. *PLoS One* 2016; 11(12): e0166684. <http://dx.doi.org/10.1371/journal.pone.0166684>
- [178] Kabir SR, Hossen A, Zubair A, *et al.* A new lectin from the tuberos rhizome of *Kaempferia rotunda*: isolation, characterization, antibacterial and antiproliferative activities. *Protein Pept Lett* 2011; 18(11): 1140-9. <http://dx.doi.org/10.2174/092986611797200896>
- [179] Akhbari M, Kord R, Jafari Nodoshan S, Hamed S. Analysis and evaluation of the antimicrobial and anticancer activities of the essential oil isolated from *Foeniculum vulgare* from Hamedan, Iran. *Nat Prod Res* 2019; 33(11): 1629-32. <http://dx.doi.org/10.1080/14786419.2017.1423310>
- [180] Krstić NM, Matić IZ, Juranić ZD, Novaković IT, Sladić DM. Steroid dimers - *In vitro* cytotoxic and activities. *J Steroid Biochem Mol Biol* 2014; 143: 365-75. <http://dx.doi.org/10.1016/j.jsbmb.2014.06.005>
- [181] Mondal M, Hossain MS, Das N, *et al.* Phytochemical screening and evaluation of pharmacological activity of leaf Methanolic extract of *Colocasia affinis* Schott. *Clinical Phytoscience* 2019; 5: 8. <http://dx.doi.org/10.1186/s40816-019-0100-8>

- [182] Matthews RS. *Artemia salina* as a test organism for measuring superoxide-mediated toxicity. *Free Radic Biol Med* 1995; 18(5): 919-22.
[http://dx.doi.org/10.1016/0891-5849\(94\)00205-X](http://dx.doi.org/10.1016/0891-5849(94)00205-X)
- [183] Movahhedini N, Barar J, Azad FF, Barzegari A, Nazemiyeh H. Phytochemistry and biologic activities of *Caulerpa peltata* native to Oman sea. *Iran J Pharm Res* 2014; 13(2): 515-21.
- [184] Carballo JL, Hernández-Inda ZL, Pérez P, García-Grávalos MD. A comparison between two brine shrimp assays to detect *in vitro* cytotoxicity in marine natural products. *BMC Biotechnol* 2002; 2: 17.
<http://dx.doi.org/10.1186/1472-6750-2-17>
- [185] Caldwell GS, Bentley MG, Olive PJW. The use of a brine shrimp (*Artemia salina*) bioassay to assess the toxicity of diatom extracts and short chain aldehydes. *Toxicol* 2003; 42(3): 301-6.
[http://dx.doi.org/10.1016/S0041-0101\(03\)00147-8](http://dx.doi.org/10.1016/S0041-0101(03)00147-8)
- [186] Unuofin JO, Otunola GA, Afolayan AJ. Toxicity assessment of *Kedrostis africana* cogn : a medicinal plant used in the management of obesity in south africa using brine shrimp (*Artemia Salina* Linn.) Assay. *Int J Pharm Sci Res* 2017; 8(9): 3719-25.
- [187] Shaala NMA, Zulkifli SZ, Ismail A, Azmai MNA, Mohamat-Yusuff F. lethal concentration 50 (LC₅₀) and effects of diuron on morphology of brine shrimp *Artemia salina* (Branchiopoda: Anostraca) Nauplii. *Procedia Environ Sci* 2015; 30: 279-84.
<http://dx.doi.org/10.1016/j.proenv.2015.10.050>

CHAPTER II

Using *Artemia salina* model as a screening method for general toxicity

This chapter resume that *Artemia salina* is a good model for screening general toxicity used to identify toxic samples (synthetic and natural product compounds or even nanosystems) and was used in the following 9 articles:

1. Ntungwe N, E.; Marçalo, J.; Garcia, C.; Reis, C.; Teodósio, C.; Oliveira, C.; Oliveira, C.; Roberto, A. Biological activity screening of seven *Plectranthus* species. *J. Biomed. Biopharm. Res.* 2017, 14, 95–108, doi:10.19277/BBR.14.1.153.
2. Luís M T Frija, Ntungwe Epole, Przemysław Sitarek, Armando J. L. Pombeiro. In Vitro Assessment of Antimicrobial, Antioxidant, and Cytotoxic Properties of Saccharin–Tetrazolyl and –Thiadiazolyl Derivatives: The Simple Dependence of the pH Value on Antimicrobial. 2019, 12(4):167, *Pharmaceuticals*, DOI: 10.3390/ph12040167
3. Garcia C, Ntungwe E, Rebelo A, Bessa C, Stankovic T, Dinic J, Díaz-Lanza A, P Reis C, Roberto A, Pereira P, Cebola MJ, Saraiva L, Pesic M, Duarte N, Rijo P. Parvifloron D from *Plectranthus strigosus*: Cytotoxicity Screening of *Plectranthus* spp. Extracts. *Biomolecules*. 2019 Oct 17;9(10). pii: E616. doi: 10.3390/biom9100616.
4. Ribeiro, N., Galvão, A. M., Gomes, C. S. B., Ramos, H., Pinheiro, R., Saraiva, L., Epole N., Vera I., Patrícia R., Isabel C., Filipa R., Rita C., João C., Isabel C. (2019). Naphthoylhydrazones: coordination to metal ions and biological screening. *New Journal of Chemistry*. 1 - 44 doi:10.1039/c9nj01816f
5. Tatu Rimpiläinen, Joana Andrade, Alexandra Nunes, Epole Ntungwe, Ana S. Fernandes, João R. Vale, João Rodrigues, João Paulo Gomes, Patricia Rijo and Nuno R. Candeias. Aminobenzylated 4-Nitrophenols as Antibacterial Agents Obtained from 5-Nitrosalicylaldehyde through a Patis Borono–Mannich Reaction. *ACS Omega* 2018, 3, 16191–16202.
6. Mota Ana Henriques, Andrade Joana Marçalo, Ntungwe Epole, Pereira Paula, Cebola Maria João, Bernardo-Gil Maria Gabriela, Molpeceres Jesús, Rijo Patrícia, Viana Ana Semedo, Ascensão Lia, and Pinto Reis Catarina. Green Extraction of *Sambucus nigra* L. for Potential Application in Skin Nanocarriers. *Green Materials*. 0 0:0, 1-13. 2020. <https://doi.org/10.1680/jgrma.18.00074>

7. Rimpilainen T, Nunes A, Calado R, Fernandes AS, Andrade J, Ntungwe E, et al. Increased antibacterial properties of indoline-derived phenolic Mannich bases. *European Journal of Medicinal Chemistry* 2021: 113459. <https://doi.org/10.1016/j.ejmech.2021.113459>.
8. Neto, I; Domínguez-Martín, E.M.; Ntungwe, E; Reis, C.P.; Pesic, M.; Faustino, C.; Rijo, P. Dehydroabiatic Acid potential as Biofilm-Mediated Infections Treatment. *Pharmaceutics* 2021, 13, 825. <https://doi.org/10.3390/pharmaceutics13060825>.
9. Ntungwe, E; Isca, V.M.S.; Díaz-lanza, A.M.; Afonso, C.A.M.; Rijo, P. General Toxicity screening of Royleanone derivatives using an *Artemia salina* model. 2021, 1–9, doi:10.19277/bbr.18.1.254.

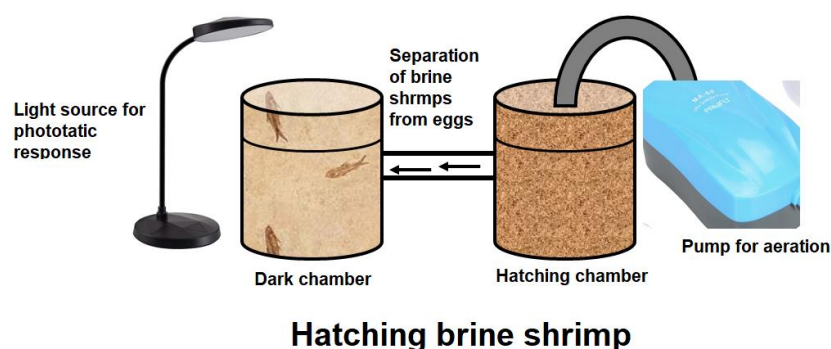
Introduction

Invertebrate animals have been used as models for research since the late 1800s because of their unique biological characteristics, such as small body size and short lifespan. These study systems are cornerstones of biological and biomedical research and provide key insights into toxicity study [1,2].

In recent years *Artemia salina* has drawn interest as a test laboratory animal. *A. salina* has gained popularity as a test organism for short-term toxicity testing. This is because of its ease of culture, short generation time, and cosmopolitan distribution [3]. Its use as a test organism is based on cellular mechanisms that may occur via necrosis, characterized by loss of membrane integrity, death of cell, or apoptosis, a genetic program of controlled cell death [4]. The significant correlation between the brine shrimp assay and in vitro growth inhibition of human solid tumor cell lines demonstrated by the National Cancer Institute (NCI, USA) further boost the use of *A. salina* for toxicity testing. This was the case in the articles discussed below and is significant because it shows the value of this bioassay as a pre-screening tool for antitumor drug research [5–7] thus widely used for the screening of bioactive compounds, extracts, and nano formulations. These findings suggest that the *A. salina* test can be used as a preliminary test to determine the general toxicity of a wide range of samples.

Methodology of *A. salina* Bioassay employed in the papers below.

Artemia salina eggs (dry cyst) were hatched in artificial seawater at 25–30 °C under aeration. A container with two connected chambers with a simple handmade communicating vessel was used for brine shrimp hatching. The eggs were placed in one of two compartments of a container separated by a boundary plate. The compartment with the eggs was covered to maintain a dark ambiance. The other compartment was illuminated to attract the phototactic newly hatched larvae through perforations on the boundary plate. After 48 h, the brine shrimps that had moved to the illuminated compartment were collected and used in the lethality assay. The samples were evaluated for their effect on the survival of *A. salina* according to the procedure described by Alanís-Garza et al. [8]. The assay was performed in 24 well plates containing groups of 10–15 nauplii randomly selected to a final volume of 1mL. The samples were exposed to the *Artemia* nauplii for 24 h at a concentration of 10ppm diluted in natural seawater. The number of dead larvae was recorded after 24 hours and used to calculate the lethal concentration (%). In the negative control, larvae were incubated in seawater and potassium dichromate was used as the positive control. Three independent experiments were performed. Standard deviations (SD) were calculated and results expressed as a mean of replicates \pm SD.



We employed this model during this project for preliminary toxicity study in different works such as:

ANNEX I: In this work, a test of lethality to *Artemia salina* (brine shrimp) was employed to evaluate the general toxicity of synthesised aminoalkylphenols from 5-nitrosalicylaldehyde through a Patis borono– Mannich multicomponent reaction. The results obtained from the *A. salina* bioassay were in correlation with those of in vitro noncancer human cells model [9].

ANNEX II: *Artemia salina* was exploited in this study for determine the general toxicity of the four synthesised mixed-azole compounds of benzisothiazole–tetrazolyl and benzisothiazole–thiadiazolyl (N-(1H-tetrazol-5-yl)-N-(1,1-dioxo-1,2-benzisothiazol-3-yl)amine (TS), N-(2-methyl-2H-tetrazol-5-yl)-N-(1,1-dioxo-1,2-benzisothiazol-3-yl) amine (2MTS), N-(1-methyl-2H-tetrazol-5-yl)-N-(1,1-dioxo-1,2-benzisothiazol-3-yl) amine (TSMT) and 3-[(5-methyl-1,3,4-thiadiazol-2-yl) sulfanyl]-1,2-benzisothiazole 1,1-dioxide (MTSB). It was observed that all these compounds had low general toxicity in *A. salina* model which is in agreement with the cytotoxicity study as none of these compounds reduced the viability of human cancer cells in the range of concentrations tested [10].

ANNEX III: In this study, the synthesis of 3-hydroxyl-2-naphthoylhydrazones containing pyrrole (HL1), furane (HL2), and thiophene (HL3) moieties and their V(IV)O-, Cu(II)- and Zn(II)-complexes are reported. The general toxicity of the above compounds was evaluated with the help of Brine shrimp lethality bioassay with the Cu complexes being the most bioactive [11].

ANNEX IV: Herein, we reported the general toxicity study of 31 *Plectranthus* extracts obtained from 16 *Plectranthus* spp. The Preliminary evaluation of general Toxicity on *A. salina* Model reveals *P. strigosus* to be the most toxic [12].

ANNEX V: In the article “Biological activity screening of seven *Plectranthus* species: Pesquisa de atividade biológica de sete espécies de *Plectranthus*” by Ntungwe *et al*, seven *Plectranthus* speies were evaluated by the brine shrimp lethality assay to screen for their toxicity [13].

ANNEX VII: In this work, we studied the supercritical fluids extracts obtained from fresh and dried elderberries of *Sambucus nigra* L.: A (dried berries, ethanol absolute), B (dried berries,

ethanol 96%), C (dried berries, ethanol 70%) and D (fresh berries, ethanol 96%). Their preliminary toxicity was evaluated in order to select the most active extract for encapsulation in polymeric nano particles (NPs). Although no toxic effect was observed in *A. salina* model, this model once more proven to be useful in toxicity study [14].

ANNEX VII: Here, novel aminoalkylphenols were identified as particularly promising, after MIC and minimum bactericidal concentrations (MBC) determination against a panel of reference strain Gram-positive bacteria, and further confirmed against 40 clinical isolates (*Staphylococcus aureus*, *Staphylococcus epidermidis*, *Enterococcus faecalis*, *Enterococcus faecium*, and *Listeria monocytogenes*). The *A. salina* was used to determine the general toxicity and these same two aminoalkylphenols displayed low toxicity against this model [15].

ANNEX VIII: In this work, dehydroabietic acid (DHA) was studied. DHA is an abietane diterpenoid and possesses a characteristic aromatic ring C, particularly for these types of compounds. The abietic acids are strong antibacterial agents with DHA generally being the most potent. The present work is focused on the antimicrobial and toxicological studies of DHA, and DHA-alginate beads were produced for protection of DHA from degradation and *A. salina* was used to assess if the compound had antimicrobial and not cytotoxic properties [16].

ANNEX IX: In this work, the *A. salina* bioassay was used for the preliminary assessment of general toxicity in natural products thereby guiding the determination of possible biological activities. We report the general toxicity of some derivatives from 6,7-dehydroroyleanone and 7 α -acetoxy-6 β -hydroxyroyleanone compounds [17].

References

- [1] Morley EL, Jones G, Radford AN. The importance of invertebrates when considering the impacts of anthropogenic noise 2013; 281.
- [2] Wilson-Sanders SE. Invertebrate models for biomedical research, testing, and education 2011; 52: 126–52.
- [3] Papadopoulos AI, Lazaridou E, Mauridou G, Touraki M. Glutathione S-transferase in the branchiopod *Artemia salina* 2004; 144: 295–301.
- [4] Ntungwe N E, Marçalo J, Garcia C, Reis C, Teodósio C, Oliveira C, et al. Biological activity screening of seven *Plectranthus* species 2017; 14: 95–108.
- [5] Gajardo GM, Beardmore JA. The brine shrimp *Artemia*: Adapted to critical life conditions 2012; 3 JUN: 1–8.
- [6] Parra AL, Yhebra RS, Sardiñas IG, Buela LI. Comparative study of the assay of *Artemia salina* L. and the estimate of the medium lethal dose (LD50 value) in mice, to determine oral acute toxicity of plant extracts 2001; 8: 395–400.
- [7] Campus Y. Evaluation of the Antibacterial Activity and Toxicity of Isolated Arctiin From the Seeds of *Centaurea Sclerolepis* *Centaurea Sclerolepis* Tohumlarında İzole Edilen Arctiin 'In 2006; 35: 103–9.
- [8] Alanís-Garza BA, González-González GM, Salazar-Aranda R, Waksman de Torres N, Rivas-Galindo VM. Screening of antifungal activity of plants from the northeast of Mexico 2007; 114: 468–71.
- [9] Rimpiläinen T, Andrade J, Nunes A, Ntungwe E, Fernandes AS, Vale JR, et al. Aminobenzylated 4-Nitrophenols as Antibacterial Agents Obtained from 5-Nitrosalicylaldehyde through a Pétasis Borono-Mannich Reaction 2018; 3: 16191–202.
- [10] Frija LMT, Ntungwe E, Sitarek P, Andrade JM, Toma M, Śliwiński T, et al. In vitro assessment of antimicrobial, antioxidant, and cytotoxic properties of saccharin-tetrazolyl and -thiadiazolyl derivatives: The simple dependence of the pH value on antimicrobial activity 2019; 12: 1–14.
- [11] Ribeiro N, Galvão AM, Gomes CSB, Ramos H, Pinheiro R, Saraiva L, et al. Naphthoylhydrazones: coordination to metal ions and biological screening 2019; 43: 17801–18.
- [12] Garcia C, Ntungwe E, Rebelo A, Bessa C, Stankovic T, Dinic J, et al. Parvifloron D from *Plectranthus strigosus*: Cytotoxicity screening of *Plectranthus* spp. extracts 2019; 9.

- [13] Ntungwe N E, Domínguez-Martín EM, Roberto A, Tavares J, Isca VMS, Pereira P, et al. *Artemia* species: An Important Tool to Screen General Toxicity Samples 2020; 26: 2892–2908.
- [14] Mota AH, Andrade JM, Ntungwe EN, Pereira P, Cebola MJ, Bernardo-Gil MG, et al. Green extraction of *Sambucus nigra* L. for potential application in skin nanocarriers 2020: 1–13.
- [15] Rimpilainen T, Nunes A, Calado R, Fernandes AS, Andrade J, Ntungwe E, et al. Increased antibacterial properties of indoline-derived phenolic Mannich bases. *European Journal of Medicinal Chemistry* 2021: 113459.
- [16] Neto, I; Domínguez-Martín, E.M.; Ntungwe, E.; Reis, C.P.; Pesic, M.; Faustino, C.; Rijo, P. Dehydroabietic Acid potential as Biofilm-Mediated Infections Treatment. *Pharmaceutics* 2021, 13, 825.
- [17] Ntungwe, E.; Isca, V.M.S.; Díaz-lanza, A.M.; Afonso, C.A.M.; Rijo, P. General Toxicity screening of Royleanone derivatives using an *Artemia salina* model. 2021, 1–9.

CHAPTER III

Article 2

Preliminary Biological Activity Screening of *Plectranthus* spp. Extracts for the Search of Anticancer Lead Molecules

Epole Ntungwe ^{1,2}, Eva María Domínguez-Martín ^{1,2}, Catarina Teodósio ¹, Silvia Teixidó Trujillo ³, Natalia Armas- Capote ³, Lucilia Saraiva ⁴, Ana María Díaz-Lanza ², Noélia Duarte ⁵ and Patrícia Rijo ^{1,5*}

^a CBIOS – Universidade Lusófona Research Center for Biosciences & Health Technologies, Universidade Lusófona de Humanidades e Tecnologias, Campo Grande 376, .1749-024 Lisboa, Portugal; ntungweepolengolle@yahoo.com (E.N.); evam.dominguez@uah.es (E.M.D.-M.); catarina.teodosio@gmail.com(C.T.)

² Department of Biomedical Sciences, Faculty of Pharmacy, University of Alcalá de Henares, Ctra. A2, Km 33.100 – Campus Universitario, 28805 Alcalá de Henares, Spain; ana.diaz@uah.es

³ Centro Atlántico del Medicamento S.A., Avenida Trinidad 61, 7^a Planta, Torre Agustín Arévalo. 38204. La Laguna, Tenerife, Spain; teixido.silvia@gmail.com (S.T.T.); nataliaarmas@ceamedsa.com (N.A.C.)

⁴ LAQV/REQUIMTE, Laboratório de Microbiologia, Departamento de Ciências Biológicas, Faculdade de Farmácia, Universidade do Porto, Rua de Jorge Viterbo Ferreira n.º 228, 4050-313, Porto, Portugal; lucilia.saraiva@ff.up.pt

⁵ Instituto de Investigação do Medicamento (iMed.Ulisboa), Faculdade de Farmácia, Universidade de Lisboa, 1649-003 Lisboa, Portugal; mduarte@ff.ulisboa.pt







* Correspondence author: patricia.rijo@ulusofona.pt

Pharmaceuticals 2021, 14, 402.

<https://doi.org/10.3390/ph14050402>

Article

Preliminary Biological Activity Screening of *Plectranthus* spp. Extracts for the Search of Anticancer Lead Molecules

Epole Ntungwe ^{1,2} , Eva María Domínguez-Martín ^{1,2} , Catarina Teodósio ¹, Silvia Teixidó-Trujillo ³, Natalia Armas Capote ³, Lucilia Saraiva ⁴ , Ana María Díaz-Lanza ² , Noélia Duarte ⁵  and Patrícia Rijo ^{1,5,*} 

- ¹ CBIOS—Universidade Lusófona Research Center for Biosciences & Health Technologies, Universidade Lusófona de Humanidades e Tecnologias, Campo Grande 376, 1749-024 Lisboa, Portugal; ntungweepolengolle@yahoo.com (E.N.); evam.dominguez@uah.es (E.M.D.-M.); catarina.teodosio@gmail.com (C.T.)
- ² Department of Biomedical Sciences, Faculty of Pharmacy, University of Alcalá de Henares, Ctra. A2, Km 33.100—Campus Universitario, 28805 Alcalá de Henares, Spain; ana.diaz@uah.es
- ³ Centro Atlántico del Medicamento S.A., Avenida Trinidad 61, 7ª Planta, Torre Agustín Arévalo, 38204 La Laguna, Tenerife, Spain; teixido.silvia@gmail.com (S.T.-T.); nataliaarmas@ceamedsa.com (N.A.C.)
- ⁴ LAQV/REQUIMTE, Laboratório de Microbiologia, Departamento de Ciências Biológicas, Faculdade de Farmácia, Universidade do Porto, Rua de Jorge Viterbo Ferreira n.º 228, 4050-313 Porto, Portugal; lucilia.saraiva@ff.up.pt
- ⁵ Instituto de Investigação do Medicamento (iMed.U.Lisboa), Faculdade de Farmácia, Universidade de Lisboa, 1649-003 Lisboa, Portugal; mduarte@ff.ulisboa.pt
- * Correspondence: patricia.rijo@ulusofona.pt



Citation: Ntungwe, E.; Domínguez-Martín, E.M.; Teodósio, C.; Teixidó-Trujillo, S.; Armas Capote, N.; Saraiva, L.; Díaz-Lanza, A.M.; Duarte, N.; Rijo, P. Preliminary Biological Activity Screening of *Plectranthus* spp. Extracts for the Search of Anticancer Lead Molecules. *Pharmaceuticals* **2021**, *14*, 402. <https://doi.org/10.3390/ph14050402>

Academic Editor: Maria Matilde Soares Duarte Marques

Received: 6 April 2021
Accepted: 20 April 2021
Published: 23 April 2021

Publisher's Note: MDPI stays neutral with regard to jurisdictional claims in published maps and institutional affiliations.



Copyright: © 2021 by the authors. Licensee MDPI, Basel, Switzerland. This article is an open access article distributed under the terms and conditions of the Creative Commons Attribution (CC BY) license (<https://creativecommons.org/licenses/by/4.0/>).

Abstract: *Plectranthus* species (Lamiaceae) have been employed in traditional medicine and this is now validated by the presence of bioactive abietane-type diterpenoids. Herein, sixteen *Plectranthus* acetonic extracts were prepared by ultrasound-assisted extraction and their biological activity was screened. The antimicrobial activity of each extract was screened against yeasts, and Gram-positive and Gram-negative bacteria. The *P. hadiensis* and *P. mutabilis* extracts possessed significant activity against *Staphylococcus aureus* and *Candida albicans* (microdilution method). Moreover, all extracts showed antioxidant activity using the DPPH method, with *P. hadiensis* and *P. mutabilis* extracts having the highest scavenging activities. Selected by the *Artemia salina* model, *P. hadiensis* and *P. ciliatus* possessed low micromolar anti-proliferative activities in human colon, breast, and lung cancer cell lines. Furthermore, the most bioactive extract of *P. hadiensis* leaves and the known abietane diterpene, 7 α -acetoxy-6 β -hydroxyroyleanone isolated from this plant, were tested against the aggressive type triple negative breast cancer (MDA-MB-231S). *P. hadiensis* extract reduced the viability of MDA-MB-231S cancer cell line cells, showing an IC₅₀ value of 25.6 μ g/mL. The IC₅₀ value of 7 α -acetoxy-6 β -hydroxyroyleanone was 5.5 μ M (2.15 μ g/mL), suggesting that this lead molecule is a potential starting tool for the development of anti-cancer drugs.

Keywords: *Plectranthus*; royleanone; 7 α -acetoxy-6 β -hydroxyroyleanone; *ent*-abietane; antitumoral activity; antimicrobial activity; antioxidant

1. Introduction

Over the centuries, plants and natural products derived from plants have been the basis of traditional medicine. Nowadays, plant-based medicines have been playing an important role in drug discovery and development. They are also widely employed in various public health practices as they are safe, cost-effective, and possess unique chemical diversity [1,2]. Cancer remains one of the leading causes of death globally, with approximately 18.1 million new cases and 9.6 million cancer-related deaths in 2018, according to the World Health Organization [3]. Furthermore, several types of chemotherapies used are ineffective and generate unwanted adverse side effects [4,5]. Similarly, there is an increasing number of cases of bacterial infections that are resistant to current antibiotics and are

difficult or impossible to treat [6]. Currently, there is an emerging interest in developing drugs that overcome the problems stated above by using natural compounds.

Plectranthus L' Herit. is a major genus of the Lamiaceae family comprising about 300 species mainly distributed in the summer-rainfall savannahs and forested regions of tropical Africa, Asia, and Australia [7,8]. Most of the *Plectranthus* species are soft trailing semi-succulent to succulent herbs or shrubs and their stems, leaves, roots, and tubers are frequently used as traditional medicines for the treatment of various illnesses, including respiratory, digestive, and liver ailments [9]. Phytochemical studies on some species of *Plectranthus* revealed the presence of a large number of diterpenes and triterpenes [10,11]. Isolated terpenes from *Plectranthus* species are reported to possess antibacterial [12–14], antitumoral [15–18], antifungal [12,19], insecticidal [20], and antiplasmodial [20] activities. Moreover, our group has been focused on the phytochemical study of *Plectranthus* species and we have reported abietane diterpenoids with diverse bioactivity [16,17,21–25]. Therefore, the screening of other *Plectranthus* spp. extracts aiming at finding new sources of biologically active natural products is warranted.

Herein, sixteen *Plectranthus* species were screened for their bioactivity (antioxidant, antimicrobial activities, and general toxicity) and the main compound of the most bioactive extract was identified. To the best of our knowledge, the scientific literature concerning these species is scarce or even non-existent. *P. hadiensis* was earlier reported to have ethnopharmacological activity and to be a rich source of ent-abietane diterpenes [11]. This work aims to screen the antimicrobial, antioxidant, and cytotoxic properties of several *Plectranthus* spp. extracts and identifying the component in the most bioactive extract that may be responsible for its bioactivity.

2. Results and Discussion

All sixteen *Plectranthus* spp. extracts were prepared using ultrasound-assisted extraction in acetone. Previous studies of *Plectranthus* species showed that acetonic extracts are rich in diterpenoids, and high extraction yields are obtained when the ultrasound extraction method is carried out [21]. Therefore, using this extraction method, sixteen acetonic extracts of *Plectranthus* spp. were prepared. The extraction of all extracts was done in triplicate under the same conditions. All extracts were solubilized in DMSO (10 mg/mL) and stored at $-20\text{ }^{\circ}\text{C}$ until further analysis for their biological assays. *P. mutabilis* had the highest extraction yield (30.00% *w/w*) (Table 1).

The antioxidant activity of the extracts was quantitatively determined using the DPPH (2,2-diphenyl-1-picrylhydrazyl) scavenging radical assay. The antioxidant activity of the extracts was compared with quercetin, a well-known pure compound used as a positive control to understand the potential antioxidant activity of the extracts screen. The antioxidant activity indicates the capacity to quench reactive oxygen species (ROS), leading to decreased oxidative stress [26]. The results of the free radical scavenging capacity of extracts at a concentration of 10 $\mu\text{g/mL}$ are shown in Table 1. *P. mutabilis* and *P. hadiensis* had the highest scavenging activity of 46.14% and 36.24%, respectively. These results are also in agreement with other studies with *Plectranthus* extracts, in which *P. madagascarensis*, *P. neochilus*, *P. barbatus* and *P. verticillatus* extracts showed free radical scavenging abilities [27]. This could be due to the presence of abietane diterpenes known for their antioxidant activity. Recently, findings concerning the antioxidant activity of abietane diterpenes isolated from *Plectranthus* spp. suggest that the quinone moiety present in these compounds is probably responsible for their biological activity [28]. The presence of the 12-OH group and the carbonyl group at position C-7 (*p*-position) could serve as hydrogen- and/or electron-donating moieties, resulting in the formation of stable quinone derivatives [29].

To evaluate the antimicrobial activity, the extracts were screened against Gram-positive (*Staphylococcus aureus*, *Enterococcus faecalis*) and Gram-negative (*Pseudomonas aeruginosa* and *Escherichia coli*) bacteria and yeasts (*Candida albicans* and *Saccharomyces cerevisiae*) using the well diffusion assay. The antimicrobial activity of each acetonic extract was first screened by

the well diffusion method at a concentration of 1 mg/mL. Only *P. hadiensis* and *P. mutabilis* extracts showed antimicrobial activity against *S. aureus* with inhibition zones of 16 mm and 15 mm, respectively. None of the extracts showed significant antibacterial activity against *E. faecalis* and Gram-negative bacteria. These results are in agreement with previous works on *Plectranthus* spp. [17,30] showing that only Gram-positive bacteria are sensitive to *Plectranthus* acetonic extracts [27,31]. When the zone of inhibition of the extracts was compared with the negative control, it was found that nine extracts (*P. ciliatus*, *P. welshii*, *P. mzumbulensis*, *P. inflexus*, *P. lucidus*, *P. xerophylus*, *P. lippio*, *P. hadiensis*, and *P. mutabilis*.) exhibited antimicrobial activity against *C. albicans* (10–11 mm). The remaining did not display any antimicrobial effects, showing inhibition zones similar to the negative control (data not shown).

Table 1. Extraction yields (dry weight % *w/w*), antioxidant activity, and general toxicity of sixteen *Plectranthus* spp. acetonic extracts.

| Scientific Name | Yield (% <i>w/w</i>) ^a | Antioxidant Activity ^b (%) | General Toxicity | |
|--|---------------------------------------|---------------------------------------|------------------|-----------------------------|
| | | | * Mortality (%) | LC ₅₀ (µg/mL) ** |
| <i>P. swynnertonii</i> S. Moore † | 3.89 | 20.24 ± 0.01 | 65.88 ± 5 | 0.036 ± 1.69 |
| <i>P. ciliatus</i> E. Mey † | 11.86 | 13.21 ± 0.01 | 60.14 ± 0.44 | 0.504 ± 1.13 |
| <i>P. mutabilis</i> Codd. † | 30.03 | 46.14 ± 0.02 | 51.50 ± 0.07 | 0.984 ± 2.92 |
| <i>P. hadiensis</i> (Forssk.) Schweinf. Ex Sprenger † | 13.49 | 36.24 ± 0.04 | 43.65 ± 3.04 | 0.88 ± 4.87 |
| <i>P. cylindraceus</i> Hochst, ex Benth † | 9.68 | 19.19 ± 0.07 | 43.50 ± 5.66 | 0.55 ± 1.96 |
| <i>P. lucidus</i> (Benth.) Van Jaarsv. and T.J. Edwards † | 6.29 | 23.96 ± 0.09 | 38.81 ± 3.75 | 1.053 ± 4.61 |
| <i>P. inflexus</i> (Thunb.) Vahl ex Benth † | 10.97 | 0.16 ± 0.05 | 38.70 ± 3.35 | 0.986 ± 2.87 |
| <i>P. lippio</i> . Druce | 2.09 | 30.5 ± 0.14 | 24.70 ± 6.22 | N/A |
| <i>P. crassus</i> N.E.Br. † | 7.77 | 27.27 ± 0.01 | 31.16 ± 1.29 | N/A |
| <i>P. mzimvubuensis</i> Van Jaarsv. † | 7.79 | 22.47 ± 0.05 | 33.95 ± 1.63 | N/A |
| <i>P. xerophylus</i> Codd | 10.16 | 20.15 ± 0.02 | 30.48 ± 3.24 | N/A |
| <i>P. welshii</i> | 2.15 | 15.06 ± 0.03 | 23.71 ± 0.60 | N/A |
| <i>P. petiolaris</i> E. Mey ex Benth. | 11.07 | 14.45 ± 0.01 | 23.42 ± 4.15 | N/A |
| <i>P. woodii</i> Gürke | 8.51 | 13.04 ± 0.01 | 29.95 ± 6.01 | N/A |
| <i>P. welwitschii</i> (Briq. Codd) | 3.59 | 12.63 ± 0.03 | 25.17 ± 5.54 | N/A |
| <i>P. spicatus</i> E. Mey | 4.75 | 10.57 ± 0.02 | 27 ± 0.28 | N/A |
| Positive control | N/A | 99.47 ± 0.10 | 98.89 ± 2.48 | N/A |
| DMSO | N/A | N/A | 21.87 ± 0.44 | N/A |

^a (mg of extracts/ g of the dried plant). ^b Antioxidant activity (%): Quercetin a potent free radical scavenging capacity was used as a positive control. Data are mean ± SD. * Screening of the *Plectranthus* spp. extracts for general toxicity at a concentration of 10 µg/mL using the *Artemia salina* test (24 h). ** LC₅₀ values (µg/mL) for the most active extracts. Positive control = Potassium dichromate (10 µg/mL). Data are mean ± SD was calculated from three independent experiments and compared to DMSO († *p* < 0.001). Lethal concentration (%) = (Total *A.salina* – Alive *A.salina*)/(Total *A.salina*) × 100 was used to calculate the lethal concentration of all extracts. N/A—not applicable.

As the initial screening using the well diffusion assay identified *P. hadiensis* and *P. mutabilis* extracts as possessing the most promising antimicrobial activities, further studies were carried out to evaluate the minimum inhibitory concentration (MIC) and minimum bactericidal concentration (MBC) or minimum fungicidal concentration (MFC) against the susceptible strains (Table 2). The MIC values ranged from 3.91 µg/mL to 125 µg/mL. *P. hadiensis* was the most active extract, exhibiting a MIC value of 3.91 µg/mL against the methicillin-resistant *S. aureus* strain (MRSA), similar to that observed for the positive control (1.95 µg/mL). The MBC/MFC values ranged from 62.5 to 250 µg/mL. It is possible to conclude that the extracts are mainly bacteriostatic rather than bactericidal [32].

To identify the most promising extracts with cytotoxic activity, the screening of general toxicity using the *Artemia salina* model was carried out. This assay was employed to screen the sixteen extracts because it is low-cost, rapid, convenient, and requires only a relatively small amount of sample [31,33]. All of the acetonic extracts were tested at 10 µg/mL with values ranging from 23.42 to 65.88% mortality (see Table 1). The most active extracts were further studied to obtain the LC₅₀ values at concentrations of 0.1, 0.5, and 1 mg/mL,

after 24 h of exposure. The most toxic extracts (*P. mutabilis*, *P. swynnertonii*, *P. hadiensis*, *P. ciliatus*, and *P. cylindraceus*) with $LC_{50} \leq 1 \mu\text{g/mL}$ (see Table 1) were then evaluated on human-derived cancer cell lines.

Table 2. MIC and MBC/MFC ($\mu\text{g/mL}$) values of the most active acetonic extracts.

| Extracts | MIC ($\mu\text{g/mL}$) | | | MBC/MFC ($\mu\text{g/mL}$) | | |
|---------------------|--------------------------|-------|--------------------|------------------------------|------|--------------------|
| | <i>S. aureus</i> | MRSA | <i>C. albicans</i> | <i>S. aureus</i> | MRSA | <i>C. albicans</i> |
| Positive Control | 3.91 | 1.95 | <0.48 | - | - | - |
| <i>P. mutabilis</i> | 31.25 | 31.25 | 125 | 250 | 250 | 125 |
| <i>P. hadiensis</i> | 15.62 | 3.91 | 62.5 | 250 | 250 | 62.5 |

Positive controls (1 mg/mL): Gram-positive = vancomycin, Gram-negative = norfloxacin, yeast = nystatin, Negative control = DMSO, methicillin-resistant *Staphylococcus aureus* = MRSA.

The cytotoxic activity was determined by the sulforhodamine B (SRB) assay in three different cancer cell lines: colon colorectal carcinoma (HCT116), human breast adenocarcinoma (MCF-7), and lung cancer carcinoma (NCI-H460). The IC_{50} values in all the cell lines tested ranged from 2.25 $\mu\text{g/mL}$ to 36 $\mu\text{g/mL}$ (Table 3). According to the National Cancer Institute (NCI), crude extracts that possess $IC_{50} \leq 500 \mu\text{g/mL}$ are of potential interest for further studies [34] and a possible candidate for further development of cancer therapeutic agents. Thus, most of the selected extracts showed potential values, and *P. hadiensis* and *P. ciliatus* seem to be potential sources of lead anticancer molecules. *P. ciliatus* extract was most active against the colon cell line (HCT116), whereas the *P. hadiensis* extract was the most active against the breast (MCF-7) and lung (NCI-H460) cell lines with the lowest IC_{50} value in the MCF-7 cell lines. For this reason, this extract was further tested against the aggressive type triple-negative breast cancer (MDA-MB-231S). MCF-7 hormone receptors expressing breast cancers have a more favorable prognosis as opposed to triple-negative breast cancer (TNBC), which is characterized by a poor treatment outcome [35]. This cell line is a highly metastatic triple-negative breast cancer cell line that does not display estrogenic receptors (ER), progesterone receptors (PR), or human epidermal growth factor receptor 2 (HER2), and is thus difficult to treat [21]. *P. hadiensis* acetonic extract had a growth inhibition effect on MDA-MB-231 cancer cells (IC_{50} value of 25.6 $\mu\text{g/mL}$, Table 3). Many studies have attributed the cytotoxicity of *Plectranthus* extracts to the presence of royleanone-type abietane diterpenoids with known anticancer activities [18,36]. The abietane-type diterpenoid royleanones are a highly bioactive group of lead molecules, important for the development of new anticancer drugs [22]. Given the good levels of bioactivity of *P. hadiensis* extract in all the cell lines tested, it was selected to identify its main bioactive component.

Table 3. IC_{50} ($\mu\text{g/mL}$) values for five selected acetonic extracts in HCT116, MCF-7, H460 and MDA-MB231S cell lines.

| | HCT116 * | H460 * | MCF-7 * | MDA-MB231S ** |
|------------------------|------------------|------------------|------------------|-----------------|
| <i>P. hadiensis</i> | 3.45 \pm 0.35 | 3.00 \pm 0.10 | 2.90 \pm 0.10 | 25.6 |
| <i>P. ciliatus</i> | 2.25 \pm 0.75 | 6.45 \pm 0.05 | 6.70 \pm 0.30 | N/A |
| <i>P. swynnertonii</i> | 7.95 \pm 0.35 | 13.50 \pm 0.50 | 15.05 \pm 0.02 | N/A |
| <i>P. cylindraceus</i> | 10.25 \pm 0.75 | 12.50 \pm 0.50 | 12.00 \pm 1.00 | N/A |
| <i>P. mutabilis</i> | 28.00 \pm 2.00 | 36.00 \pm 2.00 | 35.00 \pm 1.00 | N/A |
| <i>Doxorubicin</i> | 0.05 \pm 3.24 | 0.29 \pm 2.32 | 0.08 \pm 4.10 | 0.07 \pm 0.01 |

* The concentration that reduces growth by 50% (IC_{50}) was determined by sulforhodamine B assay after 48 h treatment. Data are mean \pm SEM of 4–5 independent experiments. ** IC_{50} ($\mu\text{g/mL}$) of the most bioactive *P. hadiensis* acetonic extract in MDA-MB231S cancer cell lines. DMSO was used as the negative control. N/A—not applicable.

To unveil the chemical profile of the most bioactive *P. hadiensis* acetonic extract, and to identify the main compound responsible for the tested bioactivity, an HPLC–DAD study was carried out. The chromatogram revealed that the known *ent*-abietane diterpene,

7 α -acetoxy-6 β -hydroxyroyleanone, Roy (Figure 1) was the major compound in the extract (Supplementary Material). To isolate this diterpene, a bio-guided column and the preparative chromatographic procedure were carried out. Its structure was confirmed through comparison of its spectroscopic data (Supplementary Material) to those described in the literature [12,29,37].

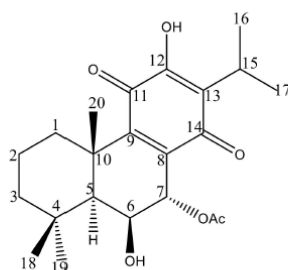


Figure 1. Chemical structure of 7 α -acetoxy-6 β -hydroxyroyleanone.

In previous studies, 7 α -acetoxy-6 β -hydroxyroyleanone showed cytotoxic activity against three human cell lines, namely, sensitive non-small cell lung carcinoma, NCI-H460 cell line (IC_{50} 2.7 ± 0.4), multidrug-resistant non-small cell lung carcinoma cell line with P-glycoprotein overexpression, NCI-H460/R (IC_{50} 3.1 ± 0.4), and human embryonal bronchial epithelial (MCR-5) cells (IC_{50} 8.6 ± 0.4) [21,38]. Given its cytotoxic properties, the presence of this compound in *P. hadiensis* acetic extract may partially explain the foreseen properties of the extract. To further explore its cytotoxicity, additional studies were performed.

The preliminary toxicity of the isolated 7 α -acetoxy-6 β -hydroxyroyleanone (Roy) was evaluated using the Brine shrimp lethality bioassay, which gave a percentage mortality of 30.95%. The cytotoxicity of 7 α -acetoxy-6 β -hydroxyroyleanone was further tested in the TNBC, MDA-MB231S cell line using the MTT assay. It had an IC_{50} value of $5.5 \mu M = 2.15 \mu g/mL$ (Supplementary Information Figure S4), being approximately 12-fold more active than the corresponding extract (MDA-MB231S IC_{50} value = $25.6 \mu g/mL$). This diterpene has also exhibited cytotoxic activity against breast, renal, melanoma, and central nervous system cancer cell lines [24,29,30]. It was also found to induce apoptosis in the H7PX glioma cell line, through the G2/M cell cycle arrest and DSBs (double-strand breaks) [39]. The cytotoxicity of 7 α -acetoxy-6 β -hydroxyroyleanone could be due to its royleanone-type scaffold and by its high lipophilicity, which facilitates penetration into the interior of the cell membrane [21,22,29,39]. Moreover, 7 α -acetoxy-6 β -hydroxyroyleanone was found to exhibit better activity against Gram-positive bacteria, and more importantly, against MRSA strains than some of the existing antibiotics [37]. Roy is found in many other *Plectranthus* species like *P. madagascariensis*, *P. grandidentatus*, *P. actites*, *P. amboinicus*, *P. sanguineus*, *P. argentatus*, and thus can be considered as a chemomarker of the *Plectranthus* genus [21,22].

3. Materials and Methods

3.1. Plant Material

All *Plectranthus* spp. studied in this work (Table 1) were grown in the “Parque Botânico da Tapada da Ajuda”, Lisbon-Portugal from cuttings provided by the Kirstenbosch National Botanical Gardens, South Africa. Plants were collected between 2007 and 2008, always in June and September. Voucher specimens were deposited in the Herbarium “João de Carvalho e Vasconcelos” of the Instituto Superior de Agronomia, Lisboa (LISI), Portugal. The plant names were verified with the Plant List [40].

Extraction Procedure

Plant extracts were obtained by the ultra-sonication method, adding 30 mL of acetone to 3 g of ground dry plants (*P. hadiensis* leaves and the whole plant for the remaining *Plectranthus* spp.), sonicated for 1 h, and filtered (Whatman No 5 paper, Inc., Clifton, NJ, USA). The extraction procedure was repeated three times until complete extraction [41]. The liquid samples were evaporated at 40–50 °C using a rotary evaporator (Sigma-Aldrich, IKA HBR 4 basic heating bath, Essen, Germany). All extracts were solubilized in DMSO (10 mg/mL, except for the exceptions that are mentioned) and stored at –20 °C until further analysis.

3.2. Phytochemical Study of *P. Hadiensis*

3.2.1. HPLC-DAD Fingerprint Analysis

Extract profiling was performed with an Agilent Technologies 1260 Infinity II Series system with diode array detector (DAD; Agilent, Santa Clara, CA, USA), equipped with an Eclipse XDB-C18, (250 × 4.0 mm i.d., 5 µm) column, from Merck and ChemStation Software (Hewlett-Packard, Alto Palo, CA, USA). Four detection wavelengths were selected: 254, 270, 280, and 360 nm. The mobile phase consisted of a mixture of methanol (A), acetonitrile (B), and 0.3% (*w/v*) trifluoroacetic acid in ultrapure water (C). The employed method was modified from the one previously published Matías et al. [21] as follows: 0 min, 15% A, 5% B, and 80% C; 10 min, 70% A, 30% B, and 0% C; 25 min, 70% A, 30% B, and 0% C; and 28 min, 15% A, 5% B, and 80% C. The flow rate was set at 1 mL/min at room temperature and the injection volume was 20 µL. Solvents were previously filtered and degassed through a 0.22 µm membrane filter. The major peak from the *P. hadiensis* leaves extract was identified by co-elution, comparing the retention time and UV-vis spectrum overlaid with an authentic standard (Supplementary Materials Figures S2 and S3).

3.2.2. Isolation and Structural Characterization of 7 α -Acetoxy-6 β -Hydroxyroyleanone

The *P. hadiensis* extract was fractionated by normal phase column chromatography over silica gel using mixtures of n-hexane: EtOAc (8: 2) as eluents to give 3 fractions (A, B, and C) in order of increasing polarity. Fraction B was further studied using preparative thin-layer chromatography (n-hexane/ AcOEt 7:3) on pre-coated TLC sheets (Merck 7747, Darmstadt, Germany) giving 4 fractions B1 to B4. Visualization of spots was performed under visible light and UV light (λ 254 and 366 nm) followed by spraying with a mixture of H₂SO₄: AcOH: H₂O (4:80:16) and heating. Fraction B2 was further purified by preparative chromatography affording its major compound, 7 α -acetoxy-6 β -hydroxyroyleanone. The NMR spectra were collected on a Bruker Fourier 300 spectrometer (¹H 300 MHz, ¹³C 75 MHz) using CDCl₃ as the solvent. ¹H and ¹³C chemical shifts are expressed in δ (ppm) and the proton coupling constants (J) in hertz (Hz) Supplementary Materials Table S1.

3.3. DPPH Radical Scavenging Assay

The free radical scavenging activity was measured by the DPPH method, as described by Rijo et al. [26]. Briefly, 10 µL of each extracted sample (1 mg of dry plant extract/mL) were added to a 990 µL solution of DPPH (0.002% in methanol). The mixture was incubated for 30 minutes in the dark, at room temperature. The absorbance (Abs) was measured at 517 nm (U-1500 Hitachi Instruments, Inc; USA). The positive control used was quercetin (10 mg/mL in methanol). An absorbance control (Abs_{control}) containing 10 µL of methanol and 990 µL of DPPH was also prepared. Assays were carried out in triplicate and the free radical scavenging activity was calculated using Equation (1):

$$\text{Scavenging activity (\%)} = \frac{\text{Abs}_{\text{control}} - \text{Abs}_{\text{sample}}}{\text{Abs}_{\text{control}}} \times 100 \quad (1)$$

3.4. Antimicrobial Screening Assays

3.4.1. Microorganism Used

The microorganisms used in this study were obtained from the American Type Culture Collection (ATCC). They included five strains *Enterococcus faecalis* ATCC 29212, *Escherichia coli* ATCC 25922, *Pseudomonas aeruginosa* ATCC 27853, *Staphylococcus aureus* ATCC 25923, *Saccharomyces cerevisiae* ATCC 2601, *Staphylococcus aureus*. CIP were obtained from the CIP 106760, and the yeast strain *Candida albicans* ATCC 10231.

3.4.2. Well Diffusion Method

The antimicrobial activity of each obtained extract was evaluated against two Gram-positive bacteria (*E. faecalis* and *S. aureus*), two Gram-negative bacteria (*E. coli* and *P. aeruginosa*), and two yeasts (*S. cerevisiae* and *C. albicans*), according to Rijo et al. [41]. The extracts were diluted in DMSO from 10 mg/mL to a final concentration of 1 mg/mL. Stock solutions of reference antibiotics (vancomycin, norfloxacin, and nystatin) were also prepared at 1 mg/mL in DMSO.

In aseptic conditions, Petri dishes containing 20 mL of solid Mueller–Hinton for bacteria, or *Sabouraud* Dextrose Agar culture medium (from Biokar Diagnostics), for yeasts, were inoculated with 0.1 mL of bacterial suspension matching a 0.5 McFarland standard solution and uniformly spread on the medium surface using a sterile swab. Wells of approximately 5 mm in diameter were made in the medium, using a sterile glass Pasteur pipette, and 50 µL of each extract were added into the wells. A positive control of vancomycin for Gram-positive bacteria, norfloxacin for Gram-negative bacteria, and nystatin for yeasts, and a negative control of DMSO, were used in the assay. Plates were incubated at 37 °C for 24 h. The antimicrobial activity was evaluated by measuring the diameter (mm) of the inhibition zone formed around the wells and compared to controls.

3.4.3. Minimum Inhibitory Concentration (MIC) and Minimum Bactericidal Concentration (MBC)/ Minimum Fungicidal Concentration (MFC)

The MIC and MBC/MFC were determined using the microdilution technique proposed by National Committee for Clinical Laboratory Standards (NCCLS) [42]. Briefly, 100 µL of Mueller–Hilton broth for bacteria and *Sabouraud* for yeasts was placed into each well of a 96 microplate, under aseptic conditions. Each extracted sample (100 µL), the appropriate positive control of each microorganism, and negative controls at a concentration of 1 mg/mL, were added to the first well. Using a multichannel micropipette, a 1:2 microdilution series was made. A standardized bacterial suspension (10 µL), corresponding to 0.5 McFarland of each microorganism, was then placed in all wells. Finally, the plates were incubated at 37 °C for 24 h. The MIC was determined when no growth was detected in the well of the microplate. Each measurement was performed in triplicate using 96 well microtiter plates with enrichment. A total of 10 µL was withdrawn from the microplate and sown in a Petri dish to verify the MBC/MFC, which was determined when there was no visible microbial growth on the plates [43].

3.5. Evaluation of General Toxicity on *Artemia salina* Model

To evaluate the general toxicity of the different extracts and *ent*-abietane diterpene 7 α -acetoxy-6 β -hydroxyroyleanone, a test of lethality to *Artemia salina* (brine shrimp) was performed as described by Ntungwe et al. [31]. *A. salina* eggs, dry cyst (JBL GmbH and Co. KG, D-67141 Neuhofen Germany), were hatched in artificial seawater at 25–30 °C under aeration with a concentration of 35 g/L. A handmade container with two connected chambers was used for brine shrimp hatching. The eggs were placed in one of two compartments of a container separated by a boundary plate. The cysts were then incubated (in thermostat cabinet AQUA LYTIC[®], Camberley, Surrey, United Kingdom) for 48 h at 24 °C. The compartment with the eggs was covered to maintain a dark ambiance. The other compartment was illuminated to attract the phototropic newly hatched nauplii through perforations on the boundary plate. The brine shrimps that had moved to the illuminated

compartment were collected and used in the lethality assay. Ten to fifteen nauplii were transferred into 24-well plates containing artificial seawater, and 100 μL of each sample was added to the wells (final volume per well: 1 mL). After 24 h exposure to the samples (24 °C), the number of dead nauplii (mortality rate (%)) was determined (Equation (2)). In addition, LC_{50} (Lethal Concentration, 50%) values ($\mu\text{g}/\text{mL}$) were calculated for the most toxic extracts. DMSO was used as the solvent and was kept at 10% (*v/v*) in all samples tested. Potassium dichromate was used as the positive control. All samples were tested in triplicates-at a concentration of 10 ppm for each sample.

$$(\text{Lethal concentration (\%)}) = \frac{\text{Total A. salina} - \text{Alive A. salina}}{\text{Total A. salina}} \times 100 \quad (2)$$

3.6. Cytotoxicity Screening Assays

3.6.1. Cells and Cell Culture

Human colon (HCT116), breast adenocarcinoma (MCF-7), lung carcinoma (H460), and triple-negative breast cancer, MDA-MB-231S, cell lines were purchased from ATCC (Rockville, MD, USA). Cell lines were routinely cultured in 293 RPMI-1640 with ultra-glutamine or DMEM (MDA-MB-231 cells) medium from Lonza (VWR, 294 Carnaxide, Portugal) supplemented with 10% fetal bovine serum from Gibco (Alfagene, Carcavelos, Portugal) and maintained in a humidified atmosphere at 37 °C with 5% CO_2 .

3.6.2. Sulphorhodamine Assay

The cytotoxicity of five of the most toxic extracts on the brine shrimp lethality bioassay was carried out using the sulforhodamine B (SRB) assay as previously described [17,44,45]. Briefly, the extracts were tested in different cancer cell lines: colon colorectal carcinoma (HCT116), human breast adenocarcinoma (MCF-7), and lung cancer carcinoma (H460). Cells were plated in 96-well plates at a final density of 5.0×10^3 cells/well and incubated for 24 h. Cells were then exposed to serial dilutions of each extract (from 1.56 to 50 $\mu\text{g}/\text{mL}$). The effect of the extracts was analyzed following 48 h incubation, using the sulforhodamine B (SRB) assay. Briefly, following fixation with 10% trichloroacetic acid from Scharlau (Sigma-Aldrich, Sintra, Portugal), plates were stained with 0.4% SRB from Sigma-Aldrich (Sintra, Portugal) and washed with 1% acetic acid. The bound dye was then solubilized with 10 mM Tris Base and the absorbance was measured at 510 nm in a microplate reader (Biotek Instruments Inc., Synergy, MX, USA). The solvent of the extracts (DMSO) corresponding to the maximum concentration used in these assays (0.25%) was included as a control. The concentration of extract that causes a 50% reduction in the net protein increase in cells (IC_{50}) was determined for all tested extracts. Data are mean \pm SEM of 4–5 independent experiments.

3.6.3. MTT Assay

MDA-MB231S cell line was grown in DMEM L050-500 culture medium Biowest supplemented with 10% fetal bovine serum, L-glutamine, and penicillin-streptomycin at 37 °C and 5% CO_2 . For the MTT assay, 1000 cells/well were placed in a 96-well plate and the compound to be tested was added 24 h after sowing.

The extract and compound were prepared as stock solutions in DMSO (Scharlau; SU01531000) at a concentration of 20 mg/mL in the case of the extract (which allowed us to use a reduced DMSO percentage at higher concentrations) and 10 mM in the case of the compound. They were stored at 4 °C. The extract and compound were prepared at different concentrations. For the extract, the following dilutions were made: 80 $\mu\text{g}/\text{mL}$, 40 $\mu\text{g}/\text{mL}$, 20 $\mu\text{g}/\text{mL}$, 10 $\mu\text{g}/\text{mL}$, and 2 $\mu\text{g}/\text{mL}$ in culture medium. For the compound, the following dilutions were prepared: 10 μM , 3 μM , 1 μM , 0.3 μM , and 0.1 μM . Each concentration was assayed in triplicate in a 96-well plate.

After 48 h of treatment with the compound or extract, the cells were incubated for 2 h with MTT. After this time, the culture medium was removed, and the formazan crystals

were dissolved by adding 200 μ L of DMSO. The absorbance of each well was measured at 595 nm.

3.7. Statistical Analysis

The results were expressed as the mean value \pm SD. Comparisons were performed within groups by the analysis of variance, using the ANOVA with Dunnett's post-test. Significant differences between control and experimental groups were assessed using GraphPad Prism version 5.00 for Windows, GraphPad Software, San Diego, CA, USA, www.graphpad.com, accessed on 5 February 2021. A probability level $p < 0.05$ was considered to indicate statistical significance.

4. Conclusions

Natural products are known to be an important source of new anticancer agents. This study investigated the diverse biological activity of sixteen *Plectranthus* extracts. Among the studied extracts, *P. hadiensis* leaves and *P. mutabilis* had the highest percentage extraction yield, antimicrobial and antioxidant activities. *P. hadiensis* and *P. ciliatus* were the most cytotoxic extract against HCT116, MCF-7, and H460 cancer cell lines. 7 α -acetoxy-6 β -hydroxyroyleanone was isolated from the most cytotoxic extract (*P. hadiensis*) and was found to be 12 times more bioactive than the extract in the MDA-MB-231S cell line (triple-negative breast cancer). Therefore, it is noteworthy that 7 α -acetoxy-6 β -hydroxyroyleanone present in the most cytotoxic extract has interesting antitumoral activities in different cancer cell lines and might thus be responsible for the biological activity of this extract. However further phytochemical studies should be done to find out more compounds that could contribute to the cytotoxicity of *P. hadiensis*.

Supplementary Materials: The following are available online at <https://www.mdpi.com/article/10.3390/ph14050402/s1>, Figure S1: 1H-NMR data information for 7 α -acetoxy-6 β -hydroxyroyleanone, Figure S2: HPLC chromatograms (270 nm) of *P. hadiensis* leaves showing the major compound, 7 α -acetoxy-6 β -hydroxyroyleanone, Figure S3: UV spectrum of 7 α -acetoxy-6 β -hydroxyroyleanone, Figure S4. Concentration-response curves (IC₅₀ μ M) for 7 α -acetoxy-6 β -hydroxyroyleanone; Table S1: NMR spectroscopy data characterization, ¹H NMR (300 MHz, CDCl₃), ¹³C (75 MHz, CDCl₃).

Author Contributions: Conceptualization, P.R.; methodology, E.N., L.S., C.T., S.T.-T. and N.A.C.; validation, L.S., A.M.D.-L. and P.R.; investigation, E.N., L.S., C.T., S.T.-T. and N.A.C.; writing—original draft preparation, E.N.; writing—review and editing, E.M.D.-M., L.S., A.M.D.-L., P.R. and N.D.; supervision, N.D. and P.R. All authors have read and agreed to the published version of the manuscript.

Funding: This research was funded by Fundação para a Ciência e Tecnologia (FCT) projects UIDB/04567/2020, UIDP/04567/2020, CBIOS/COFAC/FIPID/1/2019 and COFAC/ILIND/CBIOS/1/2020. The authors gratefully acknowledge Fundação para a Ciência e Tecnologia (FCT) for the financial support under the reference CBIOS/COFAC/FIPID/1/2019, UIDB/50006/2020, UID/MULTI/04378/2013 and the project (3599-PPCDT) PTDC/DTP-FTO/1981/2014-POCI-01-0145-FEDER-016581 and the predoctoral FPU 2019 fellowship from the University of Alcalá awarded to E.M.D.-M.

Data Availability Statement: Not applicable.

Acknowledgments: This work was supported by PADDIC 2019 (ALIES-COFAC) as part of the PhD Program in Health Sciences from Universidad de Alcalá and Universidade Lusófona de Humanidades e Tecnologias.

Conflicts of Interest: The authors declare no conflict of interest. The funders had no role in the design of the study; in the collection, analyses, or interpretation of data; in the writing of the manuscript, or in the decision to publish the results.

References

- Wu, C.; Lee, S.L.; Taylor, C.; Li, J.; Chan, Y.M.; Agarwal, R.; Temple, R.; Throckmorton, D.; Tyner, K. Scientific and Regulatory Approach to Botanical Drug Development: A U.S. FDA Perspective. *J. Nat. Prod.* **2020**, *83*, 552–562. [CrossRef] [PubMed]
- Newman, D.J.; Cragg, G.M. Natural Products as Sources of New Drugs over the Nearly Four Decades from 01/1981 to 09/2019. *J. Nat. Prod.* **2020**, *83*, 770–803. [CrossRef]
- World Health Organization (WHO). Fact Sheet on Cancer. Available online: <https://www.who.int/news-room/fact-sheets/detail/cancer> (accessed on 5 February 2021).
- Zhang, X.; Zhang, S.; Yang, Y.; Wang, D.; Gao, H. Natural barrigenol-like triterpenoids: A comprehensive review of their contributions to medicinal chemistry. *Phytochemistry* **2019**, *161*, 41–74. [CrossRef] [PubMed]
- Alam, A.; Jaiswal, V.; Akhtar, S.; Jayashree, B.S.; Dhar, K.L. Isolation of isoflavones from *Iris kashmiriana* Baker as potential anti proliferative agents targeting NF-kappaB. *Phytochemistry* **2017**, *136*, 70–80. [CrossRef] [PubMed]
- Saksham Garg, A.R. A Current Perspective of Plants as an Antibacterial Agent: A Review. *Curr. Pharm. Biotechnol.* **2020**, *21*, 1588. [CrossRef] [PubMed]
- Arumugam, G.; Swamy, M.K.; Sinniah, U.R. *Plectranthus amboinicus* (Lour.) Spreng: Botanical, Phytochemical, Pharmacological and Nutritional Significance. *Molecules* **2016**, *21*, 369. [CrossRef] [PubMed]
- Al Musayeb, N.M.; Amina, M.; Al-Hamoud, G.A.; Mohamed, G.A.; Ibrahim, S.R.M.; Shabana, S. Plectrabarbene, a new abietane diterpene from *Plectranthus barbatus* aerial parts. *Molecules* **2020**, *25*, 2365. [CrossRef] [PubMed]
- Garcia, C.; Silva, C.O.; Monteiro, C.M.; Nicolai, M.; Gonz, I.; Ana, M.D. Anticancer properties of the abietane diterpene 6,7-dehydroroyleanone obtained by optimized extraction. *Future Med. Chem.* **2018**, *10*. [CrossRef] [PubMed]
- Pereira, M.; Matias, D.; Pereira, F.; Reis, C.; Simões, M.F.; Rijo, P. Antimicrobial screening of *Plectranthus madagascariensis* and *P. neochilus* extracts. *Biomed. Biopharm. Res.* **2015**, *12*, 127–138. [CrossRef]
- Garcia, C.; Teodósio, C.; Oliveira, C.; Oliveira, C.; Díaz-Lanza, A.; Reis, C.; Duarte, N.; Rijo, P. Naturally Occurring *Plectranthus*-derived Diterpenes with Antitumoral Activities. *Curr. Pharm. Des.* **2019**, *24*, 4207–4236. [CrossRef]
- Abdissa, N.; Frese, M.; Sewald, N. Antimicrobial abietane-type diterpenoids from *Plectranthus punctatus*. *Molecules* **2017**, *22*, 1919. [CrossRef]
- Pirttimaa, M.; Nasereddin, A.; Kopelyanskiy, D.; Kaiser, M.; Yli-Kauhaluoma, J.; Oksman-Caldentey, K.M.; Brun, R.; Jaffe, C.L.; Moreira, V.M.; Alakurtti, S. Abietane-Type Diterpenoid Amides with Highly Potent and Selective Activity against *Leishmania donovani* and *Trypanosoma cruzi*. *J. Nat. Prod.* **2016**, *79*, 362–368. [CrossRef]
- Isca, V.M.S.; Andrade, J.; Fernandes, A.S.; Paix, P.; Uriel, C.; Mar, A. In Vitro Antimicrobial Activity of Isopimarane-Type Diterpenoids. *Molecules* **2020**, *25*, 4250. [CrossRef]
- Mesquita, L.S.F.; Matos, T.S.; Do Nascimento Ávila, F.; Da Silva Batista, A.; Moura, A.F.; De Moraes, M.O.; Da Silva, M.C.M.; Ferreira, T.L.A.; Nascimento, N.R.F.; Monteiro, N.K.V.; et al. Diterpenoids from Leaves of cultivated *Plectranthus ornatus*. *Planta Med.* **2020**. [CrossRef]
- Śliwiński, T.; Sitarek, P.; Skąła, E.; Isca, V.M.S.; Synowiec, E.; Kowalczyk, T.; Bijak, M.; Rijo, P. Diterpenoids from *Plectranthus* spp. As potential chemotherapeutic agents via apoptosis. *Pharmaceuticals* **2020**, *13*, 123. [CrossRef]
- Garcia, C.; Ntungwe, E.; Rebelo, A.; Bessa, C.; Stankovic, T.; Dinic, J.; Díaz-Lanza, A.; Reis, C.P.; Roberto, A.; Pereira, P.; et al. Parvifloron D from *Plectranthus strigosus*: Cytotoxicity screening of *Plectranthus* spp. extracts. *Biomolecules* **2019**, *9*, 616. [CrossRef]
- Cretton, S.; Saraux, N.; Monteillier, A.; Righi, D.; Marcourt, L.; Genta-Jouve, G.; Wolfender, J.L.; Cuendet, M.; Christen, P. Anti-inflammatory and antiproliferative diterpenoids from *Plectranthus scutellarioides*. *Phytochemistry* **2018**, *154*, 39–46. [CrossRef]
- Simões, M.F.; Rijo, P.; Duarte, A.; Barbosa, D.; Matias, D.; Delgado, J.; Cirilo, N.; Rodriguez, B. Two new diterpenoids from *Plectranthus* species. *Phytochem. Lett.* **2010**, *3*, 221–225. [CrossRef]
- Mothana, R.A.; Al-Said, M.S.; Al-Musayeb, N.M.; El Gamal, A.A.; Al-Massarani, S.M.; Al-Rehaily, A.J.; Abdulkader, M.; Maes, L. In vitro antiprotozoal activity of abietane diterpenoids isolated from *Plectranthus barbatus* andr. *Int. J. Mol. Sci.* **2014**, *15*, 8360–8371. [CrossRef]
- Matias, D.; Nicolai, M.; Saraiva, L.; Pinheiro, R.; Faustino, C.; Diaz Lanza, A.; Pinto Reis, C.; Stankovic, T.; Dinic, J.; Pesic, M.; et al. Cytotoxic Activity of Royleanone Diterpenes from *Plectranthus madagascariensis* Benth. *ACS Omega* **2019**, *4*, 8094–8103. [CrossRef]
- Garcia, C.; Isca, V.M.S.; Pereira, F.; Monteiro, C.M.; Ntungwe, E.; Sousa, F.; Dinic, J.; Holmstedt, S.; Roberto, A.; Diaz-Lanza, A.; et al. Royleanone Derivatives from *Plectranthus* spp. as a Novel Class of P-Glycoprotein Inhibitors. *Front. Pharmacol.* **2020**, *11*, 1711. [CrossRef]
- Isca, V.M.S.; Ferreira, R.J.; Garcia, C.; Monteiro, C.M.; Dinic, J.; Holmstedt, S.; André, V.; Pesic, M.; Dos Santos, D.J.V.A.; Candeias, N.R.; et al. Molecular Docking Studies of Royleanone Diterpenoids from *Plectranthus* spp. as P-Glycoprotein Inhibitors. *ACS Med. Chem. Lett.* **2020**, *11*, 839–845. [CrossRef]
- Isca, V.M.S.; Sencanski, M.; Filipovic, N.; Dos Santos, D.J.V.A.; Gašparović, A.Č.; Saraiva, L.; Afonso, C.A.M.; Rijo, P.; García-Sosa, A.T. Activity to breast cancer cell lines of different malignancy and predicted interaction with protein kinase C isoforms of royleanones. *Int. J. Mol. Sci.* **2020**, *21*, 3671. [CrossRef]
- Saraiva, N.; Costa, J.G.; Reis, C.; Almeida, N.; Rijo, P.; Fernandes, A.S. Anti-migratory and pro-apoptotic properties of parvifloron d on triple-negative breast cancer cells. *Biomolecules* **2020**, *10*, 158. [CrossRef]
- Padmapriya, R.; Ashwini, S.; Raveendran, R. In vitro antioxidant and cytotoxic potential of different parts of *Tephrosia purpurea*. *Res. Pharm. Sci.* **2017**, *12*, 31–37. [CrossRef]

27. Rijo, P.; Batista, M.; Matos, M.; Rocha, H.; Jesus, S.; Simões, M.F. Screening of antioxidant and antimicrobial activities on *Plectranthus* spp. extracts. *Biomed. Biopharm. Res.* **2012**, *9*, 225–235. [CrossRef]
28. Andrade, J.M.; Domínguez-Martín, E.M.; Nicolai, M.; Faustino, C.; Rodrigues, L.M.; Rijo, P. Screening the dermatological potential of plectranthus species components: Antioxidant and inhibitory capacities over elastase, collagenase and tyrosinase. *J. Enzym. Inhib. Med. Chem.* **2021**, *36*, 257–269. [CrossRef]
29. Ndjoubi, K.O.; Sharma, R.; Badmus, J.A.; Jacobs, A.; Jordaan, A.; Marnewick, J.; Warner, D.F.; Hussein, A.A. Antimycobacterial, Cytotoxic, and Antioxidant Activities of Abietane Diterpenoids Isolated from *Plectranthus madagascariensis*. *Plants* **2021**, *10*, 175. [CrossRef]
30. Matias, D.; Nicolai, M.; Fernandes, A.S.; Saraiva, N.; Almeida, J.; Saraiva, L.; Faustino, C.; Díaz-Lanza, A.M.; Reis, C.P.; Rijo, P. Comparison study of different extracts of *Plectranthus madagascariensis*, *P. neochilus* and the rare *P. porcatus* (lamiaceae): Chemical characterization, antioxidant, antimicrobial and cytotoxic activities. *Biomolecules* **2019**, *9*, 179. [CrossRef]
31. Ntungwe, N.E.; Marçalo, J.; Garcia, C.; Reis, C.; Teodósio, C.; Oliveira, C.; Oliveira, C.; Roberto, A. Biological activity screening of seven *Plectranthus* species. *J. Biomed. Biopharm. Res.* **2017**, *14*, 95–108. [CrossRef]
32. Mogana, R.; Adhikari, A.; Tzar, M.N.; Ramliza, R.; Wiart, C. Antibacterial activities of the extracts, fractions and isolated compounds from *Canarium patentinervium* miq. Against bacterial clinical isolates. *BMC Complement. Med. Ther.* **2020**, *20*, 55. [CrossRef] [PubMed]
33. Ntungwe, N.E.; Domínguez-Martín, E.M.; Roberto, A.; Tavares, J.; Isca, V.M.S.; Pereira, P.; Cebola, M.-J.; Rijo, P. *Artemia* species: An Important Tool to Screen General Toxicity Samples. *Curr. Pharm. Des.* **2020**, *26*, 2892–2908. [CrossRef] [PubMed]
34. Srisawat, T.; Chumkaew, P.; Heed-Chim, W.; Sukpondma, Y.; Kanokwiroon, K. Phytochemical screening and cytotoxicity of crude extracts of vatica diospyroides Symington type LS. *Trop. J. Pharm. Res.* **2013**, *12*, 71–76. [CrossRef]
35. Kathryn, J.; Sireesha, V.; Stanley, L. Triple Negative Breast Cancer Cell Lines: One Tool in the Search for Better Treatment of Triple Negative Breast Cancer. *Breast Dis.* **2012**, *32*, 35–48. [CrossRef]
36. Burmistrova, O.; Simões, M.F.; Rijo, P.; Quintana, J.; Bermejo, J.; Estévez, F. Antiproliferative activity of abietane diterpenoids against human tumor cells. *J. Nat. Prod.* **2013**, *76*, 1413–1423. [CrossRef]
37. Bernardes, C.E.S.; Garcia, C.; Pereira, F.; Mota, J.; Pereira, P.; Cebola, M.J.; Reis, C.P.; Correia, I.; Piedade, M.F.M.; Minas Da Piedade, M.E.; et al. Extraction Optimization and Structural and Thermal Characterization of the Antimicrobial Abietane 7 α -Acetoxy-6 β -hydroxyroyleanone. *Mol. Pharm.* **2018**, *15*, 1412–1419. [CrossRef]
38. Abdel-Mogib, M.; Albar, H.A.; Batterjee, S.M. Chemistry of the genus *Plectranthus*. *Molecules* **2002**, *7*, 271–301. [CrossRef]
39. Sitarek, P.; Toma, M.; Ntungwe, E.; Kowalczyk, T.; Skala, E.; Wiczfinska, J.; Śliwiński, T.; Rijo, P. Insight the biological activities of selected abietane diterpenes isolated from *Plectranthus* spp. *Biomolecules* **2020**, *10*, 194. [CrossRef]
40. The Plant List. Version 1.1. 2013. Available online: <http://www.theplantlist.org/> (accessed on 1 January 2021).
41. Rijo, P.; Matias, D.; Fernandes, A.S.; Simões, M.F.; Nicolai, M.; Reis, C.P. Antimicrobial plant extracts encapsulated into polymeric beads for potential application on the skin. *Polymers* **2014**, *6*, 479–490. [CrossRef]
42. CLSI Padronização dos Testes de Sensibilidade a Antimicrobianos por Disco-difusão. In *Norma Aprovada—Oitava Edição*; NCCLS: Wayne, PA, USA, 2003; Volume 23, ISBN 1-56238-485-6.
43. Brandão, F.; Isabel, M.; Ramos, L.; Miyagusku, L. Antimicrobial activity of hydroalcoholic extracts from genipap, baru and taruma. *Cienc. Rural* **2017**, *47*, 6–11. [CrossRef]
44. Leão, M.; Soares, J.; Gomes, S.; Raimundo, L.; Ramos, H.; Bessa, C.; Queiroz, G.; Domingos, S.; Pinto, M.; Inga, A.; et al. Enhanced cytotoxicity of prenylated chalcone against tumour cells via disruption of the p53-MDM2 interaction. *Life Sci.* **2015**, *142*, 60–65. [CrossRef]
45. Soares, J.; Pereira, N.A.; Monteiro, Â.; Leão, M.; Bessa, C.; Dos Santos, D.J.; Raimundo, L.; Queiroz, G.; Bisio, A.; Inga, A.; et al. Oxazoloisoindolinones with in vitro antitumor activity selectively activate a p53-pathway through potential inhibition of the p53-MDM2 interaction. *Eur. J. Pharm. Sci.* **2015**, *66*, 138–147. [CrossRef]

CHAPTER IV

Article 3

One new C₂₀-nor-abietane and three abietane-type diterpenoids from *Plectranthus mutabilis* Codd. leaves as modulators of P-glycoprotein activity

Epole Ntungwe^{a,b}, Sofija Jovanović Stojanov^c, Noélia Duarte^d, Nuno R. Candeias^{e,f}, Lucilia Saraiva^g, Ana María Díaz-Lanza^b, Máté Vágvölgyi^h, Attila Hunyadi^h, Milica Pešić^c, Patrícia Rijo^{a,d*}

CBIOS – Universidade Lusófona's Research Center for Biosciences & Health Technologies, Campo Grande 376, 1749-024, Lisbon, Portugal

^b Department of Biomedical Sciences, Faculty of Pharmacy, University of Alcalá, 28801 - Alcalá de Henares (Madrid), Spain

^c Institute for Biological Research "Siniša Stanković" - National Institute of Republic of Serbia, University of Belgrade, Bulevar despota Stefana 142, 11060 Belgrade, Serbia.

^d Research Institute for Medicines (iMED.Ulisboa), Faculdade de Farmácia, Universidade de Lisboa, Av. Prof. Gama Pinto, 1649-003 Lisboa, Portugal

^e Faculty of Engineering and Natural Sciences, Tampere University, Korkeakoulunkatu 8, 33101 Tampere, Finland

^f LAQV-REQUIMTE, Department of Chemistry, University of Aveiro, 3810-193 Aveiro, Portugal

^g LAQV - Faculty of Pharmacy of University of Porto, Rua de Jorge Viterbo Ferreira, 228 4050-313, Porto, Portugal

^h Institute of Pharmacognosy, Interdisciplinary Excellence Centre, University of Szeged, Eötvös str. 6. 6720 Szeged, Hungary

* Corresponding author:

E-mail address: patricia.rijo@ulusofona.pt (P. Rijo)

In revision

Highlights

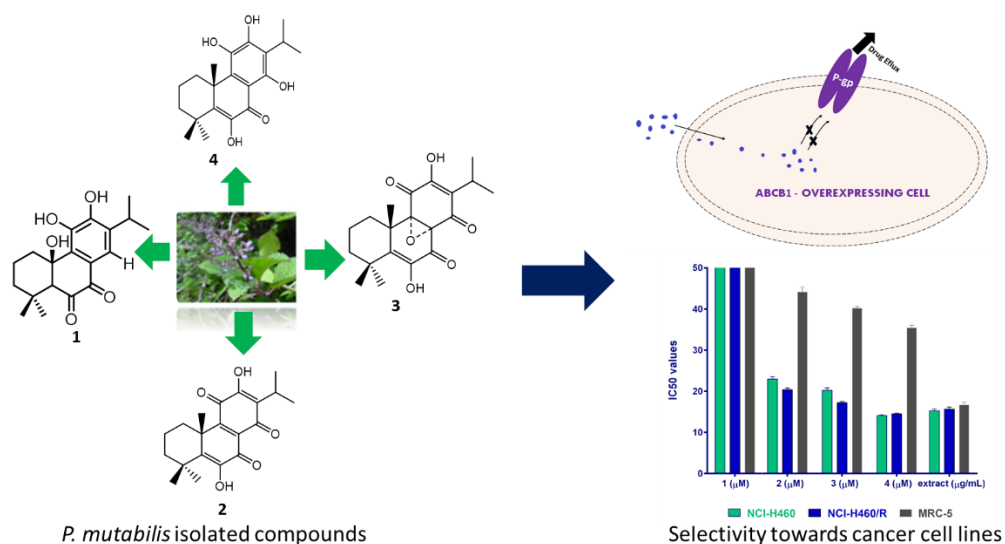
- One new C₂₀-*nor*-abietane (**1**) and three abietane-type diterpenes (**2 – 4**) were isolated from *P. mutabilis* acetone extract.
- The acetone extract and isolated diterpenes **1 - 4** are not substrates for P-glycoprotein.
- Diterpenes **1 - 4** do not affect the expression of P-glycoprotein, while the extract significantly increases P-glycoprotein expression.
- Diterpenes **2 – 4** inhibit P-glycoprotein activity after longer exposure.
- Diterpenes **2 - 4** show selectivity towards cancer cells and have the potential to reverse doxorubicin resistance.

Abstract

The emergence of drug resistance greatly hinders the efficacy of chemotherapy. P-gp is one of the major contributors to multidrug resistance (MDR) as it protects MDR cancer cells by effluxing cytotoxic drugs. Diterpenoids from *Plectranthus* spp. are known as P-gp modulators. Bioguided fractionation of *P. mutabilis* extract was performed by chromatographic methods, and structure elucidation of the isolated compounds done by spectroscopic methods. Moreover, the extract profile and quantification of each isolated compound were determined by HPLC-DAD. In this extract, one new *nor*-abietane diterpene, mutabilol (**1**), was isolated along with three known abietanes, coleon-U-quinone (**2**), 8 α ,9 α -epoxycoleon-U-quinone (**3**), and coleon U (**4**). Moreover, an additional acetoxy derivative of an abietane diterpenoid (**5**) was tentatively identified using HPLC-MS/MS. The concentration of coleon U in this acetone extract was found to be 96 ± 0.048 $\mu\text{g}/\text{mg}$. Compounds **2 - 4** were found to be selective towards the cancer cell lines and their anticancer effect was not compromised by P-gp activity in NCI-H460/R cells. Importantly **2, 3, and 4** were able to inhibit P-gp activity in NCI-H460/R cells at longer exposure of 72 h and consequently revert doxorubicin (DOX) resistance in subsequent combined treatment. None of the compounds influenced the P-gp expression in NCI-H460/R cells, while the extract significantly increased it. Our study identified abietane

diterpenoids from *P. mutabilis* that can evade MDR in cancer cells and inhibit P-gp activity in prolonged treatment.

Graphical Abstract



Keywords: *Plectranthus mutabilis*, abietane diterpenoids, anticancer effect, multidrug resistance, P-glycoprotein

Introduction

The resistance of cancer cells to a wide spectrum of anticancer agents continues to be a major obstacle to successful cancer chemotherapy. Potential factors for multidrug resistance (MDR) includes enhanced drug detoxification, decreased drug uptake, increased intracellular levels of reactive oxygen species (ROS), enhanced DNA repair, overexpression of drug efflux transporters belonging to the ATP Binding Cassette (ABC) family of transporters such as P-glycoprotein (P-gp/ABCB1), multidrug resistance-associated proteins (MRP1, MRP2), and breast cancer resistance protein (BCRP) [1,2]. In order to combat MDR in cancer, three strategies have been under study: 1) developing inhibitor/modulators of ABC-transporters that block the ligand-binding site of the transporter thus impeding the efflux of anticancer drugs. ii) searching for anticancer drugs that are not substrates for ABC-transporters [3], and iii) exploiting collateral sensitivity to selectively kill MDR cancer cells [4]. ABC transporters

possess a wide substrate spectrum including toxic compounds, metabolic products, antibiotics, proteins, lipids, sugars, ions, and anticancer drugs [5,6]. There is no final list of substrates and therefore it is of utmost importance to study the interaction between new anticancer agents and ABC transporters.

The most well-known and widely studied ABC transporter is P-glycoprotein (P-gp). P-gp is an energy-dependent efflux protein that actively exports lipophilic compounds across extra and intra-cellular membranes [7]. It extrudes a wide range of therapeutic drugs from cancer cells including paclitaxel, doxorubicin, daunorubicin, epirubicin, mitoxantrone, vincristine, and vinblastine [8], decreasing their intracellular concentration and rendering their efficacy [9].

In this context, natural products are considered as an alternative source of drugs to fight cancer MDR [10] and have emerged as the fourth generation of MDR inhibitors. Phytochemical studies on *Plectranthus* (Lamiaceae) genus revealed the presence of bioactive compounds, in particular abietane-type diterpenoids [11–15]. Previous studies from our group showed that royleanones from the *Plectranthus* genus can inhibit P-gp activity [16,17] suggesting that abietanes may constitute a new class of P-gp modulators.

P. mutabilis Codd. is a succulent herb grown mainly in South Africa [18]. The essential oils analysis of this plant only revealed the presence of nepetoidins A and B [19]. Besides, in a preliminary screening study, *P. mutabilis* extract was found to have cytotoxic activity in different cancer cell lines [20]. It is, therefore, necessary to enrich the phytochemical information of this plant in literature and identify the compounds that may be responsible for its cytotoxicity. In this work, the isolated compounds and the acetone extract were tested against sensitive and MDR non-small cell lung carcinoma cells as well as normal embryonic lung fibroblasts to assess: i) their selectivity towards cancer cells, ii) their effects against MDR phenotype, iii) the interaction with P-gp, and iv) the potential to sensitize MDR cancer cells to doxorubicin (DOX).

Material and methods

General experimental procedures

Optical rotations were obtained using a Jasco P-2000 polarimeter. IR spectra were determined on an FTIR PerkinElmer® Spectrum 400 (PerkinElmer Inc, Waltham, MA, USA) equipped with an attenuated total reflectance (ATR) device. NMR spectra of compounds **1**, **3** and **4** were recorded on a Bruker® - Biospin Fourier spectrometer (¹H 300 MHz; ¹³C 75), and compound **2** recorded on a Bruker Avance NEO 500 MHz spectrometer (¹H 500 MHz; ¹³C 126. MHz), using CDCl₃ and CD₃OD as solvent. Low-resolution mass spectra were recorded on a Kratos MS25RF spectrometer (70 eV). HRMS were performed in a Thermo Scientific Q Exactive hybrid quadrupole-Orbitrap mass spectrometer (Thermo Scientific™ Q Exactive™ Plus). Column chromatography was carried out on SiO₂ (Merck 9385), Combiflash Rf+ instrument (Teledyne ISCO, Lincoln, NE, USA) equipped with diode array and evaporative light scattering detection (DAD-ELSD), and preparative HPLC on kinetex 5u XB-C18 100A, 250 x 21.2mm using spot prep II liquid chromatography. TLC was performed on precoated SiO₂ F254 plates (Merck 7747, Darmstadt, Germany) and visualized under UV light (λ 254 and 366 nm) and by spraying with a mixture of H₂SO₄: AcOH: H₂O (1:20:4) followed by heating. The extracts were evaporated using a Rotavapor® R-300 system (Buchi, Interface I-300, 9230 Flawil Switzerland). HPLC was carried out on Agilent Technologies 1260 Infinity II Series system with diode array detector (DAD; Agilent, Santa Clara, CA, USA), equipped with an Eclipse XDB-C18, (250 x 4.0 mm i.d., 5μm) column, from Merck and ChemStation Software (Hewlett-Packard, Alto Palo, CA, USA).

Plant material

Plectranthus mutabilis Codd. was grown in the Parque Botânico da Tapada da Ajuda in Lisbon, Portugal from cuttings provided by the Kirstenbosch National Botanical Gardens, South Africa, and were collected between 2007 and 2008, always in June and September. The plant was dried at room temperature and stored protected from light and humidity. Voucher specimens were deposited in the Herbarium “João de Carvalho e Vasconcellos” of the “Instituto Superior de Agronomia”, Lisboa (LISI), Portugal with a voucher number of 651/2007. The plant name has been checked with www.theplantlist.org [21].

Extraction, bioguided fractionation and isolation

The air-dried powdered *P. mutabilis* Codd. leaves (0.71 kg) were extracted with acetone (5 x 8.75 L each 1h) at room temperature for 4 weeks using the ultrasound-assisted extraction method (ultrasound apparatus from VWR). After filtration and evaporation of the solvent under reduced pressure at 40 °C a crude extract (44.07 g) was obtained. This extract was subjected to flash column chromatography over silica gel (Merck 9385, 200 g) using mixtures of *n*-hexane: EtOAc (1:0 to 0:1) and EtOAc: MeOH (1:0 to 0:1) as eluents. According to differences in composition as indicated by TLC, ten crude fractions were obtained (A1 to A10).

A bioguided isolation was done by evaluating the general toxicity of the crude fractions using the *Artemia salina* model [22]. The most bioactive fraction (A7), eluted with *n*-hexane: EtOAc (80:20), was fractionated by column chromatography over silica gel (100g) using *n*-hexane: EtOAc (9:1) as eluent to give 9 fractions (B₁-1 to B₁-9). The fractions B₁-5 were subjected to column chromatography (silica gel, 152g) using *n*-hexane: CH₂Cl₂ (3:2) as eluent to obtain five fractions (C₁-1 to C₁-5). Fraction C₁-4 was purified employing a Combiflash instrument on polyamide stationary phase (100 g) using gradient elution with CH₂Cl₂: MeOH (1: 0 to 3: 22) at a flow rate of 60 mL/min that afforded compound 2 (3.7 mg; 0.0084 % m/m).

Subsequently, fraction C₁-5 (divided into two aliquots) was successively rechromatographed using the Combiflash system with polyamide columns (120 g and 25g), and with flow rates of 60 mL/min and 30 mL/min respectively in gradient elution mode with CH₂Cl₂: MeOH (1: 0 to 9:1) as eluents, to afford compound 4 (152.1 mg; 0.3451% m/m).

Fraction E₂-1 was further separated by means of preparative reverse- phase high performance liquid chromatography (RP-HPLC) using 53% aqueous acetonitrile as mobile phase, to afford compound 3 (63 mg; 0.143 % m/m). Fraction C₁-3 was further purified by flash column chromatography (silica gel, 24g; 25 mL/min) on the Combiflash instrument with *n*-hexane: EtOAc (87.5:12.5) and subsequently, by reverse-phase flash chromatography (C18; 30 g; 35 mL/min) with MeOH: H₂O (55% to 100% MeOH) to afford compound 1 (10.2 mg; 0.023 % m/m).

NMR analysis

Compound **1**: (Mutabilol). Purple solid; m.p., 119-120 °C; $[\alpha]_D^{22} +121.2$ (c 1.2, acetone); IR ν_{\max} cm^{-1} (ATR): 3388.3, 1779.3, 1656.3. For NMR data, see **Table IV.1**; HRMS m/z 333.1694 $[\text{M} + \text{H}]^+$ (calcd. for $\text{C}_{19}\text{H}_{25}\text{O}_5$, 333.1697).

Compound **2**: (Coleon U quinone). Orange solid; m.p. 113-115 °C; IR ν_{\max} cm^{-1} (ATR) 3657.2, 3476.9, 1167.6, 2925.9, 1651.3, 1458.8, 1334.1, 1269.2; HRMS m/z 345.1711 $[\text{M} + \text{H}]^+$ (calcd. for $\text{C}_{20}\text{H}_{25}\text{O}_5$, 345.1697).

Compound **3**: (8 α ,9 α -Epoxycoleon U quinone). Yellow solid; m.p. 137–141 °C; IR ν_{\max} cm^{-1} (ATR): 3450.0, 3357.0, 2965.3, 2920.9, 2875.4, 1682.5, 1614.5, 1462.0, 1328.1, 1249.6, 1166.2. ^1H NMR (300 MHz, CDCl_3): δ 7.02 (1H, s, OH), 6.34 (1H, s, OH), 3.13 (1H, sept, p, $J = 7.1$, H-15), 2.78 (1H, s, H-1 β), 1.77 (d, $J = 2.0$, H-1 α), 1.75 (1H, s, H-2 β), 1.73 (1H, s, H-3 α), 1.61 (1H, s, H-2 α), 1.53 (s, 3H, H-20), 1.40 (1H, s, H-3 β), 1.39 (s, 3H, H-19), 1.36 (s, 3H, H-18), 1.24 (d, $J = 2.5$, 3H, H-16), 1.21 (d, $J = 2.6$, 3H, H-17). To the best of our knowledge, ^1H data is fully described here for the first time.

^{13}C NMR data were in agreement with the literature [22]. HRMS m/z 361.1658 $[\text{M} + \text{H}]^+$ (calcd. for $\text{C}_{20}\text{H}_{25}\text{O}_6$, 361.1646).

Compound **4**: (Coleon U). Orange solid; m.p. 158–161 °C; IR (ATR, cm^{-1}): 3458.8, 3407.8, 2957.8, 2934.9, 2871.9, 1621.5, 1594.6; HRMS m/z 345.1708 $[\text{M}-\text{H}]^-$ (calcd. for $\text{C}_{20}\text{H}_{25}\text{O}_5$, 345.1707). For NMR data of compounds **2**, **3** and **4** see **supplementary information S.IV**.

UHPLC-MS/MS Analysis

The UHPLC-MS/MS experiments were carried out on a Waters Acquity™ Ultra High Performance LC (Waters®, Ireland) system equipped with a binary pump, solvent degasser, auto sampler, and column oven.

Chromatographic separation was achieved on a Purospher® STAR RP-18 2 μm (2.1 x 50 mm) column with an injection volume of 10 μL and column temperature 35°C. A mobile phase consisting of 0.1% HCOOH in Milli-Q water (eluent A) and acetonitrile (eluent B) was used with the following gradient program at 0.3 mL/min flow rate: 0–6 min 60%A, 6–10 min 5%A, and 10.10–15 min at 16% A. Tandem mass spectrometry (MS/MS) detection was performed on a Waters Acquity™ triple quadrupole (Waters®, Ireland) using an electrospray ionization source in positive mode (ESI+) and negative (ESI-) ionization modes, which was set to operate at 120 °C. The search for compounds in the extract was done in MRM (multiple reaction monitoring) mode, using cone voltages and collision energies previously optimized for each

compound and two mass transitions (MRM1 and MRM2), to optimize the selectivity and sensitivity. MassLynx® software (Waters, version 4.1) was used for data acquisition and processing. The samples were diluted (1:10) in acetonitrile and filtered through PTFE filters before analysis.

HPLC-DAD Analysis

The identification and quantification of major compounds (Coleon U quinone (**1**), 8 α ,9 α -Epoxycoleon U quinone (**2**), Coleon U (**3**), Mutabilol (**4**), in *P. mutabilis* extracts were performed using high-performance liquid chromatography (HPLC-DAD). The mobile phase consisted of a mixture of methanol (A), acetonitrile (B), and 0.3% trifluoroacetic acid in water (C) used as follows: 0 min, 15% A, 5% B, and 80% C; 2 min, 70% A, 30% B, and 0% C; 10 min, 70% A, 30% B, and 0% C; and 15 min, 15% A, 5% B, and 80% C. The time of analysis was 15 min, including the stabilization of the RP-18 column. The injection volume was 20 μ L, the flow rate was set at 1 mL/min and the detection wavelength was 270nm for compounds **2** and **3**, and 254nm for compounds **1** and **4**. *P. mutabilis* extract was dissolved in acetone at 10mg/mL. Reference standards were prepared in a concentration range of 0.750–0.030 mg/mL for Coleon U, 0.580–0.020 mg/mL for Coleon U quinone, 0.380–0.050 mg/mL for mutabilol and 0.460–0.040 mg/mL for 8 α ,9 α -epoxycoleon U quinone. Compound identification was based on the comparison of retention time and ultraviolet (UV) spectra overlay with authentic standards. All analyses were performed in triplicate. The limit of detection (LOD) and limit of quantification (LOQ) were calculated based on the standard deviation of the response and the slope using three independent analysis curves. LOD and LOQ were calculated as $3.3\sigma/S$ and $10\sigma/S$, respectively, where σ is the standard deviation of the response and S is the slope of the calibration curve.

Computational Studies

All calculations were carried out using the Gaussian09 (Gaussian09, 2019) software package without symmetry constraints. Density Functional Theory (DFT) [24] was used for optimizing geometries of the quinones in the gas phase. All calculations have been performed using the

PBE1PBE functional and 6-31G (d, p) basis set [25–28]. That functional uses a hybrid generalized gradient approximation (GGA), including a 25% mixture of Hartree-Fock (Hartree-Fock exchange with DFT exchange-correlation, given by Perdew, Burke, and Ernzerhof functional (PBE) [30,31]. Frequency calculations were performed to confirm the nature of the stationary points, yielding nonimaginary frequency for the optimized geometries. Natural Population Analysis (NPA) [31–38] was performed as implemented on Gaussian 16 to study the electronic structure of the optimized species. Fukui functions were plotted with Multiwfn [39] and visualized with Chemcraft 1.8 (Zhurko, G. A. Chemcraft). The parameters used to visualize the Fukui function in the Chemcraft program were a style of lines, a scale of 0.75, values ranging from -0.001 to 0.005, and a contour value of 0.002609. The condensed Fukui functions were calculated according to the following equations [37,40]:

$$f_k^+ = [q_k(N + 1) - q_k(N)], \text{ for nucleophilic attack (1)}$$

$$f_k^- = [q_k(N) - q_k(N - 1)], \text{ for electrophilic attack (2)}$$

$$f_k^0 = \left[\frac{q_k(N+1) - q_k(N-1)}{2} \right], \text{ for radical attack (3)}$$

where k is the numbering of the atomic site and q_k stands for the total natural population in the neutral (N), anionic (N+1), and cationic (N-1) species.

Cytotoxicity study

Cell culture

NCI-H460 (human non-small cell lung carcinoma) and normal embryonic lung fibroblast (MRC-5) cell lines were purchased from the American Type Culture Collection, Rockville, MD. NCI-H460/R cells were selected from NCI-H460 cells by continuous exposure to stepwise increasing concentrations of DOX and possess the overexpression of P-gp as well as MDR phenotype [41]. MDR cancer cell line (NCI-H460/R) and its sensitive counterpart (NCI-H460) were grown in RPMI 1640 medium supplemented with 10% FBS, 2 mM L-glutamine, and 10,000 U/ml penicillin, 10 mg/ml streptomycin, 25 µg/ml amphotericin B solution. MRC-5 cells were cultured in DMEM supplemented with 10% FBS, 4 g/l glucose, 2 mM L-glutamine, and 5000 U/ml penicillin, 5 mg/ml streptomycin solution. All cell lines were sub-cultured at 72 h

intervals using 0.25% trypsin/EDTA and seeded into a fresh medium at 16 000 cells/cm² and maintained at 37°C in a humidified 5% CO₂ atmosphere.

MTT assay

MTT assay was used to assess the viability of NCI-H460, NCI-H460/R, and MRC-5 cells (AppliChem GmbH, Taufkirchen, Germany). After reaching the confluence in 25 cm² tissue flasks, NCI-H460, NCI-H460/R, and MRC-5 cells were trypsinized. Cells were seeded at the optimal density determined in initial experiments: 2000 cell/well into flat-bottomed 96-well tissue culture plates. Following the overnight incubation in 100 µl of the appropriate medium, cells were treated with **1**, **2**, **3**, **4** (2, 5, 10, 20, and 50 µM) or extract (2, 5, 10, 20 and 50 µg/ml) for 72 h. Besides, the combined effects of **2**, **3**, and **4** with DOX were evaluated in NCI-H460/R cells. Therefore, increasing concentrations of DOX (0.1, 0.2, 0.5, 1, and 2 µM) were administrated after 72 h pre-treatment with **2**, **3**, and **4** applied in 3 different concentrations (1, 2, and 5 µM). The sensitization of NCI-H460/R cells was studied 72 h after DOX administration. After treatment, MTT was added to each well in a final concentration of 0.2 mg/ml for 4 h. Formazan product was dissolved in 200 µl of DMSO, and the absorbance was measured at 540 nm using an automatic LKB 5060-006 Micro Plate Reader (Vienna, Austria). IC₅₀ values were defined as a concentration of the drug that inhibited cell growth by 50% and was obtained by nonlinear regression analysis using GraphPad Prism 6.0 software (La Jolla, CA, USA), while Dunnett's multiple comparisons test in Two-way ANOVA was used to determine significant differences among treatment strategies (doxorubicin alone vs. combinations with **2**, **3**, and **4**). Relative selectivity towards cancer cells was calculated as a relation between IC₅₀ value obtained in MRC-5 cells and IC₅₀ for NCI-H460 or NCI-H460/R cells.

Rhodamine 123 accumulation assay

The accumulation of rhodamine 123 (Rho123), which is a fluorescent P-gp substrate, was measured by flow cytometry. The intensity of the fluorescence is proportional to Rho123 accumulation in the cell. NCI-H460 and NCI-H460/R cell lines were seeded in adherent 6-well plates and grown overnight. Cells were treated with 5 and 10 µM of **1**, **2**, **3**, and **4** and with 10 µg/ml of extract for 30 min. Tariquidar (TQ) applied at 50 nM was used as a positive control for Rho123 accumulation. Rho123 (2.5 µM) was simultaneously added with the investigated compounds and the cells were incubated at 37°C in 5% CO₂ for 30 min. To assess the indirect

effect on P-gp activity, NCI-H460 and NCI-H460/R cells were treated with the **1**, **2**, **3**, and **4** (5, and 10 μ M) and extract (5, and 10 μ g/ml) 72 h before Rho123 administration. The cells were then trypsinized, pelleted by centrifugation, washed with PBS, and placed in ice-cold PBS. The samples were kept on ice in the dark until the analysis on CyFlow Space Partec flow cytometer (Sysmex Partec GmbH, Görlitz, Germany). The fluorescence of Rho123 was detected on fluorescence channel 1 (FL1-H) at 530 nm. A minimum of 20,000 events was collected for each sample and the obtained results were analyzed using Summit software v. 4.3 (Dako Colorado Inc., Fort Collins, CO, USA).

Flow cytometric analysis of P-gp expression

P-gp expression level in NCI-H460, NCI-H460/R cells was measured by flow cytometry. All cell lines were seeded in adherent 6-well plates and treated with 5 and 10 μ M of **1**, **2**, **3**, and **4** and with 5 and 10 μ g/ml of extract for 72 h. Cells were also treated with 50 nM TQ, a non-competitive P-gp inhibitor, which served as a positive control. NCI-H460 cells with almost null expression of P-gp were used as a negative control. At the end of the incubation period, cells were collected by trypsinization, washed with PBS, and directly immuno-stained by FITC-conjugated anti-ABCB1 antibody according to the protocol provided by the manufacturer (BD Biosciences, Weybridge, Berkshire, UK). The samples were kept in the dark until the analysis. The fluorescence of FITC-conjugated anti-ABCB1 was detected on fluorescence channel 1 (FL1-H) at 530 nm of CyFlow Space Partec flow cytometer (Sysmex Partec GmbH, Görlitz, Germany). A minimum of 20,000 events was collected for each sample after gating to exclude cell debris and dead cells. The obtained results were analyzed using Summit software v. 4.3 (Dako Colorado Inc., Fort Collins, CO, USA).

Results and Discussion

The acetone extract of the air-dried powdered leaves of *P. mutabilis* was subject to a bioguided chromatographic fractionation based on its toxicity on the *Artemia salina* model [20](**supplementary information**). Crude fraction A7 was the most active against this model and was further studied. A new C₂₀ *nor*-abietane, named mutabilol [(+)-5*S*,10*R*-10,11,12-trihydroxy-6,7-dioxo-20-*nor*abiet-8,11,13-triene, **1**) was isolated, together with three known abietane diterpenes, coleon-U-quinone (**2**), 8 α ,9 α -epoxycoleon-U-quinone (**3**) and coleon U

(4) (Figure IV.1). Their structures were elucidated by spectroscopic methods (IR, and 1D and 2D-NMR) and HRMS. Compound **2** was previously isolated from *P. argentatus* [42], *P. sanguineus* [43], *P. madagascariensis* [44–46], and *P. forsteri* [47]. Compound **3** was found in *P. punctatus* [48], *P. sanguineus* [43], and compound **4** was isolated from *P. madagascariensis* [13,45,49], *P. forsteri* [47], *P. grandidentatus* [50], and *P. argentatus* [47]. Their spectroscopic data were in agreement with those reported in the literature [23,42,47].

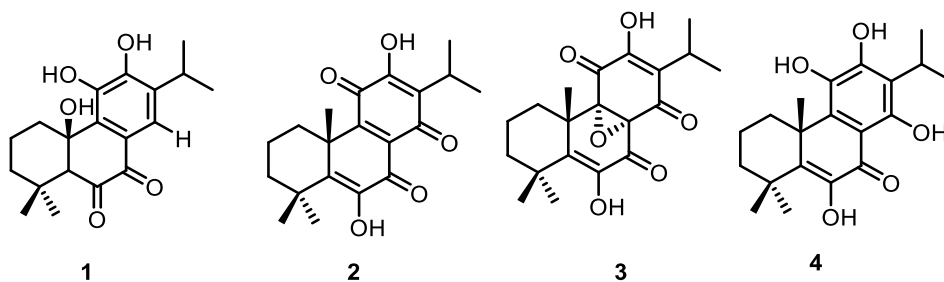


Figure IV.1. Structures of compounds 1–4 from *P. mutabilis*

Compound **1**, named mutabilol, was isolated as a purple solid. Its molecular formula was determined as $C_{19}H_{24}O_5$ from the HRMS that showed a protonated molecular ion at 333.1694 indicative of 8 degrees of unsaturation. In the IR spectrum, characteristic absorption bands for a hydroxyl group (3388.3 cm^{-1}) and carbonyl groups (1779.3), including a conjugated one (1656.3 cm^{-1}) were observed. The $^1\text{H-NMR}$ spectrum (Supplementary information) indicated the presence of an isopropyl substituent evidenced from the characteristic downfield signal at δ_{H} 3.16 (1H, sept, $J = 7.1\text{ Hz}$, H-15) and two doublet methyl groups at δ_{H} 1.18 (3H, d, $J = 6.9\text{ Hz}$, CH_3 -16), and 1.17 (3H, d, $J = 6.9\text{ Hz}$, CH_3 -17). Moreover, $^1\text{H NMR}$ spectrum also showed the signals for one aromatic proton at δ_{H} 7.23 (H-14), a tertiary methine signal at δ_{H} 1.26 (H-5), two singlet methyl groups at δ_{H} 1.29 and 0.94 (H-18 and H-19), and three hydroxyl groups at δ_{H} 8.05 (12-OH), 7.76 (10-OH), and 7.56 (11-OH). The $^{13}\text{C-NMR}$, HMBC and HSQC (supplementary information) displayed resonances of nineteen carbons corresponding to four methyl groups, three methylenes, three methines (one sp^2 carbon at 115.9), and nine quaternary carbons (including one oxygenated at 54.2 and two carbonyl groups at 176.4 and 178.9).

The ^1H - and ^{13}C -NMR spectra of compound **1** were similar to those of coleon V (Supplementary information) [23]. The main differences were the absence of the C-20 methyl group signal (δ_{C} 23.6) that together with a downfield quaternary carbon at δ_{C} 54.2 suggested the presence of an extra hydroxyl group at C-10 and the nor-abietane structure. Moreover, the absence of a hydroxyl group at C-14 was indicated by the signal at δ_{H} 7.23 instead of δ_{H} 13.47, and the downfield shift of C-14 (δ_{C} 115.9).

These structural features were confirmed by 2D NMR data analysis (COSY, HMQC and HMBC (**Figure IV.2**)). In particular, the $^2\text{J}_{\text{C-H}}$ correlations observed between the quaternary carbon at δ_{C} 54.2 and H1- β (δ_{H} 2.85) and H-5 (δ_{H} 1.26) corroborated the presence of the hydroxyl group at C-10. The cross-peak between the carbonyl signal at δ_{C} 176.4 and H-5 was used to assign its position at C-6. Furthermore, the long-range correlation of C-14 (115.96) to H-15 (δ_{H} 3.16) confirmed the absence of a hydroxyl group at C-14.

Based on the above evidence, the structure of compound **1** was identified as (+)-(5*S*,10*R*)-10,11,12-trihydroxy-6,7-dioxo-20-nor-abieta-8,11,13-triene.

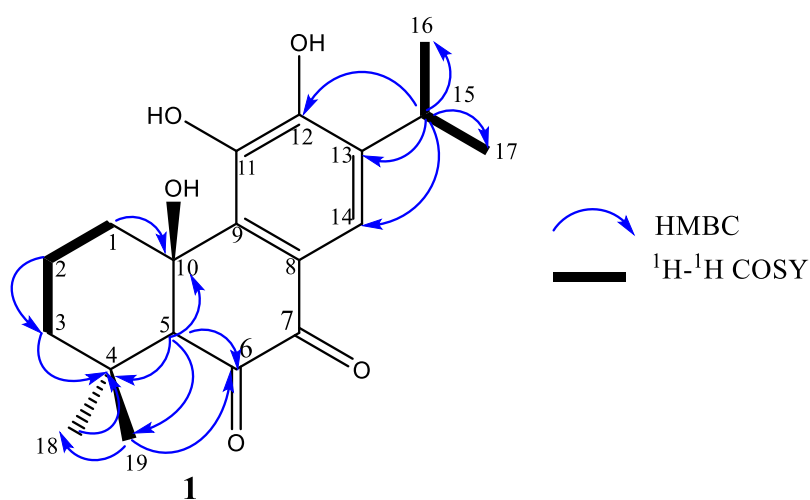


Figure IV.2. Key ^1H - ^1H COSY (bold lines) and HMBC (blue arrows) correlations of compound **1**

Table IV.1. NMR data of compound 1 (CD₃OD, 1H 500 MHz, 13C 126 MHz; δ in ppm, J in Hz)

| Position | δ_{H} | δ_{C} |
|------------|----------------------------------|---------------------|
| 1 α | 1.78 (m) | 35.8 |
| 1 β | 2.84 (m) | |
| 2 α | 1.56 (m, $J = 3.4$) | 18.7 |
| 2 β | 1.70 (m, $J = 14.0$, 3.4 Hz) | |
| 3 α | 2.89 (m) | 32.9 |
| 3 β | 1.64 (m) | |
| 4 | | 34.7 |
| 5 | 1.26 (s) | 42.4 |
| 6 | | 176.4 |
| 7 | | 178.9 |
| 8 | | 125.3 |
| 9 | | 153.2 |
| 10-OH | 7.76 (s) | 54.2 |
| 11-OH | 7.56 (s) | 170.6 |
| 12-OH | 8.05 (s) | 175.5 |
| 13 | | 118.8 |
| 14 | 7.23 (s) | 115.96 |
| 15 | 3.16 (sept, $J =$ 7.1) | 24.8 |
| 16 | 1.18 (d, $J = 6.9$) | 21.5 |
| 17 | 1.17 (d, $J = 6.9$) | 19.5 |
| 18 | 0.94 (d, $J = 4.9$) | 28.2 |

LC-MS/MS was used to study the fragmentation pattern of the isolated compounds and further analyse the presence of diterpenoids in the acetone extract. Compound **1** yielded its deprotonated ion at m/z 331 $[M-H]^-$. Its MS/MS spectra showed fragments at 303 due to the loss of -CO group $[M-H-CO]^-$ and m/z 313 resulting from the loss of water $[M-H-H_2O]^-$. Other product ions at m/z 298 $[M-H-H_2O-CH_3]^-$, 285 $[M-H-CO-H_2O]^-$ and 259 $[M-2H-CO-C_3H_7]^-$ were

also detected at low abundance. Compound **(2)** showed a protonated ion at m/z 345 $[M+H]^+$ that generated fragments m/z 111 and m/z 233 resulting from the fragmentation at the 11,13-positions of the C-ring [51]. Fragment m/z 303 corresponds to the loss of the propene unit $[M+H-43Da]^+$ and 327 from the loss of H_2O $[M+H-H_2O]^+$. The fragmentation of the parent ion of compound **3** (m/z 359 $[M-H]^-$) produced an ion at m/z 300 $[M-H-C_3H_7O]^-$ and a base peak at m/z 285 $[M-H-2CO-H_2O]^-$ [42]. The fragment ion at m/z 272 $[M-H-C_3H_7O-CO]^-$ was also observed. Compound **4** showed a deprotonated ion at m/z 345 $[M-H]^-$ and a base peak at m/z 330 due to the loss of a methyl group.

The UHPLC-MS/MS analysis revealed an additional compound in the extract. This compound exhibited a protonated ion at 389 $[M+H]^+$. Its MS/MS spectrum showed an abundant fragment ion at m/z 347 that was attributed to the loss of a propene unit $[M+H-C_3H_6]^+$, suggesting the presence of the characteristic isopropyl group of abietane diterpenoids. The presence of a small fragment ion at m/z 330 $[M+H-C_2H_3O_2]^+$ suggested the loss of an acetoxy group (59 Da) (Supplementary information). The above finding suggests that this compound could be an acetoxy derivative of an abietane diterpenoid. More work is ongoing for the proper identification of this compound.

HPLC–DAD Profiling of *P. mutabilis* acetonic extract

In the present study, *P. mutabilis* extract was found to contain four abietane diterpenoids. HPLC analysis revealed the presence of the following compounds mutabilol $tR = 9.20$ (**1**), Coleon U quinone $tR = 10.22$ (**2**), $8\alpha,9\alpha$ -Epoxycoleon U quinone, $tR = 9.43$ (**3**), Coleon U, $tR = 11.80$ (**4**). The HPLC quantification of the four isolated abietane diterpenoids is represented in **Table IV.2** below with compound **4** being the major compound in the extract. Coleon U quinone appears to be an oxidation product of coleon U, as it was only present in the crude extract in small quantities. These were in agreement with the results obtained by Diogo *et al*, from *P. madagascariensis* Benth. [13] and Wellsow *et al.*, 2006, where Coleon U quinone only appeared in significant amounts during the isolation process [47].

Table IV.2. Abietane Diterpenoids compositions of the extract from *P. mutabilis* by HPLC–DAD

| Compounds | Concentration μg/mg | LOD μg/mg | LOQ μg/mg |
|--|------------------------|--------------|--------------|
| Mutabilol (1) | 51±0.008 | 1.120 | 3.39 |
| Coleon U quinone (2) | 35±0.005 | 0.102 | 0.310 |
| 8α,9α-Epoxycoleon U quinone (3) | 36±0.018 | 0.828 | 2.510 |
| Coleon U (4) | 96±0.048 | 0.78 | 2.35 |

Results are expressed as average ± standard deviation (SD) of three determinations. LOD (limit of detection) and LOQ (limit of quantification). Compounds **2** and **3** were quantified at 270 nm and compounds **1** and **4** at 254 nm.

Biosynthetic relation between 2-4

The biosynthetic relationship between compounds **2-4** was considered employing a computational study. While Coleon U **4** is the undoubted precursor of **2** and **3**, the formation of epoxyquinone **3** can be formulated straight from Coleon U **4** or from its quinone **2**. To get insight into the formation of epoxyquinone **3**, the electron density-based local reactivity descriptors condensed Fukui indexes have been determined for the three compounds, together with the bond dissociations energies (BDEs) of the O-H bonds of Coleon U **4**. Herein, Fukui functions have the capability of identifying nucleophilic and electrophilic regions in molecules, as well as the propensity of certain regions to undergo a radical attack.

Figure IV.3 depicts the results of the electrophilic (f_k^-), nucleophilic (f_k^+), and radical (f_k^0) Fukui functions in the gas phase, where the positions with higher Fukui indexes have been indicated. In **Table IV.3** is presented the bond dissociation energies of the O-H bonds present in Coleon U **4**. The BDE of the O-H at the C11 position is significantly lower than any of the other O-H bonds, which indicates that under oxidative radical conditions the removal of this hydrogen radical will trigger the oxidative process of the hydroquinone to quinone **2**. The analysis of the Fukui reactivity descriptors of **2** and **4** point to the carbon atoms of the hydroquinone moiety as the most nucleophilic region of the molecule while the quinone portion becomes the most electrophilic region in **2**. This observation suggests that the installation of epoxide in **2** to form **3** would occur via the nucleophilic conjugate addition by an oxygen-carrier group (eg. hydroperoxide). On the other hand, the oxygen atom in the epoxide of **3** is more likely to have its origin in electrophilic molecular oxygen making Coleon U **4** a suitable biosynthetic precursor considering its nucleophilic character around the

hydroquinone core. With this in mind, the formation of anions **4**¹¹ and **4**¹⁴ was considered, and the electrophilic Fukui functions (f_k^-) of both anions were analyzed (**Figure IV.4**). The difference of 25 kcal/mol in the Gibbs free energy of formation of both anions indicates that the hydroxyl deprotonation at position 11 is preferable. The analysis of the electrophilic Fukui function (f_k^-) indicates position C9 as the second most nucleophilic atom (0.136 condensed index), only overpassed by the anionic oxygen. A similar analysis for the electrophilic Fukui function (f_k^-) for anion **4**¹⁴ indicates C11 as the most nucleophilic carbon, although having a close condensed index to C9 and C13 (0.138 vs 0.122-0.124).

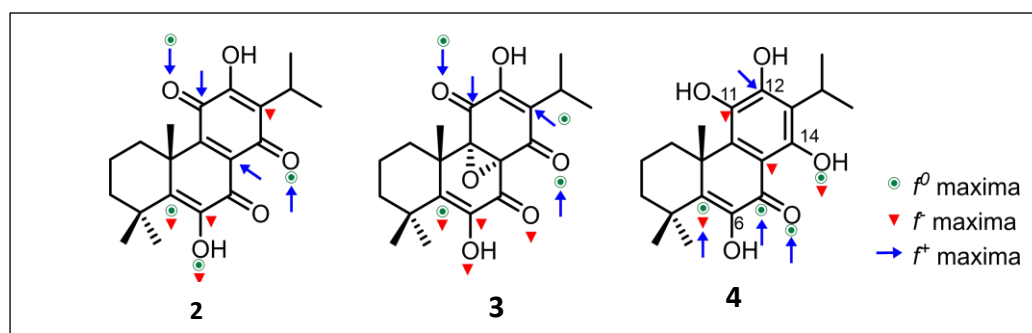


Figure IV.3. Electrophilic (f_k^-), nucleophilic (f_k^+) and radical (f_k^0) Fukui functions of 2-4. The higher condensed Fukui indexes are indicated as green circles, red triangles, and blue arrows, respectively representing the sites in the molecules that are most susceptible for a radical attack, most nucleophilic, and most electrophilic.

Table IV.3. Hydrogen Bond Dissociation Energies (BDEs; kcal/mol) of O-H bonds in **4**.

| Position of OH in 4 | O-H Bond Dissociation Energy (kcal/mol) |
|----------------------------|---|
| C6 | 103.8 |
| C11 | 84.1 |
| C12 | 103.0 |
| C14 | 116.5 |

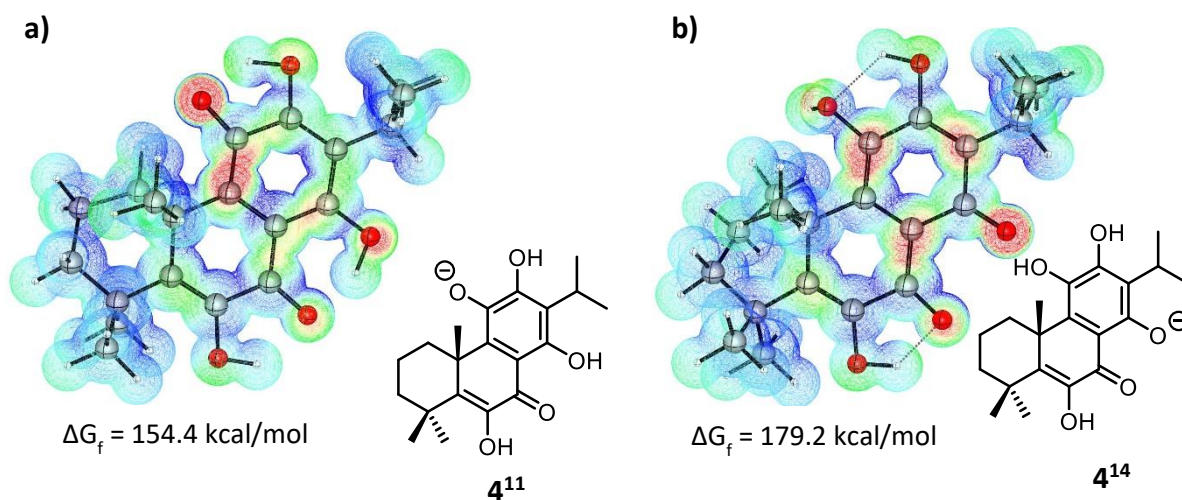
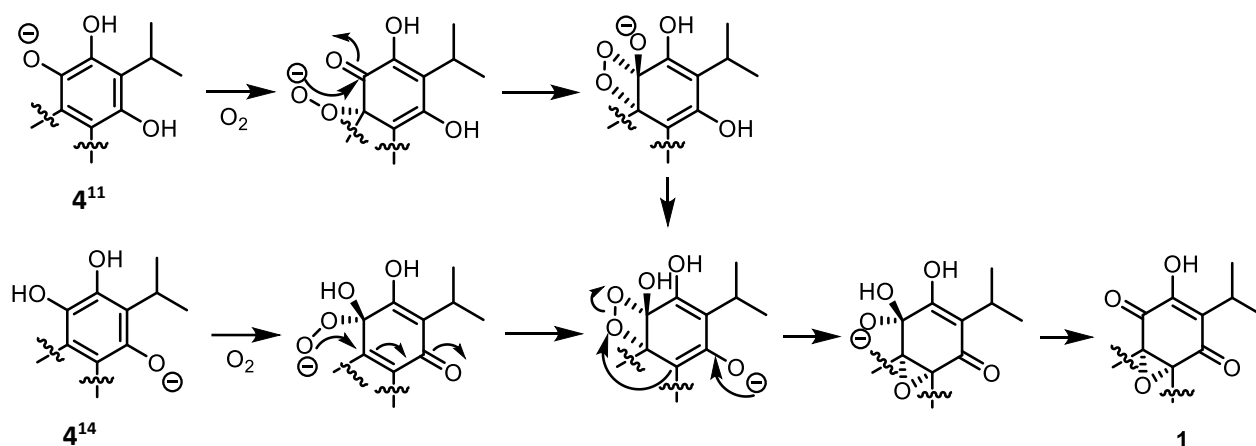


Figure IV.4. Electrophilic Fukui functions (f_k^-) and Gibbs energy for the formation of anions derived from deprotonation of Coleun U (4**) at hydroxyl positions on C11 a) and C14 b)**

With this in mind, two paths are suggested as plausible for the formation of epoxide **3** from **4** (**Scheme IV.1**). Upon hydroxyl deprotonation of **4** at the C11 position, the anion $\mathbf{4}^{11}$ reacts with molecular oxygen at C9 to form a hydroperoxide, which undergoes nucleophilic attack at C11 carbonyl to deliver a dioxetane. A proton exchange places the anion at the oxygen at C14 position, followed by dioxetane opening delivers the epoxide. Alternatively, the same dioxetane can be reached from anion $\mathbf{4}^{14}$ through the electrophilic attack at molecular oxygen by C11, as corroborated by the higher nucleophilic Fukui condensed index, followed by conjugate addition. While the formation of $\mathbf{4}^{11}$ is more favorable than the formation of $\mathbf{4}^{14}$, given its lower Gibbs free energy of formation, the oxygen electrophilic addition to C9 formulated in the first path should be hampered by stereochemical constraints. Furthermore, the formation of epoxyquinones [52,53] through electrophilic attack by phenol bearing carbons (such as in C11) has been reported in bacteria [54], fungi [55] and in mammals in the biosynthesis of vitamin K epoxide [56,57].



Scheme IV.1

Selectivity towards cancer cells

The viability of human cancer cells was compared with that of human normal cells upon treatment with the acetone extract and diterpenes **1-4**, isolated from *P. mutabilis*. The model system used in the study comprises human non-small cell lung carcinoma cells (NCI-H460), its MDR variant with P-gp expression (NCI-H460/R), and human embryonic pulmonary fibroblasts (MRC-5). Cell viability was assessed by the MTT assay. The largest reduction of cancer cell viability (metabolic activity) was observed with coleon U - compound **4** (IC₅₀ ≈ 14 μM) against the NCI-H460 and NCI-H460/R expressed with P-gp which also showed the highest selectivity index at 2.5 (**Table IV.4**). Compounds **2** and **3** (coleon U quinone and 8α,9α-epoxycoleon U quinone, respectively) showed similar inhibition of cancer cell viability (IC₅₀ ≈ 20 μM) and a similar selectivity index of 2.0 (**Table IV.4**). New identified compound **1** - mutabilol was inactive against all three cell lines displaying IC₅₀ over the highest concentration for compounds used in the study (**Table IV.4**). The acetone extract showed similar activity against cancer and normal cells with a selectivity index of 1.0 (**Table IV.4**). Previous results on coleon U activity against NCI-H460 cells assessed by sulforhodamine B (SRB) test showed significantly lower IC₅₀ value ≈ 3 μM [13,58]. Due to different detection methods of SRB (labeling cellular proteins,[59] and MTT (labeling vital mitochondria, (Cory et al., 1991), we can assume that the anticancer effect of coleon U is rather cytostatic or antiproliferative than cytotoxic. This could be also true for coleon U quinone, and 8α,9α-epoxycoleon U quinone. Further investigations should be directed to elucidate the mechanism of abietane diterpenoids against cancer cell growth.

Coleon U quinone was tested by another research group, in normal human keratinocytes (HaCaT) using the MTT assay [45]. The IC₅₀ value obtained was two-fold higher ($\approx 98 \mu\text{M}$) than that obtained in MRC-5 cells (**Table IV.4**) suggesting even a greater selectivity of coleon U quinone (compound **2**) towards cancer cells.

Importantly, the presence of MDR phenotype (P-gp overexpression) in NCI-H460/R did not affect the inhibitory effect of **2**, **3**, **4**, and the extract, implying that they are not substrates for P-gp. Similar results were obtained with another representative of abietane diterpenoids – namely, 6,7-dehydroroyleanone, 7 α -acetoxy-6 β -hydroxyroyleanone 6 β ,7 α -dihydroxyroyleanone, 7 α -formyloxy-6 β -hydroxyroyleanone and coleon U, which showed selectivity for non-small lung carcinoma cells and their multidrug-resistant variant [13]. These royleanones equally significantly inhibited sensitive and P-gp overexpressing cancer in NCI-H460/R cell lines [12,16].

Table IV.4. Inhibition of cell viability assayed by MTT in non-small cell lung cancer cells (NCI-H460 and NCI-H460/R) and embryonic pulmonary fibroblasts (MRC-5).

| Compounds | NCI-H460 | NCI-H460/R | MRC-5 | Selectivity index ^a |
|------------|-------------------------------|-------------------|-------------------|--------------------------------|
| 1 | > 50 | > 50 | > 50 | n.a. |
| 2 | 22.96 \pm 0.56 ^b | 20.37 \pm 0.43 | 44.13 \pm 1.19 | 2.0 |
| 3 | 20.23 \pm 0.59 | 17.26 \pm 0.26 | 40.22 \pm 0.44 | 2.0 |
| 4 | 14.11 \pm 0.19 | 14.50 \pm 0.18 | 35.47 \pm 0.56 | 2.5 |
| extract | 15.30 \pm 0.37 ^c | 15.66 \pm 0.47 | 16.68 \pm 0.69 | 1.0 |
| Paclitaxel | 0.0006 \pm 0.0001 | 0.117 \pm 0.013 | 0.523 \pm 0.001 | 872 |

^aSelectivity index was calculated as a relation between IC₅₀ for MRC-5 cells and IC₅₀ for NCI-H460 or NCI-H460/R cells

^bIC₅₀ values in μM for compounds,

^cIC₅₀ values in $\mu\text{g}/\text{mL}$ for extract

Interaction with P-gp activity

We further investigated the influence of compounds and extract on P-gp activity using Rho123 accumulation assay in MDR NCI-H460/R cells. Rho123 is a P-gp substrate suitable for studying by flow cytometry. Increased accumulation of Rho123 implies P-gp inhibition, while its decreased accumulation implies P-gp stimulation. Compounds (**1**, **2**, **3**, and **4**) were applied in concentrations of 5 or 10 μ M, while the extract was applied in concentrations of 5 or 10 μ g/mL. Compounds and extract were simultaneously combined with 2.5 μ M of Rho123 for short exposure of only 30 min. Tariquidar (TQ), a known third-generation inhibitor of P-gp, efficient in the nanomolar range, was used as a positive control for Rho123 accumulation as well as untreated sensitive NCI-H460 cells (**Table IV.5**). Fluorescent activity ratio (FAR) and sensitivity index (SI) clearly showed that TQ increases the accumulation of Rho123 and thus inhibits P-gp activity. All tested compounds, as well as extract, showed the opposite effect on P-gp activity by decreasing the Rho123 accumulation in NCI-H460/R cells. This finding implies that compounds and extract stimulate P-gp activity in a direct interaction assessed after 30 min.

Table IV.5. Rho123 accumulation assay, 30 min simultaneous treatment with tested compounds, shows direct interaction with P-gp and interference with its activity (inhibition or stimulation)

| Compounds/(Cell Lines) | | MFI ^a | FAR \pm S.E. ^b | SI \pm S.E. ^c |
|------------------------|---------------|------------------|------------------------------|--------------------------------|
| NCI-H460 ^d | | 2479.3 | 3.06 \pm 0.61 | |
| NCI-H460/R | | 811.1 | | 32.71 \pm 1.65 |
| TQ | 50 nM | 3004.0 | 3.70 \pm 0.54 ^e | 121.16 \pm 0.88 ^e |
| Extract | 5 μ g/mL | 339.5 | 0.42 \pm 0.20 ^f | 13.69 \pm 3.24 ^f |
| | 10 μ g/mL | 307.7 | 0.38 \pm 0.20 | 12.41 \pm 3.15 |
| 1 | 5 μ M | 265.9 | 0.33 \pm 0.21 | 10.72 \pm 3.55 |
| | 10 μ M | 254.5 | 0.31 \pm 0.22 | 10.26 \pm 3.63 |
| 2 | 5 μ M | 277.3 | 0.34 \pm 0.20 | 11.18 \pm 3.29 |
| | 10 μ M | 242.0 | 0.30 \pm 0.20 | 9.76 \pm 3.44 |
| 3 | 5 μ M | 289.7 | 0.36 \pm 0.20 | 11.68 \pm 3.29 |
| | 10 μ M | 276.6 | 0.34 \pm 0.21 | 11.16 \pm 3.41 |
| 4 | 5 μ M | 173.5 | 0.21 \pm 0.24 | 7.00 \pm 3.99 |
| | 10 μ M | 109.7 | 0.14 \pm 0.29 | 4.43 \pm 4.71 |

^a The measured mean fluorescence intensity (MFI) was used for the calculation of the fluorescence activity ratio (FAR).

^b via the following equation: $FAR = MFI_{MDRtreated}/MFI_{MDRcontrol}$.

^c The sensitivity index (SI) was calculated based on the measured mean fluorescence intensity (MFI) expressed via the following equation: $SI = (MFI_{MDRtreated} \times 100)/MFI_{sensitive\ control}$.

^d Sensitive cancer cell lines and their MDR counterparts used in the study: non-small cell lung carcinoma-NSCLC (NCI-H460 and NCI-H460/R).

^e TQ was applied as a positive control for P-gp inhibition (red labeled FAR and SI values).

^f Extract and 4 tested compounds exerted a stimulating effect on P-gp (blue labeled FAR and SI values).

To show whether this stimulation persists over a longer treatment period, we studied Rho123 accumulation after 72 h treatment with compounds and extract (**Table IV.6**). After 72 h treatment, all compounds, as well as extract, increased the Rho123 accumulation when lower concentration was applied (5 μ M or 5 μ g/mL, respectively) (**Table IV.5**). All compounds except **4** and extract increased Rho123 accumulation when 10 μ M was administered. Compound **2** showed a concentration-dependent effect according to FAR and SI values (**Table IV.6**). However, 10 μ M of **4** decreased the accumulation of Rho123 as well as 10 μ g/mL of extract. Considering that **4** is the most abundant compound in the extract (**Table IV.2**), this result was not surprising. Therefore, **4** exerted the strongest inhibition of P-gp with 5 μ M (FAR = 2.45) but also the strongest stimulation of P-gp with 10 μ M (FAR = 0.49) (**Table IV.6**).

According to the Rho123 accumulation profile, we assume that these compounds, also present in the extract, bind close or within the nucleotide-binding domain region (NBD) of P-gp inducing its stimulation and consequent high consumption of ATP necessary for the P-gp functioning. Therefore, compounds and extract can exhaust or even deplete ATP over a longer period of treatment. This we confirmed in the Rho123 accumulation study after 72 h treatment with compounds and extract. However, the strongest stimulation of P-gp achieved with 10 μ M of **4** (FAR = 0.14, **Table IV.5**) was reduced but persisted over time (FAR = 0.49, **Table IV.6**). As **4** is the most abundant and the most potent component of the extract, its Rho123 accumulation profile was similar to the one obtained with the extract (**Table IV.6**). Further studies should be undertaken to reveal the effect of abietane diterpenoids on the P-gp ATPase activity.

Table IV.6. Rho123 accumulation assay, 30 min load after 72 h treatment with tested compounds and extract, shows the indirect effect on P-gp activity (inhibition or stimulation)

| Compounds/(Cell Lines) | | MFI ^a | FAR±S.E. ^b | SI±S.E. ^c |
|------------------------|---------|------------------|------------------------|--------------------------|
| NCI-H460 ^d | | 2151.0 | 4.19±0.45 | |
| NCI-H460/R | | 513.7 | | 23.88±2.22 |
| TQ | 50nM | 3004.0 | 3.70±0.54 ^e | 121.16±0.88 ^e |
| Extract | 5µg/mL | 654.0 | 1.27±0.96 ^e | 30.40±2.14 |
| | 10µg/mL | 473.4 | 0.92±0.96 ^f | 22.01±2.14 |
| 1 | 5 µM | 595.3 | 1.16±0.98 | 27.68±2.18 |
| | 10 µM | 573.0 | 1.12±1.03 | 26.64±2.29 |
| 2 | 5 µM | 669.6 | 1.30±1.00 | 31.13±2.22 |
| | 10µM | 991.3 | 1.93±0.86 | 46.09±1.90 |
| 3 | 5 µM | 711.6 | 1.39±0.98 | 33.08±2.19 |
| | 10 µM | 666.1 | 1.30±1.02 | 30.97±2.26 |
| 4 | 5 µM | 1258.8 | 2.45±0.78 | 58.52±1.73 |
| | 10 µM | 253.0 | 0.49±1.25 | 11.76±2.78 |

^a The measured mean fluorescence intensity (MFI) was used for the calculation of the fluorescence activity ratio (FAR).

^b via the following equation: $FAR = MFI_{MDRtreated} / MFI_{MDRcontrol}$.

^c The sensitivity index (SI) was calculated based on the measured mean fluorescence intensity (MFI) expressed via the following equation: $SI = (MFI_{MDRtreated} \times 100) / MFI_{sensitive\ control}$.

^d Sensitive cancer cell lines and their MDR counterparts used in the study: non-small cell lung carcinoma-NSCLC (NCI-H460 and NCI-H460/R).

^e Red labeled FAR and SI values indicate P-gp inhibiting activity of tested compounds/concentrations.

^f Blue labeled FAR, and SI values indicate P-gp stimulating effect of tested compounds/concentrations.

Effects on P-gp expression

The effect on P-gp (ABCB1) expression was assessed by flow cytometry using FITC conjugated ABCB1 antibody after 72 h treatment of NCI-H460/R cells with compounds and extract. NCI-H460 cells with almost null expression of ABCB1 were used as a negative control, while treatment with TQ in NCI-H460/R cells was used as a positive control. Namely, TQ inhibition of P-gp activity strongly induces P-gp expression as a compensative mechanism. The results showed that none of the tested compounds had influence on ABCB1 expression in NCI-H460/R cells, while the extract significantly increased ABCB1 expression in a concentration-dependent manner (**Figure IV.5**). The increase in ABCB1 expression induced by 10 µg/mL of extract was like the one achieved by 50 nM of TQ (**Figure IV.5**). According to our

results, the extract can increase resistance by stimulating P-gp expression. Therefore, it would not be wise to use the extract in combination with chemotherapeutics which are P-gp substrates.

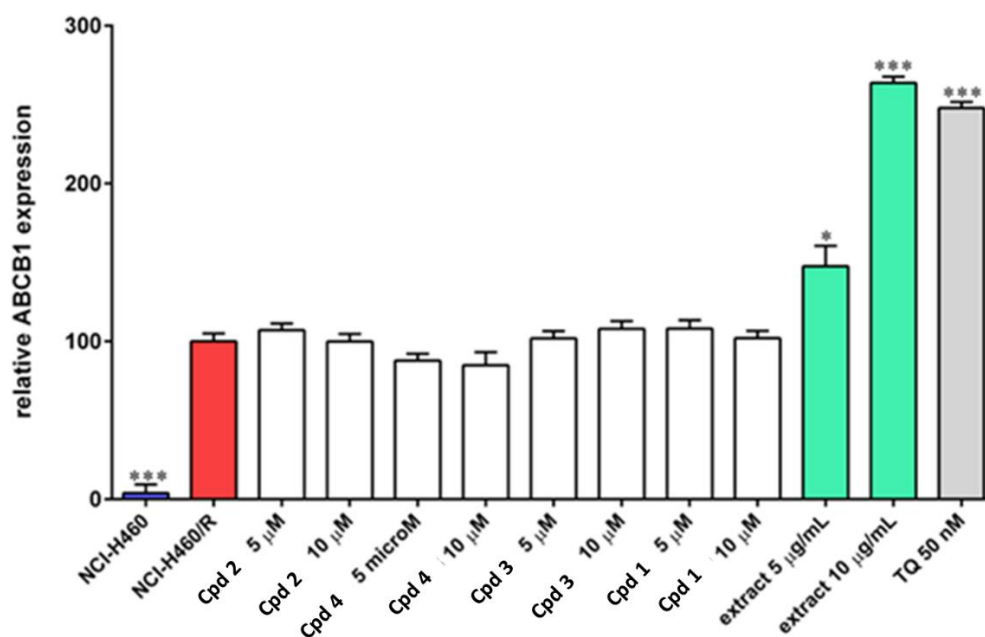


Figure IV.5. Effects of compounds and extract on the ABCB1 expression. Mean fluorescence of untreated NCI-H460/R cells was set to 100 and used for the comparison of other mean fluorescence (untreated NCI-H460 cells and treated NCI-H460/R cells) in GraphPad Prism 6 software (unpaired t-test). Mean fluorescence was calculated from three independent experiments. Significant difference to untreated NCI-H460/R cells was considered if $p < 0.05$ (*), $p < 0.001$ (***)

Our findings prompted us to investigate the sensitizing effect of **2**, **3**, and **4** in NCI-H460/R cells. These three compounds showed an anticancer effect in MTT assay (**Table IV.4**); a considerable increase of Rho123 accumulation after 72 h when applied in 5 μM (**Table IV.6**); and no influence on the ABCB1 expression in NCI-H460/R cells (**Figure IV.5**).

Reversal of DOX resistance

NCI-H460/R cells were developed by the continuous exposure of NCI-H460 cells to the step-wise increasing concentrations of DOX [41]. Therefore, we studied the sensitization of NCI-

H460/R cells to DOX which was combined with **2**, **3**, and **4**. DOX (0.1, 0.2, 0.5, 1 and 2 μ M) was administrated after 72 h pre-treatment with **2**, **3**, and **4** applied in three concentrations below their IC₅₀ (1, 2, and 5 μ M).

Table IV.7. Reversal of DOX resistance in NCI-H460/R cells pre-treated with 1, 2, and 3, assayed by MTT

| <i>Compounds</i> | <i>Concentration</i> | <i>IC₅₀ for DOX</i> | <i>Relative reversal index</i> |
|------------------|----------------------|--------------------------------|--------------------------------|
| <i>DOX</i> | | 1.620±0.084 | |
| 2 | 1 μ M | 0.565±0.012 | 2.867 ^{***} |
| | 2 μ M | 0.482±0.010 | 3.361 ^{***} |
| | 5 μ M | 0.217±0.004 | 7.465 ^{***} |
| 3 | 1 μ M | 0.820±0.016 | 1.976 ^{***} |
| | 2 μ M | 0.345±0.007 | 4.696 ^{***} |
| | 5 μ M | 0.343±0.006 | 4.723 ^{***} |
| 4 | 1 μ M | 0.625±0.013 | 2.592 ^{***} |
| | 2 μ M | 0.540±0.012 | 3.000 ^{***} |
| | 5 μ M | 0.268±0.006 | 6.045 ^{***} |

All subsequent combinations of all compounds with DOX showed significant reversal potential expressed as Relative reversal index (**Table IV.7**). Relative reversal index was calculated as the ratio between IC₅₀ value for DOX alone and IC₅₀ value for DOX in combination with a compound. The most potent sensitization of NCI-H460/R cells to DOX was achieved with 5 μ M of **2** and **4** with relative reversal index 7.465 and 6.045, respectively (Annex 6, Supplementary information. Fig. SI-5). A recent study from our group showed the abietane diterpenoid 7 α -acetoxy-6 β -benzoyloxy-12-O-(4-chloro) benzoylroyleanone enhanced the sensitivity of cancer cells to DOX. Importantly, IC₅₀ concentrations (0.5 and 1 μ M) can reverse DOX resistance towards cancer cells and thus may be useful in combination with classic chemotherapeutics [16].

Conclusion:

Plectranthus mutabilis Codd. leaves are a valuable source of abietane diterpenoids and a C₂₀-nor-abietane with coleon U as a major constituent in the acetone extract. A biosynthetic relation between **2**, **3** and **4** based on computational data indicates that both the quinone **2** and the epoxyquinone **3** are formed directly from Coleon U. Compounds isolated from *Plectranthus mutabilis* Codd. are not P-gp substrates because the presence of MDR phenotype did not affect their antimetabolic activity studied by MTT. Besides, these compounds do not change the expression of P-gp after 72 h treatment. Although these diterpenoids stimulated P-gp activity in a direct interaction after 30 min application, longer exposure led to the decreased activity of P-gp. This unique mechanism needs to be clarified in further research by assessing the effects on P-gp ATPase activity and ATP levels in MDR cancer cells. Finally, our results showed the potential of **2**, **3**, and **4** to reverse DOX resistance and increase its efficacy towards cancer cells. Therefore, we identified diterpenoids from *Plectranthus mutabilis* Codd. which could be considered as MDR modulators in cancer. New derivatives and their structure-activity studies are important to reinforce abietanes as a new family of P-gp modulators.

Patents

Not Applicables

Conflict of interest

The authors declare no conflict of interest nor competing for financial interest.

Supplementary Materials: The following are available online at www.mdpi.com/xxx/s1, Figure S.IV.1: Key ¹H–¹H COSY (bold lines), HMBC (blue arrows) and NOESY (red arrows) correlations of **2**, **3** and **4**. **S.IV.2:** ¹H NMR Data (δ) for Compounds 2-4, Table S.IV.1. ¹³C-NMR data of compounds 2-4 δ, (1, 3, 4-126 MHz, 2- 75 MHz), Figure S.IV.2: Screening of the *P. mutabilis* column fractions for general toxicity at a concentration of 10 ppm using the *Artemia salina* test, Figure **S.IV.3**. Calibration curves for the HPLC quantification of diterpenoids from the acetonic extract of *P. Mutabilis*, Figure SI-4: ¹H NMR– compound 1, Figure **S.IV.5:** COSY – Compound 1, Figure **S.IV.6:** HMBC– compound 1, Figure **S.IV.7:** HSQC– compound 1, Figure **S.IV.8:** ¹³C–NMR compound 1, Figure **S.IV.9:** ESI- Comparison of chromatographic profiles of isolated compounds with *P. mutabilis* leaves extract, Figure **S.IV.10:** MS/MS

spectrum Mutabilol, 1 (ESI-), Figure **S.IV.11**: MS/MS spectrum of Coleon U quinone, 2 (ESI+), Figure **S.IV.12**: MS/MS spectrum of $8\alpha,9\alpha$ -epoxycoleon U quinone, 3 (ESI-), Figure **S.IV.13**: MS/MS spectrum of Coleon U, 4 (ESI-), Figure **S.IV.14**: MS/MS spectrum of acetoxy derivative of an abietane diterpenoid, 5 (ESI+), Figure **S.IV.14**. Reversal of DOX resistance in NCI-H460/R cells in subsequent treatment with compounds 2, 3, and 4, Figure **S.IV.15**: Single treatment with compounds 2, 3, and 4 in NCI-H460/R cells assessed by MTT after 144 h (control treatments of combined effect with DOX), Table **S.IV.2** Atomic coordinates for all the optimized species (PBE1PBE/6-31G**).

References

1. Ma, Y.; Yin, D.; Ye, J.; Wei, X.; Pei, Y.; Li, X.; Si, G.; Chen, X.Y.; Chen, Z.S.; Dong, Y.; et al. Discovery of Potent Inhibitors against P-Glycoprotein-Mediated Multidrug Resistance Aided by Late-Stage Functionalization of a 2-(4-(Pyridin-2-yl)phenoxy)pyridine Analogue. *J. Med. Chem.* **2020**, *63*, 5458–5476, doi:10.1021/acs.jmedchem.0c00337.
2. Efferth, T.; Kadioglu, O.; Saeed, M.E.M.; Seo, E.J.; Mbaveng, A.T.; Kuete, V. *Medicinal plants and phytochemicals against multidrug-resistant tumor cells expressing ABCB1, ABCG2, or ABCB5: a synopsis of 2 decades*; Springer Netherlands, 2020; Vol. 7; ISBN 0123456789.
3. Abdelfatah, S.; Böckers, M.; Asensio, M.; Kadioglu, O.; Klinger, A.; Fleischer, E.; Efferth, T. Isopetasin and S-isopetasin as novel P-glycoprotein inhibitors against multidrug-resistant cancer cells. *Phytomedicine* **2020**, 153196, doi:10.1016/j.phymed.2020.153196.
4. Szakács, G.; Hall, M.D.; Gottesman, M.M.; Boumendjel, A.; Kachadourian, R.; Day, B.J.; Baubichon-Cortay, H.; Di Pietro, A. Targeting the achilles heel of multidrug-resistant cancer by exploiting the fitness cost of resistance. *Chem. Rev.* **2014**, *114*, 5753–5774, doi:10.1021/cr4006236.
5. Stefan, S.M. Multi-target ABC transporter modulators: What next and where to go? *Future Med. Chem.* **2019**, *11*, 2353–2358, doi:10.4155/fmc-2019-0185.
6. Michael W and SM Stefan The A-B-C of small-molecule ABC transport protein modulators: From inhibition to activation—a case study of multidrug resistance-associated protein 1 (ABCC1) 2019, 1–51.
7. Gonçalves, B.M.F.; Cardoso, D.S.P.; Ferreira, M.J.U. Overcoming multidrug resistance: Flavonoid and terpenoid nitrogen-containing derivatives as ABC transporter modulators. *Molecules* **2020**, *25*, doi:10.3390/molecules25153364.
8. Kryczka, J.; Boncela, J. Cell migration related to MDR-another impediment to effective chemotherapy? *Molecules* **2018**, *23*, doi:10.3390/molecules23020331.
9. Wang, S.; Wang, S.Q.; Teng, Q.X.; Yang, L.; Lei, Z.N.; Yuan, X.H.; Huo, J.F.; Chen, X.B.; Wang, M.; Yu, B.; et al. Structure-Based Design, Synthesis, and Biological Evaluation of New Triazolo[1,5- a]Pyrimidine Derivatives as Highly Potent and Orally Active ABCB1 Modulators. *J. Med. Chem.* **2020**, *63*, 15979–15996, doi:10.1021/acs.jmedchem.0c01741.

10. Xiao, Z.; Morris-natschke, S.L.; Lee, K.; Evaluation, D.; Medica, M.; Medica, M.; Carolina, N.; Hill, C. Strategies for the Optimization of Natural Leads to Anticancer Drugs or Drug Candidates. *HHS Public Access* **2017**, *36*, 32–91, doi:10.1002/med.21377.Strategies.
11. Sitarek, P.; Toma, M.; Ntungwe, E.; Kowalczyk, T.; Skała, E.; Wieczfinska, J.; Śliwiński, T.; Rijo, P. Insight the biological activities of selected abietane diterpenes isolated from *Plectranthus* spp. *Biomolecules* **2020**, *10*, 1–13, doi:10.3390/biom10020194.
12. Garcia, C.; Silva, C.O.; Monteiro, C.M.; Nicolai, M.; Viana, A.; Andrade, J.M.; Barasoain, I.; Stankovic, T.; Quintana, J.; Hernández, I.; et al. Anticancer properties of the abietane diterpene 6,7-dehydroroyleanone obtained by optimized extraction. *Future Med. Chem.* **2018**, *1*, 1177–1189, doi:10.4155/fmc-2017-0239.
13. Matias, D.; Nicolai, M.; Saraiva, L.; Pinheiro, R.; Faustino, C.; Diaz Lanza, A.; Pinto Reis, C.; Stankovic, T.; Dinic, J.; Pesic, M.; et al. Cytotoxic Activity of Royleanone Diterpenes from *Plectranthus madagascariensis* Benth. *ACS Omega* **2019**, *4*, 8094–8103, doi:10.1021/acsomega.9b00512.
14. Śliwiński, T.; Sitarek, P.; Skała, E.; Isca, V.M.S.; Synowiec, E.; Kowalczyk, T.; Bijak, M.; Rijo, P. Diterpenoids from *Plectranthus* spp. As potential chemotherapeutic agents via apoptosis. *Pharmaceuticals* **2020**, *13*, 1–16, doi:10.3390/ph13060123.
15. Cretton, S.; Saraux, N.; Monteillier, A.; Righi, D.; Marcourt, L.; Genta-Jouve, G.; Wolfender, J.L.; Cuendet, M.; Christen, P. Anti-inflammatory and antiproliferative diterpenoids from *Plectranthus scutellarioides*. *Phytochemistry* **2018**, *154*, 39–46, doi:10.1016/j.phytochem.2018.06.012.
16. Garcia, C.; Isca, V.M.S.; Pereira, F.; Monteiro, C.M.; Ntungwe, E.; Sousa, F.; Dinic, J.; Holmstedt, S.; Roberto, A.; Díaz-Lanza, A.; et al. Royleanone Derivatives From *Plectranthus* spp. as a Novel Class of P-Glycoprotein Inhibitors . *Front. Pharmacol.* **2020**, *11*, 1711.
17. Isca, V.M.S.; Ferreira, R.J.; Garcia, C.; Monteiro, C.M.; Dinic, J.; Holmstedt, S.; André, V.; Pesic, M.; Dos Santos, D.J.V.A.; Candeias, N.R.; et al. Molecular Docking Studies of Royleanone Diterpenoids from *Plectranthus* spp. as P-Glycoprotein Inhibitors. *ACS Med. Chem. Lett.* **2020**, *11*, 839–845, doi:10.1021/acsmchemlett.9b00642.
18. Codd, L.E. *Plectranthus* (Labiatae) and allied genera in Southern Africa. *Bothalia* **1975**, *11*, 371–442, doi:10.4102/abc.v11i4.1482.

19. Grayer, R.J.; Eckert, M.R.; Veitch, N.C.; Kite, G.C.; Marin, P.D.; Kokubun, T.; Simmonds, M.S.J.; Paton, A.J. The chemotaxonomic significance of two bioactive caffeic acid esters, nepetoidins A and B, in the Lamiaceae. *Phytochemistry* **2003**, *64*, 519–528, doi:10.1016/S0031-9422(03)00192-4.
20. Ntungwe, E.; Mar, E.; Teod, C.; Teixid, S.; Capote, N.A.; Saraiva, L.; Mar, A. Preliminary Biological Activity Screening of *Plectranthus* spp. Extracts for the Search of Anticancer Lead Molecules. *Pharmaceuticals* **2021**, 1–11.
21. The Plant List. Version 1.1. 2013. Available online: <http://www.theplantlist.org/> (accessed on 1 January 2021).
22. Ntungwe N, E.; Domínguez-Martín, E.M.; Roberto, A.; Tavares, J.; Isca, V.M.S.; Pereira, P.; Cebola, M.-J.; Rijo, P. Artemia species: An Important Tool to Screen General Toxicity Samples. *Curr. Pharm. Des.* **2020**, *26*, 2892–2908, doi:10.2174/1381612826666200406083035.
23. Miyase, T.; Riiedi, P.; Conrad Hans, E. Leaf-gland Pigments: Coleons U, V, W, 14-O-Formyl-coleon-V, and two Royleanones from *Plectranthus myrianthus* BRIQ.; cis- and trans-A/B-6,7-Dioxoroyleanon. *Helv. Chim. Acta* **1977**, *13*, 4–6.
24. Yang, P.R. and W. Density Functional Theory of Atoms and Molecules. Oxford University Press: New York. *Density Funct. Theory Atoms Mol.* **1989**, *47*, 10101.
25. Ditchfield, R.; Hehre, W.J.; Pople, J.A. Self-consistent molecular-orbital methods. IX. An extended gaussian-type basis for molecular-orbital studies of organic molecules. *J. Chem. Phys.* **1971**, *54*, 720–723, doi:10.1063/1.1674902.
26. Hariharan, P.C.; Pople, J.A. Accuracy of AHn equilibrium geometries by single determinant molecular orbital theory. *Mol. Phys.* **1974**, *27*, 209–214, doi:10.1080/00268977400100171.
27. Gordon, M.S. The isomers of silacyclopropane. *Chem. Phys. Lett.* **1980**, *76*, 163–168, doi:10.1016/0009-2614(80)80628-2.
28. Hariharan, P.C.; Pople, J.A. The influence of polarization functions on molecular orbital hydrogenation energies. *Theor. Chim. Acta* **1973**, *28*, 213–222, doi:10.1007/BF00533485.
29. W. J. Hehre, L. Radom, P. v. R. Schleye, J.P. Ab Initio Molecular Orbital Theory. *J. Comput. Chem.* **1986**, *7*, 379–379, doi:10.1002/jcc.540070314.

30. Perdew, J.P. Density-functional approximation for the correlation energy of the inhomogeneous electron gas. *Phys. Rev. B* **1986**, *33*, 8822–8824, doi:10.1103/PhysRevB.33.8822.
31. Carpenter, J.E. Extension of Lewis structure concepts to open-shell and excited-state molecular species, Ph.D. thesis, University of Wisconsin, Madison. *WI* **1987**.
32. Carpenter, J.E.; Weinhold, F. Analysis of the geometry of the hydroxymethyl radical by the “different hybrids for different spins” natural bond orbital procedure. *J. Mol. Struct. THEOCHEM* **1988**, *169*, 41–62, doi:10.1016/0166-1280(88)80248-3.
33. Foster, J.P.; Weinhold, F. Natural Hybrid Orbitals. *J. Am. Chem. Soc.* **1980**, *102*, 7211–7218, doi:10.1021/ja00544a007.
34. Reed, A.E.; Weinhold, F. Natural bond orbital analysis of near-Hartree-Fock water dimer. *J. Chem. Phys.* **1983**, *78*, 4066–4073, doi:10.1063/1.445134.
35. Reed, A.E.; Weinhold, F. Natural localized molecular orbitals. *J. Chem. Phys.* **1985**, *83*, 1736–1740, doi:10.1063/1.449360.
36. Reed, A.E.; Weinstock, R.B.; Weinhold, F. Natural population analysis. *J. Chem. Phys.* **1985**, *83*, 735–746, doi:10.1063/1.449486.
37. Reed, A.E.; Curtiss, L.A.; Weinhold, F. Intermolecular Interactions from a Natural Bond Orbital, Donor—Acceptor Viewpoint. *Chem. Rev.* **1988**, *88*, 899–926, doi:10.1021/cr00088a005.
38. F. Weinhold, J.E.C. The Structure of Small Molecules and Ions. *Plenum* **1988**.
39. Lu, T.; Chen, F. Multiwfn: A multifunctional wavefunction analyzer. *J. Comput. Chem.* **2012**, *33*, 580–592, doi:10.1002/jcc.22885.
40. Parr, R.G.; Yang, W. Density Functional Approach to the Frontier-Electron Theory of Chemical Reactivity. *J. Am. Chem. Soc.* **1984**, *106*, 4049–4050, doi:10.1021/ja00326a036.
41. Pesic, M.; Markovic, J.Z.; Jankovic, D.; Kanazir, S.; Markovic, I.D.; Rakic, L.; Ruzdijic, S. Induced resistance in the human non small cell lung carcinoma (NCI-H460) cell line in vitro by anticancer drugs. *J. Chemother.* **2006**, *18*, 66–73, doi:10.1179/joc.2006.18.1.66.
42. Alfredo Carlos Alder, P.R. and C.H.E. Polar Diterpenoids from Leaf-Glands of *Pfeetranthus argentatus* S.T. BLAKE. *Helv. CHIMICA ACTA* **1984**, *67*, 1–8.

43. Matloubi-Moghadam, F.; Rüedi, P.; Eugster, C.H. Drüsefarbstoffe aus Labiaten: Identifizierung von 17 Abietanoiden aus *Plectranthus sanguineus* BRITTEN. *Helv. Chim. Acta* **1987**, *70*, 975–983, doi:10.1002/hlca.19870700407.
44. Kubínová, R.; Pořízková, R.; Navrátilová, A.; Farsa, O.; Hanáková, Z.; Bačinská, A.; Čížek, A.; Valentová, M. Antimicrobial and enzyme inhibitory activities of the constituents of *Plectranthus madagascariensis* (Pers.) Benth. *J. Enzyme Inhib. Med. Chem.* **2014**, *29*, 749–752, doi:10.3109/14756366.2013.848204.
45. Ndjoubi, K.O.; Sharma, R.; Badmus, J.A.; Jacobs, A.; Jordaan, A.; Marnewick, J.; Warner, D.F.; Hussein, A.A. Antimycobacterial, Cytotoxic, and Antioxidant Activities of Abietane Diterpenoids Isolated from *Plectranthus madagascariensis*. *Plants* **2021**, *175*, doi:https://doi.org/10.3390/plants10010175.
46. Etsassala, N.G.E.R.; Ndjoubi, K.O.; Mbira, T.J.; Pearce, B.; Pearce, K.; Iwuoha, E.I.; Hussein, A.A.; Benjeddou, M. Glucose-Uptake Activity and Cytotoxicity of Diterpenes and Triterpenes Isolated from Lamiaceae Plant Species. *Molecules* **2020**, *25*, 1–10, doi:10.3390/molecules25184129.
47. Wellsow, J.; Grayer, R.J.; Veitch, N.C.; Kokubun, T.; Lelli, R.; Kite, G.C.; Simmonds, M.S.J. Insect-antifeedant and antibacterial activity of diterpenoids from species of *Plectranthus*. *Phytochemistry* **2006**, *67*, 1818–1825, doi:10.1016/j.phytochem.2006.02.018.
48. Abdissa, N.; Frese, M.; Sewald, N. Antimicrobial abietane-type diterpenoids from *Plectranthus punctatus*. *Molecules* **2017**, *22*, 1–11, doi:10.3390/molecules22111919.
49. Matias, D.; Nicolai, M.; Fernandes, A.S.; Saraiva, N.; Almeida, J.; Saraiva, L.; Faustino, C.; Díaz-Lanza, A.M.; Reis, C.P.; Rijo, P. Comparison study of different extracts of *Plectranthus madagascariensis*, *P. Neochilus* and the rare *P. porcatus* (Lamiaceae): Chemical characterization, antioxidant, antimicrobial and cytotoxic activities. *Biomolecules* **2019**, *9*, 1–13, doi:10.3390/biom9050179.
50. Rijo, P.; Gaspar-Marques, C.; Simões, M.F.; Jimeno, M.L.; Rodríguez, B. Further diterpenoids from *Plectranthus ornatus* and *P. grandidentatus*. *Biochem. Syst. Ecol.* **2007**, *35*, 215–221, doi:10.1016/j.bse.2006.10.011.

51. Vinodh, G.; Naveen, P.; Venkatesan, C.S.; Rajitha, G.; Shree, A.J. Pharmacological Evaluation of Abietane Diterpenoids from *Plectranthus bishopianus* as Potent Antibacterial, Antioxidant and Their Cytotoxic Agents. *Nat. Prod. J.* **2018**, *9*, 229–237, doi:10.2174/2210315508666181120105219.
52. Bugg, T.D.H. Dioxygenase enzymes: Catalytic mechanisms and chemical models. *Tetrahedron* **2003**, *59*, 7075–7101, doi:10.1016/S0040-4020(03)00944-X.
53. Thibodeaux, C.J.; Chang, W.C.; Liu, H.W. Enzymatic chemistry of cyclopropane, epoxide, and aziridine biosynthesis. *Chem. Rev.* **2012**, *112*, 1681–1709, doi:10.1021/cr200073d.
54. Shen, B.; Gould, S.J. Opposite Facial Specificity for two Hydroquinone Epoxidases: (3-si,4-re)-2,5-Dihydroxyacetanilide Epoxidase from *Streptomyces* LL-C10037 and (3-re,4-,si)-2,5-Dihydroxyacetanilide Epoxidase from *Streptomyces* MPP 3051. *Biochemistry* **1991**, *30*, 8936–8944, doi:10.1021/bi00101a004.
55. Priest, J.W.; Light, R.J. Patulin Biosynthesis: Epoxidation of Toluquinol and Gentsyl Alcohol by Particulate Preparations from *Penicillium patulum*. *Biochemistry* **1989**, *28*, 9192–9200, doi:10.1021/bi00449a035.
56. Hubbard, B.R.; Ulrich, M.M.W.; Jacobs, M.; Vermeer, C.; Walsh, C.; Furie, B.; Furie, B.C. Vitamin K-dependent carboxylase: Affinity purification from bovine liver by using a synthetic propeptide containing the γ -carboxylation recognition site. *Proc. Natl. Acad. Sci. U. S. A.* **1989**, *86*, 6893–6897, doi:10.1073/pnas.86.18.6893.
57. Seung Wook Ham and Paul Dowd On the Mechanism of Action of Vitamin K. A New Nonenzymic Model. *J. Am. Chem. Soc.* **1990**, 1660–1661, doi:10.1021/ja00160a073.
58. Marques, C.G.; Pedro, M.; Simões, M.F.A.; Nascimento, M.S.J.; Pinto, M.M.M.; Rodriguez, B. Effect of abietane diterpenes from *Plectranthus grandidentatus* on the growth of human cancer cell lines. *Planta Med.* **2002**, *68*, 839–840, doi:10.1055/s-2002-34407.
59. Skehan, P.; Storeng, R.; Scudiero, D.; Monks, A.; McMahon, J.; Vistica, D.; Warren, J.T.; Bokesch, H.; Kenney, S.; Boyd, M.R. New Colorimetric Cytotoxicity Assay for Anticancer-Drug Screening. *J. Natl. Cancer Inst.* **1990**, *82*, 1107–1112.

Supplementary information S.IV

Structure elucidation

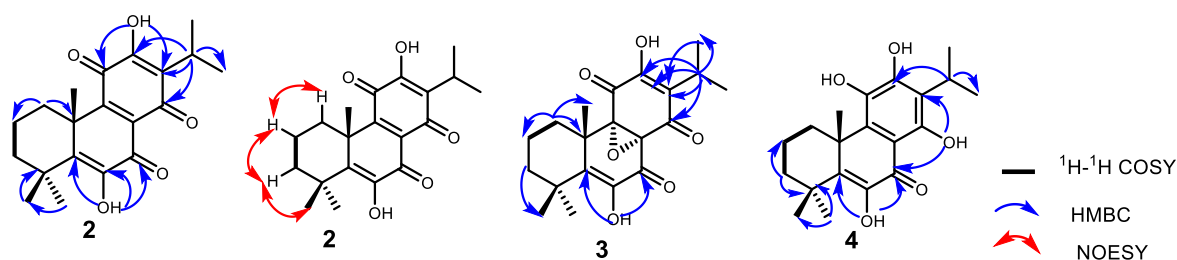


Figure S.IV.1: Key ^1H - ^1H COSY (bold lines), HMBC (blue arrows) and NOESY (red arrows) correlations of **2**, **3** and **4**.

S.IV.2: ^1H NMR Data (δ) for Compounds 2-4

Compound **2**: (Coleon U quinone). ^1H -NMR (500 MHz, CDCl_3): δ 7.09 (1H, s, 6-OH), 7.07 (s, 1H, 12-OH), 3.22 (1H, *sept*, $J = 7.1$ Hz, H-15), 2.65 (1H, s, H-1 β), 1.98 (1H, m, $J = 14.9$ Hz, H-3 α), 1.90 (1H, s, H-2 β), 1.62 (1H, m, $J = 16.7$ Hz, H-2 α), 1.60 (1H, s, H-1 α), 1.64 (s, 3H, H-20), 1.45 (1H, s, H-3 β), 1.43, 1.42 (6H, d, $J = 4.9$ Hz, H-19, H-18), 1.25, 1.24 (6H d, $J = 6.9$ Hz, H-16, H-17). For ^{13}C -NMR data, see Table S.IV.3.

Compound **3**: (8 α ,9 α -Epoxy)coleon U quinone). For ^{13}C -NMR data, see Table S.IV.3.

Compound **4**: (Coleon U). ^1H NMR (500 MHz, CDCl_3): δ 12.92 (s, 1H, 14-OH), 6.98 (s, 1H, 6-OH), 6.05 (s, 1H, 11-OH), 3.21 (Sept, 1H, $J = 7.1$, H-15), 2.88 (dt, $J = 13.5, 8.9$, 1H, H-3 α), 1.87 (1H, s, H-2 β), 1.86 (s, 1H, H-3 β), 1.65 (s, 1H, H-1), 1.66 (s, 1H, H-2 α), 1.67 (s, H-20, 3H), 1.47 (s, 3H, H-18), 1.43 (s, 3H, H-19), 1.38 (d, $J = 7.2$, 3H, H-17), 1.40 (d, $J = 7.2$, 3H, H-16). For ^{13}C -NMR data, see Table S.IV.3.

Coleon V: ^1H NMR (0 to 50 ppm, Acetone- d_6): δ 13.47 (s, 1H, 14-OH), 3.51 (Sept, 1H, $J = 7.0$, H-15), 3.12 (s, 1H, H-5), 3.50 (H-1 α), 1.33 (s, 1H, H-1 β), 1.40 (s, H-20, 3H), 1.40 (s, 3H, H-18), 1.04 (s, 3H, H-19), 1.37 (d, $J = 7.0$, 3H, H-17). For ^{13}C -NMR data, see Table S.IV.3 [23].

Table S.IV.3. ¹³C-NMR data of compounds 2-4 δ, (1, 3, 4-126 MHz, 2- 75 MHz)

| | 2 | 3 | 4 | Coleon V |
|------|--------|--------|--------|----------|
| C-1 | 30.93 | 31.18 | 28.88 | 37.7 |
| C-2 | 17.84 | 17.19 | 18.35 | 18.7 |
| C-3 | 36.49 | 37.27 | 31.73 | 41.6 |
| C-4 | 36.45 | 36.09 | 36.55 | 32.8 |
| C-5 | 143.50 | 140.03 | 142.05 | 65.1 |
| C-6 | 146.93 | 140.91 | 142.98 | 200.8 |
| C-7 | 177.68 | 183.08 | 182.90 | 184.1 |
| C-8 | 126.97 | 57.26 | 105.54 | 109.5 |
| C-9 | 155.20 | 67.64 | 137.21 | 138.1 |
| C-10 | 41.57 | 39.25 | 41.13 | 44.7 |
| C-11 | 183.70 | 186.67 | 133.18 | 133.9 |
| C-12 | 150.82 | 150.82 | 150.31 | 157.4 |
| C-13 | 126.16 | 128.50 | 118.39 | 119.3 |
| C-14 | 184.48 | 186.32 | 156.74 | 163.6 |
| C-15 | 24.52 | 25.54 | 24.58 | 24.5 |
| C-16 | 19.91 | 19.34 | 20.94 | 19.9 |
| C-17 | 19.90 | 19.73 | 20.86 | - |
| C-18 | 27.64 | 28.37 | 27.18 | 21.7 |
| C-19 | 27.28 | 27.19 | 30.94 | 32.4 |
| C-20 | 29.20 | 27 | 28.06 | 23.6 |

Phytochemistry study of chromatographic column fractions

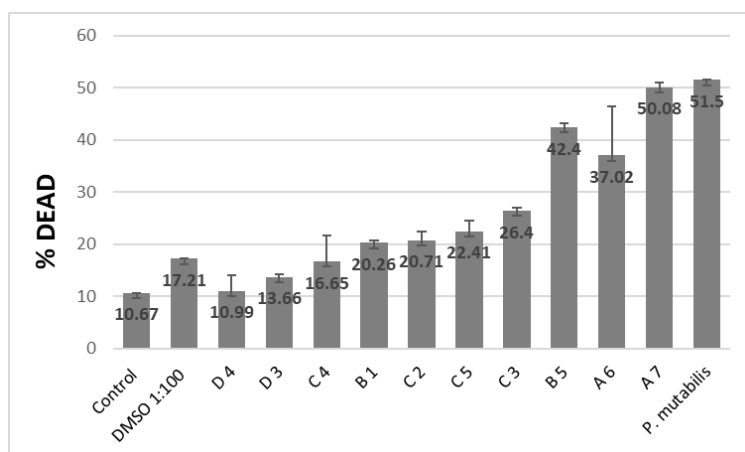


Figure S.IV.2: Screening of the *P. mutabilis* column fractions for general toxicity at a concentration of 10 ppm using the *Artemia salina* test

Formula

$$\text{Lethal concentration} = \frac{\text{Total } A. \text{ salina} - \text{Alive } A. \text{ salina}}{\text{Total } A. \text{ salina}} \quad \text{Equation (1)}$$

HPLC quantification

The chromatographic runs resulted in calibration curves for the following standards: Coleon U quinone $Y = 39655X + 1332.4$ ($R^2 = 0.9986$), $8\alpha,9\alpha$ -Epoxy-coleon U quinone $Y = 18522X - 401.77$ ($R^2 = 0.9413$), Coleon U $Y = 15528X + 583.53$ ($R^2 = 0.9995$), 7-hydro, mutabilol U $Y = 3122.5X - 84.157$ ($R^2 = 0.9865$).

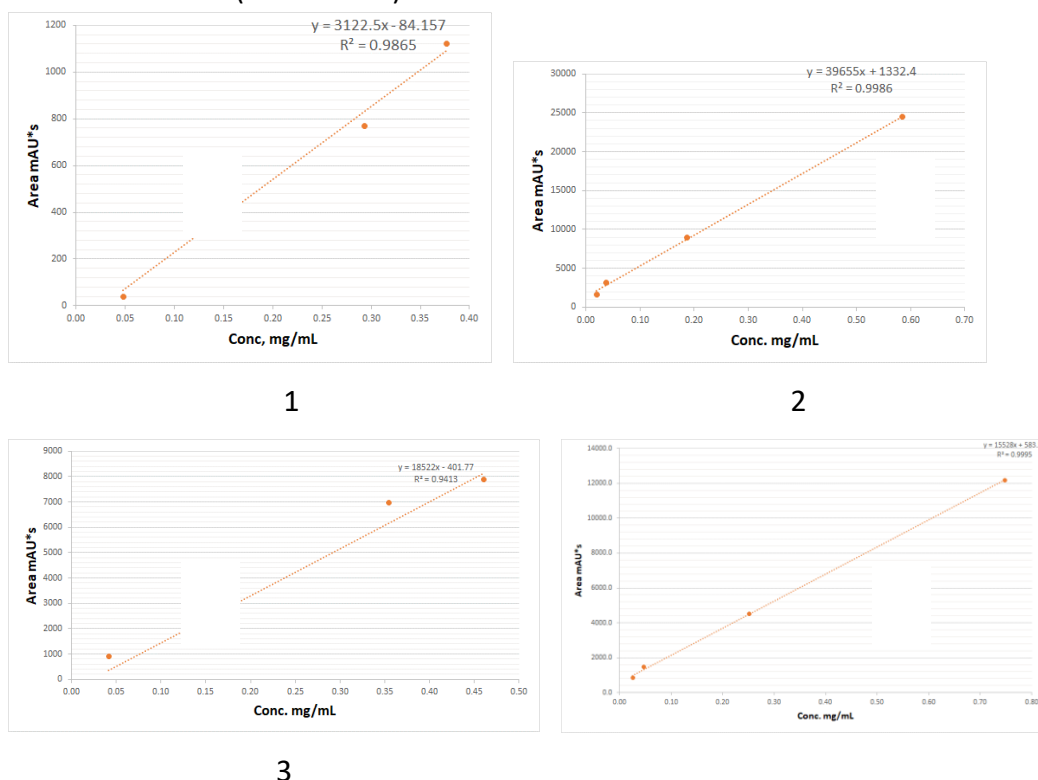


Figure S.IV.3. Calibration curves for the HPLC quantification of diterpenoids from the acetonic extract of *P. mutabilis*. UV detection at 270 nm. Mutabilol (1), Coleon U quinone (2), $8\alpha,9\alpha$ -Epoxycoleon U quinone, (3), Coleon U (4)

Figure S.IV.4: 1D and 2D- NMR data

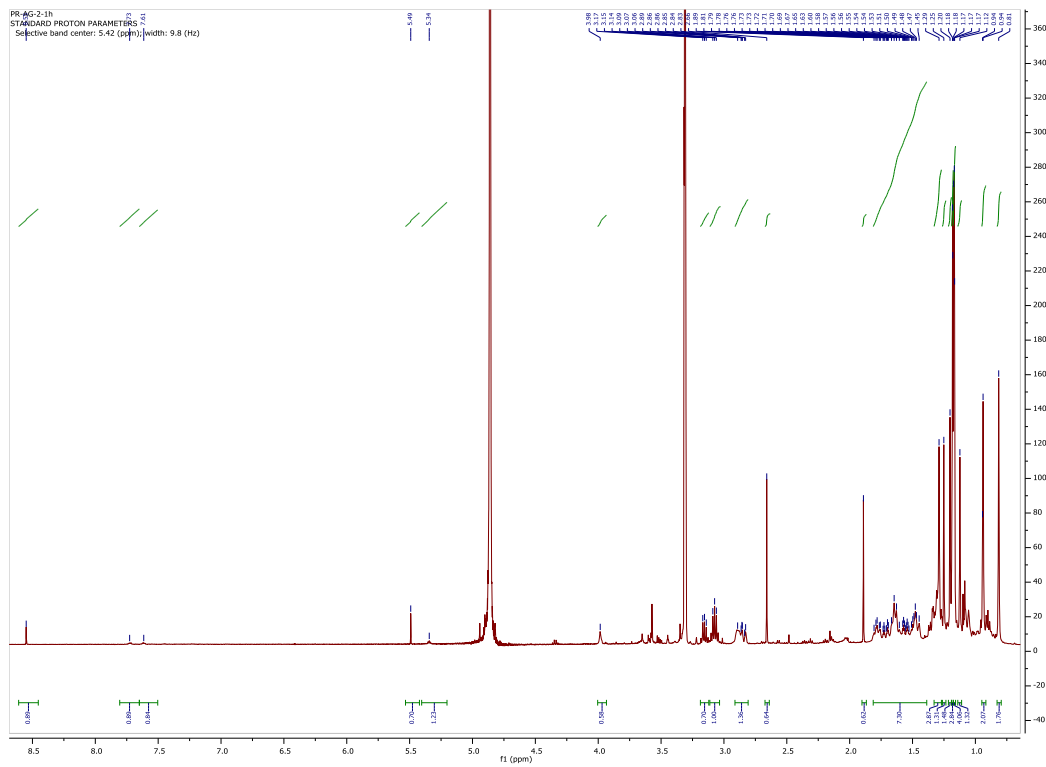
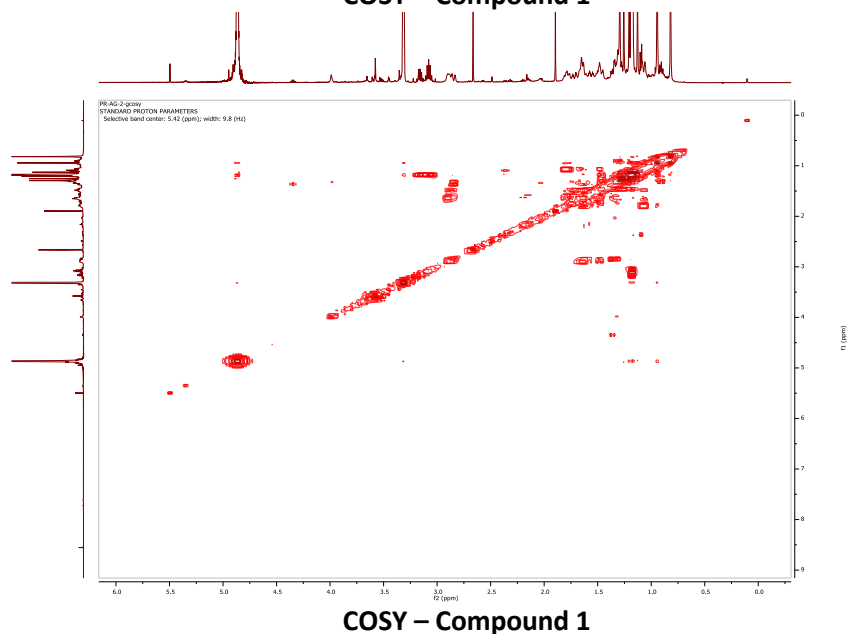


Figure S.IV.4: ¹H NMR– compound 1

COSY – Compound 1



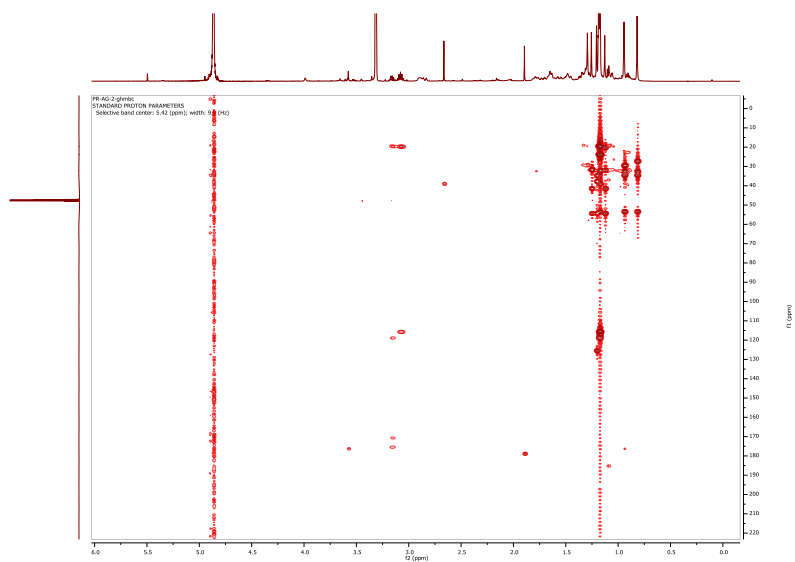


Figure S.IV.5: HMBC– compound 1

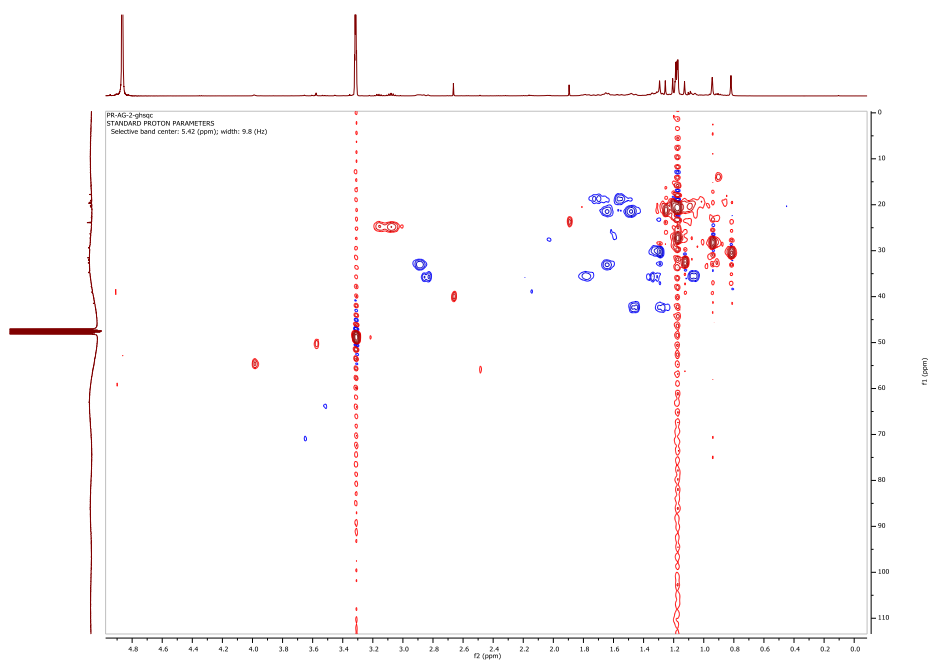


Figure S.IV.6: HSQC– compound 1

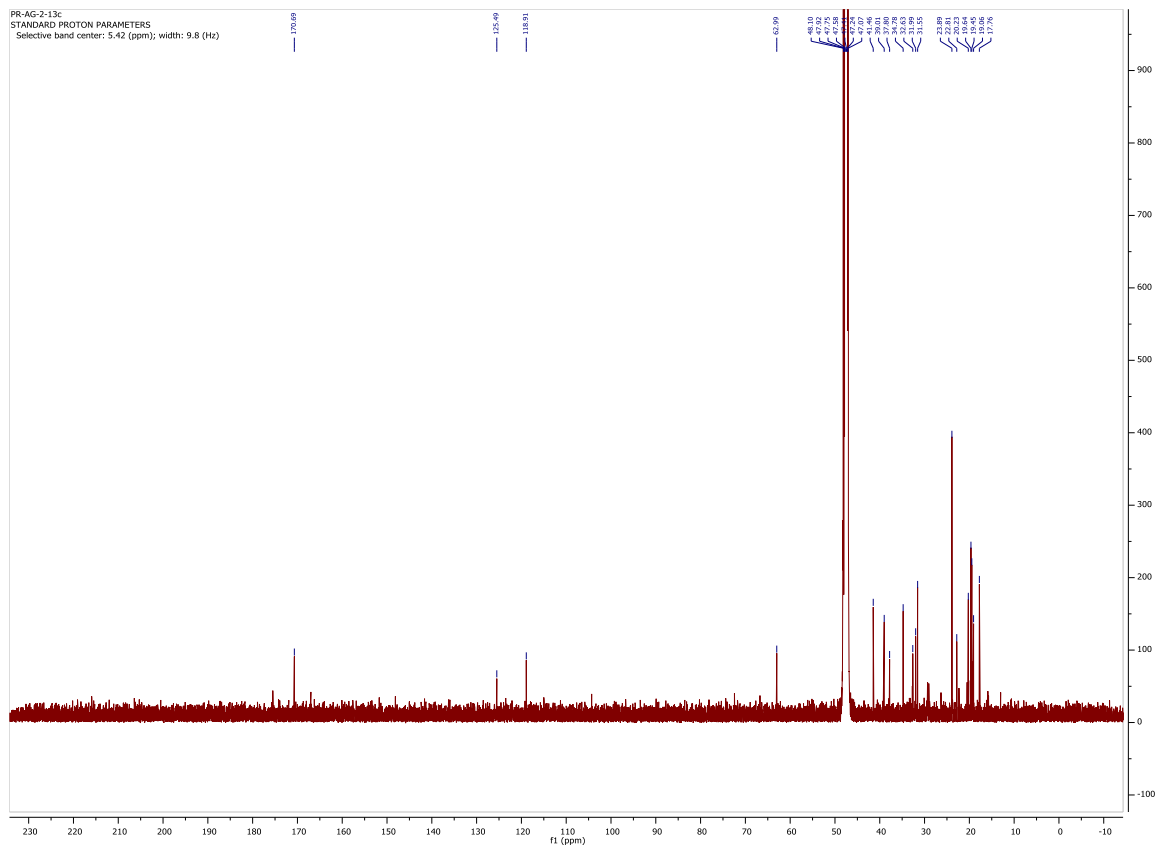


Figure S.IV.7: ^{13}C -NMR compound 1

LCMS spectra

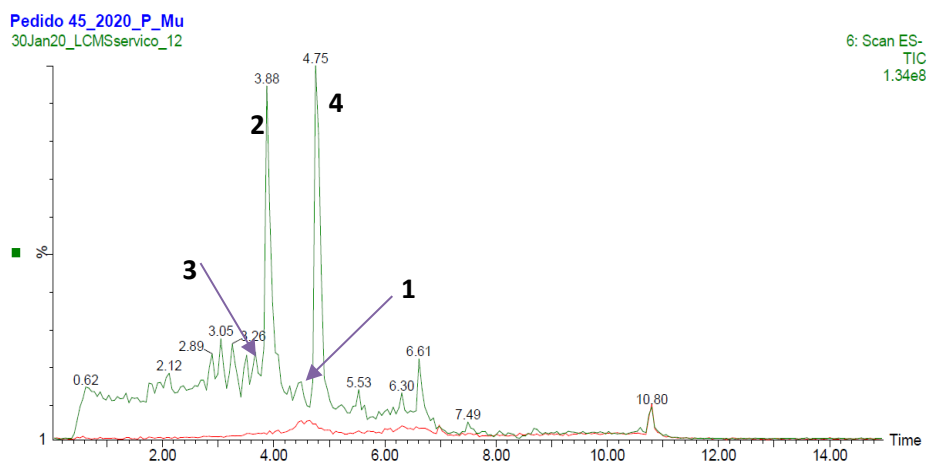


Figure S.IV.8: ESI- Comparison of chromatographic profiles of isolated compounds with *P. mutabilis* leaves extract

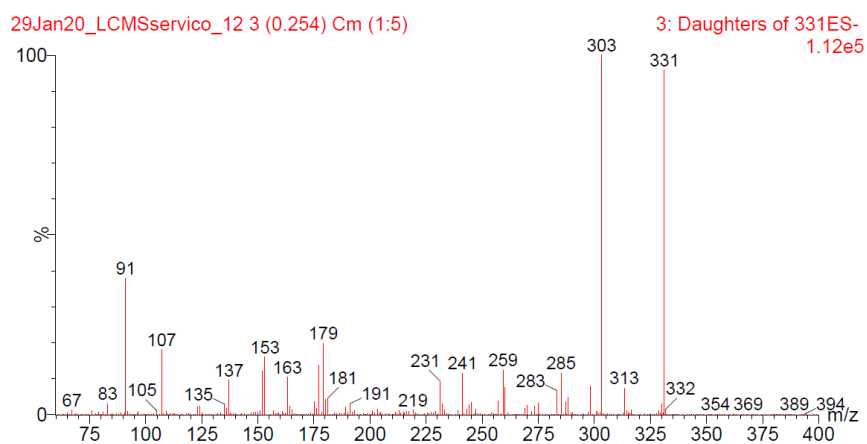


Figure S.IV.12: MS/MS spectrum Mutabilol, 1 (ESI-)

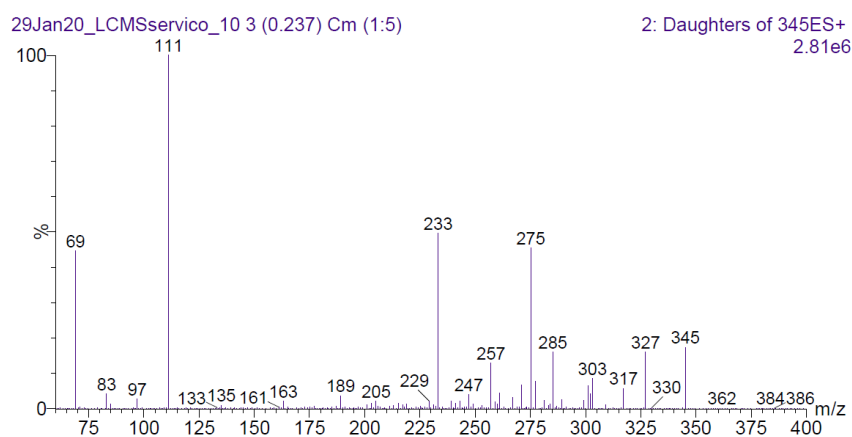


Figure S.IV.9: MS/MS spectrum of Coleon U quinone, 2 (ESI+).

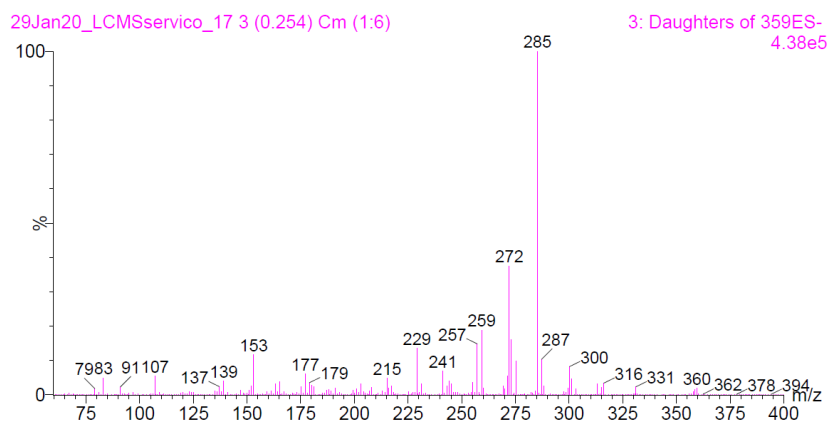


Figure S.IV.10: MS/MS spectrum of 8 α ,9 α -epoxycoleon U quinone, 3 (ESI-)

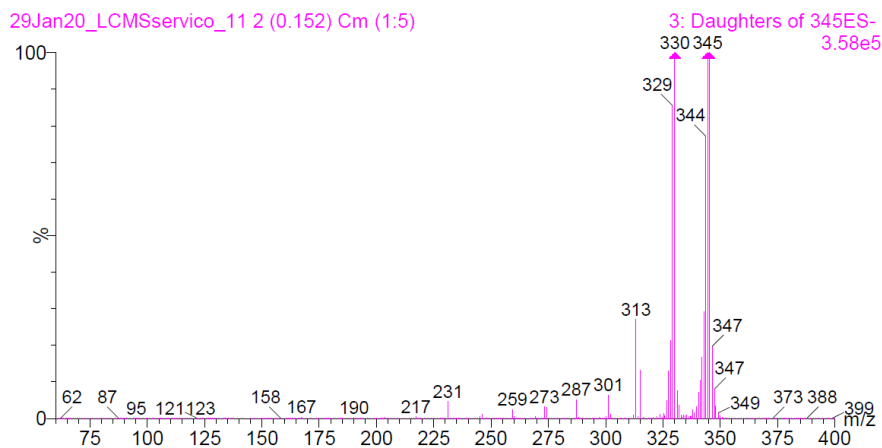


Figure S.IV.11: MS/MS spectrum of Coleon U, 4 (ESI-)

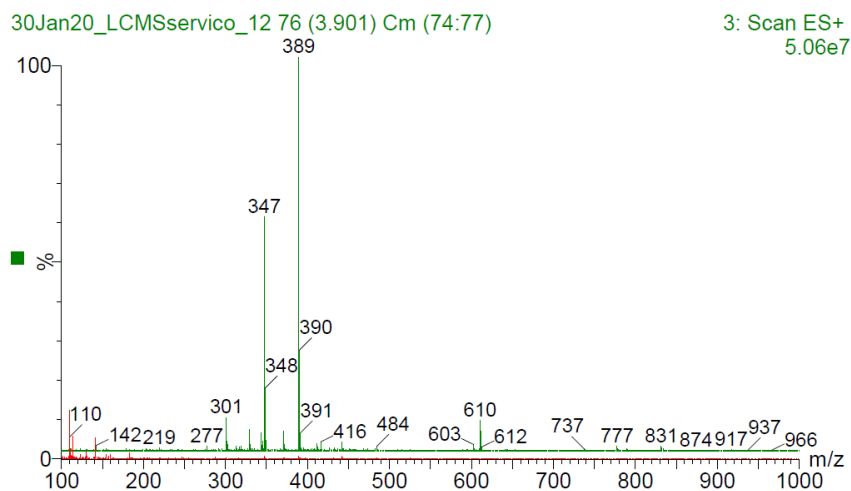


Figure S.IV.13: MS/MS spectrum of acetoxy derivative of an abietane diterpenoid, 5 (ESI+)

Effects of compounds' (2, 3, and 4) pre-treatment on doxorubicin anticancer efficacy in NCI-H460/R cells.

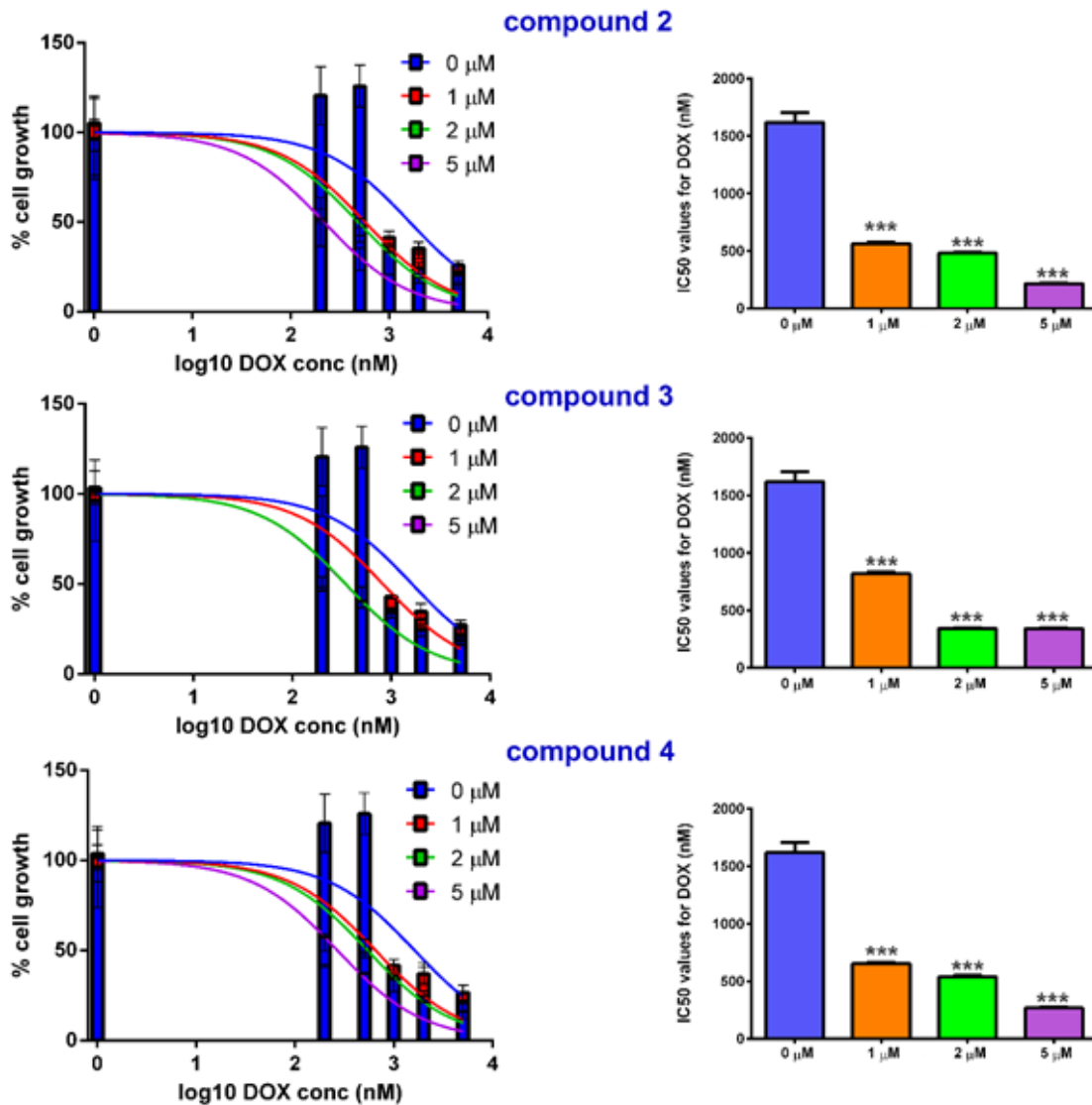


Figure S.IV.14. Reversal of DOX resistance in NCI-H460/R cells in subsequent treatment with compounds 2, 3, and 4. Left panel: Cell growth inhibition induced by combined treatments of compounds 2, 3, and 4 with DOX. Right panel: IC₅₀ values obtained by non-linear regression in GraphPad Prism 6 software. Dunnett's multiple comparisons test in Two-way ANOVA was used to determine the significant differences among treatment strategies ($p \leq 0.01$ ***). Results were obtained from three independent experiments ($n=3$).

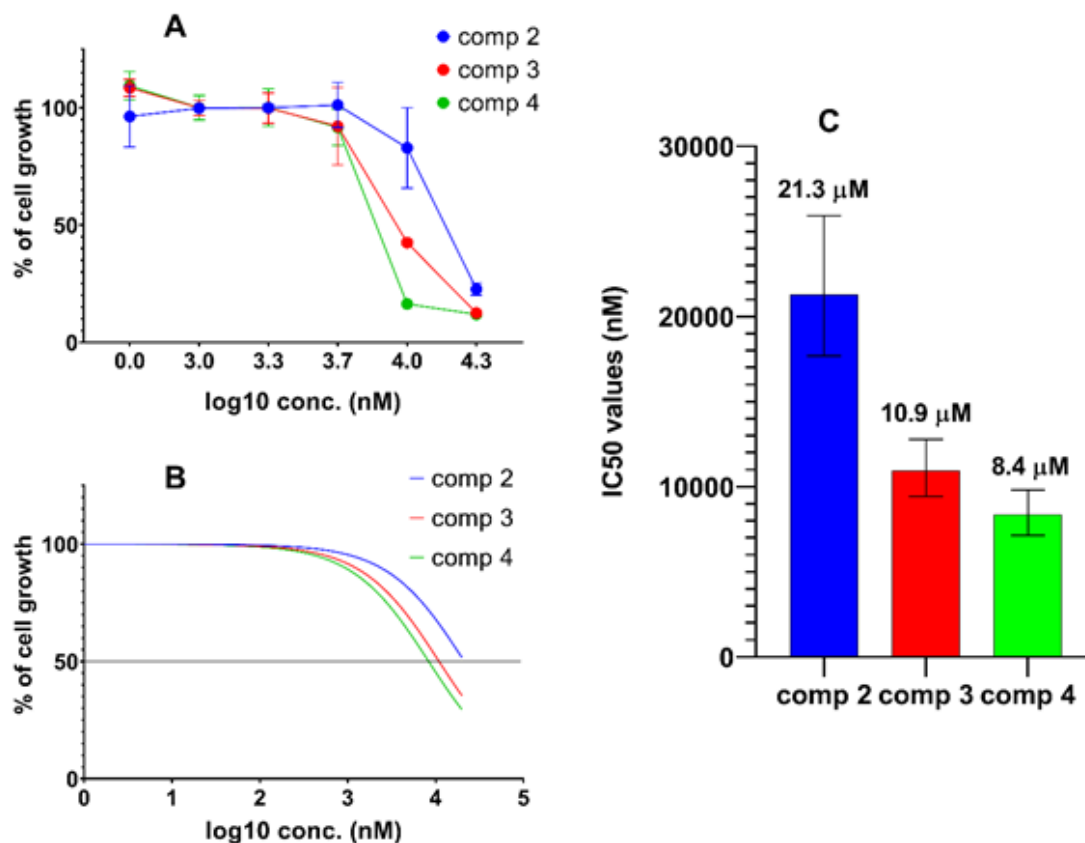


Figure S.IV.15. Single treatment with compounds 2, 3, and 4 in NCI-H460/R cells assessed by MTT after 144 h (control treatments of combined effect with DOX). A: Cell growth inhibition induced by single treatments of compounds 2, 3, and 4 with DOX. B: Non-linear regression used to calculate the IC₅₀ values of compounds 2, 3, and 4. IC₅₀ values obtained by non-linear regression in GraphPad Prism 6 software. Results were obtained from three independent experiments (n=3). The results confirmed that 1 μM, 2 μM, and 5 μM used in combination with DOX (Annex 6) did not affect the cell viability after 144 h. Only 10 μM and 20 μM inhibited the cell growth of NCI-H460/R but these concentrations were not used in combination studies

Supplementary table S.IV.4. Atomic coordinates for all the optimized species (PBE1PBE/6-31G)**

| | | | | | | | |
|----------|-----------|-----------|-----------|----------|-----------|-----------|-----------|
| 2 | | | | | | | |
| 6 | -6.510598 | -1.779398 | 1.479926 | 6 | -7.970876 | 0.780834 | 0.526030 |
| 6 | -7.531096 | -1.603413 | 0.368407 | 6 | -4.857951 | -2.000515 | -1.605359 |
| 6 | -7.307474 | -0.274144 | -0.378671 | 8 | -1.163278 | 1.737198 | -1.737323 |
| 6 | -5.812576 | -0.018174 | -0.593221 | 6 | 0.986286 | 0.324638 | -0.528563 |
| 6 | -4.825958 | -1.155550 | -0.406426 | 6 | 1.699007 | 0.251735 | 0.824911 |
| 6 | -5.089506 | -1.926752 | 0.933919 | 6 | 1.714161 | -0.497542 | -1.598615 |
| 6 | -5.366542 | 1.169179 | -1.066715 | 8 | -0.050959 | -2.275970 | 0.352379 |
| 6 | -3.943581 | 1.513549 | -1.210878 | 8 | -2.525781 | -2.918256 | 0.154374 |
| 6 | -2.953974 | 0.524590 | -0.753593 | 1 | -6.923503 | -2.842398 | 1.921557 |
| 6 | -3.377117 | -0.723779 | -0.434745 | 1 | -6.759040 | -1.111726 | 2.130090 |
| 6 | -1.510904 | 0.937819 | -0.622889 | 1 | -8.627158 | -1.700757 | 0.544753 |
| 6 | -0.472386 | -0.095410 | -0.446381 | 1 | -7.460960 | -2.453773 | -0.522227 |
| 6 | -0.894182 | -1.359908 | -0.221952 | 1 | -4.938619 | -3.051636 | 0.707898 |
| 6 | -2.329027 | -1.744994 | -0.194396 | 1 | -4.541494 | -1.721600 | 1.771359 |
| 6 | -8.047669 | -0.299977 | -1.726809 | 8 | -6.200604 | 2.218359 | -1.299660 |
| 6 | -7.912939 | 0.853667 | 0.482813 | 8 | -3.713876 | 2.738489 | -1.444515 |
| 6 | -5.002622 | -2.112785 | -1.626524 | 1 | -7.874686 | 0.784651 | -2.218774 |
| 8 | -1.221045 | 2.121411 | -0.617078 | 1 | -9.063991 | -0.409872 | -1.664477 |
| 6 | 0.971841 | 0.335494 | -0.440785 | 1 | -7.577087 | -0.947221 | -2.459824 |
| 6 | 1.617160 | 0.126924 | 0.933379 | 1 | -7.848015 | 1.786667 | 0.125447 |
| 6 | 1.770777 | -0.359399 | -1.548369 | 1 | -7.543005 | 0.763414 | 1.532449 |
| 8 | -0.074167 | -2.390575 | 0.001545 | 1 | -9.042667 | 0.569773 | 0.609945 |
| 8 | -2.564906 | -2.935325 | 0.002661 | 1 | -4.228832 | -2.887377 | -1.502349 |
| 1 | -6.749353 | -2.654558 | 2.093775 | 1 | -4.509025 | -1.405917 | -2.456032 |
| 1 | -6.564028 | -0.914745 | 2.151569 | 1 | -5.871125 | -2.333887 | -1.832805 |
| 1 | -8.549068 | -1.599820 | 0.774760 | 1 | 0.979702 | 1.366977 | -0.864337 |
| 1 | -7.486513 | -2.457066 | -0.318685 | 1 | 2.722705 | 0.626192 | 0.723699 |
| 1 | -4.854243 | -2.978326 | 0.758105 | 1 | 1.747569 | -0.775651 | 1.195022 |
| 1 | -4.379997 | -1.583076 | 1.693833 | 1 | 1.189752 | 0.863483 | 1.575539 |
| 8 | -6.161903 | 2.186470 | -1.447177 | 1 | 2.747508 | -0.149447 | -1.696743 |
| 8 | -3.675186 | 2.602544 | -1.711526 | 1 | 1.227695 | -0.388612 | -2.572182 |
| 1 | -7.942714 | 0.654833 | -2.247310 | 1 | 1.735790 | -1.558682 | -1.335069 |
| 1 | -9.114581 | -0.484354 | -1.556422 | 1 | -0.617776 | -3.061528 | 0.479165 |
| 1 | -7.670931 | -1.092420 | -2.380480 | 1 | -5.592493 | 2.946103 | -1.538704 |
| 1 | -7.802699 | 1.826473 | 0.004438 | 8 | -3.133581 | 0.332438 | 0.838177 |
| 1 | -7.442070 | 0.906951 | 1.468878 | | | | |
| 1 | -8.980987 | 0.658432 | 0.628634 | 4 | | | |
| 1 | -4.336068 | -2.971832 | -1.527847 | 6 | -6.539897 | -1.866714 | 1.404408 |
| 1 | -4.778572 | -1.581526 | -2.556133 | 6 | -7.528184 | -1.654080 | 0.271925 |
| 1 | -6.026808 | -2.480901 | -1.686551 | 6 | -7.271879 | -0.300086 | -0.416740 |
| 1 | 0.957918 | 1.410772 | -0.646814 | 6 | -5.766223 | -0.044190 | -0.567457 |
| 1 | 2.645796 | 0.501904 | 0.923930 | 6 | -4.782098 | -1.201830 | -0.412312 |
| 1 | 1.644007 | -0.932990 | 1.201810 | 6 | -5.125485 | -2.051483 | 0.857620 |
| 1 | 1.069645 | 0.667305 | 1.711312 | 6 | -5.311494 | 1.164463 | -0.964650 |
| 1 | 2.796856 | 0.022105 | -1.562115 | 6 | -3.887488 | 1.505751 | -1.038522 |
| 1 | 1.330132 | -0.172787 | -2.532362 | 6 | -2.897853 | 0.522539 | -0.718219 |
| 1 | 1.811879 | -1.440490 | -1.389355 | 6 | -3.309580 | -0.789600 | -0.381366 |
| 1 | -0.667247 | -3.158729 | 0.123952 | 6 | -1.522950 | 0.884001 | -0.770010 |
| 1 | -5.524776 | 2.870780 | -1.745435 | 6 | -0.512496 | -0.046120 | -0.488727 |
| | | | | 6 | -0.936879 | -1.333075 | -0.167708 |
| 3 | | | | 6 | -2.301702 | -1.700976 | -0.120620 |
| 6 | -6.648287 | -1.920306 | 1.398714 | 6 | -7.959443 | -0.273250 | -1.792066 |
| 6 | -7.578543 | -1.661558 | 0.227975 | 6 | -7.916025 | 0.789936 | 0.465451 |
| 6 | -7.318589 | -0.275319 | -0.390202 | 6 | -4.915408 | -2.086798 | -1.686420 |
| 6 | -5.814200 | -0.000583 | -0.517928 | 8 | -1.166100 | 2.127058 | -1.095326 |
| 6 | -4.833267 | -1.151465 | -0.310408 | 6 | 0.946797 | 0.352766 | -0.542234 |
| 6 | -5.193170 | -2.015248 | 0.941757 | 6 | 1.629028 | 0.222449 | 0.823449 |
| 6 | -5.376336 | 1.208694 | -0.940049 | | | | |
| 6 | -3.966314 | 1.614547 | -1.037916 | 6 | 1.711296 | -0.411152 | -1.628269 |
| 6 | -2.918923 | 0.663334 | -0.539225 | 8 | -0.032597 | -2.288730 | 0.113004 |
| 6 | -3.392424 | -0.682827 | -0.121824 | 8 | -2.483160 | -3.049729 | 0.139947 |
| 6 | -1.472665 | 0.856571 | -0.960313 | 1 | -6.810123 | -2.737367 | 2.011736 |
| 6 | -0.463904 | -0.076639 | -0.421563 | 1 | -6.568300 | -1.002111 | 2.077068 |
| 6 | -0.885499 | -1.296990 | -0.010697 | 1 | -8.558598 | -1.662595 | 0.644943 |
| 6 | -2.307902 | -1.727413 | -0.012737 | | | | |
| 6 | -7.992770 | -0.204383 | -1.771819 | | | | |

| | | | |
|---|-----------|-----------|-----------|
| 1 | -7.458368 | -2.483774 | -0.442579 |
| 1 | -5.009135 | -3.111091 | 0.593207 |
| 1 | -4.410913 | -1.814750 | 1.656950 |
| 8 | -6.103788 | 2.207285 | -1.296959 |
| 8 | -3.618908 | 2.685885 | -1.376549 |
| 1 | -7.831126 | 0.700656 | -2.270452 |
| 1 | -9.033160 | -0.459680 | -1.672649 |
| 1 | -7.557323 | -1.041041 | -2.459795 |
| 1 | -7.792137 | 1.781695 | 0.032763 |
| 1 | -7.483966 | 0.805568 | 1.470607 |
| 1 | -8.987918 | 0.584586 | 0.561986 |
| 1 | -4.218866 | -2.927925 | -1.628658 |
| 1 | -4.678381 | -1.495624 | -2.574760 |
| 1 | -5.926215 | -2.483750 | -1.798583 |
| 1 | 0.955817 | 1.412120 | -0.815679 |
| 1 | 2.658899 | 0.590851 | 0.765710 |
| 1 | 1.659068 | -0.818952 | 1.154653 |
| 1 | 1.103737 | 0.809990 | 1.582720 |
| 1 | 2.741764 | -0.045120 | -1.690745 |
| 1 | 1.244709 | -0.272132 | -2.608260 |
| 1 | 1.743618 | -1.482312 | -1.412310 |
| 1 | -0.546784 | -3.091870 | 0.297128 |
| 1 | -5.469292 | 2.926628 | -1.491434 |
| 1 | -3.154553 | -3.155574 | 0.821621 |
| 1 | -2.004938 | 2.627255 | -1.275839 |

4¹¹

| | | | |
|---|-----------|-----------|-----------|
| 6 | -6.588713 | -2.302216 | 1.048832 |
| 6 | -7.557057 | -1.698986 | 0.021789 |
| 6 | -7.243777 | -0.255859 | -0.408492 |
| 6 | -5.754100 | -0.055395 | -0.711254 |
| 6 | -4.778294 | -1.187374 | -0.431559 |
| 6 | -5.155460 | -1.756187 | 0.957607 |
| 6 | -5.293724 | 1.142333 | -1.125620 |
| 6 | -3.863486 | 1.470623 | -1.253215 |
| 6 | -2.888881 | 0.519420 | -0.867965 |
| 6 | -3.312709 | -0.771827 | -0.411212 |
| 6 | -1.516584 | 0.888410 | -0.916383 |
| 6 | -0.513219 | -0.010970 | -0.527492 |
| 6 | -0.949982 | -1.264179 | -0.111337 |
| 6 | -2.334155 | -1.694427 | -0.052505 |
| 6 | -8.104115 | 0.055550 | -1.643528 |
| 6 | -7.642850 | 0.695189 | 0.736517 |
| 6 | -4.868303 | -2.283662 | -1.526406 |
| 8 | -1.157322 | 2.117283 | -1.341241 |
| 6 | 0.949850 | 0.371239 | -0.571956 |
| 6 | 1.587296 | 0.322334 | 0.820330 |
| 6 | 1.729730 | -0.502038 | -1.560231 |
| 8 | -0.147148 | -2.253289 | 0.279274 |
| 8 | -2.455942 | -2.930569 | 0.340575 |
| 1 | -6.582791 | -3.391164 | 0.917599 |
| 1 | -6.967439 | -2.130413 | 2.064115 |
| 1 | -8.583656 | -1.715632 | 0.413284 |
| 1 | -7.581223 | -2.328118 | -0.874290 |
| 1 | -4.421093 | -2.526192 | 1.210682 |
| 1 | -5.021343 | -0.937207 | 1.675215 |
| 8 | -6.076582 | 2.221517 | -1.401973 |
| 8 | -3.617790 | 2.649072 | -1.666614 |
| 1 | -7.976346 | 1.090689 | -1.964533 |
| 1 | -9.164323 | -0.115955 | -1.414813 |
| 1 | -7.828098 | -0.599596 | -2.477066 |
| 1 | -7.428783 | 1.732863 | 0.470278 |
| 1 | -7.095240 | 0.454824 | 1.653576 |
| 1 | -8.716484 | 0.601364 | 0.947224 |
| 1 | -4.146719 | -3.067311 | -1.276458 |
| 1 | -4.602867 | -1.850013 | -2.495554 |

| | | | |
|---|-----------|-----------|-----------|
| 1 | -5.861258 | -2.732138 | -1.615703 |
| 1 | 0.991631 | 1.406327 | -0.928156 |
| 1 | 2.641077 | 0.626757 | 0.779275 |
| 1 | 1.535083 | -0.691442 | 1.228115 |
| 1 | 1.065460 | 0.993607 | 1.510011 |
| 1 | 2.783970 | -0.199386 | -1.602992 |

| | | | |
|---|-----------|-----------|-----------|
| 1 | 1.309858 | -0.417392 | -2.567731 |
| 1 | 1.682769 | -1.552776 | -1.259379 |
| 1 | -0.909996 | -2.938340 | 0.455328 |
| 1 | -5.400408 | 2.892608 | -1.647350 |
| 1 | -2.008909 | 2.581618 | -1.557241 |

4¹⁴

| | | | |
|---|-----------|-----------|-----------|
| 6 | -6.520498 | -1.852272 | 1.409718 |
| 6 | -7.527305 | -1.667740 | 0.287061 |
| 6 | -7.293646 | -0.317173 | -0.416164 |
| 6 | -5.790935 | -0.042483 | -0.564987 |
| 6 | -4.784920 | -1.180054 | -0.425877 |
| 6 | -5.107880 | -2.025720 | 0.851928 |
| 6 | -5.342244 | 1.161537 | 0.959507 |
| 6 | -3.898362 | 1.554616 | -1.063391 |
| 6 | -2.897226 | 0.596766 | -0.739348 |
| 6 | -3.311655 | -0.730117 | -0.406714 |
| 6 | -1.478244 | 0.989267 | -0.772182 |
| 6 | -0.497859 | -0.056914 | -0.479688 |
| 6 | -0.939532 | -1.318005 | -0.187829 |
| 6 | -2.323002 | -1.656081 | -0.144593 |
| 6 | -7.985816 | -0.310954 | -1.788464 |
| 6 | -7.956156 | 0.771850 | 0.451222 |
| 6 | -4.909851 | -2.077335 | -1.688252 |
| 8 | -1.101603 | 2.145478 | -1.036108 |
| 6 | 0.961299 | 0.324559 | -0.524476 |
| 6 | 1.652595 | 0.168210 | 0.833366 |
| 6 | 1.729003 | -0.418330 | -1.622123 |
| 8 | -0.066485 | -2.332523 | 0.086790 |
| 8 | -2.546693 | -3.024119 | 0.106364 |
| 1 | -6.776084 | -2.716170 | 2.036541 |
| 1 | -6.555750 | -0.975145 | 2.066759 |
| 1 | -8.556396 | -1.693780 | 0.669215 |
| 1 | -7.442998 | -2.501702 | -0.422021 |
| 1 | -4.967015 | -3.085322 | 0.605589 |
| 1 | -4.389849 | -1.765159 | 1.641269 |
| 8 | -6.117267 | 2.214014 | -1.287714 |
| 8 | -3.752793 | 2.741821 | -1.427875 |
| 1 | -7.848651 | 0.659822 | -2.272427 |
| 1 | -9.062882 | -0.497481 | -1.678117 |
| 1 | -7.573791 | -1.082841 | -2.446007 |
| 1 | -7.801618 | 1.760161 | 0.018044 |
| 1 | -7.541811 | 0.783838 | 1.464443 |
| 1 | -9.034513 | 0.579871 | 0.526977 |
| 1 | -4.202983 | -2.909742 | -1.627127 |
| 1 | -4.679389 | -1.482018 | -2.576081 |
| 1 | -5.918724 | -2.485460 | -1.803212 |
| 1 | 0.942562 | 1.391208 | -0.779613 |
| 1 | 2.691620 | 0.521140 | 0.786919 |
| 1 | 1.662388 | -0.879214 | 1.151903 |
| 1 | 1.132239 | 0.752077 | 1.599633 |
| 1 | 2.769112 | -0.069809 | -1.677588 |
| 1 | 1.263770 | -0.248719 | -2.598491 |
| 1 | 1.739785 | -1.496638 | -1.433370 |
| 1 | -0.642484 | -3.104635 | 0.208990 |
| 1 | -5.381816 | 2.875577 | -1.484367 |
| 1 | -3.007706 | -3.097411 | 0.9 |

CHAPTER V

Article 4

Self-Assembly Nanoparticles of Natural Bioactive Abietane Diterpenes

Epole Ntungwe ^{1,2}, Eva María Domínguez-Martín ^{1,2}, Gabrielle Bangay ^{1,2}, Catarina Garcia^{1,2}, Iris Guerreiro¹, Eleonora Colombo³, Lucilia Saraiva ⁴, Ana María Díaz-Lanza ², Andreia Rosatella^{1,5}, Marta M. Alves ⁶, Daniele Passarella³ Catarina Reis ⁵, and Patrícia Rijo ^{1,5*}

- ¹ CBIOS – Universidade Lusófona’s Research Center for Biosciences & Health Technologies, Campo Grande 376, 1749-024, Lisbon, Portugal; epole.ntungwe@ulusofona.pt; evam.dominguez@uah.es
- ² University of Alcalá de Henares, Faculty of Pharmacy, Department of Biomedical Sciences, Pharmacology Area (Pharmacognosy Laboratory), New antitumor compounds: Toxic action on leukemia cells research group. Ctra. A2, Km 33.100 – Campus Universitario, 28805. Alcalá de Henares, Madrid, Spain; ana.diaz@uah.es
- ³ Dipartimento di Chimica, Università degli Studi di Milano, Via Golgi 19, 20133 Milano, Italy; eleonora.colombo@unimi.it
- ⁴ LAQV - Faculty of Pharmacy of University of Porto, Rua de Jorge Viterbo Ferreira, 228 4050-313, Porto, Portugal; lucilia.saraiva@ff.up.pt
- ⁵ iMed.Ulisboa, Faculdade de Farmácia da Universidade de Lisboa, Av. Prof. Gama Pinto, 1649-003 Lisboa, Portugal; andrea.rosatella@ulusofona.pt
- ⁶ Centro de Química Estrutural, Instituto Superior Técnico, Universidade de Lisboa, Av. Rovisco Pais, 1, 1049-001 Lisboa, Portugal; martamalves@tecnico.ulisboa.pt

* Corresponding author:

E-mail address: patricia.rijo@ulusofona.pt (P. Rijo)

Int. J. Mol. Sci. 2021, 22, 10210.

<https://doi.org/10.3390/ijms221910210>

Article

Self-Assembly Nanoparticles of Natural Bioactive Abietane Diterpenes

Epole Ntungwe ^{1,2,†}, Eva María Domínguez-Martín ^{1,2,†}, Gabrielle Bangay ^{1,2}, Catarina Garcia ^{1,2}, Iris Guerreiro ¹, Eleonora Colombo ³, Lucilia Saraiva ⁴, Ana María Díaz-Lanza ², Andreia Rosatella ^{1,5}, Marta M. Alves ⁶, Catarina Pinto Reis ⁵, Daniele Passarella ³ and Patricia Rijo ^{1,5,*}

Citation: Ntungwe, E.; Domínguez-Martín, E.M.; Bangay, G.; Garcia, C.; Guerreiro, I.; Colombo, E.; Saraiva, L.; Díaz-Lanza, A.M.; Rosatella, A.; Alves, M.M.; et al. Self-Assembly Nanoparticles of Natural Bioactive Abietane Diterpenes. *Int. J. Mol. Sci.* **2021**, *22*, 10210. <https://doi.org/10.3390/ijms221910210>

Academic Editor: Guido R. M. M. Haenen

Received: 14 August 2021
Accepted: 16 September 2021
Published: 22 September 2021

Publisher's Note: MDPI stays neutral with regard to jurisdictional claims in published maps and institutional affiliations.



Copyright: © 2021 by the authors. Licensee MDPI, Basel, Switzerland. This article is an open access article distributed under the terms and conditions of the Creative Commons Attribution (CC BY) license (<http://creativecommons.org/licenses/by/4.0/>).

- ¹ CBIO5—Niversidade Lusófona's Research Center for Biosciences & Health Technologies, Campo Grande 376, 1749-024 Lisbon, Portugal; epole.ntungwe@ulusofona.pt (E.N.); evam.dominguez@uah.es (E.M.D.-M.); gabrielle.bangay@gmail.com (G.B.); catarina.g.garcia@gmail.com (C.G.); iris.c.f.guerreiro@gmail.com (I.G.); andreia.rosatella@ulusofona.pt (A.R.)
 - ² Pharmacology Area (Pharmacognosy Laboratory), New Antitumor Compounds: Toxic Action on Leukemia Cells Research Group, Faculty of Pharmacy, Department of Biomedical Sciences, University of Alcalá de Henares, Ctra. A2, Km 33.100—Campus Universitario, 28805 Alcalá de Henares, Spain; ana.diaz@uah.es
 - ³ Department of Chemistry, University of Milan, Via Golgi 19, 20133 Milano, Italy; eleonora.colombo@unimi.it (E.C.); daniele.passarella@unimi.it (D.P.)
 - ⁴ LAQV—Faculty of Pharmacy of University of Porto, Rua de Jorge Viterbo Ferreira 228, 4050-313 Porto, Portugal; lucilia.saraiva@ff.up.pt
 - ⁵ iMed.Ulisboa, Faculdade de Farmácia da Universidade de Lisboa, Av. Prof. Gama Pinto, 1649-003 Lisboa, Portugal; catarinapinto@ff.ulisboa.pt
 - ⁶ Centro de Química Estrutural, Instituto Superior Técnico, Universidade de Lisboa, Av. Rovisco Pais, 1, 1049-001 Lisboa, Portugal; martamalves@tecnico.ulisboa.pt
- * Correspondence: patricia.rijo@ulusofona.pt
† These authors contributed equally to this work.

Abstract: Different approaches have been reported to enhance penetration of small drugs through physiological barriers; among them is the self-assembly drug conjugates preparation that shows to be a promising approach to improve activity and penetration, as well as to reduce side effects. In recent years, the use of drug-conjugates, usually obtained by covalent coupling of a drug with biocompatible lipid moieties to form nanoparticles, has gained considerable attention. Natural products isolated from plants have been a successful source of potential drug leads with unique structural diversity. In the present work three molecules derived from natural products were employed as lead molecules for the synthesis of self-assembled nanoparticles. The first molecule is the cytotoxic royleanone 7 α -acetoxy-6 β -hydroxyroyleanone (Roy, 1) that has been isolated from hairy colesus (*Plectranthus haidensis* (Forssk.) Schweinf.) ex Sprenger leaves in a large amount. This royleanone, its hemisynthetic derivative 7 α -acetoxy-6 β -hydroxy-12-benzoyloxyroyleanone (12BzRoy, 2) and 6,7-dehydroroyleanone (DHR, 3), isolated from the essential oil of thicket colesus (*P. madagascariensis* (Pers.) Benth.) were employed in this study. The royleanones were conjugated with squalene (sq), oleic acid (OA), and/or 1-bromododecane (BD) self-assembly inducers. Roy-OA, DHR-sq, and 12BzRoy-sq conjugates were successfully synthesized and characterized. The cytotoxic effect of DHR-sq was previously assessed on three human cell lines: NCI-H460 (IC₅₀ 74.0 \pm 2.2 μ M), NCI-H460/R (IC₅₀ 147.3 \pm 3.7 μ M), and MRC-5 (IC₅₀ 127.3 \pm 7.3 μ M), and in this work Roy-OA NPs was assayed against Vero-E6 cells at different concentrations (0.05, 0.1, and 0.2 mg/mL). The cytotoxicity of DHR-sq NPs was lower when compared with DHR alone in these cell lines: NCI-H460 (IC₅₀ 10.3 \pm 0.5 μ M), NCI-H460/R (IC₅₀ 10.6 \pm 0.4 μ M), and MRC-5 (IC₅₀ 16.9 \pm 0.5 μ M). The same results were observed with Roy-OA NPs against Vero-E6 cells as was found to be less cytotoxic than Roy alone in all the concentrations tested. From the obtained DLS results, 12BzRoy-sq assemblies were not in the nano range, although Roy-OA NP assemblies show a promising size (509.33 nm), Pdl (0.249), zeta potential (-46.2mV), and spherical morphology from SEM. In addition, these NPs had a low release of Roy at physiological pH 7.4 after 24 h. These results suggest the nano assemblies can act as prodrugs for the release of cytotoxic lead molecules.

Keywords: royleanones; self-assembly; nanoparticles; squalene; oleic acid; 1-bromododecane

1. Introduction

Many established and newly developed therapeutics are poorly water-soluble, limiting their bioavailability [1] and adequate drug delivery. Nanoparticles (NPs) have recently gained an increase in interest in the scientific community due to their advantages in increasing and effectively overcoming some pharmacokinetic limitations, such as drug bioavailability and possible side effects due to targeted delivery to specific tissues [2]. Important desired characteristics of nanoparticles are a large loading capacity for one or more therapeutics, a long circulation half-life, protection of the therapeutic agent during circulation, limited side effects, and an effective and selective release of therapeutics at the target site [2,3]. Several nanoplatforms already exist. These include polymer-based nanoparticles, lipid-based NPs, and nanosuspensions [4]. Lipid-based NPs are promising due to their high biocompatibility, ease of production, and solubilization capacity retention upon administration [1]. Lipid-based NPs can be divided into three different groups: liposomes, solid lipid NPs, and self-nano-emulsifying drug delivery systems (SNEDDS). The last one has received more attention from researchers due to its easy formulation. They consist of amphiphilic molecules with a lipid and a surfactant phase that, in an aqueous medium, mimic the self-assembly behavior that occurs in nature [4,5], forming highly ordered structures. This spontaneous assembly occurs due to non-covalent interactions such as van der Waals interactions, hydrogen bonding, and electrostatic interactions. Thus, it is possible to obtain fine and stable nanoemulsions upon gentle agitation. This is especially interesting for industrialization and commercialization because no extra energy needs to be added [4]. By using self-assembling conjugates it is possible to increase the loading capacity of the NPs and eliminate the need of a carrier [6]. This overcomes important drawbacks of nanomedicines including the use of many excipients, low drug loading efficiency, and crystallization [7,8].

To form self-assembling NPs, the conjugate is usually formed by covalent coupling of the drug with biocompatible lipidic moieties [9]. These molecules can be connected through smart linkers, which release the drug when an internal or external stimulus is applied, ensuring targeted delivery and controlled drug release [10]. A multitude of smart linkers (hydrazone, azo, peptide, disulfide, etc.) are available, each with unique advantages and disadvantages [11], and the most frequently used are redox-sensitive linkers. For instance, the high concentration of glutathione (GSH) in tumor cells cleaves these linkers, and the drug is released. The use of these types of linkers has been demonstrated for NPs of multiple cytotoxic agents [12]. Squalene is a lipidic moiety and a natural precursor of many steroids that spontaneously form self-assembling NPs in water, with an unusually high drug content. Since squalene is well tolerated, it makes it an ideal component of the drug delivery system [7,9,13]. Another attractive option commonly used as lipidic moieties is fatty acids due to their biodegradability and biosafety. Previous studies have concluded that oleic acid and 1-bromododecane can improve the stability of anti-cancer drugs and accomplish targeted delivery of the drug [6,14,15].

Plectranthus plants have historically been used in traditional medicine and are a known source of bioactive products, particularly royleanones, with pharmacological activities, including antiproliferative properties [11,16]. On one hand, 7 α -acetoxy-6 β -hydroxyroyleanone (Roy), for example, is the main metabolite of *P. hadiensis* leaf extracts [17], and it has been shown to have cytotoxicity against different cancer cell lines. It regulates MDR by inhibiting P-glycoprotein [18,19]; thus, is an interesting component for the development of new cancer treatments. The presence of hydroxyl groups at positions 6 and 12 of this cytotoxic molecule makes it an attractive lead for derivatization for the drug discovery process. 7 α -Acetoxy-6 β -hydroxy-12-benzoyloxyroyleanone (12BzRoy) is a de-

derivative of Roy obtained through a benzoylation reaction and has shown improved cytotoxic activity in different cancer cell lines. On the other hand, 6,7-dehydroroyleanone (DHR) is the main component of *P. madagascariensis* essential oil and was isolated from this plant, and it has been reported to have antioxidant, antimicrobial, and cytotoxic activities [11,20].

In this study the synthesis of lipid-drug conjugates based on three abietane diterpenes (Roy, its derivative 12BzRoy, and DHR, Figure 1) is described, which self-assemble in water, in a way to increase the bioavailability. The NPs of these lipid-drug conjugates were characterized, and their properties as well as their cytotoxicity in different cancer cell lines were accessed.

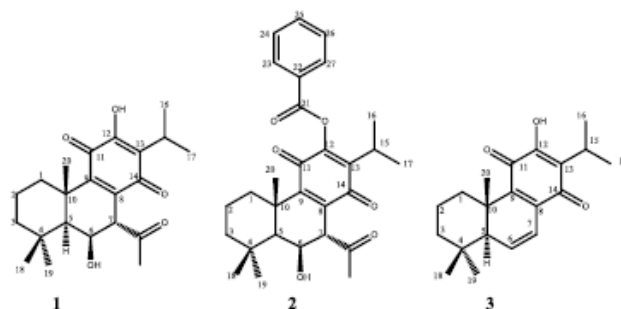


Figure 1. Chemical structures of the abietane diterpenes: (1) 7 α -acetoxy-6 β -hydroxyroyleanone, Roy; (2) 7 α -acetoxy-6 β -hydroxy-12-benzyloxyroyleanone, 12BzRoy; (3) 6,7-dehydroroyleanone DHR.

2. Results and Discussion

2.1. Hemisynthesis of Self-Assembly Nanoparticles Conjugates

Hemisyntheses were performed with Roy, 12BzRoy, and DHR lead molecules using squalene (Sq), oleic acid (OA), and 1-bromododecane (BD) as self-assembly inducers. Unfortunately, only two conjugates were successfully synthesized: 12BzRoy-Sq (7) and Roy-OA conjugates (5), with overall yields of 20.4% and 90.9%, respectively (Figure 2).

The NMR analysis showed that, in the case of 12BzRoy, squalene was added to the C-6 hydroxyl group (6-OH), that was confirmed by the absence of the 6-OH around 7 ppm in the $^1\text{H-NMR}$ spectra Figure S1. In addition, the slight chemical shift of 7 β -H from 5.70 to 5.30 and H-6 α from 4.34 to 4.22 also confirmed the presence of the squalene moiety at position 6 of 12BzRoy molecule. For the Roy-OA conjugate, the presence of 6-OH and no change in the chemical shift of 7 β -H (5.64 ppm) and 6 α -H (4.31 ppm) of the lead molecule Roy suggests that oleic acid was added on position 12. This is in agreement with our previous work on derivatization of Roy, where position 12 was proven to be more active [11]. In addition, the number of protons of the oleic acid ethylene group in the synthesized product is proportional to one molecule of Roy, indicating the presence of one oleic acid molecule in the conjugate at position 12. DHR-Sq (9) structure was confirmed by NMR (Figure S2) and was in agreement with the literature [21].

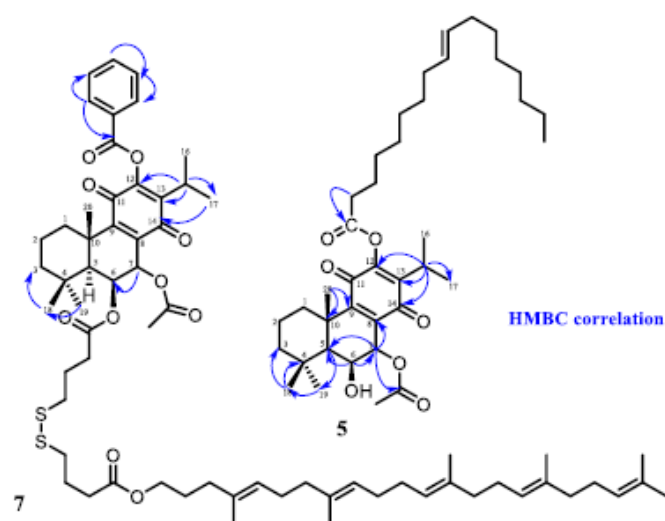


Figure 2. HMBC correlations of derivatives Roy-OA (5) and 12BzRoy-Sq (7).

2.2. Nanoassemblies: Preparation and Characterization

After the synthesis of the Roy and 12BzRoy conjugates, the respective self-assembled nanoparticles (NP) were prepared. In a way to confirm the formation of the NPs, FTIR spectra main peaks and the corresponding functional groups were identified for all samples tested (drug conjugate and its corresponding self-assembled NP). In the IR spectrum of compound 5 (Roy-OA conjugate), characteristic absorption bands for a hydroxyl group (3454 cm^{-1}) at the 6 position, C–H alkane stretching (2923 cm^{-1}), and ester groups (1725 cm^{-1}) at positions 12 and 7 were evident. The peak at 1667 cm^{-1} was attributed to the carbonyl groups and at 1459 cm^{-1} to the methyl groups. In the Roy-OA self-assembled nanoparticle, there was a clear difference in the spectrum. The peak at 2923 cm^{-1} due to C–H alkane stretching disappeared, suggesting some structure modification of Roy-OA conjugate in an organized nanoparticle arrangement (Figure 3). In addition, the carbonyl region (around 1600 cm^{-1}) in the Roy-OA self-assembled NP was also different from its conjugate. These results were similar to the FTIR analysis of 12BzRoy-Sq self-assembled NP when compared with the 12BzRoy-Sq conjugate. For example, displayed bands at 2924 cm^{-1} attributed to C–H alkane stretching and 1643 cm^{-1} for carbonyl groups (Figure 4) were not seen in the spectrum of 12BzRoy-Sq NP, further confirming the formation of the NPs.

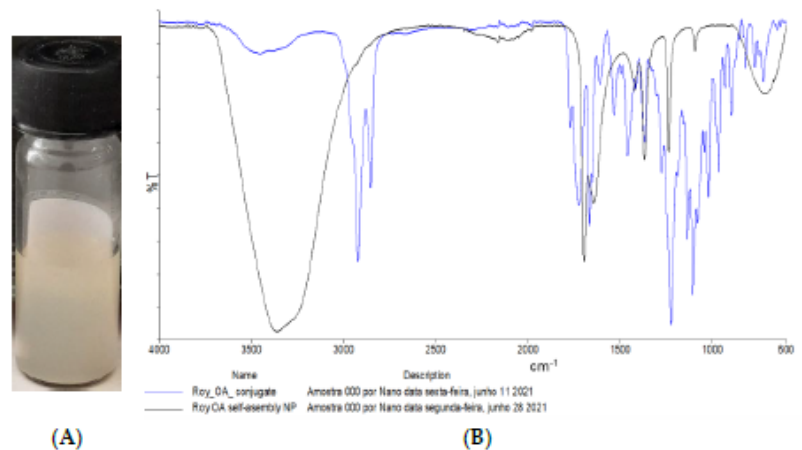


Figure 3. (A) Aqueous solution of nanoassemblies. (B) FTIR of Roy-OA conjugate 5 (blue) and its self-assembled NPs (black).

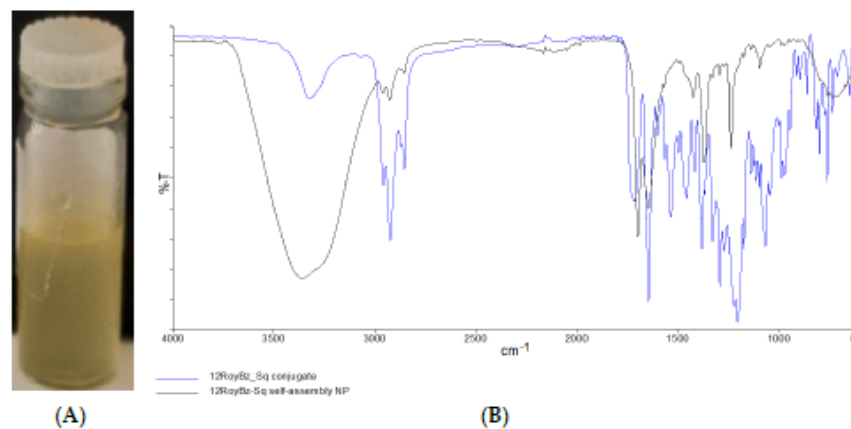


Figure 4. (A) Aqueous solution of nanoassemblies. (B) FTIR of 12BzRoy-Sq conjugate 7 (blue) and its self-assembled NP (black).

The mean size value, polydispersity, and zeta potential of the NPs were determined. In terms of size, it was observed that 12BzRoy-Sq was bigger than the Roy-OA NPs. The size of the 12BzRoy-Sq NPs was different from that previously observed for squalene-based heteronanoparticles [7,9], indicating that the larger nature of the 12BzRoy-Sq NPs could be due to the agglomeration in water; hence, these are not suitable for drug delivery. The zeta potential was negative in both cases, with the Roy-OA being more negative. This observation implies a better stability of these NPs. The Pdl of Roy-OA was smaller, indicating a narrower and homogenous size distribution (Table 1). Since the 12BzRoy-Sq NPs size was not in the nano range, only Roy-OA NPs were further characterized.

Table 1. Size and Zeta Potential Measurements (mean \pm SD, n= 3 at least).

| Sample | Size (nm) | Pdl | Zeta Potential (mV) |
|------------------------|----------------------|-------------------|---------------------|
| ROY-OA NP Assembly | 509.33 \pm 4.29 | 0.249 \pm 0.012 | -46.2 \pm 0.4 |
| 12BzRoy-Sq NP Assembly | 2739.33 \pm 100.50 | 0.731 \pm 0.187 | -28.9 \pm 1.2 |

The morphology for successful fabrication of self-assembled NPs was further confirmed by SEM. Observations showed that NPs in the Roy-OA assembly had a round shape morphology with homogenous sizes ranging from 80 to 50 nm in diameter (Figure 5b).

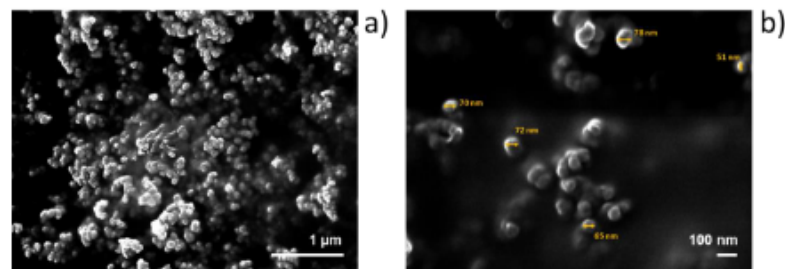


Figure 5. Scanning electron microscopy (SEM) images of Roy-OA NPs at (a) lower ($\times 25,000$) and (b) higher ($\times 70,000$) magnifications.

2.3. In Vitro Release Studies

The evaluation of Roy release from the self-assembled NPs in PBS at physiologic pH 7.4 was used to establish the release profile of Roy from the Roy-OA NP. As illustrated in Figure 6, Roy showed a slow release, since after 24 h approximately 8.35 % was released from the NPs. The release profile was continually sustained over the first 24 h of the assay; however, a bulk amount of the drug was not released from the NP, and Roy was found to degrade over time. Importantly, the amount of Roy released is enough to exhibit cytotoxic activity against cancer cell lines (Figure 7 and 8). These results were in agreement with those of Luo *et al.*, where oleic acid conjugated to Paclitaxel (PTX) was used as control. The results showed that there was almost no PTX released from PTX-OA NPs after incubation in PBS (pH 7.4) [15].

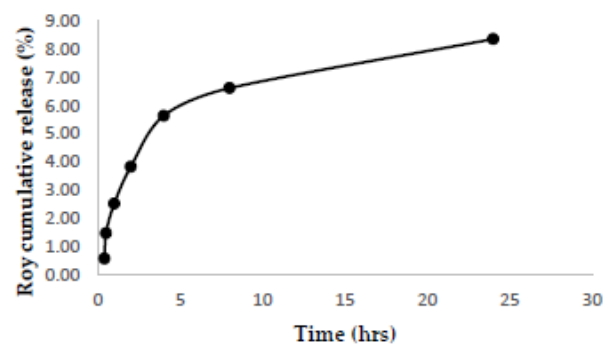


Figure 6. Cumulative release of Roy from Roy-OA NP in phosphate buffer saline adjusted to pH 7.4.

2.4. Biological activity study

2.4.1. Preliminary toxicity assay

The general toxicity of Roy-OA NP and its lead molecule was assessed using the *Artemia salina* model. The results revealed that Roy-OA NP had no toxicity against this model and was eight times less toxic than the corresponding lead molecule, Roy. These suggest that the Roy-OA NP may act as a prodrug.

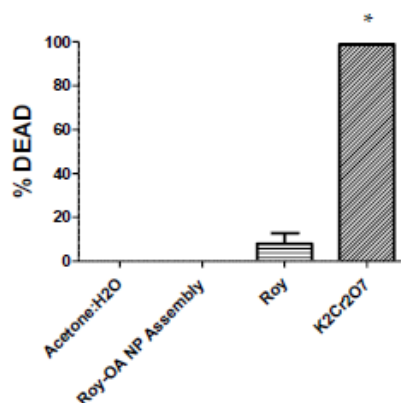


Figure 7. Brine shrimp lethal (BSLA) activity (%) against Roy and Roy-OA NP after 24 h exposure. Values are expressed as the mean \pm SD ($n = 3$). * $p < 0.0001$ comparison Acetone: H₂O vs NP. K₂Cr₂O₇ was used as the positive control.

2.4.2. Cytotoxicity study

Roy-OA nano assembly did not decrease cell viability of Vero-E6 cells even at high concentration of 200 $\mu\text{g/mL}$ as compared to Roy, where a significant reduction in cell viability in a concentration-dependent manner was observed (Figure 8). These results are consistent with those obtained from the royleanone DHR and DHR-Sq NPs previously tested against three human cancer cell lines, namely, sensitive non-small cell lung carcinoma, NCI-H460 cell line; multidrug-resistant non-small cell lung carcinoma cell line with P-glycoprotein overexpression, NCI-H460/R; and human embryonal bronchial epithelial (MCR-5) cells. DHR was more cytotoxic: NCI-H460 ($IC_{50} 10.3 \pm 0.5 \mu\text{M}$), NCI-H460/R ($IC_{50} 10.6 \pm 0.4 \mu\text{M}$), MRC-5 ($16.9 \pm 0.5 \mu\text{M}$) than DHR-sq NPs: NCI-H460 ($IC_{50} 74.0 \pm 2.2 \mu\text{M}$), NCI-H460/R ($IC_{50} 147.3 \pm 3.7 \mu\text{M}$), and MRC-5 ($IC_{50} 127.3 \pm 7.3 \mu\text{M}$) [21]. This suggests that Roy-OA nano assembly may act as a strategy to vehiculate the cytotoxic Roy. This type of strategy can allow the release of the parent drug *in vivo*, enhancing the stability and selectivity of targeted cells, eliminating the side effects, and overcomes discomfort scents of drugs. In addition, it increases drug loading efficiency and avoids the large use of excipients [8].

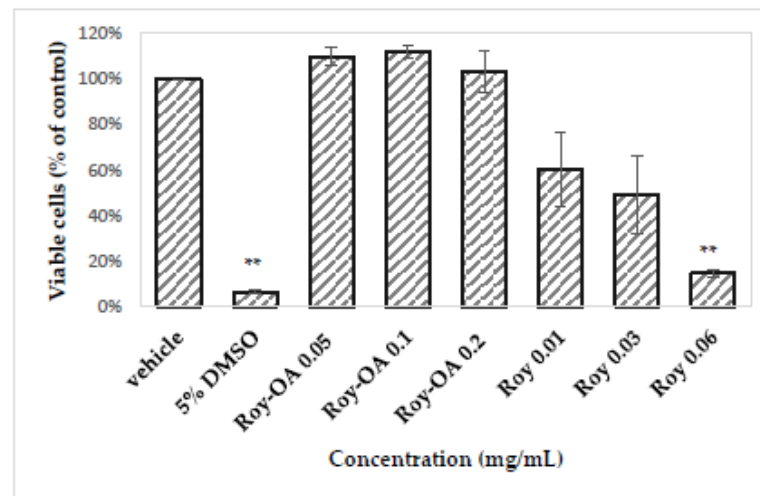


Figure 8. Cell viability was assessed on Vero-E6 cells by MTT. Results are represented as percentage of viable cells for each condition, compared to control. Statistical analysis was performed using Student's t-test for comparison between groups. **p-value <0.001.

3. Materials and Methods

3.1. Plant Material

The plant material (Figure 9), *Plectranthus madagascariensis* Benth. and *P. hadiensis* (Forssk.) Schweinf. ex Sprenger, was cultivated in Parque Botânico da Tapada da Ajuda (Instituto Superior de Agronomia, Lisbon, Portugal) from cuttings obtained from the Kirstenbosch National Botanical Garden (Cape Town, South Africa). Whole plants were collected between 2007 and 2008, always in June and September. They were deposited in the Herbarium “João de Carvalho e Vasconcelos” of the Instituto Superior de Agronomia, Lisboa (LISI), Portugal under the Voucher number 841/2007 for *P. madagascariensis* Benth and 833/2007 and 438/2010/ for *P. hadiensis*. The plant names were verified with the Plant List [22].

The extraction and isolation processes of 1 and 3 were performed according to Ntungwe *et al.*, 2021 [16], and Garcia C. *et al.*, 2018 [20], respectively. Briefly, 46.86 ± 3.51 g of dried *P. madagascariensis* was submerged in 1 L of distilled water and then submitted to hydrodistillations using a Clevenger apparatus (steam distillation) to obtain the essential oils (EOS). *P. hadiensis* extract was obtained by the ultra-sonication method, adding 30 mL of acetone to 3 g of ground dry plants sonicated for 1 h, and filtered (Whatman No 5 paper, Inc., Clifton, NJ, USA). All extractions were performed in triplicate, and the solvent was further evaporated to dryness at 40 °C on a rotary evaporator (Sigma-Aldrich, IKA HBR 4 basic heating bath, Essen, Germany).

The EOs from *P. madagascariensis* were fractionated by dry-column flash chromatography on high-purity-grade silica gel 60 (1.09385.1000; 230–400 mesh; Merck KGaA 64271 Darmstadt, Germany), with eluent of increasing polarity of *n*-hexane–EtOAc (9:1). DHR was purified by recrystallization with methanol. *P. hadiensis* extract was fractionated by normal phase column chromatography over silica gel using mixtures of *n*-hexane–EtOAc (8: 2) as eluents. Roy was obtained using preparative thin-layer chromatography (*n*-hexane/AcOEt 7:3) on pre-coated TLC sheets (Merck 7747, Darmstadt, Germany).

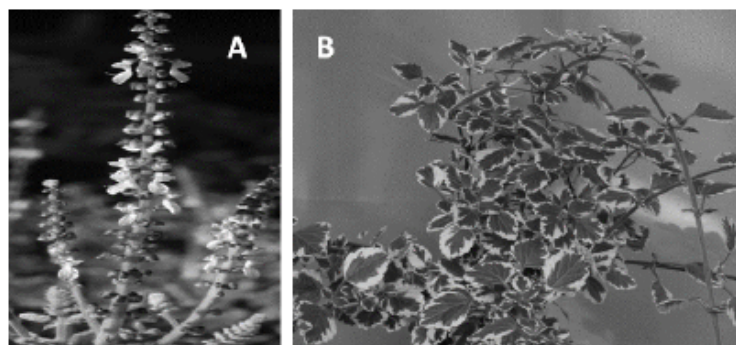


Figure 9. Illustration of *P. haitiensis* (A) and *P. madagascariensis* (B) adapted from van Jaarsveld and Thomas, 2006 [23].

3.2. Reaction Procedure

In the hemisynthetic study, the derivative (2) 7α -acetoxy- 6β -hydroxy-12-benzoyloxyroyleanone (12BzRoy) was successfully prepared from the lead molecule 1 obtained on the more reactive 12-OH by benzylation reaction (Scheme 1). The reactions, purification, identification, and stability of royleanone derivatives were carried out and previously reported in the study of Garcia *et al.*, 2020 [11].

3.3. Hemisynthesis of Drug Conjugates for Self-assembly Nanoparticles

7α -Acetoxy- 6β -hydroxyroyleanone (1), 7α -acetoxy- 6β -hydroxy-12-benzoyloxyroyleanone (2), and 6,7-dehydroroyleanone (3) were used as lead molecules in this study to prepare conjugate compounds using squalene, oleic acid, and 1-bromododecane as self-assembly inducers exploiting different methodologies.

3.3.1. Synthesis of Drug Conjugates using Squalene as a Self-assembly Inducer [7]

For the general procedure, 1-ethyl-3-(3-dimethylaminopropyl) carbodiimide hydrochloride (EDC-HCl, 0.06 mmol, VWR) and 4-dimethylaminopyridine (DMAP, 0.03 mmol, VWR) were added to a solution of squalene linker (0.04 mmol), in dry CH_2Cl_2 (1 mL, Sigma). The lead molecule (0.04 mmol) was added, and the reaction mixture was stirred at room temperature for 3–96 h. HCl 1 M (15 mL) was added and extracted with CH_2Cl_2 (5×5 mL). The organic layers were dried over Na_2SO_4 , and the solvent was removed under reduced pressure. The crude was purified by semi-preparative TLC (AcOEt/Hex). Scheme 2–3

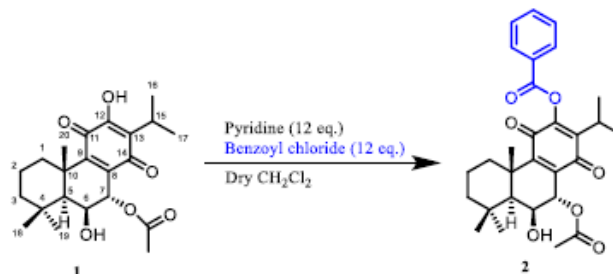
3.3.2. Synthesis of Drug Conjugates using Oleic Acid as a Self-assembly Inducer [6]

The lead molecule (82 mmol, 1 eq) was dissolved in anhydrous methylene chloride (1 mL), and then oleic acid (82 mmol, 1 eq), DMAP (1 eq, 82 mmol, VWR), and dicyclohexylcarbodiimide (DCC, 2 Eq 164 mmol, VWR) were added. The reaction mixture was stirred at ambient temperature for 12 h. After filtering, the filtrate was diluted with diethyl ether, and then the mixture was washed with 5% aqueous hydrochloric acid, water, and saturated aqueous sodium chloride. The filtrate was evaporated, and then the residue was thoroughly dried under a vacuum to get the conjugate. Scheme 2,3.

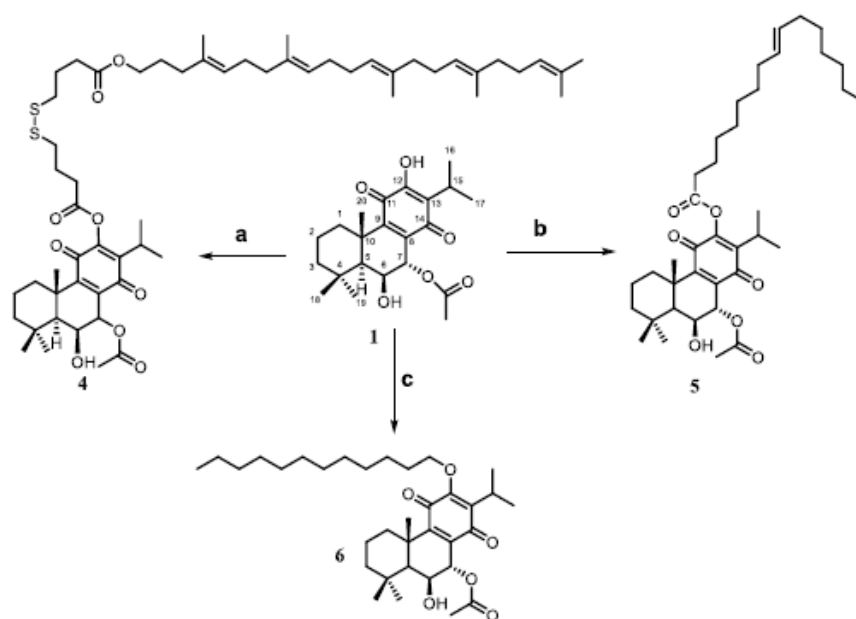
3.3.3. Synthesis of Roy-dodecane Conjugate using 1-bromododecane as Self-assembly Inducer [14]

A bromoalkane was coupled to Roy by $\text{S}_{\text{N}}2$ substitution. NaH (60% in mineral oil, 1.068 mg, 3 Eq, Sigma) was suspended in dry THF (1.5 mL, Sigma) in a three-necked flask, at 0 °C, and under argon atmosphere. A solution of Roy (10 mg, 1 eq) in dry THF was added dropwise, keeping the temperature below 0 °C. The reaction mixture was stirred

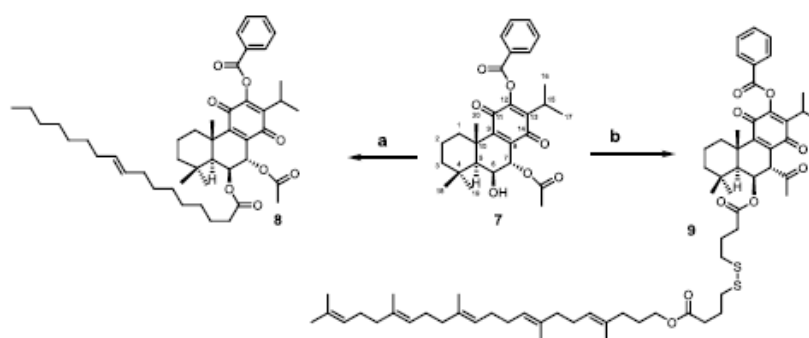
for 30 min at 0 °C and then for 20 min 25at ambient temperature. After cooling again to 0 °C, a solution of 1-bromododecane (17.82 μL, 3 eq) in dry THF (1 mL) was slowly added. The mixture was stirred at ambient temperature overnight, heated on steam. Scheme 2



Scheme 1. Reactions scheme for the synthesis of compound 2.



Scheme 2. Conjugation of 7α-acetoxy-6β-hydroxyroyleanone with self-assembly inducers: a = squalene-type chain using a labile linker, DMAP, EDC.HCL, dry CH₂Cl₂; b = oleic acid, DMAP, DCC, dry CH₂Cl₂; c = 1-bromododecane, NaH, dry THF. The reaction conditions are reported in the experimental section.



Scheme 3. Conjugation of 7 α -acetoxy-6 β -12benzyloxyroyleanone with self-assembly inducers: d = oleic acid, DMAP, DCC, dry CH₂Cl₂; e = squalene-type chain using a labile linker, DMAP, EDC.HCL, dry CH₂Cl₂. The reaction conditions are reported in the experimental section.

3.4. Characterization of Synthesized Molecules

The structures of the final product were characterized by 1D and 2D-NMR. The ¹H NMR spectra of 12BzRoy-Sq, Roy-OA, and Roy-Sq were recorded on a Bruker 300 MHz NMR spectrometer and ¹³C, HSQC, and HMBC at 100 MHz at room temperature on a Bruker® Biospin Fourier spectrometer at the Faculty of Pharmacy of the University of Lisbon. The chemical shifts (δ , ppm) were reported relative to the residual solvent peak, CDCl₃ (δ , ppm), (Aldrich 99.80%, <0.01% H₂O), 7.26 [1H] and 77.16 ppm [¹³C].

3.4.1. 12 BzRoy-Squalene conjugate

Yellow solid, yield 20.4%. ¹H NMR (300 MHz, CDCl₃) δ : 8.01 (s, 1H, H-1'), 7.98 (s, 1H, H-2'), 7.75 (s, 2H, H-6'), 7.72 (s, 1H, H-4'), 5.30 (s, 1H, H-7 β), 4.28–4.16 (m, 2H, 6 β , Sq) *, 3.48 (d, J = 7.1 Hz, 1H, Sq), 3.36 (sept, J = 7.1 Hz, 1H, H-15), 3.25 (t, J = 6.4 Hz, 2H, Sq), 2.19 (d, J = 1.9 Hz, 1H, Sq), 2.17 (s, 1H, Sq), 1.89–1.78 (m, 2H, H-2 β , H-1 β) *, 1.71–1.63 (m, 2H, H-2 α , H-3) *, 1.60 (s, 10H, Sq) *, 1.33 (s, 1H, H-5), 1.31 (s, 10H, Sq) *, 1.29 (s, 3H, Me-17), 1.28 (s, 2H, Me-16), 1.27 (s, 3H, Me-19), 1.25 (s, 10H, Sq) *, 0.95 (s, 3H, Me-18) *, 0.07 (s, 3H). * Overlapped signals

¹³C NMR (101 MHz, CDCl₃) δ : 184.32 (C-12), 183.40 (OCO-Bz), 153.20 (C-2'), 152.99 (C-14), 152.59 (C-6'), 146.65 (C-13), 140.67 (C-9), 138.61 (C-8), 136.31 (Sq), 133.21 (-4'), 126.25 (6OCO-Sq), 126.08 (C-5'), 125.81 (C-3'), 121.55 (Sq), 114.22 (-CO-Sq), 61.40 (C-7), 37.77 (C-18), 37.68 (Sq), 34.63 (C-4), 31.92 (Sq), 31.84 (C-3), 31.58 (Sq), 31.33 (Sq), 30.32 (Sq), 30.07 (Sq), 29.85 (Sq), 24.19 (C-15), 22.65 (C-19), 19.77 (C-17), 19.58 (C-16).

3.4.2. Roy-Oleic acid conjugate

Yellow solid, yield 90.9%. ¹H NMR (400 MHz, CDCl₃) δ : 5.64 (s, 1H, H-7 β), 5.35 (s, 1H, OA-CH=CH), 4.31 (s, 1H, H-6 α), 3.17 (Sept, 1H, H-15), 2.60 (q, J = 7.0, 6.5 Hz, 2H, OCO(CH₂CH₂, OA) *, 2.50–2.59 (m, J = 11.7 Hz, H-2 α , H-1 β), 2.31–2.33 (d, J = 7.6 Hz, OCO(CH₂), 2.19 (1H, s, OH-6 β), 2.09–1.95 (m, 8H, OCOCH₃, H-3 α) *, 1.77 (s, 1H, H-2 β), 1.62 (s, 3H, Me-20), 1.35 (H-5 α), 1.33 (s, 11H, OA) *, 1.23–1.20 (m, 12H, Me-17, Me-16, Me-19) *, 1.19 (s, 3H, OA), 0.94 (s, 3H, Me-19), 0.88 (s, 3H, Me-OA). *Overlapped signals

¹³C NMR (101 MHz, CDCl₃) δ : 185.39 (C-14), 175.95 (C-11), 171.11 (OCO(CH₂n), 169.70 (OCOCH₃), 152.93 (C-9), 149.75 (C-12), 139.43 (C-13), 135.65 (C-8), 68.89 (C-7), 67.39 (C-6), 49.84 (C-5), 42.34 (C-4), 39.05 (C-10), 33.88, (C-1), 33.59, (C-18), 31.35 (C-3), 27.31 (C-Oleic acid), 25.23 (C-15), 24.48 (C-2), 22.82 (C-19), 21.70 (C-20), 20.64 (C-16), 20.51 (OCOCH₃), 20.23 (C-17).

3.5. Preparation of Self-assembled Nanoparticles

Self-assembled nanoparticles were prepared by the solvent displacement method. The drug-linker conjugate was dissolved in appropriate amount acetone to give a yellow

solution of 4.0 mM in the drug. Nanoprecipitation was then induced by adding the solution dropwise and under stirring (400 rpm) to Milli-Q water (Sigma), without surfactant addition to a final concentration of 2.0 mM. The organic solvent was removed under reduced pressure, at 313 K. The turbid yellow suspension containing the nanoassemblies was stored in the dark, at 4 °C.

3.6. Physical-chemical and Morphological Characterization of Self-assembly Nanoparticles

3.6.1. Fourier Transform Infrared Spectroscopy (FTIR)

FTIR of derivatives 5 and 7 were evaluated by FTIR in a PerkinElmer® Spectrum 400 (PerkinElmer Inc, Waltham, MA, USA) equipped with an attenuated total reflectance (ATR) device. The ATR system was cleaned before each analysis by using dry paper and scrubbing it with methanol and water (50:50). The room air FTIR-ATR spectrum was used as background to verify the cleanliness and to evaluate the instrumental conditions and room interferences due to H₂O and CO₂. The spectra were obtained collecting 100 scans of each sample, between 4000 and 600 cm⁻¹, with a resolution of 4 cm⁻¹.

3.6.2. Dynamic Light Scattering (DLS)

Physical characterization of the nanoparticles in suspension was carried out by evaluation of mean particle size, polydispersity index (PDI), and surface charge (zeta potential) by DLS and electrophoretic mobility in a Malvern Zetasizer Nano S (Malvern Instruments, Worcestershire, UK). Experiments were conducted in triplicate. Results were expressed as the mean ± SD (*n* = 3).

3.6.3. Scanning Electron Microscopy (SEM) analysis

The morphology of the self-assembled nanoparticles was analyzed with a JEOL-JSM7001F scanning electron microscope (SEM) at a voltage of 25 kV. The conductivity of the NP particle assemblies was increased by adding a thin coating of conductive gold/palladium (Polaron E-5100).

3.7. *In vitro* Release Studies

The release pattern of Roy from Roy-OA NP was studied *in vitro*. Briefly, the self-assembled NPs were dissolved in 30 mL of PBS at approximately blood pH (pH 7.4, European Pharmacopoeia 7.0) under constant stirring (200 rpm) using a multi-position magnetic stirrer with heater RT series, 15, RT 15, IKA, to simulate the *in vivo* conditions [24]. Although the Roy-OA conjugate could self-assemble into NPs in Milli-Q water without any surfactant, this nanoassembly showed poor stability in PBS due to the highly hydrophobic surface. To address this issue, a small amount of Tween 80, 100 µL (Sigma-Aldrich), was added to prepare NPs for improved solubility. At appropriate time intervals, aliquots of the release medium were collected from three different points of the dissolution medium, to ensure a homogenous collection of the sample. Nanoparticles were isolated from the supernatant by centrifugation (7,000 rpm for 7 min). The amount of Roy collected from the *in vitro* release medium, at each time point, was determined by HPLC (Agilent Technologies 1260 Infinity II Series system with diode array detector (DAD; Agilent, Santa Clara, CA, USA and ChemStation Software (Hewlett-Packard, Alto Palo, CA, USA).

The mobile phase consisted of a mixture of methanol (A), acetonitrile (B), and 0.3% trifluoroacetic acid in water (C) used as follows: 0 min, 15% A, 5% B, and 80% C; 2 min, 70% A, 30% B, and 0% C; 10 min, 70% A, 30% B, and 0% C; and 15 min, 15% A, 5% B, and 80% C. The time of analysis was 15 min, including the stabilization of the RP-18 column (Eclipse XDB-C18, 250 × 4.0 mm i.d., 5 µm) column, from Merck. The injection volume was 20 µL, the flow rate was set at 1 mL/min, and the detection wavelength was 270 nm. Roy identification was based on the comparison of retention time and ultraviolet (UV)

spectra overlay with authentic standards. The assay was conducted for 72 h ($n = 3$, mean \pm SD).

3.8. Preliminary Toxicity Assay

The Brine shrimp lethality assay (BSLA) is a benchtop assay used for the preliminary toxicity evaluation. The experiment was carried out using the method described by Epole *et al.*, 2020 [25]. Brine shrimp eggs were obtained from JBL GmbH and Co. KG (Neuhofen, Germany). Briefly, *Artemia salina* cysts (brine shrimp eggs) were allowed to hatch in natural seawater, containing 35 g/L salts under constant aeration and illumination to ensure survival and maturity before use. Ten to fifteen nauplii were collected with the aid of a pipette and added to a 24-well plate. Drug conjugates and NPs were added to the corresponding wells, and the plate was stored for 24 h at 25 °C. Tests were carried out in triplicate. The negative control consisted of ten to fifteen nauplii per well in seawater without test samples, while $K_2Cr_2O_7$ was used as the positive control. After the 24 h incubation, the number of dead nauplii in each well was recorded using a microscope. Larvae were considered dead after 5 s of no movement. Death was induced on the rest of the nauplii using $K_2Cr_2O_7$ at 1 mg/mL, and the total nauplii in each well was determined. After 24 h, all dead larvae were counted, and the mortality rate (%) was determined according to equation 1. Results were analyzed using GraphPad Prism version 5.00 for Windows, GraphPad Software, San Diego, CA, USA, www.graphpad.com, accessed on 5 February 2021. The results were expressed as the mean value \pm SD, and a probability level $p < 0.05$ was considered to indicate statistical significance.

$$\text{Mortality Rate (\%)} = \frac{\text{Total Asalina-Living Asalina}}{\text{Total Asalina}} \times 100 \quad (1)$$

3.9. Cytotoxicity Study

3.9.1. Cell Culture

The Vero-E6 cells line, representative of nontumor-like kidney cells, was obtained from ATCC (Manassas, VA, USA). Cells were cultured in DMEM supplemented with 10% fetal bovine serum, 100 U/mL penicillin, and 0.1 mg/mL streptomycin. The cultures were maintained at 37 °C under a humidified atmosphere containing 5% CO_2 .

3.9.2. Cell Viability

Cell Viability was determined by the MTT assay and is based on the reduction of 3-(4, 5-dimethyl-2-thiazolyl)-2,5-diphenyl-2H-tetrazolium bromide into formazan dye by active mitochondria of living cells. The effect of Roy and its NPs on cell viability was assessed. Briefly, 6.0×10^3 Vero-E6 cells were cultured in 190 μ L of complete medium in 96-well plates. Cells were grown for 24 h at 37 °C, 5 % CO_2 , and then exposed to different concentrations of Roy (13.75, 27.5 and 55 μ M) and NPs (0.05, 0.1 and 0.2 μ M) for 24 h. MTT reduction assay was performed as previously described by Fernandes *et al.* [26]. Each condition was tested in four replicates of two independent experiments.

3.10. Statistical Analysis

The results were expressed as the mean value \pm SD. Comparisons were performed within groups using the Student's t-test. Significant differences between control and experimental groups were assessed using GraphPad Prism version 5.00 for Windows, GraphPad Software, San Diego, CA, USA, www.graphpad.com, accessed on 5 February 2021. A probability level $**p < 0.01$ was considered to indicate statistical significance.

4. Conclusions

In this study, the cytotoxic diterpenoids Roy, 12BzRoy, and DHR were explored as lead molecules for the hemi-synthesis of drug-linker conjugates. Using squalene, oleic

acid, and 1-bromododecane as inducers, derivatives 5, 7, and 9 from squalene and oleic acid linkers were successfully prepared and confirmed by 1D- and 2D-NMR. Products 4 and 8 were synthesized; however, they were highly unstable. Nano assemblies of 5 and 9 were successfully characterized, and the cytotoxicity of 5 NPs was studied. Compound 5 and its corresponding NPs were tested against the nontumor-like kidney cell lines. The results revealed that 5-NPs may be used as a strategy to deliver Roy, thereby increasing the water solubility using it as a suspension of self-assembly nanoparticles of Roy. The *in vitro* release profile of Roy in 5-NPs showed a delay on the release, which can be important issue for a potential therapeutic application of Roy.

Supplementary Materials: The following are available online at www.mdpi.com/article/10.3390/ijms221910210/s1, Figure S1: ¹H NMR for 12BzRoy-Sq (7), Figure S2: ¹H NMR for Roy-OA (5).

Author Contributions: Conceptualization, P.R.; methodology, E.N., E.M.D.-M., G.B., E.C.; C.G.; I.G.; M.M.A.; validation, L.S., A.M.D.-L., and P.R.; investigation, E.N., E.M.D.-M., E.C.; writing—original draft preparation, E.N.; writing—review and editing, L.S., A.M.D.-L., A.R., C.P.R.; D.P.; P.R.; supervision, L.S., A.M.D.-L., P.R.; All authors have read and agreed to the published version of the manuscript.

Funding: This research was funded by Fundação para a Ciência e Tecnologia (FCT) projects UIDB/04567/2020, UIDP/04567/2020, UIDB/50006/2020, UID/MULTI/04378/2013, UID/DTP/04138/2020 and UIDB/00100/2020, and INSTITUTO LUSÓFONO DE INVESTIGAÇÃO E DESENVOLVIMENTO (ILIND) for the project COFAC/ILIND/CBIOS/1/2020. The authors gratefully acknowledge Fundação para a Ciência e Tecnologia (FCT) for the financial support grant under the reference 2020.07813.BD and ID/DTP/O4567/2019-CBIOS/BI, SFRH/BD/147306/2019 and ILIND for the financial support grant PADDIC 2019 (ALIES-COFAC) as part of the PhD Program in Health Sciences from Universidad de Alcalá and Universidade Lusófona de Humanidades e Tecnologias.

Institutional Review Board Statement: Not applicable.

Informed Consent Statement: Not applicable.

Acknowledgments: The authors are grateful to Tânia Ferreira-Gonçalves (FCT reference SFRH/BD/147306/2019) for her help in particle size and zeta potential measurements.

Conflicts of Interest: The authors declare no conflict of interest.

References

- Jahangirian, H.; Lemraski, E.G.; Webster, T.J.; Rafiee-Moghaddam, R.; Abdollahi, Y. A review of drug delivery systems based on nanotechnology and green chemistry: Green nanomedicine. *Int. J. Nanomed.* **2017**, *12*, 2957–2978, doi:10.2147/IJN.S127683.
- Liu, J.; Zhang, R.; Xu, Z.P. Nanoparticle-Based Nanomedicines to Promote Cancer Immunotherapy: Recent Advances and Future Directions. *Small* **2019**, *15*, 1–21, doi:10.1002/smll.201900262.
- El-Readi, M.Z.; Althubiti, M.A. Cancer Nanomedicine: A New Era of Successful Targeted Therapy. *J. Nanomater.* **2019**, *2019*, doi:10.1155/2019/4927312.
- Sim, T.; Lim, C.; Hoang, N.H.; Joo, H.; Lee, J.W.; Kim, D. won; Lee, E.S.; Youn, Y.S.; Kim, J.O.; Oh, K.T. Nanomedicines for oral administration based on diverse nanoplatform. *J. Pharm. Investig.* **2016**, *46*, 351–362, doi:10.1007/s40005-016-0255-y.
- Wang, H.; Lu, Z.; Wang, L.; Guo, T.; Wu, J.; Wan, J.; Zhou, L.; Li, H.; Li, Z.; Jiang, D.; et al. New generation nanomedicines constructed from self-assembling small-molecule prodrugs alleviate cancer drug toxicity. *Cancer Res.* **2017**, *77*, 6963–6974, doi:10.1158/0008-5472.CAN-17-0984.
- Zhong, T.; Yao, X.; Zhang, S.; Guo, Y.; Duan, X.C.; Ren, W.; Dan, H.; Yin, Y.F.; Zhang, X. A self-assembling nanomedicine of conjugated linoleic acid-paclitaxel conjugate (CLA-PTX) with higher drug loading and carrier-free characteristic. *Sci. Rep.* **2016**, *6*, doi:10.1038/srep36614.
- Fumagalli, G.; Christodoulou, M.S.; Riva, B.; Revuelta, I.; Marucci, C.; Collico, V.; Prosperi, D.; Riva, S.; Perdicchia, D.; Bassarini, I.; et al. Self-assembled 4-(1,2-diphenylbut-1-en-1-yl)aniline based nanoparticles: Podophyllotoxin and aloin as building blocks. *Org. Biomol. Chem.* **2017**, *15*, 1106–1109, doi:10.1039/c6ob02591a.
- Li, M.; Zhao, L.; Zhang, T.; Shu, Y.; He, Z.; Ma, Y.; Liu, D.; Wang, Y. Redox-sensitive prodrug nanoassemblies based on linoleic acid-modified docetaxel to resist breast cancers. *Acta Pharm. Sin. B* **2019**, *9*, 421–432, doi:10.1016/j.apsb.2018.08.008.
- Borrelli, S.; Christodoulou, M.S.; Ficarra, I.; Silvani, A.; Cappelletti, G.; Cartelli, D.; Damia, G.; Ricci, F.; Zuchetti, M.; Dosio, F.; et al. New class of squalene-based releasable nanoassemblies of paclitaxel, podophyllotoxin, camptothecin and epothilone A. *Eur. J. Med. Chem.* **2014**, *85*, 179–190, doi:10.1016/j.ejmech.2014.07.035.

10. Hassanzadeh, P.; Atyabi, F.; Dinarvand, R. Linkers: The key elements for the creation of efficient nanotherapeutics. *J. Control. Release* **2018**, *270*, 260–267, doi:10.1016/j.jconrel.2017.12.007.
11. Garcia, C.; Isca, V.M.S.; Pereira, F.; Monteiro, C.M.; Ntungwe, E.; Sousa, F.; Dinic, J.; Holmstedt, S.; Roberto, A.; Diaz-Lanza, A.; et al. Royleanone Derivatives From *Plectranthus* spp. as a Novel Class of P-Glycoprotein Inhibitors. *Front. Pharmacol.* **2020**, *11*, 1711.
12. Ulbrich, K.; Vladimir, S.; Bakandritsos, A. Targeted Drug Delivery with Polymers and Magnetic Nanoparticles: Covalent and Noncovalent Approaches, Release Control, and Clinical Studies. *Chem. Rev.* **2016**, *116*, 5338–5431, doi:10.1021/acs.chemrev.5b00589.
13. Dosio, F.; Reddy, L.H.; Ferrero, A.; Stella, B.; Cattel, L.; Couvreur, P. Novel nanoassemblies composed of squalenoyl-paclitaxel derivatives: Synthesis, characterization, and biological evaluation. *Bioconjug. Chem.* **2010**, *21*, 1349–1361, doi:10.1021/bc100154g.
14. Bisi, A.; Mokhtar Mahmoud, A.; Allarà, M.; Naldi, M.; Belluti, F.; Gobbi, S.; Ligresti, A.; Rampa, A. Polycyclic Maleimide-based Scaffold as New Privileged Structure for Navigating the Cannabinoid System Opportunities. *ACS Med. Chem. Lett.* **2019**, *10*, 596–600, doi:10.1021/acsmchemlett.8b00594.
15. Luo, C.; Sun, J.; Liu, D.; Sun, B.; Miao, L.; Musetti, S.; Li, J.; Han, X.; Du, Y.; Li, L.; et al. Self-Assembled Redox Dual-Responsive Prodrug-Nanosystem Formed by Single Thioether-Bridged Paclitaxel-Fatty Acid Conjugate for Cancer Chemotherapy. *Nano Lett.* **2016**, *16*, 5401–5408, doi:10.1021/acs.nanolett.6b01632.
16. Ntungwe, E.; Mar, E.; Teod, C.; Teixid, S.; Capote, N.A.; Saraiva, L.; Mar, A. Preliminary Biological Activity Screening of *Plectranthus* spp. Extracts for the Search of Anticancer Lead Molecules. *Pharmaceuticals* **2021**, *14*, 1–11.
17. Bernardes, C.E.S.; Garcia, C.; Pereira, F.; Mota, J.; Pereira, P.; Cebola, M.J.; Reis, C.P.; Correia, I.; Piedade, M.F.M.; Minas Da Piedade, M.E.; et al. Extraction Optimization and Structural and Thermal Characterization of the Antimicrobial Abietane 7 α -Acetoxy-6 β -hydroxyroyleanone. *Mol. Pharm.* **2018**, *15*, 1412–1419, doi:10.1021/acs.molpharmaceut.7b00892.
18. Matias, D.; Nicolai, M.; Saraiva, L.; Pinheiro, R.; Faustino, C.; Diaz Lanza, A.; Pinto Reis, C.; Stankovic, T.; Dinic, J.; Pesic, M.; et al. Cytotoxic Activity of Royleanone Diterpenes from *Plectranthus madagascariensis* Benth. *ACS Omega* **2019**, *4*, 8094–8103, doi:10.1021/acsomega.9b00512.
19. Isca, V.M.S.; Ferreira, R.J.; Garcia, C.; Monteiro, C.M.; Dinic, J.; Holmstedt, S.; André, V.; Pesic, M.; Dos Santos, D.J.V.A.; Candeias, N.R.; et al. Molecular Docking Studies of Royleanone Diterpenoids from *Plectranthus* spp. as P-Glycoprotein Inhibitors. *ACS Med. Chem. Lett.* **2020**, *11*, 839–845, doi:10.1021/acsmchemlett.9b00642.
20. Garcia, C.; Silva, C.O.; Monteiro, C.M.; Nicolai, M.; Viana, A.; Andrade, J.M.; Barasoain, I.; Stankovic, T.; Quintana, J.; Hernández, I.; et al. Anticancer properties of the abietane diterpene 6,7-dehydroroyleanone obtained by optimized extraction. *Future Med. Chem.* **2018**, *1*, 1177–1189, doi:10.4155/fmc-2017-0239.
21. Gonçalves Garcia, C.A. Isolation, Synthesis and Nanoencapsulation of Cytotoxic Compounds from *Plectranthus* spp. Ph.D. Thesis, Universidad de Alcalá, Alcalá de Henares, Madrid, 2019.
22. The Plant List. Version 1.1. 2013. Available online: <http://www.theplantlist.org/> (accessed on 1 January 2021)
23. Ernst van Jaarsveld, *The Southern African Plectranthus and the art of turning shade to glade*, 1st Edition, Fernwood press, South Africa, 2006.
24. Silva, C.O.; Molpeceres, J.; Batanero, B.; Fernandes, A.S.; Saraiva, N.; Costa, J.G.; Rijo, P.; Figueiredo, I.V.; Faisca, P.; Reis, C.P. Functionalized diterpene parvifloron D-loaded hybrid nanoparticles for targeted delivery in melanoma therapy. *Ther. Deliv.* **2016**, *7*, 521–544, doi:10.4155/tde-2016-0027.
25. Ntungwe, N., E.; Domínguez-Martín, E.M.; Roberto, A.; Tavares, J.; Isca, V.M.S.; Pereira, P.; Cebola, M.-J.; Rijo, P. Artemia species: An Important Tool to Screen General Toxicity Samples. *Curr. Pharm. Des.* **2020**, *26*, 2892–2908, doi:10.2174/1381612826666200406083035.
26. Fernandes, A.S.; Gaspar, J.; Cabral, M.F.; Rueff, J.; Castro, M.; Batinic-Haberle, I.; Costa, J.; Oliveira, N.G. Protective role of ortho-substituted Mn(III) N-alkylpyridylporphyrins against the oxidative injury induced by tert-butylhydroperoxide. *Free Radic. Res.* **2010**, *44*, 430–440, doi:10.3109/10715760903555844.

CONCLUSIONS

In this study, sixteen plants from the *Plectranthus* genus (**Table III. 1**) often used as traditional medicines for the treatment of various illnesses, including respiratory, digestive, and liver ailments were selected. The acetone extracts of these *Plectranthus* species were done by ultrasound-assisted extraction and were screened for their antioxidant, antimicrobial, and general toxicity bioactivities. Five most bioactive extracts (*P. mutabilis*, *P. swynnertonii*, *P. hadiensis*, *P. ciliatus*, and *P. cylindraceus*) were selected and tested in three different cancer cell lines, colon colorectal carcinoma (HCT116), human breast adenocarcinoma (MCF-7), and lung cancer carcinoma (NCI-H460). *P. mutabilis*, and *P. hadiensis* were the most bioactive and the compounds that may be responsible for their biological activity determined.

P. hadiensis acetone extract was briefly profiled by HPLC-DAD and revealed 7-acetoxy-6-hydroxyroyleanone (Roy) to be the major compound in the extract. Roy was isolated from this extract and its biological activity determined. Its cytotoxicity against the more aggressive MDA-MB-231S cancer cell lines reveals that Roy was approximately 12 times more cytotoxic than *P. hadiensis* extract. These results indicate that Roy could be a prospective starting point for the development of anticancer drugs.

The phytochemical study of the second most bioactive *P. mutabilis* extract, with limited information in the literature was studied. This extract was subjected to different chromatographic techniques leading to the isolation of three known abietane diterpenes (coleon-U-quinone (**2**), 8 α ,9 α -epoxycoleon-U-quinone (**3**) and coleon U (**4**)) and one new nor-abietane (+)-5*S*,10*R*-10,11,12-trihydroxy-6,7-dioxo-20-norabieta-8,11,13-triene, given the common name mutabilol). The structures of these compounds were elucidated using different spectroscopic techniques and HRMS. In addition, the results from HPLC-MS/MS showed an additional peak which based on its m/z and fragmentation pattern was tentatively identified as 12-O-acetylcoleon-U-quinone (**5**).

The HPLC profile of *P. mutabilis* extract was also done and each of the isolated compounds quantified. The cytotoxicity of Compounds **2–4** was done against NCI-H460, its multidrug resistant variant overexpressed with P-gp NCI-H460/R and normal MRC-5 cell lines.

Compounds **2-4** were selective towards the cancer cell lines and were not substrates for P-gp as they inhibited P-gp activity in NCI-H460/R cells at longer exposure of 72 h. They

also showed the ability to regress doxorubicin (DOX) resistance in subsequent combined treatment. Compound **1** was inactive against all three cell lines in the range of concentrations (2 to 50 μ M) tested. Most importantly, none of the isolated compounds suborned to P-gp expression in NCI-H460/R cells, while the extract remarkably increased it.

The cytotoxicity of Roy previously isolated from *P. hadiensis* and its derivative 7 α -acetoxy-6 β -benzoyloxyroyleanone (12BzRoy) with improved bioactivity were further employed in the last chapter of this work. These compounds have a very low aqueous solubility and therefore there was a need to address this problem. Self-assembled nanoparticles were thus prepared with the help squalene, oleic acid and 1-bromododecane as linkers able to self-assemble in water. The nanoparticles from Roy-oleic acid (Roy-OA) were the most promising and were characterized based on size, Pdl, zeta potential and morphology. The size of the Roy-OA NP was confirmed by the SEM \sim 100nm. Roy release profile from the Roy-OA nano assemblies was determined and only small amount of Roy was released (7.99%). The bioactivity of the Roy-OA nanoparticles and Roy was evaluated using the *Artemia salina* model. These NPs had no toxicity against this model and thus the Roy-OA NP could act as a prodrug to release the cytotoxic Roy.

Our study identified abietane diterpenoids from *P. mutabilis* that can evade MDR in cancer cells and inhibit P-gp activity in prolonged treatment. Also, Roy-OA nano assemblies were successfully prepared, characterized and this method has proven to be effective in increasing the solubility of Roy in aqueous solvents.

ANNEXES

General Toxicity screening of Royleanone derivatives using an *Artemia salina* model

Avaliação da toxicidade geral de derivados de Roileanonas pelo ensaio de letalidade de Artemia salina

Epole Ntungwe^{1,2}, Vera M. S. Isca^{1,3}, Ana María Díaz-Lanza², Carlos A. M. Afonso³, Patrícia Rijo^{1,3*}

¹CBIOS – Center Research for Biosciences & Health Technologies, Lisbon, Portugal

²Department of Biomedical Sciences, Faculty of Pharmacy, University of Alcalá, Spain

³Med.U.Lisboa, Faculdade de Farmácia da Universidade de Lisboa, Portugal

*corresponding author: patricia.rijo@ulusofona.pt

Abstract

Cancer is the second leading cause of death globally. World Health Organization recorded an estimated 9.6 million deaths attributed to cancer in 2018. There is an urgent need for new anticancer drugs with novel modes of action. Natural products remain a valuable source for the identification and development of novel treatment options for cancer. *Plectranthus* species are well-known medicinal species used extensively for the treatment of different illnesses. These species are rich in diterpenoids which are reported to be responsible for various pharmacological activities including cytotoxic activities. Brine shrimp (*Artemia salina*) is broadly used in lethality studies and this model is a convenient starting point for cytotoxicity study when screening for general toxicity of natural products. This assay is based on their ability to kill a laboratory cultured nauplii. In this work, we report the general toxicity of some derivatives from 6,7-dehydroroyleanone (1) and 7 α -acetoxi-6 β -hydroxyroyleanone (2) compounds. The *A. salina* bioassay is a simple, rapid, and low-cost test, and is very useful for preliminary assessment of general toxicity in natural products thereby guiding the determination of possible biological activities.

Keywords: *Artemia salina*, general toxicity, Royleanone, *Plectranthus*

Resumo

O cancro é a segunda principal causa de morte no mundo, A Organização Mundial da Saúde registou cerca de 9,6 milhões de mortes atribuídas ao cancro em 2018. Assim existe uma grande urgência por novos fármacos anticancerígenos. Os produtos naturais continuam a ser uma importante fonte para a identificação e desenvolvimento de novos tratamentos para o cancro. O género *Plectranthus* engloba espécies de plantas bem conhecidas pelas suas propriedades medicinais e amplamente utilizadas no tratamento de algumas doenças. Estas plantas são ricas em diterpenóides, compostos estes que apresentam diversas atividades farmacológicas interessantes, incluindo efeitos citotóxicos. O camarão marinho (*Artemia salina*) é amplamente utilizado em estudos de letalidade e é um ponto de partida vantajoso para a pesquisa de toxicidade geral de produtos naturais. Este ensaio é baseado na capacidade que os produtos naturais apresentam para matar náuplios criados em laboratório. Neste trabalho relatamos a toxicidade geral de alguns derivados preparados a partir dos compostos 6,7-dehidroileanona (1) e 7 α -acetoxi-6 β -hidroxiroileanona (2). O bioensaio de *A. salina* é um teste simples, rápido e de baixo custo, muito útil para a avaliação preliminar da toxicidade geral de produtos naturais, orientando assim para possíveis atividades biológicas.

Palavras-chave: *Artemia salina*, toxicidade geral, Roileanonas, *Plectranthus*

Received / Recabido: 23/02/2021
Accepted / Aceite: 20/04/2021
Electronic Edition: www.alies.pt

Introduction

During the past three decades, there has been significant progress in both the understanding and treatment of cancer. However, cancer remains the second leading cause of non-communicable disease deaths in the world. In 2018, there were over 18 million new cancer cases and approximately 10 million people died from the disease globally (1,2).

Medicinal plants are considered potential sources for drug development and many novel products. Natural products play a relevant role in cancer therapy today. Substantial numbers of anticancer agents used in the clinic are either natural or derived from natural products from various sources such as plants, animals, and microorganisms (also of marine origin) (3,4). During the last few decades, a wide range of cytotoxic agents were discovered from plants, and some of these are used as anti-cancer drugs. Paclitaxel (Taxol), for example, one of the most known chemotherapy drugs of natural origin, was derived from the bark of *Taxus brevifolia* and is one of the most active cancer chemotherapeutic drugs (5).

Artemia salina, commonly known as brine shrimp, is a tiny halophilic invertebrate belonging to the Phylum Arthropoda and Subphylum Crustacean, and play an important role in saline aquatic and marine ecosystems. In addition to usage as feedstuff in aquaculture, it is also highly valued for its larvae's application in toxicity detection (6). *A. salina* has gained popularity as a test organism for short-term toxicity testing because of its ease of culture, short generation time, and cosmopolitan distribution (7). In addition, its dormant brine shrimp eggs remain viable for many years and are therefore a suitable biological source (8). Other advantages of using brine shrimp in toxicity testing include (i) rapidity (i.e. 28–72 h from hatching to the first endpoint), (ii) cost-effectiveness, (iii) the availability of nauplii hatched from commercial durable cysts (eggs) (i.e., homogeneity of the population, availability all-year-round without the necessity of culturing) (9). Its use as a test organism is based on cellular mechanisms that may occur via necrosis, characterized by loss of membrane integrity, death of cell or apoptosis, a genetic program of controlled cell death (10). The significant correlation between the brine shrimp assay and *in vitro* growth inhibition of human solid tumor cell lines demonstrated by the National Cancer Institute (NCI, USA) further boosts the use of *A. salina* for general toxicity testing (11–14). This correlation is significant because it shows the value of this bioassay as a pre-

Introdução

Durante as últimas três décadas, houve um progresso significativo na compreensão e tratamento do cancro. No entanto, o cancro continua a ser a segunda causa de morte por doenças não transmissíveis no mundo. Em 2018, havia mais de 18 milhões de novos casos de cancro e aproximadamente 10 milhões de pessoas morreram da doença, em todo o mundo (1,2).

As plantas medicinais são importantes fontes de obtenção no desenvolvimento de novos medicamentos e produtos. Os produtos naturais desempenham um papel relevante no tratamento do cancro, com um número substancial de agentes anticancerígenos, de uso clínico atual, provenientes de origem natural ou derivados de produtos naturais, de várias fontes, como plantas, animais e microrganismos (também de origem marinha) (3,4). Durante as últimas décadas, uma vasta gama de agentes citotóxicos foi descoberta em plantas, alguns dos quais são utilizados atualmente no tratamento do cancro. O paclitaxel (Taxol), por exemplo, obtido a partir da casca de *Taxus brevifolia*, é um dos quimioterápicos mais conhecidos de origem natural em quimioterapia e dos mais ativos (5).

Artemia salina, popularmente conhecido como artémia, é um minúsculo invertebrado halófilo pertencente ao Filo Arthropoda e Subfilo Crustáceo, que desempenha um papel importante nos ecossistemas salinos aquáticos. Além do seu uso como alimento na aquicultura, também é altamente valorizado pelo seu uso de larvas na avaliação da toxicidade geral (6). O uso de *A. salina* ganhou ênfase em estudos de triagem de toxicidade, de curto prazo. Isso deve-se à sua facilidade de cultura, curto tempo de geração e distribuição cosmopolita (7). Além disso, os ovos de artémia permanecem viáveis por muitos anos e são, portanto, uma fonte biológica adequada (8). Outras vantagens do uso de artémia em testes de toxicidade incluem: (i) rapidez (ou seja, 28-72 h desde a eclosão do ovo até o primeiro ponto final); (ii) custo-benefício; (iii) a disponibilidade de náuplios nascidos de cistos duráveis comerciais (ovos) (ou seja, homogeneidade da população e disponibilidade durante todo o ano, sem a necessidade de cultivo) (9). O seu uso como organismo-teste é baseado em mecanismos celulares que podem ocorrer via necrose, caracterizada pela perda da integridade da membrana, morte celular ou apoptose, programa genético de morte celular controlada (10). O National Cancer Institute (NCI, EUA) evidenciou uma correlação significativa entre o ensaio de artémia e a inibição do crescimento *in vitro* de linhas de células tumorais sólidas humanas,

screening tool for antitumor drug research (15–17). In the present study, we evaluated the general toxicity of 6,7-dehydroroyleanone (1) and 7 α -acetoxy-6 β -hydroxyroyleanone (2) derivatives using the *A. salina* model.

Materials and Methods

Plant Material

The plant materials, *P. madagascarensis* Benth. and *P. grandidentatus* Gürke were cultivated in Parque Botânico da Tapada da Ajuda (Instituto Superior Agrário, Lisbon, Portugal) from cuttings obtained from the Kirstenbosch National Botanical Garden (Cape Town, South Africa). The extraction and isolation processes of compounds 1 and 2 (Figure 1) were performed according to Garcia C. et al., 2018 (19) and Bernardes C.E.S. et al, 2018 (20), respectively.

Reaction Procedures

The reactions, purification, identification, and stability of royleanone derivatives were carried out and previously reported in the study of Garcia et al. 2020 (21), Schemes 1 and 2.

o que apoia fortemente o uso do modelo de *A. salina* em testes de toxicidade geral (11–14). Isso é significativo porque mostra o valor deste bioensaio como uma ferramenta de pré-triagem para a pesquisa de fármacos antitumorais (15–18). No presente estudo, a toxicidade geral de dezassete derivados obtidos a partir de 6,7-dehidroroileanona (1) e de 7 α -acetoxi-6 β -hidroxiroileanona (2) foi avaliada no ensaio de letalidade de *A. salina*.

Materiais e Metodos

Material vegetal

As plantas *P. madagascarensis* Benth e *P. grandidentatus* Gürke foram cultivadas no Parque Botânico da Tapada da Ajuda (Instituto Superior Agrário, Lisbon, Portugal) a partir de estacas obtidas do *Kirstenbosch National Botanical Garden* (Cidade do Cabo, África do Sul). Os processos de isolamento e extração dos produtos naturais 1 e 2 (Figura 1) foram realizados segundo Garcia C. et al., 2018 (19) e Bernardes C.E.S. et al, 2018 (20), respetivamente.

Procedimentos das Reações

As reações e a purificação, identificação e estabilidade dos derivados de roileanona foram realizadas no estudo de Garcia et al. 2020 (21), Esquemas 1 e 2.

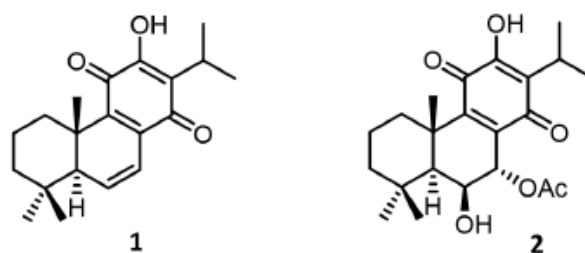
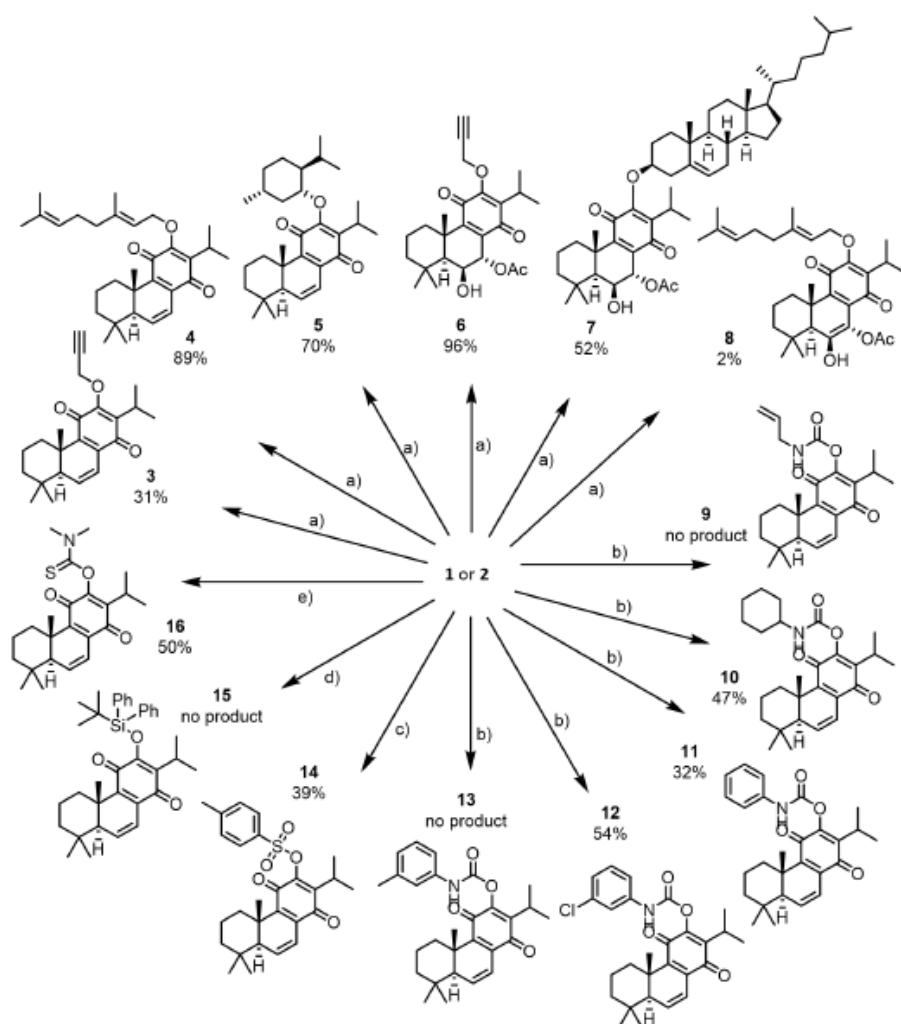
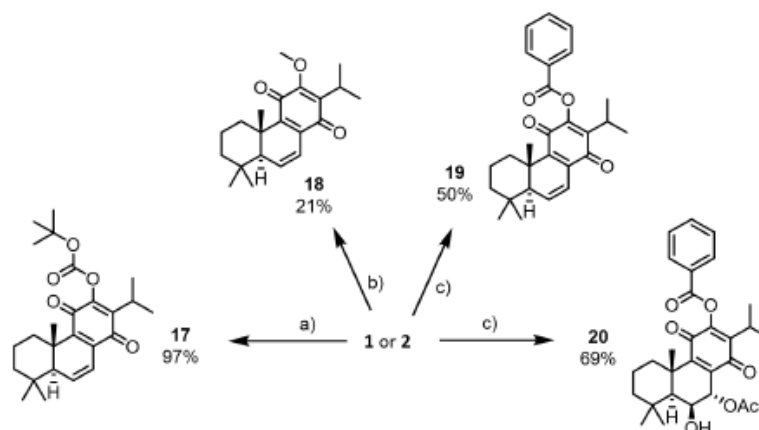


Figure 1 -6,7-dehydroroyleanone (1) and 7 α -acetoxy-6 β -hydroxyroyleanone (2)
Figura 1. 6,7-dehidroroileanona (1) e 7 α -acetoxi-6 β -hidroxiroileanona (2)



Scheme 1 - Reactions of natural products 1 and 2 that produce unstable derivatives: a) Triphenylphosphine (5 eq.), DIAD (5 eq.), corresponding alcohol (5 eq.), and dry THF, under atmosphere inert, derivatives 3 to 8; b) DMAP (5 eq.), corresponding isocyanate (in excess), and dry CH_2Cl_2 , under inert conditions, expected derivatives 9 to 13; c) triethylamine (4.5 eq.), DMAP (0.3 eq.), *p*-toluenesulfonyl chloride (3 eq.), and dry CH_2Cl_2 , derivative 14; d) imidazole (2 eq.), TBDPSCl (in excess), and dry CH_2Cl_2 , expected derivative 15; e) dimethylthiocarbamoyl chloride (1.2 eq.), NaH (1 eq.), NaI (0.5 eq.), and THF, derivative 16.

Esquema 1 - Reações dos produtos naturais 1 e 2 que conduziram a derivados instáveis: a) Trifenilfosfina (5 eq.), DIAD (5 eq.), álcool correspondente (5 eq.) e THF seco, sob atmosfera inerte, derivados 3 to 8; b) DMAP (5 eq.), isocianato correspondente (em excesso) e CH_2Cl_2 seco, sob atmosfera inerte, derivados esperados 9 to 13; c) trietilamina (4.5 eq.), DMAP (0.3 eq.), cloreto de *p*-toluenosulfonil (3 eq.) e CH_2Cl_2 seco, derivado 14; d) imidazole (2 eq.), TBDPSCl (em excesso) e CH_2Cl_2 seco, derivado esperado 15; e) cloreto de dimetiltiocarbamoilo (1.2 eq.), NaH (1 eq.), NaI (0.5 eq.) e THF, derivado 16.



Scheme 2 - Reactions of 1 and 2 that afford stable derivatives: a) DMAP (0.5 eq.), Boc₂O (2.2 eq.), and dry CH₂Cl₂, derivative 17; b) CH₃I (8.4 eq.), Ag₂O (8.4 eq.), and dry CH₂Cl₂, derivative 18; c) Pyridine (12 eq.), benzoyl chloride (12 eq.), and dry CH₂Cl₂, derivatives 19 and 20.

Esquema 2 - Reações de 1 e 2 que originaram derivados estáveis: a) DMAP (0.5 eq.), Boc₂O (2.2 eq.) e CH₂Cl₂ seco, derivado 17; b) CH₃I (8.4 eq.), Ag₂O (8.4 eq.) e CH₂Cl₂ seco, derivado 18; c) Piridina (12 eq.), cloreto de benzoilo (12 eq.) e CH₂Cl₂ seco, derivados 19 e 20.

Assessment of preliminary toxicity - Brine shrimp lethality bioassay

Samples of each tested compound were prepared at a concentration of 100 ppm in a salt medium (Brine shrimp salt obtained from JBL GmbH and Co. KG, D-67141, Neuhofen Germany) at a concentration of 35 g/L. A 24-well plate was used, and around 10 to 15 larvae were added to each well containing salt medium. Afterward, each compound was added (100 µL) to the corresponding wells, and the plate was stored for 24 h at 25°C. After 24 h, the number of dead larvae in each well was recorded. To determine the total number of larvae in each well, death was induced on the remaining living larvae by adding potassium dichromate (K₂Cr₂O₇) at 1 mg/mL.

After 24 h, all dead larvae were counted and the mortality rate (%) was determined according to Equation 1. Dimethyl sulfoxide (DMSO) at the same concentration of the samples (100 ppm) was used as a negative control. Four replicates were used for each test, and the assay was performed in triplicate.

$$\text{Mortality Rate (\%)} = \frac{(\text{Total } A. \text{ salina} - \text{Living } A. \text{ salina})}{(\text{Total } A. \text{ salina})} \times 100 \quad [\text{Eq. 1}]$$

Avaliação da toxicidade geral - Bioensaio de letalidade de Artémia

As amostras analisadas foram preparadas a uma concentração de 100 ppm, em meio salino (Sal para camarão marinho adquirido a JBL GmbH and Co. KG, D-67141 Neuhofen, Alemanha) à concentração de 35g/L. Numa placa de 24 poços, colocaram-se aproximadamente 10 a 15 larvas, em meio salino, em cada poço. De seguida, cada composto foi adicionado (100 µL) ao poço correspondente e a placa armazenada por 24h a 25°C. Após 24h, o número de larvas mortas em cada poço foi registado. De modo a determinar o número total de larvas em cada poço, a morte das larvas vivas remanescentes foi induzida, pela adição de dicromato de potássio (K₂Cr₂O₇) a 1 mg / mL.

Após 24h, todas as larvas mortas foram contadas e a taxa de mortalidade (%) determinada de acordo com a Equação 1. O controlo negativo utilizado foi o dimetilssulfóxido (DMSO), na mesma concentração das amostras (100 ppm). Quatro réplicas foram usadas para cada teste, e o ensaio foi realizado em triplicado.

$$\text{Taxa de letalidade (\%)} = \frac{(A. \text{ salina total} - A. \text{ salina vivos})}{(A. \text{ salina total})} \times 100 \quad [\text{Eq. 1}]$$

Statistical Analysis

The results were expressed as the mean value \pm SD. Comparisons were performed within groups by the analysis of variance using the ANOVA test. Significant differences between control and experimental groups were assessed by the SigmaStat software (StatSoft, Tulsa, OK, USA). A probability level $p < 0.05$ was considered to indicate statistical significance.

Results and discussion

Hemi-synthesis of royleanone derivatives

Several hemi-synthetic reactions were performed to prepare a small library of compounds of enhanced cytotoxic potential. Both natural compounds **1** and **2** (Figure 1) were subjected to short-time microwave-assisted Mitsunobu and benzylation reactions. Natural compound **2** was also subjected to a carbamylation, tosylation, methylation, and introduction of Boc (*tert*-butyloxycarbonyl) and TBDPS (*tert*-butyldiphenylsilyl) groups. The predicted structures and the isolated derivatives (**3** to **20**) are shown in Schemes 1 and 2.

The introduction of Boc group (**17**), methylation (**18**), and benzylation (**19** and **20**) reactions were accomplished with success, affording pure products with overall good yields (97% for derivative **17**, 28% for methylated derivative **18**, and 50% and 69% for benzylation derivatives **19** and **20**, respectively), scheme 2. Unfortunately, products **3** to **16** (Scheme 1) displayed a high rate of decomposition, occurring especially after isolation.

Evaluation of general toxicity using *A. salina* model

Although some of the expected derivatives were not formed due to their chemical (in)stability, the general toxicity of all the obtained derivatives was assessed. The general toxicity was assessed through the brine shrimp lethality bioassay. Figure 2 illustrates the mortality rate (%) of *A. salina* after 24 h of exposure to the diterpenoid compounds tested.

According to the results, natural product **1** displays moderate toxic activity (36.68% at 100 ppm). The unstable tosylation derivative (**9**) presented the highest mortality rate (81.87%). Overall, in agreement with this model, the chemical modifications induced in natural royleanone **1** structure through microwave-assisted Mitsunobu reactions, enhanced the toxic activity in all derivatives (**3** to **5**). Likewise, stable methylated **18** and

Análise Estatística

Os resultados foram expressos como valores médios \pm desvios padrão. As comparações foram realizadas dentro dos grupos pela análise de variância, utilizando o teste ANOVA. As diferenças significativas entre os grupos controle e experimental foram avaliadas pelo software SigmaStat (StatSoft, Tulsa, OK, EUA). O nível de significância $p < 0,05$ foi considerado para indicar significância estatística.

Resultados e discussão

Hemi-síntese de derivado de royleanone

Diversas reações hemi-sintéticas foram realizadas com o objetivo de preparar uma pequena biblioteca de compostos com elevado potencial citotóxico. Os compostos naturais **1** e **2** (Figura 1) foram submetidos a reações de Mitsunobu, assistidas por micro-ondas, e de benzoilação. Reações de carbamoilação, tosilção, metilação e introdução dos grupos Boc (*tert*-butiloxicarbonil) e TBDPS (*tert*-butildifenilsilil) também foram testadas no composto **2**. As estruturas previstas e os derivados isolados (**3** a **20**) estão apresentados nos Esquemas 1 e 2.

As reações de introdução do grupo Boc (**17**), metilação (**18**) e benzoilação (**19** e **20**) originaram produtos puros com bons rendimentos gerais (97% para o derivado **17**, 28% para o derivado metilado **18** e 50% e 69% para os benzoilados **19** e **20**, respetivamente), Esquema 2. Infelizmente, os produtos **3** a **16** (Esquema 1) apresentaram uma elevada taxa de decomposição, ocorrendo especialmente após o isolamento.

Avaliação da toxicidade geral através do ensaio de letalidade de *A. salina*

Alguns dos derivados esperados não se formaram devido à sua instabilidade química. No entanto, avaliou-se a toxicidade geral de todos os derivados obtidos. A toxicidade geral foi avaliada através do bioensaio de letalidade de artémia. A Figura 2 ilustra a taxa de mortalidade (%) de *A. salina* após 24 h de exposição aos diterpenóides.

De acordo com os resultados apresentados, o produto natural **1** apresenta uma atividade tóxica moderada (36.68% à concentração de 100 ppm). O derivado tosilado instável (**9**) é responsável pela taxa de mortalidade mais elevada do ensaio (81.87%).

benzoylated 19 derivatives increased the toxicity of the original scaffold (1). The derivatives 9 - 11, 10, and 11 displayed the lowest mortality rate.

Natural royleanone 2 appears to be slightly less toxic than 1 (30.95% at 100 ppm), but similarly, the Mitsunobu derivatives increased the toxicity of the lead molecule (compounds 6 to 8). The benzoylated product of 2 (compound 20) also slightly increased the toxicity of the original scaffold.

Considering that only derivatives 17 to 20 were stable, that 18 was obtained with a lower yield, and that 17 displayed lower toxicity, this shows that compounds 19 and 20 (both esters) were the most promising of the targets produced.

De um modo geral, as modificações induzidas na estrutura do composto natural 1, por reações de Mitsunobu assistidas por micro-ondas, conduziram a um aumento da toxicidade em todos os derivados (3 to 5). Do mesmo modo, os derivados estáveis 18 (metilado) e 19 (benzoilado) aumentaram a toxicidade verificada no composto de partida (1). Os derivados 9 - 11, 10 e 11 apresentaram a menor taxa de mortalidade.

A roileanona natural 2 apresenta valores de toxicidade ligeiramente inferiores a 1 (30.95% à concentração de 100 ppm). À semelhança do que se verificou com 1, os derivados de Mitsunobu (compostos 6 a 8) obtidos a partir de 2 foram responsáveis por um aumento da toxicidade comparativamente com ao composto de partida. Adicionalmente, o produto benzoilado de 2 (composto 20) aumentou ligeiramente a toxicidade verificada em 2.

Considerando que apenas os derivados 17 a 20 são estáveis, o derivado 18 foi obtido com baixo rendimento e o 17 apresentou baixa toxicidade, os resultados demonstram que os compostos 19 e 20 (ambos ésteres) são os mais promissores.

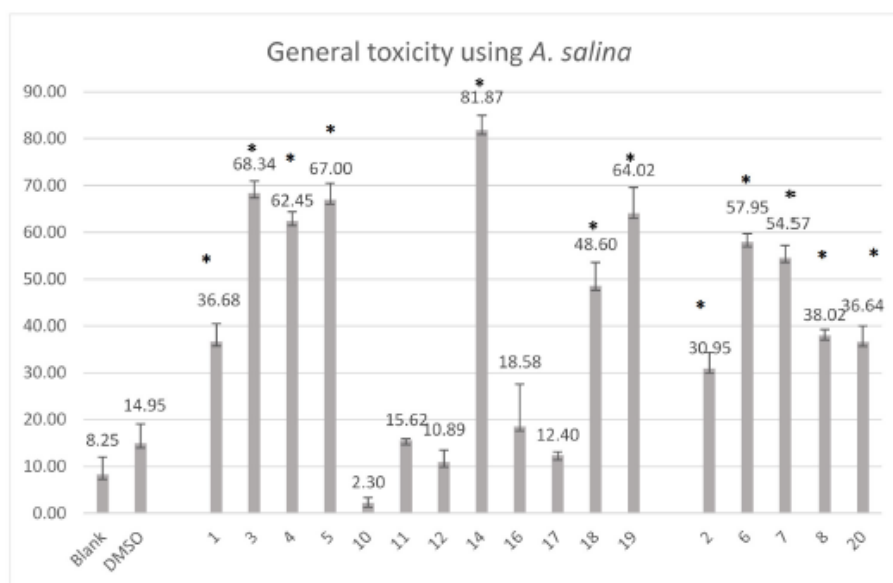


Figure 2 - Mortality rate (%) of *Artemia salina* after 24 h exposure to royleanones. Values are expressed as the mean \pm SD (n = 3). * $p < 0.05$ comparison DMSO vs compounds.

Figura 2 -Taxa de letalidade (%) de *Artemia salina* após 24 h de exposição às roileanonas. Os valores são expressos como a média \pm DP (n = 3). * $p < 0,05$ comparação DMSO vs compostos.

Conclusions

The reactivity of two natural royleanones **1** and **2** was explored. Several hemi-synthetic reactions were performed, and the obtained products were limited by stability issues: the derivatives **3** to **16** tend to degrade after isolation. Successful results were obtained when performing methylation and benzylation, as with the introduction of a BOC group, affording pure compounds (**17** to **20**), with overall good yields.

General toxicity using the *A. salina* model has been established for the obtained products. As such, products **3** to **8**, **14**, and **18** to **20** have increased the toxicity of the lead compound. Products **19** and **20** displayed the best results regarding their stability and high toxicity, thus suggesting that the formation of esters is a more convenient approach for future derivatives.

Authors Contributions Statement

EN, VI - experimental and original writing; AD - visualisation; CA - methodology, supervision; PR - conceptualization, supervision, final writing

Funding

Support for this work was provided by Fundação para a Ciência e a Tecnologia (FCT) through projects UIDP/04567/2020 e UIDB/04567/2020 and PhD grant SFRH/BD/137671/2018.

Conflict of Interest

The authors report no conflicts of interest.

Conclusões

A reatividade de duas roileanonas naturais **1** e **2** foi estudada através de várias reações hemi-sintéticas. Os produtos obtidos apresentaram alguns problemas de estabilidade: os derivados **3** a **16** degradaram no processo de isolamento. No entanto foram obtidos produtos puros e estáveis, com bons rendimentos globais, nas reações de metilação, benzoilação e introdução do grupo BOC (**17** a **20**).

A toxicidade geral através do modelo de *A. salina* foi avaliada para os derivados preparados. Os derivados **3** a **8**, **14** e **18** a **20** aumentaram a toxicidade do composto natural de partida. Os produtos **19** e **20** apresentaram os melhores resultados quanto à estabilidade e elevada toxicidade, sugerindo que a formação de ésteres é uma abordagem mais conveniente para futuros derivados.

Declaração Sobre as Contribuições do Autor

EN, VI - experimental e escrita original; AD - visualização; CA - metodologia, supervisão; PR - concepção, supervisão, edição final

Financiamento

Os autores agradecem à FCT pelo apoio financeiro para este trabalho através dos projetos UIDP/04567/2020 e UIDB/04567/2020 e bolsa de Doutoramento SFRH/BD/137671/2018.

Conflito de Interesses

Os autores não têm conflitos de interesse a reportar.

References / Referências

- World Health Organization (WHO), fact sheet on Cancer. Available online: <https://www.who.int/news-room/fact-sheets/detail/cancer> (accessed on 5 February 2021).
- Tobore T. O. (2019). On the need for the development of a cancer early detection, diagnostic, prognosis, and treatment response system. *Future science OA*, 6(2), FSO439. <https://doi.org/10.2144/fsoa-2019-0028>
- Nobili, S., Lippi, D., Witort, E., Donnini, M., Bausi, L., Mini, E., & Capaccioli, S. (2009). Natural compounds for cancer treatment and prevention. *Pharmacological research*, 59(6), 365–378. <https://doi.org/10.1016/j.phrs.2009.01.017>
- Taviano, M. F., Rashed, K., Filocamo, A., Cacciola, F., Dugo, P., Mondello, L., Bisignano, C., Acquaviva, R., D'Arrigo, M., & Miceli, N. (2018). Phenolic profile and biological properties of the leaves of *Ficus vasta* Forssk. (Moraceae) growing in Egypt. *BMC complementary and alternative medicine*, 18(1), 161. <https://doi.org/10.1186/s12906-018-2210-0>
- Seca, A., & Pinto, D. (2018). Plant Secondary Metabolites as Anticancer Agents: Successes in Clinical Trials and Therapeutic Application. *International journal of molecular sciences*, 19(1), 263. <https://doi.org/10.3390/ijms19010263>
- Zhang, Y., Mu, J., Han, J., & Gu, X. (2012). An improved brine shrimp larvae lethality microwell test method. *Toxicology mechanisms and methods*, 22(1), 23–30. <https://doi.org/10.3109/15376516.2011.583297>.
- Papadopoulos, A.I.; Lazaridou, E.; Mauridou, G.; Touraki, M. (2004). Glutathione S-transferase in the branchiopod *Artemia salina*. *Marine Biology*, 144, 295–301, doi:10.1007/s00227-003-1203-8.
- Ntungwe N, E., Domínguez-Martín, E. M., Roberto, A., Tavares, J., Isca, V., Pereira, P., Cebola, M. J., & Rijo, P. (2020). *Artemia* species: An Important Tool to Screen General Toxicity Samples. *Current pharmaceutical design*, 26(24), 2892–2908. <https://doi.org/10.2174/1381612826666200406083035>
- Libralato, G.; Prato, E.; Migliore, L.; Cicero, A.M.; Manfra, L. (2016) A review of toxicity testing protocols and endpoints with *Artemia* spp. *Ecological Indicators*, 69, 35–49, doi:10.1016/j.ecolind.2016.04.017.
- Ntungwe N, E.; Marçalo, J.; Garcia, C.; Reis, C.; Teodósio, C.; Oliveira, C.; Roberto, A. (2017) Biological activity screening of seven *Plectranthus* species. *Biomedical and Biopharmaceutical Research*, 14(1), 95–108, doi:10.19277/BBR.14.1.153.
- Zengin, G., Ferante, C., Senkardes, I., Gevrenova, R., Zheleva-Dimitrova, D., Menghini, L., Orlando, G., Recinella, L., Chiavaroli, A., Leone, S., Brunetti, L., Picot-Allain, C., Rengasamy, K. R., & Mahomoodally, M. F. (2019). Multidirectional biological investigation and phytochemical profile of *Rubus sanctus* and *Rubus ibericus*. *Food and chemical toxicology : an international journal published for the British Industrial Biological Research Association*, 127, 237–250. <https://doi.org/10.1016/j.fct.2019.03.041>.
- Krstić, N. M., Matic, I. Z., Juranić, Z. D., Novaković, I. T., & Sladić, D. M. (2014). Steroid dimers-in vitro cytotoxic and antimicrobial activities. *The Journal of steroid biochemistry and molecular biology*, 143, 365–375. <https://doi.org/10.1016/j.jsbmb.2014.06.005>
- Olivares-Bañuelos, T., Gutiérrez-Rodríguez, A. G., Méndez-Bellido, R., Tovar-Miranda, R., Arroyo-Helguera, O., Juárez-Portilla, C., Meza-Menchaca, T., Aguilar-Rosas, L. E., Hernández-Kelly, L., Ortega, A., & Zepeda, R. C. (2019). Brown Seaweed *Egregia menziesii*'s Cytotoxic Activity against Brain Cancer Cell Lines. *Molecules* (Basel, Switzerland), 24(2), 260. <https://doi.org/10.3390/molecules24020260>
- Logarto Parra, A., Silva Yhebra, R., Guerra Sardiñas, I., & Iglesias Buela, L. (2001). Comparative study of the assay of *Artemia salina* L. and the estimate of the medium lethal dose (LD50 value) in mice, to determine oral acute toxicity of plant extracts. *Phytomedicine : international journal of phytotherapy and phytopharmacology*, 8(5), 395–400. <https://doi.org/10.1078/0944-7113-00044>.
- Gajardo, G. M., & Beardmore, J. A. (2012). The brine shrimp *Artemia*: adapted to critical life conditions. *Frontiers in physiology*, 3, 185. <https://doi.org/10.3389/fphys.2012.00185>.
- Arsilanyolu, M.; Erdemgil, F. Z. (2006) Evaluation of the Antibacterial Activity and Toxicity of Isolated Arctiin From the Seeds of *Centaurea Sclerolepis*. *Journal of Faculty of Pharmacy of Ankara University*, 35 (2), 103–109. https://doi.org/10.1501/Eczfak_0000000052
- Mayorga, P., Pérez, K. R., Cruz, S. M., & Cáceres, A. (2010). Comparison of bioassays using the anostracan crustaceans *Artemia salina* and *Thamnocephalus platyurus* for plant extract toxicity screening. *Revista Brasileira de Farmacognosia*, 20(6), 897-903. <https://dx.doi.org/10.1590/S0102-695X2010005000029>.
- Logarto Parra, A., Silva Yhebra, R., Guerra Sardiñas, I., & Iglesias Buela, L. (2001). Comparative study of the assay of *Artemia salina* L. and the estimate of the medium lethal dose (LD50 value) in mice, to determine oral acute toxicity of plant extracts. *Phytomedicine : international journal of phytotherapy and phytopharmacology*, 8(5), 395–400. <https://doi.org/10.1078/0944-7113-00044>.
- Garcia, C., Silva, C. O., Monteiro, C. M., Nicolai, M., Viana, A., Andrade, J. M., Barasoain, I., Stankovic, T., Quintana, J., Hernández, I., González, I., Estévez, F., Díaz-Lanza, A. M., Reis, C. P., Afonso, C. A., Pesic, M., & Rijo, P. (2018). Anticancer properties of the abietane diterpene 6,7-dehydroroyleanone obtained by optimized extraction. *Future medicinal chemistry*, 10(10), 1177–1189. <https://doi.org/10.4155/fmc-2017-0239>.
- Bernardes, C., Garcia, C., Pereira, F., Mota, J., Pereira, P., Cebola, M. J., Reis, C. P., Correia, I., Piedade, M., Minas da Piedade, M. E., & Rijo, P. (2018). Extraction Optimization and Structural and Thermal Characterization of the Antimicrobial Abietane 7 α -Acetoxy-6 β -hydroxyroyleanone. *Molecular pharmaceutics*, 15(4), 1412–1419. <https://doi.org/10.1021/acs.molpharmaceut.7b00892>.
- Garcia, C., Isca, V., Pereira, F., Monteiro, C. M., Ntungwe, E., Sousa, F., Dinic, J., Holmstedt, S., Roberto, A., Diaz-Lanza, A., Reis, C. P., Pesic, M., Candéias, N. R., Ferreira, R. J., Duarte, N., Afonso, C., & Rijo, P. (2020). Royleanone Derivatives From *Plectranthus* spp. as a Novel Class of P-Glycoprotein Inhibitors. *Frontiers in pharmacology*, 11, 557789. <https://doi.org/10.3389/fphar.2020.557789>
- Bessa, C., Soares, J., Raimundo, L., Loureiro, J. B., Gomes, C., Reis, F., Soares, M. L., Santos, D., Dureja, C., Chaudhuri, S. R., Lopez-Haber, C., Kazanietz, M. G., Gonçalves, J., Simões, M. F., Rijo, P., & Saraiva, L. (2018). Discovery of a small-molecule protein kinase C δ -selective activator with promising application in colon cancer therapy. *Cell death & disease*, 9(2), 23. <https://doi.org/10.1038/s41419-017-0154-9>.

Biological activity screening of seven *Plectranthus* species

Pesquisa de actividade biológica de sete espécies de Plectranthus

Epole Ntungwe N.¹, Joana Marçalo¹, Catarina Garcia¹, Catarina Reis², Catarina Teodósio¹, Carolina Oliveira¹, Cláudia Oliveira¹, Amílcar Roberto¹, Patricia Rijo^{1,2*}

¹ CBIOS - Research Center for Biosciences & Health Technologies, U. Lusófona de Humanidades e Tecnologias, Campo Grande 376, 1749-024 Lisboa, Portugal

² Instituto de Investigação do Medicamento (iMed.U.Lisboa), Faculdade de Farmácia, Universidade de Lisboa, 1649-003 Lisboa, Portugal

Email: patricia.rijo@ulusofona.pt

Abstract

Natural products from *Plectranthus* spp. plants have an ethnopharmacological use, inspiring several scientific investigations. As such, this work aims to perform a biological activity screening in order to scientifically validate the use of these plants. Assays on in vitro acetylcholinesterase (AChE) inhibition, antioxidant effects, antimicrobial activity and *Artemia salina* lethality were performed on seven *Plectranthus* spp. extracts (*P. swynnertonii*, *P. welwischii*, *P. woodii*, *P. cylindraceus*, *P. spicatus*, *P. ramosior* and *P. petiolaris*). Acetonic extracts were obtained by sonication (10% w/v), where *P. ramosior* had the highest yield of dry extract (13.49% w/w). In the AChE inhibition assay, only *P. cylindraceus* extract decreased enzymatic activity (30.2 ± 3.78%). The antimicrobial activity was screened using the well diffusion method, against Gram positive and negative bacteria and yeast. *P. ramosior* extract showed not only an inhibition zone against *S. aureus* and *C. albicans* (15 and 11 mm, respectively), but also the highest scavenging activity (DPPH method, 36.4 ± 0.04%). On the lethality test in *A. salina*, *P. swynnertonii* extract was the most toxic (LC50 = 0.036 mg/L). These preliminary results showed that *P. cylindraceus*, *P. ramosior* and *P. swynnertonii* are potential bioactive extracts for further isolation and antimicrobial and cytotoxic studies.

Keywords: *Plectranthus*, Acetylcholinesterase, Antioxidant, Antimicrobial, Toxicity

Resumo

Os produtos naturais das espécies de plantas *Plectranthus* têm um uso etnofarmacológico, suscitando vários estudos científicos. Neste trabalho pretendeu-se validar cientificamente estas plantas, realizando uma pesquisa de atividades biológicas. Extratos de sete espécies de *Plectranthus* (*P. swynnertonii*, *P. welwischii*, *P. woodii*, *P. cylindraceus*, *P. spicatus*, *P. ramosior* e *P. petiolaris*) foram testados na inibição da acetilcolinesterase in vitro (AChE), atividades antioxidante e antimicrobiana, e toxicidade em *Artemia salina*. Os extratos acetónicos foram obtidos por ultrassons (10% m/v), dos quais *P. ramosior* obteve o rendimento de extração mais elevado (13,49% m/m). Todos os extratos foram testados, no entanto apenas o *P. cylindraceus* obteve inibição da atividade da AChE (30,2 ± 3,78%). A atividade antimicrobiana foi avaliada usando o método de difusão em poços, contra bactérias Gram-positivas, -negativas e leveduras. *P. ramosior* revelou não só inibição contra *S. aureus* e *C. albicans* (15 e 11 mm, respetivamente), como também a mais elevada atividade antioxidante (método DPPH, 36,4 ± 0,04%). No ensaio em *A. salina* *P. swynnertonii* foi o extrato mais tóxico (LC50 = 0,036 mg/L).

Os resultados preliminares obtidos neste trabalho, revelam a potencial biotividade dos extratos de *P. cylindraceus*, *P. ramosior* e *P. swynnertonii*, sugerindo o posterior isolamento dos compostos bioativos, e continuidade dos estudos antimicrobianos e citotóxicos.

Palavras chave: *Plectranthus*, Acetilcolinesterase, Antioxidante, Antimicrobiana, Toxicidade

Received / Recebido: 15/03/2017

Accepted / Aceite: 28/04/2017

Electronic Edition: www.alies.pt

Introduction

Plectranthus L' Her. genus belongs to the Lamiaceae family together with other commercially important plant genera, such as, *Salvia*, *Ocimum* or *Mentha*, with a rich diversity of ethnobotanical uses in traditional medicine ^(1,2). The scientific validation on the traditional medicine of these plants is an important issue, to search for pharmacological activities and through drug development. In fact, there has been an increasing interest on the *Plectranthus* genus for the investigation of its therapeutic values ^(3,4). Regarding this, the herein described study evaluated several biological activities of seven *Plectranthus* species (*P. swymertonii* S. Moore, *P. welwischii* Briq. Codd, *P. woodii* Gürke, *P. cylindraceus* Hochst ex Benth, *P. spicatus* E. Mey ex Benth, *P. ramosior* Benth. Van Jaarsv., and *P. petiolaris* E. Mey ex Benth, Druce).

According to the references of this study, scientific information on the analyzed *Plectranthus* spp. is scarce and with no phytochemical studies (except for *P. cylindraceus*). To the best of our knowledge, this is the first report comprising the evaluation of acetylcholinesterase inhibition, antioxidant and antimicrobial activities, as well as the *Artemia salina* lethality assay of the seven *Plectranthus* species.

Alzheimer's disease (AD) is the most common cause of dementia, a progressive neurodegenerative disorder associated with memory and cognition impairment, that remains until the end of the patient life ⁽⁵⁾. Reversible inhibition of the acetylcholinesterase (AChE) enzyme is considered as one of the prime therapeutic strategies for the treatment of AD ^(6,7). Eserine, tacrine, donepezil, rivastigmine and galanthamine are the only drugs currently approved for the treatment of AD; however, these drugs are known to have severe side effects for frequent clinical use ⁽⁸⁾. Therefore, there is an urgent need to search for new drugs. *Plectranthus* spp. could be an important source to find novel compounds that can simultaneously protect neurons from oxidative stress and selectively inhibit AChE.

Humans are often exposed to free radicals which are generated from normal metabolic processes in the body. Free radicals are not always harmful, however, high level of free radicals may disturb the normal cellular mechanism by inducing oxidative damage to DNA, protein and lipids which ultimately result in chromosomal instability and mutation ⁽⁹⁾. Moreover, overproduction of free radicals may reduce the potency of the biological defense system to detoxify these radicals which result in oxidative stress. The oxidative stress might play a role in the risk of development of several metabolic

Introdução

O género *Plectranthus* L' Her. pertence à família Lamiaceae juntamente com outros géneros de plantas comercialmente importantes, como *Salvia*, *Ocimum* ou *Mentha*, que possuem uma diversidade rica de usos etnobotânicos na medicina tradicional ^(1,2). A procura de atividades farmacológicas até o desenvolvimento de fármacos, através da validação científica da medicina tradicional destas plantas é um assunto importante. Na verdade, tem havido um aumento na pesquisa de interesses terapêuticos do género *Plectranthus* ^(3,4). Assim, no presente estudo são descritas várias atividades biológicas de sete espécies de *Plectranthus* (*P. swymertonii* S. Moore, *P. welwischii* Briq. Codd, *P. woodii* Gürke, *P. cylindraceus* Hochst ex Benth, *P. spicatus* E. Mey ex Benth, *P. ramosior* Benth. Van Jaarsv., e *P. petiolaris* E. Mey ex Benth, Druce).

De acordo com as referências deste estudo, as informações científicas sobre *Plectranthus* spp. são escassas, e sem estudos fitoquímicos (exceto para *P. cylindraceus*). Tanto quanto é do nosso conhecimento, este é o primeiro relatório que inclui a avaliação da inibição da acetilcolinesterase, atividades antioxidantes e antimicrobianas, bem como o ensaio de letalidade de *Artemia salina* das sete espécies de *Plectranthus*.

A doença de Alzheimer (AD) é a causa mais comum de demência, um distúrbio neurodegenerativo progressivo associado à perda de memória e cognição, que permanece até o final da vida do paciente ⁽⁵⁾. A inibição reversível da enzima acetilcolinesterase (AChE) é considerada como uma das principais estratégias terapêuticas para o tratamento da AD ^(6,7). Os únicos fármacos aprovados atualmente para o tratamento da AD são a eserina, tacrina, donepezilo, rivastigmina e galantamina. No entanto, estes fármacos são conhecidos por terem efeitos secundários graves em uso clínico frequente ⁽⁸⁾. Assim sendo, há uma urgente necessidade de procurar novos medicamentos. As *Plectranthus* spp. podem ser uma fonte essencial para encontrar novos compostos, que possam simultaneamente proteger os neurónios contra o stress oxidativo e inibir seletivamente a AChE. Os seres humanos são frequentemente expostos a radicais livres que são gerados a partir de processos metabólicos normais no corpo. Os radicais livres nem sempre são prejudiciais, no entanto, o alto nível de radicais livres pode perturbar o mecanismo celular normal, induzindo danos oxidativos ao DNA, proteínas e lipídios que, em última análise, resultam em instabilidade cromossômica e mutações ⁽⁹⁾. Além disso, a superprodução de radicais livres pode reduzir a potência do sistema de defesa biológico para desintoxicar estes radicais, re-

diseases such as cancer, cardiovascular diseases, diabetes, obesity, neurodegenerative and ageing-related disorders^(9,10). Regarding the antioxidant properties of the Lamiaceae family and future phytochemical evaluation of active compounds, there are several related reports of *Plectranthus* spp. extracts that suggest these plants as an important study motif⁽³⁾.

The antimicrobials of natural origin usually present complex chemical structures, which may be important for specific interactions and recognition of potential macromolecular targets in the pathogenic microorganisms. These active natural products are, generally, secondary plant metabolites biosynthesized to fight and prevent the proliferation of plant pathogenic microorganisms⁽¹¹⁾. Some species of the *Plectranthus* genus have ethnopharmacological applications, with antimicrobial activity often cited. Indeed, it is known that both the metabolites and extracts of several *Plectranthus* spp. have exhibited activity against Gram-positive and Gram negative bacteria and yeasts⁽¹²⁻¹⁴⁾.

Brine shrimp lethality assay is a technique commonly used to investigate the toxic potential of plant extracts⁽¹⁵⁾. This is based on cellular mechanisms that may occur via necrosis, characterised by loss of membrane integrity, death of cell or apoptosis, a genetic program of controlled cell death⁽¹⁶⁾. Brine Shrimp Lethality Assay (BSLA) has been applied as an alternative bioassay technique to screen the toxicity of plant extracts, toxicity of heavy metals and metal ions, toxicity of cyanobacteria and algae, cytotoxicity of dental materials, toxicity of nanoparticles, as well as screening of marine natural products⁽¹⁷⁾. This test is economical and utilises small amount of test material^(18,19). The present study was therefore designed to evaluate the potential toxicity (using *A. salina*) of the seven *Plectranthus* spp.

Methods and Materials

Chemicals: Acetone, dimethyl sulfoxide (DMSO) and acetylcholine iodide (Sigma). Tacrine, HEPES buffer and Ellman reagent (Fluka Chemie AG). Mueller-Hinton and *Sabouraud dextrose Agar*, vancomycin, norfloxacin, nystatin, 2,2-diphenyl-1-picrylhydrazyl (DPPH), Quercetin, Butylated hydroxytoluene (BHT),

sultando no *stress* oxidativo. O *stress* oxidativo pode ter um papel crucial no risco de desenvolvimento de várias doenças metabólicas como cancro, doenças cardiovasculares, diabetes, obesidade, distúrbios neurodegenerativos e doenças associadas ao envelhecimento^(9,10). Vários estudos têm vindo a avaliar os extratos de *Plectranthus* spp. tendo em conta as suas propriedades antioxidantes e futura avaliação fitoquímica de compostos ativos, transformando estas plantas num importante motivo de estudo⁽³⁾.

Os compostos antimicrobianos de origem natural geralmente apresentam estruturas químicas complexas que podem ser importantes nas interações específicas e reconhecimento de alvos macromoleculares potenciais, nos microrganismos patogénicos. Estes produtos naturais ativos são, em geral, metabolitos secundários vegetais biosintetizados para combater e prevenir a proliferação de microrganismos patogénicos das plantas⁽¹¹⁾. Algumas espécies do género *Plectranthus* têm aplicações etnofarmacológicas com atividade antimicrobiana frequentemente citada. De facto, sabe-se que tanto os metabolitos como os extratos de várias *Plectranthus* têm demonstrado atividade contra bactérias Gram-positivas e negativas e leveduras⁽¹²⁻¹⁴⁾.

O ensaio de letalidade em *Artemia salina* é uma técnica usual para avaliar o potencial tóxico de extratos vegetais⁽¹⁵⁾. Este ensaio é baseado no mecanismo celular que pode ocorrer através de necrose, caracterizada pela perda da integridade da membrana, morte da célula ou apoptose, um programa genético de morte celular controlada⁽¹⁶⁾. O ensaio de letalidade em *A. salina* (BSLA) tem vindo a ser aplicado como uma técnica alternativa de bioensaio para examinar a toxicidade de extratos de plantas, toxicidade de metais pesados e iões metálicos, toxicidade de cianobactérias e algas, citotoxicidade de materiais dentários, toxicidade de nanopartículas, bem como no rastreio de produtos marinhos naturais⁽¹⁷⁾. Este teste é económico e necessita apenas de uma pequena quantidade de amostra^(18,19). O presente estudo foi portanto concebido para avaliar a potencial toxicidade (utilizando o modelo de *A. salina*) das sete espécies de *Plectranthus*.

Métodos

Reagentes: Acetona, dimetilsulfóxido (DMSO) e iodeto de acetilcolina (Sigma). Tacrina, tampão HEPES e reagente de Ellman (Fluka Chemie AG). Agar Mueller-Hinton e *Sabouraud Dextrose*, vancomicina, norfloxacin, nistatina, 2,2-difenil-1-picrilhidrazilo (DPPH), quercetina, hidroxitolueno butilado (BHT), metanol,

Methanol, JBL *Artemia* salt, JBL *Artemia* eggs (JBL GmbH and Co. KG, D-67141 Neuhausen Germany).

Equipment: Rotary evaporator (K Ika-WERKE, GMBH & CO.KG; D-79219 Staufen Germany), spectrophotometer U-1500 Hitachi Instruments, Inc USA., microscope (E, CETI Belgium), 24 well microplates, aquarium air pump (HI-FLO™ Single Type 4000), Thermostat Cabinet AQUA LYTIC®, TLC silica gel 60F₂₅₄ 20x20(Merck KGaA), Whatman, Inc., Clifton, NJ, USA and ultrasound apparatus from VWR.

Plant material

All plant materials of *Plectranthus swynnertonii* S. Moore, *P. welwischii* (Briq. Codd), *P. woodii* Gürke, *P. cylindraceus* Hochst, ex Benth, *P. spicatus* E. Mey ex Benth., *P. ramosior* Benth. Van Jaarsv., *P. petiolaris* E. Mey ex Benth, Druce were grown in the Parque Botânico da Tapada da Ajuda from cuttings provided by the Kirstenbosch National Botanical Gardens, South Africa, and were collected between 2007 and 2008, always in June and September, and voucher specimens were deposited in the Herbarium “João de Carvalho e Vasconcelos” of the “Instituto Superior de Agronomia”, Lisboa (LISI), Portugal.

Microorganisms

Enterococcus faecalis ATCC 29212, *Escherichia coli* ATCC 25922, *Pseudomonas aeruginosa* ATCC 27853, *Staphylococcus aureus* ATCC 25923, *Saccharomyces cerevisiae* ATCC 2601 and *Candida albicans* ATCC 10231.

Extract preparation

Plant extracts were prepared by a sonication extraction method (10 % (w/v)). This was performed by adding 30 mL of acetone to 3 g of grinded dry plant leaves three times, sonicating for 1 hour for each extraction, and filtering (Whatman N° 5 paper, Inc., Clifton, NJ, USA.)⁽⁴⁴⁾ after each sonication. The liquid samples were evaporated using a rotary evaporator at 40-50°C. The extracts were prepared at the concentration of 10 mg/mL in DMSO. The extraction yield (% w/w) for each of the extracts was determined (Equation 1).

$$\text{Equation 1: \% Yield (w/w)} = \frac{\text{Weight of extract (g)}}{\text{Weight of dried plant (g)}} \times 100$$

$$\text{Equação 1: \% Rendimento (m/m)} = \frac{\text{Resíduo seco (g)}}{\text{Planta seca (g)}} \times 100$$

JBL *Artemia* salt, JBL *Artemia* eggs (JBL GmbH e Co. KG, D-67141 Neuhausen Alemanha).

Equipamento: Evaporador rotativo (K Ika-WERKE, GMBH & CO.KG; D-79219 Staufen Alemanha), Espectrofotômetro U-1500 Hitachi Instruments, Inc USA., Microscópio óptico (E, CETI Bélgica), microplacas de 24 poços, Bomba de ar de aquário (HI-FLO™ Single Type 4000), Armário com termóstato AQUA LYTIC®, sílica gel de TLC 60F₂₅₄ 20x20(Merck KGaA), Whatman, Inc., Clifton, NJ, USA e aparelho de ultrassons da VWR.

Material vegetal

Todo o material das plantas *Plectranthus swynnertonii* S. Moore, *P. welwischii* (Briq. Codd), *P. woodii* Gürke, *P. cylindraceus* Hochst, ex Benth, *P. spicatus* E. Mey ex Benth., *P. ramosior* Benth. Van Jaarsv. e *P. petiolaris* E. Mey ex Benth, Druce cresceu no Parque Botânico da Tapada da Ajuda, provenientes de porções de caules vindos do “Kirstenbosch National Botanical Gardens”, África do Sul, e foi recolhido entre 2007 e 2008, sempre em Junho e Setembro e variados espécimes foram plantados no Herbário “João de Carvalho e Vasconcelos” do “Instituto Superior de Agronomia”, Lisboa (LISI), Portugal.

Microorganismos

Enterococcus faecalis ATCC 29212, *Escherichia coli* ATCC 25922, *Pseudomonas aeruginosa* ATCC 27853, *Staphylococcus aureus* ATCC 25923, *Saccharomyces cerevisiae* ATCC 2601 e *Candida albicans* ATCC 10231.

Preparação dos extratos

Os extratos das plantas foram preparados utilizando um método de extração por ultrassons (10 % (m/v)). Adicionaram-se 30 mL de acetona a 3 g de folhas trituradas de planta seca, três vezes durante 1 hora cada extração, e filtrou-se usando filtros Whatman papel N° 5 (Whatman, Inc., Clifton, NJ, USA.)⁽²⁰⁾. Os extratos obtidos foram evaporados usando o evaporador rotativo a 40-50 °C. O extratos foram depois colocados em Eppendorfs e dissolvidos em DMSO a uma concentração de 10 mg/mL. O rendimento de extração foi determinado para cada um dos extratos (Equação 1).

In vitro Acetylcholinesterase inhibition

Acetylcholinesterase enzymatic activity was evaluated in accordance with the method described by Rijo *et al.*,⁽²⁰⁾ using a microplate reader. All tests were carried out in triplicate with tacrine as the positive control. The acetonic extracts were tested at a concentration of 0.1 µg/mL, and the inhibition percentage values were calculated according to Equation 2 and 3.

$$\text{Equation 2: Velocity reaction of control or inhibitor} = \frac{\text{Corrected absorbance (nm)}}{\text{Time (min)}}$$

$$\text{Equação 2: Velocidade da reação do controlo ou inibidor} = \frac{\text{Absorvência corrigida (nm)}}{\text{Tempo (min)}}$$

$$\text{Equation 3: Inhibition (\%)} = 100 - \left(\frac{100 \times \text{Velocity reaction of inhibitor}}{\text{Velocity reaction of control}} \right)$$

$$\text{Equação 3: Inibição (\%)} = 100 - \left(\frac{100 \times \text{Velocidade da reação do inibidor}}{\text{Velocidade da reação controlo}} \right)$$

Atividade da acetilcolinesterase *in vitro*

A atividade enzimática da acetilcolinesterase foi avaliada de acordo com o método descrito por Rijo *et al.*,⁽²⁰⁾ usando um leitor de microplacas (Secção 2.2). Todos os testes foram executados em triplicado usando tacrina como controlo positivo. Os extratos das plantas foram testados a uma concentração de 0,1 µg/mL de acordo com as equações em Equação 2 e 3.

Antimicrobial activity: Well Diffusion Method

The antimicrobial activity of each prepared extract was evaluated against two Gram-positive bacteria (*E. faecalis* and *S. aureus*), two Gram-negative bacteria (*E. coli* and *P. aeruginosa*) and two yeasts (*S. cerevisiae* and *C. albicans*). Previously prepared extracts as described previously were reconstituted in DMSO at 1 mg/mL concentration. Stock solutions of reference antibiotics (vancomycin, norfloxacin and nystatin) were also prepared at 1 mg/mL in DMSO.

In aseptic conditions, Petri dishes containing 20 mL of solid Mueller-Hinton, or *Sabouraud Dextrose Agar* culture medium for yeasts, were inoculated with 0.1 mL of bacterial suspension matching a 0.5 McFarland standard solution and uniformly spread on the medium surface using a sterile swab. Wells of approximately 5 mm in diameter were made in the medium, using a sterile glass Pasteur pipette, and 50 µL of each extract were added into the wells. A positive control of vancomycin for Gram-positive bacteria, norfloxacin for Gram-negative bacteria and nystatin for yeasts and a negative control of DMSO were used in the assay. Plates were incubated at 37 °C for 24 hours. The antimicrobial activity was evaluated by measuring the diameter (mm) of the inhibition zone formed around the wells and compared to controls⁽⁶⁾.

Atividade antimicrobiana: Método de difusão em poços

A atividade antimicrobiana de cada extrato preparado foi avaliada contra seis espécies bacterianas e leveduras obtidas de "American Type Culture Collection" (ATCC), nomeadamente *Enterococcus faecalis* ATCC 29212, *Escherichia coli* ATCC 25922, *Pseudomonas aeruginosa* ATCC 27853, *Staphylococcus aureus* ATCC 25923, *Saccharomyces cerevisiae* ATCC 2601 e *Candida albicans* ATCC 10231. O ensaio de difusão em poços foi usado para selecionar os extratos com atividade antimicrobiana.

Os extratos preparados anteriormente de acordo com o descrito na secção 2.5 foram reconstituídos em DMSO a uma concentração de 1 mg/mL. As soluções *stock* dos antibióticos de referência (vancomicina, norfloxacin e nistatina) foram também preparadas a uma concentração de 1 mg/mL em DMSO.

Em condições assépticas, as caixas de Petri que continham 20 mL de meio de cultura de Agar Mueller-Hinton sólido e *Sabouraud Dextrose* (para as leveduras) foram inoculadas com 0,1 mL de suspensão bacteriana de acordo com a escala 0,5 da solução de McFarland e a suspensão foi uniformemente espalhada na superfície do meio usando um cotonete estéril. Foram feitos poços com aproximadamente 5 mm de diâmetro no meio com uma pipeta de Pasteur de vidro esterilizada, e foram co-

Determination of Antioxidant Activity (DPPH)

The antioxidant activity of all extracts was measured by DPPH method, as described by Rijo *et al.* (20) 10 µL of each extract sample were added to a 990 µL solution of DPPH (0.002% in methanol). The mixture was incubated for 30 minutes at room temperature. The absorbance was measured at 517 nm against a corresponding blank and the antioxidant activity was calculated using Equation 4.

$$\text{Equation 4: AA (\%)} = \frac{A_{\text{DPPH}} - A_{\text{sample}}}{A_{\text{DPPH}}} \times 100$$

$$\text{Equação 4: AA (\%)} = \frac{A_{\text{DPPH}} - A_{\text{amostra}}}{A_{\text{DPPH}}} \times 100$$

AA is the antioxidant activity, A DPPH is the absorption of DPPH against the blank and A sample is the absorption of the extract or control against the blank. Tests were carried out in triplicate at a sample concentration at 1 mg of dry plant extract/mL. The reference standard used for this procedure was quercetin, used in the same conditions as the samples.

Brine shrimp lethality bioassay

In order to evaluate the toxicity of the different extracts, a test of lethality to *Artemia salina* brine shrimp was performed (18). Concentrations of 10 ppm of each extract were tested. The number of dead larvae was recorded after 24 hours and used to calculate the lethal concentration (%), according to Equation 5.

$$\text{Equation 5: Lethal concentration (\%)} = \frac{\text{Total nauplii} - \text{Alive nauplii}}{\text{Total nauplii}}$$

$$\text{Equação 5: Concentração letal (\%)} = \frac{\text{Náuplios totais} - \text{Náuplios vivos}}{\text{Náuplios totais}}$$

locados 50 µL de cada extrato nesses poços. O controlo positivo usado foi a vancomicina para bactérias Gram-positivas, a norfloxacinina para bactérias Gram-negativas, a nistatina para fungos e leveduras e o controlo negativo usado foi o DMSO. As placas foram incubadas a 37 °C durante 24 horas. A atividade antibacteriana foi avaliada por medição do diâmetro (mm) da zona de inibição formada à volta dos poços e comparando-os com o diâmetro dos controlos observados.

Determinação da atividade antioxidante (DPPH)

Para avaliar a capacidade de recaptação de radicais do extrato, foi usado o método do DPPH (20). Foram adicionados 10 µL de extrato de planta (amostra) a 990 µL de solução de DPPH (0,002% em metanol). A mistura foi incubada durante 30 minutos à temperatura ambiente. A absorvência foi medida a 517 nm contra o correspondente branco e a atividade antioxidante foi calculada de acordo com a Equação 4:

Em que AA é a atividade antioxidante, A DPPH é a absorvência do DPPH contra o branco e A amostra é a absorvência do extrato ou controlo contra o branco. Os testes foram feitos em triplicado. Os extratos foram testados a uma concentração final de 10 µg/mL.

Bioensaios de letalidade em Artemia salina

Com o objetivo de avaliar a toxicidade dos diferentes extratos foi realizado um teste de letalidade usando o modelo *Artemia salina* (18). Foram testadas concentrações de 10 ppm de cada extracto. O número de larvas mortas foi registado após 24h e utilizado para calcular a percentagem (%) de concentração letal, de acordo com a Equação 5.

Results

Extraction yield: Seven *Plectranthus* species were used in this study. The amount of dry extract weight of each *Plectranthus* species is presented in Figure 1. *P. ramosior* had the highest extraction yield (13.49 % w/w), followed by *P. petiolaris* while *P. welwischii* had the least extraction yield (3.59 % w/w).

In vitro Acetylcholinesterase inhibition: The AChE percentage inhibition was evaluated in all extracts at a concentration of 1 mg/mL, and once more *P. cylindraceus* ($30.2 \pm 3.78\%$ inhibition) extract was the most active, as is shown in Figure 2.

Os extratos ativos (acima dos 40 %) foram novamente testados às concentrações de 0.1, 0.5 e 1 ppm. O número de larvas mortas foi registrado e usado para calcular a Concentração Letal, 50% (LC_{50}) que foi determinada após 24 horas e a contagem foi feita usando um microscópio. Os valores de LC_{50} menores ou iguais a 1 ppm foram considerados ativos.

Resultados

Rendimento: Sete espécies do gênero *Plectranthus* foram usadas neste estudo. A quantidade dos extratos secos de cada uma das espécies de *Plectranthus* está apresentada na Figura 1. *P. ramosior* teve a maior rendimento de extração (13,49% m/m), seguido pelo *P. petiolaris* enquanto que o *P. welwischii* obteve o resultado mais baixo (3,59 % m/m).

Inibição da acetilcolinesterase in vitro: A inibição de AChE foi avaliada em todos os extratos (1 mg/mL), e uma vez mais o extrato *P. cylindraceus* ($30,2 \pm 3,78\%$ inibição) foi o mais ativo, como representado na Figura 2.

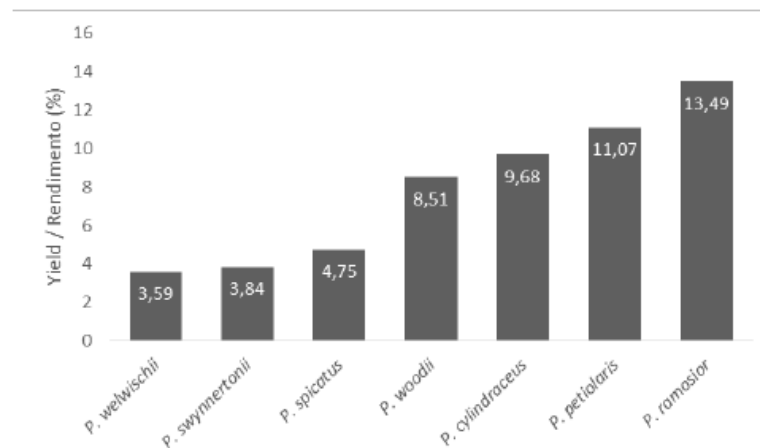


Figure 1 / Figura 1- Percentage yield (dry weight % w/w) of seven *Plectranthus* species / Rendimento (resíduo seco % m/m) das sete espécies de *Plectranthus*.

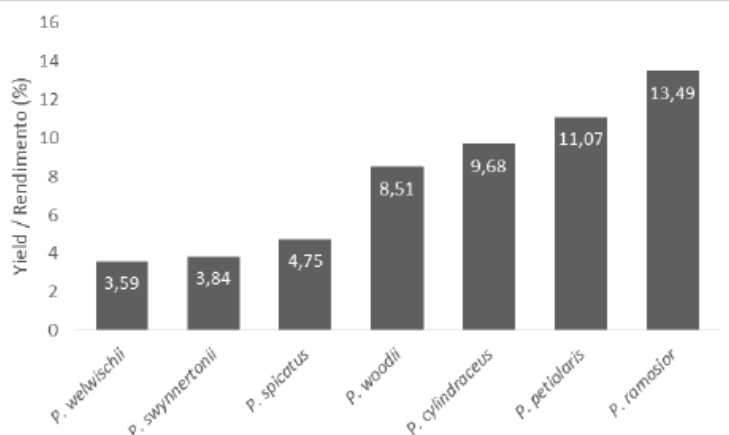


Figure 2 / Figura 2 - Acetylcholinesterase (AChE) percentage inhibition for seven Plectranthus species at 1 mg/mL / Percentagem de inibição da acetilcolinesterase (AChE) para as sete espécies de Plectranthus a 1 mg/mL.

Antimicrobial activity: The antimicrobial activity of the extracts was evaluated by the well diffusion method. Considering all extracts, the acetonic extract of *P. ramosior* obtained was the more bioactive. *P. ramosior* was active against both *S. aureus* and *C. albicans* (Table 1). None of the extracts showed significant antibacterial activity against Gram-negative bacteria with inhibition zones identical to that obtained with the negative control DMSO (5 mm).

Antioxidant activity (DPPH assay)

The antioxidant activity of the *Plectranthus* spp. acetonic extracts in study was evaluated using the DPPH method. The antioxidant activity of the extracts was qualitatively determined using the DPPH radical assay in TLC⁽¹⁴⁾ and all the extracts studied yielded positive results. The extracts were then quantified, and *P. ramosior* showed the highest scavenging activity (36.24 %) and *P. spicatus* the least (10.57 %) (Figure 3).

Brine shrimp lethality bioassay

In this study, *Artemia salina* model was preliminary used to assess the toxicity of all extracts⁽¹⁹⁾. Only three of the extracts were toxic to *A. salina*, as shown in Figure 4. The active extracts (LC above 40 %) were further determined at concentrations of 0.1, 0.5 and 1 ppm. The number of dead larvae was recorded and used to calculate the Lethal Concentration, 50% (LC₅₀), after 24 h. LC₅₀ values less than or equal to 1 ppm were considered active (Table 2).

Atividade antimicrobiana: A atividade antimicrobiana dos extratos foi avaliada pelo método de difusão em poços. Considerando todos os extratos, o extrato de *P. ramosior* obtido foi o mais bioativo. *P. ramosior* foi ativo contra *S. aureus* e *C. albicans* (Tabela 1). Nenhum dos extratos mostrou atividade antibacteriana significativa contra bactérias Gram-negativas com zonas de inibição idênticas às obtidas com o controle negativo DMSO (5 mm).

Atividade antioxidante:

A atividade antioxidante dos extratos de *Plectranthus* foi avaliada pelo método de DPPH. A atividade antioxidante dos extratos foi qualitativamente determinada utilizando o ensaio de radical DPPH em TLC⁽¹²⁾ e todos os extratos estudados produziram resultados positivos. Os extratos foram então quantificados e extrato de *P. ramosior* apresentou a maior atividade antioxidante (36.24%) enquanto que o *P. spicatus* obteve o resultado menor (10.57%) (Figura 3).

Bioensaio da letalidade em *Artemia salina*:

O modelo de *A. salina* foi utilizado preliminarmente para avaliar a toxicidade de todos os extratos neste estudo⁽¹⁹⁾. Apenas três dos extratos foram considerados tóxicos para *A. salina*, como mostrado na Figura 4. Os extratos ativos (LC acima de 40%) foram adicionalmente determinados a concentrações de 0,1; 0,5 e 1 ppm. O número de náuplios mortos foi registrado e utilizado para calcular a Concentração Letal, 50% (LC₅₀), após 24 horas. Valores de LC₅₀ inferiores ou iguais a 1 ppm foram considerados ativos (Tabela 2).

Table 1/ Tabela 1 - Antimicrobial activity of the acetonic extracts obtained by the well diffusion method (mm) / Atividade antimicrobiana dos extratos acetônicos, obtida pelo método de difusão em poços (mm).

| | Gram - | | Gram + | | Yeast/Leveduras | |
|--|-----------|-----------|-----------|-----------|-----------------|-----------|
| | <i>Pa</i> | <i>Ec</i> | <i>Sa</i> | <i>Ef</i> | <i>Sc</i> | <i>Ca</i> |
| Positive control/ Controlo positivo | 32 | 33 | 21 | 20 | 29 | 29 |
| Negative control/ Controlo negativo | 5 | 5 | 5 | 5 | 5 | 5 |
| <i>P. spicatus</i> | 5 | 5 | 5 | 5 | 5 | 5 |
| <i>P. cylindraceus</i> | 5 | 5 | 5 | 5 | 5 | 5 |
| <i>P. swynertonii</i> | 5 | 5 | 5 | 5 | 5 | 5 |
| <i>P. petiolaris</i> | 5 | 5 | 5 | 5 | 5 | 5 |
| <i>P. ramosior</i> | 5 | 5 | 15 | 5 | 5 | 11 |
| <i>P. welwischii</i> | 5 | 5 | 5 | 5 | 5 | 5 |
| <i>P. woodii</i> | 5 | 5 | 5 | 5 | 5 | 5 |

Pa – *Pseudomonas aeruginosa*; *Ec* – *Escherichia coli*; *Sa* – *Staphylococcus aureus*; *Ef* – *Enterococcus faecalis*; *Sc* – *Saccharomyces cerevisiae*; *Ca* – *Candida albicans*.

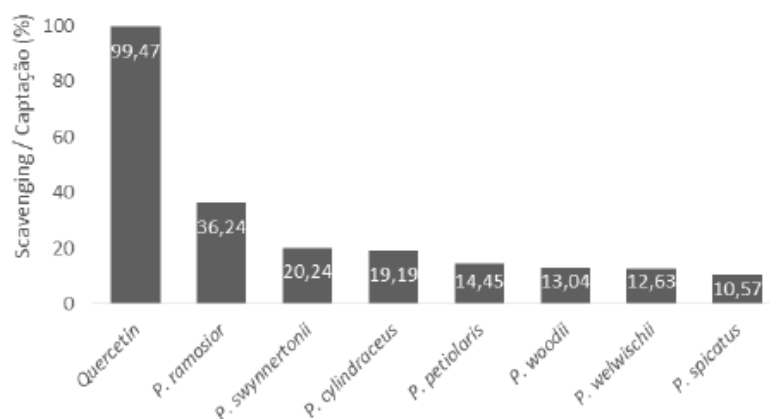


Figure 3 / Figura 3 - Antioxidant activity of extracts under study tested at a concentration of 10 µg/mL / Atividade antioxidante dos extratos em estudo tesados à concentração de 10 µg/mL.

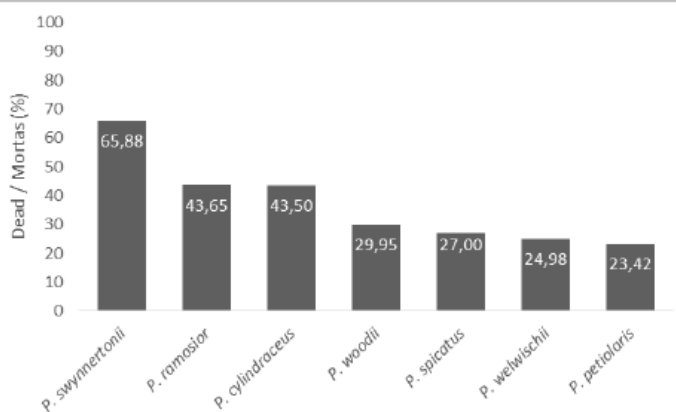


Figure 4 / Figura 4 - Screening of seven *Plectranthus* spp. extracts for toxicity at a concentration of 10 ppm using the *Artemia salina* test / Pesquisa de atividade de extratos de sete espécies de *Plectranthus* para toxicidade à concentração de 10 ppm usando o teste de *Artemia salina*.

Table 2 / Tabela 2 - LC₅₀ values (mg/L) for the most active extracts using the *Artemia salina* test / Valores de LC₅₀ (mg/L) para os extratos mais ativos usando o teste de *Artemia salina*.

| <i>Extracts/Extratos</i> | <i>LC₅₀ (mg/L)</i> |
|--------------------------|-------------------------------|
| <i>P. ramosior</i> | 0,88 |
| <i>P. cylindraceus</i> | 0,504 |
| <i>P. swynnertonii</i> | 0,036 |

Discussion

In the present study, the acetylcholinesterase inhibition, antioxidant and antimicrobial activities and *Artemia salina* toxicity of seven *Plectranthus* spp. (*P. swynertonii*, *P. welwischii*, *P. woodii*, *P. cylindraceus*, *P. spicatus*, *P. ramosior* and *P. petiolaris*) were investigated. The acetonetic extracts of the seven *Plectranthus* species were prepared using an ultrasound-assisted extraction method. Yields of extraction were determined for all prepared extracts, and the *P. ramosior* acetonetic extract revealed higher yields (Figure 1). Thus, the enhanced yield extraction of *P. ramosior* is related to the greater extent of cell rupture of the plant material. This is probably due to the ultrasound extraction that causes the migration of compounds from the plant material, providing an enriched extract compared to the other extracts in study⁽²⁰⁾.

Regarding *in vitro* AChE inhibition, *P. cylindraceus* acetonetic extract showed the highest inhibition (Figure 2), and may have the highest content in rosmarinic acid, since a correlation between rosmarinic acid content and AChE inhibition capacity has been reported previously for four other *Plectranthus* species (*P. ecklonii*, *P. fruticosus*, *P. lanuginosus* and *P. verticillatus*)⁽²⁰⁾. The AChE inhibition of these *Plectranthus* spp. under study was relatively low comparing to some of the synthetic medicines used, e.g. tacrine, donepezil and rivastigmine that have been reported to cause gastrointestinal disturbances and problems associated with bioavailability. Therefore, the search for new AChE inhibitors with higher efficacy, particularly from natural products, should be an important issue for search.

In vitro tests for screening antimicrobial activity were performed using Gram-positive bacteria (*S. aureus* and *E. faecalis*), Gram-negative bacteria (*P. aeruginosa* and *E. coli*) and yeasts (*C. albicans* and *S. cerevisiae*). The antimicrobial activity assay was carried out by the preliminary well diffusion method. Only *P. ramosior* acetonetic extract showed an inhibition growth against *S. aureus* and *C. albicans*, with no significant inhibition against Gram-negative bacteria. This results were in agreement with previous results for other *Plectranthus* spp. which also did not show antimicrobial activity against Gram negative bacteria⁽¹⁴⁾.

There has been a growing interest to find natural antioxidants, including volatile chemicals, in plants due to their inhibiting oxidative damage⁽³⁾. The acetonetic extracts under study showed low antioxidant activity. In previous studies on *Plectranthus* spp. extracts, the high content in rosmarinic acid was associated to high antioxidant activity and high AChE inhibition, on aque-

Discussão

No presente estudo, foi avaliada a inibição da acetilcolinesterase, as atividades antioxidantes e antimicrobianas e a toxicidade no modelo *Artemia salina* de sete espécies de *Plectranthus* (*P. swynertonii*, *P. welwischii*, *P. woodii*, *P. cylindraceus*, *P. spicatus*, *P. ramosior* e *P. petiolaris*). Os extratos acetônicos das sete espécies de *Plectranthus* foram preparados utilizando um método de extração assistido por ultrassons. Os rendimentos de extração foram determinados para todos os extratos preparados, e o extrato acetônico de *P. ramosior* revelou maiores rendimentos (Figura 1). Assim, o rendimento de extração de *P. ramosior* está relacionado com a maior extensão da ruptura celular do material vegetal. Isto é provavelmente devido à extração de ultrassons que causa a migração de compostos a partir do material vegetal, proporcionando um extrato enriquecido em comparação com os outros extratos em estudo⁽²⁰⁾.

Em relação à inibição da AChE *in vitro*, o extrato acetônico de *P. cylindraceus* mostrou a maior inibição (Figura 2) e pode estar relacionado com o maior teor de ácido rosmarinico, uma vez que foi relatada uma correlação entre o conteúdo de ácido rosmarinico e a capacidade de inibição da AChE em quatro outras espécies de *Plectranthus* (*P. ecklonii*, *P. fruticosus*, *P. lanuginosus* e *P. verticillatus*)⁽²⁰⁾. A inibição da AChE destas espécies de *Plectranthus* em estudo foi relativamente baixa em comparação com alguns dos medicamentos sintéticos utilizados, como a tacrina, donepezilo e rivastigmina, que foram relatados como causadores de distúrbios gastrointestinais e problemas associados à sua biodisponibilidade. Portanto, a busca por novos inibidores da AChE, particularmente a partir de produtos naturais, com maior eficácia deve ser um assunto importante a pesquisar.

Realizaram-se testes *in vitro* para rastreamento da atividade antimicrobiana utilizando bactérias Gram-positivas (*S. aureus* e *E. faecalis*), bactérias Gram-negativas (*P. aeruginosa* e *E. coli*) e leveduras (*C. albicans* e *S. cerevisiae*). Na atividade antimicrobiana realizada pelo método preliminar de difusão em poços, apenas o extrato *P. ramosior* mostrou uma inibição do crescimento contra *S. aureus* e *C. albicans*, e não mostrou uma inibição significativa contra bactérias Gram-negativas. Estes resultados estão de acordo com resultados anteriores para outras plantas do gênero *Plectranthus* que também não mostraram atividade antimicrobiana contra bactérias Gram-negativas⁽¹²⁾.

Tem havido um interesse crescente para encontrar antioxidantes naturais, incluindo produtos químicos voláteis, nas plantas devido à inibição do dano oxidativo

ous extracts⁽²⁰⁾. Since the acetonic extracts in study showed moderate AChE inhibition and also moderate antioxidant activity, the rosmarinic acid content should be low, as well as other antioxidant extract constituents. Although these results showed that *P. ramosior* was the most antioxidant, the activity was only moderate in comparison with the controls, and, additionally its AChE % inhibition was low. Hence this extract is not a potential starting point for the search of drugs that inhibit oxidative damage and may consequently prevent inflammatory conditions, ageing and neurodegenerative diseases (such as Alzheimer's disease)⁽¹⁸⁾.

In this study, the brine shrimp lethality assay (*Artemia salina*) was preliminary used to search for the toxicity of all extracts prepared. Only three extracts were considered toxic to *A. salina* (lethality > 40%), and for those the LC₅₀ was evaluated. *P. swynnertonii* extract was the most toxic with LC₅₀ value of 0.036 mg/L, followed by *P. cylindraceus* (LC₅₀ 0.50 mg/L) and *P. ramosior* (LC₅₀ value 0.88 mg/L). *P. cylindraceus* extract showed the highest AChE % inhibition and was also toxic to the *Artemia* model. Hence, this extract is an interesting starting point for future phytochemical studies to identify which compounds are responsible for the biological activities shown.

P. ramosior acetonic extract seemed to be the most promising extract regarding its activity: it had effect on growth inhibition against bacteria and yeast, had antioxidant activity and revealed high toxicity to *A. salina* model. However, the antimicrobial activity might be due to its toxicity and this should be further investigated. Other bioactivity studies should be carried out in order to unravel other potential bioactivities and its bioactive compounds.

Consequently, this bioactivity screening of *Plectranthus* extracts is important as a preliminary study to select which plants should be investigated for further phytochemical studies. Moreover, future studies on *P. ramosior* and other active extracts (such as *P. cylindraceus*, *P. swynnertonii* and *P. petiolaris*) could be done to determine which are the bioactive compounds and their structural elucidation (by spectroscopic methods), and confirm the bioactivity of these compounds that are responsible for the biological activity revealed in this study.

Conclusion

In the present study, seven species of *Plectranthus* were analysed to evaluate their acetylcholinesterase inhibition, antimicrobial and antioxidant activities and toxicity. None of the extracts showed high acetylcholinesterase

(3). Os extratos acetônicos estudados mostraram baixa atividade antioxidante. Em estudos anteriores sobre extratos de *Plectranthus*, o alto teor de ácido rosmarinico foi associado a alta atividade antioxidante e alta inibição da AChE, em extratos aquosos⁽²⁰⁾. Uma vez que os extratos de acetona no estudo mostraram uma inibição moderada da AChE bem como a atividade antioxidante, o teor de ácido rosmarinico deve ser baixo. Embora estes resultados tenham mostrado que *P. ramosior* foi o mais antioxidante, a atividade foi apenas moderada em comparação com os controles e, adicionalmente, a sua inibição de AChE foi baixa. Por conseguinte, este extrato não é um potencial ponto de partida para a pesquisa de fármacos que imibem o dano oxidativo, podendo consequentemente prevenir condições inflamatórias, envelhecimento e doenças neurodegenerativas (como a doença de Alzheimer)⁽¹⁸⁾.

O ensaio de letalidade no modelo da *Artemia salina*, foi utilizado preliminarmente para pesquisar a toxicidade de todos os extratos preparados neste estudo. Apenas três extratos foram considerados tóxicos para *A. salina* (letalidade > 40%), e para os que foram avaliados a LC₅₀. O extrato de *P. swynnertonii* foi o mais tóxico com LC₅₀ de 0,036 mg/L, seguido do *P. cylindraceus* (LC₅₀ - 0,50 mg/L) e *P. ramosior* (LC₅₀ - 0,88 mg/L). O extrato de *P. cylindraceus* apresentou a maior inibição de AChE e também foi tóxico para o modelo de *Artemia*. Assim, este extrato é um ponto de partida interessante para futuros estudos fitoquímicos, de modo a poder identificar quais os compostos que são responsáveis pelas atividades biológicas mostradas.

O extrato acetônico de *P. ramosior* parece ser o extrato mais promissor em relação às atividades biológicas estudadas: obteve efeito sobre a inibição do crescimento contra bactérias e leveduras em estudo, obteve atividade antioxidante e revelou alta toxicidade ao modelo de *A. salina*. No entanto, a actividade antimicrobiana pode ser devida à sua toxicidade e isto deve ser investigado mais a fundo. Outros estudos de bioactividade devem ser realizados para desvendar outras potenciais bioactividades e quais os compostos bioactivos responsáveis pelas actividades reveladas.

Consequentemente, este rastreio de bioactividade de extractos de *Plectranthus* é importante como um estudo preliminar, para seleccionar quais as plantas que devem ser investigadas para estudos fitoquímicos adicionais. Além disso, estudos futuros sobre *P. ramosior* e outros extratos ativos (como *P. cylindraceus*, *P. swynnertonii* e *P. petiolaris*) podem ser realizados para revelar quais são os compostos bioativos e sua elucidação estrutural (por métodos espectroscópicos) e confirmar a bioatividade desses compostos que são responsáveis pela atividade biológica revelada.

ase inhibition or antioxidant activities. Only *P. ramosior* acetonic extract exhibited antimicrobial activity, showing positive results against the Gram-positive bacteria and yeasts tested. Three extracts were toxic against the brine shrimp, with *P. swynnertonii* being the most toxic. *P. ramosior* acetonic extract exhibited antimicrobial activity. This preliminary study allows the selection of which plants should be chosen for future studies. Further studies should be undertaken to identify the bioactive compounds responsible for these bioactivities of the active extracts. (*P. ramosior*, *P. swynnertonii*, *P. cylindraceus* and *P. petiolaris*).

Conflict of interest

The authors declares that there are no financial or personal relationships that could be viewed as a potential conflict of interest.

Conclusão

No presente estudo, sete espécies de *Plectranthus* foram analisadas para avaliar a inibição da acetilcolinesterase, atividades antimicrobiana e antioxidante, e toxicidade. Nenhum dos extratos mostrou elevada inibição de acetilcolinesterase ou atividade antioxidante. Somente o extrato acetônico de *P. ramosior* mostrou resultados positivos contra bactérias Gram-positivas e leveduras testadas. Três extratos foram tóxicos contra o modelo de *A. salina*, sendo *P. swynnertonii* o mais tóxico. O extrato acetônico de *P. ramosior* exibiu atividade antimicrobiana. Este estudo preliminar permite selecionar quais as plantas que devem ser escolhidas em estudos futuros. Outros estudos devem ser realizados para identificar os compostos bioativos responsáveis por essas bioatividades dos extratos ativos (*P. ramosior*, *P. swynnertonii*, *P. cylindraceus* e *P. petiolaris*).

Conflito de Interesses

Os autores declaram não existir qualquer relação de natureza financeira ou pessoal que possa ser entendida ou representar um potencial conflito de interesses.

References/Referências

1. Lukhoba CW, Simmonds MSJ, Paton AJ. Plectranthus: A review of ethnobotanical uses. *J Ethnopharmacol.* 2006;103(1):1–24.
2. Rice LJ, Brits GJ, Potgieter CJ, Van Staden J. Plectranthus: A plant for the future? *South African J Bot.* 2011;77(4):947–59.
3. Rijo P, Batista M, Matos M, Rocha E, Jesus S, Simões M. Screening of antioxidant and antimicrobial activities on Plectranthus spp. extracts. *Biomed Biopharm Res.* 2012;9(2):225–35.
4. Rijo P, Matias D, Fernandes AS, Simões MF, Nicolai M, Reis CP. Antimicrobial plant extracts encapsulated into polymeric beads for potential application on the skin. *Polymers (Basel).* 2014;6(2):479–90.
5. Davinelli S, Sapere N, Zella D, Bracale R, Intriери M, Scapagnini G. Pleiotropic Protective Effects of Phytochemicals in Alzheimer's Disease. *Oxid Med Cell Longev.* 2012;2012:1–11.
6. Tabet N. Acetylcholinesterase inhibitors for Alzheimer's disease: anti-inflammatory in acetylcholine clothing! *Age Ageing.* 2006;35(4):336–8.
7. Colović MB, Krstić DZ, Lazarević-Pašti TD, Bondžić AM, Vasić VM. Acetylcholinesterase inhibitors: pharmacology and toxicology. *Curr Neuropharmacol.* 2013;11(3):315–35.
8. Sung SH, Kang SY, Lee KY, Park MJ, Kim JH, Park JH, et al. (+)-Alpha-viniferin, a stilbene trimer from Caragana chamlague, inhibits acetylcholinesterase. *Biol Pharm Bull.* 2002;25(1):125–7.
9. Duracková Z. Some current insights into oxidative stress. *Physiol Res.* 2010;59(4):459–69.
10. Bonomini F, Rodella LF, Rezzani R. Metabolic syndrome, aging and involvement of oxidative stress. *Aging Dis.* 2015;6(2):109–20.
11. Guimarães DO, Momesso L da S, Pupo MT. Antibióticos: importância terapêutica e perspectivas para a descoberta e desenvolvimento de novos agentes. *Quim Nova.* 2010;33(3):667–79.
12. Kubínová R, Pořízková R, Navrátilová A, Farza O, Hanáková Z, Bačinská A, et al. Antimicrobial and enzyme inhibitory activities of the constituents of Plectranthus madagascariensis (Pers.) Benth. *J Enzyme Inhib Med Chem.* 2014;29(5):749–52.
13. Albar H. Phytochemical composition and antimicrobial activities of the essential oil from Plectranthus tenuiflorus growing in Saudi Arabia. *KauEduSa.* 2002;1–9.
14. Rijo P, Batista M, Matos M, Rocha H, Jesus S, Simões MF. Screening of antioxidant and antimicrobial activities on Plectranthus spp. extracts. *Biomed Biopharm Res.* 2012;9(2):225–35.
15. Karchesy YM, Kelsey RG, Constantine G, Karchesy JJ. Biological screening of selected Pacific Northwest forest plants using the brine shrimp (*Artemia salina*) toxicity bioassay. *Springerplus.* 2016;5:510–8.
16. Chen X, Guo C, Kong J. Oxidative stress in neurodegenerative diseases. *Neural Regen Res.* 2012;7(5):376–85.
17. Hamidi MR, Jovanova B, Panovska TK. Toxicological evaluation of the plant products using Brine Shrimp (*Artemia salina* L.) model. *Maced Pharm Bull.* 2014;60(1):9–18.
18. Alanis-Garza BA, González-González GM, Salazar-Aranda R, Waksman de Torres N, Rivas-Galindo VM. Screening of antifungal activity of plants from the northeast of Mexico. *J Ethnopharmacol.* 2007;114(3):468–71.
19. Meyer B, Ferrigni N, Putnam J, Jacobsen L, Nichols D, McLaughlin J. Brine Shrimp: A Convenient General Bioassay for Active Plant Constituents. *Planta Med.* 1982;45(5):31–4.
20. Rijo P, Falé PL, Serralheiro ML, Simões MF, Gomes A, Reis C. Optimization of medicinal plant extraction methods and their encapsulation through extrusion technology. *Measurement.* 2014;58:249–55.

Article

Characterization of Kefir Produced in Household Conditions: Physicochemical and Nutritional Profile, and Storage Stability

Emília Alves ^{1,2}, Epole N. Ntungwe ^{1,2}, João Gregório ¹, Luis M. Rodrigues ¹, Catarina Pereira-Leite ^{1,3}, Cristina Caleja ⁴, Eliana Pereira ⁴, Lillian Barros ⁴, M. Victorina Aguilar-Vilas ², Catarina Rosado ^{1,*} and Patrícia Rijo ^{1,5,*}

- ¹ CBIOS—Research Center for Biosciences & Health Technologies, Universidade Lusófona's, Campo Grande 376, 1749-024 Lisboa, Portugal; emilia.alves@ulusofona.pt (E.A.); p5999@ulusofona.pt (E.N.N.); joao.gregorio@ulusofona.pt (J.G.); monteiro.rodrigues@ulusofona.pt (L.M.R.); catarina.leite@ulusofona.pt (C.P.-L.)
- ² Department of Biomedical Sciences, Faculty of Pharmacy, University of Alcalá, Carretera Madrid-Barcelona, Km 33.100, 28805 Alcalá de Henares, Madrid, Spain; mvictorina.aguilar@uah.es
- ³ LAQV, REQUIMTE, Departamento de Ciências Químicas, Faculdade de Farmácia, Universidade do Porto, Rua de Jorge Viterbo Ferreira 228, 4050-313 Porto, Portugal
- ⁴ Centro de Investigação de Montanha (CIMO), Instituto Politécnico de Bragança, Campus de Santa Apolónia, 5300-253 Bragança, Portugal; ccaleja@ipb.pt (C.C.); eliana@ipb.pt (E.P.); lillian@ipb.pt (L.B.)
- ⁵ Instituto de Investigação do Medicamento (iMed.Ulisboa), Faculdade de Farmácia, Universidade de Lisboa, 1649-003 Lisboa, Portugal
- * Correspondence: catarina.rosado@ulusofona.pt (C.R.); prijo@ff.ulisboa.pt (P.R.)



Citation: Alves, E.; Ntungwe, E.N.; Gregório, J.; Rodrigues, L.M.; Pereira-Leite, C.; Caleja, C.; Pereira, E.; Barros, L.; Aguilar-Vilas, M.V.; Rosado, C.; et al. Characterization of Kefir Produced in Household Conditions: Physicochemical and Nutritional Profile, and Storage Stability. *Foods* **2021**, *10*, 1057. <https://doi.org/10.3390/foods10051057>

Academic Editor: Francesco Visioli

Received: 9 April 2021

Accepted: 7 May 2021

Published: 11 May 2021

Publisher's Note: MDPI stays neutral with regard to jurisdictional claims in published maps and institutional affiliations.



Copyright: © 2021 by the authors. Licensee MDPI, Basel, Switzerland. This article is an open access article distributed under the terms and conditions of the Creative Commons Attribution (CC BY) license (<https://creativecommons.org/licenses/by/4.0/>).

Abstract: Kefir, a traditional fermented food, has numerous health benefits due to its unique chemical composition, which is reflected in its excellent nutritional value. Physicochemical and microbial composition of kefir obtained from fermented milk are influenced by the type of the milk, grain to milk ratio, time and temperature of fermentation, and storage conditions. It is crucial that kefir characteristics are maintained during storage since continuous metabolic activities of residual kefir microbiota may occur. This study aimed to examine the nutritional profile of kefir produced in traditional in use conditions by fermentation of ultra-high temperature pasteurized (UHT) semi-skimmed cow milk using argentinean kefir grains and compare the stability and nutritional compliance of freshly made and refrigerated kefir. Results indicate that kefir produced under home use conditions maintains the expected characteristics with respect to the physicochemical parameters and composition, both after fermentation and after refrigerated storage. This work further contributes to the characterization of this food product that is so widely consumed around the world by focusing on kefir that was produced in a typical household setting.

Keywords: kefir; household conditions; storage time influence; nutritional composition; fatty acid profile; particle size; polydispersity index; zeta potential

1. Introduction

Traditional kefir has been consumed for centuries [1,2] due to its high nutritional value and is therefore considered a health promoting food [3]. Several health benefits have been attributed to kefir, mainly justified by the bioactivity of metabolites produced during fermentation [4,5], such as improved lactose digestion and tolerance [6], anti-inflammatory effect [7,8], antimicrobial activity [9], antioxidant activity [10], antitumor activity [11], wound healing [9,12], modulation of the immune system [13], and growth inhibition of pathogenic microorganisms [14,15]. Traditional kefir production uses kefir grains as starter culture, differentiating it from other fermented foods [16]. Kefir grains can maintain their activity as long as they are preserved and incubated under appropriate conditions, due to their extremely stable microbial composition [17–19]. The microorganisms usually found in the grains are homo and heterofermentative lactic acid bacteria (LAB), Lactobacillaceae

family (genera *Lactobacillus* and *Leuconostoc*) and Streptococcaceae family (genera *Lactococcus* and *Streptococcus*), acetic acid bacteria Acetobacteraceae family (genera *Acetobacter*) and yeasts Saccharomycetaceae family (genera *Kluyveromyces* and *Saccaromyces*) [20–24]. The viability of kefir grains is guaranteed through maintenance of the bacterial/yeast ratio achieved by continuous fermentation cycles that lead to their biomass increase [2,20,25]. This increment is dependent on temperature, pH, washing of grains, renewal of milk, and presence of nutrients [16,25–27]. Grain preservation for household kefir production can be achieved either by continuous fermentation cycles, and assured for ten weeks of propagation [17], or by freezing at $-20\text{ }^{\circ}\text{C}$ [19]. The microbiological composition of kefir grains depends on their origin [20,28–30].

Kefir's microbiota is different from that of the grains [16]. The physicochemical and microbial composition of kefir fermented milk is influenced by the type of the milk, grain to milk ratio, time and temperature of fermentation, and storage conditions [31–35]. Traditional kefir typically uses cow's milk as substrate [30,33]. Although whole, semi-skimmed, or skimmed milk can be used [32,36], the latter creates a kefir with significantly lower nutritional quality [29]. Grain to milk ratio, usually varying between 2% and 10% (*w/v*), influences the kefir microbial profile, and higher rates of grain inoculum increase lactic acid levels, providing sharper pH lowering [14,31,36]. The viscosity is also affected, since higher percentages of kefir grain inoculate produce a more acidic, but less viscous, kefir [31,36]. Lactose content is the main nutritional compound influenced by the amount of grain inoculum and smaller ratios of inoculate results in kefir with higher lactose levels [21,36].

Typical kefir fermentation occurs at temperatures between 20 and 25 °C for approximately 24 h, with pH varying between 4.2 and 4.6 [14,31,37]. During fermentation, the chemical composition of kefir changes mainly due to lactose conversion by homofermentative LAB, first into lactic acid, causing the pH to drop and acidity to increase [21,38], followed by the remaining hydrolyzation into glucose and galactose by the enzymatic activity of β -galactosidase present in the grains [39]. Further into the fermentation cycle heterofermentative LAB convert glucose into CO_2 , ethanol and lactic acid, the latter being the most predominant organic acid after fermentation, and in this environment proteins are converted into peptides [34,36,40,41]. The production of lactic acid contributes to the antimicrobial effect of kefir, and since it acts as a natural preservative, allows the homemade product to have a low contamination risk [14,24,42].

The chemical composition of kefir reflects its nutritional value and the recommended quality standards for kefir are at least 2.8% protein, less than 10% fat, and at least 0.6% lactic acid [43]. Kefir can be consumed immediately after grain separation or may be refrigerated for later consumption [4,25,41]. Fermented milk characteristics must be maintained during storage; however, since continuous metabolic activities of residual kefir microbiota may occur, the composition of refrigerated kefir may be affected during storage [19,34,36,44]. Kefir can maintain a shelf life of 3–12 days [25]. During refrigerated storage at 4 °C, viscosity is reported to decrease abruptly with time [34,36], while total fat, lactose, dry matter, and pH remain constant until 14 days of storage [32,36,40] and lactic acid slightly increases after 7 days storage [40]. Although the lipolytic activity in milk fat by LAB is limited, it can still contribute to the production of free fatty acids [45].

This work aimed to study kefir produced in representative household conditions, characterizing the properties, nutritional composition, and stability of a freshly made and 48 h refrigerated beverage. To date, information on homogeneity and stability of traditional kefir is scarce, and to the best of our knowledge, this is the first study to provide information on kefir produced by simulating representative home use conditions. The innovative character of this study also resides in the fact that, in addition to the usual parameters for physicochemical analysis and composition, the fatty acid profile, particle size, polydispersity index (Pdl), zeta potential, and Fourier Transform Infrared Spectroscopy (FTIR) spectra analysis were also included in the global evaluation of kefir.

2. Materials and Methods

2.1. Kefir Grains Storage and Kefir Production

Kefir grains CIDCA AGK1 were obtained from the Centro de Investigación y Desarrollo en Criotecnología de Alimentos (CIDCA), La Plata, Argentina. Microbiological characterization of these grains has been described elsewhere [20,46,47]. Kefir grains were maintained in milk and preserved by storage in a freezer at -20 ± 2 °C, which proved to be the best method for grain preservation and can also be used to maintain the grains for household kefir production [19]. After this type of storage, the grains were activated before use in fermentation [27]. For activation, grains were left to defrost at room temperature for 12 h, after which they were placed in semi-skimmed milk at 20 ± 1 °C for 24 h. The activation step was repeated three times.

Kefir beverage samples were produced by fermentation for 24 h of a commercial ultra-high temperature pasteurized (UHT) semi-skimmed cow milk of Portuguese provenance (Nova Açores[®], S. Miguel, Portugal), with CIDCA AGK1 kefir grains using a grain inoculum of 10% (*w/v*), at a temperature of 20 ± 1 °C. After fermentation, grains were separated from the fermented milk by filtration through a plastic sieve and used as starter culture for the next kefir batch, under the same conditions. Samples of fermented milk kefir were collected after filtration.

2.2. Activity of Kefir Grains

2.2.1. Biomass Growth

Kefir grain biomass increase was measured over 8 days, with daily inoculations in milk. Kefir grains were sub-cultured by successive passage of the total amount of grains in increasing volumes of milk to maintain a concentration of 10% (*w/v*) [19]. Rinsing of the grains was made with milk, because growth of the grains is retarded when they are rinsed with water after each sieving [27]. Kefir grains were separated from fermented milk by filtration using a plastic sieve. Grains were rinsed with milk at room temperature and left to dry on a filter paper at room temperature (20 ± 1 °C), after which kefir grains were weighed using an analytical scale (KERN ALJ220-4NM (KERN & Sohn GmbH, Balingen, Germany)) for gravimetric determination. After weighing, kefir grains were used as a new inoculum, maintaining the grain to milk ratio. Samples were made in duplicate. Biomass growth rate was determined gravimetrically, and increment percentage was calculated. All measurements were made in triplicate.

2.2.2. Acidification Kinetic

Kefir fermentation of milk was carried out at 20 ± 1 °C and samples of fermented milk were collected every 2 h until a stabilized pH value was reached. Measurements were made using a Metrohm 827 pH lab[®] digital meter (Metrohm AG, Herisau, Switzerland). Samples were made in duplicate. All measurements were made in triplicate.

2.3. Viable Microorganisms and Inhibitory Activity Test

2.3.1. Bacterial and Yeasts Counts

Determination of LAB and yeast counts were made by conventional culture techniques [48]. Tryptone water (Sigma-Aldrich, St. Louis, MO, USA) at a concentration of 1 g/L was used to prepare the dilutions for the microbiological analyses. Ten-fold dilutions in 0.1% sterile tryptone water were plated in each medium. LAB counts were quantified on De Man, Rogosa and Sharpe (MRS) agar plates (Oxoid, Hampshire, UK), which were incubated at 30 ± 1 °C for 24 h, and then for another 24 h, under the same conditions. Yeast counts were quantified on Yeast-Extract Glucose Chloramphenicol (YGC) agar plates (Oxoid, Hampshire, UK), which were incubated at 30 ± 1 °C for 48 h. Counts were expressed in total colony-forming units per milliliter. Measures were made in duplicate.

2.3.2. Inhibitory Activity Test

Inhibitory activity of kefir fermented milk was evaluated on the growth of *Escherichia coli* using conventional culture techniques [48]. *E. coli* counts were quantified on Eosin Methylene Blue Agar (EMB) agar plates (Oxoid, Hampshire, UK), which were incubated at 37 ± 1 °C for 24 h. A known *E. coli* strain (ATCC 25922) was used as control. Measures were made in duplicate.

2.4. Physicochemical Characteristics of Kefir Beverage

2.4.1. Particle Size, Polydispersity Index, and Zeta Potential

The particle size and PDI were analyzed, by dynamic light scattering, for milk (control), kefir immediately after the 24 h fermentation period (t0), and kefir after storage at 5 ± 1 °C for 24 and 48 h (t24 and t48, respectively). Zeta potential was also evaluated at the same time points by an electrophoretic mobility technique using a Delsa™ Nano C from Beckman Coulter, Inc. (Brea, CA, USA). All analyses were run in triplicate at room temperature (20 ± 1 °C) after diluting the samples with distilled water. Dilutions of 1:50 or 1:125 were used in the case of unfermented or kefir fermented milk, respectively.

2.4.2. Fourier Transform Infrared Spectroscopy (FTIR)

Kefir samples (t0, t24, and t48) obtained after freeze-drying were evaluated by FTIR in a PerkinElmer® Spectrum 400 (PerkinElmer Inc, Waltham, MA, USA) equipped with an attenuated total reflectance (ATR) device. The ATR system was cleaned before each analysis by using dry paper and scrubbing it with methanol and water (50:50). The room air FTIR-ATR spectrum was used as background to verify the cleanliness and to evaluate the instrumental conditions and room interferences due to H₂O and CO₂. The spectra were obtained collecting 100 scans of each sample, between 4000 and 600 cm⁻¹, with a resolution of 4 cm⁻¹. The FTIR analysis was also performed for unfermented milk as a control sample.

2.4.3. Viscosity and pH

The viscosity and pH were evaluated for both control and kefir samples (t0, t24, and t48). Viscosity was measured using a Brookfield Ametek DV3T® rheometer (AMETEK Brookfield, Middleboro, MA, USA) with a SV18 spindle, at 30 rpm. Measurements were performed at 25.2 ± 0.2 °C and readings were recorded for 1 min. pH was measured using a Metrohm 827 pH lab® digital meter (Metrohm AG, Herisau, Switzerland). Samples were made in duplicate, and all measurements were made in triplicate.

2.5. Nutritional Analysis of Kefir Beverage

For chemical analysis, both control and kefir samples (t0, t24, and t48) were frozen at -80 °C for 24 h, after which all samples were freeze-dried in a Labconco FreeZone 25® (Labconco, Kansas City, MO, USA) using a surface condenser temperature of -50 °C and 400 mTorr for 24 h. Samples were weighed before freezing and after freeze-drying for mass determination. The contents of protein, fat, carbohydrates, and ash were determined according to the official analysis methodologies AOAC [49] and following a procedure previously reported by Barros et al. [50]. Protein was determined considering the total nitrogen content and using the specific conversion factor for milk (6.38). Total fat content was analyzed as fatty acids and expressed as triglyceride equivalents. Ash was determined by gravimetry. Total carbohydrate content was determined by difference, as follows: 100- (weight in grams (protein + fat + water + ash + alcohol) in 100 g of food) [51]. Dry matter was calculated as the sum of total fat, protein, ash, and carbohydrates content. Total energy was calculated following the Equation:

$$\text{Energy (kcal)} = 4 \times (\text{g protein} + \text{g carbohydrates}) + 9 \times (\text{g fat}).$$

All samples were also evaluated regarding the sugar content, following an extraction procedure previously described [50]. Samples were then filtered through 0.2 μm Whatman nylon filters into a 1.5 mL vial for liquid chromatography analysis. The HPLC system was coupled to a refraction index (RI) detector and the free sugars were identified by comparison with standards and further quantified considering the internal standard and results were expressed in g per 100 g [50]. In addition, all samples were also evaluated for fatty acids content, which were extracted from all the samples and determined by gas chromatography coupled with a flame ionization detector (GC-FID, DANI model GC 1000, Contone, Switzerland) using a procedure previously described by Barros et al. [50]. The results were expressed as relative percentage of each fatty acid (%). Two batches of all samples were made, and all analyses were performed in duplicate.

2.6. Statistical Analysis

Results were expressed as mean \pm standard deviation (SD). Linear regression was used to assess grains biomass growth. Differences over the groups were identified using one-way ANOVA analysis of variance. Different letters show significant differences by Tukey Post hoc multiple comparison tests. When homogeneity was not guaranteed, Games-Howell post-hoc tests were used. All analyses were performed using the SPSS statistical package version 25 (SPSS Inc., Chicago, IL, USA) with a level of significance of 0.05.

3. Results

3.1. Activity of Kefir Grains

3.1.1. Biomass Growth

Biomass growth of kefir grains, incubated at 20 ± 1 $^{\circ}\text{C}$, for successive 24 h periods over 8 days, expressed in weight (g), is showed in Figure 1.

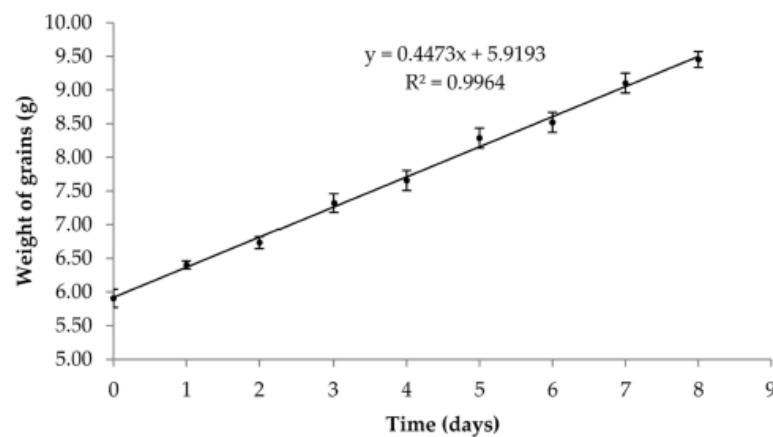


Figure 1. Increment of kefir grains biomass (g), incubated at 20 $^{\circ}\text{C}$ for 24 h periods, over 8 days (mean \pm SD, $n = 3$).

Our results showed that after 8 days of successive fermentations the biomass grains had an increment of 60% when compared to the initial weight of the grains. We found that our CIDCA AGK1 grains had a mean 24 h biomass growth of $6 \pm 2\%$, after fermentation at 20 $^{\circ}\text{C}$.

3.1.2. Acidification Kinetic

The acidification rate of milk measured during kefir fermentation are showed in Figure 2.

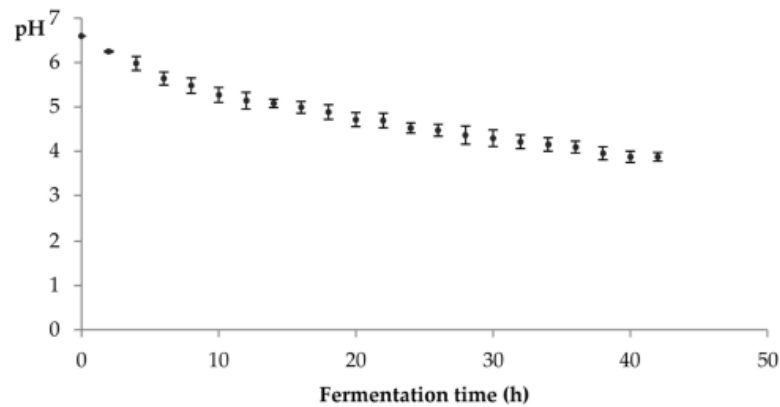


Figure 2. Acidification rate during fermentation at 20 °C, until pH stabilization (mean ± SD, $n = 3$).

As expected, during fermentation the pH value of kefir dropped from the value of 6.6 of unfermented milk, reaching a mean value of 4.5 ± 0.1 at the end of 24 h. After 42 h, the mean pH value of the kefir beverage stabilized at 3.9 ± 0.1 .

3.2. Viable Microorganisms and Inhibitory Activity Test

The viable LAB and yeast counts, as well as coliforms found in the kefir analysis are presented in Table 1.

Table 1. Viable LAB and yeast counts (CFU/mL) and coliforms (CFU/mL) of kefir made from CIDCA AGK1 grains.

| | Kefir Beverage |
|--------------------|-----------------|
| LAB (CFU/mL) | 7×10^7 |
| Yeasts (CFU/mL) | 2×10^6 |
| Coliforms (CFU/mL) | Absent |

The microbiological analysis of our kefir revealed 7×10^7 CFU/mL of LAB and 2×10^6 CFU/mL of yeast. Furthermore, the absence of coliforms (*E. coli*) was also confirmed (Table 1).

3.3. Physicochemical Characteristics of Kefir Beverage

3.3.1. Particle Size, Pdl, and Zeta Potential

The hydrodynamic diameter, Pdl, and zeta potential of unfermented milk and kefir beverages, according to storage conditions, are presented in Table 2. In all cases, nanometric diameters (250–439 nm) were found for all beverages, with Pdl values lower than 0.3, and zeta potential values smaller than -30 mV. Kefir at t_0 showed a particle size and a Pdl significantly higher ($p < 0.0001$ and $p < 0.0001$, respectively) than control, but no statistical difference was observed for zeta potential ($p = 0.483$). 24 h refrigerated kefir presented a smaller particle size ($p < 0.0001$), a smaller Pdl ($p = 0.001$) and also a smaller zeta potential ($p = 0.013$) compared to kefir at t_0 , but no differences were observed throughout storage for these parameters ($p = 0.975$, $p = 0.575$, and $p = 0.996$, respectively).

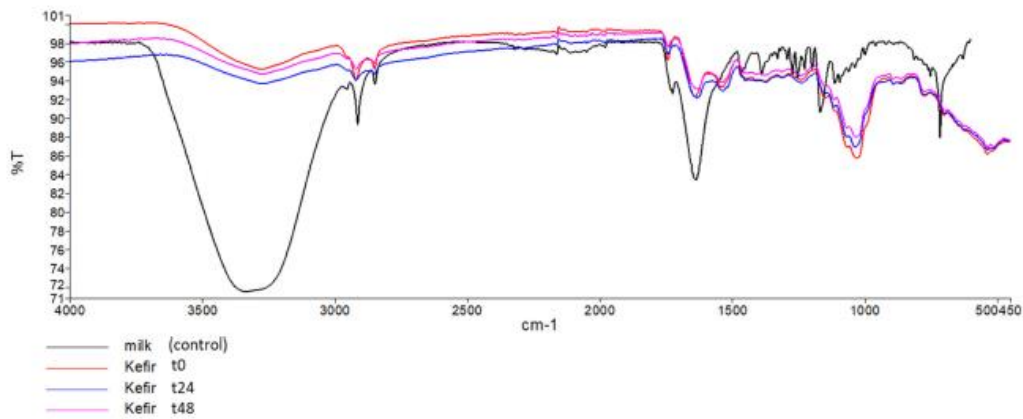
Table 2. Hydrodynamic diameter, PDI, and zeta potential of control and kefir samples (t0, t24, and t48) (mean \pm SD, $n = 3$).

| | Control | | Kefir | |
|---------------------|------------------------------|--------------------------------|--------------------------------|------------------------------|
| | | t0 | t24 | t48 |
| Diameter (nm) | 280 \pm 5 ^b | 439 \pm 42 ^a | 256 \pm 6 ^b | 249 \pm 1 ^b |
| PdI | 0.18 \pm 0.01 ^b | 0.295 \pm 0.006 ^a | 0.231 \pm 0.008 ^c | 0.22 \pm 0.02 ^c |
| Zeta potential (mV) | -35 \pm 2 ^a | -38 \pm 1 ^a | -31 \pm 2 ^b | -30 \pm 3 ^b |

^{a-c} Means within the same row with different superscripts are significantly different $p < 0.05$.

3.3.2. FTIR

FTIR spectra were collected for unfermented milk and for kefir samples (t0, t24, and t48) (Figure 3). The control spectrum showed the presence of a broad band at 3335.99 cm^{-1} : it was attributed to -OH stretching in hydroxyl groups associated with carbohydrate structures. The peaks at 2915.49 cm^{-1} are associated with C-H bending in fatty acids, 1639.26 cm^{-1} correlates to the carbonyl (C=O) stretching or N-H and C-H bending vibration of the milk proteins. The bands 2915 and 2856.7 cm^{-1} may be due to the anti-symmetric and symmetric stretching of CH_2 groups from the fatty milk components.

**Figure 3.** FTIR spectra of control and kefir samples (t0, t24, and t48).

From Figure 3 we can observe a very strong overlap between the spectral signals of milk (control) and kefir samples: t0, t24, and t48. This is evident throughout the full-recorded spectral region, suggesting a high similarity in the composition between the samples.

3.3.3. Viscosity and pH

After a 24 h fermentation, kefir showed a mean pH value of 4.60 ± 0.05 , which was significantly lower than that of the control ($p < 0.0001$). No statistical difference in pH values was observed between samples t0 and t24 ($p = 0.116$) and between both refrigerated samples ($p = 0.168$). However, the pH value decreased between t0 and t48 ($p = 0.014$). Kefir at t0 showed a mean viscosity of 32 ± 4 mPa.s, which was significantly higher than that of the control ($p < 0.0001$). The viscosity of kefir decreased after a refrigerated storage period of 24 h ($p = 0.043$). However, no significant difference in viscosity was observed between both refrigerated samples ($p = 0.732$) (Table 3).

Table 3. Physical parameters of control and kefir samples (t0, t24, and t48) (mean \pm SD, $n = 6$).

| | Control | Kefir | | |
|-------------------|------------------------------|------------------------------|--------------------------------|------------------------------|
| | | t0 | t24 | t48 |
| pH | 6.60 \pm 0.00 ^a | 4.60 \pm 0.05 ^b | 4.54 \pm 0.02 ^{b,c} | 4.50 \pm 0.04 ^c |
| Viscosity (mPa.s) | 2.11 \pm 0.01 ^b | 32 \pm 4 ^a | 26 \pm 2 ^c | 24 \pm 4 ^c |

^{a-c} Means within the same row with the different superscripts are significantly different $p < 0.05$.

3.4. Nutritional Analysis of Kefir Beverage

The nutritional content, evaluated by fat, protein, carbohydrates, ash, lactose, and lactic acid content, as well as the energy value of unfermented milk and the kefir samples immediately after 24 h fermentation at 20 °C, and after 24 h and 48 h of cold storage at 5 \pm 1 °C, is shown in Table 4.

Table 4. Nutritional composition of control and kefir samples (t0, t24, and t48) (mean \pm SD, $n = 4$).

| | Control | Kefir | | |
|-----------------------|-------------------------------|------------------------------|--------------------------------|------------------------------|
| | | t0 | t24 | t48 |
| Energy (kcal/100 mL) | 48.2 \pm 0.4 ^a | 43.8 \pm 0.6 ^b | 44.5 \pm 0.8 ^b | 44 \pm 2 ^b |
| Carbohydrates (% w/v) | 5.14 \pm 0.08 | 4.9 \pm 0.2 | 5.0 \pm 0.1 | 5.0 \pm 0.2 |
| Lactose (% w/v) | 4.74 \pm 0.05 ^a | 4.1 \pm 0.2 ^b | 3.75 \pm 0.08 ^b | 3.8 \pm 0.2 ^b |
| Proteins (% w/v) | 2.8 \pm 0.1 | 3.2 \pm 0.2 | 3.1 \pm 0.1 | 3.15 \pm 0.05 |
| Total Fat (% w/v) | 1.81 \pm 0.03 | 1.28 \pm 0.04 | 1.32 \pm 0.09 | 1.3 \pm 0.3 |
| Lactic acid (% w/v) | 0.02 \pm 0.00 ^b | 0.59 \pm 0.07 ^a | 0.63 \pm 0.01 ^a | 0.61 \pm 0.05 ^a |
| Ash (% w/v) | 0.50 \pm 0.01 ^a | 0.58 \pm 0.02 ^b | 0.59 \pm 0.01 ^{a,b} | 0.59 \pm 0.02 ^b |
| Dry matter (% w/w) | 10.28 \pm 0.04 ^a | 9.9 \pm 0.1 ^b | 10.05 \pm 0.09 ^b | 10.0 \pm 0.2 ^b |

^{a,b} Means within the same row with different superscript letters show significant statistical differences ($p < 0.05$).

Kefir at t0 showed a mean nutritional composition of 1.28 \pm 0.04 g/100 mL of fat, 3.15 \pm 0.19 g/100 mL of protein and 4.91 \pm 0.19 g/100 mL of carbohydrates. As macronutrients are concerned no difference was observed in fat, protein, and carbohydrates content due to fermentation or storage ($p = 0.071$, $p = 0.071$ and $p = 0.449$, respectively). Energy, ash, and dry matter (DM) were different between t0 and control ($p = 0.002$, $p = 0.011$ and $p = 0.028$, respectively). Finally, the lactose content in control was significantly higher than in kefir ($p = 0.011$) with a 13.6% decrease during fermentation. Consequently, the lactic acid content in kefir was significantly higher than that of the control ($p = 0.001$). No differences were found between kefir samples for lactose and lactic acid ($p = 0.100$ and $p = 0.580$, respectively).

The content of fatty acids of unfermented milk and kefir beverages was also determined, and the results are presented in Table 5. All samples evidenced the presence of 18 fatty acids, comprising saturated (SFA), monounsaturated (MUFA), and polyunsaturated (PUFA) fatty acids.

Table 5. Fatty acids profile of control and kefir samples (t0, t24, and t48) (relative frequency, mean \pm SD, $n = 4$).

| Fatty Acids (%) | Control | Kefir | | |
|-----------------|--------------------------------|--------------------------------|------------------------------|------------------------------|
| | | t0 | t24 | t48 |
| C6:0 | 3.86 \pm 0.05 | 3.6 \pm 0.2 | 3.3 \pm 0.1 | 3.7 \pm 0.1 |
| C8:0 | 2.12 \pm 0.03 ^a | 2.07 \pm 0.07 ^a | 1.95 \pm 0.05 ^b | 2.18 \pm 0.05 ^a |
| C10:0 | 4.41 \pm 0.02 | 4.5 \pm 0.3 | 4.1 \pm 0.2 | 4.6 \pm 0.1 |
| C11:0 | 0.10 \pm 0.00 | 0.2 \pm 0.1 | 0.2 \pm 0.1 | 0.2 \pm 0.1 |
| C12:0 | 5.5 \pm 0.1 ^b | 5.3 \pm 0.1 ^b | 5.2 \pm 0.2 ^b | 5.6 \pm 0.1 ^a |
| C13:0 | 0.12 \pm 0.01 | 0.10 \pm 0.00 | 0.10 \pm 0.01 | 0.11 \pm 0.02 |
| C14:0 | 14.62 \pm 0.02 | 14.3 \pm 0.2 | 14.2 \pm 0.3 | 14.1 \pm 0.9 |
| C14:1 | 1.15 \pm 0.02 | 1.18 \pm 0.06 | 1.20 \pm 0.07 | 1.11 \pm 0.04 |
| C15:0 | 1.18 \pm 0.00 ^b | 1.17 \pm 0.02 ^b | 1.14 \pm 0.03 ^b | 1.23 \pm 0.01 ^a |
| C15:1 | 0.25 \pm 0.01 ^b | 0.27 \pm 0.01 ^{a,b} | 0.26 \pm 0.01 ^b | 0.28 \pm 0.01 ^a |
| C16:0 | 39.34 \pm 0.02 ^b | 38.4 \pm 0.3 ^c | 38.9 \pm 0.5 ^c | 39.9 \pm 0.2 ^a |
| C16:1 | 1.57 \pm 0.01 ^a | 1.61 \pm 0.06 ^a | 1.57 \pm 0.08 ^a | 1.38 \pm 0.07 ^b |
| C17:0 | 0.61 \pm 0.02 ^b | 0.61 \pm 0.02 ^b | 0.61 \pm 0.05 ^b | 0.70 \pm 0.05 ^a |
| C18:0 | 5.71 \pm 0.02 | 5.64 \pm 0.06 | 5.7 \pm 0.1 | 5.74 \pm 0.09 |
| C18:1n-9 | 18.4 \pm 0.1 ^b | 19.4 \pm 0.3 ^a | 19.8 \pm 0.3 ^a | 18.0 \pm 0.7 ^a |
| C18:2n-6 | 0.79 \pm 0.03 | 1.4 \pm 0.3 | 1.52 \pm 0.07 | 0.7 \pm 0.7 |
| C18:3n-3 | 0.023 \pm 0.001 ^b | 0.123 \pm 0.003 ^a | 0.12 \pm 0.00 ^a | 0.15 \pm 0.01 ^a |
| C20:0 | 0.21 \pm 0.01 | 0.32 \pm 0.03 | 0.31 \pm 0.06 | 0.32 \pm 0.08 |
| SFA | 77.81 \pm 0.07 ^b | 76.1 \pm 0.5 ^a | 75.6 \pm 0.3 ^a | 78.5 \pm 1.2 ^a |
| MUFA | 21.37 \pm 0.09 ^b | 22.4 \pm 0.3 ^a | 22.8 \pm 0.3 ^a | 20.7 \pm 0.7 ^b |
| PUFA | 0.82 \pm 0.03 | 1.4 \pm 0.4 | 1.6 \pm 0.1 | 0.8 \pm 0.6 |

SFA—saturated fatty acids; MUFA—monounsaturated fatty acids; PUFA—polyunsaturated fatty acids. ^{a-c} Means within the same row with different superscript letters are significantly different ($p < 0.05$).

SFA content of kefir at t0 was significantly lower than control ($p = 0.012$), which is supported by the differences observed between the samples regarding palmitic acid content ($p = 0.029$). No differences were observed for the remaining SFA, between these samples. Within SFA, palmitic acid (C16:0) stands out as the major fatty acid followed by and myristic acid (C14:0). MUFA content of kefir at t0 was significantly higher than that of control ($p = 0.008$), which may be mainly supported by the difference observed between the samples regarding oleic acid content ($p = 0.014$). No differences were observed for the remaining MUFA, between these samples. Within MUFA, oleic acid (C18:1n-9) represents the major component. PUFA content showed no difference between all samples ($p = 0.050$), which may be supported by the fact that linoleic acid (C18:2n-6), the major PUFA component, also remained constant ($p = 0.083$), despite the content of α -linolenic acid (C18:3n-3) increased slightly after fermentation ($p = 0.023$).

Between t24 and t0, no difference was observed in SFA and MUFA content ($p = 0.389$ and $p = 0.460$, respectively). Within SFA, only C8:0 evidenced a very small decrease ($p = 0.041$), while within MUFA no change was observed. Between t48 and t0, no difference was observed in the SFA content ($p = 0.083$). Within SFA, lauric acid (C12:0), pentadecylic acid (C15:0), palmitic acid and margaric acid (C17:0) presented a very small increase ($p = 0.022$, $p = 0.009$, $p = 0.002$ and $p = 0.048$, respectively). MUFA content decreased ($p = 0.031$), with only palmitoleic acid (C16:1) reflecting that decrease ($p = 0.002$).

4. Discussion

Kefir grains are traditionally cultured in milk at room temperature, which is considered to be between 20 and 25 °C [36,41]. The traditional use, combined with the fact that 20 °C is in the range of typical indoor conditions of a Portuguese house [52], thus reflecting the domestic scenario of preparation of kefir, justifies the choice of the fermentation temperature in our study. It is widely known that biomass increase and lactose consumption rise at higher incubation temperatures [37]. Nevertheless, Londero et al. [53] found that

biomass growth, acidification capacity, and maintenance of the chemical composition are optimized at a fermentation temperature of 20 °C.

Increment of the grains biomass during fermentation highlights the microbial growth resulting of the balance within the microbiota of the grains [25,53,54]. This biomass increase is mainly due to the production of protein and polysaccharides by its microbiota within the grains matrix, which can be transferred to the fermented milk [54]. Our grains presented a mean biomass increment of $6 \pm 2\%$ after a 24 h fermentation of semi-skimmed milk at 20 °C, which is consistent with the results of DeSainz et al. [55], that found a biomass increase of $7.2 \pm 0.1\%$ after 24 h fermentation at 35 °C. Interestingly, using a mathematical model Zajšek and Goršek [37] observed a linear trend between fermentation temperature and increase of biomass grains, that predicted an increase of 7.034 g/L in biomass grain growth for a temperature of 20 °C. Our results showed a ten-fold higher growth, which shows a considerable disparity between a mathematical model and a real fermentation scenario. The growth behavior of our grains (Figure 1) was contrary to the results found by Pop et al. [56] using a grain inoculum of 4.5% (*w/v*) to ferment skimmed milk at 25 °C and showing a significant biomass decrease after 24 h. This may be justified by the fact that our study used semi-skimmed milk, thus making Pop's justifications, nutrient depletion or increase acidity, less robust arguments to justify growth behavior of our grains. Moreover, the fat content of the milk may be of significant importance, as demonstrated by Schoevers and Britz [27], who reported that higher milk fat content impairs grain growth by inhibition of nutrient exchange. The authors also found that the lowest increase in biomass happened when low fat milk was used, and their results using this milk type and a grain to milk ratio of 1% (*w/v*) showed a biomass increase around 50% after 8 days [27]. The increase of 60.07% in biomass that we found may also be justified by the use of a grain inoculum of 10% (*w/v*).

The mean pH value of 4.5 ± 0.1 that was verified after 24 h of fermentation is in agreement with that found by Garrote et al. [31], using the same type of grain inoculum. The acidification rate observed during fermentation in our work (Figure 2) is consistent with the literature [21,31,36,37,41] and may reflect the LAB capability to acidify the milk [37,41]. Both pH and lactic acid variation during fermentation of kefir represent an indirect measure of the biological activity of the grains [57]. LAB population present high sensitivity to low pH values, which contributes to their decline, being that the main reason why kefir does not become more acidic through time [31,36].

Interestingly, despite the home use production conditions, the resulting kefir (Table 1) is in conformity with the recommendations of *Codex Alimentarius* for fermented milks (Codex Stan 243-2003), thus complying with a number of total micro-organisms of at least 10^7 colony-forming units (CFU)/mL and a yeast number not less than 10^4 CFU/mL [43].

After fermentation, we found that the mean particle size of kefir (439 ± 42 nm) predictably increased significantly compared to the unfermented milk (280 ± 54 nm) and decreased again after 24 h-refrigerated storage (256 ± 6 nm), remaining stable for another 24 h of cold storage (249 ± 1 nm). According to the literature [58], casein micelles aggregation is promoted by increase of acidification, protein content, fat content and temperature, thus these factors may directly affect particle growth in kefir beverage. The pH decrease observed in freshly made kefir (Table 3) may be at the root of the initial aggregation of casein micelles into larger clusters. After refrigerating the kefir beverage for 24 h, the size of casein micelles probably decreased due to the effect of low temperatures on protein aggregation. In fact, it was already reported that the higher the temperature, the higher the particle size of fermented milk [58]. Moreover, it is noteworthy that, after 24 h of refrigerated storage, the particle size of kefir is in reasonable agreement with the results recently presented by Beirami-Serizkani et al. [59]. Another 24 h of refrigerated storage did not alter the particle size of kefir, probably due to the fact that, during this period, the temperature remained constant, as well as no pronounced alterations were found in pH values (Table 3) and protein or fat content (Table 4) of the kefir beverage.

The degree of non-uniformity of a population's size distribution within a given sample, represented by PDI, suggests the degree of heterogeneity of the sample. A homogeneous sample, perfectly uniform regarding the particle size, shows a PDI value of zero, while a heterogeneous sample, highly polydisperse with multiple particle size populations has a PDI of 1 [60]. The stability of a sample, given by the zeta potential, is a measure of the magnitude of electrostatic repulsion/attraction or charges between particles [58] and increases with the homogeneity of the size distribution [60]. Zeta potential depends on factors like temperature, acidity, and viscosity, and a highly negative/positive zeta potential foresees a more stable dispersion, while values lower than $|\pm 30|$ mV can indicate colloidal instability, which can lead to aggregation [61]. Concerning the particle size distribution of the analyzed samples, given by PDI (Table 2), it is remarkable that all beverages display uniform particle size distributions ($PDI < 0.3$). Despite that, the increase in particle size of kefir in comparison with unfermented milk also resulted in an increase of PDI, which was almost recovered by the decrease of particle size upon refrigerated storage for 24 h and 48 h (Table 2). In addition, the zeta potential values recorded for all samples (< -30 mV, Table 2) indicate that all beverages display good colloidal stability. It is noteworthy that the zeta potential of unfermented milk was in line with a previous report of its variation with milk pH [62]. According to our results, the zeta potential of kefir is similar to that of unfermented milk, slightly increasing with refrigerated storage (Table 2). This is not in agreement with the data reported by Beirami-Serizkani et al. [59], showing that the different preparation procedures of kefir drinks may influence the colloidal stability of the resulting beverage.

FTIR spectrum analysis of unfermented semi-skimmed milk (Figure 3) was consistent with the literature [63]. Using FTIR spectra, we confirm that the physicochemical properties of the milk change during the fermentation process. However, from the strong overlap between the kefir spectral signals (Figure 3) we corroborate that its physicochemical properties are maintained during refrigerated storage, which is consistent with the results obtained from the other analysis performed in this study.

The variations in pH and viscosity found in our kefir samples (Table 3) are similar to those reported the literature [21,36,44]. The pH value of kefir was significantly lower than that of milk, remaining constant in the first 24 h of refrigeration and showing a slight decrease of 2% at the end of 48 h (Table 3). Similar results after 2 days of storage were reported by Leite et al. [21]. Irigoyen et al. [36] also reported no variations in pH during kefir storage, and attributed it to the presence of yeast in the grains, since the production of lactic acid by LAB is slower in the presence of yeasts than in pure culture [38,44].

After a 24 h fermentation, kefir revealed a significantly higher viscosity compared to the unfermented milk (Table 3). This can be in part attributed to the production of kefir's exclusive polysaccharide, kefiran, which, in addition to constituting the grain structure, can also be found dissolved in the liquid, thus contributing to the rheology of the fermented beverage [64]. The decrease observed in kefir's viscosity after the first 24 h refrigerated storage period (Table 3) can be attributed to the hydrolysis of the polysaccharide kefiran together with the reduction observed in the LAB responsible for the polysaccharide's production [34]. Throughout storage, a decrease in viscosity and phase separation (syneresis), due to the aggregation of casein micelles and subsequent precipitation are the most typical events that may impair the quality of kefir [65]; however, these changes only become evident in periods of storage longer than seven days [34,36,44]. Nevertheless, our data showed no difference in viscosity during storage, which may be attributed to a limited storage time (only 48 h).

The nutritional composition of kefir is influenced by milk composition, origin of the grains, temperature, and duration of fermentation and storage conditions [31,36]. As explained previously, our kefir prepared in a typical home use setting fulfills the requirements the *Codex Alimentarius* (Table 4) and is in accordance with data reported by other authors [21,36,66]. Whilst typical cow milk presents a carbohydrate content between 4.7 and 4.9 g/100 mL, reflecting essentially lactose content [67], kefir has a carbohydrate

content around 11.9 g/100 g, also reflecting the presence of polysaccharide kefiran [54]. Our data for unfermented milk were consistent with the literature [67], but no difference was observed in carbohydrate content, neither during fermentation or storage. It is noteworthy that in spite the small lactose decrease observed after fermentation, the carbohydrate profile of kefir is expected to be different from that of the source milk, due to the presence of polysaccharide kefiran in kefir (not quantified in this study).

After 24 h fermentation we observed a decrease of 13.6% in lactose level and an increase in lactic acid content which is consistent with the literature [21,33,36,38,44], and may be explained by the hydrolysis of lactose and production of lactic acid in the initial LAB lactose metabolism [21,44]. These results are in line with those reported by Irigoyen et al. [36], who observed a 20–25% decrease in lactose during 24 h fermentation. Assadi et al. [68] reported much lower levels of lactose after 24 h of fermentation even though producing identical content of lactic acid. Throughout the storage period no changes were observed in lactose and lactic acid content of kefir, which is consistent with results reported for similar time storage [36,40,44]. Guzel-Seydim et al. [40] reported that during cold storage of kefir, lactic acid production may be impaired possible due to the decrease of LAB concentration attributed to pH drop [31,36]. Diversity in results involving lactose degradation and lactic acid production, in kefir fermentation, may be attributed to differences in grain to milk ratio and in different origins of kefir grains [21].

Even though, our data did not reveal any changes in fat, protein; and carbohydrates content, a small decrease in energy content was observed between milk and kefir, possibly due to variation of carbohydrates and fat, despite no statistical significance was found.

DM in freshly made kefir may range between 9.4% and 11.1%, and it is expected to change accordingly with the variation of fat and lactose comparatively with the source milk [36,38]. Our data are consistent with these, once we observed a slightly decrease of DM content after fermentation, which is consistent with the lactose variation also observed. Assadi et al. [68] observed only 5.56% of DM in kefir, however their value was also consistent with the much lower lactose level they found compared with the source milk. After 48 h storage, no differences were observed for both lactose and total fat and consequently also for DM. However, Irigoyen et al. [36] reported a DM content decrease after 48 h storage which is consistent with the fat content decrease verified in their study.

Milk proteins are affected by proteolytic activity of the kefir grains, producing different peptides and nonprotein nitrogen compounds, thus contributing to the protein profile of kefir [69]. However, during fermentation and storage, casein content does not change significantly, suggesting a low degree of casein proteolysis, contrary to the nonprotein nitrogen compounds derived from whey protein, that increase both in fermentation and in storage [70]. Even though the protein profile has not been determined in our work, its results are hereby supported, since no differences in the total protein content of kefir and unfermented milk were observed (Table 4). Moreover, utilization of protein nitrogen by bacteria during fermentation is limited, since their preferential energy source are carbohydrates [71]. Contrary results were reported by Vieira et al. [32], showing an increased protein level during fermentation, which were explained by the interaction between stress response proteins and lipid membrane unsaturation in bacterial cells, since fermentation is a stress factor for LAB [32].

Total fat composition of kefir was identical to that of the source milk (Table 4), which is consistent with the literature [32,36], and also no difference was observed during refrigerated storage [32,36,40]. However, the fatty acid profile of freshly made and refrigerated kefir differs (Table 5). Kefir at t0 presented a decrease of 2% in SFA and an increase of 5% MUFA, these variations being identically reflected in the content of palmitic acid (C16:0) and oleic acid (C18:1n-9), respectively. These results are in line with the literature [32,72] and are useful in order to consolidate the potential health benefits of kefir [73]. Vieira et al. [32], justified the change in SFA and PUFA with the increase of desaturase activity of LAB during fermentation [74] since the conversion ratio of saturated into unsaturated fatty acids can be attributed to desaturase activity [75]. Even though, in our data, PUFA content

showed an increase after fermentation, the difference was not statistically significant. PUFAs are known to affect the aroma profile of kefir, and since an increase of PUFA would lead to a loss of the typical scent [76], it is confirmed that in our particular setting conditions the olfactive characteristics of kefir are maintained. In the first 24 h of refrigerated storage no change in fatty acids profile was noted, and after 48 h storage, only a slightly decrease in MUFA was observed. Contrary results were found by Vieira et al. [32], who reported higher MUFA and lower SFA content during storage, which was attributed to the ability of LAB to increase the production of free fatty acids by lipolysis of milk fat during the cold storage [77]. The differences observed in kefir's fatty acids profiles, according to other authors, may be justified by the different origin of the grains since each bacterial community may present a unique fatty acids production [21,32].

5. Conclusions

Our results showed that the kefir produced under home use conditions using UHT milk is able to fulfill the *Codex Alimentarius* requirements and maintains its characteristics with respect to the physicochemical composition, both after fermentation, as well as during 48 h of refrigerated storage. Whereas fat, protein; and carbohydrate content suffered no significant changes over fermentation, lactic acid increased, and lactose decreased, as expected. The fatty acids profile of the milk and kefir samples changed during fermentation revealing a decrease in SFA, an increase in MUFA, and no change in PUFA. Refrigerated storage did not significantly impact nutritional composition and fatty acids profile, thus attesting for the stability of kefir under these conditions.

To the best of our knowledge, this is the first study to aggregate information on detailed composition, homogeneity; and stability after refrigeration, of kefir produced using CIDCA AGK1 grains in a traditional in use setting. This work further contributes to the characterization of this food that is so widely consumed around the world by focusing on kefir that was produced in typical home use conditions.

Author Contributions: Conceptualization, C.R. and P.R.; methodology, E.A.; software, E.A. and J.G.; validation, L.B., P.R. and C.R.; investigation, E.A., E.N.N., C.C. and E.P.; writing—original draft preparation, E.A.; writing—review and editing, P.R., C.R., C.C. and L.B.; visualization, C.P.-L., L.M.R., M.V.A.-V., C.R. and P.R.; supervision, P.R.; funding acquisition, P.R. All authors have read and agreed to the published version of the manuscript.

Funding: This work was financed by the Foundation for Science and Technology (FCT, Portugal) through projects UIDB/04567/2020 and UIDP/04567/2020 to CBIOS.

Data Availability Statement: Data available on request due to restrictions e.g., privacy or ethical. The data presented in this study are available on request from the corresponding author.

Acknowledgments: Emilia Alves and Epole Ntungwe acknowledge ALIES, Portugal for the grant PADDIC 2019–2020 and 2020–2021. The authors gratefully thank Professor Angela Leon, from the Centro de Investigación y Desarrollo en Criotecnología de Alimentos (CIDCA), Universidad de La Plata, Argentina, for providing the CIDCA AGK1 kefir grains. The authors are grateful to the Foundation for Science and Technology (FCT, Portugal) for financial support through national funds FCT/MCTES to CIMO (UIDB/00690/2020). L. Barros would like to thank the national funding by FCT, P.I., through the institutional scientific employment program-contract. To the project AllNat for the contract of C. Caleja (Project AllNat POCI-01-0145-FEDER-030463) and to the Project Mobilizador Norte-01-0247-FEDER-024479: ValorNatural[®] for the contract of E. Pereira.

Conflicts of Interest: The authors declare no conflict of interest.

References

1. Wouters, J.T.M.; Ayad, E.H.E.; Hugenholtz, J.; Smit, G. Microbes from raw milk for fermented dairy products. *Int. Dairy J.* **2002**, *12*, 91–109. [[CrossRef](#)]
2. Bourrie, B.C.T.; Willing, B.P.; Cotter, P.D. The Microbiota and Health Promoting Characteristics of the Fermented Beverage Kefir. *Front. Microbiol.* **2016**, *7*, 647. [[CrossRef](#)]

3. Vinderola, C.G.; Duarte, J.; Thangavel, D.; Perdígón, G.; Farnworth, E.; Matar, C. Immunomodulating capacity of kefir. *J. Dairy Res.* **2005**, *72*, 195–202. [[CrossRef](#)]
4. Farnworth, E.R. Kefir—A complex probiotic. *Food Sci. Technol. Bull. Funct. Foods* **2005**, *2*, 1–17. [[CrossRef](#)]
5. Ahmed, Z.; Wang, Y.; Ahmad, A.; Khan, S.T.; Nisa, M.; Ahmad, H.; Afreen, A. Kefir and Health: A Contemporary Perspective. *Crit. Rev. Food Sci. Nutr.* **2013**, *53*, 422–434. [[CrossRef](#)]
6. Hertzler, S.R.; Clancy, S.M. Kefir improves lactose digestion and tolerance in adults with lactose maldigestion. *J. Am. Diet. Assoc.* **2003**, *103*, 582–587. [[CrossRef](#)] [[PubMed](#)]
7. Rodrigues, K.L.; Carvalho, J.C.T.; Schneedorf, J.M. Anti-inflammatory properties of kefir and its polysaccharide extract. *Inflammopharmacology* **2005**, *13*, 485–492. [[CrossRef](#)] [[PubMed](#)]
8. Iraporda, C.; Romanin, D.E.; Rumbo, M.; Garrote, G.L.; Abraham, A.G. The role of lactate on the immunomodulatory properties of the nonbacterial fraction of kefir. *Food Res. Int.* **2014**, *62*, 247–253. [[CrossRef](#)]
9. Rodrigues, K.L.; Caputo, L.R.G.; Carvalho, J.C.T.; Evangelista, J.; Schneedorf, J.M. Antimicrobial and healing activity of kefir and kefir extract. *Int. J. Antimicrob. Agents* **2005**, *25*, 404–408. [[CrossRef](#)]
10. Liu, J.-R.; Chen, M.-J.; Lin, C.-W. Antimutagenic and Antioxidant Properties of Milk–Kefir and Soymilk–Kefir. *J. Agric. Food Chem.* **2005**, *53*, 2467–2474. [[CrossRef](#)] [[PubMed](#)]
11. Gao, J.; Gu, F.; Ruan, H.; Chen, Q.; He, J.; He, G. Induction of apoptosis of gastric cancer cells SGC7901 in vitro by a cell-free fraction of Tibetan kefir. *Int. Dairy J.* **2013**, *30*, 14–18. [[CrossRef](#)]
12. Huseini, H.E.; Rahimzadeh, G.; Fazeli, M.R.; Mehrzama, M.; Salehi, M. Evaluation of wound healing activities of kefir products. *Burns* **2012**, *38*, 719–723. [[CrossRef](#)]
13. Carasi, P.; Racedo, S.M.; Jacquot, C.; Romanin, D.E.; Serradell, M.A.; Urdaci, M.C. Impact of Kefir Derived *Lactobacillus kefir* on the Mucosal Immune Response and Gut Microbiota. *J. Immunol. Res.* **2015**, *2015*, 361604. [[CrossRef](#)] [[PubMed](#)]
14. Garrote, G.L.; Abraham, A.G.; De Antoni, G.L. Inhibitory Power of Kefir: The Role of Organic Acids. *J. Food Prot.* **2000**, *63*, 364–369. [[CrossRef](#)]
15. Iraporda, C.; Júnior, M.A.; Neumann, E.; Nunes, Á.C.; Nicoli, J.R.; Abraham, A.G.; Garrote, G.L. Biological activity of the non-microbial fraction of kefir: Antagonism against intestinal pathogens. *J. Dairy Res.* **2017**, *84*, 339–345. [[CrossRef](#)]
16. Simova, E.; Beshkova, D.; Angelov, A.; Hristozova, T.; Frengova, G.; Spasov, Z. Lactic acid bacteria and yeasts in kefir grains and kefir made from them. *J. Ind. Microbiol. Biotechnol.* **2002**, *28*, 1–6. [[CrossRef](#)] [[PubMed](#)]
17. Vardjan, T.; Lorbeg, P.M.; Rogelj, I.; Majhenič, A.Č. Characterization and stability of lactobacilli and yeast microbiota in kefir grains. *J. Dairy Sci.* **2013**, *96*, 2729–2736. [[CrossRef](#)]
18. Witthuhn, R.C.; Cilliers, A.; Britz, T.J. Evaluation of different preservation techniques on the storage potential of Kefir grains. *J. Dairy Res.* **2005**, *72*, 125–128. [[CrossRef](#)]
19. Garrote, G.; Abraham, A.; De Antoni, G. Preservation of Kefir Grains, a Comparative Study. *LWT* **1997**, *30*, 77–84. [[CrossRef](#)]
20. Garrote, G.L.; Abraham, A.G.; De Antoni, G.L. Chemical and microbiological characterisation of kefir grains. *J. Dairy Res.* **2001**, *68*, 639–652. [[CrossRef](#)] [[PubMed](#)]
21. Leite, A.M.O.; Leite, D.C.A.; Del Aguila, E.M.; Alvares, T.S.; Peixoto, R.S.; Miguel, M.A.L.; Silva, J.T.; Paschoalin, V.M.F. Microbiological and chemical characteristics of Brazilian kefir during fermentation and storage processes. *J. Dairy Sci.* **2013**, *96*, 4149–4159. [[CrossRef](#)]
22. Pogačić, T.; Sinko, S.; Zamberlin, Š.; Samaržija, D. Microbiota of Kefir Grains. *Mljekarstvo* **2013**, *63*, 3–14.
23. Zheng, J.; Wittouck, S.; Salvetti, E.; Franz, C.M.A.P.; Harris, H.M.B.; Mattarelli, P.; O’Toole, P.W.; Pot, B.; Vandamme, P.; Walter, J.; et al. A taxonomic note on the genus *Lactobacillus*: Description of 23 novel genera, emended description of the genus *Lactobacillus* Beijerinck 1901, and union of *Lactobacillaceae* and *Leuconostocaceae*. *Int. J. Syst. Evol. Microbiol.* **2020**, *70*, 2782–2858. [[CrossRef](#)] [[PubMed](#)]
24. Bengoa, A.A.; Iraporda, C.; Garrote, G.L.; Abraham, A.G. Kefir micro-organisms: Their role in grain assembly and health properties of fermented milk. *J. Appl. Microbiol.* **2019**, *126*, 686–700. [[CrossRef](#)] [[PubMed](#)]
25. Garrote, G.L.; Abraham, A.G.; De Antoni, G.L. Characteristics of kefir prepared with different grain [ratio] milk ratios. *J. Dairy Res.* **1998**, *65*, 149–154. [[CrossRef](#)]
26. Rattray, F.P.; O’Connell, M.J. Fermented Milks—Kefir. In *Encyclopedia of Dairy Sciences*; Fuquay, J.W., Fox, P.F., McSweeney, P.L.H., Eds.; Academic Press Inc.: London, UK, 2011; pp. 518–524.
27. Guzel-Seydim, Z.; Kok-Tas, T.; Ertekin-Filiz, B.; Seydim, A.C. Effect of different growth conditions on biomass increase in kefir grains. *J. Dairy Sci.* **2011**, *94*, 1239–1242. [[CrossRef](#)] [[PubMed](#)]
28. Schoevers, A.; Britz, T.J. Influence of different culturing conditions on kefir grain increase. *Int. J. Dairy Technol.* **2003**, *56*, 183–187. [[CrossRef](#)]
29. Rea, M.C.; Lennartsson, T.; Dillon, P.; Drinan, F.D.; Reville, W.J.; Heapes, M.; Cogan, T.M. Irish kefir-like grains: Their structure, microbial composition and fermentation kinetics. *J. Appl. Bacteriol.* **1996**, *81*, 83–94. [[CrossRef](#)]
30. Nielsen, B.; Gürakan, G.C.; Ünlü, G. Kefir: A Multifaceted Fermented Dairy Product. *Probiotics Antimicrob. Proteins* **2014**, *6*, 123–135. [[CrossRef](#)] [[PubMed](#)]
31. Wszolek, M.; Tamime, A.; Muir, D.; Barclay, M. Properties of Kefir made in Scotland and Poland using Bovine, Caprine and Ovine Milk with Different Starter Cultures. *LWT* **2001**, *34*, 251–261. [[CrossRef](#)]

32. Vieira, C.P.; Álvares, T.S.; Gomes, L.S.; Torres, A.G.; Paschoalin, V.M.F.; Conte-Junior, C.A. Kefir Grains Change Fatty Acid Profile of Milk during Fermentation and Storage. *PLoS ONE* **2015**, *10*, e0139910. [CrossRef]
33. Gul, O.; Mortas, M.; Atalar, I.; Dervisoglu, M.; Kahyaoglu, T. Manufacture and characterization of kefir made from cow and buffalo milk, using kefir grain and starter culture. *J. Dairy Sci.* **2015**, *98*, 1517–1525. [CrossRef]
34. Magra, T.L.; Antoniou, K.D.; Psomas, E.I. Effect of milk fat, kefir grain inoculum and storage time on the flow properties and microbiological characteristics of kefir. *J. Texture Stud.* **2012**, *43*, 299–308. [CrossRef]
35. Hecec, C.; Ulusoy, B.; Kaynarca, D. Effect of Different Fermentation Conditions on Composition of Kefir Microbiota. *Int. Food Res. J.* **2019**, *26*, 401–409.
36. Irigoyen, A.; Arana, I.; Castiella, M.; Torre, P.; Ibáñez, F. Microbiological, physicochemical, and sensory characteristics of kefir during storage. *Food Chem.* **2005**, *90*, 613–620. [CrossRef]
37. Zajšek, K.; Goršek, A. Modelling of batch kefir fermentation kinetics for ethanol production by mixed natural microflora. *Food Bioprod. Process.* **2010**, *88*, 55–60. [CrossRef]
38. Barukčić, L.; Gracin, L.; Jambrak, A.R.; Božanić, R. Comparison of chemical, rheological and sensory properties of kefir produced by kefir grains and commercial kefir starter. *Mljekarstvo* **2017**, *67*, 169–176. [CrossRef]
39. De Vrese, M.; Keller, B.; Barth, C.A. Enhancement of intestinal hydrolysis of lactose by microbial β -galactosidase (EC 3.2.1.23) of kefir. *Br. J. Nutr.* **1992**, *67*, 67–75. [CrossRef]
40. Guzel-Seydim, Z.; Seydim, A.C.; Greene, A.K. Organic Acids and Volatile Flavor Components Evolved During Refrigerated Storage of Kefir. *J. Dairy Sci.* **2000**, *83*, 275–277. [CrossRef]
41. Otles, S.; Cagindi, O. Kefir: A Probiotic Dairy—Composition, Nutritional and Therapeutic Aspects. *Pak. J. Nutr.* **2003**, *2*, 54–59. [CrossRef]
42. Walsh, A.M.; Crispie, F.; Kilcawley, K.; O’Sullivan, O.; O’Sullivan, M.G.; Claesson, M.J.; Cotter, P.D. Microbial Succession and Flavor Production in the Fermented Dairy Beverage Kefir. *mSystems* **2016**, *1*, e00052-16. [CrossRef]
43. Codex Alimentarius International Food Standards. *Codex Standard for Fermented Milks (Codex Stan CXS 243-2003) Codex Alimentarius*; FAO: Rome, Italy; ISBN 5856420187. Available online: <http://www.fao.org/fao-who-codexalimentarius/codex-texts/list-standards/en/> (accessed on 12 January 2021).
44. Gronnevik, H.; Falstad, M.; Narvhus, J.A. Microbiological and chemical properties of Norwegian kefir during storage. *Int. Dairy J.* **2011**, *21*, 601–606. [CrossRef]
45. Kim, Y.J.; Liu, R.H. Increase of Conjugated Linoleic Acid Content in Milk by Fermentation with Lactic Acid Bacteria. *J. Food Sci.* **2002**, *67*, 1731–1737. [CrossRef]
46. Hamet, M.F.; Londero, A.; Medrano, M.; Verccammen, E.; Van Hoorde, K.; Garrote, G.L.; Huys, G.; Vandamme, P.; Abraham, A.G. Application of culture-dependent and culture-independent methods for the identification of *Lactobacillus kefirifaciens* in microbial consortia present in kefir grains. *Food Microbiol.* **2013**, *36*, 327–334. [CrossRef]
47. Diosma, G.; Romanin, D.E.; Rey-Burusco, M.F.; Londero, A.; Garrote, G.L. Yeasts from kefir grains: Isolation, identification, and probiotic characterization. *World J. Microbiol. Biotechnol.* **2014**, *30*, 43–53. [CrossRef]
48. Clinical and Laboratory Standards Institute (CLSI). *Performance Standards for Antimicrobial Susceptibility Testing*; Clinical and Laboratory Standards Institute (CLSI): Wayne, PA, USA, 2020.
49. AOAC. *Official Methods of Analysis of AOAC International*, 20th ed.; Latimer, G., Ed.; AOAC International: Gaithersburg, MD, USA, 2016; ISBN 0935584870.
50. Barros, L.; Pereira, E.; Calhelha, R.C.; Dueñas, M.; Carvalho, A.M.; Santos-Buelga, C.; Ferreira, I.C. Bioactivity and chemical characterization in hydrophilic and lipophilic compounds of *Chenopodium ambrosioides* L. *J. Funct. Foods* **2013**, *5*, 1732–1740. [CrossRef]
51. Food and Agriculture Organization. Food Energy—Methods of Analysis and Conversion Factors. Food and Nutrition Paper 77. 2003. Available online: <http://www.fao.org/3/Y5022E/Y5022E00.htm> (accessed on 3 March 2021).
52. Instituto Português do Mar e da Atmosfera—IPMA. Clima de Portugal Continental. Available online: <https://www.ipma.pt/pt/educativa/tempo.clima/> (accessed on 10 February 2021).
53. Londero, A.; Hamet, M.F.; De Antoni, G.L.; Garrote, G.L.; Abraham, A.G. Kefir grains as a starter for whey fermentation at different temperatures: Chemical and microbiological characterisation. *J. Dairy Res.* **2012**, *79*, 262–271. [CrossRef] [PubMed]
54. Guzel-Seydim, Z.B.; Kok-Tas, T.; Greene, A.K.; Seydim, A.C. Review: Functional Properties of Kefir. *Crit. Rev. Food Sci. Nutr.* **2011**, *51*, 261–268. [CrossRef] [PubMed]
55. Abraham, A.G.; De Antoni, G.L. Characterization of kefir grains grown in cows’ milk and in soya milk. *J. Dairy Res.* **1999**, *66*, 327–333. [CrossRef] [PubMed]
56. De Sainz, I.; Redondo-Solano, M.; Solano, G.; Ramirez, L. Short communication: Effect of different kefir grains on the attributes of kefir produced with milk from Costa Rica. *J. Dairy Sci.* **2020**, *103*, 215–219. [CrossRef]
57. Pop, C.R.; Apostu, S.; Salanță, L.; Rotar, A.M.; Sincic, M.; Mabon, N.; Socaciu, C. Influence of Different Growth Conditions on the Kefir Grains Production, used in the Kefiran Synthesis. *Bull. Univ. Agric. Sci. Vet. Med. Cluj-Napoca Food Sci. Technol.* **2014**, *71*, 147–153. [CrossRef]
58. Irigoyen, A.; Ortigosa, M.; Torre, P.; Ibáñez, F. Influence of Different Technological Parameters in the Evolution of PH during Fermentation of Kefir. *Milchwissenschaft* **2003**, *58*, 631–633.

59. Hahn, C.; Sramek, M.; Nöbel, S.; Hinrichs, J. Post-processing of concentrated fermented milk: Influence of temperature and holding time on the formation of particle clusters. *Dairy Sci. Technol.* **2012**, *92*, 91–107. [CrossRef]
60. Beirami-Serizkani, F.; Hojjati, M.; Jooyandeh, H. The effect of microbial transglutaminase enzyme and Persian gum on the characteristics of traditional kefir drink. *Int. Dairy J.* **2021**, *112*, 104843. [CrossRef]
61. Danaei, M.; Dehghankhold, M.; Ataei, S.; Davarani, F.H.; Javanmard, R.; Dokhani, A.; Khorasani, S.; Mozafari, M.R. Impact of Particle Size and Polydispersity Index on the Clinical Applications of Lipidic Nanocarrier Systems. *Pharmaceutics* **2018**, *10*, 57. [CrossRef] [PubMed]
62. Teimouri, S.; Abbasi, S.; Scanlon, M.G. Stabilisation mechanism of various inulins and hydrocolloids: Milk-sour cherry juice mixture. *Int. J. Dairy Technol.* **2018**, *71*, 208–215. [CrossRef]
63. Tan, T.J.; Wang, D.; Moraru, C.I. A physicochemical investigation of membrane fouling in cold microfiltration of skim milk. *J. Dairy Sci.* **2014**, *97*, 4759–4771. [CrossRef] [PubMed]
64. Nicolaou, N.; Xu, Y.; Goodacre, R. Fourier transform infrared spectroscopy and multivariate analysis for the detection and quantification of different milk species. *J. Dairy Sci.* **2010**, *93*, 5651–5660. [CrossRef]
65. Rimada, P.S.; Abraham, A.G. Kefiran improves rheological properties of glucono- δ -lactone induced skim milk gels. *Int. Dairy J.* **2006**, *16*, 33–39. [CrossRef]
66. Şanlı, T.; Sezgin, E.; Şenel, E.; Benli, M. The effect of transglutaminase on some physicochemical and sensory properties of the Turkish drinking yoghurt Ayran. *Int. J. Dairy Technol.* **2013**, *66*, 410–416. [CrossRef]
67. Sarkar, S. Potential of kefir as a dietetic beverage—A review. *Br. Food J.* **2007**, *109*, 280–290. [CrossRef]
68. INSA Tabela Composição Alimentos. 2019. Available online: <http://portfir.insa.pt/foodcomp/search> (accessed on 25 March 2021).
69. Assadi, M.M.; Pourahmad, R.; Moazami, N. Use of isolated kefir starter cultures in kefir production. *World J. Microbiol. Biotechnol.* **2000**, *16*, 541–543. [CrossRef]
70. Dallas, D.C.; Citerne, F.; Tian, T.; Silva, V.L.; Kalanetra, K.M.; Frese, S.A.; Robinson, R.C.; Mills, D.A.; Barile, D. Peptidomic analysis reveals proteolytic activity of kefir microorganisms on bovine milk proteins. *Food Chem.* **2016**, *197*, 273–284. [CrossRef] [PubMed]
71. Alm, L. Effect of Fermentation on Proteins of Swedish Fermented Milk Products. *J. Dairy Sci.* **1982**, *65*, 1696–1704. [CrossRef]
72. Neis, E.P.J.G.; DeJong, C.H.C.; Rensen, S.S. The Role of Microbial Amino Acid Metabolism in Host Metabolism. *Nutrients* **2015**, *7*, 2930–2946. [CrossRef] [PubMed]
73. Guzel-Seydim, Z.B.; Seydim, A.C.; Greene, A.K.; Taş, T. Determination of antimutagenic properties of acetone extracted fermented milks and changes in their total fatty acid profiles including conjugated linoleic acids. *Int. J. Dairy Technol.* **2006**, *59*, 209–215. [CrossRef]
74. Molina, S.; Moran-Valero, M.; Martin, D.; Vázquez, L.; Vargas, T.; Torres, C.; De Molina, A.R.; Reglero, G. Antiproliferative effect of alkylglycerols as vehicles of butyric acid on colon cancer cells. *Chem. Phys. Lipids* **2013**, *175–176*, 50–56. [CrossRef]
75. Guerzoni, M.E.; Lanciotti, R.; Cocconcelli, P.S. Alteration in cellular fatty acid composition as a response to salt, acid, oxidative and thermal stresses in *Lactobacillus helveticus*. *Microbiology* **2001**, *147*, 2255–2264. [CrossRef]
76. Nantapo, C.T.W.; Muchenje, V.; Hugo, A. Atherogenicity index and health-related fatty acids in different stages of lactation from Friesian, Jersey and Friesian \times Jersey cross cow milk under a pasture-based dairy system. *Food Chem.* **2014**, *146*, 127–133. [CrossRef] [PubMed]
77. Cais-Sokolińska, D.; Wójtowski, J.; Pikul, J.; Danków, R.; Majcher, M.; Teichert, J.; Bagnicka, E. Formation of volatile compounds in kefir made of goat and sheep milk with high polyunsaturated fatty acid content. *J. Dairy Sci.* **2015**, *98*, 6692–6705. [CrossRef] [PubMed]

Article

Parvifloron D from *Plectranthus strigosus*: Cytotoxicity Screening of *Plectranthus* spp. Extracts

Catarina Garcia ^{1,2}, Epole Ntungwe ^{1,2}, Ana Rebelo ^{1,2}, Cláudia Bessa ³, Tijana Stankovic ⁴, Jelena Dinic ⁴, Ana Díaz-Lanza ², Catarina P. Reis ⁵, Amílcar Roberto ¹, Paula Pereira ^{1,6}, Maria-João Cebola ^{1,6}, Lucília Saraiva ³, Milica Pesic ⁴, Noélia Duarte ^{5,*} and Patrícia Rijo ^{1,5,*}

- ¹ Research Center for Biosciences & Health Technologies (CBIOS), Universidade Lusófona de Humanidades e Tecnologias, 1749-024 Lisboa, Portugal; catarina.g.garcia@gmail.com (C.G.); ntungweepolengolle@yahoo.com (E.N.); ana.rebelo1490@gmail.com (A.R.); amilcar.roberto@ulusofona.pt (A.R.); paulapereira1@sapo.pt (P.P.); m.joao.cebola@gmail.com (M.-J.C.)
- ² Department of Biomedical Sciences, Faculty of Pharmacy, University of Alcalá, Campus Universitario, 28871 Alcalá de Henares, Spain; ana.diaz@uah.es
- ³ LAQV/REQUIMTE, Laboratório de Microbiologia, Departamento de Ciências Biológicas, Faculdade de Farmácia, Universidade do Porto, Rua de Jorge Viterbo Ferreira n. 228, 4050-313 Porto, Portugal; claudiasantos26@gmail.com (C.B.); lucilia.saraiva@ff.up.pt (L.S.)
- ⁴ Institute for Biological Research, “Siniša Stanković”, University of Belgrade, Despota Stefana 142, 11060 Belgrade, Serbia; tijana.andjelkovic@ibiss.bg.ac.rs (T.S.); jelena.dinic@ibiss.bg.ac.rs (J.D.); camala@ibiss.bg.ac.rs (M.P.)
- ⁵ Instituto de Investigação do Medicamento (iMed.Ulisboa), Faculdade de Farmácia, Universidade de Lisboa, 1649-003 Lisboa, Portugal; catarinareis@ff.ulisboa.pt
- ⁶ CERENA—Centre for Natural Resources and the Environment, Instituto Superior Técnico (IST), Universidade de Lisboa, Av. Rovisco Pais, 1049-001 Lisbon, Portugal
- * Correspondence: mduarte@ff.ulisboa.pt (N.D.); patricia.rijo@ulusofona.pt (P.R.)

Received: 23 September 2019; Accepted: 13 October 2019; Published: 17 October 2019



Abstract: The *Plectranthus* genus is commonly used in traditional medicine due to its potential to treat several illnesses, including bacterial infections and cancer. As such, aiming to screen the antibacterial and cytotoxic activities of extracts, sixteen selected *Plectranthus* species with medicinal potential were studied. In total, 31 extracts obtained from 16 *Plectranthus* spp. were tested for their antibacterial and anticancer properties. Well diffusion method was used for preliminary antibacterial screening. The minimum inhibitory concentration (MIC) and minimal bactericidal concentration (MBC) values of the five most active acetonic extracts (*P. aliciae*, *P. japonicus*, *P. madagascariensis* var. “Lynne”, *P. stylesii*, and *P. strigosus*) were determined. After preliminary toxicity evaluation on *Artemia salina* L., their cytotoxic properties were assessed on three human cancer cell lines (HCT116, MCF-7, and H460). These were also selected for mechanism of resistance studies (on NCI-H460/R and DLD1-TxR cells). An identified compound—parvifloron D—was tested in a pair of sensitive and MDR-Multidrug resistance cancer cells (NCI-H460 and NCI-H460/R) and in normal bronchial fibroblasts MRC-5. The chemical composition of the most active extract was studied through high performance liquid chromatography with a diode array detector (HPLC-DAD/UV) and liquid chromatography–mass spectrometry (LC–MS). Overall, *P. strigosus* acetonic extract showed the strongest antimicrobial and cytotoxic potential that could be explained by the presence of parvifloron D, a highly cytotoxic diterpene. This study provides valuable information on the use of the *Plectranthus* genus as a source of bioactive compounds, namely *P. strigosus* with the potential active ingredient the parvifloron D.

Keywords: *Plectranthus*; *P. strigosus*; antimicrobial; cytotoxicity; parvifloron D

1. Introduction

The *Plectranthus* genus (Lamiaceae) comprises nearly 350 different species with a vast distribution and is recognized for its rich bio- and ethnobotanical diversity [1–3] (see Supplementary Materials, Figure S1). Its antibacterial, antifungal, antiviral, and antiproliferative potential have been well-described in literature [2]. These characteristics contribute to its popular use in traditional medicine, mainly through herbal preparations, thus having major importance in the provision of primary health care [3–5].

Cancer is still one of the major leading causes of death worldwide and the success of anticancer therapies is dependent on the development of multidrug resistance (MDR) [5,6]. Plants have long been used for the treatment of cancer and there are notable anticancer plant-derived drugs used in clinical practice, namely vinca alkaloids (vinblastine and vincristine) and paclitaxel [7,8]. In addition, several plant-derived products, namely terpenoids, and extracts have been described for their capability to inhibit P-glycoprotein (P-gp), and thus modulate MDR [9].

Terpenoids are also considered as responsible for the antimicrobial properties attributed to the aforementioned genus [3]. The increasing resistance to antibiotics and rising range of infections have become a public health-concerning issue [10].

Diterpenes are frequently found in the *Plectranthus* genus and are compounds of high interest, considering their wide spectrum of biological activity, characterized by antimicrobial and anti-inflammatory activity, but also, anticancer properties [11]. The majority of diterpene metabolites isolated from *Plectranthus* spp. belong to abietane, kaurane, and labdane classes [11]. The more prominent functional groups are phenol or quinone diterpenes belonging to royleanone, coleon, or parvifloron abietanes, which have been shown to be potent anticancer agent classes [12,13]. It is known that the major component of the essential oil of *P. madagascariensis* is the diterpene 6,7 dehydroroyleanone, which is easily identified due to its characteristic orange reddish color [14,15] and has already shown cytotoxic properties [16,17]. On the other hand, it is also ascribed antitumoral activity by a number of other *Plectranthus* species such as *P. amboinicus*, *P. barbatus*, and *P. hadiensis* [2], so the screening of their extracts is a significant achievement. Other previous studies showed that natural compounds with antitumor activity, isolated from *Plectranthus*, induce apoptosis by caspases activation. The discovery of natural tumor-promoting phorbol esters acting as protein kinase C (PKC) activators led to a new interest in the role of these proteins, but also, and more importantly, to new studies focusing on diterpenes as PKC modulators. It is known that some of the PKC isoforms are implied in tumoral regression, while others are involved in tumoral invasion, so modulating its activity is an important issue [18]. Having this in mind, the present study was aimed at screening the antimicrobial and cytotoxic properties of several *Plectranthus* spp. extracts. These goals were accomplished by comparing the efficacy of 31 plant extracts and identifying the bioactive component responsible for the extracts activity.

2. Experimental

2.1. Plant Material

Plectranthus spp. (Lamiaceae family) were cultivated in Instituto Superior de Agronomia Campus (Lisbon University), from seeds provided by the herbarium of the Botanical Garden of Lisbon, Portugal. The air dried and powdered whole plants were selected based on their ethnopharmacological features: *Plectranthus aliciae* (Codd) van Jaarsv. and Edwards, *Plectranthus amboinicus* (Lour.) Spreng., *Plectranthus barbatus* Andrews, *P. ecklonii* Benth., *P. fruticosus* L'Hér., *Plectranthus hadiensis* (Forssk.) Schweinf. ex Spreng. var. *hadiensis*, *P. hereroensis* Engl., *Plectranthus japonicus* Koidz., *Plectranthus madagascariensis* (Pers.) Benth. var. *madagascariensis*, *P. madagascariensis* (Pers.) Benth. var. 'Lynne', *Plectranthus malvinus* van Jaarsv. and T.J. Edwards, *Plectranthus oertendahlü* Th. Fr., *Plectranthus reflexus* van Jaarsv. and T.J. Edwards, *Plectranthus stylesii* Edwards, *P. strigosus* Benth. ex E.Mey., and *Plectranthus zuluensis* T. Cooke. The plant names were verified with the Index Kewensis [19]. The plants were grown in Parque Botânico da Tapada da Ajuda from cuttings provided through the Kirstenbosch National Botanical Gardens, South Africa; were collected between 2007 and 2008, always in June and September;

and voucher specimens were deposited in the Herbarium “João de Carvalho e Vasconcellos” of the “Instituto Superior de Agronomia”, Lisboa (LISI), Portugal [20].

Traditional uses of the mentioned plants and their voucher numbers are displayed in Table S1.

2.2. Extraction Procedure of *Plectranthus* spp.

Thirty-one extracts were prepared from sixteen different *Plectranthus* species. The air-dried leaves of each plant were milled in a kitchen mill and weighed. The extraction procedure was carried out in triplicate in an ultrasonic (US) bath (Bandelin SONOREX RK 510H, Berlin, Germany) for 60 min at 25 °C—using acetone, ethanol, and/or methanol—in a concentration of 10% (*w/v*). The suspensions were then filtered using Filtrir Laurent—Prat demas 150 mm (Couze-St-Front, France). After each filtration, the solvent was removed in a rotary evaporator (Sigma-Aldrich, IKA HBR 4 basic heating bath, Essen, Germany) at 40 °C. After submitting the suspensions to ultrasounds three times, the final extracts were weighed, and the yield of extraction determined. The percentage yield for each extract was determined (Figure S2).

2.3. Microorganisms Used and Growth Conditions

Bacterial strains *Enterococcus faecalis* (ATCC 29212), *Escherichia coli* (ATCC 25922), *Pseudomonas aeruginosa* (ATCC 27853), and *Staphylococcus aureus* (ATCC 25923), and yeast strains *Candida albicans* (ATCC 10231) and *Saccharomyces cerevisiae* (ATCC 9763) were chosen based on their clinical and pharmacological importance. In addition, *S. cerevisiae* was added due to its general toxicity screening value. The tested bacteria were precultivated on Mueller Hinton agar and yeasts in Sabouraud agar (Biokar diagnostics, Allonne, France). Cultures of microorganisms were grown at 37 °C (30 °C for the yeasts) for 24 h and were maintained on respective agar slants at 4 °C.

2.4. Antimicrobial Screening Assays

2.4.1. Well Diffusion Method

The extracts were reconstituted in DMSO—Dimethyl Sulfoxide—to a 1 mg/mL concentration as well as the stock solutions of reference antibiotics (vancomycin and norfloxacin, Gram-positive and -negative, respectively). Nystatin was used as the positive control for the yeasts. Afterwards, Petri dishes containing 20 mL of solid Mueller–Hinton culture medium (Sabouraud for the yeasts) were inoculated with 100 µL of microorganism suspension (correspondent to a 0.5 McFarland standard solution). The inocula were evenly harvested on the medium surface using a sterile swab [20]. Wells of approximately 5 mm in diameter were punched aseptically in the medium, with a sterile glass Pasteur pipette and 50 µL of each extract and antimicrobial agent were introduced into the well [20,21]. The solvent DMSO was used as negative control. Plates were then incubated at 37 °C (30 °C for the yeasts) for 24 h. The antimicrobial activity was then evaluated by measuring the diameter (mm) of the inhibition zone formed around the wells and the results compared to positive and negative controls [20]. This method was tested at least in triplicate.

2.4.2. Determination of Minimum Inhibitory Concentration

Only extracts that showed inhibitory activity on the well diffusion method were tested for this method, so only the bacteria were active. After screening the antimicrobial activity of the plant extracts, the microplate broth microdilution method was performed for those that were considered active (inhibition zone > 10 mm). As such, 100 µL of liquid Mueller–Hilton medium was distributed in each well of a 96-well plate. The first well of each row contained 100 µL of extract, the positive control, or negative control solutions (1 mg/mL concentration). Serial dilutions were made to 1:2 proportion between each row of wells (1.95–500 µg/mL range). Finally, 10 µL of bacterial suspension of 0.5 McFarland density were added to each well. Plates were then incubated at 37 °C for 24 h, allowing the bacterial growth. The latter was measured with an absorbance microplate reader (Thermo Scientific

Multiskan FC, Loughborough, UK) set to 620 nm. All assays were carried out in triplicate for each tested microorganism [20].

2.4.3. Determination of Minimal Bactericidal Concentration

After concluding the minimum inhibitory concentration (MIC) assay, the minimal bactericidal concentration (MBC) assay was done accordingly to the agar dilution method. Thus, a swab from each well where no growth was observed—containing the tested extract concentration series—was plated on a Mueller Hinton Agar [21–23]. The Petri plates were then incubated for 24 h at 37 °C, for further evaluation. The lowest concentration that revealed no visible bacterial growth after subculturing was taken as its MBC. Only the bacteria showed inhibition growth.

2.5. Cell Lines and Reagents

2.5.1. Chemicals

MTT (3-(4,5-dimethyl-2-thiazolyl)-2, 5-diphenyl-2H-tetrazolium bromide), rhodamine 123 (Rho123), and dimethylsulfoxide (DMSO) were acquired from Sigma-Aldrich Chemie GmbH. Fetal bovine serum (FBS), RPMI 1640 medium (Roswell Park Memorial Institut), DMEM (Dulbecco's Modified Eagle Medium), penicillin–streptomycin solution, antibiotic–antimycotic solution, L-glutamine, and trypsin/EDTA were purchased from PAA (Vienna, Austria).

2.5.2. Cell Culture Maintenance

Human colon (HCT116) and breast (MCF-7) adenocarcinoma, and non-small cell lung carcinoma (NCI-H460) cell lines were purchase from ATCC. All cancer cells were cultured in RPMI-1640 medium with ultraglutamine (Lonza, VWR, Carnaxide, Portugal), and supplemented with 10% fetal bovine serum (FBS; Gibco, Alfacene, Carcavelos, Portugal). Cells were maintained at 37 °C in a humidified atmosphere of 5% CO₂.

Sensitive non-small cell lung carcinoma NCI-H460, colorectal carcinoma DLD1 cell lines, and normal human embryonal bronchial fibroblasts MRC-5 were purchased from American Type Culture Collection (Rockville, MD, USA).

NCI-H460 and DLD1 cells were maintained in RPMI 1640 medium containing 10% heat in activated FBS, 2 mM L-glutamine, 4.5 g/L glucose, 10,000 U/mL penicillin, 10 mg/mL streptomycin, and 25 mg/mL amphotericin B solution at 37 °C in a humidified 5% CO₂ atmosphere. NCI-H460/R cells were originally selected from NCI-H460 cells and cultured in a medium containing 100 nM doxorubicin (DOX) [23]. DLD1-TxR cells were selected by continuous exposure to stepwise increasing concentrations of paclitaxel (PTX) from DLD1 cells [24].

MRC-5 cells were cultured in DMEM supplemented with 10% FBS, 4 g/L glucose, L-glutamine (2 mM), and 5000 U/mL penicillin, 5 mg/mL streptomycin solution at 37 °C in a humidified 5% CO₂ atmosphere.

All cell lines were subcultured at 72 h intervals using 0.25% trypsin/EDTA and seeded into a fresh medium at the density of 8000 cells/cm².

2.6. Preliminary Evaluation of General Toxicity on *Artemia salina* Model

Aiming at the evaluation of the preliminary toxicity of the selected *Plectranthus* spp. extracts, a lethality test on *Artemia salina* L. was carried out [25]. The general toxicity on *A. salina* was tested according to the method of Zhang et al. 2012 [26], with slight alterations.

Brine shrimp cysts (obtained from JBL GmbH and Co. KG, D-67141 Neuhofen Germany) were hatched in artificial sea water with a concentration of 35 g/L. A container with two connected chambers with a simple handmade communicating vessel was used for brine shrimp hatching. An air pump inserted in the container ensured a regular air flow supply, thus saturating the artificial sea water for successful hatching. The cysts were then incubated for 48 h at 24 °C. Each extract was tested at a

concentration of 100 ppm. To do so, ten to fifteen nauplii were transferred into wells of 24-well plates containing artificial sea water, and 100 μ L of each extract was added to the wells (final volume per well: 1 mL). After 24 h exposure to the extracts (24 °C), the number of dead nauplii (mortality rate (%)) was determined (Equation (1)). Also, LC₅₀ (Lethal Concentration, 50%) values (μ g/mL) were calculated for the most toxic extracts. DMSO was used as the solvent and was kept at 10% (v/v) in all samples tested.

$$\text{Mortality rate (\%)} = \frac{\text{Total nauplii} - \text{Alive nauplii}}{\text{Total nauplii}} \quad (1)$$

2.7. Cytotoxicity Screening

Sulforhodamine B Assay for the Assessment of Extracts Effects

The effect of plant extracts on the *in vitro* growth of human tumor cell lines was evaluated using the sulforhodamine B (SRB) assay, as described [27,28]. Briefly, cells were seeded in 96-well plates, at a final density of 5.0×10^3 cells/well, and incubated for 24 h. Cells were then incubated with serial dilutions of plant extracts (from 1.56 to 50 μ g/mL) for 48 h. The solvent (DMSO) was used as negative control at the same concentration as the maximum tested in the assay. The concentration of compound that causes a 50% reduction in the net protein increase in cells during treatment (GI₅₀, growth inhibition of 50%) was subsequently calculated.

NCI-H460, NCI-H460/R, DLD1, and DLD1-TxR cells grown in 25 cm² tissue flasks were trypsinized, seeded into flat-bottomed 96-well tissue culture plates (2×10^4 cells/well), and incubated overnight. Treatments with extracts (5–100 μ g/mL) lasted 72 h. The cellular proteins were stained with SRB, following slightly modified protocol of Skehan et al. [28]. Briefly, the cells in 96-well plates were fixed in 50% trichloroacetic acid (50 μ L/well) for 1 h at 4 °C, rinsed in tap water, and stained with 0.4% (w/v).

SRB in 1% acetic acid (50 μ L/well) for 30 min at room temperature. The cells were then rinsed three times in 1% acetic acid to remove the unbound stain. The protein-bound stain was extracted with 200 μ L 10 mM Tris base (pH 10.5) per well. The optical density was read at 540 nm with correction at 670 nm in a LKB 5060-006 Micro plate Reader (Vienna, Austria). The concentration of each drug that inhibited cell growth by 50%. (IC₅₀) was calculated by nonlinear regression analysis using log (inhibitor) vs. normalized response in GraphPad Prism 6 software. Values represent means \pm SE (Standard Error) from at least three independent experiments, each performed in triplicate.

2.8. Liquid Chromatography–Mass Spectrometry Analysis

Liquid chromatography–mass spectrometry (LC–MS)/MS analyses were performed on a Waters Alliance 2695 high performance liquid chromatography (HPLC) separation module connected to a Micromass Quattro Micro triple Quadrupole (Waters, Dublin, Ireland) Mass Spectrometer equipped with a Waters electrospray ionization (ESI) source. Mass spectrometer was operated in positive mode and spectra were recorded in the *m/z* 60 to 800 Da range. In order to optimize detection conditions, a standard solution of parvifloron D was infused in the mass spectrometer and capillary and cone voltages, and collision energy were tuned to maximize (recursor ion > product ion) transition signal. ESI capillary voltage was optimized to 3 kV, cone voltage was set on 30 V. Source and desolvation temperature were adjusted to 120 °C and 350 °C, respectively. High purity nitrogen (N₂) was used as drying gas and as a nebulizing gas. Ultra-high purity argon (Ar) was used as collision gas. A reversed phase WatersTM Atlantis C-18 (Waters, Milford, MA, USA; 5 μ m \times 2.1 mm \times 150 mm) was used, with an injection volume of 15 μ L. The mobile phase consisted in 0.5% formic acid in Milli-Q water (eluent A) and acetonitrile (eluent B). A flow rate of 0.2 mL/min was used, with the following gradient program: 0–15 min from 60% to 20% A, 15–20 min at 20% A, 20–30 min 60% A. MassLynx software (Waters, version 4.1) was used for data acquisition and processing.

The quantification of the identified compound was carried out in an Agilent Technologies 1200 Infinity Series system with diode array detector (DAD; Agilent, Santa Clara, CA, USA), equipped

with a Zorbax XDB-C18, (250 × 4.0 mm i.d., 5µm) column, from Merck and ChemStation Software (Hewlett-Packard, Alto Palo, CA, USA). Each extract was analyzed (after 20 µL injection) and a gradient elution mixture composed of solution A (methanol), solution B (acetonitrile), and solution C (0.3% trichloroacetic acid in water) was used as follows: 0 min, 15% A, 5% B, and 80% C; 20 min, 70% A, 30% B, and 0% C; 25 min, 70% A, 30% B, and 0% C; and 28 min, 15% A, 5% B, and 80% C. The flow rate was set at 1 mL.min⁻¹. For quantification and identification purposes, the compounds present in the samples were compared with calibration standards. Compound identification was based on ultraviolet (UV) spectra comparison and retention time. The time of analysis was of 28 min, including the stabilization of the RP-18 column. All analyses were performed in triplicate.

2.9. Anticancer Effects of the Identified Compound

The anticancer properties of the parvifloron D present in the most active extract were assessed through the use of a model system of NCI-H460 and its resistant counterpart NCI-H460/R, along with normal human embryonal bronchial fibroblasts MRC-5. MTT test was applied after 72 h incubation with diterpenes, applied within a range of concentrations 2.5–50 µM.

2.9.1. Cell Viability Assessed by MTT Assay

MTT assay is based on the reduction of 3-(4, 5-dimethyl-2-thizoly)-2,5-diphenyl-2H-tetrazolium bromide into formazan dye by active mitochondria of living cells. Briefly, cells grown in 25 cm² tissue flasks were trypsinized, seeded in 96-well tissue culture plates (2,000 cells/well), and incubated overnight in 100 mL of appropriate medium. After 24 h, cells were treated with increasing concentrations of parvifloron D (2.5–50 µM). All treatments lasted 72 h. At the end of treatment period, 100 mL of MTT solution (1 mg/mL) was added to each well and plates were incubated at 37 °C for 4 h. Formazan product was dissolved in 200 mL DMSO. The absorbance of obtained dye was measured at 540 nm using an automatic microplate reader (LKB 5060-006 Micro Plate Reader, Vienna, Austria).

Relative cell growth rate (CG) was determined according to the following equation:

$$CG (\%) = (A \text{ treated sample} / A \text{ untreated control}) \times 100, \quad (2)$$

where A is absorbance. IC₅₀ value was defined as concentration of each drug that inhibited cell growth by 50%. IC₅₀ was calculated by nonlinear regression analysis using log (inhibitor) vs. normalized response in GraphPad Prism 6 software.

2.9.2. Assay for P-gp Inhibiting Activity

The function of P-gp was analyzed by flow-cytometry utilizing the ability of its substrate Rho123 to emit fluorescence. Studies were carried out with parvifloron D. Dex-VER was used as a positive control. The MDR cells (NCI-H460/R) were grown to 80% confluence in 75 cm² flasks, trypsinized, and resuspended in 5 mL centrifuge tubes in a Rho123-containing medium (5 µM Rho123). The cells were treated with Dex-VER and parvifloron D (5 µM) and incubated at 37 °C in 5% CO₂ for 30 min. The cells were washed with cold phosphate-buffered saline, and analyzed using a flow cytometer. The samples were washed twice, resuspended in 1.0 mL CyFlow Space flow cytometer (Partec, Münster, Germany). The mean fluorescence intensity (MFI) of Rho123 was assessed on fluorescence channel 1. At least 10,000 events were assayed for each sample.

2.9.3. Effects of Compounds on Microtubule

The effect of the identified compound on interphase on microtubules, mitotic spindles, nuclear morphology, and cell cycle was assessed. In order to do so, human lung carcinoma A549 cells were incubated for 20 h with serial concentrations of the diterpene ranging from 10 nM to 200 µM.

The DNA content was analyzed by flow cytometry using a BD FACSVerser™ cytometer (BD Biosciences, San Jose, CA, USA). Cells were collected and centrifuged at 500× g, washed with phosphate buffer saline (PBS), and resuspended in 50 µL of PBS. Following dropwise addition of 1 mL

of ice-cold 75% ethanol, fixed cells were stored at $-20\text{ }^{\circ}\text{C}$ for 1 h. Samples were then centrifuged at $500\times g$ and washed with PBS before resuspension in 1 mL of PBS containing $50\text{ }\mu\text{g/mL}$ propidium iodide and $100\text{ }\mu\text{g/mL}$ RNase A, and incubation for 1 h at $37\text{ }^{\circ}\text{C}$ in the dark. The percentage of cells with decreased DNA staining, composed of apoptotic cells resulting from either fragmentation or decreased chromatin, was counted (minimum of 10,000 cells per experimental condition). Cell debris was excluded from analysis by selective gating based on anterior and right angle scattering.

3. Results and Discussion

The acetic, ethanolic, and/or methanolic extracts of several *Plectranthus* species (Figure S1) were evaluated concerning their antimicrobial activity through the well diffusion method and further MIC and MBC determination. Furthermore, in order to evaluate their cytotoxic properties, toxicity assays were performed on *Artemia salina* L. and different cancer cell lines.

All 31 extracts were screened at a fixed concentration (1 mg/mL). Overall, five extracts demonstrated inhibitory activities against either or both *Enterococcus faecalis* (ATCC 29212) and *Staphylococcus aureus* (ATCC 25923) bacterial strains (Table S2). All other extracts did not display antibacterial effects, showing inhibition zones lower than 10 mm (data not shown). The extracts prepared with acetone revealed better antimicrobial activity, particularly against Gram-positive bacteria.

A significant inhibition zone was recorded for the acetic extracts of *P. aliciae* and *P. madagascariensis* var. "Lynne", for both Gram-positive bacteria used (*E. faecalis* and *S. aureus*), with results similar to those of positive control. The remaining active extracts, however, showed selectivity only against *S. aureus*.

Regarding the results obtained on the well diffusion test, only Gram-positive bacteria were taken into account on these assays. Thus, in order to assess the lowest growth inhibitory concentration of the most promising *Plectranthus* spp. extracts, minimum inhibitory concentration values (MIC) were determined. Their bacteriostatic and bactericidal properties were also evaluated (Table 1) MIC values ranged from 15.6 to $125\text{ }\mu\text{g/mL}$, while MBC values ranged from >62.5 to $250\text{ }\mu\text{g/mL}$.

Table 1. Minimum inhibitory concentration (MIC) and minimum bactericidal concentration (MBC) values of *Plectranthus* spp. acetic extracts against tested bacteria (results expressed in $\mu\text{g/mL}$).

| Acetic Extracts | Gram-Positive Bacteria | | | |
|------------------------------------|---------------------------------|-------|-------------------------------|-----|
| | <i>E. faecalis</i> (ATCC 29212) | | <i>S. aureus</i> (ATCC 25923) | |
| | MIC | MBC | MIC | MBC |
| <i>P. aliciae</i> | 15.6 | 125 | 62.5 | 125 |
| <i>P. japonicus</i> | 62.5 | 125 | 62.5 | 125 |
| <i>P. madagascariensis</i> 'Lynne' | 15.6 | >125 | 125 | 125 |
| <i>P. strigosus</i> | 15.6 | >62.5 | 125 | 125 |
| <i>P. stylesii</i> | 31.3 | >125 | 62.5 | 250 |
| Positive control (VAN) | 1.95 | | 7.82 | |
| Negative control (DMSO) | >500 | | >500 | |

VAN—vancomycin (1 mg/mL); NOR—norfloxacin (1 mg/mL).

Comparing the MBC and MIC values of the selected extracts, and having in mind that a bactericidal effect is associated to a MBC no more than four times the MIC value [21], it is possible to conclude that the extracts are mainly bactericidal rather than bacteriostatic.

The preliminary evaluation of toxicity on *Artemia salina* is a fairly easy and inexpensive method and is particularly interesting when testing plant extracts as it can be used as a prescreen of their potential antitumor activities. This assay also helps in gaining a preliminary understanding of which extracts may deserve additional testing. All 31 extracts were tested (data not shown), but only five of them exhibited toxic effects with values ranging from 13.62 to $110.76\text{ }\mu\text{g/mL}$ (Table 2). Curiously, these five acetic extracts were the same that induced *S. aureus* growth inhibition. The lowest LC_{50} , and consequently, the highest toxic potential, was attributed, once again, to the activity of *P. strigosus*. On the contrary, the least toxic extract was attributed to *P. stylesii*.

Table 2. *A. salina* general toxicity results LC₅₀ (µg/mL) of acetonic extracts of the selected *Plectranthus* spp.

| Acetonic Extracts | Mortality Rate (%) at 100 ppm Concentration | LC ₅₀ (µg/mL) |
|--|---|--------------------------|
| <i>P. aliciae</i> | 16.71 ± 1.01 | 53.48 |
| <i>P. japonicus</i> | 21.85 ± 0.35 | 38.9 |
| <i>P. madagascariensis</i> var “Lynne” | 9.67 ± 0.93 | 91.7 |
| <i>P. stylesii</i> | 16.30 ± 0.99 | 110.76 |
| <i>P. strigosus</i> | 42.88 ± 2. 21 | 13.62 |
| DMSO | 22.50 ± 3.54 | N.A. |

N.A.—non applicable.

The GI₅₀ values were also determined for each of the 31 extracts, in HCT116, MCF-7, and NCI-H460 cell lines, and the observed reduction in the cell growth was compared to the growth of cells treated with DMSO only (set as 100% growth). The results are summarized in Figure 1 below. The data bars not shown refer to a GI₅₀ value equal or higher than 50 µg/mL.

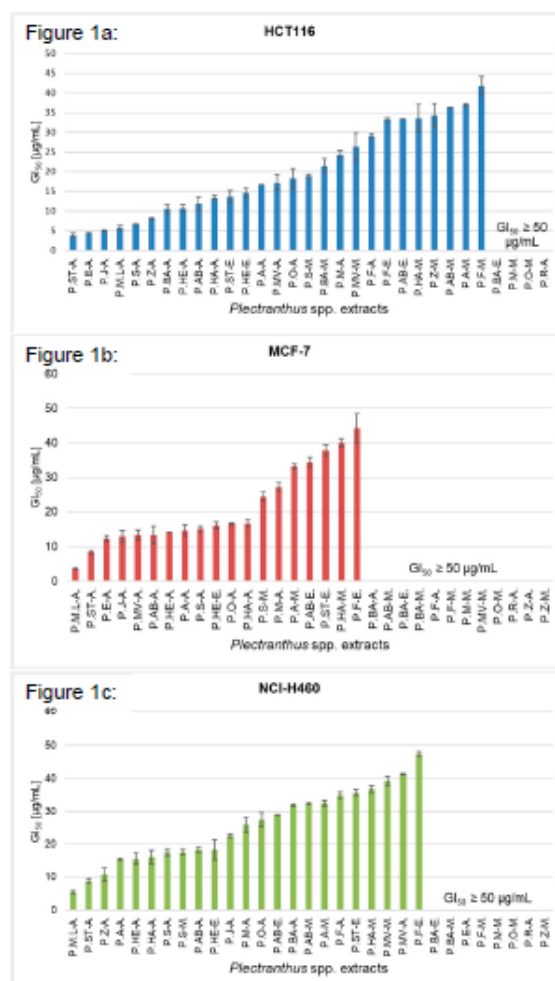


Figure 1. Growth inhibition of 50% (GI₅₀) values (µg/mL) of *Plectranthus* spp. extracts in HCT116 (a), MCF-7 (b), and NCI-H460 (c) cells were determined after 48 h treatment using the SRB assay. Data are mean ± SEM (n = 3,4). Doxorubicin was used as a positive control (GI₅₀: 54.00 ± 3.24 ng/mL in HCT116, 85.17 ± 4.10 ng/mL in MCF-7, 292.01 ± 2.32 ng/mL in NCI-H460 cells).

According to the results, acetic extracts revealed better cytotoxic effects. Five of these—*P. aliciae*, *P. japonicus*, *P. madagascariensis* var. “Lynne”, *P. stylesii*, and *P. strigosus*—have consistently exhibited a broad cytotoxic potential. When analyzing GI_{50} on the three tested cell lines, values ranged between 3.47 to 16.67 $\mu\text{g/mL}$, showing effective growth inhibition against specific cell lines.

P. strigosus acetic extract displayed the highest overall anticancer potential, given its growth inhibitory activities towards HCT116 ($GI_{50} = 3.78 \pm 0.49 \mu\text{g/mL}$), MCF-7 ($GI_{50} = 8.35 \pm 0.57 \mu\text{g/mL}$), and NCI-H460 ($GI_{50} = 8.75 \pm 0.70 \mu\text{g/mL}$). On the other hand, the highest inhibitory growth activities on MCF-7 and NCI-H460 cell lines were attributed to the effect of *P. madagascariensis* var. “Lynne” ($GI_{50} = 3.47 \pm 0.15 \mu\text{g/mL}$ and 5.39 ± 0.48 , respectively).

The extract with the lowest anticancer potential was *P. reflexus* methanolic extract, for which GI_{50} was not reached in the screened range in all tested cell lines ($GI_{50} \geq 50 \mu\text{g/mL}$).

Overall, *Plectranthus* spp. extracts recorded a broader cytotoxic activity against HCT116, given that 27 out of the 31 extracts tested have GI_{50} lower than 50 $\mu\text{g/mL}$.

According to the results obtained in the previous screening (Figure 1), the most promising *Plectranthus* spp. extracts were tested in MDR cell lines with P-gp overexpression: NCI-H460/R (non-small cell lung carcinoma cell line) and DLD1-TxR (colorectal adenocarcinoma cell line). The effects of the five selected acetic extracts were assessed by SRB assay after 72 h, and their IC_{50} values were determined (Figure 2). *P. strigosus* acetic extract exerted an overall best effect in both non-small cell lung carcinoma and colorectal adenocarcinoma cells, which showed IC_{50} values of 5.64 $\mu\text{g/mL}$ (NCI-H460), 11.09 $\mu\text{g/mL}$ (NCI-H460/R), 2.41 $\mu\text{g/mL}$ (DLD1), and 2.51 $\mu\text{g/mL}$ (DLD1-TxR).

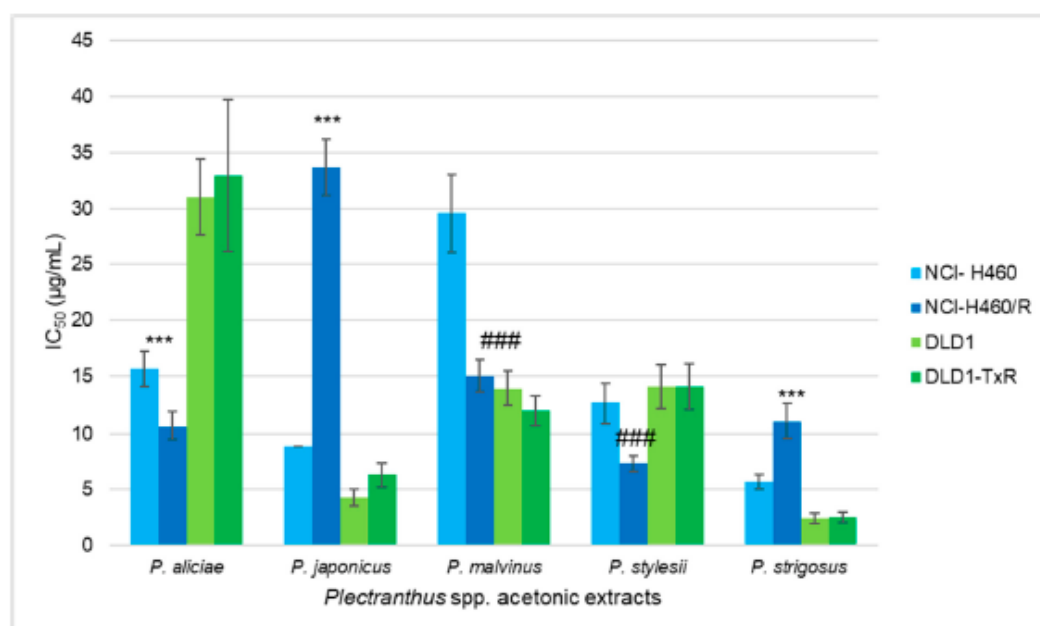


Figure 2. Sensitivity of MDR (MultiDrug Resistance) cancer cells and their corresponding sensitive cells to acetic *Plectranthus* extracts. The IC_{50} (half maximal inhibitory concentration) was determined using SRB assay after 72 h treatment with acetic extracts. Statistical analysis was performed in GraphPad Prism 6 by two-way ANOVA: *** indicates the resistance to the specific extract ($p < 0.001$); ### indicates the collateral sensitivity to the specific extract ($p < 0.001$).

All five extracts exerted similar results towards colorectal adenocarcinoma cells (DLD1 and DLD1-TxR). Thus, their efficacy might not depend on the presence of a MDR phenotype. Acetic extracts from *P. aliciae*, *P. japonicus*, and *P. strigosus* were less active against non-small cell lung carcinoma MDR cells (NCI-H460/R) in comparison with their sensitive counterparts (NCI-H460). Interestingly,

resistant NCI-H460/R were more sensitive to extracts from *P. malvinus* and *P. stylesii* showing collateral sensitivity, the phenomenon when MDR cells are more vulnerable than corresponding sensitive cells.

In order to assess the chemical composition of the most active extract (*P. strigosus* acetonetic extract), and in an attempt to identify the compounds responsible for the referred activity, a combination of HPLC–DAD (diode array detector)–MS techniques were carried out. The HPLC–MS analysis showed two main peaks at 19.8 and 22.0 min, which revealed a UV spectrum characteristic of quinone methide diterpenes [29]. The ESI mass spectra of the compounds pointed to the presence of parvifloron E or F (peak at 19.8 min, m/z 451 $[M + H]^+$) and parvifloron D (peak at 22 min, m/z 435 $[M + H]^+$). The presence of parvifloron D was confirmed through MS/MS analysis by comparison with a standard compound. MS/MS spectra showed product ions at m/z 297 (base peak) and m/z 279, corresponding to the loss of the ester moiety ($[M-C_7H_5O_3 + H]^+$) and ester moiety and H_2O ($[M-C_7H_5O_3-H_2O + H]^+$), see Supplementary Materials, Figure S3. The 19.8 min compound displayed a similar fragmentation pattern corresponding to the same diterpenic scaffold, with one more hydroxyl group on the aromatic ring substituent. Therefore, this compound was tentatively identified as parvifloron E. The quantification of parvifloron D was performed through HPLC–DAD/UV and was found to be present in the acetonetic extract of *P. strigosus* with a relative concentration of 9%.

Given its antitumor properties [30], the presence of the latter may explain, to a certain extent, the foreseen toxic properties of *P. strigosus* acetonetic extract. In order to further explore its cytotoxicity, additional studies were performed on this compound.

Afterwards, the preliminary toxicity evaluation of parvifloron D on *Artemia salina* L. resulted in a 76.6% mortality rate on this species after 24 h incubation.

In addition, its cytotoxic activity was further evaluated on NCI-H460 and NCI-H460/R cell lines. To determine whether parvifloron D is selective towards cancer cells, the cytotoxic effect in normal embryonic bronchial fibroblasts (MRC-5) was also evaluated.

As expected, this diterpene demonstrated high cytotoxicity and exerted a similar activity in all three cell lines, with IC_{50} ranging from 1.7 to 1.9 μ M. Interestingly, it also showed the same efficacy in sensitive and MDR cancer cells, which implies that parvifloron D is able to evade P-gp efflux activity (Figure 3A). However, it was equally active against normal cells (Figure 3A). Parvifloron D was also tested regarding its potential to inhibit P-gp activity in NCI-H460/R cells. Unfortunately, parvifloron D was not able to increase the Rhodamine 123 accumulation in P-gp overexpressing cells (Figure 3B). Considering its high cytotoxic potential, further examinations of parvifloron D should be performed. Its mechanism in cancer and normal cells, with respect to the application of lower concentrations and different time scheduling, are necessary to clarify whether this compound should be developed as an anticancer agent.

In order to check whether this abietane diterpene was a microtubule stabilizer agent, A549 cell morphologies in the IC_{50} culture plates were examined with an inverted microscope, after 20 h incubation with parvifloron D. Paclitaxel was used as control tubulin specific drug. All microtubule targeting drugs, stabilizers, or depolymerizers in contact with A549 cell lines induced the appearance of round cells (mitotic cells) that detach from the plate. However, parvifloron D only displayed a cytotoxic effect rather than cytostatic, with no mitotic blockage, practically ruling out an action on mitotic spindle microtubules (data not shown). These results suggest that the antibacterial and anticancer activities of the acetonetic extract of *P. strigosus* are attributed to the presence of parvifloron D. These results correlate to the representative HPLC–DAD/UV ($\lambda = 254$ nm) chromatogram of acetonetic extract of *P. strigosus* and UV DAD spectra of peaks. The prepared acetonetic extract of *P. strigosus* ($c = 0.67$ mg/mL) was revealed to have Parvifloron D (9% (w/w)) in its composition.

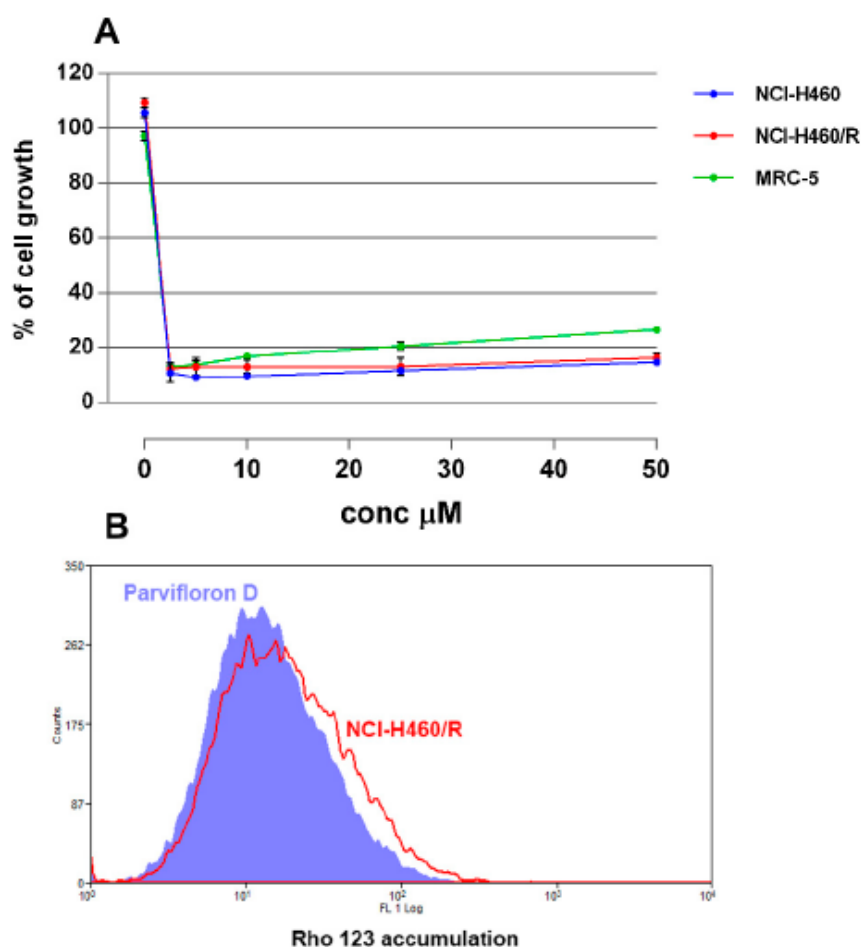


Figure 3. Anticancer effects of parvifloron D. The cytotoxicity was assessed by MTT—3-(4,5-Dimethylthiazol-2-yl)-2,5-diphenyltetrazolium bromide—assay after 72 h treatment in NCI-H460, NCI-H460/R, and MRC-5 cells (A). Rho 123 accumulation was evaluated as an indicator of P-glycoprotein (P-gp) function in NCI-H460/R cells untreated and treated with parvifloron D (B).

4. Conclusions

Overall, the screening of the *Plectranthus* spp. through several extracts carried out in this work was motivated by the possibility of enlightening the cytotoxic activities of these species. Acetone extracts have been proven to possess higher overall antimicrobial and cytotoxic activity. Comparing the results of the well diffusion method with the corresponding GI₅₀ (μg/mL) values obtained in cancer cells, it can be concluded that the extracts with antimicrobial properties in *S. aureus* were also those with the lowest GI₅₀ values. Therefore, among the 31 *Plectranthus* spp. extracts, the acetonic extracts from *P. aliciae*, *P. japonicus*, *P. malvinus* van Jaarsv. and T.J. Edwards, *P. strigosus*, and *P. stylesii* were selected as promising candidates for further examination. To the best of our knowledge, this study provides the first insight on the biological activities of some *Plectranthus* spp. such as *P. aliciae*, *P. madagascariensis* var. “Lynne”, and *P. stylesii*. More importantly, it has also allowed the assignment of components that might be responsible for their activity, such as the abietane diterpene parvifloron D. Overall, the acetonic extract of *P. strigosus* revealed the best cytotoxic potential.

For the reasons mentioned above, the results demonstrated that the *Plectranthus* genus may contain therapeutically useful compounds against both Gram-positive bacteria and some solid cancer cell lines including those with MDR phenotype.

Supplementary Materials: The following are available online at <http://www.mdpi.com/2218-273X/9/10/616/s1>, Figure S1: Selected *Plectranthus* spp. photos: *P. aliciae* (left) and *P. stylesii* (right). Table S1. *Plectranthus* spp. voucher numbers and respective traditional medicine uses. Table S2: Antimicrobial activity of *Plectranthus* spp. extracts using the well diffusion method (zone of inhibition in mm). Figure S2. Percentage yield of the *Plectranthus* spp. extracts (expressed in percentage dry weight (% w/w)) according to the extracting solvents used. Figure S3. *Parvifloron* D Mass Spectroscopy spectra (MS/MS spectra).

Author Contributions: Conceptualization, P.R.; methodology, C.G., E.N., A.R. (Ana Rebelo), C.B.; software, T.S., J.D.; validation, L.S., M.P., P.R. and N.D.; investigation, C.G., C.B., J.D.; writing—original draft preparation, C.G.; writing—review and editing, A.D.-L., C.P.R., A.M., P.R., P.P., M.-J.C.; visualization, N.D., A.R. (Amílcar Roberto); supervision, P.R.

Funding: This research and APC were funded by Fundação para a Ciência e Tecnologia (FCT) grant number UID/DTP/04567/2016, UID/QUI/50006/2019 and UID/DTP/04567/2019.

Acknowledgments: This work was supported by PADDIC 2016 and 2017 (ALIES-COFAC) as part of the PhD Program in Health Sciences from Universidad de Alcalá and Universidade Lusófona de Humanidades e Tecnologias. The authors acknowledge Fundação para a Ciência e Tecnologia (FCT) for the financial support under the reference UID/DTP/04567/2016–CBIOS/PRUID/B11/2017, UID/QUI/50006/2019, UID/DTP/04567/2019 and REDE/1518/REM/2005 for the LC-MS experiments at Faculdade de Farmácia da Universidade de Lisboa. The authors would like to thank Isabel Barasoain from e Centro de Investigaciones Biológicas Consejo Superior de Investigaciones Científicas Ramiro de Maeztu, 9, 28040 Madrid, Spain for the microtubule work. This work was performed within the framework of COST Actions CM1407 (Challenging organic syntheses inspired by nature—from natural products chemistry to drug discovery) and CA17104 (New diagnostic and therapeutic tools against multidrug resistant tumor).

Conflicts of Interest: The authors declare no conflict of interest.

References

- Rice, L.J.; Brits, G.J.; Potgieter, C.J.; Van Staden, J. *Plectranthus*: A plant for the future? *S. Afr. J. Bot.* **2011**, *77*, 947–959. [CrossRef]
- Lukhoba, C.W.; Simmonds, M.S.; Paton, A.J. *Plectranthus*: A review of ethnobotanical uses. *J. Ethnopharmacol.* **2006**, *103*, 1–24. [CrossRef] [PubMed]
- Rijo, P.; Batista, M.; Matos, M.; Rocha, H.; Jesus, S.; Simões, M.F. Screening of antioxidant and antimicrobial activities on *Plectranthus* spp. extracts. *Biomed. Biopharm. Res.* **2012**, *9*, 225–235. [CrossRef]
- Rijo, P.; Faustino, C.; Simões, M.F. Antimicrobial natural products from *Plectranthus* plants. In *Microbial Pathogens and Strategies for Combating Them: Science, Technology and Education*, 2nd ed.; Méndez-Vilas, A., Ed.; Formatec Research Center: Badajoz, Spain, 2013.
- Saeed, M.E.M.; Meyer, M.; Hussein, A.; Efferth, T. Cytotoxicity of South-African medicinal plants towards sensitive and multidrug-resistant cancer cells. *J. Ethnopharmacol.* **2016**, 209–223. [CrossRef] [PubMed]
- WHO. Cancer. Available online: <https://www.who.int/news-room/fact-sheets/detail/cancer> (accessed on 15 October 2019).
- Cragg, G.M.; Newman, D.J. Natural products: A continuing source of novel drug leads. *Biochim. Biophys. Acta (BBA) Bioenerg.* **2013**, *1830*, 3670–3695. [CrossRef] [PubMed]
- Newman, D.; Cragg, G. Natural products as sources of new drugs over the 30 years. *J. Nat. Prod.* **2012**, *23*, 311–335. [CrossRef] [PubMed]
- Abdallah, H.M.; Al-Abd, A.M.; El-Dine, R.S.; El-Halawany, A.M. P-glycoprotein inhibitors of natural origin as potential tumor chemo-sensitizers: A review. *J. Adv. Res.* **2015**, *6*, 45–62. [CrossRef]
- WHO. Antimicrobial Resistance. Available online: <https://www.who.int/antimicrobial-resistance/en/> (accessed on 15 October 2019).
- Wellsow, J.; Grayer, R.J.; Veitch, N.C.; Kokubun, T.; Lelli, R.; Kite, G.C.; Simmonds, M.S. Insect-antifeedant and antibacterial activity of diterpenoids from species of *Plectranthus*. *Elsevier Phytochem.* **2016**, *67*, 1818–1825. [CrossRef]
- Marques, C.G.; Pedro, M.; Simões, M.F.; Nascimento, M.S.; Pinto, M.M.; Rodriguez, B. Effect of abietane diterpenes from *Plectranthus grandidentatus* on the growth of human cancer cell lines. *Planta Med.* **2002**, *68*, 839–840. [CrossRef]
- Rijo, P.; Duarte, A.; Francisco, A.P.; Semedo-Lemsaddek, T.; Simões, M.F. In Vitro antimicrobial activity of royleanone derivatives against Gram-positive bacterial pathogens. *Phytother. Res.* **2014**, *28*, 76–81. [CrossRef]

14. Ascensão, L.; Figueiredo, A.C.; Barroso, J.G.; Pedro, L.G.; Schripsema, J.; Deans, S.G.; Scheffer, J.J.C. *Plectranthus madagascariensis*: Morphology of the glandular trichomes, essential oil composition, and its biological activity. *Int. J. Plant. Sci.* **1998**, *159*, 31–38. [CrossRef]
15. Kubínová, R.; Pořízková, R.; Navrátilová, A.; Farsa, O.; Hanáková, Z.; Bačinská, A.; Cížek, A.; Valentová, M. Antimicrobial and enzyme inhibitory activities of the constituents of *Plectranthus madagascariensis* (Pers.) Benth. *J. Enzyme Inhib. Med. Chem.* **2014**, *29*, 749–752. [CrossRef] [PubMed]
16. Areche, C.; Schmeda-Hirschmann, G.; Theoduloz, C.; Rodríguez, J.A. Gastroprotective effect and cytotoxicity of abietane diterpenes from the Chilean *Lamiaceae*. *Sphacele Chamaedryoides* (Balbis) Briq. *J. Pharm. Pharmacol.* **2009**, *61*, 1689–1697. [CrossRef] [PubMed]
17. Kusumoto, N.; Aburai, N.; Ashitani, T.; Takahashi, K.; Kimura, K.-I. Pharmacological Prospects of Oxygenated Abietane-Type Diterpenoids from *Taxodium distichum* Cones. *Adv. Biol. Chem.* **2014**, *4*, 109–115. [CrossRef]
18. Matias, D.; Bessa, C.; Simões, M.F.; Reis, C.P.; Saraiva, L.; Rijo, P. Natural products as lead Protein Kinase C modulators for cancer therapy. *Studies Nat. Prod. Chem.* **2016**, *50*, 45–79.
19. ePIC. Index Kewensis. *Royal Botanic Gardens, Kew, UK*. Available online: <http://epic.kew.org/index.htm> (accessed on 9 October 2019).
20. Rijo, P.; Matias, D.; Fernandes, A.S.; Simões, M.F.; Nicolai, M.; Reis, C.P. Antimicrobial plant extracts encapsulated into polymeric beads for potential application on the skin. *Polymers* **2014**, *6*, 479–490. [CrossRef]
21. Balouiri, M.; Sadiki, M.; Ibsouda, S.K. Methods for in vitro evaluating antimicrobial activity: A review. *J. Pharm. Anal.* **2016**, *6*, 71–79. [CrossRef]
22. Karygianni, L.; Cecere, M.; Skaltsounis, A.L.; Argyropoulou, A.; Hellwig, E.; Aligiannis, N.; Wittmer, A.; Al-Ahmad, A. High-level antimicrobial efficacy of representative Mediterranean natural plant extracts against oral microorganisms. *Biomed. Res. Int.* **2014**, *2014*, 839019. [CrossRef]
23. Pesic, M.; Markovic, J.Z.; Jankovic, D.; Kanazir, S.; Markovic, I.D.; Rakic, L.; Ruždijic, S. Induced resistance in the human non small cell lung carcinoma (NCI-H460) cell line in vitro by anticancer drugs. *J. Chemother.* **2006**, *18*, 66–73. [CrossRef]
24. Podolski-Renić, A.; Anđelković, T.; Banković, J.; Tanić, N.; Ruždijic, S.; Pešić, M. The role of paclitaxel in the development and treatment of multidrug resistant cancer cell lines. *Biomed. Pharmacother.* **2011**, *65*, 345–353. [CrossRef]
25. Alanís-Garza, B.A.; González-González, G.M.L.; Salazar-Aranda, R.; Waksman de Torres, N.; Rivas-Galindo, V.M. Screening of antifungal activity of plants from the northeast of Mexico. *J. Ethnopharmacol.* **2007**, *114*, 468–471. [CrossRef] [PubMed]
26. Zhang, Y.; Mu, J.; Han, J.; Gu, X. An improved brine shrimp larvae lethality microwell test method. *Toxicol. Mech. Methods* **2012**, *22*, 23–30. [CrossRef] [PubMed]
27. Soares, J.; Pereira, N.A.; Monteiro, Â.; Leão, M.; Bessa, C.; Dos Santos, D.J.; Raimundo, L.; Queiroz, G.; Bisio, A.; Inga, A. Oxazoloisoindolinones with in vitro antitumor activity selectively activate a p53-pathway through potential inhibition of the p53–MDM2 interaction. *Eur. J. Pharm. Sci.* **2015**, *66*, 138–147. [CrossRef] [PubMed]
28. Skehan, P.; Storeng, R.; Scudiero, D.; Monks, A.; McMahon, J.; Vistica, D.; Warren, J.T.; Bokesch, H.; Kenney, S.; Boyd, M.R. New colorimetric cytotoxicity assay for anticancer—Drug screening. *J. Natl. Cancer Inst.* **1990**, *82*, 1107–1112. [CrossRef] [PubMed]
29. Alder, A.C.; Rüdi, P.; Eugster, C.H. Drüsenfarbstoffe aus tropischen Labiaten: Parviflorones from *Plectranthus strigosus* Benth. *Helv. Chim. Acta* **1984**, *67*, 1531–1534. [CrossRef]
30. Burmistrova, O.; Perdomo, J.; Simões, M.F.; Rijo, P.; Quintana, J.; Estévez, F. The abietane diterpenoid parvifloron D from *Plectranthus ecklonii* is a potent apoptotic inducer in human leukemia cells. *Phytomedicine* **2015**, *22*, 1009–1016. [CrossRef]



© 2019 by the authors. Licensee MDPI, Basel, Switzerland. This article is an open access article distributed under the terms and conditions of the Creative Commons Attribution (CC BY) license (<http://creativecommons.org/licenses/by/4.0/>).



Article

In Vitro Assessment of Antimicrobial, Antioxidant, and Cytotoxic Properties of Saccharin–Tetrazolyl and –Thiadiazolyl Derivatives: The Simple Dependence of the pH Value on Antimicrobial Activity

Luís M. T. Frija ^{1,*}, Epole Ntungwe ², Przemysław Sitarek ³, Joana M. Andrade ²,
Monika Toma ⁴, Tomasz Śliwiński ⁴, Lília Cabral ⁵, M. Lurdes S. Cristiano ⁵, Patrícia Rijo ^{2,6,*}
and Armando J. L. Pombeiro ¹

¹ Centro de Química Estrutural (CQE), Instituto Superior Técnico, Universidade de Lisboa, Av. Rovisco Pais, 1049-001 Lisboa, Portugal; pombeiro@ist.utl.pt

² CBIOS—Research Center for Health Sciences & Technologies, ULusófona de Humanidades e Tecnologias, Campo Grande 376, 1749-024 Lisboa, Portugal; ntungweepolengolle@yahoo.com (E.N.); p5319@ulusofona.pt (J.M.A.)

³ Department of Biology and Pharmaceutical Botany, Medical University of Lodz, Muszyńskiego Street 1, 90-151 Łódź, Poland; przemyslaw.sitarek@umed.lodz.pl

⁴ Laboratory of Medical Genetics, Faculty of Biology and Environmental Protection, University of Lodz, 90-151 Lodz, Poland; monika.toma@biol.uni.lodz.pl (M.T.); tomasz.sliwinski@biol.uni.lodz.pl (T.Ś.)

⁵ Department of Chemistry and Pharmacy (FCT) and Center of Marine Sciences (CCMar), Universidade do Algarve, P-8005-039 Faro, Portugal; liliacabral80@gmail.com (L.C.); mcristi@ualg.pt (M.L.S.C.)

⁶ iMed.Ulisboa - Research Institute for Medicines, Faculdade de Farmácia, Universidade de Lisboa, Av. Prof. Gama Pinto, 1649-003 Lisboa, Portugal

* Correspondence: luisfrija@tecnico.ulisboa.pt (L.M.T.F.); patricia.rijo@ulusofona.pt (P.R.)

Received: 4 October 2019; Accepted: 7 November 2019; Published: 12 November 2019



Abstract: The antimicrobial, antioxidant, and cytotoxic activities of a series of saccharin–tetrazolyl and –thiadiazolyl analogs were examined. The assessment of the antimicrobial properties of the referred-to molecules was completed through an evaluation of minimum inhibitory concentration (MIC) and minimum bactericidal concentration (MBC) values against Gram-positive and Gram-negative bacteria and yeasts. Scrutiny of the MIC and MBC values of the compounds at pH 4.0, 7.0, and 9.0 against four Gram-positive strains revealed high values for both the MIC and MBC at pH 4.0 (ranging from 0.98 to 125 µg/mL) and moderate values at pH 7.0 and 9.0, exposing strong antimicrobial activities in an acidic medium. An antioxidant activity analysis of the molecules was performed by using the DPPH (2,2-diphenyl-1-picrylhydrazyl) method, which showed high activity for the TSMT (*N*-(1-methyl-2*H*-tetrazol-5-yl)-*N*-(1,1-dioxo-1,2-benzisothiazol-3-yl) amine, **7**) derivative (90.29% compared to a butylated hydroxytoluene positive control of 61.96%). Besides, the general toxicity of the saccharin analogs was evaluated in an *Artemia salina* model, which displayed insignificant toxicity values. In turn, upon an assessment of cell viability, all of the compounds were found to be nontoxic in range concentrations of 0–100 µg/mL in H7PX glioma cells. The tested molecules have inspiring antimicrobial and antioxidant properties that represent potential core structures in the design of new drugs for the treatment of infectious diseases.

Keywords: saccharin; tetrazole; 1,3,4-thiadiazole; H7PX glioma cells; antimicrobial screening; antioxidant capacity

1. Introduction

In 1878, 1,2-benzisothiazole-3-one 1,1-dioxide (**1**, Figure 1), commercially known as saccharin, was discovered accidentally by Fahlberg during an investigation of the oxidation of *o*-toluenesulfonamide [1,2]: it was published by Remsen and Fahlberg one year later [3]. For more than a century, saccharin has been commonly used as a noncaloric artificial sweetener in the form of its water-soluble salts (mainly sodium, ammonium, and calcium), and it is the principal sweetening component of diabetic diets. For about three decades (since reports on carcinogenicity in laboratory animals were published), the debate on its toxicity to humans has not reached a consensus [4–6]. Numerous *N*-substituted derivatives of saccharin have been assessed for *in vitro* biological activity [7–10]. For example, first-row transition metal saccharinates as well as dioxovanadium(VI), dioxouranium(VI), and cerium(IV) saccharinates have been classified as protease inhibitors, and several metal(II) saccharinates have displayed superoxide dismutase-like activity [11]. Besides, structure–activity relationship studies have shown that the saccharin scaffold is an effective element for the development of inhibitors of human leukocyte elastase (HLE), cathepsin G (Cat G), and proteinase 3 (PR3), as well as antimycobacterium and central nervous system agents [9,12–14]. Recently, different saccharin-based antagonists have been recognized for their interferon-signaling pathways, showing antitumor activity through the inhibition of cancer-related isoforms in humans [15]. It should also be noted that the first non-benzoannelated 4-amino-2,3-dihydroisothiazole 1,1-dioxide, which lacks a 3-oxo group, has been described and shows anti-HIV-1 activity. Additionally, saccharin and isothiazolyl derivatives have been used in agriculture as herbicides, fungicides, and pesticides [16].

Azole-type heterocyclic cores on the genesis
of the molecules tested in this study:

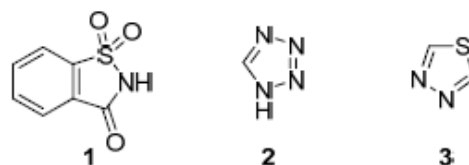


Figure 1. Structures of 1,2-benzisothiazole-3-one 1,1-dioxide (**1**, saccharin), 1*H*-tetrazole (**2**), and 1,3,4-thiadiazole (**3**).

Tetrazole (CN₄H₂) and its derivatives have attracted much attention as well due to their practical applications. The tetrazolic acid fragment –CN₄H has acidity similar to the carboxylic acid group –CO₂H and is almost allosteric with it, but it is metabolically more stable at the physiologic pH [17]. Hence, synthetic methodologies leading to the replacement of –CO₂H groups by –CN₄H groups in biologically active molecules are of major relevance [18]. Indeed, the number of patent claims and publications related to medicinal uses of tetrazolyl derivatives continues to grow rapidly and cover a wide range of applications: tetrazoles have been found, for instance, in compounds with antihypertensive, antiasthmatic, antitubercular, antimalarial, and antibiotic activity [19–22]. Several tetrazole derivatives have shown potential as anticonvulsants and anticancer and anti-HIV-1 drugs [23–25]. Tetrazoles have also had important applications in agriculture as plant growth regulators, herbicides, fungicides [26], and stabilizers in photography and photoimaging [27]. Due to the high enthalpy of formation, tetrazole decomposition results in the liberation of two nitrogen molecules and a significant amount of energy. Therefore, several tetrazole derivatives have been explored as explosives, propellant components for missiles, and gas generators for airbags (applicable to the automobile industry) [28]. In addition, various tetrazole-based compounds have good coordination properties and are able to form stable complexes with several metal ions. This ability is successfully used in analytical chemistry for the removal of heavy metal ions from liquids and in chemical systems formulated for metal protection against corrosion [29]. Many physical, chemical, physicochemical, and biological properties of tetrazoles are closely related to their ability to behave as acids and bases. In the tetrazole ring, the four nitrogen atoms connected

in succession are able to be involved in proteolytic processes. This heterocyclic system is unusual in structure and unique in terms of acid–base characteristics.

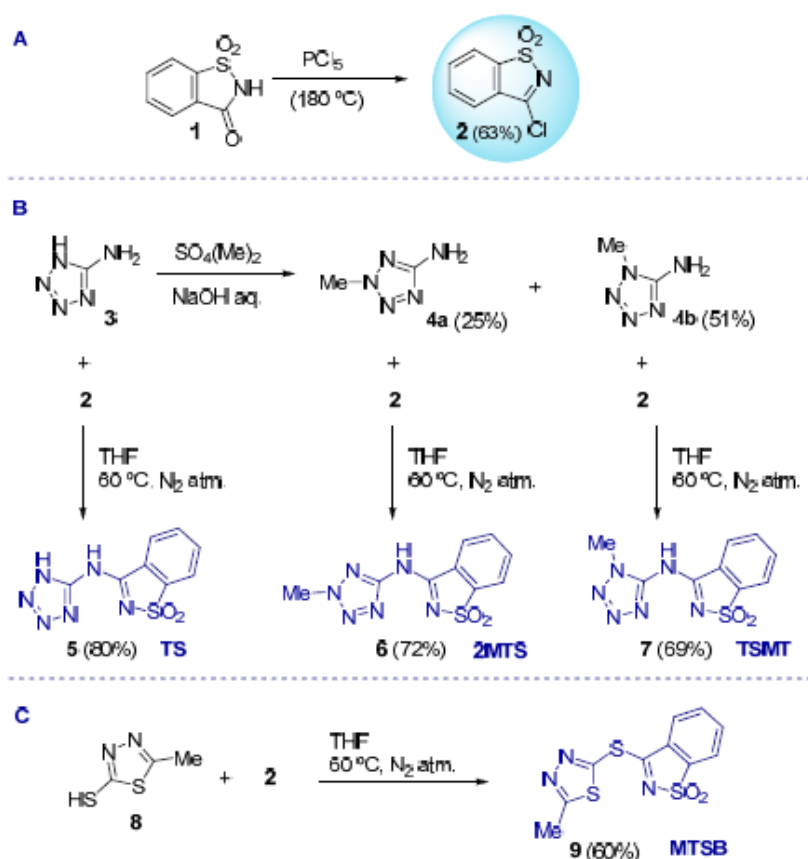
In line with what is mentioned above for saccharin and tetrazole derivatives, the 1,3,4-thiadiazole scaffold represents an important class of core structures that are of great interest mainly because of their various biological activities and respective therapeutic applications. The 1,3,4-thiadiazole ring is a very weak base, possesses relatively high aromaticity, and is moderately stable in aqueous acid solutions although it is vulnerable to ring cleavage with an aqueous base [30]. Besides, this heterocyclic ring is very electron-deficient due to the electron-withdrawing effect of the nitrogen atoms and is relatively inert toward electrophilic substitution but susceptible to nucleophilic attack, whereas when substitutions are introduced into the 2' or 5' position of this ring, it is highly activated and readily reacts to produce varied derivatives [31]. To some extent, these specific properties lead to the application of 1,3,4-thiadiazole derivatives in pharmaceutical, agricultural, and material chemistry. Therefore, several 1,3,4-thiadiazole-based compounds display a broad spectrum of biological activities, such as antimicrobial [32], antituberculosis [33], antioxidant [34], anti-inflammatory [35], anticonvulsant [36], antidepressant, anxiolytic [37], antihypertensive [38], anticancer [39], and antifungal activity [40]. The most prominent thiadiazole derivative is possibly the acetazolamide [*N*-(5-sulfamoyl-1,3,4-thiadiazol-2-yl)acetamide], a very well-known carbonic anhydrase inhibitor that is used in the treatment of glaucoma [41], high-altitude illness [42], epileptic seizures [43], idiopathic intracranial hypertension [44], hemiplegic migraine [45], cystinuria [46], obstructive sleep apnea [47], and congenital myasthenic syndromes [48].

The search for new molecular entities, whether natural or synthetic, with relevant pharmacological activities for effective applications in medical practices continues to be a hot topic in health science as well as in science as a whole. This permanent search is well documented in the immense scientific literature and is mainly supported by the fact that many pathogenic organisms are able to develop mechanisms of resistance to high-activity medicines in their early lives [49–54]. In this context, and given our prior interest in the synthesis, reactivity, and bioactivity of tetrazole and thiazole derivatives, our collaborative interest was piqued by the great potential of these heterocycles for medical applications. Herein, we report on the antimicrobial, antioxidant, and cytotoxic activities of four mixed-azole compounds of benzisothiazole–tetrazolyl and benzisothiazole–thiadiazolyl.

2. Results and Discussion

2.1. Chemistry

The 3-chloro-1,2-benzisothiazole 1,1-dioxide (**2**), one of the strategic building blocks for the synthesis of the studied molecules, was first prepared through the halogenation of saccharin (**1**), as previously described (Scheme 1 (A)) [55]. The three saccharin–tetrazolyl analogs (TS (**5**), 2MTS (**6**), and TSMT (**7**)) were synthesized through a combination of the amino-tetrazoles **3**, **4a**, and **4b** with **2**, following a nucleophilic substitution reaction of the chloride anion by the amine functionality (Scheme 1 (B)). Similarly, compound **9** (MTSB) was prepared by coupling **2** and 5-methyl-1,3,4-thiadiazole-2-thiol (**8**) (Scheme 1 (C)). All of the reactions proceeded smoothly under experimental protocols originally developed by us [56–59], affording crystalline products in reasonable to very good yields.



Scheme 1. Synthesis of saccharin-tetrazolyl (TS, 2MTS, and TSMT) and saccharin-thiadiazolyl (MTSB) derivatives.

2.2. Biological Assays

2.2.1. Antimicrobial Activity

The assessment of the antibacterial properties of compounds TSMT, MTSB, TS, and 2MTS was determined through minimum inhibitory concentration (MIC) and minimum bactericidal concentration (MBC) values against Gram-positive (*Staphylococcus aureus* and *Enterococcus faecalis*), Gram-negative (*Pseudomonas aeruginosa* and *Escherichia coli*), and yeast (*Saccharomyces cerevisiae* and *Candida albicans*) strains obtained from the American Type Culture Collection (ATCC) (Table 1). The MIC value corresponding to the lowest concentration at which no visible growth was observed was assessed by the microdilution method [60]. For MBC evaluation, the bacterial suspension in the wells was homogenized, serially diluted, spread in triplicate on appropriate medium, and incubated at 37 °C. All compounds and respective positive controls were tested at the same concentration of 500 µg/mL.

Table 1. Minimum inhibitory concentration (MIC) and minimum bactericidal concentration (MBC) values of TSMT, MTSB, TS, and 2MTS (obtained through the microdilution method against Gram-positive bacteria, Gram-negative bacteria, and yeast strains (in μM)).

| Sample | <i>E. faecalis</i> | | <i>S. aureus</i> | | <i>P. aeruginosa</i> | | <i>E. coli</i> | | <i>S. cerevisiae</i> | | <i>C. albicans</i> | |
|------------------|--------------------|--------|------------------|--------|----------------------|-------|----------------|-------|----------------------|-------|--------------------|--------|
| | MIC | MBC | MIC | MBC | MIC | MBC | MIC | MBC | MIC | MBC | MIC | MBC |
| TSMT | 236.5 | 1892.1 | 118.3 | 1892.1 | 118.3 | 946.0 | 236.5 | 473.0 | 473.0 | 946.0 | 236.5 | 1892.1 |
| MTSB | 219.0 | 1752.1 | 109.5 | 1752.1 | 109.5 | 876.1 | 219.0 | 438.0 | 438.0 | 876.1 | 219.0 | 1752.1 |
| TS | 249.8 | 1998.1 | 124.9 | 1998.1 | 124.9 | 999.0 | 249.8 | 499.5 | 499.5 | 999.0 | 249.8 | 1998.1 |
| 2MTS | 236.5 | 1892.1 | 118.3 | 1892.1 | 118.3 | 946.0 | 236.5 | 473.0 | 473.0 | 946.0 | 236.5 | 1892.1 |
| Positive control | 1.95 | nt | 1.95 | nt | 0.977 | nt | 0.488 | nt | 15.6 | nt | 7.81 | nt |
| | VAN | | VAN | | NOR | | NOR | | NYS | | NYS | |

VAN: vancomycin; NOR: norfloxacin; NYS: nystatin; nt: not tested. Data are the median values of at least three replicates.

The results of the antimicrobial assay showed that the compounds tested were bacteriostatic. This was concluded because the MBC values were much higher than the MIC values (see Table 1). The compounds were more active against the Gram-negative *P. aeruginosa* and the Gram-positive *S. aureus* bacteria. However, it seemed that the MIC and MBC values were more similar against *E. coli*. Additionally, antimicrobial tests were performed at different pH values (pH 4.0, 7.0, and 9.0), also using the microdilution method (see Tables 2–4). The microorganisms used in these tests were chosen based on the initial results from the antimicrobial screening of Gram-positive bacteria and comprised four Gram-positive strains, namely *S. aureus* CIP6538, *E. faecalis* ATCC 29212, methicillin-resistant *S. aureus* CIP106760 (MRSA), and vancomycin-resistant *E. faecalis* ATCC51299 (VRE).

Table 2. MIC and MBC values of TSMT, MTSB, TS, and 2MTS (obtained through the microdilution method against Gram-positive bacteria at pH 4.0).

| Sample | <i>S. aureus</i> CIP6538 | | <i>E. faecalis</i> ATCC51299 (VRE) | | <i>S. aureus</i> CIP106760 (MRSA) | | <i>E. faecalis</i> 29212 | |
|------------------|--------------------------|--------|------------------------------------|--------|-----------------------------------|-------|--------------------------|--------|
| | MIC | MBC | MIC | MBC | MIC | MBC | MIC | MBC |
| TSMT | 473.0 | 1892.1 | 236.5 | 1892.1 | 236.5 | 473.0 | 236.5 | 1892.1 |
| MTSB | 13.7 | 109.5 | 13.7 | 109.5 | 3.42 | 1.71 | 3.42 | 27.4 |
| TS | 62.5 | 499.5 | 31.2 | 249.8 | 3.90 | 1.95 | 7.80 | 62.5 |
| 2MTS | 29.6 | 236.5 | 14.8 | 118.3 | 3.70 | 1.85 | 473.0 | 1892.1 |
| Positive control | 1.95 | nt | 1.95 | nt | 0.977 | nt | 0.488 | nt |
| | VAN | | VAN | | NOR | | NOR | |

VAN: vancomycin; NOR: norfloxacin; NYS: nystatin; nt: not tested. Data are the median values of at least three replicates.

Table 3. MIC and MBC values of TSMT, MTSB, TS, and 2MTS (obtained through the microdilution method against Gram-positive bacteria at pH 7.0).

| Sample | <i>S. aureus</i> CIP6538 | | <i>E. faecalis</i> ATCC51299 (VRE) | | <i>S. aureus</i> CIP106760 (MRSA) | | <i>E. faecalis</i> 29212 | |
|------------------|--------------------------|--------|------------------------------------|--------|-----------------------------------|--------|--------------------------|--------|
| | MIC | MBC | MIC | MBC | MIC | MBC | MIC | MBC |
| TSMT | 473.0 | 1892.1 | 236.5 | 1892.1 | 473.0 | 1892.1 | 946.0 | 1892.1 |
| MTSB | 438.0 | 1752.1 | 219.0 | 1752.1 | 438.0 | 1752.1 | 876.1 | 1752.1 |
| TS | 499.5 | 1998.1 | 249.8 | 1998.1 | 499.5 | 1998.1 | 999.0 | 1998.1 |
| 2MTS | 473.0 | 1892.1 | 236.5 | 1892.1 | 473.0 | 1892.1 | 946.0 | 1892.1 |
| Positive control | 1.95 | nt | 1.95 | nt | 0.977 | nt | 0.488 | nt |
| | VAN | | VAN | | NOR | | NOR | |

VAN: vancomycin; NOR: norfloxacin; NYS: nystatin; nt: not tested. Data are the median values of at least three replicates.

Table 4. MIC and MBC values of TSMT, MTSB, TS, and 2MTS (obtained through the microdilution method against Gram-positive bacteria at pH 9.0).

| Sample | <i>S. aureus</i> CIP6538 | | <i>E. faecalis</i> ATCC51299 (VRE) | | <i>S. aureus</i> CIP106760 (MRSA) | | <i>E. faecalis</i> 29212 | |
|------------------|--------------------------|--------|------------------------------------|--------|-----------------------------------|--------|--------------------------|--------|
| | MIC | MBC | MIC | MBC | MIC | MBC | MIC | MBC |
| TSMT | 946.0 | 1892.1 | 473.0 | 1892.1 | 473.0 | 1892.1 | 473.0 | 1892.1 |
| MTSB | 438.0 | 1752.1 | 219.0 | 1752.1 | 438.0 | 1752.1 | 438.0 | 1752.1 |
| TS | 499.5 | 1998.1 | 499.5 | 1998.1 | 999.0 | 1998.1 | 499.5 | 1998.1 |
| 2MTS | 473.0 | 1892.1 | 473.0 | 1892.1 | 473.0 | 1892.1 | 473.0 | 1892.1 |
| Positive control | 1.95 | nt | 1.95 | nt | 0.977 | nt | 0.488 | nt |
| | VAN | | VAN | | NOR | | NOR | |

VAN: vancomycin; NOR: norfloxacin; NYS: nystatin; nt: not tested. Data are the median values of at least three replicates.

The results of the antimicrobial assays at the different pH values showed that lowering the medium pH to 4.0 had a positive effect on the compounds MTSB, TS, and 2MTS against the methicillin-resistant *S. aureus* CIP106760 (MRSA). Overall, it was attested that MTSB at pH 4.0 was the most active derivative against all Gram-positive strains. It should be noted that MTSB was the sole compound comprising the thiazazole function, and presumably, the different activity must be correlated with the type of heterocycle ring. The results for pH 7.0 and 9.0 did not provide better results than those previously obtained.

In terms of pH-dependent antimicrobial mechanisms, it should be emphasized that several antimicrobial peptides (AMPs) have increasingly been reported as potent antibiotics that utilize pH-dependent antimicrobial mechanisms [61]. Some of these antibiotics display high pH optima related to their antimicrobial activity and show activity against microbes that present low pH optima, which reflects the acidic pH generally found at their sites of action, namely the skin. This effect should be comparable to our compounds and could be the explanation for the high antimicrobial activity of our compounds at low pH. Several pH-dependent AMPs and other antimicrobial proteins have been developed for medical purposes and have successfully gone through clinical trials, namely kappacins, LL-37, histatins, lactoferrin, and their derivatives. The major examples of the therapeutic applications of these antimicrobial compounds include wound healing as well as the treatment of multiple infections. Generally, such applications involve topical administration, a source of novel biologically active agents that could aid in the fulfilment of the urgent need for alternatives to conventional antibiotics, helping to avert a return to the pre-antibiotic era: our compounds could be a key development.

2.2.2. Antioxidant Activity

The antioxidant activity of the studied compounds was evaluated using a DPPH assay, which evaluates the potential of test samples to quench DPPH radicals via hydrogen-donating ability. The antioxidant agents convert DPPH into a stable diamagnetic molecule, 1-1diphenyl-2-picryl hydrazine, through electron or hydrogen transfers. A color change from purple to yellow indicates the increasing radical scavenging activity of the test compounds. Herein, it was observed that TSMT and MTSB derivatives possessed a high free radical scavenging ability (see Figure 2). These two molecules had the highest reducing power, indicating that they were good electron/hydrogen donors and could prevent oxidative stress.

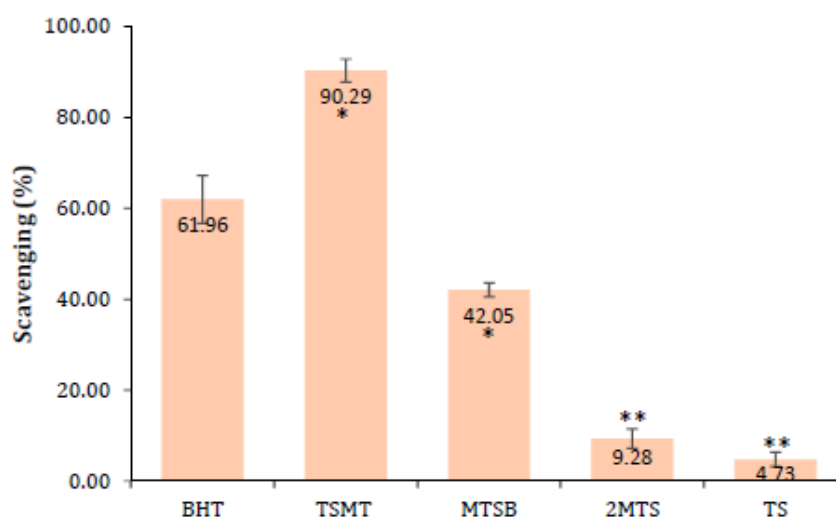


Figure 2. Antioxidant activity tested at a concentration of 10 $\mu\text{g/mL}$. The mean value \pm SD was calculated from three independent experiments and compared to butylated hydroxytoluene (BHT) (* $p < 0.05$; ** $p < 0.001$).

2.2.3. Brine Shrimp Lethality Bioassay (General Toxicity)

The *Artemia salina* test is a known, simple, fast, and low-cost test and was used in this investigation to check the general toxicity of the compounds. As a general rule, it was observed that all of the compounds exhibited low toxicity in the *Artemia salina* model (Figure 3). Nevertheless, it should be emphasized that the MTSB and TSMT derivatives presented with higher toxicity, making them potential lead therapeutic agents, and thus they must further be tested using different cell- and microorganism-based assays.

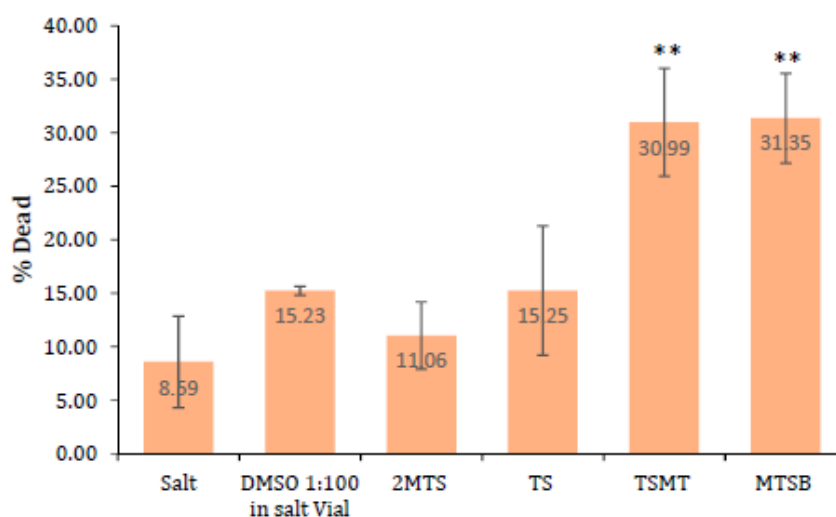


Figure 3. General toxicity screening at a concentration of 10 ppm using the *Artemia salina* test. The mean value \pm SD was calculated from three independent experiments and compared to salt (** $p < 0.001$).

2.2.4. Cell Viability after Treatment with MTSB, TS, TSMS, and 2MTS in H7PX Glioma Cells (IV Grade)

In the course of this study, H7PX cells were treated with a concentration range of 0–100 $\mu\text{g/mL}$ of the four compounds (MTSB, TS, TSMS, and 2MTS) over 24 h, after which the percentage of cell viability was determined by an MTT assay. It was demonstrated that none of the tested compounds

reduced the viability of human H7PX cells in the stated range of concentration (0–100 µg/mL) after 24 h (Figure 4). None of the compounds' IC₅₀ values were reached. Similar effects were observed with 48 h of incubation (data not shown).

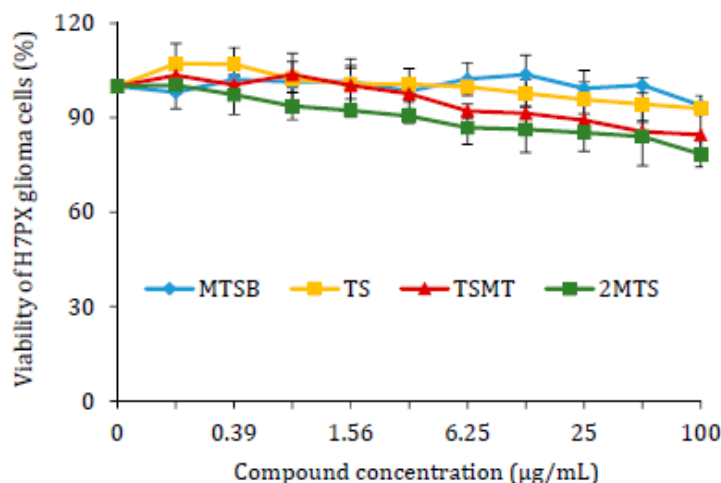


Figure 4. Effect of MTSB, TS, TSMT, and 2MTS treatment on the viability of H7PX glioma cells after 24 h of incubation (data are reported as means \pm SD of three determinations).

3. Experimental Section

3.1. Chemistry

3.1.1. General

Unless indicated otherwise, solvents and starting materials were obtained from Sigma. All chemicals used were of reagent grade without further purification before use. Column chromatography was performed using silica gel 60 MN, and aluminum-backed silica gel Merck 60 F254 plates were used for analytical thin-layer chromatography (TLC). Melting points were recorded and are uncorrected. ¹H and ¹³C NMR spectra were recorded at room temperature on a Bruker Avance II 400 (UltraShield™ Magnet, Billerica, MA, USA) spectrometer operating at 400 MHz (¹H) and 101 MHz (¹³C). The chemical shifts are reported in ppm using TMS (tetramethylsilane) as an internal standard. Carbon, hydrogen, and nitrogen elemental analyses were carried out by the Microanalytical Service of the Instituto Superior Técnico—University of Lisbon. FT-IR spectra (4000–400 cm⁻¹) were recorded on a VERTEX 70 (Bruker, Billerica, MA, USA) spectrometer using KBr pellets. Mass spectra were obtained on a VG 7070E mass spectrometer through electron ionization (EI) at 70 eV.

3.1.2. Synthetic Protocols

The synthesis of 3-chloro-1,2-benzisothiazole-1,1-dioxide (**2**), 2-methyl-(2*H*)-tetrazole-5-amine (**4a**), 1-methyl-(1*H*)-tetrazole-5-amine (**4b**), *N*-(1*H*-tetrazol-5-yl)-*N*-(1,1-dioxo-1,2-benzisothiazol-3-yl) amine (**5**) (TS), *N*-(2-methyl-2*H*-tetrazol-5-yl)-*N*-(1,1-dioxo-1,2-benzisothiazol-3-yl) amine (**6**) (2MTS), *N*-(1-methyl-2*H*-tetrazol-5-yl)-*N*-(1,1-dioxo-1,2-benzisothiazol-3-yl) amine (**7**) (TSMT), and 3-[(5-methyl-1,3,4-thiadiazol-2-yl)sulfanyl]-1,2-benzisothiazole 1,1-dioxide (**9**) (MTSB) was carried out as previously described [55,56,58,59].

3.2. Biologic Activities

3.2.1. Antioxidant Activity (DPPH Method)

The antioxidant activity of all the compounds was measured by the DPPH method, as described by Rijo et al. [62]. Accordingly, a mixture containing 10 μ L of sample and 990 μ L of DPPH solution (0.002% in methanol) was incubated for 30 min at room temperature followed by absorbance measurements at 517 nm against the corresponding blank sample. The antioxidant activity of each compound was calculated using Equation (1). AA denotes the antioxidant activity, A_{DPPH} is the absorption of DPPH against the blank, and A_{sample} represents the absorption of the compound or control against the blank. All tests were carried out in triplicate at a sample concentration of 10 μ g/mL. The reference standard used for this procedure was butylated hydroxytoluene (BHT) in the same conditions as the samples:

$$AA = \frac{A_{DPPH} - A_{Sample}}{A_{DPPH}} \times 100\%, \quad (1)$$

3.2.2. Brine Shrimp Lethality Bioassay (General Toxicity)

The general toxicity of the compounds was evaluated by the use of a test of lethality to *Artemia salina* (brine shrimp) [63]. Concentrations of 10 ppm of each sample were tested. The number of dead larvae was recorded after 24 h and was used to calculate the lethal concentration (%) according to Equation (2) (where $Total_{A. salina}$ = the total number of larvae in the assay and $Alive_{A. salina}$ = the number of alive *A. salina* larvae in the assay):

$$\text{Letal concentration} = \frac{Total_{A. salina} - Alive_{A. salina}}{Total_{A. salina}} \times 100\%, \quad (2)$$

3.2.3. Cell Culture

An H7PX primary glioblastoma cell line was cultivated in DMEM (Biowest, Nuaollé, France) supplemented with 10% FBS (Euroclone, Pero, Italy), 100 IU/mL penicillin (Sigma-Aldrich, Saint Louis, MO, USA), 100 μ g/mL streptomycin (Sigma-Aldrich, Saint Louis, MO, USA) and 50 μ g/mL gentamicin (Biowest, Nuaollé, France) in a humidified atmosphere (5% CO₂, 37 °C).

3.2.4. In Vitro Cell Viability by MTT Assay

An MTT (3-(4,5-dimethylthiazol-2-yl)-2,5-diphenyl tetrazolium bromide) assay was employed to measure the viability of H7PX cells (glioma cells in IV grade derived from patient) treated with different concentrations of TS (5), 2MTS (6), TSMT (7), or MTSB (9). Cells were seeded at 1×10^4 cells per well in 96-well culture plates and were left overnight before treatments for attachment. Subsequently, the cells were incubated for 24 h with all compounds over a range of concentrations: 0.0 (control), 0.39, 0.78, 1.56, 3.13, 6.25, 12.5, 25, 50, and 100 μ g/mL. Following this, the cells were incubated with 0.5 mg/mL of MTT at 37 °C for 1.5 h. After that, the MTT was carefully removed, and DMSO (100 μ L) was added to each well and vortexed at low speed for 5 min to fully dissolve the formazan crystals. Absorbance was measured at 570 nm with a reference at 630 nm using a Bio-Tek Synergy HT Microplate Reader (Bio-Tek Instruments, Winooski, VT, USA). All experiments were repeated in triplicate. Cell viability was expressed as a percentage relative to the untreated cells, which was defined as 100%. The study was approved by the Ethical Commission of the Medical University of Lodz, and informed consent was obtained from the patients (Nr. RNN/194/12/KE).

3.2.5. Antimicrobial Activity

Microorganisms and growth conditions: The strains used in this study comprised *Staphylococcus aureus* (ATCC 25,923 and CIP 106760), *Enterococcus faecalis* (ATCC 51,299 and ATCC29212), *Escherichia coli* ATCC 25922, *Pseudomonas aeruginosa* ATCC 27,853, and the yeasts *Candida albicans* ATCC 10,231

and *Saccharomyces cerevisiae* ATCC 2601. All bacteria were grown at 37 °C in Mueller–Hinton broth (Biokar Diagnostics, Beauvais, France), and the yeasts were grown in Sabouraud dextrose agar (Biokar Diagnostics, Allone, France).

Microdilution method (MIC determination): The minimum inhibitory concentrations (MICs) of the compounds (dissolved in the respective pH aqueous solutions) were evaluated using a twofold serial broth microdilution assay (CLSI, 2011) in Mueller–Hinton broth (MHB, Biokar Diagnostics, Beauvais, France). Overnight cultures were diluted in MHB with increasing concentrations of each compound (in μM). Vancomycin (VAN), norfloxacin (NOR), and nystatin (NYS) were used as positive controls for Gram-positive bacteria, Gram-negative bacteria, and yeasts, respectively. The negative control for the aqueous solutions at different pH values showed no inhibition growth. The cultures were incubated for 24 h at 37 °C, and Optical Density at 620 nm was measured using a Microplate Reader (Thermo Scientific Multiskan FC, Loughborough, UK). Assays were carried out in triplicate for each tested microorganism.

Minimum bactericidal concentration (MBC) assessment: To define the minimum bactericidal concentration (MBC) for each set of wells in the MIC determination, a loopful of agar was collected from the wells without any growth and inoculated on sterile Mueller–Hilton medium broth (for bacteria) through streaking. Plates inoculated with bacteria were incubated at 37 °C for 24 h. After incubation, the lowest concentration was noted as the MBC (for bacteria) at which no visible growth was observed.

3.2.6. Statistical Analysis

The values in this study are expressed as means \pm SD. The Shapiro–Wilk test was used for verification of the normality of the data. Statistical differences were determined by one-way ANOVA. The results were analyzed using STATISTICA 12.0 software (StatSoft, Tulsa, OK, USA). Differences of $p < 0.05$ were considered statistically significant.

4. Conclusions

The antimicrobial, antioxidant, and cytotoxic activities of three saccharin–tetrazolyl (TS, TSMT, and 2MTS) derivatives and one saccharin–thiadiazolyl (MTSB) derivative were addressed throughout this investigation. The antimicrobial activity of the synthesized compounds was evaluated against a series of Gram-positive and Gram-negative bacteria and yeast strains. An evaluation of the MIC and MBC values of the four derivatives was completed at pH 4.0, 7.0, and 9.0 against four Gram-positive strains (*S. aureus*, *E. faecalis*, *S. aureus* (MRSA), and *E. faecalis* (VRE)), showing high values for the MIC and MBC at pH 4.0 (ranging from 3.42 to 473.0 μM). It was attested that the derivative MTSB, the sole compound comprising the thiadiazole function, was the most active against all of the considered Gram-positive strains at pH 4.0.

In addition, the antioxidant activity of the compounds (calculated by using the DPPH method) was the highest value for TSMT (90.29% compared to the BHT positive control of 61.96%). Finally, we demonstrated for the first time that the TS, TSMT, 2MTS, and MTSB compounds did not show in vitro cytotoxic effects on H7PX glioma cells.

The present study exposed the influence of the pH of the medium on the antimicrobial activity of the TS, TSMT, 2MTS, and MTSB compounds, which is similar to well-described antimicrobial peptide antibiotics. Therefore, the use of these kinds of molecules to produce new antibiotics should be considered in the future, although further studies are needed to confirm this hypothesis.

Author Contributions: L.M.T.F. and P.R. designed the study, analyzed the data, and wrote the paper; E.N., P.S., J.M.A., M.T., and T.S. performed the biological assays; L.M.T.F. and L.C. performed the synthesis and characterization of the compounds; M.L.S.C. and A.J.L.P. were responsible for supervision and reviewing the draft.

Funding: This work was partially supported by the Foundation for Science and Technology (FCT), Portugal ((UID/QUI/00100/2019) and (UID/MULTI/04326/2019 – CCMAR)). L.M.T.F. expresses gratitude to FCT for the post doc fellowship (SFRH/BPD/99851/2014) and work contract n° IST-ID/115/2018.

Conflicts of Interest: The authors declare no conflicts of interest.

References

1. Schulze, B.; Illgen, K. Isothiazol-1,1-dioxide—Vom Süßstoff zum chiralen Auxiliar in der stereoselektiven Synthese. *J. Prakt. Chem.* **1997**, *339*, 1–14. [[CrossRef](#)]
2. Ellis, J.W.J. Overview of sweeteners. *Chem. Educ.* **1995**, *72*, 671–675. [[CrossRef](#)]
3. Remsen, I.; Fahlberg, C. On the oxidation of substitution products of aromatic hydrocarbons. IV. On the oxidation of orthotoluenesulphonamide. *J. Am. Chem. Soc.* **1879**, *1*, 426–438. [[CrossRef](#)]
4. Price, M.J.; Biava, G.C.; Oser, L.B.; Vogin, E.E.; Steinfeld, J.; Ley, L.H. Bladder tumors in rats fed cyclohexylamine or high doses of a mixture of cyclamate and saccharin. *Science* **1970**, *167*, 1131–1132. [[CrossRef](#)] [[PubMed](#)]
5. Masui, T.; Mann, M.A.; Borgeson, D.C.; Garland, M.E.; Okamura, T.; Fujii, H.; Pelling, C.J.; Cohen, M.S. Sequencing analysis of HA-RAS, KI-RAS, and N-RAS genes in rat urinary-bladder tumors induced by N-[4-(5-Nitro-2-furyl)-2-thiazolyl]formamide (FANFT) and sodium saccharin. *Terat. Carcin. Mutagen.* **1993**, *13*, 225–233. [[CrossRef](#)] [[PubMed](#)]
6. Garland, M.E.; Sakata, T.; Fisher, M.J.; Masui, T.; Cohen, M.S. Influences of Diet and Strain on the Proliferative Effect on the Rat Urinary Bladder Induced by Sodium Saccharin. *Cancer Res.* **1989**, *49*, 3789–3794. [[PubMed](#)]
7. Groutas, W.C.; Houser-Archield, N.; Chong, L.S.; Venkataraman, R.; Epp, J.B.; Huang, H.; McClenahan, J.J. Efficient inhibition of human-leukocyte elastase and cathepsin-G by saccharin derivatives. *J. Med. Chem.* **1993**, *36*, 3178–3181. [[CrossRef](#)] [[PubMed](#)]
8. Groutas, W.C.; Chong, L.S.; Venkataraman, R.; Kuang, R.; Epp, J.B.; Houser-Archield, N.; Huang, H.; Hoydal, R.J. Amino acid-derivative phthalimide and saccharin derivatives as inhibitors of human leukocyte elastase, cathepsin G, and proteinase 3. *Arch. Biochem. Biophys.* **1996**, *332*, 335–340. [[CrossRef](#)] [[PubMed](#)]
9. Groutas, W.C.; Epp, J.B.; Venkataraman, R.; Kuang, R.; Truong, T.M.; McClenahan, J.J.; Prakash, O. Design, synthesis, and in vitro inhibitory activity toward human leukocyte elastase, cathepsin G, and proteinase 3 of saccharin-derived sulfones and congeners. *Bioorg. Med. Chem.* **1996**, *4*, 1393–1400. [[CrossRef](#)]
10. Elghamry, I.; Youssef, M.M.; Al-Omair, M.A.; Elsayy, H. Synthesis, antimicrobial, DNA cleavage and antioxidant activities of tricyclic sultams derived from saccharin. *Eur. J. Med. Chem.* **2017**, *139*, 107–113. [[CrossRef](#)] [[PubMed](#)]
11. Apella, M.C.; Totaro, R.; Baran, E.J. Determination of superoxide dismutase-like activity in some divalent metal saccharinates. *Biol. Trace Elem. Res.* **1993**, *37*, 293–299. [[CrossRef](#)] [[PubMed](#)]
12. Guenther, U.; Wrigge, H.; Theuerkauf, N.; Boettcher, M.F.; Wensing, G.; Zinserling, J.; Putensen, C.; Hoeft, A. Repinotan, a selective 5-HT_{1A}-R-agonist, antagonizes morphine-induced ventilator depression in anesthetized rats. *Anesth. Analg.* **2010**, *111*, 901–907. [[PubMed](#)]
13. Malinka, W.; Ryng, S.; Sieklucka-Dziuba, M.; Rajtar, G.; Gownial, A.; Kleinrok, Z. 2-Substituted-3-oxoisothiazolo[5,4-b]pyridines as potential central nervous system and antimycobacterial agents. *Farmaco* **1998**, *53*, 504–512. [[CrossRef](#)]
14. Malinka, W.; Ryng, S.; Sieklucka-Dziuba, M.; Rajtar, G.; Gownial, A.; Kleinrok, Z. Synthesis and preliminary screening of derivatives of 2-(4-arylpiperazine-1-ylalkyl)-3-oxoisothiazolo[5,4,b]pyridines as CNS and antimycobacterial agents. *Pharmazie* **2000**, *55*, 416–425. [[PubMed](#)]
15. Csakai, A.; Smith, C.; Davis, E.; Martinko, A.; Culp, S.; Yin, H. Saccharin derivatives as inhibitors of interferon-mediated inflammation. *J. Med. Chem.* **2014**, *57*, 5348–5355. [[CrossRef](#)] [[PubMed](#)]
16. Fischer, R.; Kretschik, O.; Schenke, T.; Schenkel, R.; Wiedemann, J.; Erdelen, C.; Loesel, P.; Drewes, M.W.; Feucht, D.; Andersch, W.W. *Ger. Offen.* DE 1999244668. 1999. *Chem. Abstr.* **2001**, *134*, 4932.
17. Singh, H.; Chawla, A.S.; Kapoor, V.K.; Paul, D.; Malhotra, R.K. Medicinal chemistry of tetrazoles. *Prog. Med. Chem.* **1980**, *17*, 151–183. [[PubMed](#)]
18. Noda, K.; Saad, Y.; Kinoshita, A.; Boyle, T.P.; Graham, R.M.; Husain, A.; Karnik, S.S. Tetrazole and carboxylate receptor antagonists bind to the same subsite by different mechanisms. *J. Biol. Chem.* **1995**, *270*, 2284–2289. [[CrossRef](#)] [[PubMed](#)]
19. Mavromoustakos, T.; Kolocouris, A.; Zervou, M.; Roumelioti, P.; Matsoukas, J.; Weisemann, R. An effort to understand the molecular basis of hypertension through the study of conformational analysis of Losartan and Sarmesin using a combination of nuclear magnetic resonance spectroscopy and theoretical calculations. *J. Med. Chem.* **1999**, *42*, 1714–1722. [[CrossRef](#)] [[PubMed](#)]

20. Toney, J.H.; Fitzgerald, P.M.D.; Grover-Sharma, N.; Olson, S.H.; May, W.J.; Sundelof, J.G.; Vanderwall, D.E.; Cleary, K.A.; Grant, S.K.; Wu, J.K.; et al. Antibiotic sensitization using biphenyl tetrazoles as potent inhibitors of *Bacteroides fragilis* metallo- β -lactamase. *Chem. Biol.* **1998**, *5*, 185–196. [[CrossRef](#)]
21. Gao, C.; Chang, L.; Xu, Z.; Yan, X.-F.; Ding, C.; Zhao, F.; Wu, X.; Feng, L.-S. Recent advances of tetrazole derivatives as potential anti-tubercular and anti-malarial agents. *Eur. J. Med. Chem.* **2019**, *163*, 404. [[CrossRef](#)] [[PubMed](#)]
22. Hashimoto, Y.; Ohashi, R.; Kurosawa, Y.; Minami, K.; Kaji, H.; Hayashida, K.; Narita, H.; Murata, S. Pharmacologic Profile of TA-606, a Novel Angiotensin II-Receptor Antagonist in the Rat. *J. Cardiovasc. Pharmacol.* **1998**, *31*, 568–575. [[CrossRef](#)] [[PubMed](#)]
23. Desarro, A.; Ammendola, D.; Zappala, M.; Grasso, S.; Desarro, G.B. Relationship between Structure and Convulsant Properties of Some β -Lactam Antibiotics following Intracerebroventricular Microinjection in Rats. *Antimicrob. Agents Chemother.* **1995**, *39*, 232–237. [[CrossRef](#)] [[PubMed](#)]
24. Tamura, Y.; Watanabe, F.; Nakatani, T.; Yasui, K.; Fujii, M.; Komurasaki, T.; Tsuzuki, H.; Maekawa, R.; Yoshioka, T.; Kawada, K.; et al. Highly Selective and Orally Active Inhibitors of Type IV Collagenase (MMP-9 and MMP-2): N-Sulfonylamino Acid Derivatives. *J. Med. Chem.* **1998**, *41*, 640–649. [[CrossRef](#)] [[PubMed](#)]
25. Abell, A.D.; Foulds, G.J. Synthesis of a cis-conformationally restricted peptide bond isostere and its application to the inhibition of the HIV-1 protease. *J. Chem. Soc. Perkin Trans.* **1997**, *1*, 2475–2482. [[CrossRef](#)]
26. Sandmann, G.; Schneider, C.; Boger, P. A New Non-Radioactive Assay of Phytoene Desaturase to Evaluate Bleaching Herbicides. *Z. Naturforsch. C* **1996**, *51*, 534–538. [[CrossRef](#)] [[PubMed](#)]
27. Koldobskii, G.I.; Ostrovskii, V.A.; Poplavskii, V.S. Advances in tetrazole chemistry. *Khim. Geterotsikl. Soedin.* **1981**, *10*, 1299.
28. Ostrovskii, V.A.; Pevzner, M.S.; Kofman, T.P.; Shcherbinin, M.B.; Tselinskii, I.V. *Targets in Heterocyclic Systems. Chemistry and Properties*; Attanasi, O.A., Spinelli, D., Eds.; Societa Chimica Italiana: Rome, Italy, 1999; Volume 3, p. 467.
29. Moore, D.S.; Robinson, S.D. Catenated Nitrogen Ligands Part II. Transition Metal Derivatives of Triazoles, Tetrazoles, Pentazoles, and Hexazine. *Adv. Inorg. Chem.* **1988**, *32*, 171–239.
30. Balaban, A.T.; Oniciu, D.C.; Katritzky, A.R. Aromaticity as a cornerstone of heterocyclic chemistry. *Chem. Rev.* **2004**, *104*, 2777–2812. [[CrossRef](#)] [[PubMed](#)]
31. Hu, Y.; Li, C.-Y.; Wang, X.-M.; Yang, Y.-H.; Zhu, H.-L. 1,3,4-Thiadiazole: Synthesis, reactions, and applications in medicinal, agricultural, and materials chemistry. *Chem. Rev.* **2014**, *114*, 5572–5610. [[CrossRef](#)] [[PubMed](#)]
32. Almajan, G.L.; Barbuceanu, S.F.; Bancescu, G.; Saramet, I.; Saramet, G.; Draghici, C. Synthesis and antimicrobial evaluation of some fused heterocyclic [1,2,4]triazolo[3,4-b][1,3,4]thiadiazole derivatives. *Eur. J. Med. Chem.* **2010**, *45*, 6139–6146. [[CrossRef](#)] [[PubMed](#)]
33. Kolavi, G.; Hegde, V.; Khazi, I.; Gadad, P. Synthesis and evaluation of antitubercular activity of imidazo[2,1-b][1,3,4]thiadiazole derivatives. *Bioorg. Med. Chem.* **2006**, *14*, 3069–3080. [[CrossRef](#)] [[PubMed](#)]
34. Khan, I.; Ali, S.; Hameed, S.; Rama, N.H.; Hussain, M.T.; Wadood, A.; Uddin, R.; Ul-Haq, Z.; Khan, A.; Ali, S.; et al. Synthesis, antioxidant activities and urease inhibition of some new 1,2,4-triazole and 1,3,4-thiadiazole derivatives. *Eur. J. Med. Chem.* **2010**, *45*, 5200–5207. [[CrossRef](#)] [[PubMed](#)]
35. Hafez, H.N.; Hegab, M.I.; Ahmed-Farag, I.S.; El-Gazzar, A.B.A. A facile regioselective synthesis of novel *spiro*-thioxanthene and *spiro*-xanthene-9',2'-[1,3,4]thiadiazole derivatives as potential analgesic and anti-inflammatory agents. *Bioorg. Med. Chem. Lett.* **2008**, *18*, 4538–4543. [[CrossRef](#)] [[PubMed](#)]
36. Jatav, V.; Mishra, P.; Kashaw, S.; Stables, J.P. CNS depressant and anticonvulsant activities of some novel 3-[5-substituted 1,3,4-thiadiazole-2-yl]-2-styryl quinazoline-4(3H)-ones. *Eur. J. Med. Chem.* **2008**, *43*, 1945–1954. [[CrossRef](#)] [[PubMed](#)]
37. Clerici, F.; Pocar, D.; Guido, M.; Loche, A.; Perlini, V.; Brufani, M. Synthesis of 2-amino-5-sulfanyl-1,3,4-thiadiazole derivatives and evaluation of their antidepressant and anxiolytic activity. *J. Med. Chem.* **2001**, *44*, 931–936. [[CrossRef](#)] [[PubMed](#)]
38. Hasui, T.; Matsunaga, N.; Ora, T.; Ohayabu, N.; Nishigaki, N.; Imura, Y.; Igata, Y.; Matsui, H.; Motoyaji, T.; Tanaka, T.; et al. Identification of benzoxazin-3-one derivatives as novel, potent, and selective nonsteroidal mineralocorticoid receptor antagonists. *J. Med. Chem.* **2011**, *54*, 8616–8631. [[CrossRef](#)] [[PubMed](#)]
39. Noolvi, M.N.; Patel, H.M.; Singh, N.; Gadad, A.K.; Cameotra, S.S.; Badiger, A. Synthesis and anticancer evaluation of novel 2-cyclopropylimidazo[2,1-b][1,3,4]thiadiazole derivatives. *Eur. J. Med. Chem.* **2011**, *46*, 4411–4418. [[CrossRef](#)] [[PubMed](#)]

40. Liu, X.H.; Shi, Y.X.; Ma, Y.; Zhang, C.Y.; Dong, W.L.; Pan, L.; Wang, B.L.; Li, B.J.; Li, Z.M. Synthesis, antifungal activities and 3D-QSAR study of *N*-(5-substituted-1,3,4-thiadiazol-2-yl)cyclopropanecarboxamides. *Eur. J. Med. Chem.* **2009**, *44*, 2782–2786. [[CrossRef](#)] [[PubMed](#)]
41. Kaur, I.P.; Smitha, R.; Aggarwal, D.; Kapil, M. Acetazolamide: Future perspective in topical glaucoma therapeutics. *Int. J. Pharm.* **2002**, *248*, 1–14. [[CrossRef](#)]
42. Luks, A.M.; McIntosh, S.E.; Grissom, C.K.; Auerbach, P.S.; Rodway, G.W.; Schoene, R.B.; Zafren, K.; Hackett, P.H. Wilderness Medical Society consensus guidelines for the prevention and treatment of acute altitude illness. *Wilderness Environ. Med.* **2010**, *21*, 146–155. [[CrossRef](#)] [[PubMed](#)]
43. Wolf, P. Acute drug administration in epilepsy: A review. *CNS Neurosci. Ther.* **2011**, *17*, 442–448. [[CrossRef](#)] [[PubMed](#)]
44. Rangwala, L.M.; Liu, G.T. Pediatric idiopathic intracranial hypertension. *Surv. Ophthalmol.* **2007**, *52*, 597–617. [[CrossRef](#)] [[PubMed](#)]
45. Russell, M.B.; Ducros, A. Sporadic and familial hemiplegic migraine: Pathophysiological mechanisms, clinical characteristics, diagnosis, and management. *Lancet Neurol.* **2011**, *10*, 457–470. [[CrossRef](#)]
46. Tiselius, H.G. New horizons in the management of patients with cystinuria. *Curr. Opin. Urol.* **2010**, *20*, 169–173. [[CrossRef](#)] [[PubMed](#)]
47. Jalandhara, N.B.; Patel, A.; Arora, R.R.; Jalandhara, P. Obstructive sleep apnea: A cardiopulmonary perspective and medical therapeutics. *Am. J. Ther.* **2009**, *16*, 257–263. [[CrossRef](#)] [[PubMed](#)]
48. Schara, U.; Lochmuller, H. Therapeutic strategies in congenital myasthenic syndromes. *Neurotherapeutics* **2008**, *5*, 542–547. [[CrossRef](#)] [[PubMed](#)]
49. Superti-Furga, G.; Cochran, J.; Crews, C.M.; Frye, S.; Neubauer, G.; Prinjha, R.; Shokat, K. Where is the Future of Drug Discovery for Cancer? *Cell* **2017**, *168*, 564–565.
50. Gulçin, I. Antioxidant activity of food constituents: An overview. *Arch. Toxicol.* **2012**, *86*, 345–391. [[CrossRef](#)] [[PubMed](#)]
51. Walker, B.; Barrett, S.; Polasky, S.; Galaz, V.; Folke, C.; Engstrom, G.; Ackerman, E.; Arrow, K.; Carpenter, S.; Chopra, K.; et al. Environment. Looming global-scale failures and missing institutions. *Science* **2009**, *325*, 1345–1346. [[CrossRef](#)] [[PubMed](#)]
52. D'Costa, V.M.; King, C.E.; Kalan, L.; Morar, M.; Sung, W.W.; Schwarz, C.; Froese, D.; Zazula, G.; Calmels, F.; Debruyne, R.; et al. Antibiotic resistance is ancient. *Nature* **2011**, *477*, 457. [[CrossRef](#)] [[PubMed](#)]
53. Andersson, D.I.; Hughes, D. Antibiotic resistance and its cost: Is it possible to reverse resistance? *Nat. Rev. Microbiol.* **2010**, *8*, 260. [[CrossRef](#)] [[PubMed](#)]
54. Cassir, N.; Rolain, J.M.; Brouqui, P. A new strategy to fight antimicrobial resistance: The revival of old antibiotics. *Front. Microbiol.* **2014**, *5*, 551. [[CrossRef](#)] [[PubMed](#)]
55. Brigas, A.F.; Fonseca, C.S.C.; Johnstone, R.A.W. Preparation of 3-Chloro-1,2-Benzisothiazole 1,1-Dioxide (Pseudo-Saccharyl Chloride). *J. Chem. Res.* **2002**, *6*, 299–300. [[CrossRef](#)]
56. Frija, L.M.T.; Alegria, E.C.B.A.; Sutradhar, M.; Cristiano, M.L.S.; Ismael, A.; Kopylovich, M.N.; Pombeiro, A.J.L. Copper(II) and cobalt(II) tetrazole-saccharinate complexes as effective catalysts for oxidation of secondary alcohols. *J. Mol. Catal. A Chem.* **2016**, *425*, 283–290. [[CrossRef](#)]
57. Frija, L.M.T.; Fausto, R.; Loureiro, R.M.S.S.; Cristiano, M.L.S. Synthesis and structure of novel benzisothiazole-tetrazolyl derivatives for potential application as nitrogen ligands. *J. Mol. Catal. A Chem.* **2009**, *305*, 142–146. [[CrossRef](#)]
58. Ismael, A.; Paixão, J.A.; Fausto, R.; Cristiano, M.L.S. Molecular structure of nitrogen-linked methyltetrazole-saccharinates. *J. Mol. Struct.* **2012**, *1023*, 128–142. [[CrossRef](#)]
59. Cabral, L.; Brás, E.; Henriques, M.; Marques, C.; Frija, L.M.T.; Barreira, L.; Paixão, J.A.; Fausto, R.; Cristiano, M.L.S. Synthesis, Structure, and Cytotoxicity of a New Sulphonyl-Bridged Thiadiazolyl-Saccharinate Conjugate: The Relevance of S...N Interaction. *Chem. Eur. J.* **2018**, *24*, 3251–3262. [[CrossRef](#)] [[PubMed](#)]
60. Rijo, P.; Duarte, A.; Francisco, A.P.; Semedo-Lemsaddek, T.; Simões, M.F. In vitro antimicrobial activity of royleanone derivatives against Gram-positive bacterial pathogens. *Phytother. Res.* **2014**, *8*, 76–81. [[CrossRef](#)] [[PubMed](#)]
61. Malik, E.; Dennison, S.R.; Harris, F.; Phoenix, D.A. pH Dependent Antimicrobial Peptides and Proteins, Their Mechanisms of Action and Potential as Therapeutic Agents. *Pharmaceuticals* **2016**, *9*, 67. [[CrossRef](#)] [[PubMed](#)]

62. Rijo, P.; Falé, P.L.; Serralheiro, M.L.; Simões, M.F.; Gomes, A.; Reis, C. Optimization of medicinal plant extraction methods and their encapsulation through extrusion technology. *Measurement* **2014**, *58*, 249–255. [CrossRef]
63. Alanís-Garza, B.A.; González-González, G.M.; Salazar-Aranda, R.; Waksman de Torres, N.; Rivas-Galindo, V.M. Screening of antifungal activity of plants from the northeast of Mexico. *J. Ethnopharmacol.* **2007**, *114*, 468–471. [CrossRef] [PubMed]



© 2019 by the authors. Licensee MDPI, Basel, Switzerland. This article is an open access article distributed under the terms and conditions of the Creative Commons Attribution (CC BY) license (<http://creativecommons.org/licenses/by/4.0/>).

Article

Dehydroabietic Acid Microencapsulation Potential as Biofilm-Mediated Infections Treatment

Iris Neto ^{1,2}, Eva María Domínguez-Martín ^{1,3}, Epole Ntungwe ^{1,3}, Catarina P. Reis ², Milica Pesic ⁴, Célia Faustino ^{2,*} and Patrícia Rijo ^{1,2,*}

- ¹ CBIOS-Research Center for Biosciences & Health Technologies, Universidade Lusófona de Humanidades e Tecnologias, Campo Grande 376, 1749-024 Lisboa, Portugal; irisrbneto@gmail.com (I.N.); evam.dominguez@uah.es (E.M.D.-M.); p5999@ulusofona.pt (E.N.)
- ² Instituto de Investigação do Medicamento (iMed.U.Lisboa), Faculdade de Farmácia, Universidade de Lisboa, 1649-003 Lisboa, Portugal; catarinareis@ff.ulisboa.pt
- ³ Pharmacology Area (Pharmacognosy Laboratory), New Antitumor Compounds: Toxic Action on Leukemia Cells Research Group. Ctra. A2, Department of Biomedical Sciences, Faculty of Pharmacy, Km 33.100-Campus Universitario, University of Alcalá de Henares, Alcalá de Henares, 28805 Madrid, Spain
- ⁴ Institute for Biological Research "Sinisa Stankovic"-National Institute of Republic of Serbia, University of Belgrade 142, 11060 Belgrade, Serbia; camala@ibiss.bg.ac.rs
- * Correspondence: cfaustino@ff.ulisboa.pt (C.F.); patricia.rijo@ulusofona.pt (P.R.)

Citation: Neto, I.; Domínguez-Martín, E.M.; Ntungwe, E.; Reis, C.P.; Pesic, M.; Faustino, C.; Rijo, P. Dehydroabietic Acid potential as Biofilm-Mediated Infections Treatment. *Pharmaceutics* **2021**, *13*, 825. <https://doi.org/10.3390/pharmaceutics13060825>

Academic Editors: Maria Camilla Bergonzi, Javier Garcia-Pardo and Charles M. Heard

Received: 15 April 2021
Accepted: 31 May 2021
Published: 2 June 2021

Publisher's Note: MDPI stays neutral with regard to jurisdictional claims in published maps and institutional affiliations.



Copyright: © 2021 by the authors. Licensee MDPI, Basel, Switzerland. This article is an open access article distributed under the terms and conditions of the Creative Commons Attribution (CC BY) license (<http://creativecommons.org/licenses/by/4.0/>).

Abstract: The antimicrobial activity of dehydroabietic acid (DHA) for its use as an antibiofilm agent was tested in this work. DHA was assayed against a collection of Gram-positive, Gram-negative sensitive and resistant bacteria and yeasts through the minimum inhibitory concentration (MIC), MIC with Bioburden challenge, minimum bactericidal concentration (MBC), minimum biofilm inhibitory concentration (MBIC), MBIC with Bioburden challenge and growth curve studies. Toxicological studies (*Artemia salina*, sulforhodamine B (SRB) assay) were done to assess if the compound had antimicrobial and not cytotoxic properties. Furthermore, microencapsulation and stability studies were carried out to evaluate the chemical behavior and stability of DHA. On MIC results, Gram-positive bacteria *Staphylococcus aureus* ATCC 1228 and *Mycobacterium smegmatis* ATCC 607 presented a high efficiency (7.81 µg/mL), while on Gram-negative bacteria the highest MIC value of 125 µg/mL was obtained by all *Klebsiella pneumoniae* strains and *Escherichia coli* isolate strain HSM 303. Bioburden challenge showed that MIC, MBIC and percentage biofilm inhibition (BI) values suffered alterations, therefore, having higher concentrations. MBIC values demonstrated that DHA has a higher efficiency against *S. aureus* ATCC 43866 with a percentage of BI of 75.13% ± 0.82% at 0.49 µg/mL. Growth curve kinetic profiles of DHA against *S. aureus* ATCC 25923 were observed to be bacteriostatic. DHA-alginate beads had a average size of 2.37 ± 0.20 and 2.31 ± 0.17 × 10³ µm² with an encapsulation efficiency (EE%) around 99.49% ± 0.05%, a protection percentage (PP%) of 60.00% ± 0.05% in the gastric environment and a protection efficiency (PE%) around 88.12% ± 0.05% against UV light. In toxicological studies DHA has shown IC₅₀ of 19.59 ± 7.40 µg/mL and a LC₅₀ of 21.71% ± 2.18%. The obtained results indicate that DHA is a promising antimicrobial candidate against a wide range of bacteria and biofilm formation that must be further explored.

Keywords: dehydroabietic acid; antimicrobial resistance; biofilm; infection; microencapsulation

1. Introduction

Antimicrobial resistance (AMR) is one of the current worldwide problems in developing and developed countries, because of the misuse and overuse of antibiotics [1]. In fact, among the main causes of morbidity and mortality in developing countries are infectious diseases, causing the healthcare-acquired infections (HAI) high rates of deaths globally [2]. Actually, it is estimated that there are 700,000 deaths worldwide related to AMR, and that number will rise in 2050 approximately to 10 million deaths [3].

Currently, some microorganisms' strains have become common inhabitants in the hospital environments, such as methicillin-resistant *Staphylococcus aureus* (MRSA), vancomycin-resistant *S. aureus* (VRSA), vancomycin-resistant *Enterococcus* (VRE) and multi-drug-resistant (MDR) [4–6]. The problem aggravates considering the diminution of new antibiotics development, raising the infections specter that once were treatable may soon become untreatable [7]. This justifies why the World Health Organization (WHO) identified antimicrobial resistance as a public health concern just at the beginning of the 21st century [8], as a consequence of the quickly arise and spread of resistant microorganisms to commonly used antibiotics.

AMR to regularly employed antimicrobial agents is primarily a result of the enzymatic inactivation of the drug, a shift of its receptor or target site, altered membrane permeability (which prevents the drug to access to the inner of the bacteria) or the overexpression of efflux pumps [9–11]. Moreover, in the past, many antibiotics were developed considering the microorganisms grew in planktonic cultures, but currently it is clear that most of the bacteria live as complex communities known as biofilms. Undoubtedly, as current published works evidenced, microbial biofilms are the responsible for the treatment failure to conventional antimicrobial therapy, due to the difficulty of these drugs to penetrate and destroy biofilm matrix [12–14]. Therefore, to contain and to solve the global increasing of AMR, it is necessary to invest on novel classes of antimicrobial agents with better efficacy and mechanisms of action, to be used alone or as combination regimens with another antibiotics. Isolated compounds from herbal medicines can enrich our AMR therapeutic arsenal used solely or in combination with the current antibiotics available in the market.

Our research group has recently isolated several antimicrobial diterpenes from *Plectranthus* plants, namely royleanones and coleons, which belong to the largest group of naturally occurring abietanes [15–17]. The abietanes possess a characteristic aromatic ring C, being an example, the dehydroabietic acid (DHA) (Figure 1). The abietic acids are strong antibacterial agents with DHA generally being the most potent [18].

Antimicrobial diterpenes like DHA target cellular membranes by a combination of hydrophobic and electrostatic adsorption effects at the membrane/water interface, leading to membrane destabilization and enhanced permeability. Subsequently, disruption of the physical integrity of the membrane or translocation into the cell occurs, compromising cellular processes such as DNA replication, protein folding and synthesis. This mode of action has been shown to limit the risk of cross-resistance [19–21].

The present work is focused on the antimicrobial and toxicological studies of DHA, and DHA-alginate beads were produced for protection of DHA from degradation.

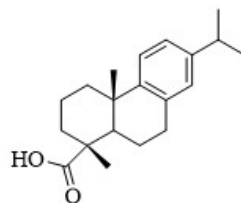


Figure 1. Chemical structure of dehydroabietic acid (DHA).

2. Materials and Methods

2.1. Reagents

Phosphate buffered saline (PBS), alginate, sulfuric acid, absolute ethanol (99.7%), trichloroacetic acid, sulforhodamine B, acetic acid and tris(hydroxymethyl)aminomethane (TRIS base) were purchased from Sigma-Aldrich® (Darmstadt, Germany). Gram's crystal violet solution, dimethyl sulfoxide (DMSO), deuterated dimethyl sulfoxide (DMSO-d₆), anhydrous chloroform, deuterated chloroform (CDCl₃), methanol, ethyl acetate (AcOEt) and calcium chloride were bought from Merck® (Lisboa, Portugal). Dehydroabietic acid was obtained from Wako® (Neuss, Germany) (FUJIFILM Wako Pure Chemical Corporation; CAS RN®: 1740-19-8, Molecular Formula: C₂₀H₂₈O₂; Molecular Weight: 300.44). Mueller–Hinton Broth (MHB), Mueller–Hinton agar (MHA), Sabouraud dextrose broth (SDB), Sabouraud dextrose agar (SDA) and tryptic soy broth (TSB) were purchased from Biokar® Diagnostics (Allonne, France).

2.2. Equipment

The microbiological assays required Greiner® Bio-one 96 well V-bottom microplates, Costar® cell culture 96 well flat-bottom microplates, a microplate reader from Thermo-Fisher Scientific (Marsiling, Singapore), incubators from Memmert, Heidolph Inkubator 1000 and Heidolph Unimax 1010 Stirrer (Heidolph Instruments GmbH & Co. KG, Schwabach, Germany), a laminar flow cabinet from FASTER Bio 48 (Milan, Italy), Xiaomi Redmi 4 (5-element lens, 1.12 µm pixels, 13 MP CMOS) Camera and a spectrophotometer from Hitachi (Santa Clara, CA, USA).

2.3. Dehydroabietic Acid Purification and Identification

DHA obtained from Wako® was purified through the process of recrystallization from methanol. The solid crystals of DHA were collected and the purity was checked by nuclear magnetic resonance (NMR) spectroscopy. The chemical structure of purified DHA was elucidated based on 1D-(¹H and ¹³C) and 2D (COSY, HSQC and HMBC) NMR spectroscopy experiments. NMR spectra were recorded in DMSO-d₆ and CDCl₃ on a 400 MHz instrument (Varian INOVA-400 Spectrometer (UNITYNOVA™ NMR Spectrometer Systems) at 400 MHz (¹H) and 75 MHz (¹³C). The chemical shifts (δ) are in ppm and the coupling constants (J) in Hertz (Hz).

2.4. Bacterial Strains and Culture Media

Preservation and culture of the test organisms were carried out accordingly to the Clinical and Laboratory Standards Institute (CLSI). Bacterial strains studied were Gram-positive bacteria (*Staphylococcus aureus* ATCC 25923 (MSSA), *S. aureus* CIP 106760 (MRSA), *S. aureus* ATCC 6538, *S. aureus* ATCC 25923, *S. aureus* ATCC 700699, *S. aureus* FFHB 25923 (MRSA), *S. aureus* 43300, *S. aureus* ATCC 43866, *S. epidermidis* ATCC 12228, *Enterococcus faecalis* ATCC 29212, *E. faecalis* ATCC 51299, *E. faecalis* V583 and *Mycobacterium smegmatis* ATCC 607), Gram-negative bacteria (*Pseudomonas aeruginosa* ATCC 9027, *Escherichia coli* ATCC 25922, *E. coli* HSM 1323, *E. coli* HSM 1465, *E. coli* HSM 3023, *Klebsiella pneumoniae* HSM 701, *K. pneumoniae* HSM 703, *K. pneumoniae* HSM 873, *K. pneumoniae* HSM 2948 and *Enterobacter cloacae* HSM 1284), a diploid fungus (*Candida albicans* ATCC 10231) and yeast (*Saccharomyces cerevisiae* ATCC 2601). For the growth and maintenance of the microorganisms, MHB, MHA, SDB and SDA were used, whereas for creating the bacterial biofilm, TSB supplemented by 1% glucose was employed. All microorganisms were cultured and incubated during 24 h at 37 °C in an aerobic workstation. In order to harvest overnight cultures, bacterial suspensions used for antibacterial assays and quantitative biofilm assays were prepared, suspending them in sterile water and adjusting the turbidity to 0.5 McFarland standard.

2.5. Bioburden Challenge

Two different organic challenges were investigated, namely 4% bovine serum albumin (BSA, Sigma-Aldrich®, Darmstadt, Germany) and human blood serum (HBS, Sigma-Aldrich®).

2.6. Cell Cultures

HaCaT cell line (normal human keratinocytes obtained from CLS-Cell Lines Service, Eppelheim, Germany). In a Dulbecco's modified eagle's medium (DMEM) supplemented with 10% fetal bovine serum (FBS), 4 g/L glucose, L-glutamine (2 mM) and 5000 U/mL penicillin, 5 mg/mL streptomycin solution and HaCaT cells were cultured. Then, HaCaT cells were subcultured at 144 h intervals using 0.25% trypsin/ethylenediaminetetraacetic Acid (EDTA) and seeded into a fresh medium at 64,000 cells/cm².

2.7. Antimicrobial Tests

2.7.1. Minimum Inhibitory Concentration Assay

The minimum inhibitory concentration (MIC) of DHA was determined through the two-fold serial broth microdilution assay following CLSI guidelines [22]. In aseptic conditions, 100 µL of the medium (MHB or SDB) was distributed in each well of a 96-well plate. Later, to the first well of each row was added 100 µL of DHA (diluted in DMSO), positive control (commercial antimicrobial: rifampicine (RIF) and vancomycin (VAN) for Gram positive bacteria; ampicillin (AMP) for Gram negative bacteria; nystatin (NYS) for yeasts), or negative control (sterile culture media) solutions at 1 mg/mL concentration. Additionally, DMSO was used as negative control as the solvent used to dissolve DHA, at this high concentration DMSO was not toxic as previously described [15–17,23]. Using a multichannel micropipette, a serial dilution was made to 1:2 proportion between each row of wells (50,000–0.49 mg/L range). Finally, 10 µL of bacterial suspension was added to every well, and plates were covered and incubated at 37 °C for 24 h. The bacterial growth was measured with an absorbance microplate reader (Thermo Scientific Multiskan FC, Loughborough, UK) set to 595 nm. Assays were carried out at least in triplicate for each tested microorganism.

2.7.2. Minimum Bactericidal Concentration Assay

The minimum bactericidal concentration (MBC) was determined according to the procedure recommended by the CLSI [22]. MBC was defined as the lowest concentration of DHA at which a complete absence of growth of bacterial colonies on the agar surface was observed compared with a non-treated control. Assays were carried out at least in triplicate for each tested microorganism.

2.7.3. Minimum Inhibitory Concentration Assay with the Bioburden Challenge

The MICs with the Bioburden challenge were measured as described above (Section 2.7.1.). After the addition of the bacterial suspension to the wells, 10 µL of BSA 4% and HBS solutions were added to the wells, and the plates were incubated for 24 h at 37 °C. The bacterial growth was measured with an absorbance microplate reader set to 595 nm. Assays were carried out at least in triplicate for each tested microorganism.

2.7.4. Biofilm Formation Assay

Biofilm formation of the selected strains was detected by an optimized semiquantitative assay in 96-well polystyrene microtiter plates as previously described [23]. Overnight cultures of clinical strains were diluted at 0.5 McFarland standard in TSB containing 1% glucose and dispensed into 96-well flat-bottom plates (300 µL/well). After 24 h of static incubation at 37 °C, the plates were washed gently three times with PBS (pH 7.2) to remove unattached bacteria, fixed at 60 °C for 60 min in an incubator, and stained with crystal violet 1% (*w/v*) for 15 min at room temperature. Wells were then thoroughly

washed with running tap water. Biofilm formation was quantified by adding 150 μL of absolute ethanol into each well for 30 min, and then scanned at 595 nm using a 96-well plate spectrophotometer to determine the optical density of the stained biofilms. Sterile culture media was used as a negative control.

According to their biofilm-forming ability, the selected strains were divided into four groups, as measured by OD values at 595 nm (OD_{595}). The cut-off OD value (OD_c) was defined as three standard deviations (SD) above the mean OD of the negative control (Equation 1). The OD value of a tested strain was expressed as its average. The strains were divided into the following groups: $\text{OD}_{595} \leq \text{OD}_c$ = no biofilm producer (-); $\text{OD}_c < \text{OD}_{595} \leq 2 \times \text{OD}_c$ = weak biofilm producer (+); $2 \times \text{OD}_c < \text{OD}_{595} \leq 4 \times \text{OD}_c$ = moderate biofilm producer (++); $4 \times \text{OD}_c < \text{OD}_{595}$ = strong biofilm producer (+++). Assays were carried out at least in triplicate for each tested microorganism [24].

$$\text{OD}_c = \bar{X} \times \text{OD} \times \text{Negative control} + (3 \times \text{SD} \times \text{Negative control}) \quad (1)$$

2.7.5. Inhibition Properties of Dehydroabiatic Acid on Biofilm Formation

By two-fold dilution and crystal violet staining methods, the effect of DHA on biofilm formation was assayed.

The minimum biofilm inhibitory concentration (MBIC) of the compounds was determined using the two-fold serial broth microdilution assay. In aseptic conditions, 100 μL of TSB containing 1% glucose medium was distributed in each well of a 96-well microplate. Next, to the first well of each row were added 100 μL of DHA, the positive control or negative control solutions at 1 mg/mL concentration. Using a multichannel micropipette, a serial dilution was made to 1:2 proportion between each row of wells (50,000–0.49 mg/L range). Lastly, 20 μL of bacterial suspension was added to every well, and plates were covered and incubated at 37 $^\circ\text{C}$ for 24 h. After the crystal violet staining method, the biofilm growth was measured with an absorbance microplate reader set to 595 nm. The percentage of biofilm formation in the presence of different concentrations of DHA was determined using Equation 2. Results are shown as mean \pm SD, $p < 0.05$.

$$\text{Biofilm Formation (\%)} = \frac{\text{OD}_{595} \text{ of the test well}}{\text{OD}_{595} \text{ of non - treated control well}} \times 100 \quad (2)$$

2.7.6. Inhibition Properties of Dehydroabiatic Acid on Biofilm Formation with Bioburden Challenge

The effect of DHA on biofilm formation with interfering substances was determined by two-fold microdilution and crystal violet staining methods, described previously (Section 2.7.1. and 2.7.4., respectively) [23,24]. The MBIC was determined employing the two-fold serial broth microdilution assay. A total of 100 μL of TSB containing the 1% glucose medium were introduced in each well of a 96-well plate under aseptic conditions. Next, to the first well of each row 100 μL of DHA was added, the positive control or negative control solutions at a 1 mg/mL concentration. Using a multichannel micropipette, a serial dilution was made to 1:2 proportion between each row of wells (50,000–0.49 mg/L range). Finally, 10 μL of bacterial suspension plus 10 μL of BSA 4% or HBS solutions were added to every well, and plates were covered and incubated at 37 $^\circ\text{C}$ for 24 h.

After the crystal violet staining method, the biofilm growth was measured with an absorbance microplate reader set to 595 nm. Using Equation 2, the percentage of biofilm formation in the presence of different concentrations of each compound was established. Assays were carried out at least in triplicate for each tested microorganism. Results are shown as mean \pm SD, $p < 0.05$.

2.7.7. Growth Curve Studies

The growth curve of DHA was determined using the method described previously [25]. Concentrations equivalent to the MIC of DHA were prepared. After overnight incubation over stirring (at 100 RPM), inoculum size of 1.0×10^8 colony forming units (CFU)/mL was chosen. DHA was prepared at different concentrations that were incorporated into test tubes containing sterile nutrient broth and inoculated with test microorganisms. Aliquots of 1.0 mL of the medium taken at time intervals of 30 min for 6 h were inoculated into nutrient agar and incubated at 37 °C for 24 h and measured with a spectrophotometer set to 620 nm. A control test (negative) consisted of test microorganisms alone without DHA.

After 24 h of incubation, the CFU was determined (data not shown). The procedure was repeated in triplicates (three independent experiments) and a graph of the absorbances against time was plotted.

2.8. Microencapsulation of Dehydroabiatic Acid

2.8.1. Production of dehydroabiatic acid-loaded calcium alginate microspheres

By the extrusion/external gelation method, DHA-alginate microspheres were prepared [26]. To a 5 mL of 2% sodium alginate solution, a volume of 1 mL of reconstituted DHA at 10 mg/mL was incorporated. Under magnetic stirring, this suspension was extruded through a fine syringe (21-gauge, diameter 0.81 mm) to 100 mL of calcium chloride 0.05 M solution for 15 min.

Gelled and hydrated microspheres were recovered by filtration. Blank microspheres were also produced.

2.8.2. Characterization of Dehydroabiatic Acid-Loaded Calcium Alginate Microspheres

The size and morphology of the calcium alginate beads were determined by direct observation, and the images were recorded digitally (Xiaomi Redmi 4 Camara). The encapsulation efficiency (EE%) of DHA-alginate microspheres was determined in triplicate through an indirect method. The absorbance (Ab_{620nm}) of the supernatant obtained in the preparation of the microspheres was measured through a spectrophotometric method previously described [27,28]. In Equation 3, as an indicator of the EE% were used calcium chloride and DHA concentration, where EE% corresponds to the encapsulation efficiency, C_i to the initial concentration of DHA and C_f to the final concentration of DHA (non-encapsulated or free DHA) present in the supernatant. Results are shown as mean \pm SD, $p < 0.05$.

$$\text{Encapsulation efficiency (\%)} = \frac{C_i - C_f}{C_i} \times 100 \quad (3)$$

2.8.3. Stability Studies of Dehydroabiatic Acid-Loaded Calcium Alginate Microspheres

2.8.3.1. Harsh Conditions Such as Gastric Environment or Low pH Study

To test the protection percentage (PP%) for DHA-alginate microspheres in acidic conditions, a forced degradation study was conducted. It was performed the acid stress reflux with HCl (0.1 M) at 60 °C for 30 min as beforehand defined [29–31]. With the same spectrophotometric method previously described the amount of DHA in the supernatant and remaining DHA in beads were quantified.

Fresh solutions of DHA and DHA-alginate microspheres were used as the controls. DHA concentration was used as the indicator of PP% using Equation 4, where PP% corresponds to the protection efficiency, C_i to the initial concentration of DHA and C_f to the final concentration of DHA (non-encapsulated or free DHA) present in the supernatant. Results are shown as mean \pm SD, $p < 0.05$.

$$\text{Protection percentage (\%)} = \frac{C_i - C_f}{C_i} \times 100 \quad (4)$$

2.8.3.2. Photostability Studies

Freeze-dried beads made from calcium alginate (200 mg) were deposited in vials containing 10 mL of water under UV light (274 nm) and left for magnetic stirring for 2 h, as previously described [26].

The amount of DHA in the supernatant and remaining in beads was quantified using the same spectrophotometric method. Fresh solutions of DHA and DHA-alginate microspheres were used as the controls. Calcium chloride and DHA concentration were used as the indicator of protection efficiency using Equation (5), where PE% corresponds to the protection efficiency, C_i to the initial concentration of DHA and C_f to the final concentration of DHA (non-encapsulated or free DHA) present in the supernatant. Results are shown as mean \pm SD, $p < 0.05$.

$$\text{Protection efficiency (\%)} = \frac{C_i - C_f}{C_i} \times 100 \quad (5)$$

2.9. Toxicological Studies

2.9.1. Sulforhodamine B Assay

HaCaT cells grown in 25 cm² tissue flasks were trypsinized, seeded into flat-bottom 96-well tissue culture plates, and incubated overnight. Later, they were seeded at 4000, 8000 and 16,000 cells/well, respectively.

Compound used as treatment were incorporated at concentration of 1–100 mM lasted 72 h. The cellular proteins were stained with sulforhodamine B (SRB) assay, following the slightly modified protocol previously described [32]. Briefly, the cells in 96-well plates were fixed in 50% trichloroacetic acid (50 mL/well) for 1 h at 4 °C, rinsed in tap water and stained with 0.4% (*w/p*) sulforhodamine B in 1% acetic acid (50 mL/well) for 30 min at room temperature. The cells were then rinsed three times in 1% acetic acid to remove the unbound stain. The protein-bound stain was extracted with 200 mL 10 mM TRIS base (pH 10.5) per well. The optical density was read at 540 nm, with correction at 670 nm. Results are shown as mean \pm SD, $p < 0.05$.

2.9.2. Artemia Salina Toxicological Study

The toxicity of DHA on *Artemia salina* was tested according to the method described previously [33–35], with some small adaptations on the hatching equipment, namely material for covering the compartments. DHA concentrations of 10 ppm were tested.

In artificial seawater (salinity concentration 30 g/L), during 48 h at 30 °C, 80 mg of brine shrimp cysts (JBL GmbH & Co., KG D-67141; Neuhofen, Germany) were incubated. Next, from the hatched cysts, ten nauplii were selected and transferred into wells of 21-well cultures plates containing artificial seawater (final volume/well 1 mL). The culture plates were incubated for 48 h at 30 °C; after every 24 h, the number of dead nauplii was counted microscopically.

The mortality was used to calculate the percentage (%) of lethal concentration, according to Equation (6). Results are shown as mean \pm SD, $p < 0.05$.

$$\text{Lethal concentration (\%)} = \frac{\text{Total nauplii} - \text{Alive nauplii}}{\text{Total nauplii}} \quad (6)$$

2.10. Statistical Analysis, Software and Databases

In order to perform statistical analysis, GraphPad Prism version 7.0a (San Diego, CA, USA) and a one-way ANOVA were used with a significance level (p -value) of 0.05. Additionally, the following software and database were used: ChemDraw 19.0 (PerkinElmer Informatics, Massachusetts, USA), MestreNova 8.1.4 (York, England), Microsoft Excel (Microsoft Office 365), PubMed-NCBI and ISI web of knowledge.

3. Results

3.1. Dehydroabietic Acid Recrystallization

Commercial DHA (purity 85–90%) was recrystallized from methanol to give white needle crystals and purity was verified by NMR. ^1H NMR(DMSO- d_6 , 400 MHz, ppm) δ 7.08 (d, 1H, $J_{11,12}$ = 8.1 Hz, H-11), 6.89 (d, $J_{12,11}$ = 8.1 Hz, 1H, H-12), 6.77 (brs, 1H, H-14), 2.72–2.68 (m, 2H, H-7, H-15, overlapped signals), 2.40–2.45 (m, 4H, 4H, H-2 α , H-2 β , H-3 α , H-3 β), 2.22 (brs, 1H, H-5), 1.90–1.98 (m, 2H, H-6 α and H-6 β), 1.58 (m, 1H, H-1 α), 1.25 (m, 1H, H-6 β), 1.08 (brs, 6H, Me-16, Me-17, overlapped signals), 1.07 (s, 3H, Me-19), 1.04 (brs, 3H, Me-20); ^{13}C NMR (DMSO- d_6 , 75 MHz, ppm) δ 179.53 (C-18), 146.80 (C-9), 145.11 (C-13), 134.16 (C-8), 126.53 (C-14), 124.12 (C-11), 123.79 (C-12), 46.43 (C-5), 44.76 (C-4), 37.83 (C-1), 36.49 (C-3), 36.32 (C-10), 32.95 (C-15), 29.61^a (C-17), 24.89 (C-19), 24.01 (C-20), 21.19^a (C-16), 18.23 (C-6) and 16.44 (C-2). ^a May be interchanged.

3.2. Antimicrobial Tests

3.2.1. Minimum Inhibitory Concentration Assay

The antimicrobial activity of DHA was screened and MIC values were determined against a collection of Gram-positive and Gram-negative bacteria and yeasts using the microdilution method. The results obtained are shown in Table 1.

Table 1. Minimum inhibitory concentration (MIC) values ($\mu\text{g/mL}$) of DHA against a collection of Gram-positive and Gram-negative bacteria, and some yeasts. Results showed as mean \pm SD, $p < 0.05$.

| Microorganism | Strain | DHA | Positive Control ^a | Negative Control ^b |
|---|--|------------|-------------------------------|-------------------------------|
| Gram-positive bacteria | <i>S. aureus</i> CIP 106760 ^c | 15.63 | RIF > 500 | 250 |
| | <i>S. aureus</i> ATCC 6538 | 15.63 | RIF < 0.49 | 250 |
| | <i>S. aureus</i> ATCC 25923 ^d | 31.25 | RIF 0.98 | 250 |
| | <i>S. aureus</i> ATCC 700699 | 62.5 | RIF < 0.49 | 250 |
| | <i>S. aureus</i> FFHB 25923 ^e | 31.25 | RIF < 0.49 | 250 |
| | <i>S. aureus</i> ATCC 43300 ^c | 125 | RIF < 0.49 | 250 |
| | <i>S. aureus</i> ATCC 43866 | >250 | RIF < 0.49 | 250 |
| | <i>S. epidermidis</i> ATCC 12228 | 7.81 | RIF < 0.49 | 250 |
| | <i>M. smegmatis</i> ATCC 607 | 7.81 | RIF < 0.49 | 250 |
| | <i>E. faecalis</i> ATCC 29212 | >125 | VAN 62.5 | 125 |
| | <i>E. faecalis</i> ATCC 51299 ^f | >125 | VAN 62.5 | 125 |
| <i>E. faecalis</i> V583 ^f | 500 | VAN 62.5 | 500 | |
| Gram-negative bacteria | <i>E. coli</i> ATCC 25922 | >125 | AMP < 0.49 | 125 |
| | <i>E. coli</i> HSM 1323 ^c | >250 | AMP < 0.49 | 250 |
| | <i>E. coli</i> HSM 1465 ^c | >250 | AMP < 0.49 | 250 |
| | <i>E. coli</i> HSM 3023 ^c | 125 | AMP < 0.49 | 250 |
| | <i>P. aeruginosa</i> ATCC 9027 | >125 | AMP 31.25 | 125 |
| | <i>K. pneumoniae</i> HSM 701 ^c | 125 | AMP < 0.49 | 250 |
| | <i>K. pneumoniae</i> HSM 703 ^c | 125 | AMP < 0.49 | 250 |
| <i>K. pneumoniae</i> HSM 873 ^c | 125 | AMP < 0.49 | 250 | |

| | | | | |
|--------|--|-------|------------|------|
| | <i>K. pneumoniae</i> HSM 2948 ^c | 125 | AMP < 0.49 | 250 |
| | <i>E. cloacae</i> HSM 1284 ^c | >250 | AMP > 500 | 250 |
| Yeasts | <i>C. albicans</i> ATCC 10231 | >125 | NYS 31.25 | 125 |
| | <i>S. cerevisiae</i> ATCC 2601 | >62.5 | NYS 31.25 | 62.5 |

^aRIF, rifampicine; VAN, vancomycin; AMP, ampicillin; NYS, nystatin; ^bDMSO; ^cMRSA; ^dMSSA; ^eFFHB strain are clinical isolates from Hospital do Barreiro, and HSM strains are clinical isolates from Hospital de Santa Maria deposited at the Microbiology Laboratory, Faculty of Pharmacy, University of Lisbon; ^fVRE. All the MIC values were evaluated using DMSO as the solvent, which was also evaluated as the negative control.

In Gram-positive reference bacteria, *S. epidermidis* ATCC 12228 and *M. smegmatis* ATCC 607, DHA demonstrated a high efficiency with a MIC value of 7.81 µg/mL (Table 1). Regarding bacteria *S. aureus* CIP 106760, a MIC value of 15.63 µg/mL was showed by DHA, having even higher efficiency than the positive control. Against the remaining bacterial pathogens tested, DHA also had a potential antibacterial effect.

Regarding Gram-negative microorganisms (Table 1), the lowest MIC value (125 µg/mL) was registered against *K. pneumoniae* isolate strains and *E. coli* isolate strain HSM 3023.

3.2.2. Minimum Bactericidal Concentration

Bactericidal activity of DHA was also screened against a collection of Gram-positive (MSSA *S. aureus* ATCC 25923 and *S. epidermidis* ATCC 12228), Gram-negative bacteria (*E. coli* ATCC 25922 and slime producer *P. aeruginosa* ATCC 9027) and yeasts (*C. albicans* ATCC 10231 and *S. cerevisiae* ATCC 2601) using the microdilution method. Regarding MBC values, low MBC/MIC ratios within each strain are typical of bactericidal agents. In a recent study [36], the abietane-type diterpenoid taxodone showed MIC and MBC values of 500 and 500 µg/mL, respectively, against both *S. aureus* and *E. coli*. However, MBC values against the specified microorganisms could not be determined for DHA in the tested concentration range, contrary to MIC values, suggesting that antimicrobial properties of DHA are mainly bacteriostatic in nature.

3.2.3. Minimum Inhibitory Concentration Assay with Bioburden

Antimicrobial activity of DHA with bioburden was screened and its MIC values were determined against Gram-positive (*S. aureus* ATCC 25923 and *S. aureus* CIP 106760) and Gram-negative (*P. aeruginosa* ATCC 9027) bacteria using the microdilution method. These strains were chosen due to their high resistance to antimicrobials (MRSA species), biofilm formation and slime production (*P. aeruginosa* ATCC 9027).

After data analysis, MIC values with bioburden suffer alterations, thus, having higher concentrations (Table 2).

Table 2. Minimum inhibitory concentration (MIC) values (µg/mL) of DHA against Gram-positive (*S. aureus* ATCC 25923 and *S. aureus* CIP 106760) and Gram-negative (*P. aeruginosa* ATCC 9027) bacteria. Results showed as mean ±SD, $p < 0.05$.

| Bacterial Strain | Biofilm Formation | Free DHA | BSA | HBS |
|---|-------------------|----------|------|------|
| <i>S. aureus</i> ATCC 25923 ^a | +++ | 31.25 | 62.5 | 250 |
| <i>S. aureus</i> CIP 106760 ^b | + | 250 | 500 | 500 |
| <i>P. aeruginosa</i> ATCC 9027 ^c | + | 500 | 1000 | 1000 |

^aMSSA; ^bMRSA; ^cslime producer. All the MIC values were evaluated using DMSO as the solvent, which was also evaluated as the negative control.

3.2.4. Inhibition Properties of Dehydroabiatic Acid on Biofilm Formation

Biofilm formation of a collection of Gram-Positive bacteria, Gram-negative bacteria and yeasts was tested by a microdilution method and the results are shown on Table 3. Among all the strains tested only clinical isolate *E. cloacae* HSM 1264 did not produce biofilm.

Table 3. Minimum biofilm inhibitory concentration (MBIC) values ($\mu\text{g/mL}$) and percentage of biofilm inhibition for DHA against a collection of Gram-positive and Gram-negative bacteria, and yeast. Results showed as mean \pm SD, $p < 0.05$.

| Microorganism | Strain | Biofilm Formation ^a | MBIC ($\mu\text{g/mL}$) | Biofilm Inhibition (%) |
|---|--|--------------------------------------|---------------------------|------------------------|
| Gram-positive bacteria | <i>S. aureus</i> ATCC 25923 ^b | +++ | 125 | 72.66 \pm 2.88 |
| | <i>S. aureus</i> ATCC 6538 | ++ | 500 | 43.64 \pm 1.58 |
| | <i>S. aureus</i> ATCC 700699 | ++ | 500 | 57.55 \pm 17.50 |
| | <i>S. aureus</i> ATCC 43300 ^c | ++ | 125 | 65.99 \pm 3.72 |
| | <i>S. aureus</i> ATCC 43866 | +++ | 0.49 | 75.13 \pm 8.82 |
| | <i>S. aureus</i> CIP 106760 ^c | + | 62.5 | 77.48 \pm 0.05 |
| | <i>S. aureus</i> FFHB 25923 ^d | ++ | 3.91 | 63.69 \pm 0.05 |
| | <i>S. epidermidis</i> ATCC 12228 | ++ | 500 | 92.56 \pm 5.72 |
| | <i>E. faecalis</i> ATCC 51299 ^e | ++ | 7.81 | 75.93 \pm 0.05 |
| | <i>E. faecalis</i> ATCC 29212 | ++ | 15.63 | 87.25 \pm 0.05 |
| | <i>E. faecalis</i> V583 ^e | ++ | 31.25 | 75.72 \pm 0.05 |
| | <i>E. coli</i> ATCC 25922 | + | 500 | 80.22 \pm 1.93 |
| | Gram-negative bacteria | <i>E. coli</i> HSM 1323 ^d | + | 250 |
| <i>E. coli</i> HSM 1465 ^d | | + | 1.95 | 80.35 \pm 13.37 |
| <i>E. coli</i> HSM 3023 ^d | | +++ | 250 | 92.58 \pm 1.18 |
| <i>K. pneumoniae</i> HSM 701 ^d | | + | 0.98 | 92.75 \pm 5.69 |
| <i>K. pneumoniae</i> HSM 703 ^d | | + | 0.98 | 94.13 \pm 2.37 |
| <i>K. pneumoniae</i> HSM 873 ^d | | +++ | 250 | 98.82 \pm 2.00 |
| <i>K. pneumoniae</i> HSM 2948 ^d | | +++ | 250 | 96.99 \pm 0.24 |
| <i>E. cloacae</i> HSM 1264 ^d | | - | ND | ND |
| <i>P. aeruginosa</i> ATCC 9027 ^f | | + | 7.81 | 64.64 \pm 10.19 |
| Yeast | <i>C. albicans</i> ATCC 10231 | + | 62.5 | 81.83 \pm 7.05 |

^a (-) no biofilm producer; (+) weak biofilm producer; (++) moderate biofilm producer; (+++) strong biofilm producer; ^b MSSA; ^c MRSA; ^d FFHB species are clinical isolates from Hospital do Barreiro and HSM strains are clinical isolates from Hospital de Santa Maria, deposited on the Microbiology Laboratory, Faculty of Pharmacy, University of Lisbon; ^e VRE; ^f slime producer. All the MIC values were evaluated using DMSO as the solvent, which was also evaluated as negative control.

The strains that are strong biofilm producers are *S. aureus* ATCC 25923, *S. aureus* ATCC 43866, clinical isolate *E. coli* HSM 3023, clinical isolate *K. pneumoniae* HSM 873 and clinical isolate *K. pneumoniae* HSM 2948. None of the Gram-negative strains demonstrated to be a moderate biofilm producer, nevertheless, in Gram-positive bacteria the strains that showed this capacity were *S. aureus* ATCC 6538, *S. aureus* ATCC 700699, *S. aureus* ATCC 43300, *S. epidermidis* ATCC 12228 and all the *E. faecalis* strains. In Gram-positive bacteria only *S. aureus* CIP 106760 demonstrated to be a weak biofilm producer followed by Gram-negative clinical isolates *E. coli* HSM 1323, *E. coli* HSM 1465, *E. coli* ATCC 25922 *K. pneumoniae* HSM 701, *K. pneumoniae* HSM 703, *P. aeruginosa* ATCC 9027 and by the yeast *C. albicans* ATCC 10231.

The MBIC of DHA on biofilm formation against a collection of Gram-positive and Gram-negative bacteria and yeasts was tested by means of the two-fold serial broth microdilution assay and results are also presented on Table 3.

The lowest MBIC value registered for DHA was achieved against Gram-positive *S. aureus* ATCC 43866, a strong biofilm producer, with a percentage of biofilm inhibition (BI) of $75.13\% \pm 8.82\%$, being achieved at $0.49 \mu\text{g/mL}$ DHA, followed by clinical isolate *K. pneumoniae* HSM 701 and clinical isolate *K. pneumoniae* HSM 703. Still according to Table 3, in Gram-positive microorganisms the lowest MBIC values were in the following order: *S. aureus* FFHB 25923 < *E. faecalis* ATCC 51229 < *E. faecalis* ATCC 29212 < *E. faecalis* V583 < *S. aureus* CIP 160760 < *S. aureus* ATCC 25923 < *S. aureus* ATCC 43300 < *S. aureus* ATCC 6538 < *S. aureus* ATCC 700699. In Gram-negative bacteria, the lowest values of MBIC were attained against clinical isolates *K. pneumoniae* HSM 701 and *K. pneumoniae* HSM 703 followed by clinical isolate *E. coli* HSM 1465, *P. aeruginosa* ATCC 9027, clinical isolates *K. pneumoniae* HSM 873, *K. pneumoniae* and *E. coli* HSM 3023 and finally *E. coli* ATCC 25922.

Although MBIC concentrations varies between the bacterial strains, BI is never below 50% except for *S. aureus* ATCC 6538 and clinical isolate *E. coli* HSM 1323, which indicates that DHA has a strong biofilm inhibition ability that merits further investigation. Therefore, inhibition properties of DHA on biofilm formation with Bioburden and growth curve studies were performed as described in the next sections.

3.2.5. Inhibition Properties of Dehydroabietic Acid on Biofilm Formation with Bioburden

In developed countries, a high economical hurdle is the high cost of chronic wounds, which are characterized by microbial complications such as local or overt infection, delaying in the healing time and spread of multiresistant microorganisms [37]. In a hope of treating germs in wounds, antiseptics is the method of choice, considering that systemic antibiotics can barely penetrate into wound biofilms and topically applied ones can easily lead to sensitization, antiseptics is the method of choice to treat germs in wounds [37].

Therefore, a MBIC study with Bioburden was conducted to demonstrate that DHA MBIC and BI do not suffer significant alterations in the presence of Bioburden. MBIC values with Bioburden for DHA was tested by means of the two-fold serial broth microdilution assay and the results are shown on Table 4.

Table 4. Minimum biofilm inhibitory concentration (MBIC) values ($\mu\text{g/mL}$) and biofilm inhibition (BI) percentage of DHA against Gram-positive (*S. aureus* ATCC 25923 and *S. aureus* CIP 106760) and Gram-negative (*P. aeruginosa* ATCC 9027) with the Bioburden challenge. Results showed as mean \pm SD, $p < 0.05$.

| Strain | Biofilm Formation | MBIC ($\mu\text{g/mL}$) | | | Biofilm Inhibition (%) | | |
|---|-------------------|---------------------------|-------|-------|------------------------|------------------|------------------|
| | | Free DHA | BSA | HBS | Free DHA | BSA | HBS |
| <i>S. aureus</i> ATCC 25923 ^a | +++ | 15.63 | 15.63 | 125 | 62.96 ± 0.15 | 45.67 ± 0.56 | 51.54 ± 1.45 |
| <i>S. aureus</i> CIP 106760 ^b | + | 250 | 250 | 500 | 50.61 ± 1.56 | 48.59 ± 4.34 | 52.03 ± 2.33 |
| <i>P. aeruginosa</i> ATCC 9027 ^c | + | 7.81 | 62.5 | 31.25 | 62.15 ± 0.89 | 43.56 ± 2.12 | 57.88 ± 1.34 |

^aMSSA; ^bMRSA; ^cslime producer. All the MBIC values were evaluated using DMSO as the solvent, which was also evaluated as the negative control.

In *S. aureus* strains, BSA demonstrates not to have any influence in MBICs, although it has in BIs values. Nevertheless, HBS has influence in both MBICs and BIs values, increasing them. In Gram-negative bacteria (*P. aeruginosa* ATCC 9027) both BSA and HBS have influence in both MBICs and BIs values by increasing them. This increase may also be due to the production of slime that this strain is known for.

3.2.6. Growth Curve Study

To study the pharmacodynamics of antimicrobial agents, the growth curve assay is the method of choice, since it examines the rate at which different concentrations of an antimicrobial drug kill bacteria, displaying the concentration-dependent and time-dependent bactericidal activities of antimicrobial agents [38].

Growth curve profiles of DHA against Gram-positive bacteria (*S. aureus* ATCC 25923) were observed to be bacteriostatic. The growth curve profile of DHA against the test microorganisms at test concentrations showed reduction in number of cells over the first four hours, when compared to the control (microorganism without antimicrobial agent). The area under the curve, which is a measure of the activity of DHA over the 15 h period, showed that DHA at concentrations of 31.25, 62.50 and 93.75 µg/mL significantly ($p < 0.05$) reduced the number of *S. aureus* ATCC 25923 cells when compared to the control (Figure 2).

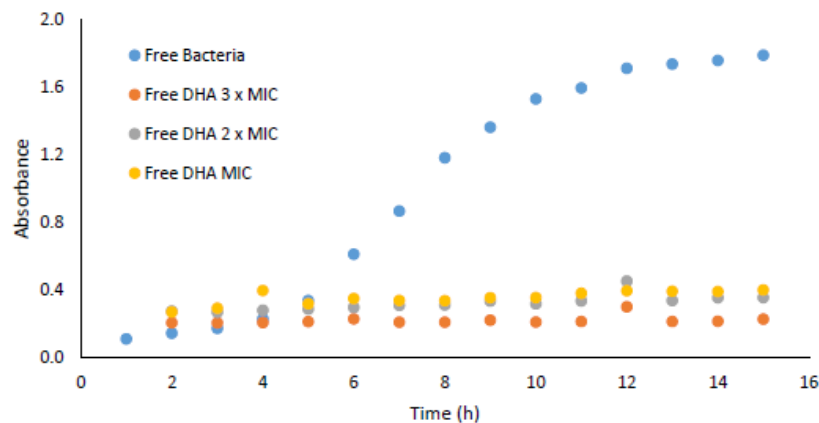


Figure 2. Graphic representation of the growth curve study results of DHA against *S. aureus* ATCC 25923.

3.3. Microencapsulation of Dehydroabietic Acid

3.3.1. Production and Characterization of Dehydroabietic Acid-Loaded Calcium Alginate Microspheres

Using the extrusion/external gelation method, DHA-alginate microspheres were successfully prepared. This technique is promptly performed, and it can be easily adapted to the industrial scale. Essentially, there are two main techniques for producing calcium alginate microspheres ((1) external and (2) internal gelation), based on the source of calcium. In (1), the external gelation method, the drops of alginate (name as droplets are gelled in a calcium chloride solution, and therefore, the calcium source is external to the droplet. In this case, gelation is initiated from the surface and works toward the inner core. On the other hand, in (2) the internal gelation method uses an inner source of calcium, where the alginate solution is preloaded within soluble calcium salt, releasing calcium ions with pH adjustment [26].

In the present work, DHA-alginate microspheres were spherical in shape and showed a mean diameter of 2.37 ± 0.20 and $2.31 \pm 0.17 \times 10^3 \mu\text{m}$ for loaded and empty particles, respectively, in the digital images (Figure 3). These images confirmed the encapsulation of DHA inside the calcium alginate microspheres since empty calcium alginate beads were transparent; meanwhile, when DHA was present, the beads changed to yellow.

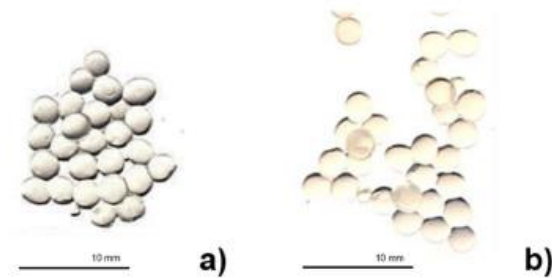


Figure 3. Digital images of (a) the empty alginate microspheres and (b) the DHA-alginate microspheres.

As a polyelectrolyte hydrocolloid, alginate has the property to interact with water, reducing its diffusion and stabilizing its presence. Such water may be retained specifically through direct hydrogen bonds or the structuring of water within extensive, but contained, inter- and intramolecular voids [26].

Therefore, the diterpene DHA was successfully encapsulated into calcium alginate microspheres, where the EE% value was very high (around $99.49\% \pm 0.05\%$). Alginate gelling features strongly depend upon its monomeric composition, sequential arrangements and the lengths of the G-blocks [26]. As previously mentioned in this work, alginate has the ability to form gels with calcium, and this is an autocoperative reaction that happens between calcium and the homopolymeric blocks of G on the alginate chain [26]. Calcium alginate gels shrink during gel formation, which leads to the loss of water and a rise in the concentration of polymer in the beads relative to that in the alginate solution. That may diminish some of the encapsulate diffusion to outside of the polymeric matrix. Herein, the physical characteristics of calcium alginate gel are also influenced by the alginate concentration and molecular size, the calcium concentration and gelling time [26]. Moreover, in the extrusion/external gelation method, a solution of sodium alginate is forced into a bath of a calcium chloride solution, and then, calcium alginate is formed as fibers (gel). Whether alginates of low viscosity are employed, a strong solution is normally created without any viscosity problems, and the calcium in the bath is not diluted as rapidly. Regularly, low G alginates, as the one used in this study, generate very flexible gels [26]. Gel fibers have very good strength in both wet and dry forms, and as with majority of polymer fibers made by extrusion, stretching while forming arises the linearity of the polymer chains and the strength of the fiber [26].

3.3.2. Stability Studies of Dehydroabiestic Acid-Loaded Calcium Alginate Microspheres

3.3.2.1. Harsh Conditions Such as Gastric Environment or Low pH Study

Hydrolysis, a chemical process that consists of the decomposition of a chemical compound with water, is one of the most common degradation chemical reactions over a wide range of pH [29–31]. Hydrolytic study under acidic and basic conditions involves catalysis by ionizable functional groups present in the molecule. For example, HCl and NaOH are employed for generating acidic and basic stress samples, respectively. The hydrolytic degradation of a new drug or molecule in acidic and alkaline condition can be studied by refluxing the drug in 0.1 M HCl/0.1 M NaOH [29–31]. When a reasonable degradation is detected, the test can be stopped at that point. Nonetheless, if no degradation of the drug is perceived under these conditions, it should be refluxed in acid/alkali of higher strength and for longer duration of time [29–31]. As an alternative, if total degradation is seen after subjecting the drugs to initial condition, acid/alkali strength can be reduced with a decrease in reaction temperature. In fact, temperature and pH are the major factors in stability of the drug/molecule prone to hydrolytic decomposition [29–31]. Most of the

drugs/molecules' hydrolysis depend on the relative concentration of hydronium and hydroxyl ions, which allow one to determine the pH at which each drug is optimally stable [29–31].

In this work, the diterpene DHA was successfully encapsulated into calcium alginate microspheres and tested in acidic conditions. Alginate microspheres were able to protect DHA against acidic conditions such as those found in the gastric environment, with a PP% around $60.00\% \pm 0.05\%$.

3.3.2.2. Photostability Studies

Photostability testing is performed to generate primary degradants (such as UV or fluorescent light) that create conditions to evaluate if a drug substance suffers unacceptable changes under light exposition [31].

In an attempt to prolong the release of pharmaceutical compounds and protect them from atmospheric agents (moisture, light, heat and/or oxidation), study of modern dosage forms as the employment of microencapsulates that incorporate active ingredients within polymers, are a very appropriate and effective process for the purpose sought [26].

DHA was maintained in calcium alginate microspheres over time (for seven days) and against UV in contrast to free (non-encapsulated) DHA. Similarly to previous studies [26], alginate proved to be a very good encapsulant material.

In this study, the DHA-alginate microspheres were very successful in protecting DHA, where the PE% value was high (around $88.12\% \pm 0.05\%$)

3.4. Toxicological Studies

3.4.1. Sulforhodamine B Assay

One of the most largely used methods for in vitro cytotoxicity screening is the SRB assay [39]. SRB is a strong-intensity bright-pink aminoxanthene dye with two sulfonic groups that bind to basic aminoacidic residues under mild acidic conditions, and dissociate under basic conditions [39]. This assay is based on the stoichiometric linking of SRB to protein components of cells that are fixed to tissue-culture 96-well plates by trichloroacetic acid, being the amount of dye extracted from stained cells directly proportional to the cell mass [39].

The toxicity effect of DHA was tested against the HaCaT cell line (normal human keratinocytes). The effects on growth of HaCaT after continuous treatment of 72 h were assessed by chemosensitivity assay SRB assay. DHA did not reduce significantly the viability number of normal cells, however it showed a half maximum inhibitory concentration (IC_{50}) of $19.69 \pm 7.40 \mu\text{g/mL}$. Nevertheless, DHA was non-toxic to normal cells (HaCaT) in the same range of concentrations in a recent study [40].

3.4.2. Artemia Salina Toxicological Study

Artemia salina model is a known, simple, fast and low-cost test and was preliminary used to assess the toxicity of DHA [41]. The compound (LC_{50} above 40%) was further assayed at a concentration of 10 ppm. The number of dead larvae was recorded and used to calculate the median lethal concentration (LC_{50}), after 24 h. LC_{50} values less than or equal to 10 ppm were considered active.

A very low mortality of *A. salina* of $21.71\% \pm 2.18\%$ was observed upon exposure to DHA, demonstrating that the compound in this preliminary toxicological study did not have a toxic effect.

4. Discussion

The main goal of this study was the screening of the antimicrobial activity of DHA against a collection of Gram-positive bacteria, Gram-negative bacteria and yeasts, the performance of toxicological assays to assess if the compound had antimicrobial and not cytotoxic properties, and microencapsulation and stability studies to evaluate the chemical behavior and stability of DHA.

In MIC studies, DHA demonstrated to have higher efficacy in Gram-positive bacteria *S. epidermidis* ATCC 12228 and *M. smegmatis* ATCC 607 (both with the lowest MIC value of 7.81 µg/mL) compared with Gram-negative bacteria, where the lowest MIC value of 125 µg/mL was obtained for all clinical isolates of *K. pneumoniae* and clinical isolate strain *E. coli*. The studies of MIC with bioburden have shown that organic challenges have influence in MIC values thus increasing them. In a more recent study [36], some carbazole derivatives from DHA have shown a MIC range between 1.9 and 100 µg/mL against *S. aureus*, but it did not specify which strain. Gu et al. [36] showed that carbazole derivatives from DHA have an enhancement efficacy against Gram-negative bacteria like *E. coli* and also against yeast like *C. albicans*, thus demonstrating the potential of DHA and its derivatives as antimicrobial agents with enhanced antimicrobial activity.

With regard to MIC values with bioburden it was expected that the MIC would have higher concentrations. In a recent study [37], antimicrobial activity with bioburden was tested for some antiseptics, and it was shown that PVP-iodine 10% has an even higher MIC value (1562.5 µg/mL) than DHA against *S. aureus* ATCC 25923. Within the same strain, it was presented that chlorhexidine with bioburden had the same MIC value as DHA, therefore, demonstrating that DHA has interest as an antimicrobial. In traumatic, surgical and burn wound infections, *S. aureus* is the most problematic microorganism. Moreover, there are other such as *P. aeruginosa*, *E. coli* and *K. pneumoniae*, which can cause chronic wound infection [38]. Therefore, it is often necessary the use of systemic and topical antibiotics or the use of antiseptic substances to avoid or eliminate the risk of wound infection. Therefore, it is imperative to find new antimicrobials.

In the biofilm formation assay, most of the tested microorganisms were biofilm producers except for clinical isolate *E. cloacae* HSM 1264. Therefore, this work had a vast collection of microorganisms with biofilm production that will be an advantage for further antimicrobial testing. Regarding the biofilm inhibition properties of DHA, the lowest MBIC value was registered against Gram-positive *S. aureus* ATCC 43866 (0.49 µg/mL; BI 75.13 ± 8.82%), which is a strong biofilm producer. In Gram-positive bacteria with Bioburden challenge only HBS had more influence in MBIC and BI, yet in Gram-negative bacteria all challenges had influence in MBIC and BI values. Notwithstanding, these results demonstrate the capability of this diterpene in the battle against resistant biofilm-producing bacteria. In a recent study [37], MBIC and BI values were obtained for some disinfectants tested against a similar collection of Gram-positive and Gram-negative bacteria and yeasts. Comparatively, DHA show better results than polyhexanide 0.1% (31.25 µg/mL; BI 43.82 ± 0.05%), triclosan 0.15% (46.88 µg/mL; BI 67.90 ± 0.05%) and chlorhexidine 0.2% (62.50 µg/mL; BI 86.14 ± 0.05%) against Gram-positive *S. aureus* ATCC 43866, and similar values against Gram-negative bacteria. MBIC values observed in yeast for the disinfectants was against *C. albicans* ATCC 10231 (62.50 µg/mL; BI 81.83% ± 7.05%).

Pathogenic bacteria can develop mechanisms to adapt and survive in specific micro-environments, which involve overcoming antibiotic killing-effects on them, causing therapeutic failure, recurrence and resistance to the infections. In fact, the biofilms formed by these bacteria existing on the surface of implanted medical devices and in deep tissues, play a meaningful role in persistent infections [39]. This is due to the formation of biofilms that are formed by complex aggregates that involved the bacteria, which are in the dormant state, because of the protection from host defense and antimicrobials by the extracellular matrix where they lived. The extracellular matrix comprising polymeric substances such as DNA, lipopolysaccharides, teichoic acids and proteins. Moreover, biofilm formation and growth, which are accompanied by finely regulated metabolic changes, also affect the bacterial response to antimicrobials [39]. The increase on the emergence of multidrug-resistant bacteria is mainly due to the limited effectiveness against biofilm-related infections [40]. Therefore, it is urgent to investigate new alternatives to these conventional antimicrobial agents, such as DHA and its derivatives.

At concentrations of 31.25, 62.50 and 93.75 µg/mL against the tested organisms (*S. aureus* ATCC 25923), DHA growth curve profiles showed antibacterial properties. This is

consistent with the fact that MBC values could not be determined in the concentration range tested against the same microorganisms used to obtain the MIC values, thus suggesting that antimicrobial properties of DHA are mainly due to bacterial growth inhibition.

Regarding microencapsulation and stability studies of DHA, encapsulation efficiency of the compound attained $99.49\% \pm 0.05\%$ and the stability studies demonstrated that DHA remained stable within alginate microspheres (PP% $60.00\% \pm 0.05\%$, PE% $88.12\% \pm 0.05\%$). Therefore, this study considers the encapsulation of the diterpene in alginate an excellent way to maintain its physicochemical characteristics.

In the *Artemia salina* toxicological study [41], DHA demonstrated not to have toxicity, and although in the SRB assay it exhibited an IC_{50} value of $19.69 \pm 7.40 \mu\text{g/mL}$, the 72 h test is considered more stressful towards the HaCaT cells than the 24 h assay as performed by Huh et al. [42]. These preliminary toxicological studies demonstrate that further studies in this area need to be performed using other methods.

To recapitulate, screening of DHA antimicrobial activity evidenced the potential inhibition of planktonic and biofilm growth in a battery of yeasts, Gram-positive and Gram-negative bacteria. Probably the diterpenoid influenced the membrane integrity in all microorganisms and helped to eradicate most biofilm cells. The significant reduction in cell attachment makes diterpenoids an ideal antiadhesive with potential as antibiofilm coating for medical devices. Diterpenes have also been frequently reported to be active against microorganisms [17]. Terpenes are thought to act at different levels in bacteria: 1) disturbing the membrane, thereby, inhibiting respiration and ion transport processes in bacterial cells; 2) altering the lipid composition of the cell membrane, and thus, cell hydrophobicity, which lead to the eradication of the biofilm [18,19]. Soon, it will be imperative to develop and optimize antimicrobial assays, in order to elucidate the mechanisms of action of diterpenes and how they perform to eradicate bacterial biofilms.

The results obtained in this study provide preliminary scientific validation upon the known ethnopharmacological uses of (dehydro)abiatic acids. Regardless of the renewed interest on natural compounds and their biological applications, it is decisive to improve the studies of DHA and its derivatives, evaluate their possible uses, understand their safety and unravel their mechanism of action on specific targets.

5. Conclusions

One of the most current serious health treats are biofilms infections, mainly because of the existence of antibiotic resistant strains. Using a unique test, as MIC, to assay planktonic (biofilm) susceptibility to antibiotics may be a possible explanation for treatment failure and the appearance of resistances. Though most of the methods performed in this study are time consuming, they are relatively not expensive and easily reproduced. Here, the results of the MIC with or without the Bioburden challenge, MBC, MBIC with or without Bioburden challenge and growth curve study have highlighted the interesting activity of DHA, acknowledge that further studies of this compound are needed: mechanism of action; optimized methods; other studies like minimal biofilm eradication concentration (MBEC), among others; the development of novel compounds with antibacterial and antibiofilm activity.

Author Contributions: Conceptualization, C.F. and P.R.; methodology, C.F., P.R., C.P.R., I.N., E.N., and M.P.; formal analysis and investigation, I.N. and C.P.R.; data analysis, I.N., P.R., C.P.R., C.F. and E.M.D.-M.; writing—original draft preparation, I.N. and E.M.D.-M.; writing—review and editing, I.N., E.M.D.-M., E.N., C.F. and P.R.; supervision, P.R., C.P.R. and C.F.; All authors have read and agreed to the published version of the manuscript.

Funding: This research was funded by Fundação para a Ciência e a Tecnologia (FCT, Portugal), through projects UIDP/04567/2020 and UIDB/04567/2020 and COFAC—Cooperativa de Formação e Animação Cultural, CRL by the Seed Funding project COFAC/ILIND/CBIOS/1/2020 and CBIOS/COFAC/FIPID/2/2019.

Institutional Review Board Statement: Not applicable.

Informed Consent Statement: Not applicable.

Data Availability Statement: Data available on request due to restrictions e.g., privacy or ethical. The data presented in this study are available on request from the corresponding author.

Acknowledgments: E.M.D-M gratefully acknowledges being the recipient of a predoctoral FPU 2019 fellowship from the University of Alcalá.

Conflicts of Interest: The authors declare no conflicts of interest.

References

- World Health Organization. *Antimicrobial Resistance: Global Report on Surveillance 2014*; WHO: Geneva, Switzerland, 2014; p. 257.
- World Health Organization. *Prevention of Hospital-Acquired Infections: A Practical Guide*; WHO: Geneva, Switzerland, 2002; p. 64.
- O'Neill, J. *Antimicrobial Resistance: Tackling a Crisis for the Health and Wealth of Nations*; Wellcome Trust: London, UK, 2014; p. 20.
- Sefton, A.M. Mechanisms of antimicrobial resistance—Their clinical relevance in the new millennium. *Drugs* 2002, 62, 557–566.
- Patel, R. Clinical impact of vancomycin-resistant enterococci. *J. Antimicrob. Chemother.* 2003, 51, 13–21.
- Mitchell, M.O. Antibacterial agents against methicillin-resistant *Staphylococcus aureus* and vancomycin-resistant *Enterococcus*. *Antimicrob. Agents Med. Chem.* 2007, 16, 243–247.
- Rice, L.B. The clinical consequences of antimicrobial resistance. *Curr. Opin. Microbiol.* 2009, 12, 476–481.
- World Health Organization Anti-Infective Drug Resistance Surveillance and Containment Team. *WHO Global Strategy for Containment of Antimicrobial Resistance*; WHO: Geneva, Switzerland, 2001; p. 99.
- Alekshun, M.N.; Levy, S.B. Molecular mechanisms of antibacterial multidrug resistance. *Cell* 2007, 128, 1037–1050.
- Palmer, A.C.; Kishony, R. Understanding, predicting and manipulating the genotypic evolution of antibiotic resistance. *Nat. Rev. Genet.* 2013, 14, 243–248.
- Delcour, A.H. Outer membrane permeability and antibiotic resistance. *Biochim. Biophys. Acta Proteins Proteom.* 2009, 1794, 808–816.
- Penesyan, A.; Gillings, M.; Paulsen, I.T. Antibiotic discovery: Combatting bacterial resistance in cells and in biofilm communities. *Molecules* 2015, 20, 5286–5298.
- Vega, N.M.; Gore, J. Collective antibiotic resistance: Mechanisms and implications. *Curr. Opin. Microbiol.* 2014, 21, 28–34.
- de la Fuente-Nunez, C.; Refuiveille, F.; Fernandez, L.; Hancock, R.E.W. Bacterial biofilm development as a multicellular adaptation: Antibiotic resistance and new therapeutic strategies. *Curr. Opin. Microbiol.* 2013, 16, 580–589.
- Gaspar-Marques, C.; Rijo, P.; Simões, M.F.; Duarte, M.A.; Rodriguez, B. Abietanes from *Plectranthus grandidentatus* and *P. hereiroensis* against methicillin- and vancomycin-resistant bacteria. *Phytomedicine* 2006, 13, 267–271.
- Rijo, P.; Simões, M.F.; Francisco, A.P.; Rojas, R.; Gilman, R.H.; Vaisberg, A.J.; Rodriguez, B.; Moiteiro, C. Antimycobacterial metabolites from *Plectranthus*: Royleanone derivatives against *Mycobacterium tuberculosis* strains. *Chem. Biodivers.* 2010, 7, 922–932.
- Rijo, P.; Esteves, M.; Simões, M.; Silva, A.; Duarte, A.; Rodriguez, B. Antimicrobial activity of 7 α -acetoxy-6 β -hydroxyroyleanone 12-O-benzoyl esters. *Planta Med.* 2008, 74, PB81.
- Hu, X.Y.; Logue, M.; Robinson, N. Antimicrobial resistance is a global problem—a UK perspective. *Eur. J. Integr. Med.* 2020, 36, 101136.
- Söderberg, T.A.; Holm, S.; Gref, R.; Hallmans, G. Antibacterial effects of zinc-oxide, rosin, and resin acids with special reference to their interactions. *Scand. J. Plast. Reconstr. Surg. Hand. Surg.* 1991, 25, 19–24.
- Findlay, B.; Zhanel, G.G.; Schweizer, F. Cationic amphiphiles, a new generation of antimicrobials inspired by the natural antimicrobial peptide scaffold. *Antimicrob. Agents Chemother.* 2010, 54, 4049–4058.
- Lai, X.Z.; Feng, Y.; Pollard, J.; Chin, J.N.; Rybak, M.J.; Bucki, R.; Epan, R.F.; Epan, R.M.; Savage, P.B. Ceragenins: Cholic acid-based mimics of antimicrobial peptides. *Acc. Chem. Res.* 2008, 41, 1233–1240.
- CLSI. *Performance Standards for Antimicrobial Susceptibility Testing*, 29th ed.; Clinical and Laboratory Standards Institute: Wayne, PA, USA, 2019; p. 25.
- Rijo, P.; Matias, D.; Fernandes, A.S.; Simões, M.F.; Nicolai, M.; Reis, C.P. Antimicrobial plant extracts encapsulated into polymeric beads for potential application on the skin. *Polymers* 2014, 6, 479–490.
- Stepanovic, S.; Vukovic, D.; Hola, V.; Di Bonaventura, G.; Djukic, S.; Cirkovic, I.; Ruzicka, F. Quantification of biofilm in microtiter plates: Overview of testing conditions and practical recommendations for assessment of biofilm production by staphylococci. *Apmis* 2007, 115, 891–899.
- Hammer, K.A.; Carson, C.F.; Riley, T.V. Influence of organic matter, cations and surfactants on the antimicrobial activity of *Melaleuca alternifolia* (tea tree) oil *In Vitro*. *J. Appl. Microbiol.* 1999, 86, 446–452.
- Boakye, Y.D.; Agyare, C.; Hensel, A. Anti-infective properties and time-kill kinetics of *Phyllanthus muellerianus* and its major constituent, geraniin. *Med. Chem.* 2016, 6, 95–104.
- Reis, C.P.; Neufeld, R.J.; Ribeiro, A.J.; Veiga, F. Nanoencapsulation, I. Methods for preparation of drug-loaded polymeric nanoparticles. *Nanomedicine* 2006, 2, 8–21.

28. Reis, C.P.; Neufeld, R.J.; Ribeiro, A.J.; Veiga, F. Nanoencapsulation II. Biomedical applications and current status of peptide and protein nanoparticulate delivery systems. *Nanomedicine* 2006, 2, 53–65.
29. Hotha, K.K.; Reddy, S.P.K.; Raju, V.K.; Ravindranath, L.K. Forced degradation studies: Practical approach-Overview of regulatory guidance and literature for the drug products and drug substances. *Int. Res. J. Pharm.* 2013, 4, 78–85.
30. Charde, M.S.; Kumar, J.; Welankiwar, A.S.; Chakole, R.D. Review: Development of forced degradation studies of drugs. *Int. J. Adv. Pharm.* 2013, 2, 34–39.
31. Guidance for Industry: Q1B Photostability Testing of New Drug Substances and Products. In Proceedings of the International Conference on Harmonisation of Technical Requirements for Registration of Pharmaceuticals for Human Use (ICH), online, 1 May 1996; p. 14.
32. Dacevic, M.; Isakovic, A.; Podolski-Renic, A.; Isakovic, A.M.; Stankovic, T.; Milosevic, Z.; Rakic, L.; Ruzdijic, S.; Pesic, M. Purine nucleoside analog-sulfinosine modulates diverse mechanisms of cancer progression in multi-drug resistant cancer cell lines. *PLoS ONE* 2013, 8, e54044.
33. Meyer, B.N.; Ferrigni, N.R.; Putnam, J.E.; Jacobsen, L.B.; Nichols, D.E.; McLaughlin, J.L. Brine shrimp: A convenient general bioassay for active plant constituents. *Planta Med.* 1982, 45, 31–34.
34. Alanís-Garza, B.A.; Gonzalez-Gonzalez, G.M.; Salazar-Aranda, R.; de Torres, N.W.; Rivas-Galindo, V.M. Screening of antifungal activity of plants from the northeast of Mexico. *J. Ethnopharmacol.* 2007, 114, 468–471.
35. Silva, C.O.; Rijo, P.; Molpeceres, J.; Figueiredo, I.V.; Ascensao, L.; Fernandes, A.S.; Roberto, A.; Reis, C.P. Polymeric nanoparticles modified with fatty acids encapsulating betamethasone for anti-inflammatory treatment. *Int. J. Pharm.* 2015, 493, 271–284.
36. Gu, W.; Qiao, C.; Wang, S.F.; Hao, Y.; Miao, T.T. Synthesis and biological evaluation of novel *N*-substituted 1*H*-dibenzo *a,c* carbazole derivatives of dehydroabiatic acid as potential antimicrobial agents. *Bioorg. Med. Chem. Lett.* 2014, 24, 328–331.
37. Liu, H.; Zhao, Y.; Zhao, D.; Gong, T.; Wu, Y.; Han, H.; Xu, T.; Peschel, A.; Han, S.; Di, Q. Antibacterial and anti-biofilm activities of thiazolidione derivatives against clinical staphylococcus strains. *Emerg. Microbes Infect.* 2015, 4, e1.
38. Daeschlein, G. Antimicrobial and antiseptic strategies in wound management. *Int. Wound J.* 2013, 10 (Suppl. 1), 9–14.
39. Ferro, B.E.; van Ingen, J.; Wattenberg, M.; van Soolingen, D.; Mouton, J.W. Time-kill kinetics of antibiotics active against rapidly growing mycobacteria. *J. Antimicrob. Chemother.* 2015, 70, 811–817.
40. Vichai, V.; Kirtikara, K. Sulforhodamine B colorimetric assay for cytotoxicity screening. *Nat. Protoc.* 2006, 1, 1112–1116.
41. Ntungwe, N.E.; Domínguez-Martín, E.M.; Roberto, A.; Tavares, J.; Isca, V.; Pereira, P.; Cebola, M.J.; Rijo, P. Artemia species: An important tool to screen general toxicity samples. *Curr. Pharm. Des.* 2020, 26, 2892–2908.
42. Huh, W.B.; Kim, J.E.; Kang, Y.G.; Park, G.; Lim, T.G.; Kwon, J.Y.; Song, D.S.; Jeong, E.H.; Lee, C.C.; Son, J.E.; et al. Brown pine leaf extract and its active component trans-communic acid inhibit UVB-induced MMP-1 expression by targeting PI3K. *PLoS ONE* 2015, 10, e0128365.

Communication

Insight the Biological Activities of Selected Abietane Diterpenes Isolated from *Plectranthus* spp.

Przemysław Sitarek ¹, Monika Toma ², Epole Ntungwe ³, Tomasz Kowalczyk ⁴,
Ewa Skala ¹, Joanna Wieczfinska ⁵, Tomasz Śliwiński ² and Patricia Rijo ^{3,6,*}

¹ Department of Biology and Pharmaceutical Botany, Medical University of Lodz, Muszyńskiego 1, 90-151 Łódź, Poland; przemyslaw.sitarek@umed.lodz.pl (P.S.); ewa.skala@umed.lodz.pl (E.S.)

² Laboratory of Medical Genetics, Faculty of Biology and Environmental Protection, University of Lodz Pomorska 141/143, 90-236 Lodz, Poland; monikatoma3@gmail.com (M.T.); tomasz.sliwinski@biol.uni.lodz.pl (T.Ś.)

³ Research Center for Biosciences and Health Technologies (CBIOS), Universidade Lusófona de Humanidades e Tecnologias, 1749-024 Lisboa, Portugal; epole.ntungwe@ulusofona.pt

⁴ Department of Molecular Biotechnology and Genetics, University of Lodz, S. Banacha 12/16, 90-237 Lodz, Poland; tomasz.kowalczyk@biol.uni.lodz.pl

⁵ Department of Immunopathology, Medical University of Lodz, Żeligowskiego 7/9, 90-752 Lodz, Poland; joanna.wieczfinska@umed.lodz.pl

⁶ Instituto de Investigação do Medicamento (iMed.U LISBOA), Faculdade de Farmácia, Universidade de Lisboa, 1649-003 Lisboa, Portugal

* Correspondence: patricia.rijo@ulusofona.pt; Tel: +351-217515500; Fax: +351-217577006

Received: 28 December 2019; Accepted: 22 January 2020; Published: 28 January 2020



Abstract: Natural compounds isolated from plants are excellent starting points in drug design and have been widely studied as anticancer agents; they hence find use in a considerable proportion of anticancer drugs. The genus *Plectranthus* (Lamiaceae) comprises a large and widespread group of species with various applications in traditional medicine. Therefore, the aim of the present study was to determine the effectiveness of treatment with four abietane diterpenoids isolated from *P. madagascariensis* and *P. ecklonii*, 6,7-dehydroroyleanone, 7 β ,6 β -dihydroxyroyleanone, 7 α -acetoxo-6 β -hydroxyroyleanone and parvifloron D, in initiating apoptosis in a glioma cell line. The pure compounds were found to exhibit anticancer effects in primary H7PX glioma cells line by inducing apoptosis G2/M cell cycle arrest and double-strand breaks, indicated by increased levels of phosphorylated H2A.X and decreasing mitochondrial membrane potential; they also influenced the expression of pro- and anti-apoptotic genes (*Bax*, *Bcl-2*, *TP53*, or *Cas-3*). Our findings indicate that these compounds may offer potential as beneficial antitumor drugs but further in vivo studies are needed.

Keywords: natural abietane diterpenes; cytotoxic activity; apoptosis; cell cycle; gene expression; H2A.X; mitochondrial membrane potential

1. Introduction

Glioblastoma multiforme (GBM) is the most malignant and most common form of primary astrocytoma, accounting for more than 60% of all brain tumors in adults [1]. Despite the development of new therapies, it demonstrates high mortality, with patients expecting a median survival period of approximately 14 to 15 months from diagnosis [2,3]. There is hence a pressing need to identify new compounds for use in therapy. The plant kingdom is a valuable source of natural compounds with potential anti-cancer activity: many metabolites of plant origin have a broad spectrum of activity and are less toxic to patients than synthetic drugs [4]. One potential source is represented by the plants of the genus *Plectranthus* [5].

The genus *Plectranthus* (Lamiaceae) is located in the tropical and warm regions of the Old World, including Africa, Australia and India [6]. Of 300 species of *Plectranthus*, 62 are reported to be used as traditional medicines, foods, ornamentals, flavorings, animal fodder and materials; however, over 85% of these species are used in medicine. *Plectranthus* is a valuable source of secondary metabolites with proven cytotoxic, antiproliferative, anti-bacterial, anti-fungal, anti-plasmodic, or anti-cancer effects [6,7]. Numerous studies attribute these biological properties to the diterpenes expressed by this genus [8–10]. Our previous studies have demonstrated that the diterpenes isolated from *Plectranthus* genus induce apoptosis in various cancer cell lines, including human myeloid leukaemia, and pancreatic, lung, melanoma, prostate, and breast cancer [11–17]. The present study focuses on the properties of abietane diterpenes (Roy, Deroy, Diroy, and Parv D) isolated from *P. madagascariensis* and *P. ecklonii*. (Figure 1).

P. madagascariensis can be found in regions of South Africa [18] and has been traditionally used for skin ailments, such as treatment of scabies and small wounds. It is also used for colds and asthma [6]. Similarly to other members of this genus, *P. madagascariensis* possesses a number of secondary metabolites with antimicrobial, antioxidant or anticancer properties [15,16]. The essential oil is a rich source of 6,7-dehydroroyleanone (Deroy), i.e., an abietane diterpene with a quinone moiety [15]. However, the acetone extracts are rich in various royleanones, including 7 β ,6 β -dihydroxyroyleanone (Diroy) and 7 α -acetoxy-6 β -hydroxyroyleanone (Roy) [18]. Another *Plectranthus* member, *P. ecklonii*, is highly rich in another abietane diterpene, parvifloron D (Parv D), which has long been known to display potent anticancer activities [19,20].

To gain a greater insight into their potential use in cancer treatment, the present study examines the apoptotic character of these *Plectranthus*-derived abietanes and their activities against a human glioma cell line.

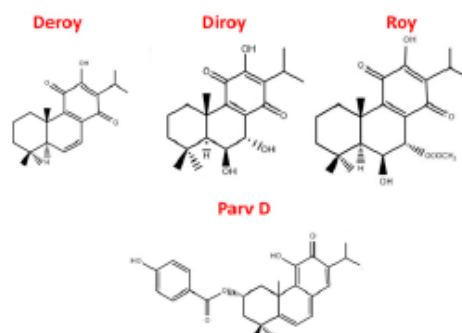


Figure 1. Abietane diterpenes isolated from *P. madagascariensis* and *P. ecklonii*.

2. Materials and Methods

2.1. Plant Material

Plectranthus ecklonii and *Plectranthus madagascariensis* (Lamiaceae family) were cultivated in Instituto Superior de Agronomia Campus (Lisbon University), from seeds provided by the Herbarium of the Botanical Garden of Lisbon, Portugal. Their growth was monitored at Parque Botânico da Tapada da Ajuda from cuttings collected in June and September in the years 2007 and 2008 (provided by the Kirstenbosch National Botanical Gardens, South Africa). Voucher specimens were deposited at Herbarium “João de Carvalho e Vasconcellos” of the “Instituto Superior de Agronomia”, Lisboa (LISI), Portugal.

2.2. Isolation and Identification of Abietane Diterpenes

The abietane diterpene 6,7-dehydroroyleanone (Deroy) was extracted from the essential oil obtained through the hydrodistillation of *P. madagascariensis* leaves and stems in a Clevenger-apparatus, while 7 β ,6 β -dihydroxyroyleanone (Diroy) and 7 α -acetoxy-6 β -hydroxyroyleanone (Roy), were isolated from acetonic extracts of the same plant. Parvifloron D (Parv D) was isolated from an acetonic extract

of the whole plant of *P. ecklonii*. The isolation and identification of all compounds were described earlier [15,19,21].

2.3. Cell Cultures

Our studies were performed on a human primary H7PX glioma cell line obtained from a cancer patient diagnosed with grade 4 glioblastoma multiforme. The study was approved by the Ethical Commission of the Medical University of Lodz, and informed consent was obtained from the patients (Nr. RNN/194/12/KE). Cell lines were maintained in an incubator with 5% CO₂ atmosphere at 100% humidity and 37 °C in DMEM medium supplemented with 10% (*v/v*) heat-inactivated Fetal Bovine Serum (FBS) and 100 U/mL penicillin, 100 µg/mL streptomycin. All cell culture media and components were purchased in Lonza (Basel, Switzerland).

2.4. Cell Viability

MTT assay was employed to measure the viability of primary H7PX glioma cells treated with different concentrations of abietane diterpenes, Deroy, Diroy, Roy, and Parv D. Briefly, cells were seeded at 1×10^4 cells per well in 96-well culture plates and left overnight. In the next step, the cells were incubated for 24 h with the test compounds over a range of concentrations: 0 (control), 0.39, 0.78, 1.56, 3.13, 6.25, 12.5, 25, 50, and 100 µg/mL. Following this, the cells were incubated with 0.5 mg/mL of 3-(4,5-dimethylthiazol-2-yl)-2,5-diphenyl tetrazolium bromide (MTT) at 37 °C for 1.5 h. After this time, MTT was carefully removed and DMSO (100 µL) was added to each well; the mixture was mixed at low speed for 5 min to fully dissolve the formazan crystals. Absorbance was measured at 570 nm with a reference at 630 nm using a Bio-Tek Synergy HT Microplate Reader (Bio-Tek Instruments, Winooski, VT, USA). All experiments were repeated in triplicate. Cell viability was expressed as a percentage relative to the untreated cells, which was defined as 100%. Cell line pictures after treatment were captured using HDCE-X5 digital microscope camera and Scopelimage9.0 software.

2.5. Apoptosis/Necrosis and Cell Cycle Detection by Flow Cytometry

In this experiment, a population of apoptotic and necrotic cells of the primary H7PX glioma cell line was detected using an annexin V-fluorescein isothiocyanate (FITC)/propidium iodide (PI) (BD Biosciences) detection kit according to the manufacturer's protocol. Briefly, the cells were plated into 6-well culture dishes (2×10^5 cells/well) for 24 h prior to the addition of all tested compounds used in this study. Following 24-h incubation with all compounds, the percentage of apoptotic/necrotic cells was determined by the annexin V-FITC/PI assay. The proportions of the H7PX cell line in different cell cycle phases was assessed using PI/RNase staining buffer (BD Biosciences). Cells were seeded as mentioned above and treated with IC₅₀ concentrations of Deroy, Diroy, Roy and Parv D. After 24-h incubation, the medium was discarded, and the cells were collected and fixed with 70% cold ethanol for at least one hour at −20°C. In the next step, the cells were suspended in staining buffer. Cell analysis was performed using CytoFlex Beckman Coulter.

2.6. ELISA Measurement of γ -H2A.X

The primary H7PX glioma cell line was cultured at a density of 1×10^4 cells per well with vehicle or with the following abietane diterpenes: Deroy, Diroy, Roy and Parv D. They were administered at the IC₅₀ concentration on black 96-well plates with a clear bottom. The level of phosphorylated H2A.X histone was determined using an H2A.X Phosphorylation Assay Kit (Millipore, Billerica, MA, USA) according to the manufacturer's protocol. Briefly, chemiluminescence detection was performed using a GloMax-Multi device (Promega). The mixtures were incubated for 30 min with 35 µM. Bleomycine as a positive control.

2.7. RNA Isolation and RT-PCR

The cells were plated into 6-well culture dishes (3×10^5 cells/well) for 24 h prior to the addition of Deroy, Diroy, Roy, and Parv D. The total RNA isolation kit (A & A Biotechnology) was used to isolate total RNA from cells treated with the compounds at the IC_{50} value. The obtained RNA was transcribed into cDNA using TranScriba Kit (A&A Biotechnology). Following this, the expression of four genes (*Bax*, *Bcl-2*, *Cas-3*, *TP53*) was measured by qRT-PCR using TaqMan[®] Real-Time PCR Master Mix (Life Technologies, Carlsbad, CA, USA) and Agilent Technologies Stratagene Mx300SP working on MxPro software Santa Clara, CA, USA). TaqMan probes (Life Technologies) were used to analyse genes and *18S rRNA* (Life Technologies) was included as a reference gene. The PCR was performed as follows: 95 °C for 10 min, 40 cycles of 95 °C for 15 s and 60 °C for 60 s.

2.8. Mitochondrial Membrane Potential (MMP)

Mitochondrial membrane potential was determined by the fluorescent probe JC-1 (5,6,6-tetrachloro-1,1,3,3-tetraethylbenzimidazolylcarbocyanine iodide). Briefly, cells were seeded into black 96-well tissue culture plates with transparent bottom (Greiner Bio-One, Monroe, NC, USA) at a density of 1×10^5 cells/well (primary H7PX glioma cells) in 50 μ L culture medium and allowed to grow overnight. The next day, cells were treated with indicated concentration IC_{50} of Deroy, Diroy, Roy and Parv D for 24 h. Finally, the cells were preincubated with 5 μ M JC-1 in the HBSS in a CO_2 incubator at 37 °C for 30 min. Prior to measurements, the cells were centrifuged ($300 \times g$ for 10 min at 22 °C) then washed twice with the HBSS. Further procedure has been described previously [22,23].

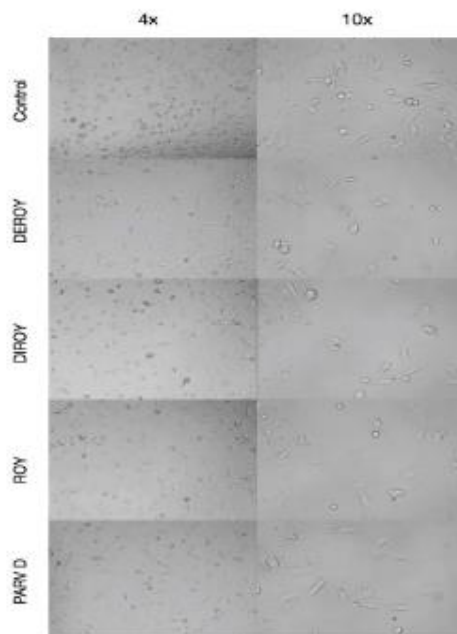
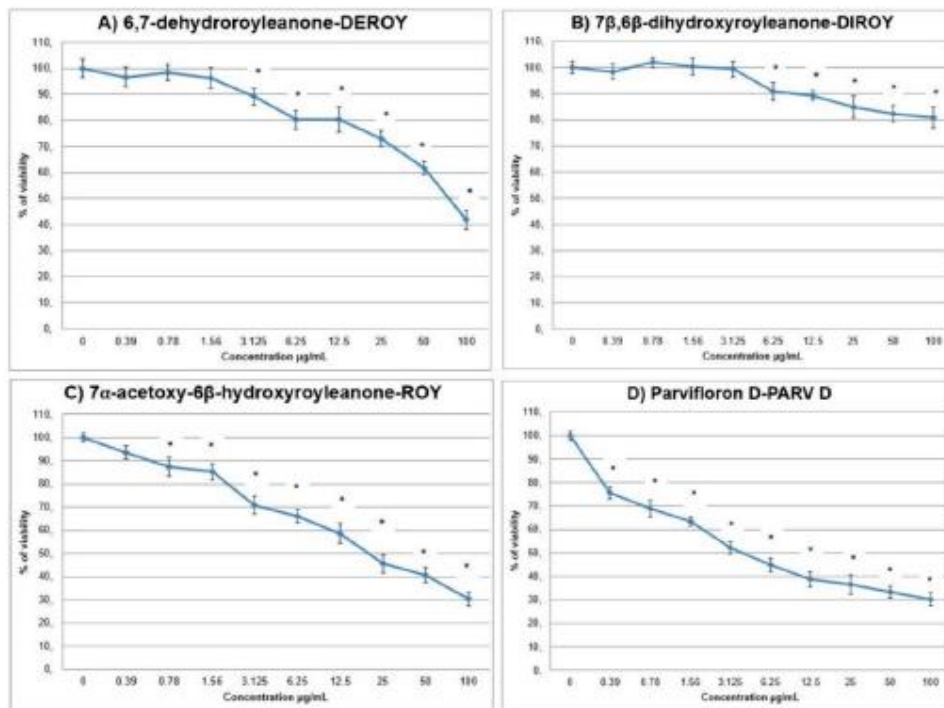
2.9. Statistical Analysis

Data are presented as the mean \pm standard error (SD) of the mean of at least three independent experiments. The Shapiro–Wilk test was used to determine the normality of the distribution of results. The Kruskal–Wallis test with multiple comparisons of average ranks and the one-way analysis of variance (ANOVA) with the Tukey post hoc test were used to determine differences between samples. Statistica 13 software was used for all calculations. * $P < 0.05$ was considered to indicate a statistically significant difference.

3. Results

3.1. Cytotoxic Activity

The primary H7PX glioma cells were treated with the four compounds (6,7-dehydroroyleanone-Deroy, 7 β ,6 β -dihydroxyroyleanone-Diroy, 7 α -acetoxy-6 β -hydroxyroyleanone-Roy and parvifloron D-Parv D) at concentrations of 0–100 μ g/mL for 24 h, and the percentage of viable cells was determined by MTT assay. It was found that all tested compounds reduced the viability of human H7PX cells but to different degree: the H7PX cells were most sensitive to Parv D, Roy and Deroy compared to Diroy in the tested range of concentrations (Figure 2A–D). Figure 2E show primary H7PH glioma cells after 24 h treatment with IC_{50} concentrations of compounds at different magnifications.



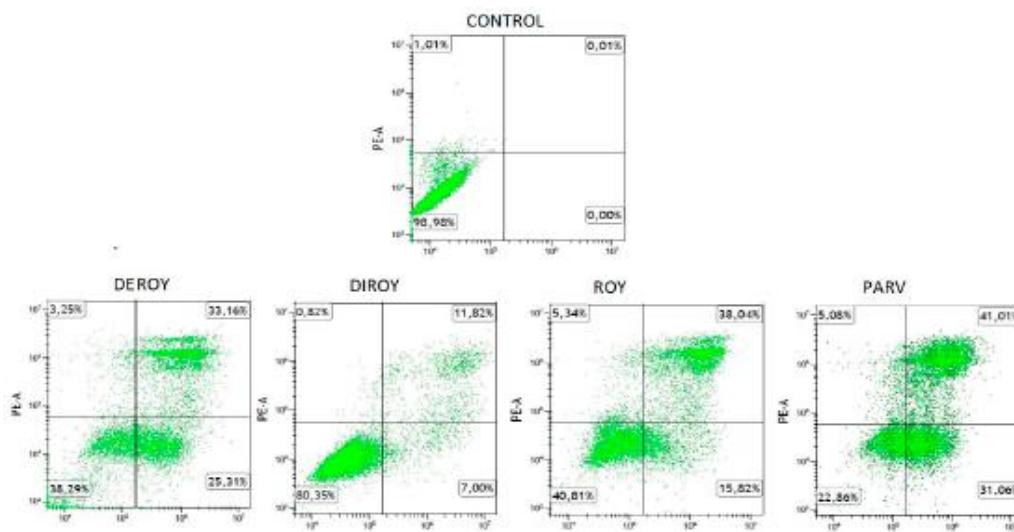
E)

Figure 2. (A–E) The effect of Deroxy, Diroy, Roy, and Parv D treatment on cell viability after 24-h incubation. The primary H7PX glioma cells were treated with different concentrations of these compounds. The y-axis shows the percentage of cell viability. Data are reported as means \pm SD of three determinations. * $P < 0.05$ vs untreated cells E. Representative photos showing primary H7PH glioma cells after 24 h treatment with IC₅₀ concentrations of given compounds at different magnifications 4 \times and 10 \times . Photos were captured with HDCE-X5 digital microscope camera using ScopeImage9.0 software.

3.2. Analysis of Apoptotic/Necrotic and Cell Cycle Distribution

Flow cytometry analysis was performed to verify whether the tested compounds induced apoptosis or necrosis and whether they resulted in an altered cell cycle distribution. The experiment showed that cell death after treatment occurred mainly through the apoptosis pathway. A greater percentage of early and late apoptosis was observed after treatment with Deroy, Diroy, Roy, and Parv D) (62%, 20%, 53%, and 73%, respectively) compared to untreated cells. Cell cycle distribution analysis revealed increased H7PX cell percentage in G2/M phase after treatment with Deroy, Diroy, Roy, and Parv D compared to the untreated cells, with the respective percentages being 51%, 23%, 58%, and 60% (Figure 3A–D).

(A)



(B)

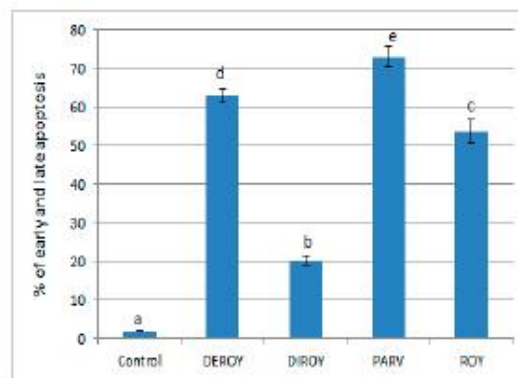
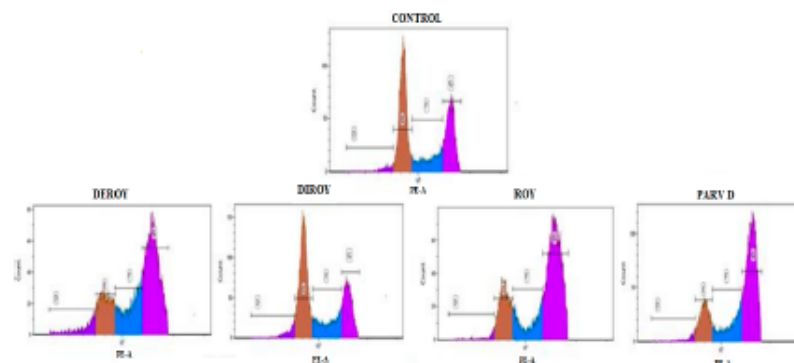


Figure 3. Cont.

(C)



(D)

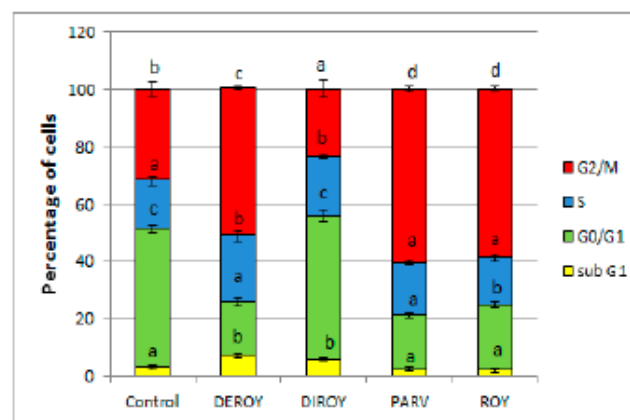


Figure 3. (A) Representative histograms of apoptosis/necrosis analysis of primary H7PX glioma cells after 24-h treatment with abietane diterpenes (B) The percentage of primary H7PX glioma cells in early and late apoptosis after 24-h treatment (C) Representative histograms of primary H7PX glioma cell cycle distribution after 24-h treatment (D) The percentages of individual cell cycle phases after 24-h treatment. The values represent mean \pm SD of three independent experiments. Different letter indicates differences at the $P < 0.05$. In all figures, Deroy (6,7-dehydroxyroyleanone), Diroy (7 β ,6 β -dihydroxyroyleanone), Roy (7 α -acetoxy-6 β -hydroxyroyleanone) and Parv D (parvifloron D).

3.3. The Level of Phosphorylated H2A.X in H7PX Cells after Treatment of Abietane Diterpenes

Increased levels of phosphorylated H2A.X, which marks indicating the presence of DSBs (double strand breaks), were observed in cells treated with the diterpenes in comparison to untreated control cells. Significant increase in the amount of phosphorylated H2A.X histone was visible after treatment with Deroy, Roy, and Parv D. The effect after treatment with Diroy was mediate (Figure 4).

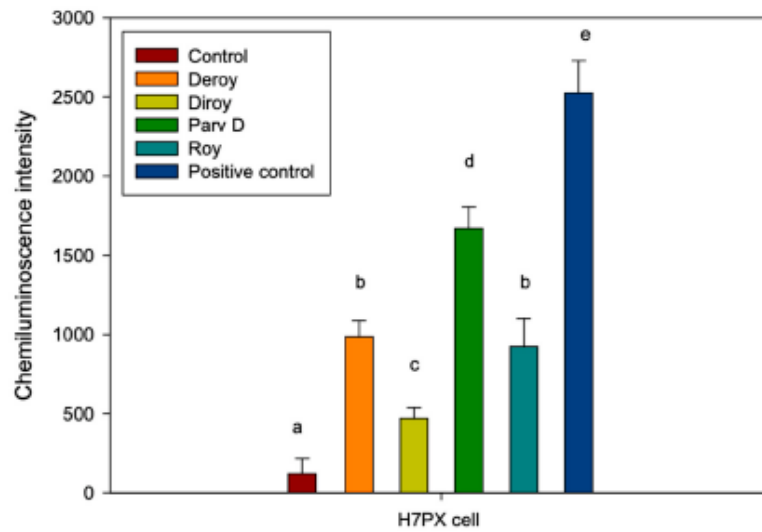


Figure 4. The levels of phosphorylated H2A.X identified in H7PX cell line treated with 6,7-dehydroroyleanone (Deroy), 7β,6β-dihydroxyroyleanone (Diroy), 7α-acetoxy-6β-hydroxyroyleanone (Roy) and parvifloron D (Parv D), indicating the presence of DSBs. Cells were treated with all compounds for 24 h. The mean values ± SD of γ-X2A.X were calculated from three independent ELISA experiments. Different letters indicate significant differences at $P < 0.05$. Bleomycine was used as a positive control.

3.4. Determination of the mRNA Expression of TP53, Bax, Bcl-2, and Cas-3 using RT-PCR

The effect of Deroy, Diroy, Roy, and Parv D treatment at IC₅₀ on gene expression was also analyzed. Following 24-h treatment, the mRNA expression of TP53, Bax, and Cas-3 was found to be significantly increased in the cells treated with all tested compounds, while that of Bcl-2 was decreased (Figure 5).

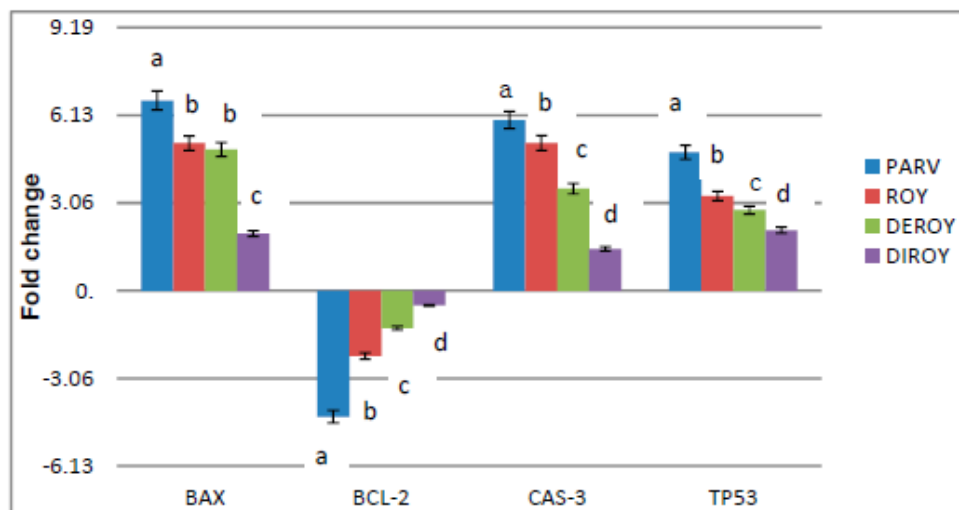


Figure 5. RT-PCR analysis of the mRNA expression of TP53, Cas-3, Bax, and Bcl-2 in H7AX glioma cells following treatment with Deroy, Diroy, Roy, and Parv D for 24 h. The transcript level of each gene was normalized to the expression of a reference gene (*18S rRNA*). Data is presented as fold change in cells treated with tested compounds versus untreated, control cells, in which the expression level of the genes was set as 1. The mean values ± SD were calculated from triplicate. The same letter at the same genes are not significantly different at the level of $P > 0.05$.

3.5. Effect of Deroy, Diroy, Roy, and Parv D on Mitochondrial Membrane Potential Loss ($\Delta\Psi_m$) in Primary H7PX Glioma Cells

The mitochondrial membrane potential was measured by staining with JC-1 after treatment with IC_{50} for each of the pure compounds (Deroy, Diroy, Roy, and Parv D), to evaluate the functional status of mitochondria. After 24 h exposure, mitochondrial membrane potential was significantly decreased in primary H7AX glioma cells after treatment with all compounds compared to the control (Figure 6). Our data suggest that mitochondrial dependent mechanism contributed to abietane diterpenes (Deroy, Diroy, Roy, and Parv D) mediated apoptosis in primary H7AX glioma cells by mitochondrial membrane depolarization.

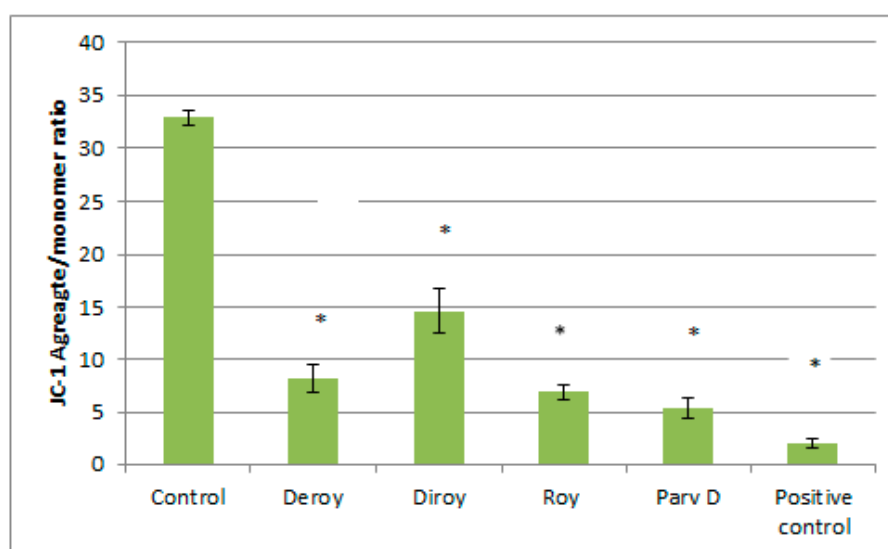


Figure 6. The effect of Deroy, Diroy, Roy, and Parv D on mitochondrial membrane potential in primary H7PX glioma cells. MMP is expressed as a ratio of 530 nm/590 nm to 485 nm/538 nm (aggregates to monomer) fluorescence, as quantified with a fluorescent plate reader after JC-1 staining. The data represent means \pm SD. * $P < 0.05$ Control vs. Deroy, Diroy, Roy, and Parv D. Temozolomide was used as a positive control.

4. Discussion

Although the plant kingdom constitutes an extraordinary reservoir of novel bioactive organic molecules, this resource was not fully appreciated until the recent worldwide surge of interest in herbal medicine [24]. Medicinal plants can biosynthesize chemical compounds with different biological properties [25], and these have long been used for treating various civilization diseases including cancer [26–29]. Cancer is an established global health problem known to account for nine million deaths globally, and is expected to increase to about 15 million by 2030 [27]. Therefore, there is a pressing need to identify new natural compounds with potential anti-cancer activity. The biological studies revealed that abietanes are active and Parv D is the most active compound. Parv D has a very apolar feature on the positions C-6 and C-7, like Deroy, which also has an apolar part on the same C-6 and C-7 positions. Roy follows this tendency in the C-6 and C-7 polarity and bioactivity. The compound Diroy is the less bioactive abietane and this is in agreement with the more polar feature on the C-6 and C-7 positions. This polar structure-activity relationship could be explained due to a better membrane interaction [11–17].

Many studies have shown that plant extracts or pure compounds isolated from plants are able to induce apoptosis in various types of cancer [22,30–32]. Although revolutions in the modern drug industry have given rise to a trend of replacing herbal remedies with modern drugs, studies of natural

compounds from herbal plants and their activities are still of interest for drug discovery; they are not only characterized by better absorption but also by lower toxicity than chemical drugs. Around 60% of drugs in current use, including anti-cancer drugs, are of plant origin. Of these, the abietane diterpenes have demonstrated strong biological activity, particularly with regard to their cytotoxic, anti-proliferative and antimicrobial potential [17,32,33]. Therefore, in recent years, many molecular studies have examined their influence on various cancer cells [15,19].

The present study describes the first evaluation of the potential of pure 6,7-dehydroroyleanone (Deroy), 7 β ,6 β -dihydroxyroyleanone (Diroy), 7 α -acetoxy-6 β -hydroxyroyleanone (Roy), and parvifloron D (Parv D) isolated from *P. madagascariensis* and *P. ecklonii* to induce apoptosis in a primary glioma cell line. These members of the Lamiaceae family are particularly interesting due to their high content of secondary metabolites, including abietane diterpenes [6].

Apoptosis is an important process because it involves several biochemical and morphological changes that eventually lead to cell death [34]. The most frequently-mutated genes, independent of those giving rise to the tumor, are the TP53 DNA damage checkpoint tumor suppressor genes [35]. The initiation of apoptosis itself is also dependent on the balance of two apoptosis regulators, *Bcl-2* and *Bax*: A balance needs to be maintained between *Bcl-2* and *Bax* expression to ensure cell survival [36], with higher *Bcl-2* expression resulting in the inhibition of apoptosis [37,38]. Current anticancer therapies, such as chemotherapeutic agents and radiotherapy, act by inducing apoptosis in various cancer cells [39]. Literature reports suggest that the common initial event in the majority of apoptotic processes involves DNA damage or damage to various other critical molecules [40,41].

The four compounds tested in the present study were found to induce apoptosis and G2/M cell cycle arrest, and increase phosphorylated H2A.X levels, by influencing the expression of pro- and anti-apoptotic genes in the H7PX glioma cell line. Of these four compounds, Deroy, Roy, and Parv D displayed stronger anticancer activity than Diroy. These findings represent the first example of apoptosis induction in a H7PX glioma cell line.

Other preliminary studies demonstrate that the same tested compounds (6,7-dehydroroyleanone, 7 α -acetoxy-6 β -hydroxyroyleanone and parvifloron D) isolated from *P. madagascariensis* and *P. ecklonii* induced apoptosis in CCRF-CEM and A549 cell lines by damaging DNA, increasing ROS levels and mitochondrial copy number, decreasing mitochondrial membrane potential and by changing the level of expression of pro and anti-apoptotic genes (manuscript in draft).

Not only did Parv D demonstrate the greatest cytotoxic effect against the tested H7PX line in the present study, it also displayed the strongest cytotoxic activity against CCRF-CEM and A549 cell lines in other experiments (manuscript in draft). Similarly, Burmistrova et al. report that Parv D displays cytotoxic activity against various leukemia cell lines, including HL-60, U-937, MOLT-3, and K-562 [6]. They propose that the mechanism of action is associated with a decrease in mitochondrial membrane potential and the release of cytochrome c, and that it may be amplified by inhibition of extracellular signal-regulated kinases (ERKs) 1/2 signaling; they also suggest it may be caused by a mechanism dependent on intracellular ROS generation in leukemia cells [19]. Santos-Rebelo et al. also report that Parv D obtained from *P. ecklonii* displayed a cytotoxic effect on pancreatic cell lines [42]. In the present study, it was found that of the four tested compounds, Parv D treatment induced the highest level of phosphorylated histone. It has been noted that increased levels of phosphorylated H2A.X are indicative of the presence of DSBs, which have been proposed as a cause of apoptosis induction in cancer cells [43]. In a previous study, Garcia et al. also reported that Parv D increased the level of mtDNA damage in a CCRF-CEM cell line [15].

While the H7PX glioma cells tested in the present study were found to be resistant to Diroy treatment across the tested range of concentrations, with cell viability scores of 80–100% being observed, the CCRF-CEM and A549 lines tested elsewhere were far more sensitive (manuscript in draft). We suspect that the difference observed in the potential of the four tested compounds may be attributed to a combination of differences in their chemical structures (functional groups) and the sensitivities of the cancer cells. Garcia et al. report that Deroy obtained from *P. madagascariensis* is able

to induce apoptosis by triggering the intrinsic cell death pathway in cancer cells through the activation of caspases-3 and caspases-9 [15]. From these promising results, three of the tested compounds demonstrate strong cytotoxic effects on the H7PX glioma human cell line; however, more research based on molecular chemistry, molecular docking analysis and ideally, in vivo studies, is needed to clarify their interactions with cellular components.

5. Conclusions

Pure parvifloron D, 7 α -acetoxy-6 β -hydroxyroyleanone and 6,7-dehydroroyleanone isolated from *P. madagascariensis* and *P. ecklonii* may exhibit anticancer effects in H7PX glioma cell line by inducing apoptosis, G2/M cell cycle arrest and DSBs (double strand breaks), indicated by elevated phosphorylated H2AX, decreasing mitochondrial membrane potential, and by changing the level of expression of pro and anti-apoptotic genes. These natural compounds may hence prove beneficial in the treatment of different cancer types. We hope that our discoveries may contribute to the development of new anticancer treatments, but further in vivo evaluation is urgently required.

Author Contributions: Conceptualization, P.S. and P.R.; methodology, M.T.; E.N. writing—original draft preparation, P.S., P.R. review and editing, E.S., T.Š., J.W.; visualization, T.K., supervision, T.Š., P.R. All authors have read and agreed to the published version of the manuscript.

Funding: This research received no external funding.

Conflicts of Interest: The authors declare no conflict of interest.

References

- Hanif, F.; Muzaffar, K.; Perveen, K.; Malhi, S.M.; Simjee, S.U. Glioblastoma Multiforme: A Review of its Epidemiology and Pathogenesis through Clinical Presentation and Treatment. *Asian Pac. J. Cancer Prev.* **2017**, *18*, 3–9.
- Aldape, K.; Zadeh, G.; Mansouri, S.; Reifenberger, G.; von Deimling, A. Glioblastoma: Pathology, molecular mechanisms and markers. *Acta Neuropathol.* **2015**, *129*, 829–848. [[CrossRef](#)]
- Cloughesy, T.F.; Cavenee, W.K.; Mischel, P.S. Glioblastoma: From molecular pathology to targeted treatment. *Annu. Rev. Pathol.* **2014**, *9*, 1–25. [[CrossRef](#)]
- Lichota, A.; Gwozdziński, K. Anticancer Activity of Natural Compounds from Plant and Marine Environment. *Int. J. Mol. Sci.* **2018**, *19*, 3533. [[CrossRef](#)]
- Rice, L.R.; Brits, G.J.; Potgieter, C.J.; Van Staden, J. *Plectranthus*: A plant for the future? *S. Afr. J. Bot.* **2011**, *77*, 947–959. [[CrossRef](#)]
- Lukhoba, C.W.; Simmonds, M.S.J.; Paton, A.J. *Plectranthus*: A review of ethnobotanical uses. *J. Ethnopharmacol.* **2006**, *103*, 1–24. [[CrossRef](#)]
- Abdel-Mogib, M.; Albar, H.A.; Batterjee, S.M. Chemistry of the genus *Plectranthus*. *Molecules* **2002**, *7*, 271–301. [[CrossRef](#)]
- Dellar, J.E.; Cole, M.D.; Waterman, P.G. Antimicrobial abietane diterpenoids from *Plectranthus elegans*. *Phytochemistry* **1996**, *41*, 735–738. [[CrossRef](#)]
- Figueiredo, N.L.; De Aguiar, S.R.M.M.; Falé, P.L.; Ascensão, L.; Serralheiro, M.L.M.; Lino, A.R.L. The inhibitory effect of *Plectranthus barbatus* and *Plectranthus ecklonii* leaves on the viability, glucosyltransferase activity and biofilm formation of *Streptococcus sobrinus* and *Streptococcus mutans*. *Food Chem.* **2010**, *119*, 664–668. [[CrossRef](#)]
- Van Zyl, R.L.; Khan, F.; Edwards, T.J.; Drewes, S.E. Antiplasmodial activities of some abietane diterpenes from the leaves of five *Plectranthus* species. *S. Afr. J. Sci.* **2008**, *104*, 62–64.
- Santos-Rebello, A.; Kumar, P.; Pillay, V.; Choonara, Y.E.; Eleutério, C.; Figueira, M.; Viana, A.S.; Ascensão, L.; Molpeceres, J.; Rijo, P.; et al. Development and Mechanistic Insight into the Enhanced Cytotoxic Potential of Parvifloron D Albumin Nanoparticles in EGFR-Overexpressing Pancreatic Cancer Cells. *Cancers* **2019**, *11*, 1733. [[CrossRef](#)]

12. Garcia, C.; Ntungwe, E.; Rebelo, A.; Bessa, C.; Stankovic, T.; Dinic, J.; Díaz-Lanza, A.; Reis, C.; Roberto, A.; Pereira, P.; et al. Parvifloron D from *Plectranthusstrigosus*: Cytotoxicity Screening of *Plectranthus* spp. Extracts. *Biomolecules* **2019**, *10*, 616. [CrossRef]
13. Matias, D.; Nicolai, M.; Fernandes, A.S.; Saraiva, N.; Almeida, J.; Saraiva, L.; Faustino, C.; Díaz-Lanza, A.M.; Reis, C.P.; Rijo, P. Comparison Study of Different Extracts of *Plectranthus madagascariensis*, *P. neochilus* and the Rare, *P. porcatus* (Lamiaceae): Chemical Characterization, Antioxidant, Antimicrobial and Cytotoxic Activities. *Biomolecules* **2019**, *9*, 179. [CrossRef]
14. Garcia, C.; Teodósio, C.; Oliveira, C.; Oliveira, C.; Díaz-Lanza, A.; Reis, C.; Duarte, N.; Rijo, P. Naturally Occurring *Plectranthus*-derived Diterpenes with Antitumoral Activities. *Curr. Pharm Des.* **2018**, *24*, 4207–4236. [CrossRef]
15. Garcia, C.; Silva, C.O.; Monteiro, C.M. Anticancer properties of the abietane diterpene 6,7-dehydroroyleanone obtained by optimized extraction. *Future Med. Chem.* **2018**, *10*, 1177–1189. [CrossRef]
16. Bernardes, C.E.S.; Garcia, C.; Pereira, F.; Mota, J.; Pereira, P.; Cebola, M.J.; Reis, C.P.; Correia, I.; Piedade, M.F.M.; Minas da Piedade, M.E.; et al. Extraction optimization, structural and thermal characterization of the antimicrobial abietane 7 α -acetoxo-6 β -hydroxyroyleanone. *Mol. Pharm.* **2018**, *15*, 1412–1419. [CrossRef]
17. Rijo, P.; Duarte, A.; Francisco, A.P.; Semedo-Lemsaddek, T.; Simões, M.F. In vitro antimicrobial activity of royleanone derivatives against gram-positive bacterial pathogens. *Phyther. Res.* **2014**, *28*, 76–81. [CrossRef]
18. Kubínová, R.; Pořízková, R.; Navrátilová, A.; Farsa, O.; Hanáková, Z.; Bačinská, A.; Cížek, A.; Valentová, M. Antimicrobial and enzyme inhibitory activities of the constituents of *Plectranthus madagascariensis* (Pers.) Benth. *J. Enzyme Inhib. Med. Chem.* **2014**, *29*, 749–752. [CrossRef]
19. Burmistrova, O.; Perdomo, J.; Simões, M.F.; Rijo, P.; Quintana, J.; Estévez, F. The abietane diterpenoid parvifloron D from *Plectranthus ecklonii* is a potent apoptotic inducer in human leukemia cells. *Phytomedicine* **2015**, *22*, 1009–1016. [CrossRef]
20. Nyila, M.A.; Leonard, C.M.; Hussein, A.A.; Lall, N. Bioactivities of *Plectranthus ecklonii* constituents. *Nat. Prod. Commun.* **2009**, *4*, 1177–1180. [CrossRef]
21. Rijo, P.; Simões, M.F.; Francisco, A.P.; Rojas, R.; Gilman, R.H.; Vaisberg, A.J.; Rodríguez, B.; Moiteiro, C. Antimycobacterial metabolites from *Plectranthus*: Royleanone derivatives against *Mycobacterium tuberculosis* strains. *Chem. Biodivers.* **2010**, *7*, 922–932. [CrossRef]
22. Sitarek, P.; Synowiec, E.; Kowalczyk, T.; Śliwiński, T.; Skala, E. An In Vitro Estimation of the Cytotoxicity and Genotoxicity of Root Extract from *Leonurus sibiricus* L. Overexpressing AtPAP1 against Different Cancer Cell Lines. *Molecules* **2018**, *23*, 2049. [CrossRef]
23. Kowalczyk, T.; Sitarek, P.; Skala, E.; Toma, M.; Wielanek, M.; Pytel, D.; Wieczfińska, J.; Szemraj, J.; Śliwiński, T. Induction of apoptosis by in vitro and in vivo plant extracts derived from *Menyanthes trifoliata* L. in human cancer cells. *Cytotechnology* **2019**, *71*, 165–180. [CrossRef]
24. Kooti, W.; Servatyari, K.; Behzadifar, M.; Asadi-Samani, M.; Sadeghi, F.; Nouri, B.; Marzouni, Z.H. Effective Medicinal Plant in Cancer Treatment, Part 2: Review Study. *J. Evid. Based Complementary Altern. Med.* **2017**, *22*, 982–995. [CrossRef]
25. Sakarkar, D.M.; Deshmukh, V.N. Ethnopharmacological review of traditional medicinal plants for anticancer activity. *Int. J. Pharm. Tech. Res.* **2011**, *3*, 298–308.
26. Cragg, G.M.; Newman, D.J. Plants as a source of anti-cancer agents. *J. Ethnopharmacol.* **2005**, *100*, 72–79. [CrossRef]
27. Desai, A.G.; Qazi, G.N.; Ganju, R.K.; El-Tamer, M.; Singh, J.; Saxena, A.K.; Bedi, Y.S.; Taneja, S.C.; Bhat, H.K. Medicinal Plants and Cancer Chemoprevention. *Curr. Drug Metab.* **2008**, *9*, 581–591. [CrossRef]
28. Badolato, M.; Carullo, G.; Cione, E.; Aiello, F.; Caroleo, M.C. From the hive: Honey, a novel weapon against cancer. *Euro. J. Med. Chem.* **2017**, *142*, 290–299. [CrossRef]
29. Aiello, F.; Armentano, B.; Polerà, N.; Carullo, G.; Loizzo, M.R.; Bonesi, M.; Maria Cappello, S.; Capobianco, L.; Tundis, R. From Vegetable Waste to New Agents for Potential Health Applications: Antioxidant Properties and Effects of Extracts, Fractions and Pinoembrin from *Glycyrrhiza glabra* L. Aerial Parts on Viability of Five Human Cancer Cell Lines. *J. Agric. Food Chem.* **2017**, *65*, 7944–7954. [CrossRef]
30. Sitarek, P.; Kowalczyk, T.; Santangelo, S.; Białas, A.J.; Toma, M.; Wieczfińska, J.; Śliwiński, T.; Skala, E. The Extract of *Leonurus sibiricus* Transgenic Roots with AtPAP1 Transcriptional Factor Induces Apoptosis via DNA Damage and Down Regulation of Selected Epigenetic Factors in Human Cancer Cells. *Neurochem. Res.* **2018**, *43*, 1363–1370. [CrossRef]

31. Skala, E.; Synowiec, E.; Kowalczyk, T.; Śliwiński, T.; Sitarek, P. Rhaponticum carthamoides Transformed Root Extract Has Potent Anticancer Activity in Human Leukemia and Lung Adenocarcinoma Cell Lines. *Oxid Med. Cell Longev.* **2018**, *9*. [CrossRef] [PubMed]
32. Burmistrova, O.; Simões, M.F.; Rijo, P.; Quintana, J.; Bermejo, J.; Estévez, F. Antiproliferative activity of abietane diterpenoids against human tumor cells. *J. Nat. Prod.* **2013**, *23*, 1413–1423. [CrossRef] [PubMed]
33. Fronza, M.; Lamy, E.; Günther, S.; Heinzmann, B.; Laufer, S.; Merfort, I. Abietane diterpenes induce cytotoxic effects in human pancreatic cancer cell line MIA PaCa-2 through different modes of action. *Phytochemistry* **2012**, *78*, 107–119. [CrossRef] [PubMed]
34. Elmore, S. Apoptosis: A Review of Programmed Cell Death. *Toxicol. Pathol.* **2007**, *35*, 495–516. [CrossRef]
35. Negrini, S.; Gorgoulis, V.G.; Halazonetis, T.D. Genomic instability—an evolving hallmark of cancer. *Nat. Rev. Mol. Cell Biol.* **2010**, *11*, 220–228. [CrossRef]
36. Huang, F.; Yang, Z.; Yu, D.; Wang, J.; Li, R.; Ding, G. Sepia ink oligopeptide induces apoptosis in prostate cancer cell lines via caspase-3 activation and elevation of Bax/Bcl-2 ratio. *Mar. Drugs* **2012**, *10*, 2153–2165. [CrossRef]
37. Tasyriq, M.; Najmuldeen, I.A.; In, L.L.; Mohamad, K.; Awang, K.; Hasima, N. 7alpha-Hydroxy-beta-Sitosterol from *Chisocheton tomentosus* Induces Apoptosis via Dysregulation of Cellular Bax/Bcl-2 Ratio and Cell Cycle Arrest by Downregulating ERK1/2 Activation. *Evid. Based Complement. Alternat. Med.* **2012**, 765316.
38. Del Poeta, G.; Ammatuna, E.; Lavorgna, S.; Capelli, G.; Zaza, S.; Luciano, F.; Ottone, T.; Del Principe, M.I.; Buccisano, F.; Maurillo, L.; et al. The genotype nucleophosmin mutated and FLT3-ITD negative is characterized by high bax/bcl-2 ratio and favourable outcome in acute myeloid leukaemia. *Br. J. Haematol.* **2010**, *149*, 383–387. [CrossRef]
39. Safarzadeh, E.; Shotorbani, S.S.; Baradaran, B. Herbal Medicine as Inducers of Apoptosis in Cancer Treatment. *Adv. Pharm. Bull.* **2014**, *4*, 421–427. [CrossRef]
40. Makin, G.; Dive, C. Apoptosis and cancer chemotherapy. *Trends Cell Biol.* **2001**, *11*, 22–26. [CrossRef]
41. Fulda, S.; Debatin, K.M. Targeting apoptosis pathways in cancer therapy. *Curr. Cancer Drug Targets* **2004**, *4*, 569–576. [CrossRef] [PubMed]
42. Santos-Rebelo, A.; Garcia, C.; Eleutério, C.; Bastos, A.; Coelho, S.C.; Coelho, M.A.N.; Molpeceres, J.; Viana, A.S.; Ascensão, L.; Pinto, J.F.; et al. Development of Parvifloron D-loaded Smart Nanoparticles to Target Pancreatic Cancer. *Pharmaceutics* **2018**, *10*, 216. [CrossRef] [PubMed]
43. Kinner, A.; Wu, W.; Staudt, C.; Iliakis, G. γ -H2AX in recognition and signaling of DNA double-strand breaks in the context of chromatin. *Nucleic Acids Res.* **2008**, *36*, 5678–5694. [CrossRef] [PubMed]



© 2020 by the authors. Licensee MDPI, Basel, Switzerland. This article is an open access article distributed under the terms and conditions of the Creative Commons Attribution (CC BY) license (<http://creativecommons.org/licenses/by/4.0/>).

Accepted manuscript
doi: 10.1680/jgrma.18.00074

Submitted: 24 September 2018

Published online in 'accepted manuscript' format: 30 January 2020

Manuscript title: Green Extraction of *Sambucus nigra* L. for Potential Application in Skin Nanocarriers

Authors: Ana Henriques Mota¹, Joana Marçalo Andrade², Epole Ntungwe³, Paula Pereira^{3,4}, Maria João Cebola^{3,4,5}, Maria Gabriela Bernardo-Gil⁴, Jesús Molpeceres⁶, Patrícia Rijo³, Ana Semedo Viana⁷, Lia Ascensão⁸, Catarina Pinto Reis^{1,9}

Affiliations: ¹Research Institute for Medicines, Faculdade de Farmácia, Universidade de Lisboa, Av. Prof. Gama Pinto, 1649-003 Lisboa, Portugal. ²Universidade Lusófona de Humanidades e Tecnologias, Campo Grande 376, 1749-024 Lisboa, Portugal. ³Research Center for Biosciences & Health Technologies, Universidade Lusófona de Humanidades e Tecnologias, Campo Grande 376, 1749-024 Lisboa, Portugal. ⁴Centro de Recursos Naturais e Ambiente, Instituto Superior Técnico, Universidade de Lisboa, Av. Rovisco Pais, 1049-001 Lisboa, Portugal. ⁵Escola Náutica Infante D. Henrique, Av. Eng. Boneville Franco, 2770-058 Paço de Arcos, Portugal. ⁶Department of Biomedical Sciences, Faculty of Pharmacy, University of Alcalá, Ctra. A2 km 33.600, 28871 Alcalá de Henares, Spain. ⁷Centro de Química e Bioquímica, Faculdade de Ciências, Universidade de Lisboa, Campo Grande 1749-016 Lisboa, Portugal. ⁸Centro de Estudos do Ambiente e do Mar (CESAM), Faculdade de Ciências da Universidade de Lisboa, Edifício C2, Campo Grande, 1749-016 Lisboa, Portugal. ⁹Biophysics and Biomedical Engineering, Faculdade de Ciências, Universidade de Lisboa, Campo Grande, 1749-016 Portugal.

2

Accepted manuscript
doi: 10.1680/jgrma.18.00074

Corresponding author: Catarina Pinto Reis, Research Institute for Medicines, Faculdade de Farmácia, Universidade de Lisboa, Av. Prof. Gama Pinto, 1649-003 Lisboa, Portugal. Tel.: +351 217946400, Fax: +351 217946470
E-mail: catarinapintoreis@gmail.com

Abstract

Sambucus nigra L. is a well-known species with a wide range of medicinal properties. In this work, supercritical fluids extracts were obtained from fresh and dried elderberries of *S. nigra* L.: A (dried berries, ethanol absolute), B (dried berries, ethanol 96%), C (dried berries, ethanol 70%) and D (fresh berries, ethanol 96%). In vitro enzymatic activities of those extracts, antioxidant activity (AA) and preliminary safety assessment were evaluated. The most promising extracts were selected for encapsulation in polymeric nanoparticles (NPs). All extracts demonstrated low to moderate AA and they did not reveal any antimicrobial activity for the bacteria and yeasts tested. No toxic effect in *Artemia salina* model was observed. Due to the antioxidant, anti-collagenase and anti-elastase activities, A and C extracts were successfully encapsulated into PLGA NPs. According to morphology analysis, empty PLGA NPs had a rounded irregular shape and seemed somewhat collapsed, while PLGA NPs loaded with extract A or C exhibited a spherical shape with a smooth surface. The encapsulation process produced a slight increase in the NPs' size. Further studies will include the optimization of extract conditions to improve the yield of extraction as well as the in vivo evaluation of these nanocarriers.

1. Introduction

The genus *Sambucus* L. from the *Adoxaceae* (Caprifoliaceae) family ^{1,2} is widely known for their traditional medicinal properties ³⁻⁷. It is commonly named elder or elderberry. *S. nigra* has a wide variety of applications in traditional medicine such as sedative agent, anti-hemorrhoid, insect repellent, as well as, to treat burns and infected wounds, neuralgia and rheumatism ^{7,8}. To the best of our knowledge, so far, a clear scientific confirmation of those properties is still lacking.

The *S. nigra* contain many antioxidants, vitamins, bioflavonoids, minerals, pectin substances, organic acids and dietary fibers ⁹⁻¹¹. Many phytochemical studies have been performed so far, revealing the presence of hexahydrofarnesyl acetone, 4-vinyl guaiacol, between flavonoids (cyanidin-3-*O*-sambubioside, CyS), cyanidin-3-*O*-glucoside (CyG, or chrysanthemine), cyanidin-3-sambubioside-5-glucoside, cyanidin-3,5-diglucoside, rutin, or quercetin-3-*O*-rutinoside, quercetin-3-*O*-glucoside, kaempferol-3-*O*-rutinoside, isorhamnetin-3-*O*-rutinoside, isorhamnetin-3-*O*-glucoside and 5-*O*-caffeoylquinic acid ^{1, 3, 7, 9, 11-13}, among others.

In terms of antioxidant activity (AA), antioxidants are protection agents, reducing oxidative damage in the human body ¹⁴. The antioxidant and pharmacological properties are generally connected with the presence of phenolic compounds (mainly, flavonoids and polyphenols) ¹⁴⁻¹⁶. Flavonoids are able to interact with free radicals involved in initiating oxidation reactions or by reactive oxygen species (ROS) produced during chain reactions ¹⁴. In previous studies, the alcoholic extract of dried elderberries is suggested to act as an antioxidant

5

by neutralization of free radicals and inhibition of the co-oxidation reactions of linoleic acid and β -carotene^{14,17}.

Over the last decades, supercritical fluid extraction (SFE) has been increasingly seen as an interesting extraction process for the production of high added-value products for the nutraceutical and functional food industries, as well as for the pharma and cosmetic industries¹⁸. The SFE technique has been extensively reported as being a more selective, overall cost-efficient and, above all, environmentally friendly. In general, this method avoids the use of organic solvents, solving the problem of its disposal when compared with conventional methods of extraction^{9,18}. Because of its "greenness", the extraction of bioactive compounds from natural sources has been one of the most important application of SFE^{18,19}.

The main scope of this study was to expand our limited knowledge on the potential therapeutic and health-promoting properties of *S. nigra* extracts produced by SFE. The aim of this work was to prepare 4 different extracts from *S. nigra* by using SFE and to verify the *in vitro* antimicrobial, antioxidant (AA), inhibitory effects on different enzymes such as collagenase (Coll), elastase (Ela), tyrosinase (Tyr) and acetylcholinesterase (AChE). It was also the aim of this work the assessment of the toxicity of *S. nigra* elderberries extracts. Then, the most promising extract(s) for potential application in prevention and/or treatment of skin disorders was encapsulated into polymeric nanoparticles (NPs) and briefly characterized in terms of size, polydispersivity index (PdI), morphology and pH. It is well known that polymeric nanoparticles (NPs) have been used to increase the stability of the encapsulated agents over the time^{20,21} and to promote the increase the skin permeation of extracts/compounds and having

great importance into future advances to medicine and pharmacy²²⁻²⁴. In this work, polylactide-co-glycolide (PLGA) was selected because it is safe (generally regarded as safe, GRAS, by FDA) and it has been demonstrated to enhance the stability the compounds and it has been widely employed in drug delivery systems²⁴⁻²⁷.

2. Materials

2.1 Biological material

Fruits of *S. nigra* were collected at the harvesting period (September to October 2016) from plants cultivated at Moimenta da Beira (Beira Alta, north of Portugal, lat. 40° 59'06"N; long. 7° 37' 03" W; 695 m alt.). Samples of fresh and dried berries were used in the extraction experiments. The drying process of the berries occurred at room temperature with low relative humidity (≤ 50 %) using carbon dioxide (N48, 99.998%) which was purchased from Air Liquid (Lisbon, Portugal). *Artemia salina* eggs and *Artemia* salt were supplied from JBL GmbH and Co. KG (Neuhofen, Germany).

2.2 Chemicals

Ethanol absolute was acquired from Riedel-deHaëen (Seelze, Germany). L-tyrosine, tyrosinase from mushroom, kojic acid, 2,2-diphenyl-1-picrylhydrazyl (DPPH), AChE, acetylcholine iodide $\geq 98\%$ (AChI), quercetin, N-succinyl-Ala-Ala-Ala-p-nitroanilide (SANA), N-[3-furyl-acryloyl]-Leu-Gly-Pro-Ala (FALGPA), Pluronic[®] F127, ursolic acid and collagenase from *Clostridium histolyticum* type IA were purchased from Sigma-Aldrich (Steinheim, Germany). The 5,5'-dithio-bis-(2-nitrobenzoic acid) (Ellman reagent, DTNB) and

Oleic Acid were purchased from Fluka Chemicals (Buchs, Switzerland). The 1,2,3,4-Tetrahydro-5-aminoacridine (tacrine) was obtained from Cayman Chemical Company (Michigan, USA). Elastase from porcine pancreas was acquired from Alfa Aesar (Karlsruhe, Germany). Tricine buffer was supplied by Amresco and Folin reagent was obtained from Merck (Darmstadt, Germany). Mueller-Hinton agar (MHA) and Sabouraud dextrose agar (SDA) were acquired from Biokar[®] Diagnostics. Purasorb[®] PLDG 5002-PLGA Ratio L/G % 50:50 (MW between 45.000 and 75.000 Da) was supplied from Purac Biomaterials (Gorinchen, Netherlands) and Epigallocatechin gallate (EGCG) was obtained from Sigma Aldrich (Saint Louis, USA). All other chemicals were of analytical grade.

3. Experimental

3.1 *Supercritical fluid extraction*

Samples of fresh and dried berries were used in the extraction experiments.

SFE experiments were carried out in the apparatus (Figure 1), following the procedure, already described elsewhere²⁸. The liquid CO₂ from the supply cylinder passed through a high-pressure tubing coil immersed in a cold (≈ 5 °C) water bath (Frigedor REG, Selecta, Barcelona, Spain) and, then, it was compressed to the desired extraction pressure by an air driven liquid pump (model MCPV-71, Haskell, Burbank, California, USA). The pressure was controlled with a back-pressure regulator (model BSH4-02-11-N/S-01129, RHPS, Amsterdam, Netherlands) and measured by a digital manometer (model DPG-111, Dwyer, Michigan, Indiana, USA). Inside the temperature-controlled oven, the fluid was heated to the desired temperature. At working conditions, SCCO flow through the material inside the extraction

8

vessel (316SS) that was placed in a temperature-controlled oven (Digital temperature controller, model TS3-50020, Dwyer, Michigan, Indiana, USA). The extraction cell was a tubular extractor of 278 mL of capacity, internal diameter $D = 37.9$ mm, height/diameter ratio $H/D = 6.5$. After leaving the extractor, the stream of CO_2 carrying the extract flow through a sequence of pressure expansion valves (Hoke, Spartanburg, SC, USA) and the stream pressure was reduced to atmospheric pressure. The extract was collected in a stainless-steel vessel. The CO_2 flow rate was measured with a flowmeter (Omega FLDC3302G, Stamford, Connecticut, USA) and the total mass of CO_2 used in the assays was measured with a gas counter (Arlete Compact LPG, Soprocom, Sintra, Portugal). Spent CO_2 was vented to the atmosphere. The tubing expansion line was always cleaned with ethanol after each extraction stage through a dedicated entry point placed in the line immediately before the first expansion valve. The residue was assured to the total yield. The supercritical conditions were maintained after solvent addition. Ethanol-containing extracts were then evaporated using a rotary evaporator with vacuum control at a temperature of 35 °C. The evaporation was repeated until constant weight was achieved. Dried extracts were kept at a -20 °C until further analysis. In the experiments where a co-solvent was used, its addition to the system was made via a liquid pump (LDC-Analytical type NSI-33R minipump, USA) linked to a liquid mass flow meter (model 5882, Flomega, Brooks Instrument, Veenendaal, The Netherlands) equipped with a rate totalizer (Beka, BA 558C, Hitchin, Hertford-shire, UK) connected to the gas line between the high-pressure tubing coil immersed in the water bath and the extraction vessel.

In this work, different ethanol degrees (100% or absolute, 96%, and 70%, v/v) were used

as co-solvent. Briefly, 30 g of ground elderberries (dried or fresh) were placed inside a 278 cm³ stainless steel pressure vessel. Extracts were obtained by SFE at 20 MPa, 40 °C and a CO₂ flow of 0.3 kg/h. The extraction time was 2 h. During the first hour, only CO₂ was used as extraction fluid, targeting the less polar components. To broaden the range of extracted compounds, in the second hour, ethanol (either ethanol absolute, ethanol 96%, v/v, or ethanol 70%, v/v) was used as co-solvent to get the more polar components. Ethanol was pumped into the extraction cell at a flow rate of 0.090 kg/h. The assays were made at 200 bars, 1 h for the extraction only with CO₂ and another hour for the extraction with CO₂ and solvent, for fresh and dried berries. Our aims were also to verify the influence of the presence of co-solvent and the presence of water in extract's activities. In this way, we analyzed the extraction of only CO₂ and CO₂ with co-solvent, testing all polarities of the compounds in our samples (extracts).

Table 1 summarizes the experimental conditions used and identifies the extracts obtained (A, B, C and D) and the extraction yield (% m/m) was calculated according Eq. 1.

$$Yield (\%) = \frac{Weight\ of\ extract\ (g)}{Weight\ of\ dried\ plant\ (g)} \times 100 \quad (1)$$

3.2 Antimicrobial activity

Antimicrobial activity was studied by using the agar well diffusion method. A preliminary antimicrobial activity screening of all the extracts was carried out using two Gram-positive bacteria (*S. aureus* ATCC 25923 and *Enterococcus faecalis* ATCC 29212), two Gram-negative bacteria (*P. aeruginosa* ATCC 27853 and *E. coli* ATCC 25922), *C. albicans* ATCC 10231 and *Saccharomyces cerevisiae* ATCC 2601. The assay followed the guidelines of the Clinical &

10

Laboratory Standards Institute (CLSI): Methods for Dilution Antimicrobial Susceptibility Tests for Bacteria That Grow Aerobically (M07-A9), 2012, protocol with slight modifications. Bacteria were cultured in Mueller-Hinton agar, while the yeasts were cultured in Sabouraud agar. Briefly, 100 μ L of a standardized microorganism suspension, corresponding to 0.5 McFarland, was used to inoculate a Petri dish of solid Mueller-Hinton medium. These suspensions were spread over the medium surface using a sterile swab. Subsequently, agar wells were made of approximately 5.0 mm in diameter with a Pasteur pipette. Then, 50 μ L of each sample, dimethyl sulfoxide (DMSO, negative control), vancomycin/norfloxacin/nystatin (all three were positive controls) and microorganisms (*S. aureus*, *E. faecalis*, *P. aeruginosa*, *E. coli*, *C. albicans* and *S. cerevisiae*), were added on each of the wells. Plates were incubated at 37 °C for 24 h. After this period of time, the diameters of the inhibition zones were measured and the results were expressed in millimetres (mm) as in previous studies²⁹.

3.3 Antioxidant activity

The AA was studied using the DPPH method previously described³⁰⁻³² because it is considered very rapid method and easily to perform. To evaluate the sample AA through the free radical scavenging test, the change in optical density of DPPH radicals was monitored. Extracts from fresh and dried elderberries were diluted with the respective solvents of extraction and a DPPH solution (0.5 mM) in ethanol 70% (v/v) was added. After 30 min, the absorbance was measured at 517 nm (Thermo Scientific Evolution 300 UV-vis, Altrincham, UK).

The inhibitory effect of DPPH was then calculated according to Eq. 2:

$$\text{Scavenging activity (\%)} = \frac{\text{Absorbance control} - \text{Absorbance sample}}{\text{Absorbance control}} \times 100 \quad (2)$$

This study was made in triplicate at a sample concentration of 0.1 mg of extract/mL and quercetin was used as the reference standard for this procedure. Linear graph of concentration versus percentage inhibition was plotted and IC₅₀ values were calculated. The AA of each sample was expressed in terms of IC₅₀ (micromolar concentration required to inhibit DPPH radical formation by 50%), calculated from the inhibition curve.

3.4 *In vitro* enzymatic activities

SFE from fresh and dried berries of *S. nigra* were also investigated for the *in vitro* inhibitory effects on several enzymes such as collagenase (Coll), elastase (Ela), tyrosinase (Tyr) and acetylcholinesterase (AChE).

3.4.1 Collagenase inhibition assay

The assay was performed in 50 mM Tricine buffer (pH 7.5 with 400 mM NaCl and 10 mM CaCl₂) according previous study³³. Coll from *Clostridium histolyticum* (EC.3.4.23.3) was dissolved in buffer for use at an initial concentration of 0.8 units/mL according to the supplier's activity data. The synthetic substrate FALGPA was dissolved in Tricine buffer to 2 mM. Absorbance at 405 nm was immediately measured after adding substrate and then continuously for 10 min. EGCG was used as a positive control at a concentration of 250 μM (0.114 mg/mL)^{33, 34}. Each plant extract was assayed in triplicate for Coll inhibition by measuring its effect on Coll activity, using a 96-well reader (Thermo Scientific Multiskan FC, Shanghai, China).

3.4.2 Elastase inhibition assay

This assay was performed in 0.2 mM Tris-HCl buffer (pH 8.0) according previous study³³. Porcine pancreatic Ela was dissolved to make a 3.33 mg/mL stock solution in sterile water. The substrate SANA was dissolved in the buffer at 1.6 mM. Ursolic acid at a concentration of 250 μ M was used as a positive control. Absorbance was measured at 405 nm immediately measured following addition of the substrate and then every 30 seconds for 3 min. The percentage inhibition for both Coll and Ela assays was calculated according to Eq. 3.

$$\text{Enzyme inhibition activity (\%)} = \left(\frac{OD_{Control} - OD_{Sample}}{OD_{Control}} \right) \times 100 \quad (3)$$

Each plant extract was tested for Ela inhibition by measuring its effect on Ela activity using 96-well reader in triplicate.

3.4.3 Tyrosinase inhibition assay

The reaction was carried out as previously described in a 50 mM PBS buffer (pH 6.8), 0.5 mM L-tyrosine, 10 mg/mL of kojic acid and 5000 U/mL of mushroom Tyr at 30 °C according previous studies^{33, 35, 36}. After incubation, absorbance was measured at 450 nm every 2 min, for a total of 10 min using 96-well reader. The velocity reaction of control or inhibitor was calculated using Eq. 4 and the enzyme inhibition activity using Eq. 3.

$$\text{Velocity reaction of control or inhibitor} = \frac{\text{Corrected absorbance}}{\text{time (min)}} \quad (4)$$

All tests were carried out in triplicate at a sample and positive control concentration of 50 μ g of extract/mL and kojic acid was used as the reference standard for this procedure.

3.4.4 Acetylcholinesterase inhibition assay

The AChE enzymatic activity was carried out as previously described in a 50 mM HEPES buffer (pH 8.0) containing 100 U of AChE and 3 μ M tacrine at 30 °C according previous studies^{31,33}. After incubation, absorbance was measured at 405 nm every 30 seconds, for a total of 3 min using a 96-well reader. All tests were carried out in triplicate with a sample and positive control concentration of 50 μ g of extract/m. Tacrine was used as the reference standard for this procedure.

3.5 Preliminary toxicity assay

This assay consists in a test where the lethality of *A. salina* L. brine shrimp was assessed by stereomicroscopic observation^{37, 38}. *A. salina* was chosen by their importance in the ecosystems. For this assay, an aquarium air pump (HI-FLOTM Single Type 4000), a thermostat Cabinet Aqua Lytic® and a stereomicroscope (CETI Belgium) were used. All the extracts were tested at a concentration of 10 mg/mL in triplicate. The number of dead *A. salina* larvae (*nauplii*) was recorded after 24 h and the lethal concentration (%) was calculated according to Eq. 5.

$$\text{Lethal concentration (\%)} = \frac{\text{Total}_{nauplii} - \text{Alive}_{nauplii}}{\text{Total}_{nauplii}} \times 100 \quad (5)$$

3.6 Encapsulation of the selected extract into polymeric nanoparticles

PLGA nanoparticles were prepared by emulsification/solvent diffusion method³⁹. Briefly, for empty nanoparticles, PLGA polymer was dissolved in a mixture acetone:ethanol (8:2, v/v) and

then added to an aqueous phase consisting of 0.1 % Pluronic[®] F127⁴⁰. For extract-loaded PLGA NPs, the same procedure was used with ratio of PLGA:extract (2:1, m/m).

3.7 *Physical-chemical and morphological characterization of PLGA nanoparticles*

Mean particle size, polydispersity index (PdI) of NPs suspension were measured by dynamic light scattering (DLS) in a Malvern Zetasizer Nano S (Malvern Instruments, Worcestershire, UK). Experiments were conducted in triplicate. Results were expressed as the mean \pm SD (n = 3).

Particle morphology was observed by scanning electron microscopy (SEM) according previous study⁴¹. For that purpose, aliquots (10 μ L) of aqueous suspensions containing empty and extract-loaded PLGA NPs were carefully scattered over a round glass coverslip previously coated with poly-L-lysine and attached to the microscope stubs surfaces. Afterwards, samples were left to dry in a desiccator, being subsequently coated with a thin layer of gold and observed on a JEOL 5200LV scanning electron microscope (JEOL Ltd., Tokyo, Japan) at an accelerating voltage of 20 kV. Images were recorded digitally.

Other method used to analyze the NPs morphology was atomic force microscopy (AFM) which it was carried out in a Multimode 8 HR Microscope (Bruker, Billerica, Massachusetts, USA). For AFM imaging, a drop of ca. 50 μ L of each sample, was placed on a freshly cleaved mica surface and allowed to adsorb for ca. 30 min. Afterwards, the samples were dried in a stream of N₂, and analyzed in intermittent mode. The images were acquired in ambient conditions (ca. 21 °C), using etched silicon tips with a resonance frequency of ca. 320 kHz (NCHV, Bruker, USA), at a scan rate of approximately 1.3 Hz. For AFM analysis, the samples

15

were prepared by centrifugation at 7378 x g (Centrifuge, Sigma Laborzentrifugen, Osterode am Harz, Germany) during 5 min, followed by resuspension in water. The pH of nanoparticle suspension was also measured (Mettler Toledo, Schwerzenbach, Switzerland).

3.8 Statistical analysis

All results were expressed as means \pm SD. The significance of differences was assessed using One-Way ANOVA for multiple comparisons between the extracts and controls, using Graph Prisma Version 5.03 (GraphPad Software, San Diego, California, USA). The differences were considered significant when $p < 0.05$.

4. Results and discussion

4.1 Yields of extractions

The yields of extraction obtained are presented in Table 1. The yields were relatively low and ranged from $0.8 \pm 0.1\%$ (m/m) for fresh berries with ethanol 96% (v/v) to $9.3 \pm 0.1\%$ (m/m) for dried berries with the same solvent. These results were similar to previous studies using myrtle berries, that presented yields between 0.2 and 3%²⁸. The low yield of extraction of fresh berries could be associated of the SFE technique.

4.2 Antimicrobial activities

In the current study, all extracts obtained from fresh and dried berries did not present any antimicrobial activity against a specific type of bacteria like the *S. aureus*, *E. faecalis*, *P. aeruginosa*, *E. coli*, *C. albicans* and *S. cerevisiae*. Some previous studies in the literature have been revealed antimicrobial activities against *S. aureus*, *B. subtilis*, *P. aeruginosa*, *E. coli*, *S.*

16

typhi and *C. albicans*. However, those extracts were not obtained by SFE⁴²⁻⁴⁵ or the type of berries was different. This activity is strongly dependent of the time of collecting, the part of the plant and the specie involved. In a previous work⁴⁶, elderberries presented an inhibition against *H. pylori*, around 30%⁴⁶. In another study, extracts of *S. nigra* presented antimicrobial activity against Gram-positive bacteria (*S. pyogenes*, *Streptococci*) and Gram-negative bacterium (*B. catarrhalis*)⁴⁷. Moreover, the Committee on Herbal Medicinal Products published in EMA⁷ reported that the freeze-dried powder formulations with elderberry presented antibacterium activity against hospital bacteria methicillin resistant *S. aureus* (MRSA)^{7,45}. Although different bacterial species were used in these reports, the antibacterial activity of *S. nigra* berries extract could not be confirmed in our results, which requires further information.

4.3 Antioxidant activity using the DPPH method

The AA of the SFE extracts obtained from *S. nigra* berries are displayed in Table 2. The extracts A and B from dried berries showed a significant AA ($p < 0.0001$), with extract A presenting the higher value when compared to the extract B. However, these activities were lower than the positive control but they were similar to those described in the literature for some plant extracts studied^{48,49}. In a specific study made by Oktyabrsky *et al.*⁵⁰, values of $11.9 \pm 2.7\%$ and $16.7 \pm 1.5\%$ were observed for the AA of plant extracts from *Arctium tomentosum* and *Lathyrus gmelinii*, respectively. In case of extracts C and D, they were not statistically significant when compared to the negative control. Extracts A and B presented statistically significant differences when compared with the negative control (DMSO), and

17

extract A was the one that exhibited the most statistically significant difference.

Therefore, we can suggest that our extract from dried berries with absolute ethanol of *S. nigra* presented a similar AA. In a particular study, Seabra *et al.*^{13,49} showed that the presence of AA was mainly due to the presence of phenolic compounds, flavonoids, CyG, CyS, anthocyanins (mainly Cyanidin-3-*O*-glucoside) and rutin and that the amount of each compound strongly depends on the used extraction conditions. By other side, a study of Dawidowicz *et al.*¹⁴ revealed that there is not a direct correlation between the level of flavonoids in the extracts and their AA. Thus, for now, our values of AA might be attributed to the characteristics of the extraction. The results of SFE strongly depend on pressure, temperature and flow rate of the supercritical CO₂ and the values of AA achieved probably mean that these parameters need to be further optimized, since the therapeutic or cosmetic application of extracts as antioxidant agents is also very important. In fact, ROS have a useful function in the skin barrier against microorganisms involved, as example, in acne⁵¹. ROS result of metabolic reactions that occur in the human body, being controlled by natural enzymatic and non-enzymatic antioxidants³². When there is an uncontrolled production of ROS and an unbalanced mechanism of antioxidant protection occur, many other diseases as cancer and accelerated ageing appear^{14, 48, 52}. In addition, the cytokine cascades are also affected by ROS producing inflammatory reactions in photo-ageing or inducing the synthesis of a series of matrix metalloproteinases and, as a consequence, producing collagen degradation in wrinkles, and causing melanocyte dysfunction in skin hyperpigmentation⁵³. Moreover, ROS also stimulate the formation of nuclear factor κ B (NF- κ B); promote TNF formation and, in

consequence, activate T lymphocytes and keratinocytes. This last activation may cause the production and the release of cytokines IL, TNF, interferon (IFN), lipopolysaccharide (LPS), etc. In the case of skin inflammation, it generally begins by CD4+ in T lymphocytes (regulated by Toll-like receptors (TLRs)), neutrophil infiltration which form ROS and protease enzymes leading to follicular wall rupture of sebaceous gland. In consequence, the composition of sebum changes (linoleic acid) causes hyperkeratinization and a reduction in skin desquamation. These changes may cause microcomedos. Microcomedos may develop to comedos and other inflammatory lesions⁵¹. Other consequences are an attenuation of the physiological levels of different antioxidants (as: α -tocopherol, ubiquinol-10, ascorbic acid and glutathione) in the epidermis and dermis⁵⁴.

4.4 *In vitro* enzymatic activities tested

4.4.1 Collagenase inhibition activity

The anti-Coll activities of the four SFE *S. nigra* extracts are presented in Table 3. The best results were found with the extract A and B. Extractions using absolute ethanol (extract A) resulted in Coll inhibition, similar or even higher than that obtained with positive control ($84.7 \pm 3.7\%$ and $84.4 \pm 0.9\%$, respectively). Overall, Coll inhibition decreases with the decrease of the alcohol concentration used in the extraction process. This trend was not observed with the other enzymes studied (Ela, Tyr and AChE). In the same extraction conditions, the difference of the Coll inhibition activity found between extract B (dried berries) and extract D (fresh berries) suggests that the drying process may also contribute to different enzyme inhibitions. The value of Coll inhibition has a high potential for therapeutic uses. In a study by Thring *et al.*

19

(2009), the anti-Coll activity was investigated in 23 plant extracts commonly found as components in cosmetic formulations and only the extract from white tea gave a value of Coll inhibition ($\approx 89\%$) higher than the obtained here for extract A³⁴. All the other extracts presented a percentage of Coll inhibition lower than that shown by white tea.

Coll is an enzyme that degrades the extracellular matrix and hydrolyses the triple-helical collagen, in physiological and *in vitro* conditions, using synthetic peptides as substrates³⁴. In cases of skin cancer, the collagen matrix is reduced, mainly due to the action of Coll, which suggests a relationship between the Coll, facilitating extracellular matrix breakdown, and tumor invasion⁵⁵.

There is a direct relationship between the content of polyphenols and the Coll inhibition^{15, 16, 34} making reasonable the assumption that extract A may have the highest content of polyphenols. The presence of polyphenols can be associated with the exhibition of a positive action on skin elasticity and skin tonus (as glycosaminoglycans and collagen I, III and IV) and the collagen (produced by connective tissue cells as fibroblasts in the skin dermis) which is responsible for the rigidity of the connective tissue^{15, 56}.

4.4.2 Elastase inhibition activity

Ela is a proteinase enzyme responsible for an increase of the tissue permeability and inflammation development, delaying wound healing by degradation of elastin, caused by cleavage of specific peptide bonds^{34, 35, 56-58}. Besides the breakdown of elastin, Ela can also cleave collagen, fibronectin and other extracellular components³⁴. The increase of dermal enzymatic activity (e.g. the increase of Ela, hyaluronidase and Tyr) is responsible for several

20

skin disorders⁵⁹.

The Ela inhibition activity of the *S. nigra* extracts by SFE is presented in Table 3. Extract C showed the highest activity that is even higher than that of ursolic acid (positive control). Extracts A and D showed modest or moderate anti-Ela activities. Moreover, under the same extraction conditions, fresh and dried berries had different percentages of Ela inhibition. Apparently, the drying process before extraction may contribute to an increase in compounds responsible for Ela inhibition. Regarding the same study of Thring et al. (2009)³⁴ mentioned above and similar to anti-Coll activity, the Ela inhibition activity of white tea showed again, among the studied extracts, the strongest anti-Ela activity ($\approx 87\%$) followed by green tea (47.2%). All the other extracts presented a percentage of Ela inhibition that was about half or less than that shown by white tea. In this context, extract C had a strong anti-Ela activity. In another study carried out in 19 different fruit extracts obtained from species of several plants showed that the extract from *Stauntonia hexaphylla* (Thunb.) Decne. presented the best anti-Ela activity ($39.2 \pm 1.5\%$); however, in our work we achieved a higher value for *S. nigra* extracts, extract C with $77.3 \pm 3.6\%$ ³⁵. Although, in the literature, a relationship between the content of polyphenols and the Ela inhibition is reported^{15, 34}. In our study, the best extract for the Ela inhibition (extract C) was not the extract with the high AA ($1.5 \pm 0.7\%$). Even so, potential inhibitors of those enzymes are important to the anti-ageing effect, anti-wrinkle and hyperpigmentation, by the prevention of skin elasticity loss and skin sagging^{34, 35, 56, 59} reason why they are used as ingredients in cosmetics and dermatological drugs⁵⁹.

4.4.3 Tyrosinase inhibition activity

The Tyr inhibition activity of the SFE *S. nigra* extracts is displayed in Table 3. The highest Tyr inhibition was obtained with extract D, with $51.9 \pm 3.1\%$ (Table 3). However, this activity was about half of the Tyr inhibition shown by the kojic acid, the reference compound used as positive control, ($97.7 \pm 3.0\%$). The difference of Tyr inhibition observed between fresh berries (extract D) and dried berries (extract B, $< 10.2\%$) suggests the drying process may lead to some loss of the anti-enzymatic activity. Regarding the study of Moon et al. (2010)³⁵, it was *Vernicia fordii* (Hensl.) that presented better Tyr inhibition ($51.0 \pm 3.4\%$) similar to our result ($51.9 \pm 3.1\%$).

Although in the literature, Tyr inhibition may be related to AA and the Tyr inhibition⁶⁰, no such relation was not found in our study, since extract D exhibited the lowest AA ($1.2 \pm 0.6\%$).

Tyr catalyzes the oxidation of phenols (such as L-tyrosine), being responsible in animals for the biosynthesis of melanin^{36, 61}. The inhibition of Tyr leads to the decrease of melanin production by the rate-control step of its synthesis³⁶. The accumulation of excessive epidermal pigments may cause some dermatological disorders, such as, melasma³⁵. For this reason, in the past few years, Tyr inhibitors have been used as drugs and in cosmetics with the aim to prevent the inhibition of enzymatic oxidation³⁵.

4.4.4 Acetylcholinesterase inhibition activity

The AChE inhibition by the *S. nigra* extracts by SFE are shown in Table 3. Extract C presented

the higher inhibition ($62.7 \pm 1.9\%$). This value was lower than the positive control ($97.9 \pm 0.8\%$). Among the possible causes of our results, we cannot forget the influence of the region or country, the time of harvest and the environmental conditions during all the process of plant maturation. The slight difference of AChE inhibition between extracts D ($37.2 \pm 3.4\%$) and B ($31.0 \pm 4.2\%$), both obtained with ethanol 96%, suggests a possible loss of enzymatic activity during the drying process of elderberries. In fact, using the same solvent of extraction, the results showed a decrease of AChE inhibition in the dried elderberries extract. Again, the relationship reported in the literature between the content of polyphenols the AChE inhibition and the AA was not verified, since extract C, with the best AChE inhibition ($62.7 \pm 1.9\%$) presented a low AA ($1.5 \pm 0.7\%$)⁶². AChE is present in keratinocytes⁶³. In epidermis, either the production or degradation of autocrine acetylcholine occurs, including the functioning membrane integrated and the cytosolic butyrylcholinesterase (BuChE), that is also presented in cell membranes. The BuChE may act as a protective mechanism for AChE⁶⁴. There exists a negative regulation of antimicrobial peptide (AMP) in the skin by the cholinergic anti-inflammatory pathway via acetylcholine (ACh)⁶⁵. Other studies also demonstrated a decrease in the permeability barrier function associated with the reduction of lipid synthesis and AMP production. Cholinergic activation in non-neuronal keratinocytes is the most important pathway, which is involved in the suppression of keratinocyte antimicrobial activity and a direct connection between stress and AMP expression in cutaneous infection has been established. Other observations revealed that in keratinocytes, the β -adrenergic activation impairs cell motility and wound closure which is a good indicator of the pathway by which stress impairs cutaneous healing. All the mediators of

the stress response can have some influence (direct or indirectly) in several key components of epidermal defense. The same study stated that the ACh released from keratinocytes is due to a pathogen challenge or wounding likely contributes to the regulation of local immune responses and potentially that of infiltrating immune cells. In the skin, keratinocytes are able to synthesize, process, store and release the ACh on the cell surface regulating the cellular processes (migration, differentiation, proliferation and apoptosis).

4.5 Toxicity assay

This assay was carried out only with extracts A and C, those that presented the highest enzymatic activities, with the exception of Tyr inhibition, and for extract A because it also presents the highest AA (Figure 2). Results suggested that both extracts were not toxic for *A. salina*. This fact may represent a high potential of *S. nigra* as source of lead molecules for drug candidates or of active ingredients for cosmetic purposes since that, in contrast with a study made by Fowles, *et al.*⁶⁶, researchers showed that limonoids from *Swietenia* species present toxicity on the model *A. salina*. The same happened with another study about the fruits of *Rubus fruticosus* also revealed that the extracts presented some toxicity on brine shrimp⁶⁷.

4.6 Physicochemical and morphological characterization of the nanoparticles

Two extracts have been selected to encapsulate into NPs (extracts A and C). Extract A present the highest AA and extract C present highest Ela inhibition, even more than the respective positive control (Ursolic acid), as well as, the highest AChE inhibition. Small NPs were produced and characterized by DLS, SEM and AFM. Empty PLGA NPs had an irregular shape

(Fig. 3A). On the contrary, extract-loaded A and C NPs had a more uniform appearance, exhibiting a spherical shape and a smooth surface (Fig. 3B-E). The NPs loaded with extract A were smaller than NPs loaded with C (Fig. 3D, E). The physical-chemical NPs characteristics are presented in Table 4.

The AFM analysis is presented in Fig. 4. Sizes of the NPs were in agreement with DLS results. For empty PLGA NPs (Fig. 4A, D), we obtained values of 201.6 ± 4.0 nm by DLS analysis vs. 258 ± 63 nm ($n = 4$) (Fig. 4D) by AFM. For PLGA NPs loaded with extract A (Fig. 4B, E), the results were 272.5 ± 2.9 nm and 314 ± 38 nm ($n = 3$) (Fig. 4E) for DLS and AFM analysis, respectively. For PLGA NPs loaded with extract C (Fig. 4 C, F) ranged 851.1 ± 22.9 nm and 758 ± 177 nm ($n = 4$) (Fig. 4F).

Encapsulation process of the extract led to a slight increase in the NPs size (as seen in Fig. 5, comparison between empty PLGA NPs and PLGA NPs extract loaded), suggesting a successful encapsulation of extract A. For encapsulation of extract C, it was verified a higher variation of NPs' size, which can be correlated with the presence of agglomerates since PDI was also higher (0.483 ± 0.034). The particle size is crucial for skin delivery. Several studies in literature demonstrated that these type of polymeric NPs are able to deliver the drug through the skin and this property is dependent of the hydrophobicity of the polymer and of the resultant size of NPs⁶⁸. The hair follicles are considered a very good pathway to those nanocarriers. Here, the critical size to easily permeate through the follicle of skin is around 200 nm⁶⁸. This value is still not consensual but analyzing our results, we observed that the best nanocarrier system for skin through hair follicle is the PLGA NPs loaded with extract A. Thus,

we decided to characterize these NPs by doing a preliminary study of NPs' stability. The variation of size of empty PLGA NPs and PLGA NPs loaded with extract A over 9 months was studied and depicted in Fig. 5. The results suggest that both cases were stable over the time, especially for empty PLGA NPs. In case of extract-loaded NPs, a higher variation of size and of PDI was observed over the time probably due to extract complexity. It is known that extracts are made of different compounds (non-polar and polar compounds) with high and low molecular weight and because of this complexity a new arrangement of NPs' structure might explain the size variation and, ultimately, particle agglomeration. The precise mechanism of re-arrangement of PLGA's structure will be performed in a near future. This observation was also observed in other studies using extracts in nanoparticles as carriers^{25, 69}.

Finally, considering the potential skin application of extract-loaded NPs, the pH of the formulation is very important factor in formulation studies. The value of pH increased when the extract was encapsulated, changing from 3.98 ± 0.10 in empty NPs to 5.01 ± 0.01 (PLGA NPs loaded with extract A) and 4.5 ± 0.01 (PLGA NPs loaded with extract C) but in all cases, the final pH is described as very compatible for skin application²².

5. Conclusion

Natural products have been widely used in cosmetics, food, and traditional medicine for thousands of years. The purpose of using plant material is to obtain new bioactive compounds in a no time-consuming and cost-effective extraction method. In this context, there has been growing interest in the application of SFE.

Our results of the current study showed that the SFE obtained from *S. nigra* berries may

26

be considered as a valuable source of bioactive molecules with potential application for prevention and/or treatment of skin disorders. Despite these promising results, particularly the enzyme inhibition activity of the extracts, there are still many gaps and it would be of interest to investigate different extraction conditions, improving the yield of extraction of SFE.

This study also shown that encapsulation of the *S. nigra* extracts may represent a suitable strategy to pursue. Our future studies will include the full assessment of the previous biological activities of the extract after loading, the identification of the major compounds of the extracts and additional *in vitro* and *in vivo* biological activities after the loading process using a safe and biocompatible carrier like PLGA NPs.

Acknowledgements

The authors are grateful to the financial support to Fundação para a Ciência e Tecnologia (FCT) under the Reference UID/DTP/04138/2019, Portugal; CESAM (UID/AMB/50017), through FCT/MEC National funds, and the co-funding by the FEDER, within the PT2020. The authors are also grateful to the financial support of this project by Régiefritas.

References

1. Tejero J, Jiménez P, Quinto E, Cordoba-Diaz D, Garrosa M, Cordoba-Diaz M, Gayoso M, & Girbés T (2015) Elderberries: a source of ribosome-inactivating proteins with lectin activity *Molecules* **20**(2): 2364–2387.
2. Ho GTT, Ahmed A, Zou Y-F, Aslaksen T, Wangensteen H, & Barsett H (2015) Structure–activity relationship of immunomodulating pectins from elderberries *Carbohydrate Polymers* **125**: 314–322.
3. Simonyi A, Chen Z, Jiang J, Zong Y, Dennis Y, Gu Z, Lu C, Fritsche KL, Greenlief CM, Rottinghaus GE, Thomas AL, Lubahn DB, Grace Y, Program N, & Sciences A (2015) Inhibition of microglial activation by elderberry extracts and its phenolic components *Life Sci* **128**: 30–38.
4. Ercisli S, Tosun M, & Akbulut M (2009) Physico-chemical characteristics of some wild grown European elderberry (*Sambucus nigra* L.) genotypes *Pharmacognosy Magazine* **5**(20): 320, <https://doi.org/10.4103/0973-1296.58153>.
5. Harokopakis E, Albzreh MH, Haase EM, Scannapieco FA, & Hajishengallis G (2006) Inhibition of proinflammatory activities of major periodontal pathogens by aqueous extracts from elder flower (*Sambucus nigra*) *Journal of Periodontology* **77**(2): 271–279.
6. Gray AM, Abdel-Wahab YHA, & Flatt PR (2000) The traditional plant treatment, *Sambucus nigra* (elder), exhibits insulin-like and insulin-releasing actions *in vitro* *The Journal of Nutrition* **130**(1): 15–20.
7. Committee on Herbal Medicinal Products (2013) Assessment report on *Sambucus nigra* L.,

- fructus *European Medicines Agency* **44**: 1–26.
8. Kite GC, Larsson S, Veitch NC, Porter EA, Ding N, & Simmonds MSJ (2013) Acyl spermidines in inflorescence extracts of elder (*Sambucus nigra* L., Adoxaceae) and elderflower drinks *Journal of Agricultural and Food Chemistry* **61(14)**: 3501–3508.
 9. Braga, F. G., Carvalho, L. M., Guedes-Pinto, H., Torres-Pereira, J. M., Neto, M. F., Monteiro A (2002) Variation of the anthocyanin content in *Sambucus nigra* L. populations growing in Portugal *Journal of Herbs, Spices & Medicinal Plants* **9(4)**: 289–295.
 10. Garofulić IE, Ganić KK, Galić I, Dragović-uzelac V, & Savić Z (2012) The influence of processing on physico-chemical parameters, phenolics, antioxidant activity and sensory attributes of Elderberry (*Sambucus nigra* L.) fruit wine *Croatian Journal of Food Technology, Biotechnology and Nutrition* **7**: 9–13.
 11. Schaal S (2010) Les plantes médicinales des pelouses calcaires de la Réserve Naturelle de Montenach Faculté de Pharmacie, Université de Lorraine.
 12. Ağalar HG, Demirci B, & Başer KHC (2014) The volatile compounds of Elderberries (*Sambucus nigra* L.) *Natural Volatiles & Essential Oils* **1(1)**: 51–54.
 13. Seabra IJ, Braga MEM, Batista MTP, & de Sousa HC (2010) Fractioned High Pressure Extraction of Anthocyanins from Elderberry (*Sambucus nigra* L.) Pomace *Food and Bioprocess Technology* **3(5)**: 674–683.
 14. Dawidowicz AL, Wianowska D, & Baraniak B (2006) The antioxidant properties of alcoholic extracts from *Sambucus nigra* L. (antioxidant properties of extracts) *LWT - Food Science and Technology* **39(3)**: 308–315.

15. Wahab NA, Rahman RA, Ismail A, Mustafa S, & Hashim P (2014) Assessment of antioxidant capacity, anti-collagenase and anti-elastase assays of Malaysian unfermented cocoa bean for cosmetic application *Natural Products Chemistry & Research* **2**(3): 1–6.
16. Ghimeray A, Jung U, Lee H, Kim Y, Ryu E, & Chang M (2015) *In vitro* antioxidant, collagenase inhibition, and *in vivo* anti-wrinkle effects of combined formulation containing *Punica granatum*, *Ginkgo biloba*, *Ficus carica*, and *Morus alba* fruits extract *Clinical, Cosmetic and Investigational Dermatology* **8**: 389–396.
17. Kołodziej B, Antonkiewicz J, Maksymiec N, & Drożdżal K (2012) Effect of traffic pollution on chemical composition of raw elderberry (*Sambucus nigra* L.) *Journal of Elemntology* (1/2012): 67–78.
18. Sánchez-Camargo A, García-Cañas V, Herrero M, Cifuentes A, & Ibáñez E (2016) Comparative study of green sub- and supercritical processes to obtain carnosic acid and carnosol-enriched Rosemary extracts with *in vitro* anti-proliferative activity on colon cancer cells *International Journal of Molecular Sciences* **17**(12): 2046–2063.
19. Silva RPF da, Rocha-Santos TAP, & Duarte AC (2016) Supercritical fluid extraction of bioactive compounds *TrAC Trends in Analytical Chemistry* **76**: 40–51.
20. Mota AH, Direito R, Carrasco MP, Rijo P, Ascensão L, Silveira Viana A, Rocha J, Eduardo-Figueira M, João Rodrigues M, Custódio L, Kuplennik N, Sosnik A, José Almeida A, Gaspar M, & Pinto Reis C (2019) Combination of hyaluronic acid and PLGA particles as hybrid systems for viscosupplementation in osteoarthritis *International Journal of Pharmaceutics* **559**: 13–22.

21. Gomes A, Ascensão L, Rijo P, Baptista M, Candeias S, Martinho N, Fernandes A, Roberto A, & Reis C (2013) Evaluation of a new topical treatment for acne with azelaic acid-loaded nanoparticles *Microscopy and Microanalysis* **19**(S4): 59–60.
22. Mota AH, Rijo P, Molpeceres J, & Reis CP (2017) Broad overview of engineering of functional nanosystems for skin delivery *International Journal of Pharmaceutics* **532**(2): 710–728.
23. Reis CP, Figueiredo IV, Carvalho RA, Jones J, Nunes P, Soares AF, Silva CF, Ribeiro AJ, Veiga FJ, Damgé C, Cabrita AMS, & Neufeld RJ (2008) Toxicological assessment of orally delivered nanoparticulate insulin *Nanotoxicology* **2**(4) 205–217.
24. Reis CP, Martinho N, Rosado C, Fernandes AS, & Roberto A (2014) Design of polymeric nanoparticles and its applications as drug delivery systems for acne treatment *Drug Development and Industrial Pharmacy* **40**(3): 409–417.
25. Pereira F, Baptista R, Ladeiras D, Madureira AM, Teixeira G, Rosado C, Fernandes AS, Ascensão L, Silva CO, Reis CP, & Rijo P (2015) Production and characterization of nanoparticles containing methanol extracts of Portuguese Lavenders *Measurement* **74**: 170–177.
26. Reis CP, Gomes A, Rijo P, Candeias S, Pinto P, Baptista M, Martinho N, & Ascensão L (2013) Development and evaluation of a novel topical treatment for acne with azelaic acid-loaded nanoparticles *Microscopy and Microanalysis* **19**(5): 1141–1150.
27. Reis CP, Silva C, Martinho N, & Rosado C (2013) Drug carriers for oral delivery of peptides and proteins: Accomplishments and future perspectives *Therapeutic Delivery* **4**(2):

- 251–265.
28. Pereira P, Bernardo-Gil MG, Cebola MJ, Mauricio E, & Romano A (2013) Supercritical fluid extracts with antioxidant and antimicrobial activities from myrtle (*Myrtus communis* L.) leaves. Response surface optimization *Journal of Supercritical Fluids* **83**: 57–64.
29. Rijo P, Matias D, Fernandes A, Simões M, Nicolai M, & Reis C (2014) Antimicrobial plant extracts encapsulated into polymeric beads for potential application on the skin *Polymers* **6**(2): 479–490.
30. Mota AH, Silva CO, Nicolai M, Baby A, Palma L, Rijo P, Ascensão L, & Reis CP (2018) Design and evaluation of novel topical formulation with olive oil as natural functional active *Pharmaceutical Development and Technology* **23**(8): 794–805.
31. Rijo P, Falé PL, Serralheiro ML, Simões MF, Gomes A, & Reis C (2014) Optimization of medicinal plant extraction methods and their encapsulation through extrusion technology *Measurement* **58**: 249–255.
32. Nicolai M, Pereira P, Vitor RF, Reis CP, Roberto A, & Rijo P (2016) Antioxidant activity and rosmarinic acid content of ultrasound-assisted ethanolic extracts of medicinal plants *Measurement: Journal of the International Measurement Confederation* **89**: 328–332.
33. Andrade JE da CM de (2016) Unravelling new ethnopharmacological roles of *Plectranthus* species: biological activity screening.
34. Thring TS, Hili P, & Naughton DP (2009) Anti-collagenase, anti-elastase and anti-oxidant activities of extracts from 21 plants *BMC Complementary and Alternative Medicine* **9**(1): 27–37.

35. Moon J-Y, Yim E-Y, Song G, Lee NH, & Hyun C-G (2010) Screening of elastase and tyrosinase inhibitory activity from Jeju Island plants *EurAsian Journal of Biosciences* **53**: 41–53.
36. Yamauchi K, Mitsunaga T, & Batubara I (2011) Isolation, identification and tyrosinase inhibitory activities of the extractives from *Allamanda cathartica* *Natural Resources* **02(03)**: 167–172.
37. Alanís-Garza BA, González-González GM, Salazar-Aranda R, Waksman de Torres N, & Rivas-Galindo VM (2007) Screening of antifungal activity of plants from the northeast of Mexico *Journal of Ethnopharmacology* **114(3)**: 468–471.
38. N. EN, Marçalo J, Garcia C, Reis C, Teodósio C, Oliveira C, Oliveira C, Roberto A, & Rijo P (2017) Biological activity screening of seven *Plectranthus* species *Biomedical and Biopharmaceutical Research* **14(1)**: 95–108.
39. Reis CP, Neufeld RJ, Ribeiro AJ, & Veiga F (2006) Nanoencapsulation I. Methods for preparation of drug-loaded polymeric nanoparticles *Nanomedicine: Nanotechnology, Biology and Medicine* **2(1)**: 8–21.
40. Dora CP, Singh SK, Kumar S, Datusalia AK, & Deep A (2010) Development and characterization of nanoparticles of glibenclamide by solvent displacement method *Acta Poloniae Pharmaceutica - Drug Research* **67(3)**: 283–290.
41. Reis CP, Roque LV, Baptista M, & Rijo P (2016) Innovative formulation of nystatin particulate systems in toothpaste for candidiasis treatment *Pharmaceutical Development and Technology* **21(3)**: 282–287.

42. Mohammadsadeghi S, Malekpour A, Zahedi S, & Eskandari F (2013) The antimicrobial activity of elderberry (*Sambucus nigra* L.) extract against gram positive bacteria, gram negative bacteria and yeast *Research Journal of Applied Sciences* **8**(4): 240–243.
43. Rodino S, Butu A, Butu M, & Cornea PC (2015) Comparative studies on antibacterial activity of licorice, elderberry and dandelion *Digest Journal of Nanomaterials and Biostructures* **10**(3): 947–955.
44. Matte AK, Deak AR, & Mata PTG (2015) Triagem fitoquímica e avaliação da atividade antibacteriana de extratos das flores de *Sambucus nigra* L. (Caprifoliaceae) *Revista Brasileira de Plantas Mediciniais* **17**(4 suppl 3): 1049–1054.
45. Hearst C, Mccollum G, Nelson D, Ballard LM, Millar BC, Goldsmith CE, Rooney PJ, Loughrey A, Moore JE, & Rao JR (2010) Antibacterial activity of elder (*Sambucus nigra* L.) flower or berry against hospital pathogens *Journal of Medicinal Plants Research* **4**(17): 1805–1809.
46. Chatterjee A, Yasmin T, Bagchi D, & Stohs SJ (2004) Inhibition of *Helicobacter pylori* *in vitro* by various berry extracts, with enhanced susceptibility to clarithromycin *Molecular and Cellular Biochemistry* **265**(1/2): 19–26.
47. Krawitz C, Mraheil MA, Stein M, Imirzalioglu C, Domann E, Pleschka S, & Hain T (2011) Inhibitory activity of a standardized elderberry liquid extract against clinically-relevant human respiratory bacterial pathogens and influenza A and B viruses *BMC Complementary and Alternative Medicine* **11**(1): 16–21.
48. Çelik SE, Özyürek M, Güçlü K, Çapanoğlu E, & Apak R (2014) Identification and

- anti-oxidant capacity determination of phenolics and their glycosides in elderflower by on-line HPLC-CUPRAC method *Phytochemical Analysis* **25(2)**: 147–154.
49. Seabra IJ, Braga MEM, Batista MT, & de Sousa HC (2010) Effect of solvent (CO₂/ethanol/H₂O) on the fractionated enhanced solvent extraction of anthocyanins from elderberry pomace *The Journal of Supercritical Fluids* **54(2)**: 145–152.
50. Oktyabrsky O, Vysochina G, Muzyka N, Samoilova Z, Kukushkina T, & Smirnova G (2009) Assessment of anti-oxidant activity of plant extracts using microbial test systems *Journal of Applied Microbiology* **106(4)**: 1175–1183.
51. Kanlayavattanakul M, & Lourith N (2011) Therapeutic agents and herbs in topical application for acne treatment *International Journal of Cosmetic Science* **33(4)**: 289–297.
52. Raafat K, & El-Lakany A (2015) Acute and subchronic *in-vivo* effects of *Ferula hermonis* L. and *Sambucus nigra* L. and their potential active isolates in a diabetic mouse model of neuropathic pain *BMC Complementary and Alternative Medicine* **15(1)**: 257–270.
53. Touitou E, & Godin B (2008) Skin nonpenetrating sunscreens for cosmetic and pharmaceutical formulations *Clinics in Dermatology* **26(4)**: 375–379.
54. Kang H-J, Huang Y-H, Lim H-W, Shin D, Jang K, Lee Y, Kim K, & Lim C-J (2016) Stereospecificity of ginsenoside Rg2 epimers in the protective response against UV-B radiation-induced oxidative stress in human epidermal keratinocytes *Journal of Photochemistry and Photobiology B: Biology* **165**: 232–239.
55. Yuan Y, & Relue P (2008) Enzymatic degradation of human skin dermis revealed by fluorescence and reflectance spectroscopy *Optics Express* **16(13)**: 9857–9868.

56. Ko RK, Kim G-O, Hyun C-G, Jung DS, & Lee NH (2011) Compounds with tyrosinase inhibition, elastase inhibition and DPPH radical scavenging activities from the branches of *Distylium racemosum* Sieb. et Zucc *Phytotherapy Research* **25**(10): 1451–1456.
57. Piwowarski JP, Kiss AK, & Kozłowska-Wojciechowska M (2011) Anti-hyaluronidase and anti-elastase activity screening of tannin-rich plant materials used in traditional Polish medicine for external treatment of diseases with inflammatory background *Journal of Ethnopharmacology* **137**(1): 937–941.
58. Hwang T-L, Shen H-I, Liu F-C, Tsai H-I, Wu Y-C, Chang F-R, & Yu H-P (2014) Ursolic acid inhibits superoxide production in activated neutrophils and attenuates trauma-hemorrhage shock-induced organ injury in rats *PLoS ONE* **9**(10): e111365–e111369.
59. Tu P, & Tawata S (2015) Anti-oxidant, anti-aging, and anti-melanogenic properties of the essential oils from two varieties of *Alpinia zerumbet* *Molecules* **20**(9): 16723–16740.
60. Popoola O, Marnewick J, Rautenbach F, Ameer F, Iwuoha E, & Hussein A (2015) Inhibition of oxidative stress and skin aging-related enzymes by prenylated chalcones and other flavonoids from *Helichrysum teretifolium* *Molecules* **20**(4): 7143–7155.
61. Krüger S, Mirgos M, & Morlock GE (2015) Effect-directed analysis of fresh and dried elderberry (*Sambucus nigra* L.) via hyphenated planar chromatography *Journal of Chromatography A* **1426**: 209–219.
62. Zhao Y, Dou J, Wu T, & Aisa H (2013) Investigating the antioxidant and acetylcholinesterase inhibition activities of *Gossypium herbaceum* *Molecules* **18**(1):

951–962.

63. Walters KA, & Roberts MS (2002) The structure and function of skin In: James Swarbrick (ed) *Dermatological and Transdermal Formulations* Marcel Dekker Inc, 15–53.
64. Schallreuter KU, Gibbons NCJ, Elwary SM, Parkin SM, & Wood JM (2007) Calcium-activated butyrylcholinesterase in human skin protects acetylcholinesterase against suicide inhibition by neurotoxic organophosphates *Biochemical and Biophysical Research Communications* **355(4)**: 1069–1074.
65. Curtis BJ, & Radek KA (2012) Cholinergic regulation of keratinocyte innate immunity and permeability barrier integrity: new perspectives in epidermal immunity and disease *Journal of Investigative Dermatology* **132(1)**: 28–42.
66. Fowles RG, Mootoo BS, Ramsewak RS, & Khan A (2012) Toxicity–structure activity evaluation of limonoids from *Swietenia* species on *Artemia salina* *Pharmaceutical Biology* **50(2)**: 264–267.
67. Ali N, Aleem U, Ali Shah SW, Shah I, Junaid M, Ahmed G, Ali W, & Ghias M (2013) Acute toxicity, brine shrimp cytotoxicity, anthelmintic and relaxant potentials of fruits of *Rubus fruticosus* Agg *BMC Complementary and Alternative Medicine* **13(1)**: 138–143.
68. Özcan İ, Azizoğlu E, Şenyiğit T, Özyazıcı M, & Özer Ö (2013) Comparison of PLGA and lecithin/chitosan nanoparticles for dermal targeting of betamethasone valerate *Journal of Drug Targeting* **21(6)**: 542–550.
69. Manea A-M, Andronescu C, Meghea A (2014) Green tea extract loaded into solid lipid nanoparticles, *U.P.B. Sci. Bull., Series B* **76(2)**: 125-136.

37

Table 1. Characteristics of SFE and respective yields

| Extract of <i>S. nigra</i> | Part of plant: berries | Solvent used | Yield of extraction (%) |
|----------------------------|------------------------|---|-------------------------|
| A | | CO ₂ (1 st hour) | 5.9 ± 0.1 |
| | | CO ₂ + Ethanol Absolute (2 nd hour) | |
| B | Dried | CO ₂ (1 st hour) | 9.3 ± 0.0 |
| | | CO ₂ + Ethanol 96% (v/v, 2 nd hour) | |
| C | | CO ₂ (1 st hour) | 4.9 ± 0.1 |
| | | CO ₂ + Ethanol 70% (v/v, 2 nd hour) | |
| D | Fresh | CO ₂ (1 st hour) | 0.8 ± 0.0 |
| | | CO ₂ + Ethanol 96% (v/v, 2 nd hour) | |

Table 2. Antioxidant activity of the extracts obtained from fresh and dried *S. nigra* berries under different extraction conditions*

| Extract | Antioxidant Activity (AA, %) |
|---|------------------------------|
| A | 19.0 ± 2.5*** |
| B | 6.7 ± 2.9** |
| C | 1.5 ± 0.7 |
| D | 1.2 ± 0.6 |
| Positive Control (Quercetin) | 95.3 ± 0.2 |
| Negative Control (respective solvent of the extraction) | 0.1 ± 0.0 |

*mean ± SD, n = 3, **p < 0.01 or ***p < 0.0001 in comparison to negative control

Table 3. *In vitro* enzymatic inhibition by the extracts obtained from fresh and dried *S. nigra* berries under different SFE conditions (mean \pm SD, n = 3)*

| Extract | Enzyme Inhibition (%) | | | |
|-------------------------|--------------------------------------|--------------------------------|--------------------------------|--------------------------------|
| | Coll | Ela | Tyr | AChE |
| A | 84.7 \pm 3.7 ^{*** and a)} | < 9.1 ^{b), +++)} | 32.6 \pm 2.5 ⁺⁺⁺⁾ | < 16.0 ^{b)} |
| B | 72.8 \pm 2.9 ^{***)} | 31.6 \pm 1.4 ⁺⁺⁺⁾ | < 10.2 ^{b)} | 31.0 \pm 4.2 ⁺⁺⁺⁾ |
| C | 45.4 \pm 0.1 ^{***)} | 77.3 \pm 3.6 ^{a)} | < 10.2 ^{b)} | 62.7 \pm 1.9 ⁺⁺⁺⁾ |
| D | 59.1 \pm 1.7 ^{***)} | 17.7 \pm 0.3 ⁺⁺⁺⁾ | 51.9 \pm 3.1 ⁺⁺⁺⁾ | 37.2 \pm 3.4 ⁺⁺⁺⁾ |
| Positive Control | 84.4 \pm 0.9 ¹⁾ | 69.9 \pm 3.7 ²⁾ | 97.7 \pm 3.0 ³⁾ | 97.9 \pm 0.8 ⁴⁾ |
| Negative Control (DMSO) | 8.3 \pm 0.8 | 9.1 \pm 0.8 | 10.2 \pm 2.5 | 16.0 \pm 0.0 |

* In all assays, the concentrations were 50 μ g of extract/mL (¹EGCG, ²Ursolic Acid, ³Kojic Acid and ⁴Tacrine were reference compounds used as positive controls, **p < 0.01 or ***p < 0.0001 in comparison to negative control, ^{a)} not statistically different to positive control, ^{b)} not statistically different to negative control, ⁺⁺⁺⁾ p < 0.0001 in comparison to positive control)

Table 4. Characterization of empty and extract-loaded PLGA NPs (mean \pm SD, n=3)

| | Empty PLGA NPs | PLGA NPs loaded with extract A | PLGA NPs loaded with extract C |
|----------------------------|-------------------|--------------------------------|--------------------------------|
| Size (d. nm) | 201.6 \pm 4.0 | 272.5 \pm 2.9 | 851.1 \pm 22.9 |
| Polydispersity index (PdI) | 0.069 \pm 0.013 | 0.238 \pm 0.013 | 0.483 \pm 0.034 |
| pH of NPs solution | 3.98 \pm 0.10 | 5.01 \pm 0.01 | 4.51 \pm 0.01 |

Figure 1. Diagram of the SFE apparatus. A – CO₂ supply cylinder, M₁-M₅ – Manometers, S₁ – Cooling Bath, LP₁ – Liquid Pump, BP – Back Pressure Regulator, CV – Check Valve, V₁-V₅ – Valves, F₂ – Liquid mass flow meter, LP₂ – Co-solvent Pump, S₂ – Heated water bath, S₃ – Collector, S₄ – Ice bath, FL – Gas flow meter, T – Thermometer, G – Gas Counter

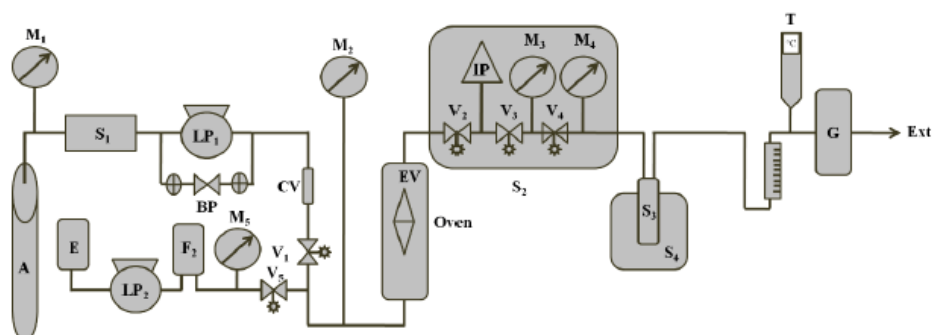


Figure 2. Screening of extracts toxicity at 10 mg/mL using *Artemia salina* test (% mean \pm SD, n=3, p < 0.0001)

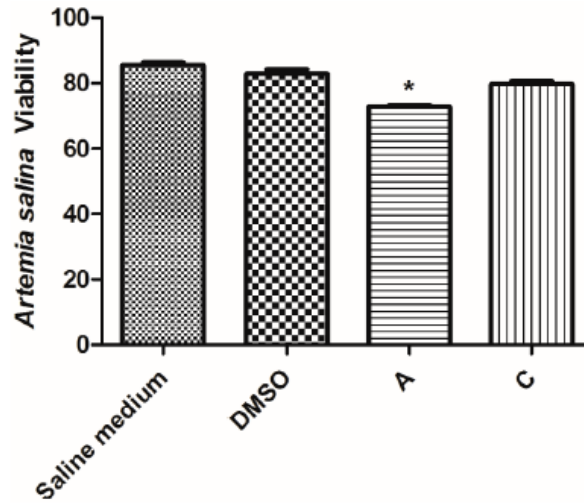


Figure 3. SEM micrographs showing the morphology of the PLGA NPs produced. A) Empty PLGA NPs; B) PLGA NPs loaded with extract C ; C) PLGA NPs loaded with extract A; D, E) Details of PLGA NPs loaded with extract C and A, respectively. Note the smaller dimension of PLGA NPs loaded with extract A. Scale bars = 1 μm (A to C) and 0.5 μm (D, E)

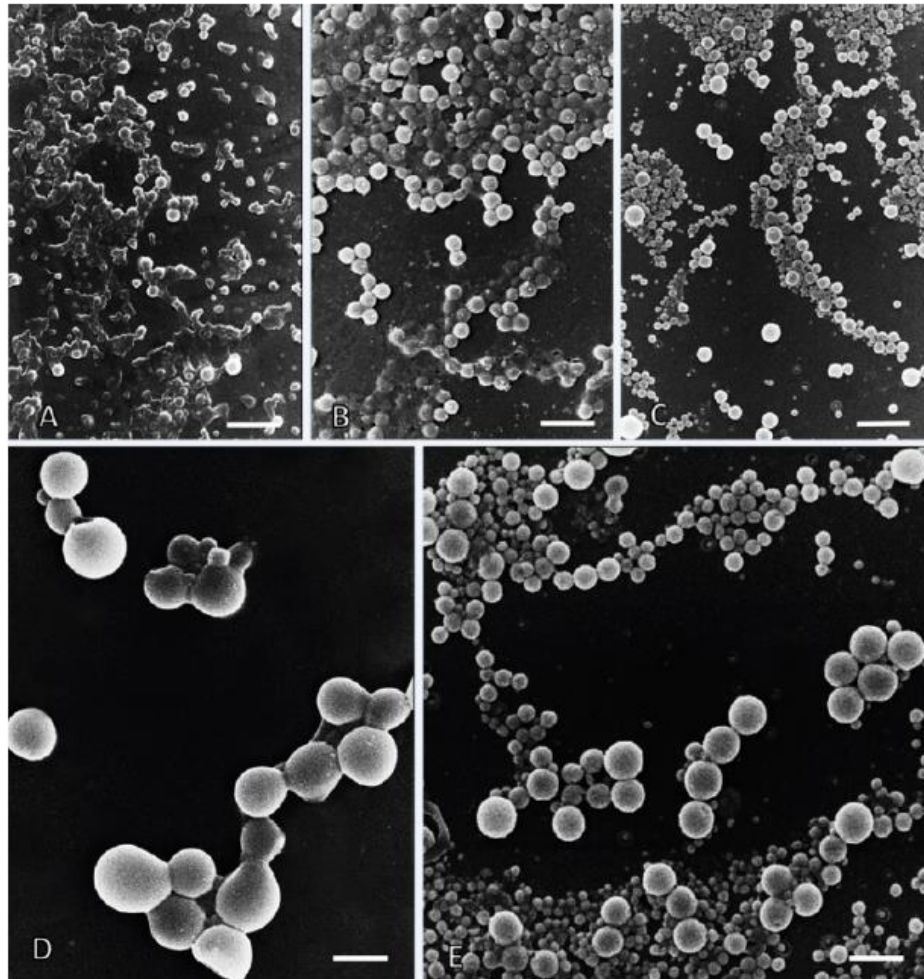


Figure 4. AFM topographic images of empty PLGA NPs (A, D), PLGA NPs loaded with extract A (B, E) and PLGA NPs loaded with extract C (C, F). 3D images (A, B, C) and cross section analysis (D, E, F).

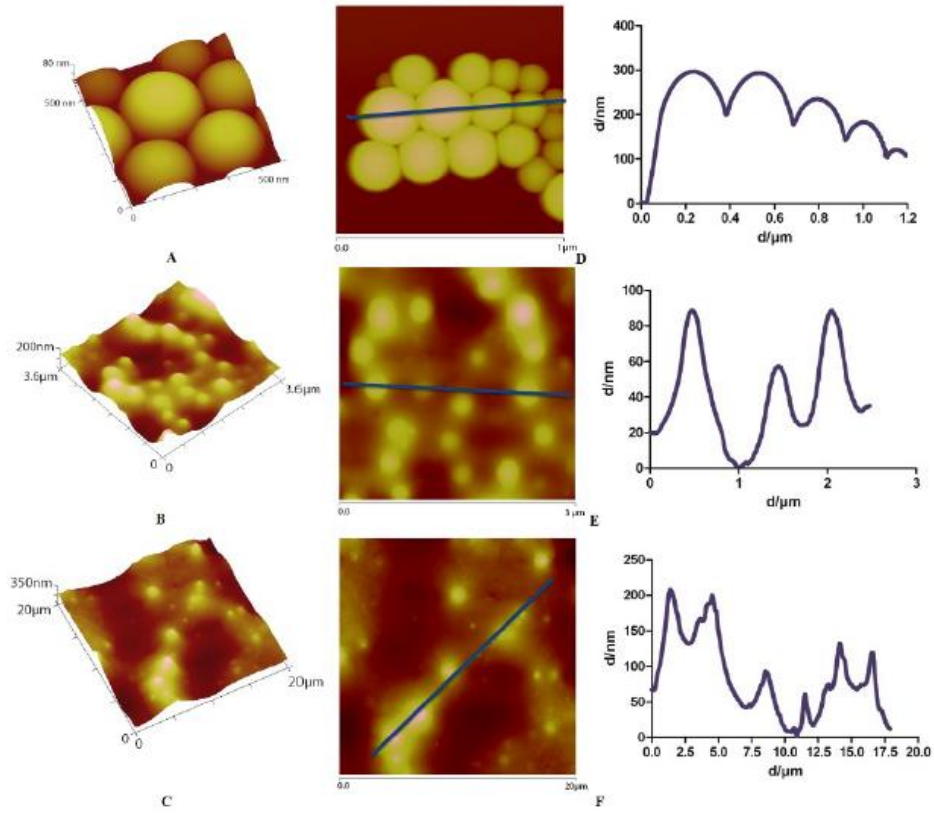
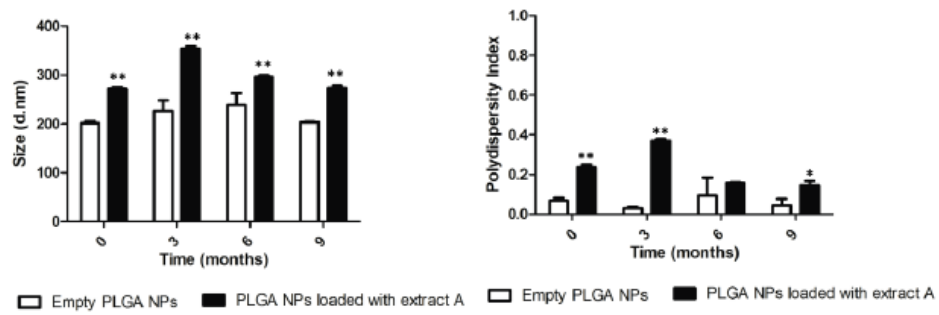


Figure 5. Preliminary stability study of size and polydispersity index (PdI) variation over the time of empty PLGA NPs (white) and PLGA NPs loaded with extract A (black) (* $p < 0.05$ and ** $p < 0.001$, PLGA NPs loaded with extract A vs Empty PLGA NPs)





Contents lists available at ScienceDirect

European Journal of Medicinal Chemistry

journal homepage: <http://www.elsevier.com/locate/ejmech>

Increased antibacterial properties of indoline-derived phenolic Mannich bases

Tatu Rimpiläinen^a, Alexandra Nunes^{b, c, d, **}, Rita Calado^b, Ana S. Fernandes^d, Joana Andrade^d, Epole Ntungwe^d, Gabriella Spengler^e, Nikolett Szemerédi^e, João Rodrigues^b, João Paulo Gomes^b, Patricia Rijo^{d, g}, Nuno R. Candeias^{a, h, *}

^a Faculty of Engineering and Natural Sciences, Tampere University, Korkeakoulunkatu 8, 33101, Tampere, Finland

^b Department of Infectious Diseases, National Institute of Health, Avenida Padre Cruz, 1649-016, Lisboa, Portugal

^c Faculty of Veterinary Medicine, Lusófona University, Campo Grande 376, 1749-024, Lisboa, Portugal

^d CBIOS-Universidade Lusófona Research Center for Biosciences & Health Technologies, Campo Grande 376, 1749-024, Lisboa, Portugal

^e Department of Medical Microbiology and Immunobiology, Faculty of Medicine, University of Szeged, Dóm tér 10, 6720, Szeged, Hungary

^f Instituto de Investigação do Medicamento (iMed.Ulissboa), Faculdade de Farmácia, Universidade de Lisboa, Av. Prof. Gama Pinto, 1649-003, Lisboa, Portugal

^h LAQV-REQUIMTE, Department of Chemistry, University of Aveiro, 3810-193, Aveiro, Portugal



ARTICLE INFO

Article history:

Received 9 March 2021

Received in revised form

6 April 2021

Accepted 7 April 2021

Available online 20 April 2021

Keywords:

Antibacterials

Aminoalkylphenols

Gram-positive

Nosocomial infections

ABSTRACT

The search for antibacterial agents for the combat of nosocomial infections is a timely problem, as antibiotic-resistant bacteria continue to thrive. The effect of indoline substituents on the antibacterial properties of aminoalkylphenols was studied, leading to the development of a library of compounds with minimum inhibitory concentrations (MICs) as low as 1.18 μM . Two novel aminoalkylphenols were identified as particularly promising, after MIC and minimum bactericidal concentrations (MBC) determination against a panel of reference strain Gram-positive bacteria, and further confirmed against 40 clinical isolates (*Staphylococcus aureus*, *Staphylococcus epidermidis*, *Enterococcus faecalis*, *Enterococcus faecium*, and *Listeria monocytogenes*). The same two aminoalkylphenols displayed low toxicity against two *in vivo* models (*Artemia salina* brine shrimp and *Saccharomyces cerevisiae*). The *in vitro* cytotoxicity evaluation (on human keratinocytes and human embryonic lung fibroblast cell lines) of the same compounds was also carried out. They demonstrated a particularly toxic effect on the fibroblast cell lines, with IC_{50} in the 1.7–5.1 μM range, thus narrowing their clinical use. The desired increase in the antibacterial properties of the aminoalkylphenols, particularly indoline-derived phenolic Mannich bases, was reached by introducing an additional nitro group in the indolyl substituent or by the replacement of a methyl by a bioisosteric trifluoromethyl substituent in the benzyl group introduced through use of boronic acids in the Petasis borono-Mannich reaction. Notably, the introduction of an additional nitro moiety did not confer added toxicity to the aminoalkylphenols.

© 2021 Elsevier Masson SAS. All rights reserved.

1. Introduction

The emergence of antimicrobial-resistant bacteria is a matter of concern for public health. The increased rate of bacterial resistance allied with the rather slow development of new antibacterial agents foreshadows a crisis. The actual global antibacterial clinical pipeline is composed of many agents that are modifications of

existing classes of antibiotics [1]. Notwithstanding the efforts done by the scientific community to address the WHO's Global Action Plan on Antimicrobial Resistance [2], especially in tackling Gram-negative bacteria, more antibacterials and of narrow scope are necessary [3]. ESKAPE pathogens (*E. faecium*, *S. aureus*, *Klebsiella pneumoniae*, *Acinetobacter baumannii*, *Pseudomonas aeruginosa*, and *Enterobacter* species) are the leading cause of nosocomial

* Corresponding author. LAQV-REQUIMTE, Department of Chemistry, University of Aveiro, 3810-193, Aveiro, Portugal.

** Corresponding author. Department of Infectious Diseases, National Institute of Health, Avenida Padre Cruz, 1649-016, Lisboa, Portugal.

E-mail addresses: alexandra.nunes@insa.min-saude.pt (A. Nunes), ncandeias@ua.pt (N.R. Candeias).

<https://doi.org/10.1016/j.ejmech.2021.113459>

0223-5234/© 2021 Elsevier Masson SAS. All rights reserved.

infections worldwide [4,5]. From these pathogens, *E. faecium* and *S. aureus* are Gram-positive, and second-generation glycopeptides such as dalbavancin and oritavancin or oxazolidinone linezolid have been described as antibacterial agents against infections by methicillin-resistant *S. aureus* (MRSA) [6,7] and vancomycin-resistant enterococci (VRE) [5,8]. Many recent developments have been done towards the treatment of multidrug-resistant Gram-positive pathogens, however, the anticipated fast evolution of resistance makes searches for new antibacterials a timely challenge [9–11].

S. aureus, *Enterococcus faecalis*, *E. faecium* and *Staphylococcus epidermidis* cause important nosocomial or healthcare-associated infections, a major cause of mortality and morbidity worldwide [12]. *Enterococcus* spp. is frequently isolated from the surgical site and bloodstream infections, but rarely found in the respiratory tract [13]. On the other hand, *S. aureus* is the primary cause of lower respiratory tract and surgical site infections, and the second leading cause of nosocomial bacteremia, pneumonia and cardiovascular infections. Coagulase-negative staphylococci (CoNS) (especially *S. epidermidis*) are isolated almost twice as often as *S. aureus* in bloodstream infections. Hospital-acquired listeriosis are often-fatal foodborne outbreak infections affecting mainly pregnant and immunocompromised patients, whose sources are difficult to identify [14,15].

Besides the patient's underlying condition, several factors contribute to the success of these nosocomial pathogens. For instance, the widespread use of broad-spectrum antibiotics promotes the emergence and re-emergence of difficult-to-treat MDR strains, with VRE, MRSA, vancomycin-resistant *S. aureus* (VRSA) and methicillin-resistant *S. epidermidis* (MRSE) on the top of the list [16,17]. Pathogens' persistence on surfaces in the hospital environment, water system, or foreign body devices (such as catheters, implants, vascular grafts, intravenous devices, respiratory equipment, prostheses, etc.) is also a determinant factor for their success. Moreover, the capacity of these pathogens to form biofilms on inert surfaces that are highly resistant to antibiotic treatments and host immune response [18–20] contributes even more for their persistence and dissemination in the health care setting.

The ability of phenolic Mannich bases to interact with living organisms [21] has been documented in several reports, biological properties such as antibacterial [22] and antitumoral [23–28], to name a few, have been described. We have previously reported the antibacterial properties of a family of aminoalkylphenols in which the indoline amine counterpart and a *para*-nitrophenol group were deemed important in conferring antimicrobial properties (Fig. 1). Tests against selected Gram-positive bacterial strains led to the identification of **1a** as a promising antibacterial agent [29]. In our follow-up work [30], the potency of such derivatives was increased by the introduction of a chlorine substituent in the *para*-position of the phenyl ring (**2a**), thus lowering the minimum inhibitory concentration (MIC) from 10.8 to 1.23 μ M for multidrug-resistant *S. aureus* and *E. faecalis*. While the influence of diverse substituents in both the phenol and phenyl rings has been evaluated in previous works, the effect of introducing different substituents on the aromatic ring of indoline was not assessed. In the present work,

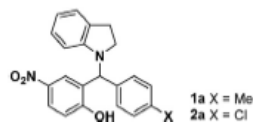


Fig. 1. Indoline-derived phenolic Mannich bases previously identified [29,30] as antibacterials.

we compile our findings on this missing link to deepen our understanding of the structure-activity relationship of this underexplored class of antimicrobial agents.

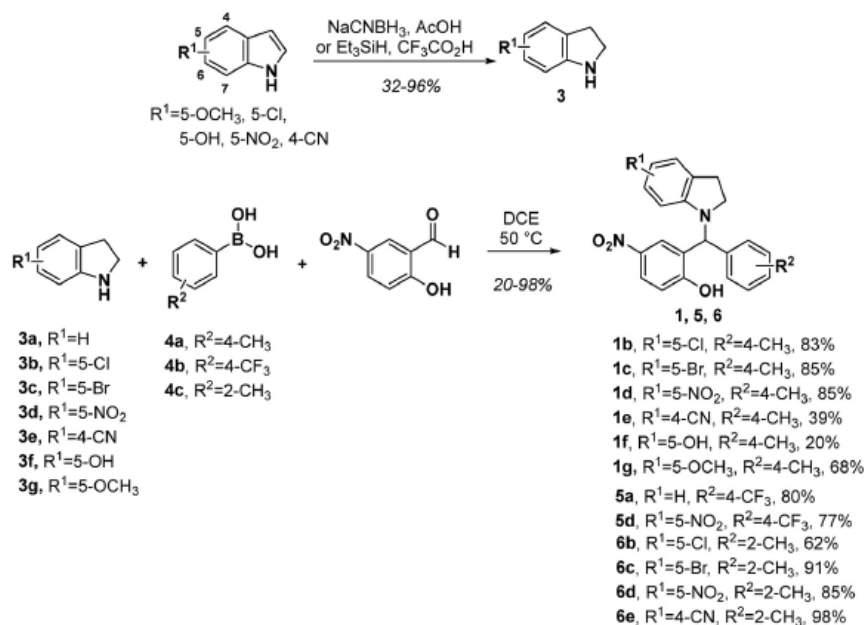
2. Results and discussion

The compounds have been prepared as previously reported, using the multicomponent Pétasis reaction [31,32] from 5-nitrosalicylaldehyde, substituted indolines **3**, and boronic acids **4** (Scheme 1). Some indolines were obtained through the reduction of commercially available indoles with either sodium cyanoborohydride or triethylsilane in trifluoroacetic acid. Specifically, Et₃SiH and trifluoroacetic acid were used for the reduction of indoles substituted with electron withdrawing groups to afford **3d** and **3e** in 96 and 70% yields, respectively. The condensation of 5-nitrosalicylaldehyde with indolines **3** in 1,2-dichloroethane, followed by reaction of the *in situ* formed iminium with the suitable boronic acid at 50 °C, provided the desired aminoalkylphenols **1**, **5**, and **6** in up to excellent yields. The procedure was successfully applied to the preparation of aminoalkylphenols derived from three different boronic acids: 4-tolyl (**4a**), 4-(trifluoromethyl)phenyl (**4b**) and 2-tolyl (**4c**) boronic acids providing aminoalkylphenols **1**, **5** and **6** respectively. All compounds were isolated by column chromatography, their purity assessed by ¹H NMR and their structures confirmed through NMR and HRMS characterization.

For the sake of comparison, the synthesized aminoalkylphenols were tested against a similar panel of Gram-positive microorganisms as for the previously reported compounds **1a** and **2a** [30]. Specifically, three *S. aureus* strains (the reference methicillin-sensitive ATCC 25923, the methicillin-resistant CIP106760, and the methicillin-sensitive ATCC 6538), two *E. faecalis* strains (the reference ATCC 29212 and the vancomycin-resistant ATCC 51299), one *S. epidermidis* strain (the vancomycin-sensitive ATCC 12228), and one *Bacillus subtilis* strain (the ATCC 6633) strains were considered and the results for the antibacterial activity of compounds in series **1**, **5** and **6**, along with that of compound **2a**, are presented in Table 1.

Notwithstanding the moderate to good minimum inhibitory concentrations previously determined for **1a**, the new 4-tolyl derivatives **1b–g** showed similar to better antibacterial properties, except in the case of *S. aureus* ATCC 6538. The presence of the nitro group in 5-position of the indolinyll makes compound **1d** particularly active with a low MIC of 1.20 μ M. On the other hand, the presence of a hydroxyl group in the same 5-position of indolinyll had a detrimental effect on the antibacterial properties. Therefore, compound **1f** was generally the least active in the series of 4-tolyl containing aminoalkylphenols **1**. Compound **1g**, containing a methylether substituent at the 5-position of indoline was not particularly active against the *S. aureus* ATCC 25923 and CIP106760 and the two *E. faecalis* strains tested when compared with others in the series of aminoalkylphenols **1**. Nevertheless, **1g** was the most potent in the same series against *S. epidermidis* ATCC 12228 and *B. subtilis* ATCC 6633.

A bioisoster replacement of the methyl group by a trifluoromethyl substituent increased the bacterial growth inhibition as observed for compounds **5a** and **5d**. Despite the higher antibacterial effect of 5-nitro in **1d** and 4-CF₃ in **5a** when compared with **1a**, the presence of both substituents in **5d** did not confer significantly better antibacterial properties than **5a**. Shuffling the methyl substituent from the 4- to the 2-position had little or no effect on the MICs of *S. aureus* or *E. faecalis* strains but led to the considerable inhibition of the growth of *S. epidermidis* and *B. subtilis*. Similar levels of growth inhibition were observed for 4-tolyl and 2-tolyl containing aminoalkylphenols **1** and **6**. Among



Scheme 1. Preparation of aminoalkylphenols studied.

Table 1

Antimicrobial activity of aminoalkylphenols **1**, **2a**, **5**, and **6** against laboratory-adapted strains. Minimum inhibitory concentrations (MIC) and minimum bactericidal concentrations (MBC) are shown in μM .

| Compd | <i>S. aureus</i> ATCC 25923 (MSSA) | | <i>S. aureus</i> ATCC 6538 | | <i>S. aureus</i> CP106760 (MRSA) | | <i>E. faecalis</i> ATCC 29212 | | <i>E. faecalis</i> ATCC 51299 (VRE) | | <i>S. epidermidis</i> ATCC 12228 | | <i>B. subtilis</i> ATCC 6633 | |
|------------------------|------------------------------------|----------------|----------------------------|----------------|----------------------------------|----------------|-------------------------------|----------------|-------------------------------------|----------------|----------------------------------|----------------|------------------------------|----------------|
| | MIC | MBC | MIC | MBC | MIC | MBC | MIC | MBC | MIC | MBC | MIC | MBC | MIC | MBC |
| 1a ^d | 21.3 | 347 | 10.8 | 43.4 | 2.71 | 5.42 | 10.8 | 86.7 | 21.7 | 173 | - ^b | - ^b | - ^b | - ^b |
| 1b | 2.30 | 36.8 | 19.8 | <1.58 | 1.15 | 4.59 | 1.15 | 9.19 | 2.30 | 9.19 | 75.4 | 37.7 | 37.7 | 151 |
| 1c | 10.1 | 81.1 | 17.8 | <1.42 | 5.07 | 20.3 | 5.07 | 81.1 | 10.1 | 162 | 9.43 | 4.71 | 4.71 | 9.43 |
| 1d | 1.20 | 38.6 | 19.3 | 77.1 | 1.20 | 4.82 | 1.20 | 9.64 | 2.41 | 154 | 18.9 | 37.7 | 18.9 | 37.7 |
| 1e | 10.7 | 85.8 | 20.3 | 40.5 | 2.68 | 21.4 | 2.68 | 42.9 | 5.36 | 172 | 37.8 | 302 | 4.71 | 9.43 |
| 1f | 67.7 | 542 | 166.2 | 332 | 67.7 | 108 | 135 | 108 | 135 | 108 | 37.8 | 302 | 2.4 | >9.43 |
| 1g | 20.0 | 160 | 20.0 | 80.0 | 10.0 | 40.0 | 10.0 | 160 | 20.0 | 160 | <1.18 | 4.71 | <1.18 | 4.71 |
| 2a ^d | 2.47 | 9.86 | 1.23 | 2.47 | 1.23 | <1.23 | 1.23 | >9.86 | 1.23 | 19.7 | - ^b | - ^b | - ^b | - ^b |
| 5a | 1.18 | 37.7 | 1.18 | 2.36 | 1.18 | 1.18 | 1.18 | 9.43 | 1.18 | 151 | <1.18 | <1.18 | <1.18 | <1.18 |
| 5d | 2.22 | 35.6 | - ^b | - ^b | 1.11 | 1.11 | 1.11 | 8.89 | 4.45 | 142 | <1.18 | 2.36 | 9.43 | 18.9 |
| 6b | 2.47 | 39.6 | 1.24 | 4.95 | 1.24 | 2.47 | 1.24 | 9.89 | 2.47 | 158 | <1.18 | 2.36 | <1.18 | 4.71 |
| 6c | 2.22 | 35.6 | 1.11 | 4.45 | 1.11 | 1.11 | 1.11 | 8.89 | 4.45 | 142 | <1.18 | <1.18 | <1.18 | <1.18 |
| 6d | 1.20 | 38.6 | 2.41 | 9.64 | 1.20 | 4.82 | 1.20 | 9.64 | 2.41 | 154 | <1.18 | 4.71 | <1.18 | 2.36 |
| 6e | 10.1 | 81.1 | 5.07 | 20.3 | 5.07 | 20.3 | 5.07 | 81.1 | 10.1 | 162 | 2.36 | 18.9 | 4.71 | 18.9 |
| CP ^e | 5.40 | - ^b | 1.35 | - ^b | <1.50 | - ^b | 3.07 | - ^b | <5.83 | - ^b | 1.95 | - ^b | 1.95 | - ^b |

^a Previously reported data [30].

^b not tested.

^c CP – positive control (Vancomycin).

the indolyl substituents, the presence of chlorine and nitro in the heterocycle has a clear positive effect in increasing the inhibition properties, as observed for **1b**, **1d**, **6b**, and **6d**. Apart from the VRE strain tested, compounds **5a**, **5d**, and **6b-d** were in general stronger bactericides than compounds **1**.

Considering that phenol compounds may exhibit antioxidant properties, scavenging the excessive amount of free radicals accumulated in the course of microbial infections and that can lead to cellular damage [33,34], we wonder if a relation between the

electronic character of the indolyl substituents and such property could be established. Therefore, the antioxidant ability of compounds **1a-1f** was investigated using the 2,2-diphenyl-1-picrylhydrazyl (DPPH) method (Fig. 2). Indeed, reduced antioxidant activity was observed for highly deactivated indolyl derivatives **1d** (5-nitro substituted) and **1e** (4-nitrile substituted) in 8% and 19%, respectively. On the other hand, unsubstituted **1a**, halogen substituted **1b** and **1c**, and hydroxy substituted **1f** indolyl derivatives showed high scavenging properties, with antioxidant

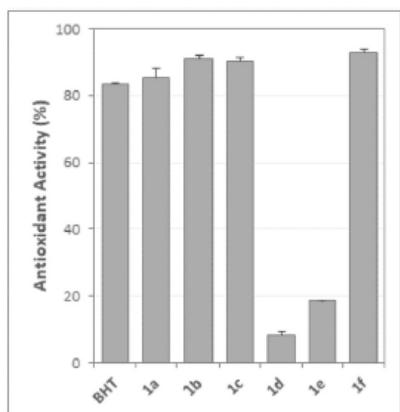


Fig. 2. Antioxidant activity of **1a-f** by DPPH method. Concentrations of 10 µg/mL (22–26 µM) of each compound were subjected to free radical scavenging test. The change in optical density of DPPH was monitored at 517 nm. Butylated hydroxytoluene (BHT) was used as the reference standard. Results are reported as percentage mean values \pm SD, based on three independent experiments.

activities higher than 80%. Despite the determined relationship between the electronic properties of the indolinyl substituents and the ability of the studied aminoalkylphenols to scavenge free radicals, the antioxidant property does not correlate with the antibacterial effect observed. This corroborates our previous observations, suggesting a mechanism of action that does not involve the scavenging of free radicals [30].

In order to disclose potential applications of the newly synthesized compounds as antibacterial agents, the most active ones, namely **5a**, **5d**, and **6b-d** were considered for further studies regarding their biocompatibility and safety. The same properties were also determined for **1d** for the sake of comparison with compounds **5d** and **6d**, as the three molecules contain a nitro group at the 5-position of the indoline moiety, which might confer additional toxicity [35].

Over the past decades, toxicity testing in pharmaceutical

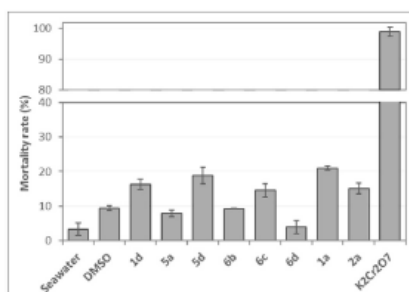


Fig. 3. General toxicity of **1d**, **5a**, **5d**, and **6b-d** in the mortality rate of *A. salina* brine shrimp model. Concentrations of 10 µg/mL (22–28 µM) of each compound were tested in an artificial seawater solution (NaCl 3.5%) with 1% of dimethylsulfoxide (DMSO, v/v). Potassium dichromate (K₂Cr₂O₇) at 10 mg/mL was used as positive toxic control, while both artificial seawater and DMSO (1%) were used as negative controls. The previously studied compounds **1a** and **2a** [30] were included for comparative purposes. The number of dead larvae was recorded after 24 h of exposure and used to calculate the lethal concentration (%). Results are reported as mean values \pm SD, based on three independent experiments.

development has been centered on animal models [36,37]. However, besides being expensive and laborious, these models cannot always be translated into the human *in vivo* responses and, more recently, have reverberated greatly social and ethical dilemmas [38]. Therefore, the use of alternative models at early phases of drug development is advised. In the present study, we select three distinct approaches to screen the general toxicity of our compounds, namely: *i*) an invertebrate animal model (*Artemia salina* brine shrimp); *ii*) a unicellular fungal model (*Saccharomyces cerevisiae*), and; *iii*) two *in vitro* human cell culture models (a keratinocyte cell line and embryonic lung fibroblast cell line). In contrast to the conventional animal models, these approaches are easy to follow, rapid, cost-effective, and have been increasingly used to screen the general toxicity in a broad spectrum of substances (such as synthetic chemicals, heavy metals, natural products, or engineered nanomaterials), constituting a convenient starting point to prioritize only the best candidates for further screening of vertebrates [38–42].

Due to their simple anatomy, brief life-cycle, and small size, which allow large-scale screenings [39], we started by evaluating the lethality of each compound on the *Artemia salina* brine shrimp (Fig. 3). Compared with the previously studied compounds **1a** and **2a** [30], we were pleased to observe that the newly developed molecules exhibited less toxicity in *A. salina* than **1a**, and were also generally less toxic than **2a**. Indeed, with exception of both **1d** and **5d**, the remaining compounds promoted a larvae lethality rate below the 15% observed for **2a**, with **6d** displaying a toxicity level similar to that seen for the artificial seawater solution (ca 3%). The most potent antibacterial agent prepared in this study (**5a**) showed very little toxicity against *A. salina* (ca. 8%), even at a concentration more than one order of magnitude higher than the MICs determined for the several strains. The brine shrimp mortality rates observed after treatment with the 5-nitro indolinyl derivatives **1d**, **5d**, and **6d** point out this last compound as being considerably less toxic. The different mortality rates observed for these three compounds indicate that the level of toxicity (even if residual) shall not be attributed to the presence of the second nitro group.

On the other hand, the yeast *S. cerevisiae* is one of the most popular and widely used eukaryotic models. Besides its rapid growth and ease of replica plating, it can be easily manipulated to evaluate multiple biological effects (inhibition of cellular growth, cytotoxicity and genotoxicity) induced by the drugs considered [40,43]. According to our results (Fig. 4), all tested compounds showed no relevant general toxicity (IC₅₀ > 100 µM) when compared to the positive control Nystatin (IC₅₀ = 3.31 µM). Overall, the obtained IC₅₀ values ranged from 121 µM for **6d** to 292 µM for **5d**, with the less active compounds (**5d**, **1a**, and **6c**) exhibiting, on

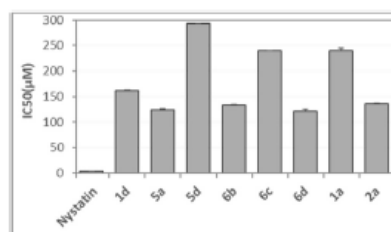


Fig. 4. General toxicity of **1d**, **5a**, **5d**, and **6b-d** in *Saccharomyces cerevisiae* model. The graph depicts the concentration at which each substance induced inhibition of 50% (IC₅₀) in *S. cerevisiae* viability. Nystatin was used as the positive control. The previously studied compounds **1a** and **2a** [30] were included for comparative purposes. Results are expressed as mean IC₅₀ values \pm SD, based on three independent experiments.

average, IC_{50} values ~2-fold higher than the others (**1d**, **5a**, **6b**, **6d** and **2a**). Moreover, the MIC values of **1d** (1.18–18.9 μ M) and **5a** (up to 1.18 μ M) are 1–2 orders of magnitude lower (161.8 and 124.3 μ M, respectively) than the IC_{50} values determined.

Despite both organism-based methods being commonly used for initial screening of general toxicity, different toxicity trends were observed for the two species. For instance, among the most active antibacterial compounds tested, *A. salina* was found to be more sensitive to **5d**, which was revealed to be the least active compound in *S. cerevisiae*. On the other hand, *S. cerevisiae* was mostly sensitive to **6d**, the least toxic compound seen for *A. salina*. Considering the different characteristics of each organism, both methods hold limitations that may underline the observed toxicity disparities. For instance, it is known that, in the brine shrimp lethality bioassay, there may be a decrease in the solubility of some chemical substances in the saline medium producing false positives due to the toxicity of the solvent itself [39,44]. Notwithstanding that no ultimate conclusions on the general toxicity of these compounds can be drawn from these protocols, the information collected is valuable in assessing the viability of this family of phenolic Mannich bases in the development of new drugs.

Finally, to unveil some of the potential applications these compounds might have, cytotoxicity was further characterized by using two widely used *in vitro* cell models of human origin: the HaCat immortalized epidermal keratinocyte line and the MRC-5 embryonic lung fibroblast line. While the former has proved to help evaluate the mechanisms of the cytotoxic and pharmacological action of various agents on the skin [45], MRC-5 cells are a suitable human lung cell model [46].

Fig. 5 shows the viability of HaCat human keratinocytes after 24 h exposure at 50 μ M of each compound under evaluation. Overall, the cytotoxic potential observed on the HaCat cells was highly heterogeneous among compounds, with cell viability ranging from 3% for **6b** (the same magnitude level as the 5% DMSO positive control) to 94% for **1d** (similar to that exhibited by non-treated cells). Among 2-tolyl analogs **6**, compound **6d** was the least cytotoxic to HaCat cells, exhibiting a cytotoxic potential 5.5- and 176-fold lower than **6c** and **6b**, respectively. The presence of a halogen in the indolyl moiety is the apparent cause for the increased cytotoxicity to **6b** and **6c** of the 2-tolyl series.

By comparing the 4-tolyl derivative **1d** and its isomer **5d** becomes evident that the cytotoxic disparities observed on HaCat viability may also rely on the influence of the substituent on the phenyl ring (Scheme 1), as the simple exchange of methyl from the

4- to the 2-positions has a prominent increasing effect on the toxicity. Moreover, likewise previously seen in the *A. salina* model (Fig. 3), the additional presence of the 5-nitro substituent in **5d** seems to confer higher toxicity in HaCat cells, when compared to its trifluoromethyl analog **5a** (Fig. 5). The most effective antibacterial, **1d** and **5a**, showed medium to almost no toxicity for HaCat cells, respectively, with **5a** displaying a cytotoxic potential 0.6-fold lower than that presented by **1d**. Notably, this represents a significant improvement when comparing with the previously studied compound **1a** [29], as 20% cell viability was observed at a 28 μ M concentration of that compound. The replacement of the methyl substituent by trifluoromethyl ameliorates the toxicity profile of the compound (*i.e.* **1a** vs **5a**) while also greatly increasing its antibacterial properties.

In contrast to that seen for HaCat cells, the cytotoxicity activity of the synthesized aminoalkylphenols under evaluation was more homogenous and efficacious on MRC-5 cells (Fig. 6), with mean IC_{50} values ranging from 1.7 μ M for **5a** to 5.8 μ M for **5d**. Surprisingly, **1d**, **5d**, and **6d**, the three molecules containing a nitro group at the 5-position of the indoline moiety, exhibited the lowest toxic effect to MRC-5 cells. Among the 2-tolyl analogs **6**, compound **6d** was the least toxic, followed by **6b** and **6c**. Despite **5a** being found to be the most toxic to MRC-5 cells, it exhibited an IC_{50} value only 0.3-fold lower than the other most effective antibacterial compound **1d**. Generally, the compounds considered for tests on MRC-5 were observed to have IC_{50} values higher than the concentration required to inhibit visible bacterial growth. While less cytotoxic than doxorubicin, the similarity between the determined MICs and IC_{50} values hampers the clinical use of these compounds in treating lower respiratory infections.

Notwithstanding the lack of a possibility to draw clear conclusions on the toxicity of the compounds tested, as no trends could be established with the toxicity models considered, compounds **1d** and **5a**, having the strongest antibacterial properties were not particularly toxic against *A. salina*, *S. cerevisiae*, and HaCat. The high and consistent toxicity of the set of compounds tested on MRC-5 can indicate that the class of aminoalkylphenols is generally toxic for these cell lines. Nevertheless, motivated by the very good bacterial growth inhibitory properties of **1d** and **5a** (previously performed with reference strains), we extended the antibacterial assays of such molecules against a larger collection of Gram-positive bacterial strains with dissimilar resistance phenotypes, including MRSA, VRE, and multidrug-resistant (MDR) strains. Overall, 40 strains from *S. aureus*, *S. epidermidis*, *E. faecalis*,

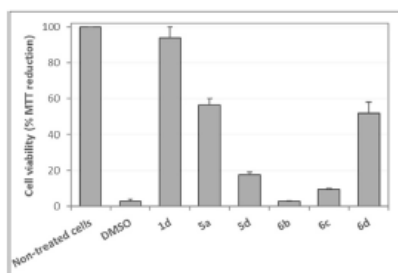


Fig. 5. Effect of the synthesized aminoalkylphenols derivatives **1d**, **5a**, **5d**, and **6b-d** on the viability of HaCat human keratinocytes, evaluated by the MTT reduction assay. Cells were treated with each compound at a final concentration of 50 μ M for 24 h and then submitted to the MTT colorimetric assay. Dimethylsulfoxide (DMSO 5%) was used as the toxic positive control. Results (reported as mean \pm SD) are expressed as percentages relative to non-treated control cells and are based on two independent experiments, each comprising four replicate cultures.

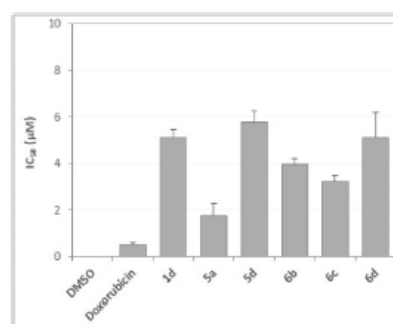


Fig. 6. IC_{50} of synthesized aminoalkylphenols derivatives **1d**, **5a**, **5d**, and **6b-d** on MRC-5 human embryonic lung fibroblast cell line. The cell viability was measured by MTT. Doxorubicin was used as a positive toxic control. IC_{50} values (reported as mean \pm SD) are based on 2 independent experiments, each comprising 4 replicate cultures.

E. faecium, and *Listeria monocytogenes* (eight clinical isolates of each species) were tested (Fig. 7 and Supplemental Table 1).

Similarly to what was previously observed for the ATCC strains, compound **5a** revealed, in general, a more significant and more consistent antibacterial effect against all clinical isolates than compound **1d**. Indeed, lower median MIC values of 4-fold for *E. faecalis* and 8-fold for the remaining species (Fig. 7) were determined for **5a**, contrasting to the milder effects determined for **1d**. The median MIC values displayed by compound **5a** ranged from 1.18 μM for *S. aureus*, *S. epidermidis* and *L. monocytogenes* to 2.36 μM for both *Enterococcus* species, while compound **1d** exhibited median MICs of 9.64 μM for all species' clinical isolates except for *E. faecalis*, for which the median MIC was 19.27 μM . Moreover, whereas compound **5a** exhibited comparable MIC values between the ATCC adapted strains and clinical isolates of both *Staphylococcus* species and *E. faecalis*, compound **1d** revealed median MIC values 2-fold higher for the *S. epidermidis* ATCC adapted strains, but at least an 8-fold lower difference for *E. faecalis* clinical isolates. Such intra-species discrepancies observed for compound **1d** may be due to: i) the dissimilar genetic background of the clinical isolates, ii) to the low number of ATCC strains tested, and iii) to the extensive *in vitro* passaging of ATCC strains.

3. Conclusions

In summary, this work presents the preparation of new phenol Mannich bases, easily prepared from the multicomponent Pétasis reaction, the assessment of their antibacterial properties, as well as their toxicity *in vivo* (on *A. salina* and *S. cerevisiae*) and *in vitro* (on keratinocyte and embryonic lung fibroblast cell lines).

This work corroborates the previous observations that this class of compounds is generally effective against multi-resistant Gram-positive bacteria. The introduction of different substituents in the indoline moiety contributed to a significant change in the antibacterial properties of previously reported analogs. The presence of an additional nitro substituent at the 5-indolyl position conferred additional antibacterial activity and decreased the antioxidant activity. Despite the noticeable effect of the indoline's substituents on the antioxidant activity, a lack of correlation between the antibacterial properties of aminoalkylphenols and such property was also

corroborated.

Apart from the increased toxic effect observed by **5d** on HaCat cell lines, the 5-nitroindolyl derivatives did not show increased toxicity when compared with other analogs. Moreover, 5-nitroindolyl derivative **1d** was determined to have increased antibacterial properties while not significantly increasing its toxicity to the eukaryotic systems considered. The presence of a trifluoromethyl substituent in the *para*-position of the aromatic ring installed by the aryl boronic acid also led to the improvement of the antibacterial properties. The 5-nitroindolyl and trifluoromethylated derivatives (**1d** and **5a**, respectively) are efficient growth inhibitors of the five Gram-positive bacterial strains tested (*S. aureus*, *S. epidermidis*, *E. faecalis*, *E. faecium*, and *L. monocytogenes*). In particular, the antibacterial efficacy of compound **5a** translates into MICs lower than 5 μM for tested reference strains and clinical isolates. While these compounds demonstrated trivial toxicity on the *in vivo* models tested, they exerted a toxic effect on normal human embryonic lung fibroblast cells indicating that the *in vivo* use of the compounds may be limited. Urged by the excellent antibacterial properties of these compounds and the urgent need to find new chemical entities that are toxic to pathogenic microorganisms, we are currently working on a system for their delivery in living organisms. Further research on understanding the mechanism of action of these compounds, and evaluation of their toxicity in other cell lines is nevertheless important to determine their full potential as antibacterial agents.

4. Materials and methods

4.1. Synthesis

4.1.1. General remarks

All reagents were obtained from Sigma-Aldrich or TCI and were used without further purification. Reactions were monitored by thin-layer chromatography carried out on precoated (Merck TLC silica gel 60 F254) aluminum plates by using UV light as a visualizing agent and cerium molybdate solution or ninhydrin as developing agents. Flash column chromatography was performed on silica gel 60 (Merck, 0.040–0.063 mm). Melting points were measured in open capillary tubes on a Büchi B-540 melting point

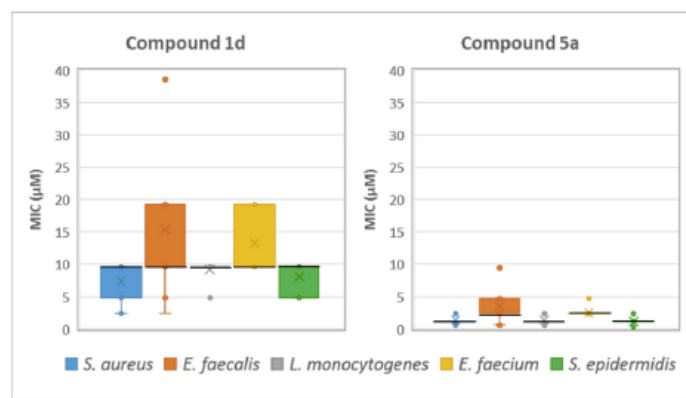


Fig. 7. MIC values of compounds **1d** and **5a** for diverse clinical isolates of *S. aureus*, *E. faecalis*, *L. monocytogenes*, *E. faecium*, and *S. epidermidis*. Boxplot chart was generated using R statistical software v. 3.4.2 and consists of boxes (median and interquartile range) and whiskers that extend to the most extreme data points that were no more than 1.5 times the interquartile range from the box. Boxes represent the variability of MIC values found among all strains from each species. The horizontal black line marks the median, while the cross ("x") within each box represents the medium MIC value. The lowest and the highest coverage values observed are represented by the extremes of the whisker below and above each box, respectively. Outliers are indicated by filled circles.

apparatus. NMR spectra were recorded with Varian Mercury 300 MHz or JEOL ECZR 500 instruments using CDCl₃, DMSO-*d*₆, or methanol-*d*₄ as solvents and calibrated using tetramethylsilane as an internal standard. Chemical shifts (δ) are reported in ppm referenced to the non-deuterated residual peak (δ 7.26 for CDCl₃, δ 2.50 for DMSO-*d*₆ and δ 3.31 for MeOH-*d*₄) or TMS peak (δ 0.00) for ¹H NMR. The same approach was used for ¹³C NMR, and the chemical shifts are referenced to the non-deuterated residual peak (δ 77.16 for CDCl₃, δ 39.50 for DMSO-*d*₆, and δ 49.00 for MeOH-*d*₄). The following abbreviations were used to describe peak splitting patterns: s = singlet, d = doublet, t = triplet, m = multiplet. Coupling constants, *J*, were reported in hertz. High-resolution mass spectra were recorded on a Waters ESI-TOF MS spectrometer. All compounds tested for antibacterial activity were established to be >95% pure upon NMR analysis.

4.1.2. Preparation of indolines 3

All indolines, except indoline (3a) and 5-bromoindoline (3c) which were obtained commercially, were synthesized by reducing commercially available indoles with sodium cyanoborohydride (Method A) or triethylsilane (Method B).

4.1.2.1. Method A. Acetic acid (10 mL) was added to a flask charged with sodium cyanoborohydride (3 mmol, 3 equiv.) and indole (1 mmol, 1 equiv.) at 0 °C, under argon. The partially frozen mixture was stirred fast for 5 min and moved to ambient temperature. The reaction was stirred until TLC indicated completion of the reaction. Acetic acid was evaporated under reduced pressure and the residue was dissolved in 15 mL of DCM. The resulting mixture was washed with 15 mL of saturated aqueous Na₂CO₃ and the aqueous layer from the washing was extracted with 3 × 5 mL of DCM. Organic extracts were combined, dried over MgSO₄, filtered, and evaporated under reduced pressure. The residue was purified by column chromatography to obtain the desired indoline.

4.1.2.2. Method B. Triethylsilane (2.6 mmol, 2.6 equiv.) was added dropwise to a stirred suspension of indole (1 mmol, 1 equiv.) in 1.5 mL of trifluoroacetic acid at ambient temperature, under argon. The reaction was heated to 50 °C and stirred until TLC indicated completion of the reaction. Trifluoroacetic acid was evaporated under reduced pressure and the residue was diluted with 5 mL of DCM. The resulting mixture was washed with 5 mL of saturated aqueous NaHCO₃ and the aqueous layer from the washing was extracted with 2 × 5 mL of DCM. Organic extracts were combined, dried over Na₂SO₄, filtered, and evaporated under reduced pressure. The residue was purified by column chromatography to obtain the desired indoline.

4.1.2.3. 5-Chloroindoline (3b). Method A provided the titled compound in 89% yield after 3 h reaction time, purified by flash chromatography using CH₂Cl₂/EtOAc (98:2) as eluent (*R*_f = 0.1, CH₂Cl₂), and having similar spectral data to previously reported.[47] ¹H NMR (300 MHz, CDCl₃) δ 6.99 (d, *J* = 1.8 Hz, 1H), 6.88 (dd, *J* = 2.3, 8.2 Hz, 1H), 6.46 (d, *J* = 8.2 Hz, 1H), 3.50 (t, *J* = 8.2 Hz, 2H, and overlapped NH), 2.94 (t, *J* = 8.5 Hz, 2H).

4.1.2.4. 5-Nitroindoline (3d). Method B provided the titled compound in 96% yield after 30 min reaction time, purified by flash chromatography using Hex/EtOAc (7:3) as eluent (*R*_f = 0.3, Hex/EtOAc 7:3), and having similar spectral data to previously reported.[48] ¹H NMR (300 MHz, CDCl₃) δ 7.99 (dd, *J* = 2.3, 8.8 Hz, 1H), 7.94 (s, 1H), 6.47 (d, *J* = 8.8 Hz, 1H), 4.53 (br. s, 1H), 3.76 (t, *J* = 8.8 Hz, 2H), 3.12 (t, *J* = 8.8 Hz, 2H).

4.1.2.5. Indoline-4-carbonitrile (3e). Method B provided the titled

compound in 70% yield after 30 min reaction time purified by flash chromatography using Hex/EtOAc (6:4) as eluent (*R*_f = 0.2, Hex/EtOAc 6:4), and having similar spectral data to previously reported.[49] ¹H NMR (500 MHz, DMSO-*d*₆) δ 7.05 (t, *J* = 7.7 Hz, 1H), 6.83 (d, *J* = 7.4 Hz, 1H), 6.72 (d, *J* = 8.0 Hz, 1H), 6.02 (br. s, 1H), 3.51 (td, *J* = 8.6, 1.1 Hz, 2H), 3.08 (t, *J* = 8.6 Hz, 2H).

4.1.2.6. Indolin-5-ol (3f). Sodium cyanoborohydride (189 mg, 3 mmol, 3 equiv.) was added in small portions to a stirred solution of 1H-indol-5-ol (133 mg, 1 mmol, 1 equiv.) in 10 mL of acetic acid at ambient temperature, under argon. The reaction was stirred for 80 min and the acetic acid was evaporated under reduced pressure. The residue was diluted with 2.5 mL of hexane, 2.5 mL of DCM, and finally basified with 3 mL of triethylamine. Solvents and the remaining triethylamine were evaporated under reduced pressure and the residue was suspended in 10 mL of diethyl ether. The suspension was filtered through a Celite pad and the pad was washed with 2 × 10 mL of Et₂O. Filtrates were combined, dried over Na₂SO₄, filtered, and evaporated under reduced pressure. The residue was purified by column chromatography (5% methanol in EtOAc) to obtain the title compound with 32% yield, with similar spectral data to previously reported (*R*_f = 0.3, EtOAc).[50, 51] ¹H NMR (300 MHz, CDCl₃) δ 6.59 (s, 1H), 6.50 (d, *J* = 8.2 Hz, 1H), 6.43 (dd, *J* = 2.3, 8.2 Hz, 1H), 4.53 (br. s, 2H), 3.46 (t, *J* = 8.2 Hz, 2H), 2.92 (t, *J* = 8.5 Hz, 2H).

4.1.2.7. 5-Methoxyindoline (3g). Method A provided the titled compound in 82% yield after 1 h reaction time, purified by flash chromatography using EtOAc as eluent (*R*_f = 0.1, EtOAc), having similar spectral data to previously reported with similar spectral data to previously reported.[52] ¹H NMR (300 MHz, CDCl₃) δ 6.69 (s, 1H), 6.52–6.52 (m, 2H), 3.67 (s, 3H), 3.46 (t, *J* = 8.2 Hz, 2H), 3.40 (br. s, 1H), 2.93 (t, *J* = 8.5 Hz, 2H).

4.1.3. Preparation of phenol Mannich bases 1, 5 and 6

4.1.3.1. General procedure. Aldehyde (0.5 mmol, 1 equiv.) and arylboronic acid (0.5 mmol, 1 equiv.) were dissolved in 5 mL of DCE and heated to 50 °C. After stirring for 5 min, indoline (0.5 mmol, 1 equiv.) was added in one portion. Stirring was continued until TLC indicated completion of the reaction. The solvent was evaporated under reduced pressure and the residue was purified by column chromatography to obtain the desired aminoalkylphenol.

4.1.3.2. 2-((5-Chloroindolin-1-yl) (p-tolyl)methyl)-4-nitrophenol (1b). Obtained in 83% yield as an off-white solid, after purification by flash chromatography using Hex/CH₂Cl₂ (3:7) as eluent (*R*_f = 0.5, CH₂Cl₂). m. p. 156–158 °C. ¹H NMR (300 MHz, CDCl₃) δ 11.39 (br. s, 1H), 8.10 (dd, *J* = 2.6, 9.1 Hz, 1H), 7.95 (d, *J* = 2.9 Hz, 1H), 7.28 (d, *J* = 8.2 Hz, 2H), 7.12–7.18 (m, 3H), 6.95 (d, *J* = 8.8 Hz, 2H), 6.38 (d, *J* = 8.2 Hz, 1H), 5.29 (s, 1H), 3.20–3.27 (m, 1H), 3.09 (q, *J* = 9.6 Hz, 1H), 2.84–3.00 (m, 2H), 2.34 (s, 3H). ¹³C NMR (75 MHz, CDCl₃) δ 162.39, 148.82, 140.83, 138.89, 134.63, 134.33, 129.87, 128.56, 127.27, 126.48, 125.17, 124.73, 117.61, 113.00, 70.06, 53.57, 28.24, 21.11. HRMS (ESI/TOF): *m/z* calcd for C₂₂H₁₉ClN₂O₃ [M]⁺, 394.1079; found 394.1061.

4.1.3.3. 2-((5-Bromoindolin-1-yl) (p-tolyl)methyl)-4-nitrophenol (1c). Obtained in 85% yield as a pale yellow solid, after purification by flash chromatography using Hex/CH₂Cl₂ (1:2) as eluent (*R*_f = 0.6, CH₂Cl₂). m. p. 146–148 °C. ¹H NMR (300 MHz, CDCl₃) δ 11.30 (br. s, 1H), 8.10 (dd, *J* = 2.9, 8.8 Hz, 1H), 7.95 (d, *J* = 2.9 Hz, 1H), 7.26–7.30 (m, 3H), 7.16–7.18 (m, 2H), 7.10 (dd, *J* = 2.1, 8.5 Hz, 1H), 6.96 (d, *J* = 8.8 Hz, 1H), 6.34 (d, *J* = 8.8 Hz, 1H), 5.30 (s, 1H), 3.20–3.27 (m, 1H), 3.05–3.14 (m, 1H), 2.85–3.01 (m, 2H), 2.34 (s, 3H). ¹³C NMR (75 MHz, CDCl₃) δ 162.35, 149.31, 140.86, 138.92,

134.72, 134.56, 130.20, 129.88, 128.58, 128.00, 126.44, 125.19, 124.73, 117.62, 114.62, 113.49, 69.88, 53.47, 28.18, 21.12. HRMS (ESI/TOF): m/z calcd for $C_{22}H_{19}BrN_2O_3^+$ [M]⁺, 438.0574; found 438.0571.

4.1.3.4. 4-Nitro-2-((5-nitroindolin-1-yl) (p-tolyl)methyl)phenol (1d). Obtained in 85% yield as an orange red solid, after purification by flash chromatography using $CH_2Cl_2/EtOAc$ (97:3) as eluent ($R_f = 0.3$, Hex/ $EtOAc$ (2:8)). m. p. 141–144 °C. ¹H NMR (500 MHz, $CDCl_3$) δ 8.17 (s, 1H), 8.13 (dd, $J = 8.9, 2.6$ Hz, 1H), 7.98 (d, $J = 2.9$ Hz, 1H), 7.91–7.94 (m, 2H), 7.18 (q, $J = 8.6$ Hz, 4H), 7.03 (d, $J = 9.2$ Hz, 1H), 6.25 (d, $J = 8.6$ Hz, 1H), 6.02 (s, 1H), 3.44–3.54 (m, 2H), 3.10 (t, $J = 8.6$ Hz, 2H), 2.36 (s, 3H). ¹³C NMR (126 MHz, $CDCl_3$) δ 160.38, 156.40, 141.22, 138.88, 138.53, 133.55, 130.90, 129.84, 128.07, 126.58, 126.42, 125.51, 125.15, 120.80, 116.65, 106.05, 60.25, 51.24, 26.96, 21.11. HRMS (ESI/TOF): m/z calcd for $C_{22}H_{19}N_3O_5^+$ [M]⁺, 405.1319; found 405.1302.

4.1.3.5. 1-((2-Hydroxy-5-nitrophenyl) (p-tolyl)methyl)indoline-4-carbonitrile (1e). Obtained in 39% yield as a pale yellow solid, after purification by flash chromatography using CH_2Cl_2 as eluent ($R_f = 0.3$, CH_2Cl_2). m. p. 182–183 °C. ¹H NMR (300 MHz, $CDCl_3$) δ 10.37 (br. s, 1H), 8.12 (dd, $J = 2.9, 8.8$ Hz, 1H), 7.98 (d, $J = 2.9$ Hz, 1H), 7.27 (d, $J = 7.6$ Hz, 2H), 7.19 (d, $J = 8.2$ Hz, 2H), 7.05–7.14 (m, 2H), 6.98 (d, $J = 8.8$ Hz, 1H), 6.62 (dd, $J = 1.8, 7.0$ Hz, 1H), 5.41 (s, 1H), 3.31–3.39 (m, 1H), 3.09–3.27 (m, 3H), 2.35 (s, 3H). ¹³C NMR (75 MHz, $CDCl_3$) δ 161.73, 151.07, 141.10, 139.11, 136.66, 134.11, 130.01, 128.58, 128.52, 126.29, 125.33, 124.81, 124.32, 117.60, 117.13, 115.42, 109.14, 68.59, 52.81, 27.93, 21.13. HRMS (ESI/TOF): m/z calcd for $C_{23}H_{19}N_3O_3^+$ [M]⁺, 385.1421; found 385.1425.

4.1.3.6. 1-((2-Hydroxy-5-nitrophenyl) (p-tolyl)methyl)indolin-5-ol (1f). Obtained in 20% yield as an orange solid, after purification by flash chromatography using Hex/ $EtOAc$ (6:4) as eluent ($R_f = 0.7$, $EtOAc$). m. p. 100–105 °C. ¹H NMR (300 MHz, $CDCl_3$) δ 8.09 (dd, $J = 2.9, 9.4$ Hz, 1H), 7.93 (d, $J = 2.9$ Hz, 1H), 7.29 (d, $J = 8.2$ Hz, 2H), 7.15 (d, $J = 8.2$ Hz, 2H), 6.94 (d, $J = 9.4$ Hz, 1H), 6.69 (d, $J = 2.3$ Hz, 1H), 6.45 (dd, $J = 2.9, 8.8$ Hz, 1H), 6.29–6.36 (m, 1H), 5.17 (s, 1H), 3.16–3.23 (m, 1H), 2.96–3.05 (m, 1H), 2.79–2.94 (m, 2H), 2.33 (s, 3H). ¹³C NMR (75 MHz, $CDCl_3$) δ 163.04, 151.63, 143.67, 140.57, 138.73, 135.29, 134.48, 129.78, 128.53, 126.91, 125.06, 124.66, 117.59, 113.58, 113.35, 112.60, 71.63, 53.95, 28.64, 21.12. HRMS (ESI/TOF): m/z calcd for $C_{22}H_{19}N_2O_4^+$ [M – H]⁺, 375.1350; found 375.1343.

4.1.3.7. 2-((5-Methoxyindolin-1-yl) (p-tolyl)methyl)-4-nitrophenol (1g). Obtained in 68% yield as a pale yellow solid, after purification by flash chromatography using Hex/ $EtOAc$ (8:2) as eluent ($R_f = 0.7$, Hex/ $EtOAc$ (1:1)). m. p. 157–158 °C. ¹H NMR (300 MHz, $CDCl_3$) δ 8.01 (dd, $J = 2.3, 8.8$ Hz, 1H), 7.87 (d, $J = 2.9$ Hz, 1H), 7.22 (d, $J = 8.2$ Hz, 2H), 7.08 (d, $J = 7.6$ Hz, 2H), 6.87 (d, $J = 8.8$ Hz, 1H), 6.69 (d, $J = 2.3$ Hz, 1H), 6.46 (dd, $J = 2.9, 8.8$ Hz, 1H), 6.32 (d, $J = 8.8$ Hz, 1H), 5.12 (s, 1H), 3.65 (s, 3H), 3.10–3.16 (m, 1H), 2.84–2.96 (m, 1H), 2.75–2.81 (m, 2H), 2.26 (s, 3H). ¹³C NMR (75 MHz, $CDCl_3$) δ 163.03, 155.85, 143.71, 140.61, 138.70, 135.34, 134.26, 129.79, 128.53, 126.93, 125.04, 124.65, 117.59, 113.19, 111.86, 111.68, 71.61, 55.65, 53.99, 28.73, 21.12. HRMS (ESI/TOF): m/z calcd for $C_{23}H_{22}N_2O_4^+$ [M]⁺, 390.1574; found 390.1574.

4.1.3.8. 2-(Indolin-1-yl(4-(trifluoromethyl)phenyl)methyl)-4-nitrophenol (5a). Obtained in 80% yield as a pale yellow solid, after purification by flash chromatography using Hex/ $EtOAc$ (7:3) as eluent ($R_f = 0.3$, Hex/ $EtOAc$ (7:3)). m. p. 115–118 °C. ¹H NMR (300 MHz, $CDCl_3$) δ 8.13 (dd, $J = 2.6, 9.1$ Hz, 1H), 7.95 (d, $J = 2.9$ Hz, 1H), 7.56–7.66 (m, 4H), 7.20 (d, $J = 7.0$ Hz, 1H), 6.92–7.05 (m, 3H), 6.49 (d, $J = 7.6$ Hz, 1H), 5.42 (s, 1H), 3.19–3.26 (m, 1H), 2.93–3.08 (m, 3H). ¹³C NMR (75 MHz, $CDCl_3$) δ 162.46, 149.89, 141.95, 140.95,

132.23, 131.27, 129.07, 127.63, 126.29, 126.24, 126.20, 126.14, 125.94, 125.49, 125.11, 124.55, 122.70, 117.91, 112.24, 70.07, 53.79, 28.47. HRMS (ESI/TOF): m/z calcd for $C_{22}H_{18}F_3N_2O_3^+$ [M+H]⁺, 415.1264; found 415.1286.

4.1.3.9. 4-Nitro-2-((5-nitroindolin-1-yl) (4-(trifluoromethyl)phenyl)methyl)phenol (5d). Obtained in 77% yield as an orange red solid, after purification by flash chromatography using $CH_2Cl_2/EtOAc$ (97:3) as eluent ($R_f = 0.1$, CH_2Cl_2). m. p. 164–167 °C. ¹H NMR (300 MHz, $CDCl_3$) δ 8.11 (dd, $J = 2.6, 9.1$ Hz, 1H), 7.89–7.91 (m, 3H), 7.60 (d, $J = 8.2$ Hz, 2H), 7.37 (d, $J = 8.2$ Hz, 2H), 6.94 (d, $J = 8.8$ Hz, 1H), 6.21 (d, $J = 9.4$ Hz, 1H), 6.01 (s, 1H), 3.36–3.43 (m, 2H), 3.07 (t, $J = 8.8$ Hz, 2H). ¹³C NMR (75 MHz, $CDCl_3$) δ 159.96, 156.12, 141.45, 141.13, 139.18, 130.61, 128.46, 126.40, 126.15, 125.89, 125.77, 125.17, 120.93, 116.65, 105.75, 59.44, 51.12, 27.04. HRMS (ESI/TOF): m/z calcd for $C_{22}H_{15}F_3N_3O_5^+$ [M – H]⁺, 458.0969; found 458.0962.

4.1.3.10. 2-((5-Chloroindolin-1-yl) (o-tolyl)methyl)-4-nitrophenol (6b). Obtained in 62% yield as a pale yellow solid, after purification by flash chromatography using Hex/ CH_2Cl_2 (8:2) as eluent ($R_f = 0.5$, CH_2Cl_2). m. p. 134–136 °C. ¹H NMR (300 MHz, $CDCl_3$) δ 8.11 (dd, $J = 2.6, 9.1$ Hz, 1H), 7.87 (d, $J = 2.9$ Hz, 1H), 7.35 (d, $J = 7.0$ Hz, 1H), 7.13–7.23 (m, 4H), 6.93–6.98 (m, 2H), 6.27 (d, $J = 8.2$ Hz, 1H), 5.69 (s, 1H), 3.23–3.28 (m, 1H), 2.92–3.10 (m, 3H), 2.38 (s, 3H). ¹³C NMR (75 MHz, $CDCl_3$) δ 162.34, 149.10, 141.08, 136.21, 136.00, 133.68, 131.25, 128.65, 128.29, 127.42, 127.17, 126.84, 126.61, 125.20, 124.49, 117.60, 112.06, 110.00, 64.22, 53.19, 28.26, 20.46. HRMS (ESI/TOF): m/z calcd for $C_{22}H_{19}ClN_2O_3^+$ [M]⁺, 394.1079; found 394.1096.

4.1.3.11. 2-((5-Bromoindolin-1-yl) (o-tolyl)methyl)-4-nitrophenol (6c). Obtained in 91% yield as an orange red solid, after purification by flash chromatography using Hex/ $EtOAc$ (8:2) as eluent ($R_f = 0.6$, Hex/ $EtOAc$ (1:1)). m. p. 158–160 °C. ¹H NMR (300 MHz, $CDCl_3$) δ 10.65 (br. s, 1H), 8.12 (dd, $J = 2.9, 8.8$ Hz, 1H), 7.88 (d, $J = 2.9$ Hz, 1H), 7.35 (d, $J = 7.6$ Hz, 1H), 7.09 (dd, $J = 2.1, 8.5$ Hz, 1H), 6.97 (d, $J = 8.8$ Hz, 1H), 6.23 (d, $J = 8.8$ Hz, 1H), 5.70 (s, 1H), 3.23–3.31 (m, 1H), 2.93–3.11 (m, 3H), 2.38 (s, 3H). ¹³C NMR (75 MHz, $CDCl_3$) δ 162.22, 149.60, 141.11, 136.15, 136.03, 134.01, 131.25, 130.32, 128.66, 128.26, 128.01, 127.16, 125.20, 124.50, 117.54, 112.41, 63.82, 53.04, 28.20, 20.43. HRMS (ESI/TOF): m/z calcd for $C_{22}H_{20}BrN_2O_3^+$ [M+H]⁺, 439.0652; found 439.0645.

4.1.3.12. 4-Nitro-2-((5-nitroindolin-1-yl) (o-tolyl)methyl)phenol (6d). Obtained in 85% yield as a dark red solid, after purification by flash chromatography using Hex/ $EtOAc$ (6:4) as eluent ($R_f = 0.2$, Hex/ $EtOAc$ (7:3)). m. p. 197–198 °C. ¹H NMR (500 MHz, $DMSO-d_6$) δ 11.58 (s, 1H), 8.15 (dd, $J = 8.9, 2.6$ Hz, 1H), 7.91 (dd, $J = 8.6, 2.3$ Hz, 1H), 7.87 (d, $J = 1.1$ Hz, 1H), 7.71 (d, $J = 2.9$ Hz, 1H), 7.27 (d, $J = 4.0$ Hz, 2H), 7.21–7.24 (m, 1H), 7.15 (d, $J = 7.4$ Hz, 1H), 7.08 (d, $J = 8.6$ Hz, 1H), 6.19 (s, 1H), 6.17 (d, $J = 9.2$ Hz, 1H), 3.37–3.48 (m, 3H), 3.06–3.16 (m, 2H), 2.15 (s, 3H). ¹³C NMR (126 MHz, $DMSO-d_6$) δ 161.92, 156.10, 139.67, 137.09, 136.27, 136.12, 130.93, 130.47, 128.02, 126.74, 126.50, 126.37, 125.86, 125.81, 124.35, 120.28, 115.85, 103.80, 54.66, 50.67, 26.25, 18.81. HRMS (ESI/TOF): m/z calcd for $C_{22}H_{18}N_3O_5^+$ [M – H]⁺, 404.1252; found 404.1221.

4.1.3.13. 1-((2-Hydroxy-5-nitrophenyl) (o-tolyl)methyl)indoline-4-carbonitrile (6e). Obtained with 98% yield as a pale yellow solid, after purification by flash chromatography using Hex/ $EtOAc$ (7:3) as eluent ($R_f = 0.5$, Hex/ $EtOAc$ (1:1)). m. p. 177–179 °C. ¹H NMR (300 MHz, $Methanol-d_4$) δ 8.10 (dd, $J = 2.6, 9.1$ Hz, 1H), 7.96 (d, $J = 2.3$ Hz, 1H), 7.14–7.22 (m, 4H), 6.95–7.01 (m, 2H), 6.79 (d, $J = 7.6$ Hz, 1H), 6.22 (d, $J = 8.2$ Hz, 1H), 6.06 (s, 1H), 3.40 (q, $J = 8.8$ Hz, 1H), 3.25–3.33 (m, 1H), 3.12–3.18 (m, 2H), 2.23 (s, 3H).

^{13}C NMR (75 MHz, Methanol- d_4) δ 162.84, 153.10, 141.85, 138.44, 137.82, 135.75, 131.83, 129.58, 128.87, 128.80, 128.50, 127.25, 126.10, 125.95, 120.22, 118.68, 116.28, 111.02, 109.14, 57.13, 51.71, 28.58, 19.45. HRMS (ESI/TOF): m/z calcd for $\text{C}_{23}\text{H}_{19}\text{N}_3\text{O}_3^+$ [M] $^+$, 385.1421; found 385.1427.

4.2. Antibacterial assays

4.2.1. Determination of MIC

For selective purposes, the antimicrobial activity of the diverse compounds was preliminarily tested against seven bacterial Gram-positive strains obtained from American Type Culture Collection (ATCC): *S. aureus* ATCC 25923 (MSSA), *S. aureus* ATCC 6538 (MSSA), *S. aureus* CIP106760 (MRSA), *E. faecalis* ATCC 29212, *E. faecalis* ATCC 51299 (VRE), *S. epidermidis* ATCC 12228 and *B. subtilis* ATCC 6633 strains.

For the most promising compounds (i.e., **1d** and **5a**), the antimicrobial activity was further evaluated against eight distinct clinical isolates of *S. aureus*, *S. epidermidis*, *E. faecalis*, *E. faecium*, and *L. monocytogenes* from the wide collection of pathogenic Gram-positive strains of the Portuguese National Institute of Health (NIH) (Supplementary Table 1).

Before each experiment, frozen stocks of all isolates were subcultured three times to check strain viability and to avoid any negative growth effect from congelation. *S. aureus*, *S. epidermidis*, *E. faecalis*, *E. faecium* and *B. subtilis* were subcultured in Mueller-Hinton (MH) agar at 35 °C whereas *L. monocytogenes* was subcultured in MH agar supplemented with 5% defibrinated horse blood and 20 mg/L β -NAD (MH-F) at 35 °C in 5% CO_2 [53].

For each compound, the minimum inhibitory concentration (MIC) was determined by the broth dilution method [54], according to the European Committee on Antimicrobial Susceptibility Testing (EUCAST) guidelines [53].

Twofold serial dilutions of the concentrated stock compound solution (1 mM) were prepared in the required growth medium for each bacterial species into a 96-well plate. For ATCC strains, vancomycin was added as the positive control. Cation-Adjusted Mueller Hinton Broth (CAMHB, BD BBL) was used for *S. aureus*, *S. epidermidis*, *E. faecalis*, *E. faecium* [53], and *B. subtilis* while CAMHB supplemented with 20 mg/L β -NAD was used for *L. monocytogenes*. For all bacterial species, inocula of 1.5×10^8 CFU/mL (one for each strain/isolate) were prepared by direct colony saline-phosphate-buffered saline (PBS) suspension, equivalent to a 0.5 McFarland standard, using colonies from the respective overnight agar plates. A 1:20 dilution of each prepared bacterial inoculum in the appropriate broth medium was subsequently used. Controls without the compound and bacterial inocula were also prepared. Plates were incubated for 16–24 h at 35 °C (and with 5% CO_2 for *L. monocytogenes*). Purity check and colony or viable cell counts of the inoculum suspensions were also evaluated in order to ensure that the final inoculum density closely approximates the intended number. This was obtained by subculturing a diluted aliquot from the growth control-well (without compound) immediately after inoculation onto a suitable nonselective agar plate for simultaneous incubation. The MIC was determined as the lowest compound concentration at which no visible growth was observed. The bacterial growth was measured with an absorbance microplate reader (Thermo Scientific Multiskan FC, Loughborough, UK) set to 600 nm. Assays were carried out in triplicate for each ATCC strain and in sextuplicate for each isolate.

4.2.2. Determination of MBC

After MIC assessment, MBC was also evaluated for each ATCC strain. Briefly, the bacterial suspension on the wells was homogenized, serially diluted, triplicate spread on appropriate medium, and

incubated. The MBC attributed to the compound concentration resulting in a 99.9% reduction in bacterial numbers. All assays were carried out in triplicate for each tested microorganism.

4.3. Toxicity evaluation

4.3.1. Brine shrimp lethality bioassay (*Artemia salina*)

For the most active antibacterial agents (**1d**, **5a**, **5d**, and **6b-d**), the toxicity was evaluated using the *Artemia salina* model, as previously described [55]. Each compound was tested at a fixed concentration of 10 ppm in artificial seawater (3.5% NaCl solution) with 1% DMSO (v/v). Potassium dichromate ($\text{K}_2\text{Cr}_2\text{O}_7$) at 10 mg/mL was used as positive toxic control, while individual artificial seawater and DMSO (1%) were included as negative controls. After 24 h of treatment, the number of survived larvae was recorded and the mortality rate (%) was determined using the following equation:

$$\text{Mortality rate (\%)} = \frac{\text{Total } A. \text{ salina} - \text{Alive } A. \text{ salina}}{\text{Total } A. \text{ salina}} \times 100\% \quad (1)$$

where,

Total *A. salina* = the total number of larvae in the assay

Alive *A. salina* = the number of surviving *A. salina* larvae in the assay

The assay was carried out in triplicate for each tested compound.

4.3.2. *Saccharomyces cerevisiae* bioassay

General toxicity studies using *Saccharomyces cerevisiae* (ATCC 2601) model were performed in a microdilution method adapted from a previous report [55]. Briefly, a volume of 100 μL was added to all the wells containing Sabouraud culture medium, and 100 μL of the samples at a concentration of 1 mg/mL were added to the first well. Serial dilutions were made in a proportion of 1:2 and 10 μL of yeast suspension was added to each well. The plates were incubated for 24 h at 37 °C and Optical Density at 525 nm was measured using a Microplate Reader (Thermo Scientific Multiskan FC, Loughborough, UK). Nystatin (NYS) was used as positive control and the assays were carried out in triplicate. Inhibition of cell growth was determined according to the formula:

$$\text{IC}_{50} = 100 - \left[\frac{\text{OD sample} - \text{OD medium control}}{\text{OD cell control} - \text{OD medium control}} \right] \times 100 \quad (2)$$

4.3.3. MTT reduction assay

4.3.3.1. Cytotoxicity in HaCat cells.

The cytotoxicity assessment in the human keratinocyte HaCat cell line was carried out using the colorimetric MTT assay, as previously described [56]. Briefly, 5×10^3 cells/well were seeded in 200 μL of culture medium (Dulbecco's Modified Eagle's Medium supplemented with 10% fetal bovine serum, 100 U/mL penicillin and 0.1 mg/mL streptomycin in 96-well plates, and incubated at 37 °C under an atmosphere with 5% CO_2 in air.

After 24 h, cells were exposed to each compound at a final concentration of 50 μM for a 24 h-period. All compounds were initially solubilized in DMSO and then further diluted in PBS, so that the final concentration of DMSO in culture medium was 0.5% in all samples, except for the positive control (DMSO 5% (v/v)). After treatment, cells were washed with culture medium, followed by the addition of MTT (0.5 mg/mL). The cells were then incubated for a further 2.5 h period and carefully washed with PBS, prior to the DMSO addition (200 μL /well) to solubilize the purple formazan

crystals resultant from the MTT reduction by mitochondrial enzymes in metabolically active cells. The MTT reduction (proportional to the number of viable cells) was measured using an absorbance microplate reader (Thermo Scientific Multiskan FC, USA) set to 595 nm. Two independent experiments were performed, each comprising four replicate cultures. Cytotoxicity results (mean \pm SD) were expressed as percentages relative to non-treated control cells.

4.3.3.2. Cytotoxicity in MRC-5 cells. The effects of increasing concentrations of each compound on MRC-5 cell (ATCC CCL-171) growth were tested in 96-well flat-bottomed microtiter plates. The cell line was purchased from LGC Promochem (Teddington, UK) and was cultured in Eagle's Minimal Essential Medium (EMEM) supplemented with non-essential amino acid mixture, a selection of vitamins, 10% heat-inactivated fetal bovine serum, 2 mM L-glutamine, 1 mM Na-pyruvate, nystatin and penicillin-streptomycin mixture (Sigma-Aldrich, USA) in concentrations of 100 U/L and 10 mg/L, respectively. The cell line was incubated at 37 °C, in a 5% CO₂, 95% air atmosphere. Each compound was diluted in 100 μ L of EMEM medium. Then, 1.5×10^4 cells in 100 μ L of medium were added to each well, except for the medium control wells. The culture plates were further incubated at 37 °C for 24 h, prior to the addition of 20 μ L of MTT (Sigma-Aldrich, Spain) (from a 5 mg/mL stock solution) to each well. After incubation at 37 °C for 4 h, 100 μ L of sodium dodecyl sulfate solution (Sigma-Aldrich, Spain) (10% in 0.01 M HCl) was added to each well and the plates were further incubated at 37 °C overnight. Cell growth was determined by measuring the optical density (OD) at 540 nm (ref. 630 nm) with a Multiskan EX ELISA reader. Inhibition of cell growth was determined according to formula (2) (see section 4.3.2). Results are expressed in terms of IC₅₀, defined as the inhibitory dose that reduced the growth of the cells exposed to the tested compounds by 50%, and presented as an average of 2 independent experiments and 4 replicates.

4.4. Antioxidant activity evaluation (DPPH method)

The antioxidant activity of compounds **1d** and **5a** was tested as previously described [30]. Briefly, a concentration of 10 μ g/mL (22–26 μ M) of each compound was subjected to the free radical scavenging test (the DPPH method). The change in optical density (OD) of DPPH radicals was monitored at 517 nm against a corresponding blank. The antioxidant activity was calculated using the following equation:

$$\text{Scavenging activity (\%)} = \frac{\text{OD control} - \text{OD sample}}{\text{OD control}} \times 100 \quad (3)$$

The reference standard used for this procedure was butylated hydroxytoluene (BHT). Tests were carried out in triplicate.

Declaration of competing interest

The authors declare that they have no known competing financial interests or personal relationships that could have appeared to influence the work reported in this paper.

Acknowledgments

Jane and Aatos Erkkö Foundation, Academy of Finland (Decision 326487) and Fundação para a Ciência e Tecnologia (UIDB/50006/2020 and CEE-CINST/2018) are acknowledged for financial support. We thank Lijo George (Faculty of Engineering and Natural Sciences, TAU) for HRMS measurements.

Appendix A. Supplementary data

Supplementary data related to this article can be found at <https://doi.org/10.1016/j.ejmech.2021.113459>.

References

- [1] U. Theuretzbacher, K. Outtersson, A. Engel, A. Karlen, The global preclinical antibacterial pipeline, *Nat. Rev. Microbiol.* 18 (2020) 275, <https://doi.org/10.1038/s41579-019-0288-0>.
- [2] Organization, W. H., Global action plan on antimicrobial resistance. https://apps.who.int/iris/bitstream/handle/10665/193736/9789241509763_eng.pdf?sequence=1. (Accessed 1 March 2021).
- [3] R.E. Duval, M. Grare, B. Demore, Fight against antimicrobial resistance: we always need new antibacterials but for right bacteria, *Molecules* 24 (2019) 3152, <https://doi.org/10.3390/molecules24173152>.
- [4] S. Santajit, N. Indrawattana, Mechanisms of antimicrobial resistance in ESKAPE pathogens, *BioMed Res. Int.* 2016 (2016), 2475067, <https://doi.org/10.1155/2016/2475067>.
- [5] Y.X. Ma, C.Y. Wang, Y.Y. Li, J. Li, Q.Q. Wan, J.H. Chen, F.R. Tay, L.N. Niu, Considerations and caveats in combating ESKAPE pathogens against nosocomial infections, *Adv. Sci.* 7 (2020) 1901872, <https://doi.org/10.1002/advs.201901872>.
- [6] R. Agarwal, S.M. Bartsch, B.J. Kelly, M. Prewitt, Y. Liu, Y. Chen, C.A. Umscheid, Newer glycopeptide antibiotics for treatment of complicated skin and soft tissue infections: systematic review, network meta-analysis and cost analysis, *Clin. Microbiol. Infect.* 24 (2018) 361, <https://doi.org/10.1016/j.cmi.2017.08.028>.
- [7] M.A.T. Blaskovich, K.A. Hansford, M.S. Butler, Z. Jia, A.E. Mark, M.A. Cooper, Developments in glycopeptide antibiotics, *ACS Infect. Dis.* 4 (2018) 715, <https://doi.org/10.1021/acinfed.7b00258>.
- [8] E. Bouza, P. Munoz, A. Burillo, The role of tedizolid in skin and soft tissue infections, *Curr. Opin. Infect. Dis.* 31 (2018) 131, <https://doi.org/10.1097/QCO.0000000000000439>.
- [9] Organization, W. H., Antibacterial agents in clinical development. https://www.who.int/medicines/areas/rational_use/antibacterial_agents_clinical_development/en/. (Accessed 1 March 2021).
- [10] M.F. Richter, P.J. Hergenrother, The challenge of converting gram-positive-only compounds into broad-spectrum antibiotics, *Ann. N. Y. Acad. Sci.* 1435 (2019) 18, <https://doi.org/10.1111/nyas.13598>.
- [11] M.Z. David, M. Dryden, T. Gottlieb, P. Tattavin, I.M. Gould, Recently approved antibacterials for methicillin-resistant *Staphylococcus aureus* (MRSA) and other gram-positive pathogens: the shock of the new, *Int. J. Antimicrob. Agents* 50 (2017) 303, <https://doi.org/10.1016/j.ijantimicag.2017.05.006>.
- [12] G. Suleyman, G. Alagaden, A.C. Bardossy, The role of environmental contamination in the transmission of nosocomial pathogens and healthcare-associated infections, *Curr. Infect. Dis. Rep.* 20 (2018) 12, <https://doi.org/10.1007/s11908-018-0620-2>.
- [13] W. Bereket, K. Hemalatha, B. Getenet, T. Wondwossen, A. Solomon, A. Zeynudin, S. Kannan, Update on bacterial nosocomial infections, *Eur. Rev. Med. Pharmacol. Sci.* 16 (2012) 1039.
- [14] B.J. Silk, M.H. McCoy, M. Iwamoto, P.M. Griffin, Foodborne listeriosis acquired in hospitals, *Clin. Infect. Dis.* 59 (2014) 532, <https://doi.org/10.1093/cid/ciu365>.
- [15] L.K. Gaul, N.H. Farag, T. Shim, M.A. Kingsley, B.J. Silk, E. Hyttia-Trees, Hospital-acquired listeriosis outbreak caused by contaminated diced celery - Texas, 2010, *Clin. Infect. Dis.* 56 (2013) 20, <https://doi.org/10.1093/cid/cis817>.
- [16] A. Facciola, G.F. Pellicano, G. Visalli, I.A. Paolucci, E. Venanzi Rullo, M. Ceccarelli, F. D'Alco, A. Di Pietro, R. Squeri, G. Nunnari, et al., The role of the hospital environment in the healthcare-associated infections: a general review of the literature, *Eur. Rev. Med. Pharmacol. Sci.* 23 (2019) 1266, https://doi.org/10.26355/eurev.201902_17020.
- [17] W.R. Miller, J.M. Munita, C.A. Arias, Mechanisms of antibiotic resistance in enterococci, *Expert Rev. Anti Infect. Ther.* 12 (2014) 1221, <https://doi.org/10.1586/14787210.2014.956092>.
- [18] M. Otto, Staphylococcal biofilms, *Curr. Top. Microbiol. Immunol.* 322 (2008) 207, https://doi.org/10.1007/978-3-540-75418-3_10.
- [19] J.H. Ch'ng, K.K.L. Chong, L.N. Lam, J.J. Wong, K.A. Kline, Biofilm-associated infection by enterococci, *Nat. Rev. Microbiol.* 17 (2019) 82, <https://doi.org/10.1038/s41579-018-0107-z>.
- [20] B.H. Lee, M. Hebraud, T. Bernardi, Increased adhesion of *Listeria monocytogenes* strains to abiotic surfaces under cold stress, *Front. Microbiol.* 8 (2017) 2221, <https://doi.org/10.3389/fmicb.2017.02221>.
- [21] G. Roman, Mannich bases in medicinal chemistry and drug design, *Eur. J. Med. Chem.* 89 (2015) 743, <https://doi.org/10.1016/j.ejmech.2014.10.076>.
- [22] G. Roman, V. Nastasa, A.C. Bostanaru, M. Mares, Antibacterial activity of Mannich bases derived from 2-naphthols, aromatic aldehydes and secondary aliphatic amines, *Bioorg. Med. Chem. Lett.* 26 (2016) 2498, <https://doi.org/10.1016/j.bmcl.2016.03.098>.
- [23] P. Doan, A. Karjalainen, J.G. Chandraseelan, O. Sandberg, O. Yli-Harja, T. Rosholm, R. Franzen, N.R. Candeias, M. Kandhavelu, Synthesis and biological screening for cytotoxic activity of N-substituted indolines and morpholines, *Eur. J. Med. Chem.* 120 (2016) 296, <https://doi.org/10.1016/j.ejmech.2021.113459>.

- jejmec.2016.05.024.
- [24] P. Doan, T. Nguyen, O. Yli-Harja, N.R. Candeias, M. Kandhavelu, Effect of alkylaminophenols on growth inhibition and apoptosis of bone cancer cells, *Eur. J. Pharmaceut. Sci.* 107 (2017) 208, <https://doi.org/10.1016/j.ejps.2017.07.016>.
- [25] A. Karjalainen, P. Doan, J.G. Chandraseelan, O. Sandberg, O. Yli-Harja, N.R. Candeias, M. Kandhavelu, Synthesis of phenol-derivatives and biological screening for anticancer activity, *Anticancer Agents Med. Chem.* 17 (2017) 1710, <https://doi.org/10.2174/1871520617666170327142027>.
- [26] P. Doan, A. Musa, N.R. Candeias, F. Emmert-Streib, O. Yli-Harja, M. Kandhavelu, Alkylaminophenol induces G1/S phase cell cycle arrest in glioblastoma cells through p53 and cyclin-dependent kinase signaling pathway, *Front. Pharmacol.* 10 (2019) 330, <https://doi.org/10.3389/fphar.2019.00330>.
- [27] H.T.T. Le, T. Rimpiläinen, S. Konda Mani, A. Murugesan, O. Yli-Harja, N.R. Candeias, M. Kandhavelu, Synthesis and preclinical validation of novel P2Y1 receptor ligands as a potent anti-prostate cancer agent, *Sci. Rep.* 9 (2019) 18938, <https://doi.org/10.1038/s41598-019-55194-8>.
- [28] H.I. Gul, M. Tugrak, M. Gul, S. Mazlumoglu, H. Sakagami, I. Gulcin, C.T. Supuran, New phenolic Mannich bases with piperazines and their bioactivities, *Bioorg. Chem.* 90 (2019) 103057, <https://doi.org/10.1016/j.bioorg.2019.103057>.
- [29] I. Neto, J. Andrade, A.S. Fernandes, C. Pinto Reis, J.K. Salunke, A. Priimägi, N.R. Candeias, P. Rijo, Multicomponent petasis-borono Mannich preparation of alkylaminophenols and antimicrobial activity studies, *ChemMedChem* 11 (2016) 2015, <https://doi.org/10.1002/cmdc.201600244>.
- [30] T. Rimpiläinen, J. Andrade, A. Nunes, E. Ntungwe, A.S. Fernandes, J.R. Vale, J. Rodrigues, J.P. Gomes, P. Rijo, N.R. Candeias, Aminobenzylated 4-nitrophenols as antibacterial agents obtained from 5-nitrosalicylaldehyde through a Pétasis borono-mannich reaction, *ACS Omega* 3 (2018) 16191, <https://doi.org/10.1021/acsomega.8b02381>.
- [31] N.R. Candeias, F. Montalbano, P. Gal, P.M.P. Gois, Boronic acids and esters in the petasis-borono Mannich multicomponent reaction, *Chem. Rev.* 110 (2010) 6169, <https://doi.org/10.1021/cr100108k>.
- [32] P. Wu, M. Givskov, T.E. Nielsen, Reactivity and synthetic applications of multicomponent Pétasis reactions, *Chem. Rev.* 119 (2019) 11245, <https://doi.org/10.1021/acs.chemrev.9b00214>.
- [33] L.A. Pham-Huy, H. He, C. Pham-Huy, Free radicals, antioxidants in disease and health, *Int. J. Biomed. Sci.* 4 (2008) 89.
- [34] S. Di Meo, P. Venditti, Evolution of the knowledge of free radicals and other oxidants, *Oxid. Med. Cell Longev.* 2020 (2020), 9829176, <https://doi.org/10.1155/2020/9829176>.
- [35] K. Nepali, H.Y. Lee, J.P. Liou, Nitro-group-containing drugs, *J. Med. Chem.* 62 (2019) 2851, <https://doi.org/10.1021/acs.jmedchem.8b00147>.
- [36] G.A. Van Norman, Limitations of animal studies for predicting toxicity in clinical trials: is it time to rethink our current approach? *JACC Basic Transl. Sci.* 4 (2019) 845, <https://doi.org/10.1016/j.jaccbts.2019.10.008>.
- [37] G.A. Van Norman, Limitations of animal studies for predicting toxicity in clinical trials: Part 2: potential alternatives to the use of animals in preclinical trials, *JACC Basic Transl. Sci.* 5 (2020) 387, <https://doi.org/10.1016/j.jaccbts.2020.03.010>.
- [38] I.A. Freires, J.C. Sardi, R.D. de Castro, P.L. Rosalen, Alternative animal and non-animal models for drug discovery and development: bonus or burden? *Pharm. Res. (N. Y.)* 34 (2017) 681, <https://doi.org/10.1007/s11095-016-2069-z>.
- [39] N.E. Ntungwe, E.M. Dominguez-Martin, A. Roberto, J. Tavares, V.M.S. Isca, P. Pereira, M.J. Cebola, P. Rijo, *Artemia* species: an important tool to screen general toxicity samples, *Curr. Pharmaceut. Des.* 26 (2020) 2892, <https://doi.org/10.2174/1381612826666200406083035>.
- [40] M. Suarez-Diez, S. Porras, F. Laguna-Teno, P.J. Schaap, J.A. Tamayo-Ramos, Toxicological response of the model fungus *Saccharomyces cerevisiae* to different concentrations of commercial graphene nanoplatelets, *Sci. Rep.* 10 (2020) 3232, <https://doi.org/10.1038/s41598-020-60101-7>.
- [41] S.K. Doke, S.C. Dhawale, Alternatives to animal testing: a review, *Saudi Pharmaceut. J.* 23 (2015) 223, <https://doi.org/10.1016/j.jsps.2013.11.002>.
- [42] Cronin, M., Non-animal approaches - the way forward, <https://op.europa.eu/s/oM5H>. (Accessed 1 March 2021).
- [43] A. Buschini, P. Poli, C. Rossi, *Saccharomyces cerevisiae* as an eukaryotic cell model to assess cytotoxicity and genotoxicity of three anticancer anthraquinones, *Mutagenesis* 18 (2003) 25, <https://doi.org/10.1093/mutage/18.1.25>.
- [44] G. Libralato, E. Prato, L. Migliore, A.M. Gcero, L. Manfra, A review of toxicity testing protocols and endpoints with *Artemia* spp., *Ecol. Indicat.* 69 (2016) 35, <https://doi.org/10.1016/j.ecolind.2016.04.017>.
- [45] M. Ermolli, C. Menne, G. Pozzi, M.A. Serra, L.A. Clerici, Nickel, cobalt and chromium-induced cytotoxicity and intracellular accumulation in human haec keratinocytes, *Toxicology* 159 (2001) 23, [https://doi.org/10.1016/s0300-483x\(00\)00373-5](https://doi.org/10.1016/s0300-483x(00)00373-5).
- [46] M. Gajdacs, G. Spengler, C. Sanmartin, M.A. Marc, J. Handzlik, E. Dominguez-Alvarez, Selenoesters and selenoanhydrides as novel multidrug resistance reversing agents: a confirmation study in a colon cancer MDR cell line, *Bioorg. Med. Chem. Lett* 27 (2017) 797, <https://doi.org/10.1016/j.bmcl.2017.01.033>.
- [47] L. Zhang, R. Qiu, X. Xue, Y. Pan, C. Xu, H. Li, L. Xu, Versatile (Pentamethylcyclopentadienyl)rhodium-2,2'-bipyridine (cp*Rh-bpy) catalyst for transfer hydrogenation of N-heterocycles in water, *Adv. Synth. Catal.* 357 (2015) 3529, <https://doi.org/10.1002/adsc.201500491>.
- [48] D.D. Li, Y.M. Chen, M.Y. Ma, Y.L. Yu, Z.Z. Jia, P.H. Li, Z.Y. Xie, Regioselective C5 nitration of N-protected indolines using ferric nitrate under mild conditions, *Synth. Commun.* 49 (2019) 1231, <https://doi.org/10.1080/00397911.2019.1580745>.
- [49] E.L. Pietniński Chlekar, R. Unwalla, T.A. Khan, R.S. Tangirala, M. Johnson, M. St Andre, J.T. Anderson, T. Kenney, S. Chiparri, C. McNally, et al., 1-(2-Hydroxy-2-methyl-3-phenoxypropyl)indoline-4-carbonitrile derivatives as potent and tissue selective androgen receptor modulators, *J. Med. Chem.* 57 (2014) 2462, <https://doi.org/10.1021/jm401625b>.
- [50] L. Chaofeng, C. Zhengxia, C. Xiaoxin, Z. Yang, L. Zhuowei, L. Peng, C. Shuhui, L. Guibai, X. Cheng, L. Zhenwei, et al., Tyrosine Kinase Inhibitor and Pharmaceutical Composition Comprising Same, 2016, p. EP3293177.
- [51] V.R. Hegde, P. Dai, C. Ladislav, M.G. Patel, M.S. Puar, J.A. Pachter, D4 dopamine receptor-selective compounds from the Chinese plant *Phoebe chekiangensis*, *Bioorg. Med. Chem. Lett* 7 (1997) 1207, [https://doi.org/10.1016/s0960-894x\(97\)00194-7](https://doi.org/10.1016/s0960-894x(97)00194-7).
- [52] M. Di Donato, M.M. Lerch, A. Lapini, A.D. Laurent, A. Iagatti, L. Bussotti, S.P. Ihrig, M. Medved, D. Jacquemin, W. Szymanski, et al., Shedding light on the photoisomerization pathway of donor-acceptor stenoisomer adducts, *J. Am. Chem. Soc.* 139 (2017) 15596, <https://doi.org/10.1021/jacs.7b09081>.
- [53] The European Committee on Antimicrobial Susceptibility Testing, Breakpoint Tables for Interpretation of MICs and Zone Diameters, 2020. Version 10.0, <http://www.eucast.org>. (Accessed 1 March 2021).
- [54] I. Wiegand, K. Hilpert, R.E. Hancock, Agar and broth dilution methods to determine the minimal inhibitory concentration (MIC) of antimicrobial substances, *Nat. Protoc.* 3 (2008) 163, <https://doi.org/10.1038/nprot.2007.521>.
- [55] L.M.T. Frija, E. Ntungwe, P. Sitarek, J.M. Andrade, M. Toma, T. Sliwinski, L. Cabral, S.C. Mi, P. Rijo, A.J.L. Pombeiro, Vitro assessment of antimicrobial, antioxidant, and cytotoxic properties of saccharin-tetrazolyl and -thiadiazolyl derivatives: the simple dependence of the pH value on antimicrobial activity, *Pharmaceuticals* 12 (2019), <https://doi.org/10.3390/ph12040167>.
- [56] T.A. Wagemaker, P. Rijo, L.M. Rodrigues, P.M. Maia Campos, A.S. Fernandes, C. Rosado, Integrated approach in the assessment of skin compatibility of cosmetic formulations with green coffee oil, *Int. J. Cosmet. Sci.* 37 (2015) 506, <https://doi.org/10.1111/ics.12225>.



Aminobenzylated 4-Nitrophenols as Antibacterial Agents Obtained from 5-Nitrosalicylaldehyde through a Petasis Borono–Mannich Reaction

Tatu Rimpiläinen,[†] Joana Andrade,[‡] Alexandra Nunes,[§] Epole Ntungwe,[‡] Ana S. Fernandes,[‡] João R. Vale,^{†,||} João Rodrigues,[§] João Paulo Gomes,[§] Patricia Rijo,^{†,||} and Nuno R. Candéias^{*,†,||}

[†]Laboratory of Chemistry and Bioengineering, Tampere University of Technology, Korkeakoulunkatu 8, 33101 Tampere, Finland

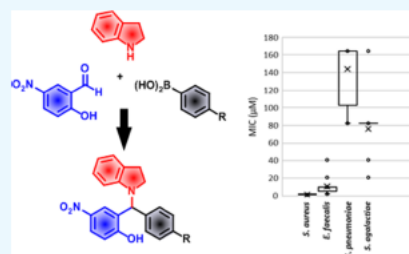
[‡]CBIOS-Universidade Lusófona Research Center for Biosciences & Health Technologies, Campo Grande 376, 1749-024 Lisboa, Portugal

[§]Department of Infectious Diseases, National Institute of Health, Avenida Padre Cruz, 1649-016 Lisboa, Portugal

^{||}Instituto de Investigação do Medicamento (iMed.U LISBOA), Faculdade de Farmácia, Universidade de Lisboa, Av. Prof. Gama Pinto, 1649-003 Lisboa, Portugal

Supporting Information

ABSTRACT: Multidrug-resistant bacteria are one of the current biggest threats to public health and are responsible for most nosocomial infections. Herein, we report the efficient and facile synthesis of antibacterial agents aminoalkylphenols, derived from 5-nitrosalicylaldehyde and prepared through a Petasis borono–Mannich multicomponent reaction. Minimum inhibitory concentrations (MICs) as low as 1.23 μ M for a chlorine derivative were determined for multidrug-resistant Gram-positive bacteria, namely, *Staphylococcus aureus* and *Enterococcus faecalis*, two of the main pathogens responsible for infections in a hospital environment. The most promising antibacterial agents were further tested against eight strains of four Gram-positive species in order to elucidate their antibacterial broadness. In vitro cytotoxicity assays of the most active aminoalkylphenol revealed considerably lower toxicity against mammalian cells, as concentrations one order of magnitude higher than the determined MICs were required to induce human keratinocyte cell death. The phenol moiety was verified to be important in deeming the antibacterial properties of the analyzed compounds, although no correlation between such properties and their antioxidant activity was observed. A density functional theory computational study substantiated the ability of aminoalkylphenols to serve as precursors of *ortho*-quinone methides.



INTRODUCTION

The discovery and development of antibiotics stands as one of mankind's greatest achievements. However, the number of infections provoked by multidrug-resistant bacteria is increasing at a remarkable pace, a problem that science has not been able to address.¹ The unrestrained use of antibiotics in the last 50 years has been advocated as one of the reasons for the colonization and infection due to drug resistant bacteria.^{2,3} It is estimated that in Europe and the United States, 48 000 people die each year because of multidrug-resistant bacterial infections,⁴ and that in 2016, there were 600 000 worldwide cases with resistance to rifampicin, of which 490 000 had multidrug-resistant tuberculosis.⁵ If no actions are taken to tackle this severe public health issue, it is foreseen that by 2050, the death toll can rise up to 10 million lives when considering drug resistance of only six pathogens.⁶ This is even more alarming in the hospital environment or other health care

facilities, where acquired infections are associated with significant morbidity and mortality, additional health care expenditure, greater use of broad spectrum antibiotics (which amplifies the emergence and reemergence of drug resistant microorganisms), and increased costs.⁷ According to WHO estimates, of every hundred hospitalized patients, 7 in developed and 10 in developing countries will acquire at least one nosocomial infection.⁸ Besides intrinsic patient factors (age, duration of hospitalization, or underlying diseases), many extrinsic factors, such as caregivers' practices, surgical operations, the use of invasive devices, administration of broad-spectrum antibiotics, or immunosuppressive agents, are risk predisposers to these infections.^{9,10} The majority of

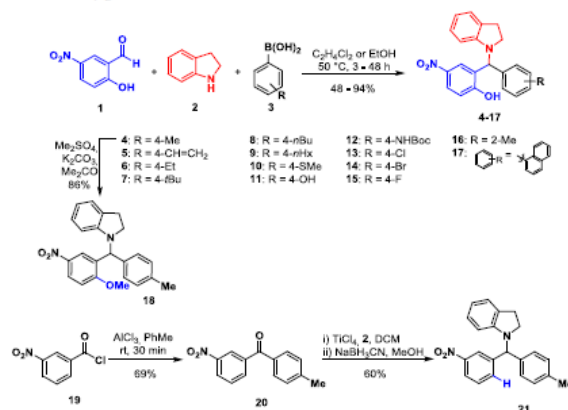
Received: September 14, 2018

Accepted: November 1, 2018

Published: November 29, 2018



Scheme 1. Preparation of Aminoalkylphenols 4–17 and Derivatives 18 and 21

Table 1. Antimicrobial Activity of Aminoalkylphenols 4–17 and Derivatives 18 and 21 against Laboratory-Adapted Strains^a

| compd. | <i>S. aureus</i> ATCC25923 (MSSA) | | <i>S. aureus</i> CIP6538 | | <i>S. aureus</i> CIP106760 (MRSA) | | <i>E. faecalis</i> 29212 | | <i>E. faecalis</i> ATCC51299 (VRE) | |
|---------|-----------------------------------|-----------------|--------------------------|-----------------|-----------------------------------|-----------------|--------------------------|-----------------|------------------------------------|-----------------|
| | MIC | MBC | MIC | MBC | MIC | MBC | MIC | MBC | MIC | MBC |
| 4 | 21.3 | 347 | 10.8 | 43.4 | 2.71 | 5.42 | 10.8 | 86.7 | 21.7 | 173 |
| 5 | 10.5 | 168 | 5.24 | 41.9 | 1.31 | 5.24 | 5.24 | 83.9 | 10.5 | 168 |
| 6 | 4.93 | 39.5 | 2.47 | 2.47 | 1.23 | <1.23 | 2.47 | 19.7 | 2.47 | 39.5 |
| 7 | 4.93 | 39.5 | 2.47 | 19.7 | 1.23 | >9.86 | 2.47 | 19.7 | 2.47 | >19.7 |
| 8 | 4.93 | 39.5 | 2.47 | 9.86 | 2.47 | <1.23 | 4.93 | >39.5 | 4.93 | 39.5 |
| 9 | 9.86 | 19.7 | 9.86 | 39.5 | 19.7 | 39.5 | 9.86 | >78.9 | 4.93 | 78.90 |
| 10 | 9.86 | 78.9 | 2.47 | 4.93 | 2.47 | 4.93 | 4.93 | 39.50 | 4.93 | 39.5 |
| 11 | 43.1 | 1379 | 8.62 | 689 | 86.2 | 1379 | 172 | 1379 | 34.5 | 1379 |
| 12 | 67.7 | 541 | 33.9 | 270 | 67.7 | 1083 | 135 | 1083 | 135 | 1083 |
| 13 | 2.47 | 9.86 | 1.23 | 2.47 | 1.23 | <1.23 | 1.23 | >9.86 | 1.23 | 19.7 |
| 14 | 2.30 | 36.8 | 1.15 | 4.59 | 1.15 | 4.59 | 1.15 | 9.19 | 2.30 | 9.19 |
| 15 | 10.7 | 85.8 | 5.36 | 21.44 | 2.68 | 21.4 | 2.68 | 42.90 | 5.36 | 171 |
| 16 | 4.93 | 9.86 | 1.23 | 4.93 | 1.23 | <1.23 | 2.47 | >19.7 | 1.23 | 39.5 |
| 17 | 4.93 | >19.7 | 1.23 | 9.86 | 2.47 | <2.47 | 4.93 | >39.5 | 2.47 | >19.7 |
| 18 | 166 | 1335 | 83.5 | 333 | 333 | 1335 | 166 | 1335 | 166 | 1335 |
| 21 | 373 | 1495 | 93.5 | 747 | 747 | 1495 | 186 | 1495 | 373 | 1495 |
| control | 5.40 ^b | nd ^e | 1.35 ^b | nd ^e | <1.50 ^c | nd ^e | 3.07 ^d | nd ^e | <5.83 ^d | nd ^e |

^aMICs and MBCs are shown in μM . ^bVancomycin used as a control. ^cNorfloxacin used as a control. ^dRifampicin used as a control. ^eNot determined.

nosocomial infections are caused by bacteria, with *Staphylococcus aureus*, *Escherichia coli*, *Pseudomonas aeruginosa*, *Enterococcus*, and *Streptococcus* spp. leading.¹¹ Despite the society being in urgent need for new antibacterial agents, the small fraction of yearly revenue per patient generated by such agents when compared with anticancer drugs have pushed the pharmaceutical companies away from their research and development programs on antibiotics.^{12,13} Opportunely, the development of antibiotics has been relaunched by small biotech companies, and alternatives to antibiotics, including “non-compound” approaches and small molecule “resistance breakers”, are growing trends in the field.¹⁴

Motivated by the antimicrobial activity of salicylaldehydes^{15–17} and their Schiff bases,¹⁸ we have recently reported the preparation and antimicrobial screening of several aminoalkylphenols.¹⁹ From screening of a library of 43

compounds, some structural features pivotal for the antibacterial activity have been identified, namely, indoline as the amine counterpart and a *para*-nitrophenol group. Promising antibacterial activity against several resistant microorganisms such as methicillin-resistant *S. aureus* (MRSA) and vancomycin-resistant enterococci (VRE), as well as other non-pathogenic Gram-positive strains, was reported for some of such derivatives. Notwithstanding the fact that aminoalkylphenols can be problematic compounds in high-throughput screenings because of their ability to form reactive quinone methides or acting as metal chelators,^{20,21} their anticancer and cytotoxic properties continue to be extensively explored.^{22,23} Almost simultaneously to our report, Roman and co-workers reported the antibacterial properties of 1-aminoalkyl 2-naphthols, in which similar properties were observed against Gram-positive bacteria.²⁴ Somewhat different structural

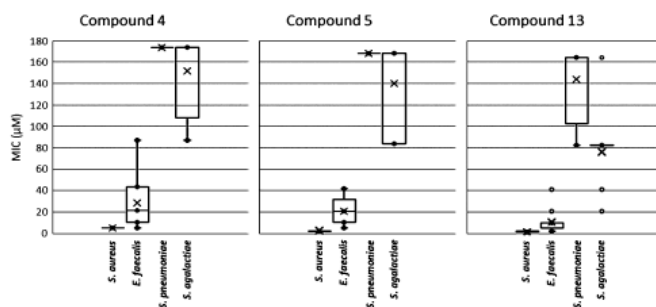


Figure 1. MIC values of compounds 4, 5, and 13 for diverse clinical isolates of *S. aureus*, *E. faecalis*, *S. pneumoniae*, and *S. agalactiae*. A boxplot chart was generated using R statistical software v. 3.4.2 and consists of boxes (median and interquartile range) and whiskers that extend to the most extreme data points that were no more than 1.5 times the interquartile range from the box. Boxes represent the variability of MIC values found among all strains from each species. The horizontal black line within each box marks the median, while the lowest and the highest coverage values observed are represented by the extremes of the whisker below and above each box, respectively. Outliers are indicated by open circles.

requirements for antibacterial activity were determined by Roman, as thiophen-2-yl derivatives showed the best activity, regardless of the nature of the amine moiety. The antibacterial properties of other Mannich bases derived from naphthol have been previously explored.²⁵ Aminoalkylphenols have also been reported to inhibit biofilm formation²⁶ and classified as anti-infectives rather than traditional antibiotics as they cure *Caenorhabditis elegans* of an *Enterococcus faecalis* infection at significantly lower concentration than the one required for in vitro bacteria growth inhibition.²⁷ After observing that the concentration required for an antibacterial effect of some promising aminoalkylphenols was generally inferior to the cytotoxic concentrations,¹⁹ we then set to expand our previous library in order to optimize the antibacterial properties.

RESULTS AND DISCUSSION

As multicomponent reactions are a remarkable tool for the easy preparation of libraries of compounds,^{28,29} our previous library of aminoalkylphenols was expanded using the Petasis borono-Mannich^{30,31} reaction (Scheme 1). Starting from 5-nitrosalicylaldehyde 1 and indoline 2, the corresponding iminium was formed in situ and trapped with different aryl boronic acids 3 to provide the desired tertiary amines 4–17. Ether 18 was prepared by methylation of the phenol functionality upon treatment of 4 with dimethyl sulfate. Tertiary amine 21, lacking the oxygen functionality in the nitroaryl substituent, was prepared by Friedel–Crafts acylation of toluene with *meta*-nitro benzoyl chloride 19 followed by reductive amination with indoline.

The selection of compounds to be prepared was reasoned based on two aspects, first, by replacing the 4-methyl substituent in 4 with other isosteres because we have previously identified position 4 of the phenyl moiety to be important in conferring the desired antibacterial activity. Therefore, the 4-methyl substituent in 4 was replaced by other alkyl substituents or heteroatoms such as thioether, hydroxyl, carbamate, and halogens. Second, in order to fully disclose the importance of the phenol moiety in the nitroaryl moiety, the methyl ether derivative 18 and tertiary amine 21 were also prepared and their antibacterial properties were evaluated.

The synthesized aminoalkylphenols 4–17 and derivatives 18 and 21 were tested against a large panel of Gram-positive microorganisms (Table 1), namely, three *S. aureus* strains (a reference ATCC, a methicillin-resistant and a non-resistant strain) and two *E. faecalis* strains (a reference ATCC and a vancomycin-resistant strain). An *E. coli* strain, representative of Gram-negative microorganisms, was also tested, although no antibacterial properties were observed for any of the compounds assayed (not shown). The modification of the para-methyl substituent to other alkyl substituents resulted in derivatives 6–8 of a similar antibacterial profile, except when a longer C₆ alkyl chain was introduced in 9. Replacing the alkyl substituent by a heteroatom functionality such as thioether, alcohol, or a carbamate also had a detrimental effect, as observed for 10–12, respectively. Gladly, the introduction of a halide such as chloride (13) or bromide (14) resulted in not only augmenting the bacterial inhibition growth but also in efficacy of killing the bacteria. Notably, a more effective activity was determined for chloro derivative 13, for which minimum inhibitory concentrations (MICs) and minimum bactericidal concentrations (MBCs) as low as 1.23 µM were determined for most of the bacteria tested. On the other hand, the presence of fluoride (15), change of the position of the methyl substituent to the 2-position (16), or replacement of the *p*-tolyl moiety by a 1-naphthyl (17) did not confer any improvement to the antibacterial characteristics of the aminoalkylphenols. Compounds 18 and 21 were poor antibacterials, as the MIC and MBC values increased by one to two orders of magnitude when compared with parental 4, hence evidencing the importance of the phenol functionality in conferring the desired properties.

In order to further elucidate the antibacterial broadness of the most promising synthesized aminoalkylphenols, compounds 4, 5, and 13 were tested against a larger panel of pathogenic Gram-positive bacterial strains with dissimilar resistance phenotypes. Overall, 32 strains from *S. aureus*, *E. faecalis*, *Streptococcus pneumoniae* (*S. pneumoniae*), and *Streptococcus agalactiae*—group B (GBS) (eight clinical isolates from each species) were tested (Figure 1 and Table S1).

In general, similar MIC values were observed for *S. aureus* and *E. faecalis* clinical isolates when compared with those seen for the ATCC adapted strains. Some exceptions occurred,

where, at some instances, a maximum of fourfold differences were observed, which may be due both to the dissimilar genetic background of the clinical isolates and to the extensive in vitro passaging of the ATCC strains. As clearly shown in Figure 1, all three selected compounds seem to be much more effective against *S. aureus* and *E. faecalis*, displaying a mean of MIC values at least 5.4-fold lower than that observed for *S. pneumoniae* and *S. agalactiae*. For the former species, for which the results were encouraging, compound 13 revealed the higher antimicrobial efficacy, given by lower and more homogeneous MIC values.

S. aureus and *E. faecalis* are among the most important bacteria causing infections in the hospital environment.^{32–34} While *S. aureus* is the primary cause of lower respiratory tract infections and surgical site infections and the second leading cause of nosocomial bacteremia, pneumonia, and cardiovascular infections, *E. faecalis* is responsible for urinary tract infections (associated with instrumentation and antimicrobial administration) followed by intra-abdominal and pelvic infection, surgical wound infection, bacteremia, endocarditis, neonatal sepsis, and rarely meningitis.¹¹ Furthermore, because of the large usage of broad-spectrum antibiotics in the hospital environment, both bacteria (mostly *S. aureus*) are able to emerge and reemerge as multidrug-resistant clones, which complicates the treatment of the caused nosocomial infections.^{35,36}

A test of lethality to *Artemia salina* brine shrimp was performed³⁷ in order to evaluate the toxicity of the different compounds, for which concentrations of 0.1 mg/mL (217–277 μ M) of each compound in dimethylsulfoxide (DMSO) were tested (Figure 2). Delightfully, a residual 15% mortality

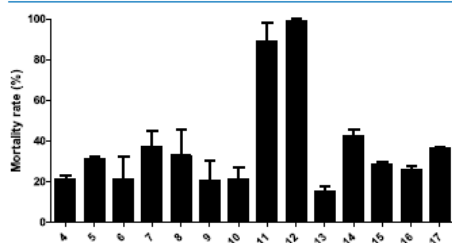


Figure 2. General toxicity of 4–17 in the mortality rate of *A. salina* brine shrimp assay was performed. Concentrations of 10 μ g/mL of each compound were tested. The number of dead larvae was recorded after 24 h and used to calculate the lethal concentration (%).

rate was observed for compound 13, while compounds 11 and 12 were highly toxic with mortality rates of 89 and 98%, respectively. Fortunately, these compounds were not active against any microorganism on the antibacterial assay. Of the remaining compounds, none held a mortality rate higher than 42%, which was observed for the bromine derivative 14, followed by compound 5 with a 31% mortality rate. For compounds 4 and 5, mortality rates of 21 and 31% were observed, respectively.

To further characterize the toxicity of the compounds, an in vitro model representative of noncancer human cells was also used. The cytotoxicity profile of compound 13 is shown in Figure 3, while other analogues were previously tested¹⁹ using the same protocol. No cytotoxic effects were observed for

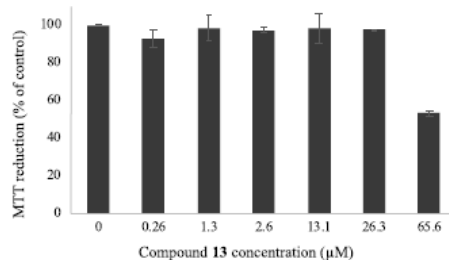


Figure 3. Cell viability of HaCat cells exposed to compound 13, as evaluated by the MTT assay. Cells were incubated with increasing concentrations of compound 13 for 24 h. Results are expressed as average values \pm SD from two independent experiments, each comprising four replicate cultures.

concentrations of compound 13 up to 26.3 μ M. Only the highest concentration tested (65.6 μ M) showed relevant cytotoxicity, decreasing cell viability to 53.4 \pm 1.5%. Compared with analogue 4 previously tested, for which a concentration of 28 μ M led to a cell viability of less than 20%,¹⁹ compound 13 shows a better safety profile.

Taking together, the common feature of the presence of the phenol moiety and the lack of significant antibacterial activity of 18 and 21, it was hypothesized that the high activity observed could be related with the antioxidant properties of phenol compounds.³⁸ Tests of antioxidant activity of compounds 4–17 using the 2,2-diphenyl-1-picrylhydrazyl (DPPH) method (Figure 4) showed that the bromine and fluorine derivatives 14 and 15 had a scavenging activity of 99 and 94%, respectively. Compounds 4 and 5 are also highly antioxidant (85 and 92%, respectively), although not being the case for the chlorine derivative 13. Furthermore, despite the decent antibacterial properties found for derivatives 6–8, their antioxidant activity was rather low (35–47%), opposing the trend observed for compounds 4 and 5. Interestingly, compound 21, lacking the hydroxyl group, showed antioxidant activity in the same range as the most antioxidant species tested. Therefore, a different main mode of action other than an antioxidant mechanism is likely to be the cause of the antibacterial properties observed.

As the identified aminoalkylphenols bear a stereogenic center in the benzylic position, the separation of both enantiomers of 4 was attempted. Hence, 4 was transformed into the corresponding Mosher's ester 22, separated through preparative thin layer chromatography and further hydrolyzed (Scheme 2). Chiral HPLC analysis of the enantiomerically enriched samples of 4 invariably revealed the presence of significant amounts of a minor enantiomer, which equilibrated to a racemic mixture upon standing in solution. Ultimately, the enantiomerically enriched samples 4a and 4b obtained (with enantiomeric ratios of 65:35 and 16:84, respectively) were also tested for their antibacterial activity (Table 2). Triggered by the difficulty in obtaining enantiomerically pure samples of 4, the putative formation of an *ortho*-quinone methide (QM)^{39,40} was considered. With this in mind, the benzyl alcohol 23, was also prepared by arylation of the 5-nitrosalicylaldehyde (Scheme 2 bottom) and its action for bacteria inhibition growth also tested (Table 2).

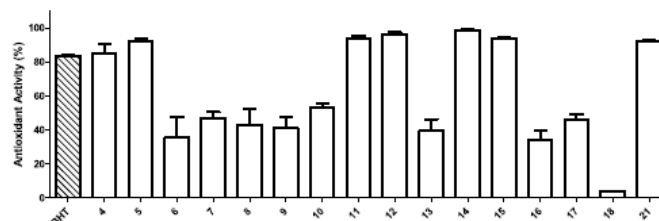
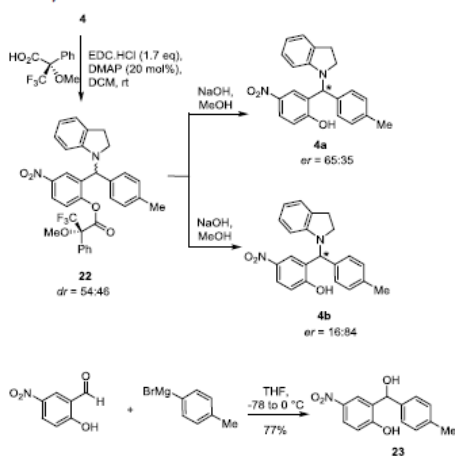


Figure 4. Antioxidant activity of 4–18 and 21, evaluated at a concentration of 10 $\mu\text{g/mL}$ (22–29 μM) by the DPPH method.

Scheme 2. Preparation of Enantiomeric Rich Samples of 4 and Synthesis of 23



The rather low antimicrobial activity observed for 23 (Table 2) clearly indicates that the antibacterial properties of 4 are not caused by the hydrolyzed QM. On the other hand, both enantiomerically enriched samples 4a and 4b showed similar levels of toxicity against bacteria as the previously tested racemate. Rokita and co-workers have showed that depending on the electronic feature of the QM, they can be stable toward water nucleophilic attack, while being trapped by nucleotides or other biomolecules.^{41,42} Specifically, the introduction of an electron-withdrawing group in the *para*-phenol position was shown to decrease the rate of the QM formation, while also decreasing its lifetime due to increased reactivity toward hydrolysis.⁴² When monitoring by ^1H NMR a solution of 4 in CDCl_3 in the presence of morpholine, we observed the

formation of the morpholine derivative in 79% yield after 96 h which was attributed to the chloroform slight acidity (Figure S5 in Supporting Information). Contrastingly, a similar experiment in $\text{DMSO-}d_6$ did not show formation of the corresponding morpholine-substituted aminoalkylphenol after 12 h (Figure S4 in Supporting Information). These observations suggest that even though the nitro substituent can decrease the ability of aminoalkylphenols to serve as QM precursors, their formation and fate is highly dependent on the acidity of the medium. An additional stability test showed that 4 remains stable in $\text{DMSO-}d_6$ at 35 $^\circ\text{C}$ for at least 11 days (Figure S6 in Supporting Information). The ability of water and acids in catalyzing nucleophilic attacks to QMs has been demonstrated both theoretically and experimentally.^{43–45} Moreover, the presence of an additional aryl substituent should facilitate the formation of the QM because of additional conjugation.

With the previous observations in mind, the formation of two QMs from 24 and 25, the latter lacking the additional phenyl ring and the nitro moiety, was considered by density functional theory (DFT)^{46a} studies in the gas phase (Figure 5), by taking into account the previously described role of bulk water in the alkylation of nitrogen nucleophiles.^{43,47,48} As expected, the formation of the QMs is a thermodynamically nonfavored process, as the overall ΔG_{form} of QM from 24 is +16.4 and ΔG_{form} of QM from 25 is 25.8 kcal/mol (Figures S1 and S2 in Supporting Information). Comparison of energy profiles in Figures S1–S3 reveals the stabilization effect of the phenyl substituent on the transition states when considering water as a proton shuttle. Additionally, this substituent and the nitro moiety induce the stabilization of the QMs, as the 25-derived QM is 10.2 kcal/mol less stable than the one derived from 24. It is worth noting that the presence of the nitro substituent induces a two-step mechanism, as zwitterion species B is a local minimum of the energy profile (see Figure S3 of Supporting Information for a similar study without the nitro substituent). On the other hand, the formation of the simplest QM from 25 seems to occur by a synchronous process where water acts as a proton shuttle resulting in indoline release. The interaction of the starting tertiary amines

Table 2. Minimum Inhibitory and Bactericidal Concentrations (μM) of 4a, 4b, and 23^a

| compd. | <i>S. aureus</i> ATCC25923 (MSSA) | | <i>S. aureus</i> CIP106760 (MRSA) | | <i>E. faecalis</i> 29212 | | <i>E. faecalis</i> ATCC51299 (VRE) | |
|-----------------|-----------------------------------|------|-----------------------------------|------|--------------------------|------|------------------------------------|------|
| | MIC | MBC | MIC | MBC | MIC | MBC | MIC | MBC |
| 4a (er = 65:35) | 5.42 | 43.4 | 10.8 | 43.4 | 1.35 | 10.8 | 10.8 | 86.7 |
| 4b (er = 16:84) | 10.8 | 86.7 | 5.42 | 43.4 | 5.42 | 43.4 | 5.42 | 43.4 |
| 23 | 168 | 1342 | 335 | 1342 | 83.9 | 671 | 167 | 1342 |

^asee Table 1 for controls.

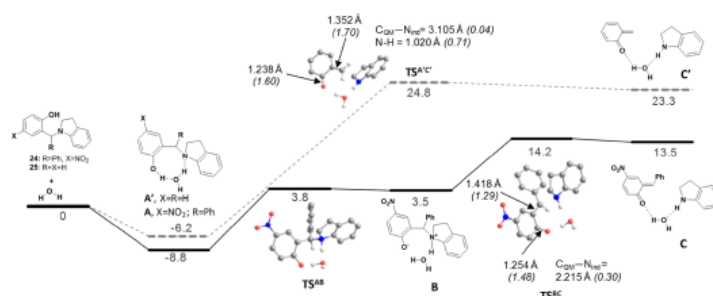


Figure 5. Gas phase energy profile (PBE1PBE/6-31G**) for formation of quinone methides from 2-(indolin-1-yl(phenyl)methyl)-4-nitrophenol (**24**, solid line) and 2-(indolin-1-ylmethyl)phenol (**25**, dashed line). Transition states are presented with bond distances and Wiberg indexes (in italics) for the more relevant bonds. Energy values are presented in kcal/mol, referring to the initial pair of tertiary amines and water.

with water results in an electronic stabilization due to formation of hydrogen bonds, even though this results in Gibbs energy increase due to the entropy contribution. The transition state for the proton exchange step in **24**, TS^{AB} , is described by a shortening of the C–O bond of the phenol moiety (1.29 Å in TS^{AB} vs 1.34 Å in **A**) accompanied by a Wiberg index¹² increase (WI = 1.28 in TS^{AB} vs 1.09 in **A**). Simultaneously, the O–H bond elongates considerably (1.31 Å in TS^{AB} vs 1.00 Å in **A**; WI = 0.27 in TS^{AB} vs 0.59 in **A**), while a new N–H bond is established ($d = 1.16$ Å, WI = 0.43 in TS^{AB} vs $d = 1.81$ Å, WI = 0.06 in **A**). The cleavage of the C–N bond represents the higher energetic barrier, characterized by the TS^{BC} , where the C–O bond becomes stronger ($d = 1.25$ Å, WI = 1.48 in TS^{BC} vs $d = 1.28$ Å, WI = 1.33 in **B**), and the C–N bond weakens ($d = 2.22$ Å, WI = 0.30 in TS^{BC} and $d = 1.55$ Å, WI = 0.83 in **B**). When similarly taking into account the water-assisted decomposition of **25** to the corresponding QM, a single late transition state $TS^{A^C'}$ was encountered. The abovementioned events are compacted in a single transition state, namely, shortening of the C–O bond ($d = 1.24$ Å, WI = 1.60 in $TS^{A^C'}$ vs $d = 1.34$ Å, WI = 1.07 in **A**), disruption of the O–H bond ($d = 1.77$ Å, WI = 0.07 in $TS^{A^C'}$ vs $d = 0.99$ Å, WI = 0.61 in **A**), formation of the N–H bond ($d = 1.02$ Å, WI = 0.71 in $TS^{A^C'}$ vs $d = 1.72$ Å, WI = 0.10 in **A**), and cleavage of the C–N bond ($d = 3.11$ Å, WI = 0.04 in $TS^{A^C'}$ vs $d = 1.50$ Å, WI = 0.92 in **A**).

Considering the low activation energy barrier for formation of the **25**-derived QM together with their increased stability as compared to the simplest QM, widely used as a nucleotide alkylating agent,^{49,50} is reasonable to suggest this path to be responsible for the antibacterial properties of the Mannich bases reported herein. Moreover, several antibiotics, namely, natural products, are known to have their antibacterial properties ground on their capability to form quinone methides and subsequently alkylate macromolecules.^{51,52} Contrarily to the recently reported 1-aminoalkyl 2-naphthols by Roman,²⁴ the antibacterial properties of the compounds described herein are highly dependent on the amine moiety.¹⁹ As indoline is released upon QM formation, other unforeseen modes of action might be the cause of the antibacterial properties. The rather lower cytotoxic levels of the studied compounds are surely dependent on the different metabolisms of the organisms tested and could be explained by a faster

kinetic profile toward QM formation in the bacterial media.^{53,54}

CONCLUSIONS

In summary, through use of Petasis borono–Mannich multicomponent reaction, starting from 5-nitrosalicylaldehyde, we were able to expand our library of aminoalkylphenols and find more potent antibacterials than the previously reported. The most active compound synthesized **13** was demonstrated to be selectively active against important bacteria responsible for nosocomial infections (*S. aureus* and *E. faecalis*), while only moderately active against *S. pneumoniae* and *S. agalactiae*. Gladly, the most active compounds against bacteria showed cytotoxicity against mammalian cells only at concentrations considerably higher than the determined MICs, as verified through an in vitro model. The phenol moiety was verified to be essential to achieve the desired antibacterial properties; however, such properties do not relate with the antioxidant properties of the compounds tested. As Mannich bases have been demonstrated to be precursors of quinone methides, a computational study was performed, and the results found are in line with such a hypothesis. As quinone methides are highly reactive, they can play a role as antibacterial agents, although not encompassing the hydrolyzed adduct. This aspect is also in agreement with the determined MICs of mixtures of different enantiomeric ratios, as both enantiomers can form a similar reactive intermediate. Nevertheless, the antibacterial mode of action of these compounds remains obscure, and further studies will be reported in due course.

EXPERIMENTAL SECTION

General Remarks. All reagents were obtained from Sigma-Aldrich or TCI and were used without further purification. The reactions were performed under argon atmosphere and monitored by thin-layer chromatography carried out on precoated (Merck TLC silica gel 60 F254) aluminium plates by using UV light as a visualizing agent and cerium molybdate solution or ninhydrin as developing agents. Flash column chromatography was performed on silica gel 60 (Merck, 0.040–0.063 mm). NMR spectra were recorded with Varian Mercury 300 MHz or JEOL ECZR 500 instruments using $CDCl_3$ or $DMSO-d_6$ as solvents and calibrated using tetramethylsilane as internal standard. Chemical shifts (δ) are reported in ppm referenced to the $CDCl_3$ residual peak (δ

7.26) or TMS peak (δ 0.00) for ^1H NMR, to CDCl_3 (δ 77.16) for ^{13}C NMR. The following abbreviations were used to describe peak splitting patterns: s = singlet, d = doublet, t = triplet, m = multiplet. Coupling constants, J , were reported in hertz. High-resolution mass spectra were recorded on a Waters ESI-TOF MS spectrometer. Elemental analysis (C, N, and H) was performed on Elementar vario EL III. All compounds tested for antibacterial activity, with exception of 12, were established to be >95% pure upon elemental analysis.

General Method for the Synthesis of Aminoalkylphenols 4–17. Indoline (56 μL , 0.50 mmol) was added to a solution of 2-hydroxy-5-nitrobenzaldehyde (83.6 mg, 0.50 mmol) and arylboronic acid (0.50 mmol) in 1,2-dichloroethane (DCE) or ethanol (EtOH; 5.0 mL) at 50 $^\circ\text{C}$. The reaction was stirred at the same temperature until it was complete as judged by TLC. The solvent was evaporated under reduced pressure, and the residue was purified by column chromatography to give the pure aminoalkylphenol.

2-(Indolin-1-yl(*p*-tolyl)methyl)-4-nitrophenol (4). After 5 h reaction in DCE, purification by column chromatography [hexane/dichloromethane (DCM) 2:3] gave 4 (155 mg, 86% yield) as an off-white solid. ^1H NMR (300 MHz, CDCl_3): δ 11.87 (br s, 1H), 8.10 (dd, J = 9.1, 2.6 Hz, 1H), 7.97 (d, J = 2.9 Hz, 1H), 7.33–7.29 (m, 2H), 7.19–7.16 (m, 3H), 7.05–7.00 (m, 1H), 6.97–6.90 (m, 2H), 6.52 (d, J = 7.6 Hz, 1H), 5.32 (s, 1H), 3.27–3.20 (m, 1H), 3.09–2.90 (m, 3H), 2.34 (s, 3H). ^{13}C NMR (75 MHz, CDCl_3): δ 162.9, 150.4, 140.9, 138.9, 135.2, 132.6, 130.0, 128.8, 127.7, 127.1, 125.2, 125.1, 124.9, 122.6, 117.8, 112.5, 70.6, 53.7, 28.6, 21.3. Elemental analysis: calcd for $\text{C}_{22}\text{H}_{20}\text{N}_2\text{O}_3 \cdot 0.19\text{H}_2\text{O}$: C, 72.64; H, 5.65; N, 7.70; found: C, 72.64; H, 5.49; N, 7.77. HRMS (ESI/TOF): m/z calcd for $\text{C}_{22}\text{H}_{21}\text{N}_2\text{O}_3^+ [\text{M} + \text{H}]^+$, 361.1547; found, 361.1566.

2-(Indolin-1-yl(4-vinylphenyl)methyl)-4-nitrophenol (5). After 48 h reaction in EtOH, purification by column chromatography (toluene) gave 5 (150 mg, 81% yield) as a light yellow solid. ^1H NMR (300 MHz, CDCl_3): δ 11.80 (br s, 1H), 8.12 (dd, J = 8.9, 2.8 Hz, 1H), 8.02 (d, J = 2.6 Hz, 1H), 7.42 (s, 4H), 7.20 (d, J = 7.0 Hz, 2H), 7.07–6.92 (m, 3H), 6.72 (dd, J = 17.7, 11.0 Hz, 1H), 6.55 (d, J = 7.9 Hz, 1H), 5.79 (d, J = 17.6 Hz, 1H), 5.38 (s, 1H), 5.31 (d, J = 10.8 Hz, 1H), 3.31–3.24 (m, 1H), 3.13–3.02 (m, 1H), 2.99–2.91 (m, 2H). ^{13}C NMR (75 MHz, CDCl_3): δ 162.8, 150.2, 140.8, 138.1, 137.5, 135.9, 132.5, 129.1, 127.6, 127.0, 126.7, 125.2, 125.0, 124.8, 122.5, 117.7, 115.1, 112.4, 70.3, 53.6, 28.5. Elemental analysis: calcd for $\text{C}_{23}\text{H}_{20}\text{N}_2\text{O}_3 \cdot 0.46\text{H}_2\text{O}$: C, 72.55; H, 5.54; N, 7.36; found: C, 72.55; H, 5.58; N, 7.15. HRMS (ESI/TOF): m/z calcd for $\text{C}_{23}\text{H}_{21}\text{N}_2\text{O}_3^+ [\text{M} + \text{H}]^+$, 373.1547; found, 373.1541.

2-(4-Ethylphenyl)(indolin-1-yl)methyl)-4-nitrophenol (6). After 48 h reaction in EtOH, purification by column chromatography (hexane/toluene 1:3) gave 6 (132 mg, 71% yield) as a light yellow solid. ^1H NMR (300 MHz, CDCl_3): δ 11.87 (br s, 1H, ArOH), 8.10 (dd, J = 8.9, 2.8 Hz, 1H), 8.00 (d, J = 2.6 Hz, 1H), 7.35 (d, J = 8.2 Hz, 2H), 7.22–7.17 (m, 3H), 7.05–6.90 (m, 3H), 6.53 (d, J = 7.6 Hz, 1H), 5.34 (s, 1H), 3.28–3.22 (m, 1H), 3.10–2.91 (m, 3H), 2.66 (q, J = 7.6 Hz, 2H), 1.24 (t, J = 7.6 Hz, 3H). ^{13}C NMR (75 MHz, CDCl_3): δ 162.9, 150.4, 145.0, 140.9, 135.4, 132.5, 128.8, 128.7, 127.6, 127.1, 125.1, 125.0, 124.9, 122.5, 117.7, 112.4, 70.6, 53.7, 28.6, 15.4. Elemental analysis: calcd for $\text{C}_{23}\text{H}_{22}\text{N}_2\text{O}_3 \cdot 0.67\text{H}_2\text{O}$: C, 71.49; H, 6.09; N, 7.25; found: C, 71.49; H, 6.10; N, 7.08. HRMS (ESI/TOF): m/z calcd for $\text{C}_{23}\text{H}_{23}\text{N}_2\text{O}_3^+ [\text{M} + \text{H}]^+$, 375.1703; found, 375.1712.

2-((4-*tert*-Butylphenyl)(indolin-1-yl)methyl)-4-nitrophenol (7). After 48 h reaction in EtOH, purification by column chromatography (hexane/toluene 3:7) gave 7 (156 mg, 78% yield) as a light yellow solid. ^1H NMR (300 MHz, CDCl_3): δ 11.89 (br s, 1H), 8.11 (dd, J = 8.9, 2.8 Hz, 1H), 8.02 (d, J = 2.6 Hz, 1H), 7.38 (s, 4H), 7.19 (d, J = 7.3 Hz, 1H), 7.05–6.90 (m, 3H), 6.54 (d, J = 7.9 Hz, 1H), 5.34 (s, 1H), 3.28–3.20 (m, 1H), 3.09–2.90 (m, 3H), 1.33 (s, 9H). ^{13}C NMR (75 MHz, CDCl_3): δ 162.9, 151.9, 150.5, 140.9, 135.2, 132.5, 128.5, 127.6, 127.1, 126.1, 125.1, 125.0, 124.9, 122.4, 117.7, 112.4, 70.6, 53.8, 34.7, 31.3, 28.5. Elemental analysis: calcd for $\text{C}_{25}\text{H}_{26}\text{N}_2\text{O}_3 \cdot 0.16\text{H}_2\text{O}$: C, 74.08; H, 6.54; N, 6.91; found: C, 74.08; H, 6.56; N, 6.76. HRMS (ESI/TOF): m/z calcd for $\text{C}_{25}\text{H}_{27}\text{N}_2\text{O}_3^+ [\text{M} + \text{H}]^+$, 403.2016; found, 403.2020.

2-((4-Butylphenyl)(indolin-1-yl)methyl)-4-nitrophenol (8). After 48 h reaction in EtOH, purification by column chromatography (hexane/toluene 1:4) gave 8 (41 mg, 19% yield) as a light yellow solid. ^1H NMR (300 MHz, CDCl_3): δ 11.88 (br s, 1H), 8.10 (dd, J = 9.1, 2.9 Hz, 1H), 7.99 (d, J = 2.6 Hz, 1H), 7.34–7.31 (m, 2H), 7.19–7.16 (m, 3H), 7.05–6.90 (m, 3H), 6.51 (d, J = 7.6 Hz, 1H), 5.31 (s, 1H), 3.26–3.18 (m, 1H), 3.09–2.90 (m, 3H), 2.60 (t, J = 7.6 Hz, 2H), 1.64–1.54 (m, 2H), 1.42–1.29 (m, 2H), 0.93 (t, J = 7.3 Hz, 3H). ^{13}C NMR (75 MHz, CDCl_3): δ 162.9, 150.5, 143.8, 140.9, 135.4, 132.6, 129.3, 128.8, 127.6, 127.1, 125.2, 125.1, 124.9, 122.5, 117.7, 112.5, 70.8, 53.7, 35.4, 33.5, 28.6, 22.5, 14.1. Elemental analysis: calcd for $\text{C}_{25}\text{H}_{26}\text{N}_2\text{O}_3 \cdot 0.19\text{H}_2\text{O}$: C, 73.97; H, 6.55; N, 6.90; found: C, 73.97; H, 6.55; N, 6.73. HRMS (ESI/TOF): m/z calcd for $\text{C}_{25}\text{H}_{27}\text{N}_2\text{O}_3^+ [\text{M} + \text{H}]^+$, 403.2016; found, 403.2020.

2-((4-Hexylphenyl)(indolin-1-yl)methyl)-4-nitrophenol (9). After 48 h reaction in EtOH, purification by column chromatography (hexane/toluene 1:4) gave 9 (140 mg, 65% yield) as a light yellow solid. ^1H NMR (300 MHz, CDCl_3): δ 11.87 (br s, 1H), 8.10 (dd, J = 8.9, 2.8 Hz, 1H), 8.00 (d, J = 2.6 Hz, 1H), 7.35–7.32 (m, 2H), 7.19–7.16 (m, 3H), 7.05–6.90 (m, 3H), 6.52 (d, J = 7.9 Hz, 1H), 5.33 (s, 1H), 3.26–3.18 (m, 1H), 3.09–2.90 (m, 3H), 2.60 (t, J = 7.3 Hz, 2H), 1.66–1.56 (m, 2H), 1.37–1.31 (m, 6H), 0.91–0.87 (m, 3H). ^{13}C NMR (75 MHz, CDCl_3): δ 162.8, 150.4, 143.8, 140.8, 135.4, 132.5, 129.2, 128.7, 127.5, 127.1, 125.1, 125.0, 124.8, 122.4, 117.6, 112.4, 70.5, 53.6, 35.7, 31.7, 31.3, 29.1, 28.5, 22.6, 14.1. Elemental analysis: calcd for $\text{C}_{27}\text{H}_{30}\text{N}_2\text{O}_3 \cdot 0.30\text{H}_2\text{O}$: C, 74.40; H, 7.07; N, 6.43; found: C, 74.40; H, 6.94; N, 6.37. HRMS (ESI/TOF): m/z calcd for $\text{C}_{27}\text{H}_{31}\text{N}_2\text{O}_3^+ [\text{M} + \text{H}]^+$, 431.2329; found, 431.2318.

2-(Indolin-1-yl(4-(methylthio)phenyl)methyl)-4-nitrophenol (10). After 48 h reaction in EtOH, purification by column chromatography (hexane/EtOAc 3:1) gave 10 (167 mg, 85% yield) as a light yellow solid. ^1H NMR (300 MHz, CDCl_3): δ 11.76 (br s, 1H), 8.11 (dd, J = 9.1, 2.9 Hz, 1H), 7.97 (d, J = 2.6 Hz, 1H), 7.35–7.32 (m, 2H), 7.26–7.17 (m, 3H), 7.05–6.90 (m, 3H), 6.51 (d, J = 7.6 Hz, 1H), 5.32 (s, 1H), 3.27–3.21 (m, 1H), 3.10–2.91 (m, 3H), 2.47 (s, 3H). ^{13}C NMR (75 MHz, CDCl_3): δ 162.8, 150.2, 140.9, 139.8, 134.5, 132.5, 129.3, 127.7, 126.74, 126.71, 125.3, 125.1, 124.8, 122.6, 117.8, 112.4, 70.2, 53.6, 28.6, 15.4. Elemental analysis: calcd for $\text{C}_{22}\text{H}_{20}\text{N}_2\text{O}_3\text{S} \cdot 0.63\text{H}_2\text{O}$: C, 65.44; H, 5.31; N, 6.94; found: C, 65.44; H, 5.31; N, 6.65. HRMS (ESI/TOF): m/z calcd for $\text{C}_{22}\text{H}_{21}\text{N}_2\text{O}_3\text{S}^+ [\text{M} + \text{H}]^+$, 393.1267; found, 393.1273.

2-((4-Hydroxyphenyl)(indolin-1-yl)methyl)-4-nitrophenol (11). After 24 h reaction in DCE, purification by column chromatography (hexane/EtOAc 4:1) gave 11 (144 mg, 80%

yield) as a yellow solid. $^1\text{H NMR}$ (300 MHz, CDCl_3): δ 8.11 (dd, $J = 9.1, 2.6$ Hz, 1H), 7.96 (d, $J = 2.9$ Hz, 1H), 7.28 (d, $J = 7.6$ Hz, 2H), 7.18 (d, $J = 7.0$ Hz, 1H), 7.05–6.90 (m, 3H), 6.81 (d, $J = 8.8$ Hz, 2H), 6.50 (d, $J = 8.2$ Hz, 1H), 5.30 (s, 1H), 3.25–3.18 (m, 1H), 3.10–2.90 (m, 3H). $^{13}\text{C NMR}$ (75 MHz, CDCl_3): 162.9, 156.1, 150.2, 140.9, 132.6, 130.4, 127.7, 127.1, 125.3, 125.1, 124.9, 122.6, 117.8, 116.1, 112.6, 70.2, 53.5, 28.6. Elemental analysis: calcd for $\text{C}_{21}\text{H}_{18}\text{N}_2\text{O}_4 \cdot 0.35\text{H}_2\text{O}$: C, 68.42; H, 5.11; N, 7.60; found: C, 68.42; H, 5.10; N, 7.32. HRMS (ESI/TOF): m/z calcd for $[\text{C}_{21}\text{H}_{18}\text{N}_2\text{O}_4 + \text{H}]^+$, 363.1339; found, 363.1339.

tert-Butyl 4-((2-Hydroxy-5-nitrophenyl)(indolin-1-yl)methyl)phenylcarbamate (12). After 24 h reaction in DCE, purification by column chromatography (hexane/EtOAc 85:15) gave **12** (215 mg, 82% yield) as a light yellow solid. $^1\text{H NMR}$ (300 MHz, CDCl_3): δ 11.80 (br s, 1H), 8.10 (dd, $J = 8.8, 2.9$ Hz, 1H), 7.95 (d, $J = 2.9$ Hz, 1H), 7.38–7.31 (m, 4H), 7.17 (d, $J = 7.0$ Hz, 1H), 7.04–6.89 (m, 3H), 6.51–6.49 (m, 2H, ArH), 5.31 (s, 1H, CH), 3.25–3.19 (m, 1H), 3.10–3.01 (m, 1H), 2.95–2.89 (m, 2H), 1.51 (s, 9H). $^{13}\text{C NMR}$ (75 MHz, CDCl_3): δ 162.9, 152.7, 150.2, 141.0, 139.0, 132.6, 132.5, 129.7, 127.7, 126.9, 125.3, 125.1, 124.9, 122.6, 119.0, 117.8, 112.5, 81.1, 70.2, 53.6, 28.6, 28.4. HRMS (ESI/TOF): m/z calcd for $[\text{C}_{26}\text{H}_{26}\text{N}_3\text{O}_5]^-$ [M – H] $^-$, 460.1878; found, 460.1863.

2-((4-Chlorophenyl)(indolin-1-yl)methyl)-4-nitrophenol (13). After 150 min reaction in DCE, purification by column chromatography (hexane/DCM, gradient from 4:6 to 3:7) gave **13** (127 mg, 67% yield) as a light yellow solid. $^1\text{H NMR}$ (300 MHz, CDCl_3): δ 11.65 (br s, 1H), 8.13 (dd, $J = 9.4, 2.9$ Hz, 1H), 7.95 (d, $J = 2.3$ Hz, 1H), 7.40–7.33 (m, 4H), 7.19 (d, $J = 7.0$ Hz, 1H), 7.05–6.91 (m, 3H), 6.49 (d, $J = 8.2$ Hz, 1H), 5.34 (s, 1H), 3.26–3.18 (m, 1H), 3.10–2.92 (m, 3H). $^{13}\text{C NMR}$ (75 MHz, CDCl_3): δ 162.6, 149.9, 140.9, 136.5, 134.9, 132.3, 130.1, 129.4, 127.6, 126.2, 125.4, 125.1, 124.6, 122.7, 117.8, 112.3, 69.9, 53.6, 28.5. Elemental analysis: calcd for $\text{C}_{21}\text{H}_{17}\text{N}_2\text{O}_3\text{Cl} \cdot 0.14\text{H}_2\text{O}$: C, 65.80; H, 4.54; N, 7.31; found: C, 65.80; H, 4.61; N, 7.12. HRMS (ESI/TOF): m/z calcd for $[\text{C}_{21}\text{H}_{18}\text{N}_2\text{O}_3\text{Cl}]^+$ [M + H] $^+$, 381.1000; found, 381.1006.

2-((4-Bromophenyl)(indolin-1-yl)methyl)-4-nitrophenol (14). After 24 h reaction in DCE, purification by column chromatography (hexane/EtOAc 3:1) gave **14** (154 mg, 72% yield) as a light yellow solid. $^1\text{H NMR}$ (300 MHz, CDCl_3): δ 11.59 (br s, 1H), 8.12 (dd, $J = 8.7, 2.8$ Hz, 1H), 7.94 (d, $J = 2.3$ Hz, 1H), 7.53–7.48 (m, 2H), 7.33–7.28 (m, 2H), 7.19 (d, $J = 7.6$ Hz, 1H), 7.04–6.91 (m, 3H), 6.48 (d, $J = 8.2$ Hz, 1H), 5.33 (s, 1H), 3.26–3.18 (m, 1H), 3.10–2.92 (m, 3H). $^{13}\text{C NMR}$ (75 MHz, CDCl_3): δ 162.7, 150.0, 141.0, 137.1, 132.5, 132.4, 130.5, 127.7, 126.3, 125.5, 125.2, 124.7, 123.1, 122.7, 117.9, 112.4, 70.0, 53.7, 28.6. Elemental analysis: calcd for $\text{C}_{21}\text{H}_{17}\text{N}_2\text{O}_3\text{Br} \cdot 0.68\text{H}_2\text{O}$: C, 57.66; H, 4.23; N, 6.40; found: C, 57.66; H, 4.24; N, 6.23. HRMS (ESI/TOF): m/z calcd for $[\text{C}_{21}\text{H}_{18}\text{N}_2\text{O}_3\text{Br}]^+$ [M + H] $^+$, 425.0495; found, 425.0498.

2-((4-Fluorophenyl)(indolin-1-yl)methyl)-4-nitrophenol (15). After 24 h reaction in DCE, purification by column chromatography (hexane/EtOAc 3:1) gave **15** (172 mg, 94% yield) as a light yellow solid. $^1\text{H NMR}$ (300 MHz, CDCl_3): δ 11.68 (br s, 1H), 8.12 (dd, $J = 8.8, 2.7$ Hz, 1H), 7.94 (d, $J = 2.3$ Hz, 1H), 7.43–7.38 (m, 2H), 7.19 (d, $J = 7.6$ Hz, 1H), 7.09–6.91 (m, 5H), 6.49 (d, $J = 8.2$ Hz, 1H), 5.35 (s, 1H), 3.24–3.18 (m, 1H), 3.10–2.91 (m, 3H). $^{13}\text{C NMR}$ (75 MHz, CDCl_3): δ 164.6, 162.8, 161.3, 150.1, 141.0, 134.1, 134.0,

132.5, 130.7, 130.6, 127.7, 126.7, 125.4, 125.2, 124.8, 122.8, 117.9, 116.5, 116.2, 112.5, 70.0, 53.7, 28.6. Elemental analysis: calcd for $\text{C}_{21}\text{H}_{17}\text{N}_2\text{O}_3\text{F} \cdot 0.87\text{H}_2\text{O}$: C, 66.38; H, 4.97; N, 7.37; found: C, 66.38; H, 4.80; N, 7.14. HRMS (ESI/TOF): m/z calcd for $[\text{C}_{21}\text{H}_{18}\text{N}_2\text{O}_3\text{F}]^+$ [M + H] $^+$, 365.1296; found, 365.1314.

2-(Indolin-1-yl(o-tolyl)methyl)-4-nitrophenol (16). After 48 h reaction in EtOH, purification by column chromatography (toluene) gave **16** (87 mg, 48% yield) as a yellow solid. $^1\text{H NMR}$ (300 MHz, CDCl_3): δ 11.31 (br s, 1H), 8.11 (dd, $J = 8.9, 2.8$ Hz, 1H), 7.93 (d, $J = 2.6$ Hz, 1H), 7.43 (d, $J = 7.3$ Hz, 1H), 7.26–7.19 (m, 4H), 7.05–6.89 (m, 3H), 6.44 (d, $J = 7.6$ Hz, 1H), 5.76 (s, 1H), 3.31–3.25 (m, 1H), 3.08–2.95 (m, 3H), 2.42 (s, 3H). $^{13}\text{C NMR}$ (75 MHz, CDCl_3): δ 162.8, 150.6, 141.0, 136.8, 136.0, 131.9, 131.2, 128.59, 128.57, 127.7, 127.21, 127.19, 125.1, 125.0, 124.6, 122.1, 117.6, 111.6, 64.6, 53.2, 28.5, 20.6. Elemental analysis: calcd for $\text{C}_{22}\text{H}_{20}\text{N}_2\text{O}_3 \cdot 0.27\text{H}_2\text{O}$: C, 72.35; H, 5.67; N, 7.67; found: C, 72.35; H, 5.63; N, 7.38. HRMS (ESI/TOF): m/z calcd for $[\text{C}_{22}\text{H}_{21}\text{N}_2\text{O}_3]^+$ [M + H] $^+$, 361.1547; found, 361.1556.

2-(Indolin-1-yl(naphthalen-1-yl)methyl)-4-nitrophenol (17). After 48 h reaction in EtOH, purification by column chromatography (toluene) gave **17** (142 mg, 72% yield) as a yellow solid. $^1\text{H NMR}$ (300 MHz, CDCl_3): δ 11.10 (br s, 1H), 8.12 (dd, $J = 8.9, 2.8$ Hz, 1H), 8.03–8.00 (m, 1H), 7.94–7.86 (m, 3H), 7.59–7.42 (m, 4H), 7.20 (d, $J = 7.0$ Hz, 1H), 7.08–7.00 (m, 2H), 6.95–6.90 (m, 1H), 6.54 (d, $J = 7.6$ Hz, 1H), 6.41 (s, 1H), 3.29–3.22 (m, 1H), 3.13–2.84 (m, 3H). $^{13}\text{C NMR}$ (75 MHz, CDCl_3): δ 162.9, 150.6, 141.2, 134.1, 133.8, 131.8, 129.6, 129.5, 127.9, 127.4, 127.3, 127.2, 126.2, 125.8, 125.3, 125.1, 125.0, 123.0, 121.9, 117.7, 111.2, 63.3, 52.6, 28.6. Elemental analysis: calcd for $\text{C}_{25}\text{H}_{20}\text{N}_2\text{O}_3 \cdot 0.33\text{H}_2\text{O}$: C, 74.61; H, 5.18; N, 6.96; found: C, 74.61; H, 5.05; N, 6.76. HRMS (ESI/TOF): m/z calcd for $[\text{C}_{25}\text{H}_{21}\text{N}_2\text{O}_3]^+$ [M + H] $^+$, 397.1547; found, 397.1563.

1-(2-Methoxy-5-nitrophenyl)(p-tolyl)methylindoline (18). Dimethyl sulfate (27.9 μL , 0.30 mmol, 1.25 equiv) was added to a solution of **4** (85.0 mg, 0.236 mmol) and K_2CO_3 (81.5 mg, 0.59 mmol, 2.5 equiv) in acetone (5.0 mL) at room temperature under argon, and the reaction mixture was stirred for 19 h. The reaction was quenched by adding 10 mL of 5% aq NaOH, and the resulting aqueous solution was extracted with DCM (4 \times 5 mL). The organic extracts were combined, dried over MgSO_4 , filtered, and evaporated under reduced pressure. The residue was purified by column chromatography (hexane/DCM 2:3) to give **18** (85 mg, 0.227 mmol, 96% yield) as a light yellow solid. $^1\text{H NMR}$ (500 MHz, CDCl_3): δ 8.39 (d, $J = 2.3$ Hz, 1H), 8.18 (dd, $J = 9.2, 2.9$ Hz, 1H), 7.18 (d, $J = 8.0$ Hz, 2H), 7.12–7.07 (m, 3H), 6.95–6.89 (m, 2H), 6.65 (t, $J = 7.4$ Hz, 1H), 6.07 (d, $J = 8.0$ Hz, 1H), 5.78 (s, 1H), 3.87 (s, 3H), 3.24–3.19 (m, 1H), 3.10 (q, $J = 8.8$ Hz, 1H), 3.02–2.89 (m, 2H), 2.33 (s, 3H). $^{13}\text{C NMR}$ (126 MHz, CDCl_3): δ 161.7, 151.8, 141.8, 137.4, 136.4, 131.9, 130.7, 129.3, 128.8, 127.2, 124.9, 124.5, 124.5, 118.3, 110.5, 108.2, 60.3, 56.4, 52.2, 28.5, 21.3. Elemental analysis: calcd for $\text{C}_{23}\text{H}_{23}\text{N}_2\text{O}_3 \cdot 0.35\text{H}_2\text{O}$: C, 72.56; H, 6.01; N, 7.36; found: C, 72.56; H, 5.63; N, 7.58. HRMS (ESI/TOF): m/z calcd for $[\text{C}_{23}\text{H}_{23}\text{N}_2\text{O}_3]^+$ [M + H] $^+$, 375.1703; found, 375.1703.

1-(3-Nitrophenyl)(p-tolyl)methylindoline (21). Anhydrous AlCl_3 (0.934 g, 7.01 mmol, 1.3 equiv) was added to a solution of 3-nitrobenzoyl chloride (1.00 g, 5.39 mmol) and dry toluene (4.0 mL). The reaction was stirred at room temperature for 30 min and then quenched by pouring the

reaction mixture into water. The aqueous layer was extracted with DCM, and the organic extract was washed with water and brine, dried over MgSO_4 , filtered, and evaporated under reduced pressure to afford 4-methyl-3'-nitrobenzophenone (**20**) (0.90 g, 69% yield) as a white solid. The product was obtained with the same spectral characterization as previously described.⁵⁵ ^1H NMR (300 MHz, CDCl_3): δ 8.60 (t, $J = 1.8$ Hz, 1H), 8.43 (dd, $J = 7.6, 2.3$ Hz, 1H), 8.12 (dt, $J = 7.9, 1.3$ Hz, 1H), 7.73–7.67 (m, 3H), 7.33 (d, $J = 7.6$ Hz, 2H), 2.47 (s, 3H).

To a solution of **20** (0.20 g, 0.83 mmol) in dry DCM (4.5 mL) was added TiCl_4 (0.10 mL, 0.90 mmol, 1.1 equiv) in dry DCM (0.90 mL). The mixture was cooled to 0 °C, and indoline (0.20 mL, 1.79 mmol, 2.16 equiv) was added. The reaction was stirred at room temperature under argon for 3 h, and sodium cyanoborohydride (0.98 mmol, 0.06 g, 1.18 equiv) in 1.5 mL of methanol was added. After an hour, the mixture was made basic (pH 10) by adding 5 M aq NaOH and filtered. The filtrate was partitioned between DCM (15 mL) and water (15 mL). The organic layer was separated, washed with water (2 \times 15 mL) and brine (15 mL), dried over MgSO_4 , filtered, and evaporated under reduced pressure. The residue was purified by column chromatography (hexane/EtOAc 92:8) to give **21** (168 mg, 60% yield) as a light yellow solid. ^1H NMR (300 MHz, CDCl_3): δ 8.26–8.25 (m, 1H), 8.14–8.10 (m, 1H), 7.75 (d, $J = 7.6$ Hz, 1H), 7.50 (t, $J = 8.2$ Hz, 1H), 7.19–7.9 (m, 5H), 6.94 (t, $J = 7.0$ Hz, 1H), 6.68 (t, $J = 7.0$ Hz, 1H), 6.15 (d, $J = 7.6$ Hz, 1H), 5.56 (s, 1H), 3.28–2.88 (m, 4H), 2.34 (s, 3H). ^{13}C NMR (75 MHz, CDCl_3): δ 151.6, 148.7, 144.6, 137.8, 136.7, 134.2, 130.7, 129.6, 128.9, 127.2, 124.7, 123.0, 122.4, 118.4, 108.4, 66.4, 51.8, 28.5, 21.2. Elemental analysis: calcd for $\text{C}_{22}\text{H}_{20}\text{N}_2\text{O}_2 \cdot 0.33\text{H}_2\text{O}$: C, 75.41; H, 5.94; N, 7.99; found: C, 75.41; H, 5.70; N, 7.88. HRMS (ESI/Q-TOF): m/z calcd for $\text{C}_{22}\text{H}_{21}\text{N}_2\text{O}_2^+ [\text{M} + \text{H}]^+$, 345.1598; found, 345.1593.

2-(Hydroxy(*p*-tolyl)methyl)-4-nitrophenol (23). A suspension of magnesium chips (194 mg, 8.00 mmol, 4 equiv) and a crystal of iodine in dry tetrahydrofuran (THF; 6.0 mL) was stirred and heated to reflux under argon. 1-Bromo-4-methylbenzene (1.37 g, 8.00 mmol, 4 equiv) in dry THF (2.0 mL) was added dropwise. The reaction mixture stirred under reflux for 50 min and then allowed to cool to room temperature. The resulting solution of *p*-tolylmagnesium bromide in THF was added dropwise to a solution of 2-hydroxy-5-nitrobenzaldehyde (2.00 mmol, 334 mg) in dry THF (4.0 mL) at –78 °C under argon. The reaction mixture was stirred for 15 min and then moved to 0 °C for another 15 min. The reaction was quenched by adding 5 mL of saturated aq NH_4Cl and then 5 mL of H_2O . Aqueous and organic layers were separated and the aqueous layer was extracted with Et_2O (2 \times 10 mL). Organic extracts were combined, dried over MgSO_4 , filtered, and evaporated under reduced pressure. The residue was purified by column chromatography (DCM/EtOAc 95:5) to give **23** (400 mg, 1.54 mmol, 77% yield) as an off-white solid. ^1H NMR (300 MHz, CDCl_3): δ ppm 9.21 (s, 1H), 8.07 (dd, $J = 9.0, 2.7$ Hz, 1H), 7.76 (d, $J = 2.5$ Hz, 1H), 7.29–7.20 (m, 4H), 6.96 (d, $J = 8.9$ Hz, 1H), 6.06 (d, $J = 1.8$ Hz, 1H), 3.03 (d, $J = 2.5$ Hz, 1H), 2.36 (s, 3H). ^{13}C NMR (75 MHz, CDCl_3): δ 161.8, 140.7, 139.2, 137.8, 130.0, 127.0, 126.9, 125.4, 124.6, 118.0, 77.0, 21.3. Elemental analysis: calcd for $\text{C}_{14}\text{H}_{13}\text{NO}_4 \cdot 0.32\text{H}_2\text{O}$: C, 63.46; H, 5.19; N, 5.29; found: C, 63.46; H, 4.99; N, 5.09. HRMS (ESI/Q-TOF): m/z calcd for $\text{C}_{14}\text{H}_{12}\text{NO}_4^+ [\text{M} - \text{H}]^+$, 258.0772; found, 258.0776.

Chiral Resolution of 2-(Indolin-1-yl(*p*-tolyl)methyl)-4-nitrophenol (4). **4** (108 mg, 0.30 mmol, 1 equiv) in dry DCM (1 mL) was added to a solution of (R)-(+)-Mosher's acid (84.3 mg, 0.36 mmol, 1.2 equiv), *N*-(3-dimethylamino-propyl)-*N*'-ethylcarbodiimide hydrochloride (98 mg, 0.51 mmol, 1.7 equiv), and DMAP (7.9 mg, 0.06 mmol, 0.2 equiv) in dry DCM (2 mL) at room temperature under argon. The reaction mixture was stirred for 72 h and then diluted with 10 mL of DCM. The solution was washed with 10 mL of saturated aq NaHCO_3 and the layers were separated. Additional 2 \times 5 mL of DCM was used to extract the aqueous layer. Organic extracts were combined, dried over MgSO_4 , filtered, and evaporated under reduced pressure. The residue was purified by column chromatography (hexane/EtOAc, gradient from 85:15 to 80:20) to give **22** (78.0 mg, 0.14 mmol, 45% yield) as a 46:54 mixture of diastereomers, determined by ^{19}F NMR. ^1H NMR (300 MHz, CDCl_3): δ 8.55 (d, $J = 2.3$ Hz, 1H), 8.49 (d, $J = 2.9$ Hz, 1H), 8.23 (dd, $J = 2.9, 1.8$ Hz, 1H), 8.20 (dd, $J = 2.6, 1.5$ Hz, 1H), 7.53 (t, $J = 8.2$ Hz, 4H), 7.45–7.27 (m, 9H), 7.11–7.03 (m, 7H), 6.94–6.89 (m, 4H), 6.80 (d, $J = 8.2$ Hz, 3H), 6.73–6.66 (m, 2H), 5.98 (d, $J = 8.2$ Hz, 1H), 5.93 (d, $J = 8.2$ Hz, 1H), 5.50 (s, 1H), 5.19 (s, 1H), 3.53 (d, $J = 1.2$ Hz, 4H), 3.44 (d, $J = 1.2$ Hz, 3H), 3.21–3.04 (m, 4H), 2.99–2.85 (m, 6H), 2.32 (s, 3H), 2.31 (s, 3H). ^{13}C NMR (126 MHz, CDCl_3): δ 164.8, 164.7, 152.4, 152.0, 151.3, 151.2, 146.5, 146.4, 137.8, 137.0, 136.5, 135.3, 135.1, 131.4, 131.0, 130.7, 130.4, 130.3, 130.2, 129.5, 129.4, 129.0, 128.9, 128.6, 128.6, 127.5, 127.3, 127.3, 125.2, 124.9, 124.5, 124.5, 124.4, 124.3, 123.9, 123.7, 123.2, 123.2, 122.1, 122.0, 118.7, 118.5, 108.5, 108.1, 85.5, 85.3, 85.0, 84.8, 84.6, 60.7, 60.1, 56.0, 55.7, 52.5, 51.9, 28.4, 21.2. ^{19}F NMR (282 MHz, CDCl_3): δ –70.91 (s, CF_3), –71.30 (s, CF_3). The diastereomers were separated by preparative thin layer chromatography, by multiple elutions with hexane/toluene 4:6 and the resulting separated diastereomers further purified from the hydrolyzed product by column chromatography (hexane/EtOAc 85:15).

22_{major} ^1H NMR (300 MHz, CDCl_3): δ 8.54 (d, $J = 2.3$ Hz, 1H, ArH), 8.20 (dd, $J = 8.8, 2.9$ Hz, 1H, ArH), 7.53 (d, $J = 7.6$ Hz, 2H, ArH), 7.40–7.35 (m, 2H, ArH), 7.32–7.27 (m, 2H, ArH), 7.08 (d, $J = 7.0$ Hz, 1H, ArH), 7.03 (d, $J = 7.6$ Hz, 2H, ArH), 6.90 (t, $J = 7.3$ Hz, 1H, ArH), 6.79 (d, $J = 8.2$ Hz, 2H, ArH), 6.69 (t, $J = 7.0$ Hz, 1H, ArH), 5.91 (d, $J = 7.6$ Hz, 1H, ArH), 5.17 (s, 1H, CH), 3.51 (d, $J = 1.2$ Hz, 3H, OCH_3), 3.12–3.04 (m, 1H, NCH_2CH_2), 2.96–2.84 (m, 3H, NCH_2CH_2), 2.30 (s, 3H, ArCH₃). ^{19}F NMR (282 MHz, CDCl_3): δ –71.31 (s). **22_{minor}** ^1H NMR (300 MHz, CDCl_3): δ 8.48 (d, $J = 2.9$ Hz, 1H, ArH), 8.20 (dd, $J = 9.1, 2.6$ Hz, 1H, ArH), 7.50 (d, $J = 7.6$ Hz, 2H, ArH), 7.44–7.30 (m, 4H, ArH), 7.08 (d, $J = 7.0$ Hz, 1H, ArH), 7.04 (d, $J = 8.2$ Hz, 2H, ArH), 6.92–6.87 (m, 3H, ArH), 6.68 (t, $J = 7.6$ Hz, 1H, ArH), 5.97 (d, $J = 8.2$ Hz, 1H, ArH), 5.48 (s, 1H, CH), 3.42 (d, $J = 1.2$ Hz, 3H, OCH_3), 3.20–3.11 (m, 1H, NCH_2CH_2), 3.08–3.02 (m, 1H, NCH_2CH_2), 2.98–2.90 (m, 2H, NCH_2CH_2), 2.31 (s, 3H, ArCH₃). ^{19}F NMR (282 MHz, CDCl_3): δ –70.93 (s).

22_{minor} (11.6 mg, 20 μmol , 1 equiv) was hydrolyzed by adding 0.01 M NaOH in methanol (2.2 mL, 1.1 equiv). The reaction mixture was stirred for 15 min and then neutralized by adding 0.1 M aq HCl (0.22 mL, 1.1 equiv). The resulting mixture was diluted with brine (3 mL) and extracted with Et_2O (3 \times 3 mL). Organic extracts were combined, dried over Na_2SO_4 , filtered, and evaporated under reduced pressure. The residue was purified by column chromatography (hexane/EtOAc, gradient from 85:15 to 80:20) to yield **4b** (7.3 mg, 20

μmol). A 16:84 enantiomeric ratio was determined by HPLC analysis of the acetate derivative of **4**, using a Chiralpak IA column (hexane/iPrOH 99:1, 1.0 mL/min, $\lambda = 254$ nm, $t_{r_{\text{minor}}} = 12.54$ min, $t_{r_{\text{major}}} = 14.16$ min). A similar procedure was applied to **22**_{major} (8.8 mg, 15 μmol), affording **4a** (4.9 mg, 13.5 μmol) in a 65:35 enantiomeric ratio determined upon subsequent derivatization to the acetate derivative and chiral HPLC analysis. The procedure for derivatization is as follows: enantiomerically enriched samples of **4** (1 mg, 2.8 μmol , 1 equiv) in 0.25 mL of dry DCM were treated with acetyl chloride (1.8 μL , 16.6 μmol , 6 equiv) and Et₃N (0.25 μL , 2.8 μmol , 1.1 equiv) in dry DCM (50 μL) at room temperature under argon. The reaction was stirred for 25 min and quenched by adding saturated aq NaHCO₃ (0.25 mL). To the resulting solution was added DCM and H₂O (0.75 mL each). The layers were separated and the aqueous layer further extracted with DCM (2 \times 1 mL). Organic extracts were combined and filtered through silica, and the solvent was removed under reduced pressure.

Antibacterial Assays. For selective purposes, the antimicrobial activity of the diverse compounds was first tested against five bacterial Gram-positive strains obtained from American Type Culture Collection (ATCC): *S. aureus* ATCC25923 (MSSA), *S. aureus* CIP6538, *S. aureus* CIP106760 (MRSA), *E. faecalis* 29212, and *E. faecalis* ATCC51299 (VRE). For the most promising compounds (i.e., compounds **4**, **5**, and **13**), the antimicrobial activity was further evaluated against eight distinct clinical isolates of *S. aureus*, *E. faecalis*, *S. pneumoniae*, and *S. agalactiae* (group B) that belong to the wide collection of pathogenic Gram-positive strains of the Portuguese National Institute of Health (NIH).

For each compound, the minimum inhibitory concentration (MIC) was determined by the broth microdilution method,⁵⁶ according to the Clinical and Laboratory Standards Institute (CLSI) guidelines.⁵⁷ Before each experiment, frozen stocks of all strains were subcultured three times in appropriate culture medium (CAMHB for *S. aureus* and *E. faecalis* and CAMHB-LHB 3.5% for streptococci) to check strain viability and to avoid any negative growth effect from congelation, and inocula of 1.5×10^8 cfu/mL (the equivalent to 0.5 McFarland) were prepared accordingly. For each microorganism, a 1:20 dilution of the prepared inoculum was used. Twofold serial dilutions of concentrated stock compound solutions (1 mM) were prepared in the required medium into 96-well plates. A control without compounds was also prepared. All cultures were incubated for 16–24 h at 35–37 °C with 5% CO₂. Purity check and colony or viable cell counts of the inoculum suspensions were also evaluated in order to ensure that the final inoculum density closely approximates the intended number. This was obtained by subculturing a diluted aliquot from the growth control well (without compound) immediately after inoculation onto a suitable nonselective agar plate for simultaneous incubation. The MIC was determined as the lowest compound concentration at which no visible growth was observed. The bacterial growth was measured with an absorbance microplate reader (Thermo Scientific Multiskan FC, Loughborough, UK) set to 620 nm.

The MBC was also evaluated. Briefly, after MIC assessment, the bacterial suspension on the wells was homogenized, serial-diluted, triplicate spread on appropriate medium and incubated. The MBC attributed to the compound concentration resulting in a 99.9% reduction in bacterial numbers. All

assays were carried out in triplicate for each tested microorganism.

DPPH Method for Antioxidant Activity. The antioxidant activity of the compounds was tested as previously described.⁵⁸ To evaluate the compounds' antioxidant potential through the free radical scavenging test, the change in optical density of DPPH radicals was monitored. The absorbance was measured at 517 nm against a corresponding blank and the antioxidant activity was calculated using the following equation

$$\text{Scavenging activity (\%)} = \frac{\text{absorbance control} - \text{absorbance sample}}{\text{absorbance control}} \times 100$$

The reference standard used for this procedure was butylated hydroxytoluene (BHT).

A. salina Mortality Bioassay. A test of mortality was performed on *A. salina* brine shrimp, of the compounds **4**–**17**, as previously described.⁵⁹ For this assay, an aquarium air pump (HI-FLOTM Single Type 4000), a thermostat Cabinet Aqua Lytic, and a stereomicroscope (CETI Belgium) were used. The number of dead nauplii was recorded after 24 h and used to calculate the percentage (%) of mortality rate, according to the equation

$$\text{Mortality rate (\%)} = \frac{\text{total}_{\text{nauplii}} - \text{alive}_{\text{nauplii}}}{\text{total}_{\text{nauplii}}}$$

Cell Culture and Cytotoxicity Assessment. The cytotoxicity profile of the compound **13** was characterized in the normal-like human keratinocytes (HaCaT cell line). HaCat cells were routinely cultured in Dulbecco's modified Eagle's medium supplemented with 10% fetal bovine serum, 100 U/mL penicillin, and 0.1 mg/mL streptomycin. Cells were kept at 37 °C, under an atmosphere containing 5% CO₂ in air. Cell viability was evaluated by the MTT assay, using a 24 h incubation protocol, according to a previously published procedure.⁶⁰ Two independent experiments were carried out, each comprising four replicate cultures.

■ ASSOCIATED CONTENT

Supporting Information

The Supporting Information is available free of charge on the ACS Publications website at DOI: 10.1021/acsomega.8b02381.

Computational details, NMR spectra, and HPLC traces (PDF)

SMILES strings of tested compounds (CSV)

■ AUTHOR INFORMATION

Corresponding Author

*E-mail: nuno.rafaelcandeias@tut.fi (N.R.C.)

ORCID

Patricia Rijo: 0000-0001-7992-8343

Nuno R. Candeias: 0000-0003-2414-9064

Author Contributions

T.R. and J.R.V. synthesized the compounds. J.A., E.N., A.S.F., and A.N. performed the biological assays. J.R. isolated and propagated the bacteria clinical isolates. J.P.G., A.N., P.R., A.S.F., and N.R.C. conceived and managed all studies. The manuscript was written through contributions of all authors.

Notes

The authors declare no competing financial interest.

ACKNOWLEDGMENTS

Janne and Aatos Erkkö Foundation, Academy of Finland (Decision 287954) and Fundação para a Ciência e a Tecnologia (UID/DTP/04567/2016) are acknowledged for the financial support. CSC—IT Center for Science Ltd, Finland is acknowledged for the allocation of computational resources.

ABBREVIATIONS

DPPH, 2,2-diphenyl-1-picrylhydrazyl; MBC, minimum bactericidal concentration; MSSA, methicillin-sensitive *Staphylococcus aureus*; QM, ortho-quinone methide

ADDITIONAL NOTES

^aDFT calculations performed at the PBE1PBE/6-31G(d,p) level with the use of the Gaussian 09 package. A complete account of the computational details and the correspondence list of references are provided in the Supporting Information. ^bWiberg indices are electronic parameters related to the electron density between atoms. They can be obtained from a natural population analysis and provide an indication of the bond strength.

REFERENCES

- Laxminarayan, R.; Duse, A.; Watal, C.; Zaidi, A. K. M.; Wertheim, H. F. L.; Sumpradit, N.; Vlieghe, E.; Hara, G. L.; Gould, I. M.; Goossens, H.; Greko, C.; So, A. D.; Bigdeli, M.; Tomson, G.; Woodhouse, W.; Ombaka, E.; Peralta, A. Q.; Qamar, F. N.; Mir, F.; Kariki, S.; Bhatta, Z. A.; Coates, A.; Bergstrom, R.; Wright, G. D.; Brown, E. D.; Cars, O. Antibiotic resistance: the need for global solutions. *Lancet Inf. Dis.* **2013**, *13*, 1057–1098.
- Tacconelli, E. Antimicrobial Use: Risk Driver of Multidrug Resistant Microorganisms in Healthcare Settings. *Curr. Opin. Infect. Dis.* **2009**, *22*, 352–358.
- Zaman, S. B.; Hussain, M. A.; Nye, R.; Mehta, V.; Mamun, K. T.; Hossain, N. A Review on Antibiotic Resistance: Alarm Bells are Ringing. *Cureus* **2017**, *9*, e1403.
- World Health Organization. Antimicrobial Resistance: Global Report on Surveillance 2014. <http://www.who.int/antimicrobial-resistance/publications/surveillance-report/en/> (accessed 28 August 2018).
- World Health Organization. Tuberculosis Factsheet. <http://www.who.int/mediacentre/factsheets/fs104/en/> (accessed 28 August 2018).
- Tackling Drug-Resistant Infections Globally: Final Report and Recommendations. *Review on Antimicrobial Resistance*, 2016.
- World Health Organization. The burden of health care-associated infection worldwide. http://www.who.int/gpsc/country_work/burden_hcai/en/ (accessed 28 August 2018).
- World Health Organization. Report on the Burden of Endemic Health Care-Associated Infection Worldwide. http://www.who.int/gpsc/country_work/burden_hcai/en/ (accessed 28 August 2018).
- Centers for Disease Control and Prevention. Types of healthcare-associated infections. Healthcare-associated infections (HAIs). www.cdc.gov/HAI/infectionTypes.html (accessed 28 August 2018).
- Allegranzi, B.; Nejad, S. B.; Combes, C.; Graafmans, W.; Attar, H.; Donaldson, L.; Pittet, D. Burden of endemic health-care-associated infection in developing countries: systematic review and meta-analysis. *The Lancet* **2011**, *377*, 228–241.
- Bereket, W.; Hemalatha, K.; Getenet, B.; Wondwossen, T.; Solomon, A.; Zeynudin, A.; Kannan, S. Update on bacterial nosocomial infections. *Eur. Rev. Med. Pharmacol. Sci.* **2012**, *16*, 1039–1044.
- Cooper, M. A.; Shlaes, D. Fix the Antibiotics Pipeline. *Nature* **2011**, *472*, 32.
- Fair, R. J.; Tor, Y. Antibiotics and Bacterial Resistance in the 21st Century. *Perspect. Medicin. Chem.* **2014**, *6*, 25–64.
- Butler, M. S.; Blaskovich, M. A.; Cooper, M. A. Antibiotics in the Clinical Pipeline at the End of 2015. *J. Antibiot.* **2017**, *70*, 3–24.
- Elo, H.; Kuure, M.; Peltari, E. Correlation of the Antimicrobial Activity of Salicylaldehydes with Broadening of the NMR Signal of the Hydroxyl Proton. Possible Involvement of Proton Exchange Processes in the Antimicrobial Activity. *Eur. J. Med. Chem.* **2015**, *92*, 750–753.
- Peltari, E.; Karhumäki, E.; Langshaw, J.; Peräkylä, H.; Elo, H. Antimicrobial Properties of Substituted Salicylaldehydes and Related Compounds. *Z. Naturforsch. C Bio. Sci.* **2007**, *62*, 487–497.
- Peltari, E.; Lehtinen, M.; Elo, H. Substituted Salicylaldehydes as Potential Antimicrobial Drugs: Minimal Inhibitory and Microbicidal Concentrations. *Z. Naturforsch. C Bio. Sci.* **2011**, *66*, 571–580.
- Shi, L.; Ge, H.-M.; Tan, S.-H.; Li, H.-Q.; Song, Y.-C.; Zhu, H.-L.; Tan, R.-X. Synthesis and Antimicrobial Activities of Schiff Bases Derived from 5-Chloro-salicylaldehyde. *Eur. J. Med. Chem.* **2007**, *42*, 558–564.
- Neto, Í.; Andrade, J.; Fernandes, A. S.; Pinto Reis, C.; Salunke, J. K.; Priimagi, A.; Candeias, N. R.; Rijo, P. Multicomponent Petasis-Boronon Mannich Preparation of Alkylaminophenols and Antimicrobial Activity Studies. *ChemMedChem* **2016**, *11*, 2015–2023.
- Bael, J. B. Observations on Screening-Based Research and Some Concerning Trends in the Literature. *Future Med. Chem.* **2010**, *2*, 1529–1546.
- Bael, J. B.; Holloway, G. A. New Substructure Filters for Removal of Pan Assay Interference Compounds (PAINS) from Screening Libraries and for Their Exclusion in Bioassays. *J. Med. Chem.* **2010**, *53*, 2719–2740.
- Roman, G. Mannich Bases in Medicinal Chemistry and Drug Design. *Eur. J. Med. Chem.* **2015**, *89*, 743–816.
- Biersack, B.; Ahmed, K.; Padhye, S.; Schobert, R. Recent Developments Concerning the Application of the Mannich Reaction for Drug Design. *Expert Opin. Drug Discov.* **2018**, *13*, 39–49.
- Roman, G.; Năstăsă, V.; Bostănar, A.-C.; Mareș, M. Antibacterial Activity of Mannich Bases Derived from 2-Naphthols, Aromatic Aldehydes and Secondary Aliphatic Amines. *Bioorg. Med. Chem. Lett.* **2016**, *26*, 2498–2502.
- Shen, A. Y.; Hwang, M. H.; Roffler, S.; Chen, C. F. Cytotoxicity and Antimicrobial Activity of Some Naphthol Derivatives. *Arch. Pharm.* **1995**, *328*, 197–201.
- Junker, L. M.; Clardy, J. High-Throughput Screens for Small-Molecule Inhibitors of *Pseudomonas aeruginosa* Biofilm Development. *Antimicrob. Agents Chemother.* **2007**, *51*, 3582–3590.
- Moy, T. I.; Conery, A. L.; Larkins-Ford, J.; Wu, G.; Mazitschek, R.; Casadei, G.; Lewis, K.; Carpenter, A. E.; Ausubel, F. M. High-Throughput Screen for Novel Antimicrobials Using a Whole Animal Infection Model. *ACS Chem. Biol.* **2009**, *4*, 527–533.
- Herrera, R. P.; Marqués-López, E. *Multicomponent Reactions: Concepts and Applications for Design and Synthesis*. John Wiley & Sons, Inc.: New Jersey, 2015.
- Zhu, J.; Wang, Q.; Wang, M.-X. *Multicomponent Reactions in Organic Synthesis*. Wiley-VCH Verlag GmbH & Co. KGaA: Weinheim, 2014.
- Guerrera, C. A.; Ryder, T. R. The Petasis-Boronon-Mannich Multicomponent Reaction. In *Boron Reagents in Synthesis*; American Chemical Society, 2016; Vol. 1236, pp 275–311.
- Candeias, N. R.; Montalbano, E.; Cal, P. M. S. D.; Gois, P. M. P. Boronic Acids and Esters in the Petasis-Boronon Mannich Multicomponent Reaction. *Chem. Rev.* **2010**, *110*, 6169–6193.
- Suleyman, G.; Alangaden, G.; Bardossy, A. C. The Role of Environmental Contamination in the Transmission of Nosocomial Pathogens and Healthcare-Associated Infections. *Curr. Infect. Dis. Rep.* **2018**, *20*, 12.

- (33) Guzman Prieto, A. M.; van Schaik, W.; Rogers, M. R.; Coque, T. M.; Baquero, F.; Corander, J.; Willems, R. J. Global Emergence and Dissemination of Enterococci as Nosocomial Pathogens: Attack of the Clones? *Front. Microbiol.* **2016**, *7*, 788.
- (34) Higuita, N. I. A.; Huycke, M. M. Enterococcal Disease, Epidemiology, and Implications for Treatment. In *Enterococci from Commensals to Leading Causes of Drug Resistant Infection*; Gilmore, M. S., Clewell, D. B., Ike, Y., Shankar, N., Eds.; Boston: Massachusetts Eye and Ear Infirmary: Boston, 2014.
- (35) Huh, K.; Chung, D. R. Changing epidemiology of community-associated methicillin-resistant *Staphylococcus aureus* in the Asia-Pacific region. *Expert Rev. Anti Infect. Ther.* **2016**, *14*, 1007–1022.
- (36) Rodríguez-Noriega, E.; Seas, C.; Guzmán-Blanco, M.; Mejía, C.; Alvarez, C.; Bavestrello, L.; Zurita, J.; Labarca, J.; Luna, C. M.; Salles, M. J. C.; Gotuzzo, E. Evolution of methicillin-resistant *Staphylococcus aureus* clones in Latin America. *Int. J. Infect. Dis.* **2010**, *14*, e560–e566.
- (37) Alanís-Garza, B. A.; González-González, G. M.; Salazar-Aranda, R.; Waksman de Torres, N.; Rivas-Galindo, V. M. Screening of Antifungal Activity of Plants from the Northeast of Mexico. *J. Ethnopharmacol.* **2007**, *114*, 468–471.
- (38) Daglia, M. Polyphenols as Antimicrobial Agents. *Curr. Opin. Biotechnol.* **2012**, *23*, 174–181.
- (39) Van De Water, R. W.; Pettus, T. R. R. *o*-Quinone Methides: Intermediates Underdeveloped and Underutilized in Organic Synthesis. *Tetrahedron* **2002**, *58*, 5367–5405.
- (40) Bai, W.-J.; David, J. G.; Feng, Z.-G.; Weaver, M. G.; Wu, K.-L.; Pettus, T. R. R. The Domestication of *ortho*-Quinone Methides. *Acc. Chem. Res.* **2014**, *47*, 3655–3664.
- (41) Zhou, Q.; Rokita, S. E. A General Strategy for Target-Promoted Alkylation in Biological Systems. *Proc. Natl. Acad. Sci. U.S.A.* **2003**, *100*, 15452–15457.
- (42) Weinert, E. E.; Dondi, R.; Colloredo-Melz, S.; Frankenfield, K. N.; Mitchell, C. H.; Preccero, M.; Rokita, S. E. Substituents on Quinone Methides Strongly Modulate Formation and Stability of Their Nucleophilic Adducts. *J. Am. Chem. Soc.* **2006**, *128*, 11940–11947.
- (43) Valentin, C. D.; Preccero, M.; Zanaletti, R.; Sarzi-Amadè, M. *o*-Quinone Methide as Alkylating Agent of Nitrogen, Oxygen, and Sulfur Nucleophiles. The Role of H-Bonding and Solvent Effects on the Reactivity through a DFT Computational Study. *J. Am. Chem. Soc.* **2001**, *123*, 8366–8377.
- (44) Chiang, Y.; Kresge, A. J.; Zhu, Y. Flash Photolytic Generation of *o*-Quinone α -Phenylmethide and *o*-Quinone α -(*p*-Anisyl)methide in Aqueous Solution and Investigation of Their Reactions in that Medium. Saturation of Acid-Catalyzed Hydration. *J. Am. Chem. Soc.* **2002**, *124*, 717–722.
- (45) Modica, E.; Zanaletti, R.; Preccero, M.; Mella, M. Alkylation of Amino Acids and Glutathione in Water by *o*-Quinone Methide. Reactivity and Selectivity. *J. Org. Chem.* **2001**, *66*, 41–52.
- (46) Parr, R. G.; Yang, W. *Density Functional Theory of Atoms and Molecules*; Oxford University Press: New York, 1989.
- (47) Preccero, M.; Di Valentin, C.; Sarzi-Amadè, M.; study, D. F. T. Modeling H-Bonding and Solvent Effects in the Alkylation of Pyrimidine Bases by a Prototype Quinone Methide: a DFT Study. *J. Am. Chem. Soc.* **2003**, *125*, 3544–3553.
- (48) Preccero, M.; Doria, F. Modeling Properties and Reactivity of Quinone Methides by DFT Calculations. In *Quinone Methides*; Wiley, 2009; pp 33–67.
- (49) Weinert, E. E.; Frankenfield, K. N.; Rokita, S. E. Time-dependent evolution of adducts formed between deoxynucleosides and a model quinone methide. *Chem. Res. Toxicol.* **2005**, *18*, 1364–1370.
- (50) Huang, C.; Rokita, S. E. DNA alkylation promoted by an electron-rich quinone methide intermediate. *Front. Chem. Sci. Eng.* **2015**, *10*, 213–221.
- (51) Thompson, D. C.; Thompson, J. A.; Sugumaran, M.; Moldéus, P. Biological and Toxicological Consequences of Quinone Methide Formation. *Chem-Biol. Interact.* **1992**, *86*, 129–162.
- (52) Wang, P.; Song, Y.; Zhang, L.; He, H.; Zhou, X. Quinone Methide Derivatives: Important Intermediates to DNA Alkylating and DNA Cross-linking Actions. *Curr. Med. Chem.* **2005**, *12*, 2893–2913.
- (53) Bolton, J. Quinone Methide Bioactivation Pathway: Contribution to Toxicity and/or Cytoprotection? *Curr. Org. Chem.* **2014**, *18*, 61–69.
- (54) Monks, T.; Jones, D. The Metabolism and Toxicity of Quinones, Quinonimines, Quinone Methides, and Quinone-Thioethers. *Curr. Drug Metab.* **2002**, *3*, 425–438.
- (55) Ghosh, P.; Ganguly, B.; Perl, E.; Das, S. A synthesis of biaryl ketones via the C-S bond cleavage of thiol ester by a Cu/Ag salt. *Tetrahedron Lett.* **2017**, *58*, 2751–2756.
- (56) Wiegand, I.; Hilpert, K.; Hancock, R. E. W. Agar and broth dilution methods to determine the minimal inhibitory concentration (MIC) of antimicrobial substances. *Nat. Protoc.* **2008**, *3*, 163–175.
- (57) CLSI. *Methods for Dilution Antimicrobial Susceptibility Tests for Bacteria That Grow Aerobically; Approved Standard*, 8th ed.; Clinical and Laboratory Standards Institute: Wayne, Pennsylvania, 2009.
- (58) Rijo, P.; Falé, P. L.; Serralheiro, M. L.; Simões, M. F.; Gomes, A.; Reis, C. Optimization of medicinal plant extraction methods and their encapsulation through extrusion technology. *Measurement* **2014**, *58*, 249–255.
- (59) Hamidi, M. R.; Jovanova, B.; Panovska, T. K. Toxicological evaluation of the plant products using Brine Shrimp (*Artemia salina* L.) model. *Maced. Pharm. Bull.* **2014**, *60*, 9–18.
- (60) Wagemaker, T. A. L.; Rijo, P.; Rodrigues, L. M.; Maia Campos, P. M. B. G.; Fernandes, A. S.; Rosado, C. Integrated approach in the assessment of skin compatibility of cosmetic formulations with green coffee oil. *Int. J. Cosmet. Sci.* **2015**, *37*, 506–510.



1 NJC

5 PAPER

Naphthoylhydrazones: coordination to metal ions and biological screening†

Cite this: DOI: 10.1039/c9nj01816f

Nádia Ribeiro,^a Adelino M. Galvão,^a Clara S. B. Gomes,^{b,ab} Helena Ramos,^c Rute Pinheiro,^c Lucília Saraiva,^c Epole Ntungwe,^d Vera Isca,^{b,da} Patrícia Rijo,^{da} Isabel Cavaco,^{b,e} Filipa Ramilo-Gomes,^{fg} Rita C. Guedes,^{b,g} João Costa Pessoa^{b,h} and Isabel Correia^{b,h*}

We report the synthesis of 3-hydroxy-2-naphthoylhydrazones containing pyrrole (HL¹), furane (HL²) and thiophene (HL³) moieties and their V(v)O-, Cu(i)- and Zn(ii)-complexes. All compounds are characterized by the usual analytical techniques and coordination of the ligands to the metal ions is discussed based on spectroscopic data (FTIR, UV-vis, EPR and NMR) as well as CAMB3LYP DFT/TDDFT calculations, indicating the formation of neutral ML₂ type complexes. The photophysical properties of ligands and complexes are disclosed. The binding to Bovine Serum Albumin (BSA) is evaluated in detail using several spectroscopic tools. Circular dichroism shows that the compounds, and particularly the ligand precursors, stabilize BSA, increasing its α -helical content. Fluorescence studies indicate the formation of 1:1 protein-compound adducts, which is corroborated by molecular docking studies that show the interaction between Trp 213 of BSA and the naphthalene rings. The general toxicity is evaluated using the *Artemia salina* lethality assay, with all compounds showing general toxicity towards the brine shrimp model. The cytotoxicity on human cancer cells (H1299, MCF7, and HCT116) is assessed for all compounds and the half-maximal inhibitory concentration (IC₅₀) values are determined to be in the range from 0.57 to 27.35 μ M. Compounds containing L¹ (pyrrole derivative) are the most cytotoxic, with the vanadium and zinc complexes performing better than the copper ones, and some of them depicting IC₅₀ values lower than 1.1 μ M. However, selectivity needs improvement as the compounds show toxicity towards *Artemia salina* and normal fibroblasts.

Received 11th April 2019,
Accepted 5th August 2019
DOI: 10.1039/c9nj01816f

see RSC.li/hcj

1 Introduction

N-Acyl or aroylhydrazones (NAH) are very useful and promising scaffolds in drug design. Their versatility arises from their modular synthesis, as they can be produced by condensation

between aldehydes or ketones with hydrazides.¹ NAH have attracted attention due to their coordination to transition metal ions and broad range of biological activity, which includes antioxidant, anti-inflammatory, antibacterial and antitumor properties.^{2–4} Many NAH have been approved as drugs and are used as therapeutics in various countries, such as nitrofurazone, a topical antibacterial agent, and nitrofurantoin, an oral antibacterial agent.⁵

Tridentate hydrazones containing phenolate groups in the coordination position form very stable metal complexes, in which the ligand binds as a (6+5)-membered chelate through the O_{phenolate}, the N_{imine} and the O_{carbonyl} atoms, with the hydrazine in either the keto or the enol form.^{2,6} In compounds containing phenolate groups on both sides of the hydrazine moiety (OH-ph-CO-NH-N=C-ph-OH) coordination occurs through the phenolate closer to the imine bond, leaving the other phenolate unbound and protonated. This has been shown for Cu(II)⁷ and V(IV).⁸

3-Hydroxy-2-naphthoylhydrazones (HNH) are molecules that contain a hydrazone and a naphthyl hydroxido group in the *ortho* position. Only a few metal complexes have been

^a Centro de Química Estrutural, Instituto Superior Técnico, Universidade de Lisboa, Portugal

^b LAQV-REQUIMTE, Departamento de Química, Faculdade de Ciências e Tecnologia, Universidade Nova de Lisboa, 2829-516, Caparica, Portugal

^c LAQV-REQUIMTE, Laboratório de Microbiologia, Departamento de Ciências Biológicas, Faculdade de Farmácia, Universidade do Porto, Porto, Portugal

^d CBOS - Research Center for Biosciences & Health Technologies, U. Lusófona de Humanidades e Tecnologias, Lisboa, Portugal

^e Instituto de Investigação do Medicamento (iMed.U.Lisboa), Faculdade de Farmácia, Universidade de Lisboa, Lisboa, Portugal

^f Departamento de Química Bioquímica e Farmácia, Universidade do Algarve, Campus de Gambeluz, 8005-139 Faro, Portugal

^g Instituto de Investigação do Medicamento (iMed.U.Lisboa), Faculdade de Farmácia, Universidade de Lisboa, Lisboa, Portugal

^h Electronic supplementary information (ESI) available. CCDC 1904521. For ESI and crystallographic data in CIF or other electronic format see DOI: 10.1039/c9nj01816f

1 reported, showing the ligand bound through the carbonyl O-atom in the enol form and the azomethine N-atom, while the phenolic O-atom remains protonated and unbound. Zaly *et al.* have reported on metal complexes of several naphthoyl hydrazone ligands derived from acetylpyridine,⁹ acetone¹⁰ and *o*-hydroxyacetophenone.^{11,12} In most cases the assignment of the ligand binding (bi, tri or tetradentate) and the structural formulae of the complexes were based on spectroscopic features (mainly FTIR).^{9,12} For the acetone derived ligand they determined metal ion stability constants by pH-potentiometry, with the following order: $(\log K) U(v)O_2 > Cu(\pi) > Zn(\pi) > Ni(\pi) > Cd(\pi) > Co(\pi)$. Some of these compounds showed antimicrobial activity against *Bacillus subtilis* and *Pseudomonas aeruginosa*.¹⁰ $Cu(\pi)$, $Ni(\pi)$ and $Zn(\pi)$ complexes containing HNH derived from *o*-hydroxyacetophenone¹¹ had their antimicrobial properties evaluated in a wide spectrum of bacterial and fungal strains. All metal complexes showed higher antibacterial activity than the ligand, with one of the Cu-complexes being the most active against all strains. $Co(\pi)$, $Gd(\pi)$, $Hg(\pi)$ and $U(v)O_2$ were also evaluated against fungi and bacteria, and all metal complexes exhibited greater antifungal activity against *Aspergillus* sp. when compared to the standard drug Miconazole and the free ligand. The antibacterial studies showed that the ligand and its complexes show moderate activity against *E. coli* and *Clostridium* sp. when compared to the standard drug Ampicillin.¹²

In 2013¹³ a series of $Cu(\pi)$, $Co(\pi)$ and $Ni(\pi)$ complexes of naphthoyl hydrazone derived from acetone were synthesized, showing structural diversity in the solid state and solution, supported by single-crystal X-ray diffraction (SC-XRD). While cobalt and nickel complexes showed distorted octahedral monomeric structures, $cis(L)[Co(HNH)_2(L)_2]$ ($L =$ pyridine) and $trans(L)[Ni(HNH)_2(L)_2]$ ($L =$ THF), with the bidentate ligands forming five-membered chelate rings, copper hydrazone complexes formed polymeric 1D-chains. Organotin(π) naphthoyl hydrazone complexes have also

1 been prepared and their molecular structures, determined by SC-XRD, showed an interesting variety of structures.¹⁴ The ligand binds tin mono- or tridentate, keeping the naphtholate oxygen unbound. The molecular structure of a $V(v)$ complex of 1-hydroxy-*N*-(3-hydroxybutyl)naphthalene-2-carbohydrazone was also reported showing the ligand tridentate through (6+5)-membered chelate rings with the naphtholate oxygen uncoordinated.¹⁵

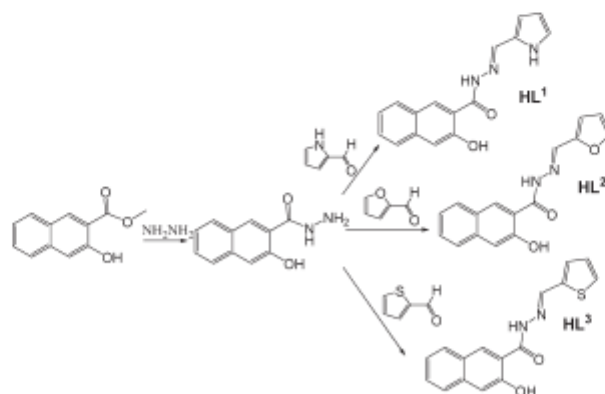
Since all these studies show an interesting coordinating behaviour for the naphthoyl hydrazone complexes, we were inspired to develop a series of ligands containing HNH and different heterocyclic rings, since it has been reported that the presence of a heterocyclic ring is key to improving the pharmacological properties of NAH.¹⁶ Metal complexes of $V(\pi)O$, $Cu(\pi)$ and $Zn(\pi)$ were prepared and characterized. The choice of the metal ions was based on their recognized therapeutic potential.^{17–21} Moreover, zinc complexes are particularly relevant since *N*-acylhydrazone zinc complexes have shown fluorescent properties.^{22,23} For instance F. Borgone *et al.*²⁴ reported on Zn-complexes with tridentate pyridinoyl hydrazone ligands and the pyridinoyl nitrogen atom in the *ortho*, *meta*, or *para* positions, which yielded complexes with diverse nuclearities and interesting photophysical properties.

2. Results and discussion

2.1. Synthesis and characterization

Three naphthoyl hydrazone Schiff base molecules were obtained from the condensation of 3-hydroxy-2-naphthoic hydrazide with heterocyclic aldehydes: pyrrole-2-carbaldehyde, 2-furaldehyde and thiophene-2-carbaldehyde (Scheme 1). The compounds were characterized by analytical techniques such as elemental analysis and mass spectrometry and the experimental values are in good agreement with the expected ones (see Experimental for details).

Additionally, several spectroscopic signatures also confirm the formation of the ligand precursors, namely, the presence of



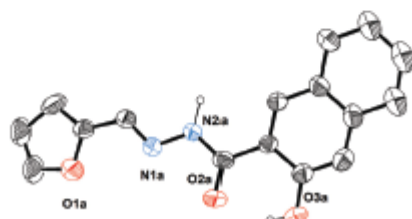
Scheme 1 Synthetic pathways for ligand precursor HL¹–HL³.

1 a singlet signal in the ^1H NMR spectra corresponding to the
 imine proton at 8.28, 7.88 and 8.67 ppm (for HL^1 , HL^2 and HL^3 ,
 respectively). Also, the FTIR spectra show distinctive bands,
 which can be assigned to the relevant functional groups. The
 5 carbonyl stretching bands appear around 1640 cm^{-1} while the
 $\nu(\text{C}=\text{N})$ stretching appears at ca. 1550 cm^{-1} ; the stretching
 corresponding to the $\nu(\text{C}-\text{O})_{\text{enph}}$ band appears around 1230
 cm^{-1} while the $\nu(\text{OH})$ band appears at 3440 cm^{-1} . The presence
 of this $\nu(\text{OH})$ band together with the weak broad bands in the
 10 1900 cm^{-1} region suggests intramolecular hydrogen bonding.⁹
 Another evidence for this H-bond is the ^1H NMR signal due to
 the proton of $(\text{OH})_{\text{enph}}$ appearing downfield at 11.48, 11.9 and
 11.25 ppm, for HL^1 , HL^2 and HL^3 , respectively. This intra-
 molecular hydrogen bond stabilizes the structure where the
 15 carbonyl faces the hydroxyl group instead of the nitrogen. For
 HL^1 it is also possible to assign a sharp band at 3410 cm^{-1} to
 the $\nu(\text{NH})$ of the pyrrole ring.

Crystals suitable for X-ray diffraction studies were obtained
 for HL^2 and the molecular structure is included in Fig. 1.
 20 Further details are given in the ESI† (Fig. S1, S2 and Tables
 S1, S2). The *E* isomer is proposed for the imine double bond
 based on this SC-XRD structure, which is similar to that
 previously reported for HL^3 .²⁵ Hydrogen bonding takes place
 between the O atoms (O_{enph} and $\text{O}_{\text{carbonyl}}$).

25 Reactions of these ligand precursors with $\text{V}(\text{IV})$, $\text{Cu}(\text{II})$ and
 $\text{Zn}(\text{II})$ salts yielded nine new complexes, which were fully
 characterized by elemental and spectroscopic techniques. The
 yields were moderate to excellent and both the elemental
 analysis and the ESI-MS spectra support the formulation ML_2 ,
 30 with the ligands behaving as monoanionic bidentate chelates,
 coordinated through the imine nitrogen and the deprotonated
 enolate oxygen of the hydrazone moiety. A general schematic
 formulation is presented in Fig. 2 for most complexes. In some
 cases different binding modes may occur, e.g., by the deprotonated
 35 naphtholate and hydrazone (see the NMR section).

2.1.1. FTIR. Most of the formulations of naphthoyl hydrazone
 complexes reported in the literature have been
 assigned based on FTIR signatures. Ligand precursors HL^1 –
 HL^3 are involved in keto-enol tautomerism; however, in the
 40 solid state they were found in the keto form as shown by the
 presence of the carbonyl band at ca. 1640 cm^{-1} (Table 1 and



45 Fig. 1 ORTEP plot of compound HL^2 , using 30% probability level ellip-
 soids. Except the NH and OH, all the hydrogen atoms were omitted for
 50 clarity. Selected distances (Å): C6a–O2a: 1.248(3); N1a–N2a: 1.384(3);
 C8a–O3a: 1.353(4); N2a–C6a: 1.335(3).

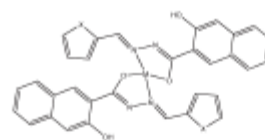


Fig. 2 General molecular formula for the complexes in this work where
 M = VO for 1, 2 and 3, M = Cu for 4, 5 and 6, and M = Zn for 7, 8 and 9; and
 where X = NH for 1, 4 and 7, X = O for 2, 5 and 8, and X = S for 3, 6 and 9.

Fig. S4, ESI†). Shifts of characteristic FTIR bands of the free
 ligand upon complexation indicate ligand coordination in a
 monoanionic bidentate fashion. The $\nu(\text{V}=\text{O})$ appears at very
 low wavenumbers suggesting a polymeric form for the V-
 complexes in the solid state. This has been previously observed
 15 and indicates $\text{V}=\text{O} \cdots \text{V}=\text{O}$ interactions, since binding of an
 O_{oxido} to a vanadium atom, *trans* to its O-oxido atom, weakens
 the bond and lowers the $\text{V}=\text{O}$ stretching frequency.^{26–30} DFT
 calculations are compatible with this analysis since the $\text{V}=\text{O}$
 20 stretching frequency is the only one overestimated by around
 120 cm^{-1} , Fig. S3 (ESI†).

For all complexes it was possible to assign M–O and M–N
 bands, which were nonexistent in the corresponding ligands'
 spectra, confirming the formation of complexes. The band for
 the stretching vibration of the hydrazone N–H, appearing at ca.
 25 3250 cm^{-1} in the ligands, is not present in the spectra of the
 complexes, as well as the carbonyl band, suggesting enolization
 and consequent binding to the metal ions. Another evidence for
 this coordination mode is the presence of a second band for the
 enolate C–O stretching vibration and a second imine (C=N)
 30 band at higher wavenumbers, making it somehow difficult to
 distinguish from the original carbonyl bands.

Additionally, the band corresponding to the C–O stretching
 vibration of the naphthoyl hydroxyl group, which appears as a
 single sharp band at ca. 1227 cm^{-1} , is split into two distinct
 35 bands in the FTIR spectra of complexes, most likely reflecting
 different chemical environments for each ligand molecule
 upon coordination to the metal center.

All complexes derived from HL^2 present spectral signatures
 identical to the ligand itself revealing that probably in the solid
 40 state a large macrostructure of polymeric composition is
 formed leaving only the terminal bonds of the ligand free to
 vibrate.

2.1.2. Photophysical properties. The UV-vis absorption
 spectra were measured in DMSO and are included in Fig. S5
 (ESI†). All ligands and complexes show strong bands in the UV
 due to transitions within the imine and carbonyl moieties.
 While for HL^1 and HL^3 complexation resulted in red shifts of
 the bands centered at ca. 330 nm, for HL^2 only the copper
 50 complex shows a large red shift. Bands assigned to $\pi \rightarrow \pi^*$
 transitions in the naphthalene aromatic ring (at ca. 270 nm) do
 not suffer significant changes when compared to the corre-
 sponding ligands, as this part of the molecule is not directly
 involved in the coordination to the metal ion.

For the Cu-complexes bands at 670 and 712 nm (for 4 and 5,
 55 respectively) due to d–d transitions are clearly distinguished in

Table 1 Characteristic FTIR bands (cm^{-1}) and assignment for ligands and complexes presented in this work

| | $\nu(\text{NH})_{\text{DMP}}$ | $\nu(\text{OH})_{\text{NapH}}$ | $\nu(\text{C-O})_{\text{NapH}}$ | $\nu(\text{C-O})_{\text{DMF}}$ | $\nu(\text{C=O})$ | $\nu(\text{C=N})$ | $\nu(\text{C=N})^a$ | $\nu(\text{V=O})$ | $\nu(\text{M-O})$ | $\nu(\text{M-N})$ |
|--------------------------------------|-------------------------------|--------------------------------|---------------------------------|--------------------------------|-------------------|-------------------|---------------------|-------------------|-------------------|-------------------|
| HL ¹ | 3409 | — | 1227 | — | 1646 | 1558 | — | — | — | — |
| HL ² | — | 3440 | 1227 | — | 1637 | 1547 | — | — | — | — |
| HL ³ | — | 3440 | 1228 | — | 1638 | 1559 | — | — | — | — |
| VO(L ¹) ₂ (1) | 3231 | 3383 | 1241/1216 | 1147 | — | 1543 | 1578 | 897 | 554 | 404 |
| VO(L ²) ₂ (2) | — | 3433 | 1242/1219 | 1296 | — | 1532 | 1574 | 906 | 555 | 401 |
| VO(L ³) ₂ (3) | — | 3440 | 1228 | 1138 | — | 1559 | 1638 | 946 | 536 | 402 |
| Cu(L ¹) ₂ (4) | 3167 | — | 1240/1219 | 1150 | — | 1554 | 1578 | — | 556 | 405 |
| Cu(L ²) ₂ (5) | — | 3444 | 1243/1221 | 1311 | — | 1537 | 1575 | — | 559 | 406 |
| Cu(L ³) ₂ (6) | — | 3440 | 1228 | 1137 | — | 1559 | 1638 | — | 534 | 401 |
| Zn(L ¹) ₂ (7) | 3187 | 3380 | 1231/1223 | 1150 | — | 1546 | 1576 | — | 547 | 428 |
| Zn(L ²) ₂ (8) | — | 3416 | 1243/1223 | 1310 | — | 1520 | 1577 | — | 554 | 409 |
| Zn(L ³) ₂ (9) | — | 3440 | 1228 | 1138 | — | 1559 | 1638 | — | 536 | 411 |

^a New C=N bond formed after enolization of the ligand and coordination to the metal ion.

the visible region, while for 6 and the V-complexes no such bands could be clearly identified, due to their low intensity and to the overlap with the long tail of the strong LMCT bands.

Fluorescence emission spectra were also measured in DMSO and are depicted in Fig. 3. Compound HL³ and its metal complexes do not show fluorescence emission due to the heavy atom effect imposed by the sulphur atom of the thiophene heterocycle. Also, 5 does not present luminescent properties. All other ligand precursors and complexes show emission centered at ca. 520–540 nm, with the following intensity order: Zn > Cu > L > VO.

2.1.3. EPR characterization. The V(ν)O and Cu(π)-complexes are paramagnetic and, thus, their EPR spectra were measured in DMF at ca. 100 K. Fig. 4 depicts the recorded spectra and the spin Hamiltonian parameters, obtained by simulation,³¹ are included in Table 2. All spectra are well resolved and show axial symmetry. For all Cu-complexes $g_x > g_y > g_z > 2.0$, indicating the $d_{x^2-y^2}$ orbital as the ground state and a square based geometry. The values obtained for the ratio g_x/g_z suggest the presence of tetrahedral distortions for 5 and 6.³² For complex 4 slightly different spin Hamiltonian parameters were obtained which suggest a different coordination mode in solution. Coordination of one or two DMF molecules, forming penta- or hexa-coordinated structures, might explain the

differences found for complex 4;³³ however, we cannot unambiguously assign a coordination mode based solely on the spectroscopic data.

The spectra of V(ν)O-complexes show the presence of two species, and these are particularly evident in the spectrum of 1, for which we were able to simulate hyperfine coupling parameters for both species. Visual inspection indicates that for all V-complexes the two coexisting species should correspond to the same type of coordination isomer. Considering the additivity relationship,³⁴ the $|A_z^{\text{DMF}}|$ for a binding mode involving the hydrazine moiety (N_{im} and C-O⁻) of both molecules in the equatorial plane has a value of $159 \times 10^{-4} \text{ cm}^{-1}$,³⁵⁻³⁷ which fits well the major species of complex 3 and the "inner" species of 1 and 2. For the "outer" species, which is the most relevant for 2, and has $|A_z|$ ca. $165 \times 10^{-4} \text{ cm}^{-1}$, the binding of one ligand in equatorial/equatorial and the other in equatorial/axial and one DMF molecule completing the equatorial plane ($2 \times \text{N}_{\text{im}}$, $1 \times \text{C-O}^-$ and $1 \times \text{DMF}$) yields an $|A_z^{\text{DMF}}| = 168 \times 10^{-4} \text{ cm}^{-1}$, and therefore this is the binding mode proposed to the other species in solution.

2.1.4. NMR characterization. 1D and 2D NMR were used to characterize the ligands and the diamagnetic Zn-complexes (see Fig. S6–S11, ESI†). The assignment of the H and C-atoms for HL¹–HL³ and its Zn-complexes is included in Table S3

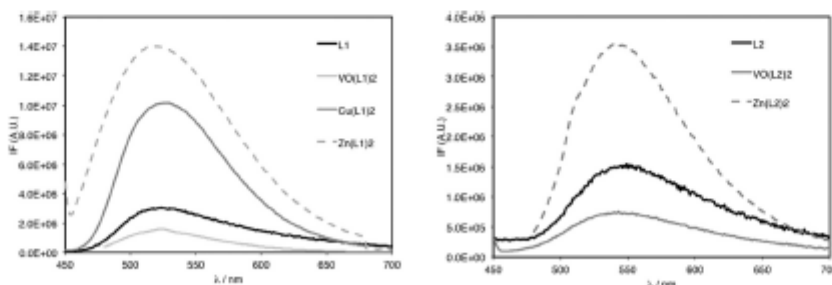


Fig. 3 Fluorescence emission spectra measured for the ligand precursors and complexes. Wavelengths used for the measurement of emission spectra: HL¹, 390 nm; VO(L¹)₂, 453 nm; Cu(L¹)₂, 435 nm; Zn(L¹)₂, 445 nm; HL², 358 nm; VO(L²)₂, 393 nm and Zn(L²)₂, 442 nm. The concentrations used were ca. 10–20 μM .

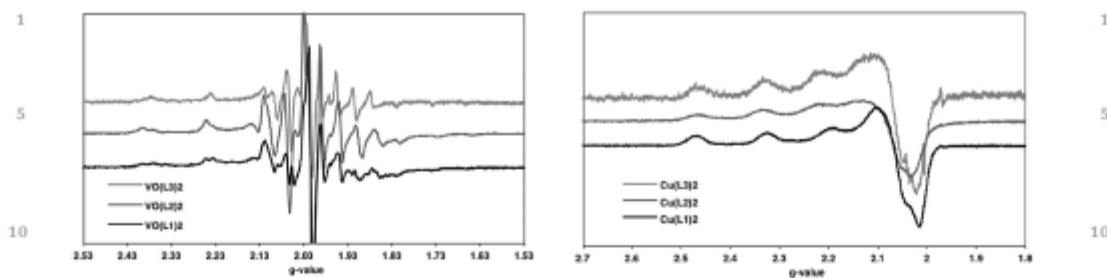


Fig. 4 First derivative X-band EPR spectra of the V^{IV} and Cu^I complexes measured at ca. 100 K in DMF. Concentration was ca. 3 mM.

Table 2 Spin Hamiltonian parameters obtained by simulation of the experimental spectra, for the $V(n)O$ and $Cu(n)$ -complexes in DMF

| Compound | g_{xy} | g_z | $ A_{xy} \times 10^4 \text{ cm}^{-1}$ | $ A_z \times 10^4 \text{ cm}^{-1}$ | g_z/A_z |
|-----------------|----------|-------|--|-------------------------------------|-----------|
| $VO(L^1)_2$ (1) | 1.980 | 1.948 | 53.8 | 165.2 | |
| | 1.980 | 1.942 | 60.1 | 161.4 | |
| $VO(L^2)_2$ (2) | 1.981 | 1.945 | 59.1 | 165.1 | |
| $VO(L^3)_2$ (3) | 1.982 | 1.952 | 54.8 | 159.1 | |
| $Cu(L^1)_2$ (4) | 2.055 | 2.256 | 18.7 | 172.6 | 131 |
| $Cu(L^2)_2$ (5) | 2.076 | 2.272 | 36.0 | 154.8 | 147 |
| $Cu(L^3)_2$ (6) | 2.062 | 2.268 | 30.9 | 156.5 | 145 |

(ESI†). The integration of the 1H NMR spectrum 7 in $DMSO-d_6$ reveals the presence of 12 protons (see Fig. 5A), consistent with the deprotonated form of HL^1 (the presence of two L^1 molecules in the Zn-complex duplicates all integrals but the ratio is maintained). The aromatic protons appear in the range 6.39 to 8.48 ppm, while the imine proton resonates at 8.70 ppm. It is possible to observe two signals downfield ($\delta > 12$ ppm), arising from one OH and one NH. Correlations from the HSQC experiment were used to assign proton signals to the corresponding carbons, while the assignments of the quaternary carbons were done based on the HMBC correlation spectrum. In the HMBC correlation spectrum (Fig. 5B), the 1H peak at 13.34 ppm shows a strong three bond coupling with C9 (δ_c , 110.23 ppm) and C7 (δ_c , 120.36 ppm), as well as a strong two bond coupling with C8 (δ_c , 155.98 ppm) and, therefore, it is assigned to the hydroxyl signal. We can conclude that the naphtholate oxygen atom is protonated and does not participate in the binding to the zinc atom. The resonance at 12.60 ppm shows a three bond coupling with C3 (δ_c , 110.96 ppm) and C2 (δ_c , 120.03 ppm), implying that this NH group corresponds to the pyrrole ring. Upon coordination the carbon atoms that suffer the highest downfield shifts are C5 (6.47 ppm), C6 (3.71 ppm) and C2 (6.06 ppm). The experimental data are in agreement with a coordination environment around $Zn(n)$ involving two O-atoms and two N-atoms from the carbonyl moieties of both ligands.

Complex 8 did not provide informative spectra in $DMSO-d_6$ and the NMR spectra were, therefore, measured in $MeOH-d_4$, which precludes the observation of NH or OH signals due to fast exchange with the solvent's deuterium atom. Integration of the 1H signals indicated the presence of two ligand molecules

and the HSQC and HMBC correlation spectra were used to clarify the structure. Although it was difficult to observe the signals from the quaternary carbons in the ^{13}C APT spectrum, the HMBC spectrum (Fig. S6A, ESI†) and particularly the presence of H16 at 8.55 ppm revealed that the signal from the carbonyl was lost, giving a clear indication of the formation of the enolate and subsequent bond formation with the $Zn(n)$ ion. The same analysis was done for 9 (Fig. S6B, ESI†), which suggested the same coordination motif. Taking all spectroscopic data into consideration a general schematic formulation is presented in Fig. 2 for all complexes, with the monoanionic ligands coordinated through the enolate and azomethine groups.

2.1.5. Stability. The stability of the ligand precursors and complexes in organic solvents and aqueous buffer (PBS, pH = 7.4) was evaluated by UV-vis spectroscopy. At biologically relevant concentrations ($< 100 \mu M$) all ligand precursors are stable in DMSO for 3 days and in PBS buffer; HL^1 and HL^2 precipitate with time, with HL^2 being stable within the same time period. The complexes are all very stable in DMSO, at least for 24 h, but most of them show precipitation at concentrations ca. 20–30 μM in aqueous buffer (see ESI†). However, the $V(n)O$ - and $Zn(n)$ -complexes of HL^2 show high stability, particularly 8. The stability of the $V(n)$ complexes towards oxidation was evaluated by ^{51}V NMR spectroscopy, using 3.5 mM solutions of the complexes in DMSO (10% $DMSO-d_6$). All compounds are stable for at least 6 h, after which small $V(v)$ peaks appear in the spectra at ca. -500 ppm. However, after 24 h the solutions are not fully oxidized (see Fig. S13, ESI†).

2.1.6. Computational calculations. All calculations were of the DFT type, carried out using GAMESS-US³⁸ version R3. The Schiff bases HL^1 – HL^3 depict two conformational isomers related to the relative conformation of the naphthoyl and hydrazone moieties. The carbonyl to enol hydrogen bonded conformer (Fig. 6B) was shown to be the most stable (by 18.5 kJ mol^{-1}) in agreement with the SC-XRD structure determined for HL^2 . However, for the reactive anionic species, in equilibrium with HL^2 , the structure with a deprotonated enol is the most stable one (Fig. 6D). The photophysics of this series of ligand precursors (see above) shows very large Stokes shifts that are incompatible with a relaxed S_1 HL^* species. TD-DFT

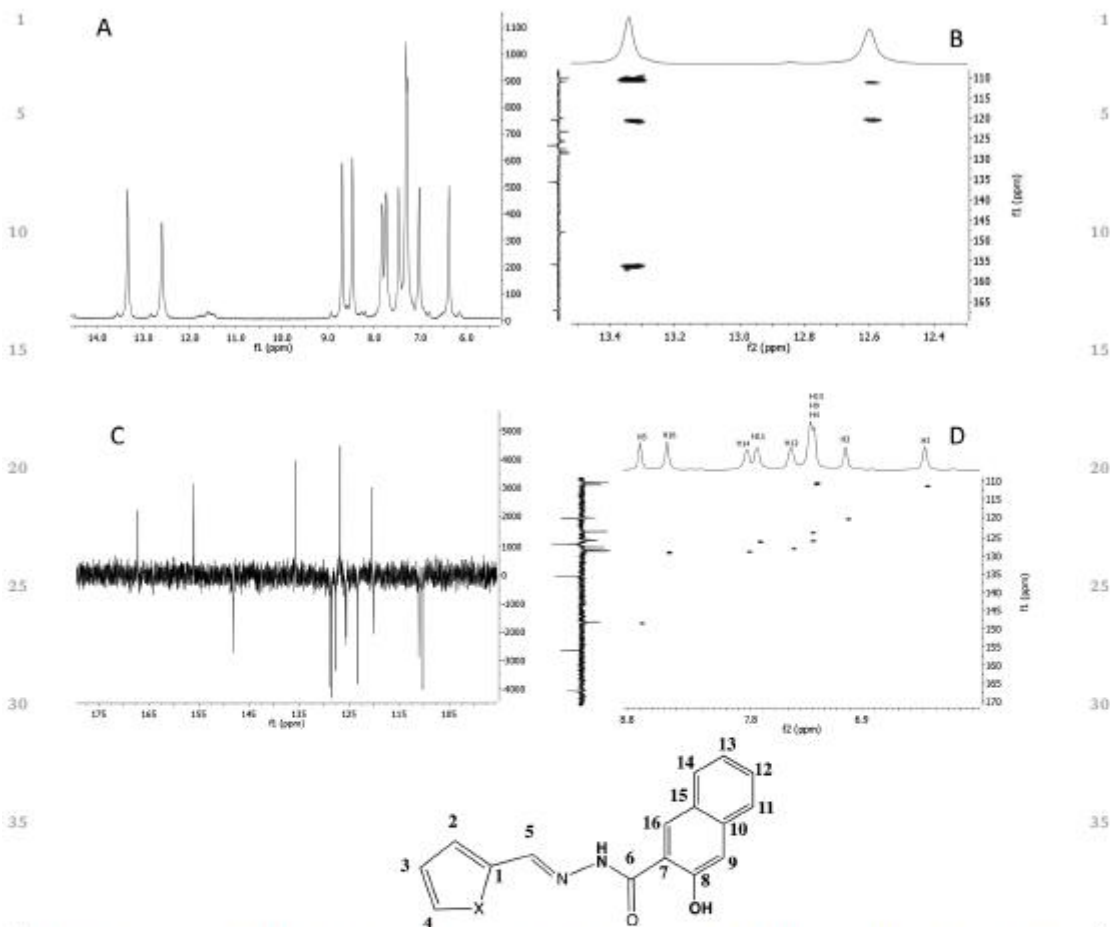


Fig. 5 (A) ^1H NMR spectrum of **7** in $\text{DMSO}-d_6$; (B) HMBSC correlation spectrum of **7** in $\text{DMSO}-d_6$ showing the OH and NH signals present at the complex's structure; (C) ^{13}C APT NMR spectrum of **7** in $\text{DMSO}-d_6$; and (D) HSQC correlation spectrum of **7** in $\text{DMSO}-d_6$. Chemical shifts are in ppm using TMS as internal reference. A general formula for the ligands is included with the atom numbering scheme used.

calculations produced a good match between the absorption spectra of HL and the emission spectra of L^- , Fig. S12 (ESI †).

The structures of vanadium, copper and zinc complexes are square pyramidal (distorted towards trigonal bipyramid), tetrahedrally distorted square planar, and tetrahedral, respectively, Fig. 7.

The photophysics of the complexes derived from HL species is more difficult to analyse since there is a dynamic equilibrium between the complex and free base, which itself is involved in an acid-base equilibrium. Upon excitation, the metal-ligand bonds become very labile and the excited base is released in a time shorter than the natural fluorescence lifetime of the complex. Hence, the emission is always coincident with the

emission of the free base. The absorption spectrum is the convolution of the spectra of both species involved in the equilibrium. For vanadium, which is predicted to have a very strong absorption at around 390 nm, the spectrum just increases around the position of the long Gaussian tail of the ligand, Fig. 8A. Copper complexes depict a very different TD-DFT absorption spectra characterized by four allowed transitions in the range 370 to 460 nm, producing a more structured absorption band, Fig. 8B. Finally, the $\text{Zn}(\text{n})$ -complexes just show two nearly degenerate transitions around 390 nm. Simulated absorption spectra of $\text{HL}^{\cdot-}$ species are very similar to those shown above with a slight blue shift of 0.1 eV, Fig. 8C.

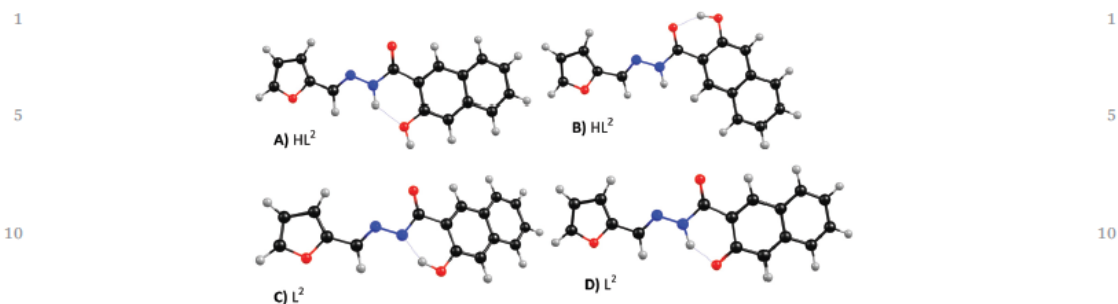


Fig. 6 (A) and (B) Conformational isomers of the naphthoyl moiety relative to the hydrazone skeleton using HL^2 as an example. (C) and (D) Structure of the most stable anionic L^2 conformers. The enolate in D is more stable by 4 kJ mol^{-1} .

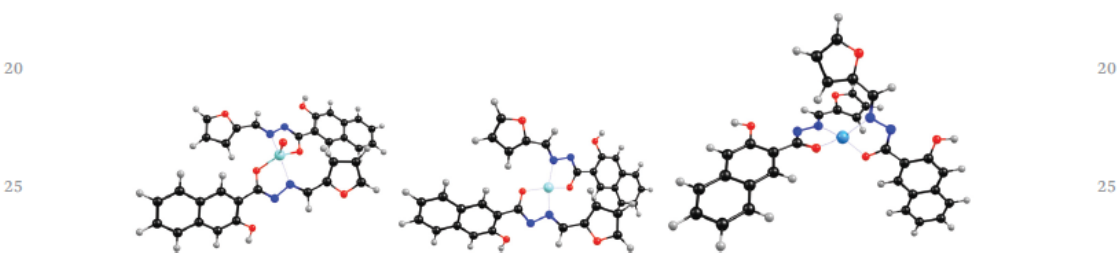


Fig. 7 DFT optimized structures of vanadium (left), copper (centre) and zinc (right) HL^2 complexes. Complexes with HL^1 and HL^3 monoanionic ligands have similar DFT calculated structures.

2.2. Interaction with BSA

Bovine serum albumin (BSA) is the most abundant protein present in cell culture media in *in vitro* assays with mammalian cells, since the addition of fetal bovine serum (FBS) is essential for cell growth. Despite the fact that BSA presents only 76% structural homology with HSA,³⁹ due to its low cost and ready availability it is also a model protein used in the evaluation of drug transport in human plasma.

2.2.1. Circular dichroism. Circular dichroism is a spectroscopic technique that has been extensively used in studies of protein folding and stability assays, intermolecular interactions and ligand binding studies. To evaluate a drug's impact on the protein secondary structure spectral changes in the far-UV range can be monitored upon incubation of the protein with the drug.

Fig. 9 and Fig. S15 (ESI[†]) show the CD spectra measured for solutions containing *ca.* $1 \mu\text{M}$ of BSA and BSA: compound molar ratios of 1 : 1 or 1 : 2. It is interesting to note that addition of the compounds leads to an increase in the intensity of the bands without any shift of the band maxima suggesting an increase in the α -helix content. This is particularly relevant for the ligand precursors, which show increases between 12–28% – Table S4 (ESI[†]) – while the complexes show only <8%.

Changes in secondary structural content has been observed for peptides and proteins upon addition of alcohols.⁴⁰ The

structure stabilization has been proposed to arise from the hydrophobicity and the strong hydrogen-bond-donating/poor hydrogen-bond-accepting property of the hydroxyl groups. Disruption of the protein's hydrogen-bond networks causing refolding to a helical configuration has been proposed. For our ligands and complexes the hydroxyl groups are available and protonated and may participate in hydrogen bonding to the BSA biomolecule.

2.2.2. UV-vis absorption. Serum albumin's UV-vis absorption spectra show two bands at *ca.* 210 and 280 nm assigned to the α -helix and the aromatic amino-acid residues, respectively. The 210 nm band is sensitive to secondary structural changes such as variation of the α -helix content and the 280 nm bands are sensitive to changes in the environment around the aromatic residues, *e.g.*, the Trp residue. Given the increase in α -helical content observed by CD spectroscopy, UV-vis absorption titrations were done for HL^1 – HL^3 and $\text{V}(\text{IV})\text{O}$ -complexes 1–3 (Fig. S16, ESI[†]). In all assays a very strong decrease (*ca.* 80%) in the intensity of the 210 nm band, accompanied by a strong red shift (to 234 nm), was observed upon addition of the compounds to BSA solution (the compounds were also added to the reference cell). Similar changes observed previously for BSA and Pt-complexes⁴¹ were attributed to perturbations of the α -helix induced by specific interactions with the complexes, which is also in agreement with our CD data.

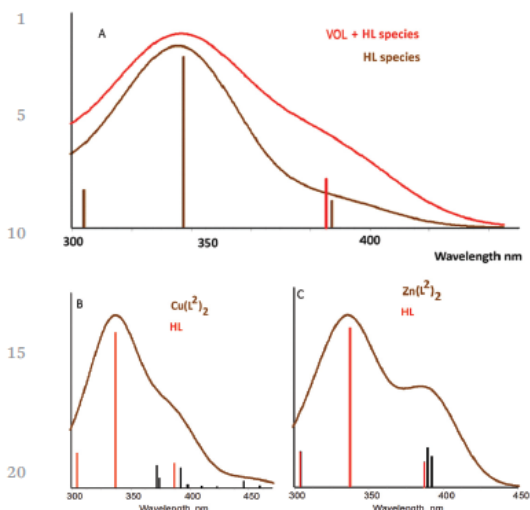


Fig. 8 TD-DFT simulated absorption spectrum of the convoluted (A) VOL + HL species; (B) CuL + HL and (C) ZnL + HL species.

Moreover, the transitions assigned to the protein's aromatic residues at 278 nm are also affected by the ligands and particularly the V-complexes, namely, an increase in the intensity of the 278 nm band of <15% for the ligand precursors, and complex 3 and an increase of 42 and 31% for complexes 1 and 2, respectively. These changes suggest that the aromatic residues, which were buried inside the hydrophobic pocket, became more exposed to the aqueous environment.

2.2.3. Fluorescence spectroscopy. Serum albumins exhibit intrinsic fluorescence emission mainly due to the presence of 1 or 2 tryptophan (Trp) residues, in HSA and BSA, respectively. In BSA Trp 134 is located on the protein surface while Trp 213 is located in a hydrophobic binding pocket of subdomain IIA. In particular Trp 213 is the most sensitive to the local

environment and its fluorescence emission easily responds to small changes induced by drug's binding to the protein.⁴⁵ Since the UV titrations suggest that Trp 213 became exposed to the solvent, fluorescence emission titrations were done for all compounds. Upon excitation at 295 nm at room temperature, BSA exhibits a strong fluorescence emission band centered at ca. 340 nm. Progressive additions of stock solutions of the compounds lead to a gradual decrease of the emission band (Fig. 10 and Fig. S17, ESI†). In the case of the ligand precursors the initial intensity was quenched to about 1/3, while with the Cu(II)-complexes the quenching followed the order $\text{Cu(L}^1\text{)}_2 < \text{Cu(L}^2\text{)}_2 < \text{Cu(L}^3\text{)}_2$. The Zn(II)-complexes followed the same order $\text{Zn(L}^1\text{)}_2 < \text{Zn(L}^2\text{)}_2 < \text{Zn(L}^3\text{)}_2$ while the oxidovanadium complexes showed a different trend: $\text{VO(L}^1\text{)}_2 < \text{VO(L}^3\text{)}_2 < \text{VO(L}^2\text{)}_2$. For some compounds a second emission band appeared at higher wavelength, but it has already been established that the presence of an isosbestic point, as in the present work, is sufficient to enable the quenching analysis without further issues.⁴²

The Stern–Volmer analysis yielded K_{SV} values in the 10^5 M^{-1} range for all compounds (Table 3). Thus, considering an average fluorescence lifetime of 6.22 ns, measured under our working conditions, this leads to bimolecular rate constants in the $10^{13} \text{ M}^{-1} \text{ s}^{-1}$ range, above the maximum limit for the diffusional quenching phenomenon ($2 \times 10^{10} \text{ M}^{-1} \text{ s}^{-1}$)⁴³ and the formation of a compound–protein adduct is expected. When small molecules bind independently to a set of equivalent sites on a macromolecule, the equilibrium between free and bound molecules can be approximately described by the Scatchard equation:

$$\log[(I_0 - I)/I] = \log K_b + n \log [Q]$$

where I_0 , I and $[Q]$ have the same meaning as in the Stern–Volmer equation, K_b is the binding constant and n is the number of binding sites.

From the values of n , we can establish a 1 : 1 compound : BSA relationship in the formation of the adduct. Binding of a small molecule to albumin is a way for it to get transported inside the

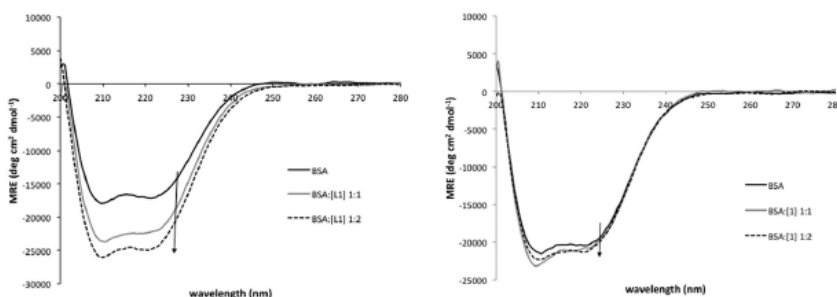


Fig. 9 Far-UV circular dichroism spectra measured for solutions containing BSA (ca. $1 \mu\text{M}$) and molar ratios of BSA : compound of 1 or 2 for HL¹ (left) and complex 1 (right). MRE is the mean residue ellipticity.

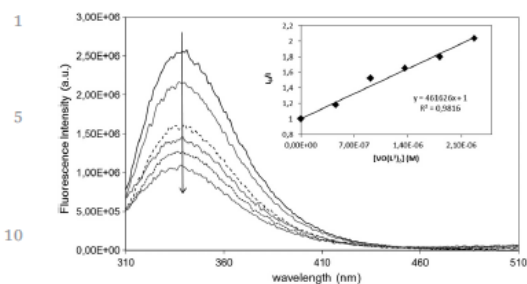


Fig. 10 Emission spectra ($\lambda_{\text{ex}} = 295 \text{ nm}$) of BSA ($1.5 \mu\text{M}$) in the absence and presence of increasing concentrations of $\text{VO}(\text{L}^2)_2 \mathbf{3}$, ($0.5\text{--}2.3 \mu\text{M}$) in 0.3% DMSO/PBS aqueous buffer, pH 7.4, after subtraction of blank emission spectra (arrow indicates the variation observed with increasing concentration of the metal compound). Inset: Stern–Volmer plots at 340 nm obtained from steady-state I_0/I measurements (I_0/I data were corrected for inner-filter-effects).

Table 3 BSA fluorescence steady state quenching experimental results after analysis with the Stern–Volmer and Scatchard equations

| | $K_{\text{SV}} (\text{M}^{-1})$ | $K_{\text{b}} (\text{M}^{-1})$ | n |
|-------------------------------|---------------------------------|--------------------------------|------|
| HL^1 | 1.64×10^5 | 2.84×10^6 | 1.22 |
| HL^2 | 3.71×10^5 | 1.07×10^5 | 0.9 |
| HL^3 | 4.67×10^5 | 1.21×10^6 | 0.99 |
| $\text{VO}(\text{L}^1)_2$ (1) | 3.03×10^5 | 5.14×10^4 | 0.87 |
| $\text{VO}(\text{L}^2)_2$ (2) | 4.69×10^5 | 5.34×10^6 | 1.00 |
| $\text{VO}(\text{L}^3)_2$ (3) | 4.62×10^5 | 8.00×10^5 | 0.96 |
| $\text{Cu}(\text{L}^1)_2$ (4) | 1.74×10^5 | 7.33×10^3 | 0.76 |
| $\text{Cu}(\text{L}^2)_2$ (5) | 3.16×10^5 | 9.29×10^4 | 0.91 |
| $\text{Cu}(\text{L}^3)_2$ (6) | 6.35×10^5 | 5.53×10^5 | 0.99 |
| $\text{Zn}(\text{L}^1)_2$ (7) | 3.03×10^5 | 4.35×10^5 | 1.03 |
| $\text{Zn}(\text{L}^2)_2$ (8) | 6.23×10^5 | 4.70×10^5 | 0.98 |
| $\text{Zn}(\text{L}^3)_2$ (9) | 1.00×10^6 | 1.30×10^6 | 1.01 |

organism to its target cells and, therefore, the binding should be reversible, which implies moderate binding constants ($10^3\text{--}10^5 \text{ M}^{-1}$), such as those obtained here for most of the compounds, except for HL^1 , HL^3 , 2 and 9, for which binding constants of the order of 10^6 M^{-1} were obtained, indicating a stronger interaction that may delay the detachment of these compounds from the protein. However, we should keep in mind the limitations of the double log Scatchard equation used to determine the binding constant and the number of binding sites, which assumes the formation of a non-fluorescent adduct, and in which $[Q]$ is set equal to $[Q]_{\text{free}}$.⁴⁴ These points are further elucidated in the time-resolved studies, which were also done, and evidence the existence of a mixed mechanism.

The linear dependence on the compound's concentration found in the steady state fluorescence quenching measurements (Stern–Volmer plots) points to a single quenching mechanism; however, time-resolved measurements regarding the average fluorescence lifetime of BSA have also shown a linear relationship with the concentration of the compounds (Fig. S18, ESI†).

The combination of these results establishes a mixed quenching mechanism with a dynamic (or collisional) component showing constants of the order of 10^4 M^{-1} in the case of HL^1 compounds (Table S5, ESI†) and in the 10^5 M^{-1} range for HL^2 and HL^3 families, still above the limit for purely collisional quenching, and, therefore, a static component of quenching also exists in these systems, corroborating again the formation of an adduct.

2.3 Docking studies

Aiming to rationalize the spectroscopic results, molecular docking studies, which aim at the determination of the binding sites of a molecule on the biological target, were carried out. Molecular interactions between the ligands and protein BSA (PDB-ID: 4JK4)⁴⁵ were studied in order to obtain insights into the binding modes. The studies were also performed for HSA protein (PDB-ID: 3LU6)⁴⁶ due to the structural similarity observed for BSA and HSA. Molecular docking studies, considering flexible ligands and a rigid protein were performed for HL^1 , HL^2 , HL^3 and for L^2 complexes. The docking assays were based on the hypothesis proposed by the spectroscopic studies, which suggests an interaction between BSA's Trp 213 and the compounds. This amino acid is part of the binding site I of BSA, located on sub-domain IIA. The binding site I of BSA consists of Trp 213, Arg 194, Asp 194, Arg 198, Ser 201, Ser 214 and Arg 217 which correspond to Trp 214, Lys 199, Arg 218, His 242 and Ala 291 of HSA (Fig. S19, ESI†).

2.3.1 Ligands – bovine serum albumin. The docked compounds occupy the region predicted by fluorescence studies. Fig. 11 shows the best binding poses obtained for HL^1 (Fig. 11a–c), HL^2 (Fig. 11d–f) and HL^3 (Fig. 11g–i). The docking scores are similar for all ligand precursors (Table S10, ESI†). Upon comparison of the poses it is possible to observe a flip of HL^1 pose when compared with HL^2 and HL^3 . However, all docked compounds' analogs interact by $\pi\text{--}\pi$ with Trp 213 as proposed by fluorescence studies (Table S8, ESI†). This interaction is observed between the naphthalene of all ligand precursors and the indole ring of tryptophan. The distance between the ligands and Trp 213 is around 3 \AA . HL^2 and HL^3 were also able to establish a hydrogen bond with Arg 194, through their O moiety. The change of heteroatom (N, O and S) in the 5-ring of the ligands doesn't appear to affect the anchoring mode of the ligands inside the pocket. The naphthalene scaffold is the determinant of the interaction with the protein, particularly with Trp 213 due to the stacking observed.

HL^1 . a. Amino acid interactions of HL^1 inside the pocket. A stacking with Trp 213 is observed; b. surface view of the 4JK4 binding pocket, with most important amino acids highlighted and HL^1 pose; c. 2D depiction of interactions of HL^1 inside the BSA pocket.

HL^2 . d. Amino acid interaction of HL^2 inside the pocket. A stacking with Trp 213 is observed; e. surface view of the 4JK4 binding pocket, with most important amino acid highlighted

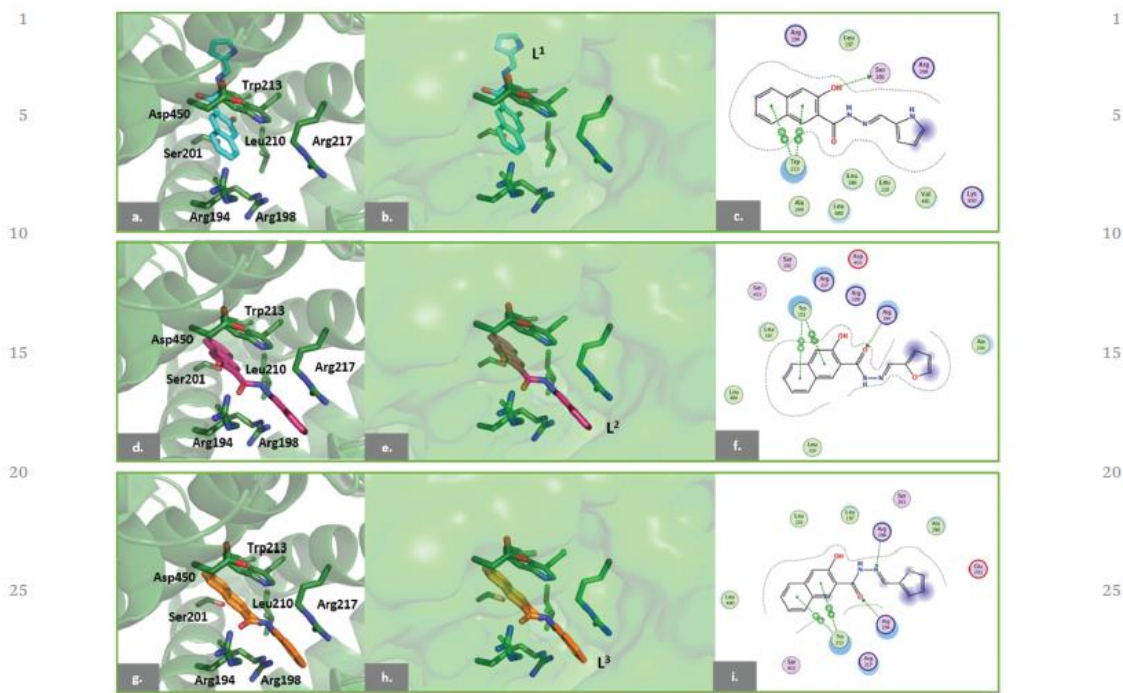


Fig. 11 Docking binding modes for BSA (PDB-ID: 4JK4).

and HL^2 pose (more similar with HL^3 pose); f. 2D depiction of interactions of HL^2 inside the BSA pocket.

HL^3 . g. Amino acid interaction of HL^3 inside the pocket. A stacking with Trp 213 is observed; h. surface view of the 4JK4 binding pocket, with most important amino acid highlighted and HL^3 pose; i. 2D depiction of interactions of HL^3 inside the BSA pocket.

2.3.2 Ligands – human serum albumin. The docked ligands HL^1 (Fig. S20j–l, ESI†) HL^2 (Fig. S20m–o, ESI†) and HL^3 (Fig. S20p–r, ESI†) occupy the same region of the binding pocket of HSA and show orientations highly resembling the crystallographic ligand. The binding poses of all ligands are analogous and our studies reveal a π – π interaction with Trp 214, similar to that observed with BSA (Table S9, ESI†). Additionally, a π –H interaction with Lys 199 is observed that seems to be key in the “anchoring” of the ligands through the naphthalene moiety (interaction not observed for BSA). The scoring values are similar for all ligands. There is no significant difference in BSA’s scores when compared with those of HSA (Table S10, ESI†).

2.3.3 L^2 complexes. To elucidate the binding mode of the complexes, additional docking studies were performed with L^2 complexes docked to BSA (PDB-ID: 4JK4) and HSA (PDB-ID:

3LU6). Interestingly, it is possible to observe different binding modes for HSA and BSA, for the same complex (Fig. 12). For the considered crystallographic structures, Trp 214 of HSA is more exposed when compared with the same amino acid for BSA, allowing the accommodation of a large complex into the pocket (Fig. 12A, B, D and E). Therefore, $VO(L^2)$ and $Cu(L^2)_2$ present a similar pose to HL^2 , with the naphthalene ring of the complex interacting by π – π stacking with HSA (Table S12, ESI†). This interaction is not clearly shown for poses of $VO(L^2)$ and $Cu(L^2)_2$ in BSA, due to the location of Trp 213 into the deep pocket and as a consequence of the stereochemical restrictions (Table S11, ESI†). Nonetheless, scores obtained for the best poses are similar and support the proposed binding mode (Table S10, ESI†).

Regarding BSA it is possible to observe interactions [mainly from $Cu(L^2)_2$ and $Zn(L^2)_2$] with Lys 294 and Pro 338. These H-acceptor and H-donor interactions, respectively, were not observed with the ligand HL^2 . However, the receptor exposure of residues Trp 213 and Arg 194 is observed for all complexes (Table S11). HSA, as mentioned before, presents similar interactions of HL^2 , mainly for $VO(L^2)_2$ and $Cu(L^2)_2$. The lengths predicted between the complexes’ naphthalene groups and Trp are consistent with HL^2 values. Additionally, to the π – π interaction, a π –H interaction is observed with Lys 199 for $VO(L^2)_2$, which is important for anchoring the complex.

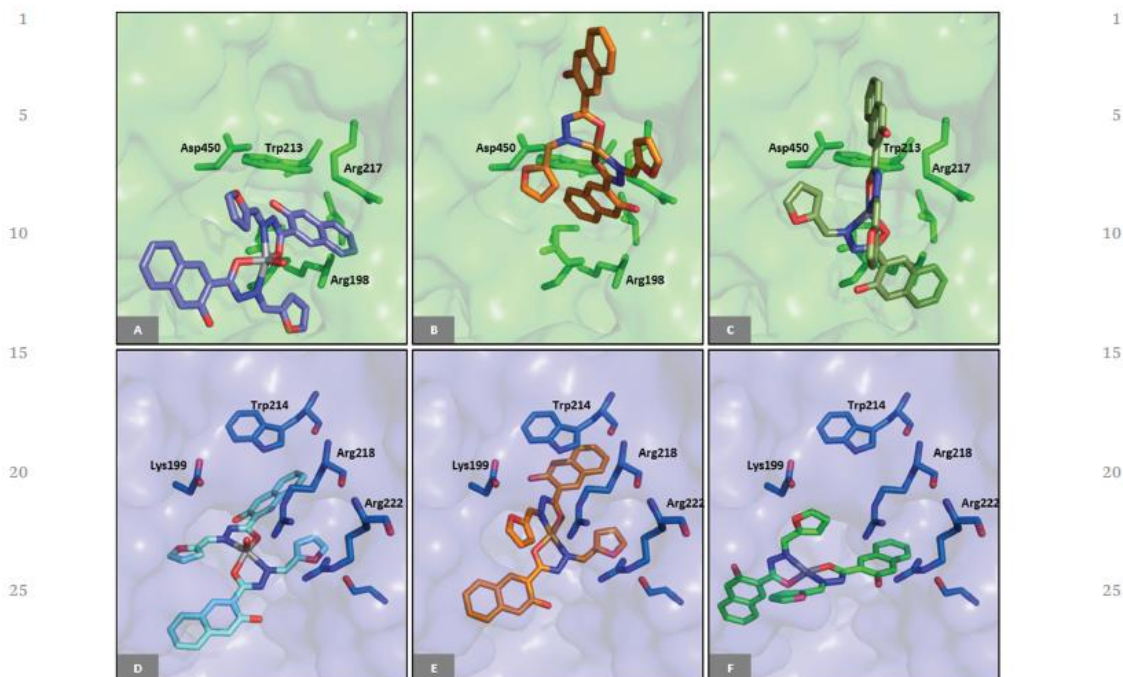


Fig. 12 Proposed docking binding modes of HL^2 complexes for BSA and HSA (PDB-ID: 4JK4 and 3LU6, respectively).

These docking results suggest a similar binding mode of the ligands for HSA and BSA. The binding mode observed by molecular modeling supports the spectroscopic hypothesis of interaction with Trp 213/214. However, further dynamic simulations should be performed to provide insights into structural modifications of the proteins (and consequent Trp exposure) in the presence of the ligands and the complexes.

Vanadium. A. Proposed interaction of $VO(L^2)_2$ inside the pocket of BSA (PDB-ID: 4JK4). D. Proposed binding mode of $VO(L^2)_2$ with HSA (PDB-ID: 3LU6).

Copper. B. Proposed interaction of $Cu(L^2)_2$ inside the pocket of BSA (PDB-ID: 4JK4). E. Proposed binding mode of $Cu(L^2)_2$ with HSA (PDB-ID: 3LU6).

Zinc. C. Proposed interaction of $Zn(L^2)_2$ inside the pocket of BSA (PDB-ID: 4JK4). F. Proposed binding mode of $Zn(L^2)_2$ with HSA (PDB-ID: 3LU6).

2.4 Biological activity

2.4.1 Antimicrobial activity. The antimicrobial activity of the compounds was screened against Gram-positive and Gram-negative bacteria and yeast (data not shown) and the results showed no relevant activity for the microorganisms tested in

comparison with the positive controls used. These results were surprising, as naphthoyl hydrazonoate complexes have shown interesting antimicrobial activity,^{10–12} but no further antimicrobial activity tests were done.

2.4.2 Brine shrimp lethality bioassay. The general toxicity of ligand precursors, Cu- and V-complexes was assessed using the *Artemia salina* model (Fig. S21, ESI†). The toxicity screening results using this model showed that all compounds display general toxicity. Particularly toxic are Cu-complexes 4 and 5 and HL^1 (% dead organisms > 70%) followed by the V-complexes 1 and 3 (% dead organisms > 50%). Thus, it is pertinent to further evaluate the compounds by other *in vitro* methods, such as cytotoxicity.

2.4.3 *In vitro* antitumor activity of compounds. The antitumor potential of the compounds was studied in the lung (H1299), breast (MCF7) and colon (HCT116) human tumor cells. For that purpose, their antiproliferative activity was tested by the sulforhodamine B (SRB) assay, for 48 h treatments. In general, the compounds showed a potent antiproliferative activity, with half-maximal inhibitory concentration (IC_{50}) values lower than 30 μM (Table 4). All compounds showed to be more potent in the colon and breast cancer cells (with IC_{50} values lower than 7 μM), than in the lung cancer cells (IC_{50} values ranging from 7 to 27.50 μM).

Table 4 IC₅₀ values (μM) of the compounds tested in the lung (H1299), breast (MCF7), p53 wild-type colon (HCT116 p53+/+) and p53 depleted (HCT116 p53-/-) human cancer cell lines as well as normal fibroblasts (HFF) for 48 h of incubation. Results are the mean of at least 4 independent biological SRB assays (±SEM)

| Compound | H1299 | MCF7 | HCT116+/+ | HCT116-/- ^a | HFF ^a |
|--------------------------------------|--------------|-------------|-------------|------------------------|------------------|
| HL ¹ | 7.35 ± 1.55 | 1.15 ± 0.05 | 1.4 ± 0.1 | 2.5 ± 0.3 | 10.5 ± 0.5 |
| HL ² | 27.5 ± 0.5 | 9.7 ± 0.3 | 13.5 ± 0.5 | | |
| HL ³ | 16.6 ± 1.7 | 3.59 ± 0.26 | 6.54 ± 0.1 | 4.9 ± 0.5 | 2.3 ± 0.25 |
| VO(L ¹) ₂ (1) | 7.0 ± 0.8 | 0.73 ± 0.12 | 1.12 ± 0.28 | <1.88 | <1.88 |
| VO(L ²) ₂ (2) | 20.5 ± 1.5 | 3.65 ± 0.25 | 7.25 ± 0.45 | 5.4 ± 0.2 | <1.88 |
| VO(L ³) ₂ (3) | 16.0 ± 1.0 | 1.37 ± 0.22 | 2.54 ± 0.82 | 1.37 ± 0.22 | <1.88 |
| Cu(L ¹) ₂ (4) | 18.0 ± 2.0 | 4.4 ± 0.1 | 5.65 ± 0.05 | 3.65 | 8.75 ± 0.55 |
| Cu(L ²) ₂ (5) | 9.25 ± 0.03 | 4.55 ± 0.26 | 5.24 ± 0.11 | | |
| Cu(L ³) ₂ (6) | 7.3 ± 2.7 | 1.21 ± 0.26 | 1.3 ± 0.1 | | |
| Zn(L ¹) ₂ (7) | 10.3 ± 2.7 | 0.57 ± 0.18 | 0.60 ± 0.28 | | |
| Zn(L ²) ₂ (8) | 11.35 ± 2.35 | 5.22 ± 0.94 | 6.62 ± 0.08 | | |
| Zn(L ³) ₂ (9) | 9.05 ± 1.95 | 1.6 ± 0.1 | 2.25 ± 0.05 | 2.89 | 15.1 ± 3.4 |

^a Results are the mean of 1 or 2 independent biological SRB assays (±SEM).

HL¹, containing the pyrrole ring, was the most active ligand of the series with its complexes showing IC₅₀ values below 6 μM (in breast and lung cell lines), with coordination to copper decreasing its activity in all cell lines. HL², containing furane, was the least cytotoxic ligand precursor, as well as its complexes, but complexation increased its cytotoxicity. For HL³, the thiophene derivative, complexation increased at least twice the cytotoxicity (as measured by the IC₅₀ values) in all cell lines and for all metal ions (except 3 in H1299). Overall, the vanadium and zinc complexes perform better than the copper ones, particularly in the breast and colon cell lines, with complexes 1 and 7, both derived from HL¹, showing IC₅₀ values lower than 1.1 μM.

In general, the complexes perform better than mixed ligand aroylhydrazone Cu(II) complexes,⁷ which were not cytotoxic (except one compound) for most cell lines, which included MCF7, colon and lung adenocarcinoma cell lines. They also compare well with results obtained with several aroylhydrazones and salicylaldehyde isonicotinoyl hydrazine, a known iron chelator, that were tested against MCF7 and HL-60 cell lines;⁴ and with Sn-HNH complexes, which were also tested in similar cell lines.⁴⁷

In order to understand the role of p53, the tumor suppression protein, a p53 depleted cell line (HCT116-/-) was also used to evaluate the cytotoxicity of selected compounds. However, the IC₅₀ values determined in the colon cancer cells with different p53 status were similar, showing no selectivity for p53.

The selectivity for tumor cells was evaluated for a few compounds using a fibroblast cell line (HFF) but all compounds showed to be cytotoxic also for this normal cell line, indicating rather non-specific toxicity. Overall, the antiproliferative studies show interesting results but the selectivity towards cancer cells need to be improved.

3. Conclusions

Nine new transition metal complexes (V^{IV}O, Cu^I and Zn^{II}) were prepared from three naphthoylhydrazones obtained from the

condensation of 3-hydroxy-2-naphthoic hydrazide with aldehydes derived from pyrrole, furane and thiophene. Analytical and spectroscopic data indicate a ML₂ stoichiometry, with the ligand molecules bound monoanionically, through the hydrazoneate moiety, which was also corroborated by DFT theoretical calculations. These also gave support to the photophysical characterization, in which all luminescent compounds showed an emission band at ca 540 nm, which is coincident with the emission from the free base, L⁻.

Studies on the interaction of the compounds with BSA showed an interesting behavior, involving the formation of a protein-adduct, and K_{SV} constants around 10⁵ M⁻¹. The binding of the compounds stabilizes the protein, increasing the formation of α-helices through H-bonding with the naphthoyl OH groups. All conditional binding constants are in the range (10³-10⁵ M⁻¹), showing moderate to strong binding. Molecular docking studies, which suggested π-π stacking interactions between the protein Trp 213 and the naphthalene aromatic rings, corroborated the binding near BSA's Trp 213. The preliminary biological screening showed no antimicrobial activity. Notwithstanding, the compounds depict general toxicity towards the *Artemia salina* model, particularly HL¹ and copper complexes 4 and 5. The cytotoxicity screening, done with three cancer cell lines, evidenced the high activity of the compounds, against the breast and colon cancer cell lines, with IC₅₀ values lower than 7 μM. No correlation was found with the p53 tumor suppression protein. Interestingly, compounds containing HL¹ were those depicting lower IC₅₀ values, but coordination to Cu(II) decreased the activity against all cell lines. Those containing HL² were the least cytotoxic, but complexation increased cytotoxicity. Binding to metals normally increased the cytotoxicity against all cell lines in the case of compounds containing HL³.

Contrary to many other series of compounds,⁴⁸⁻⁵¹ in the cytotoxicity tests overall the vanadium and zinc complexes performed better than the copper ones. Globally the results suggest that some of the new compounds present high cytotoxicity; however, selectivity for cancer cells needs improvement

1 and nanoparticle formulation will be considered in future
2 studies.

5 4. Experimental

4.1 Materials and apparatus

Methyl-3-hydroxy-2-naphthoate (TCI), hydrazine monohydrate (Sigma-Aldrich), pyrrole-2-carboxaldehyde (Aldrich), 2-furaldehyde (Aldrich) and thiophene-2-carboxaldehyde (Aldrich) were used as received. The metal salts $\text{VOCl}_2 \cdot 2\text{H}_2\text{O}$ (Carlo Erba), $\text{CuCl}_2 \cdot 2\text{H}_2\text{O}$ (Merck), and $\text{ZnCl}_2 \cdot 2\text{H}_2\text{O}$ (Riedel-de-Haën) were used as supplied. Methanol (Aldrich) and dimethyl sulfoxide (Carlo Erba) were p.a. grade and used without further purification. Millipore[®] water was used throughout all the experiments with biological macromolecules. Phosphate buffered saline (PBS) was purchased from Sigma-Aldrich as tablets readily soluble in water (deionized water) giving 0.01 M solutions in phosphate (and NaCl 0.138 M; KCl 0.0027 M), pH 7.4 at 25 °C. Bovine Serum Albumin (BSA) was purchased from Sigma-Aldrich (A7030, Lot# SLBT 4132). All other materials not mentioned here were either p.a. or reagent grade.

Elemental analysis for C, H, N and S was carried on a FISIONS EA 1108 CHNS-O apparatus. Cu, V and Zn analyses were carried out by ICP-OES in *Laboratório de Análises do IST* using a PerkinElmer *Optima 2000 DV*, after calcination of the samples at 800 °C and solubilization of the residue in hot HNO_3 . All the ^1H , ^{13}C and ^{51}V NMR spectra, as well as the 2D NMR experiments, were recorded at ambient temperature on a Bruker Avance II + 400 (UltraShieldTM Magnet) spectrometer (400.13 MHz for ^1H and 100.62 MHz for ^{13}C). The samples were dissolved in 0.5 mL of dimethyl sulfoxide- d_6 ($\text{DMSO}-d_6$), with the exception of $\text{Zn}(\text{L}^2)_2$, 8, which was dissolved in 0.5 mL of CD_3OD . The chemical shifts are reported in ppm using tetramethylsilane as internal reference. The ^{51}V NMR spectra were measured in DMSO with 10% $\text{DMSO}-d_6$ and referenced to VOCl_3 at 0 ppm. The infrared spectra were recorded on a JASCO FT/IR 4100 spectrophotometer and the UV-visible absorption spectra were recorded on a PerkinElmer Lambda 35 UV-vis spectrophotometer with 10.0 mm quartz cuvettes. A 500-MS Varian Ion Trap Mass Spectrometer was used to measure ESI-MS spectra of methanolic solutions of the compounds in both positive and negative modes. The first derivative X-band EPR spectra of the frozen solutions (frozen in liquid nitrogen, ca 100 K) were recorded on a Bruker ESP 300E spectrometer. The spectrometer was operated at ~9.51 GHz with a frequency modulation of 100 kHz. Fluorescence measurements were carried out on a SPEX[®] Fluorolog spectrofluorimeter (Horiba Jobin Yvon) in a FL3-11 configuration, equipped with a xenon lamp and in a 10.0 mm quartz cuvette. The instrumental response was corrected by means of a correction function provided by the manufacturer.

4.2 Synthesis

4.2.1 Synthesis of the ligands

55 *3-Hydroxy-2-naphthoic hydrazide*. Methyl-3-hydroxy-2-naphthoate (2 g, ~10 mmol) was suspended in 15 mL of methanol (MeOH)

and the mixture was stirred and heated at ca 50 °C till the compound dissolved completely. 2 mL of hydrazine monohydrate (~40 mmol) were added and the solution became bright yellow. The mixture was left to reflux for 3 h and a yellow precipitate was obtained from the orange solution. After cooling to room temperature the mixture was filtered, washed with cold water and the yellow solid was dried under vacuum. Yield: 1.437 g (71.5%). Elem. an. [Found (calc.)]: C, 65.2% (65.34%), H, 5.0% (4.98%), N, 13.9% (13.85%). ESI-MS m/z 243.13 (calc for $[\text{L} + \text{H}_2\text{O} + \text{Na}]^+$ 243.21). ^1H NMR (δ , ppm; $\text{DMSO}-d_6$) 4.73 (2H, NH_2); aromatic: 7.26, 7.33, 7.49, 7.74, 7.81 and 8.44; 10.16 (1H, OH) and 11.90 (1H, NH).

HL¹. 297 mg of 3-hydroxy-2-naphthoic hydrazide (1.47 mmol) were suspended in 10 mL of MeOH. 146 mg of pyrrole-2-carboxaldehyde (ca. 1.6 mmol) were dissolved in 10 mL of MeOH and added dropwise to the first suspension. A few drops of glacial acetic acid were added and the mixture was left to reflux for 4 h. After cooling to room temperature it was left overnight in the refrigerator to complete the precipitation. The light yellow solid was collected by filtration, washed with cold MeOH and dried under vacuum. Yield: 304 mg (74.8%). Elem. an. [Found (calc. for $\text{C}_{16}\text{H}_{13}\text{N}_3\text{O}_2$)]: C, 68.6% (68.81%), H, 4.5% (4.69%), N, 14.9% (15.05%). ESI-MS m/z 280.16 (calc. for $[\text{L} + \text{H}]^+$ 280.29); 278.50 (calc. for $[\text{L} - \text{H}]^-$ 278.29). ^1H NMR (δ , ppm; $\text{DMSO}-d_6$) 6.17, 6.54, 6.95 (pyrrolyl ring); naphthalene: 7.31, 7.36, 7.51, 7.76, 7.91 and 8.46; 8.28 (HC=N, imine); OH: 11.48; NH (hydrazide): 11.74 and NH (pyrrole): 11.6. ^{13}C NMR (δ , ppm; $\text{DMSO}-d_6$) 109.4 (pyr); 110.56; 113.97 (pyr); 119.93; 122.93; 123.8 (pyr); 125.84; 126.68; 126.75 (pyr); 128.17; 128.64; 129.8; 135.8; 141.7 (imine); 154.49 (naph); 163.49 (carbonyl). FTIR (cm^{-1} , KBr pellet): 3410 (sharp, pyrrolyl NH); 3244; 3050 (NH on Schiff base moiety); 1645 (carbonyl); 1625; 1559 (imine); 1532; 1228 (naphthol, OH).

HL². A procedure similar to the one used for *HL¹* was followed using 2-furaldehyde (145 μL ; ~2 mmol) instead of pyrrole-2-carboxaldehyde. A pale yellow solid was obtained. Yield: 207.6 mg (50.2%). Elem. an. [Found (calc. for $\text{C}_{16}\text{H}_{12}\text{N}_2\text{O}_3$)]: C, 68.5% (68.56%), H, 4.3% (4.32%), N, 9.8% (9.99%). ESI-MS m/z 281.12 (calc. for $[\text{L} + \text{H}]^+$ 281.28); 279.54 (calc. for $[\text{L} - \text{H}]^-$ 279.28). ^1H NMR (δ , ppm; $\text{DMSO}-d_6$) 6.66 (1H, fur); 6.97 (1H, fur); 7.32 (1H, naph); 7.35 (1H, naph) 7.51 (1H, naph); 7.76 (1H, naph); 7.88 (1H, imine); 7.9 (1H, naph); 8.35 (1H, fur); 8.43 (1H, naph); 11.3 (NH); 11.9 (OH). ^{13}C NMR (δ , ppm; $\text{DMSO}-d_6$) furanyl: 112.7; 114; 138.5; 149; naphthalene: 110.8; 120; 124; 126.25; 127; 128.6; 129; 130; 136; 154; imine: 146; carbonyl: 163.7. FTIR (cm^{-1} , KBr pellet): 3244, 3059 (NH on Schiff base moiety); 3440 (OH, stretching), 1637 (carbonyl); 1545 (imine); 1231 (naphthol, OH).

HL³. A procedure similar to the one used for *HL¹* was followed using thiophene-2-carboxaldehyde (160 μL ; ~1.7 mmol) instead of pyrrole-2-carboxaldehyde. A dark yellow solid was collected, washed with cold EtOH and diethyl ether and dried under vacuum. Yield: 440.6 mg (99%). Elem. an. [Found (calc. for $\text{C}_{16}\text{H}_{12}\text{N}_2\text{O}_2\text{S}_2$)]: C, 64.5% (64.85%), H, 4.1% (4.08%), N, 9.5% (9.45%), S, 10.7% (10.82%). ESI-MS m/z 297.12

1 (calc. for $[L + H]^+$ 297.34); 295.15 (calc. for $[L - H]^-$ 295.34). ^1H NMR (δ , ppm; DMSO- d_6) 7.17 (thioph); 7.32 (naph); 7.36 (naph); 7.51 (thioph + naph); 7.71 (thioph); 7.76 (naph); 7.91 (naph); 8.4 (naph); 8.67 (imine); 11.25 (OH); 11.93 (NH). ^{13}C NMR (δ , ppm; DMSO- d_6) 110.76; 120.7; 124; 126.1; 127; 128.2; 128.4 (thioph); 128.9; 129.5 (thioph); 130.4; 131.6 (thioph); 136; 139 (thioph); 143.72 (imine); 154.19; 163.76 (carbonyl). FTIR (cm^{-1} , KBr pellet): 3440 (OH, stretching), 3246; 3058 (NH on Schiff base moiety); 1639 (carbonyl); 1621; 1600; 1558 (imine); 1227 (naphthol, OH).

4.2.2 Synthesis of complexes. The synthesis of the complexes followed the general procedure: 2 eq. of the corresponding ligand precursor were deprotonated in MeOH using 2 eq. of sodium acetate. Then 1 eq. of either $\text{CuCl}_2 \cdot 2\text{H}_2\text{O}$, $\text{VOCl}_2 \cdot 2\text{H}_2\text{O}$ or $\text{ZnCl}_2 \cdot 2\text{H}_2\text{O}$ was added and the mixture was left to stir at $\sim 40^\circ\text{C}$ for 2.5 h. For the oxidovanadium(IV) complexes, degassed MeOH and N_2 atmosphere were used throughout the synthetic procedure. The solid compounds formed in these reactions were collected by filtration, washed with cold MeOH and dried under vacuum.

$\text{VO}(\text{L}^1)_2$ (1). A brown solid was obtained. Yield: 87.5 mg (70%). Elem. an. (%) found C, 61.1; H, 4.0; N, 13.0 and V, 8.4 [calc. for $\text{C}_{32}\text{H}_{24}\text{N}_6\text{O}_5\text{V} \cdot 0.5\text{MeOH}$: C, 61.04; H, 4.10; N, 13.14 and V, 7.97]. ESI-MS m/z 654.82 [calc. for $[\text{ML}_2 + \text{MeOH} - \text{H}]^-$ 654.15]. FTIR (cm^{-1} , KBr pellet): 3383 (broad); 3231 (medium broad); 1642; 1612; 1578; 1543; 1241; 1216; 1147; 897; 554; 404.

$\text{VO}(\text{L}^2)_2$ (2). A brown solid was obtained. Yield: 129.6 mg (68.6%). Elem. an. (%) found C, 60.4; H, 3.5; N, 8.5 and V, 7.8 [calc. for $\text{C}_{32}\text{H}_{22}\text{N}_4\text{O}_5\text{V} \cdot 0.5\text{H}_2\text{O}$: C, 60.58; H, 3.65; N, 8.83 and V, 8.03]. ESI-MS m/z 644.28 [calc. for $[\text{ML}_2 + \text{H}_2\text{O} + \text{H}]^+$ 644.09]; 658.44 [calc. for $[\text{ML}_2 + \text{MeOH} + \text{H}]^+$ 658.09]. FTIR (cm^{-1} , KBr pellet): 3433 (broad); 1640; 1532; 1296; 1242; 1219; 906; 555; 401.

$\text{VO}(\text{L}^3)_2$ (3). A dark brown solid was obtained. Yield: 164.8 mg (99%). Elem. an. (%) found C, 52.9; H, 3.4; N, 7.6; S, 8.81 [calc. for $\text{C}_{32}\text{H}_{22}\text{N}_4\text{O}_5\text{S}_2\text{V} \cdot 4\text{H}_2\text{O}$: C, 52.67; H, 4.14; N, 7.68; S, 8.79]. ESI-MS m/z 688.96 [calc. for $[\text{ML}_2 + \text{MeOH} - \text{H}]^-$ 688.61]. FTIR (cm^{-1} , KBr pellet): 3445 (broad); 3253; 3057; 1642; 1621; 1600; 1559; 1511; 1449; 1361; 1319; 1228; 1174; 1151; 1068; 1044; 973; 949; 873; 855; 834; 748; 707; 627; 473.

$\text{Cu}(\text{L}^1)_2$ (4). A light brown solid was obtained. Yield: 105 mg (84.7%). Elem. an. (%) found C, 61.6; H, 4.0; N, 13.1 and Cu, 10.0 [calc. for $\text{C}_{32}\text{H}_{24}\text{CuN}_6\text{O}_4 \cdot 0.5\text{MeOH}$: C, 61.36; H, 4.12; N, 13.21 and Cu, 9.99]. ESI-MS m/z 618.27 [calc. for $[\text{ML}_2 - \text{H}]^-$ 618.12]; 654.39 [calc. for $[\text{ML}_2 + \text{Cl}]^-$ 654.12]. FTIR (cm^{-1} , KBr pellet): 3430 (broad); 3167; 1578; 1554; 1240; 1219; 1150; 556; 405.

$\text{Cu}(\text{L}^2)_2$ (5). A light green solid was obtained. Yield: 131.5 mg (84%). Elem. an. (%) found C, 61.4; H, 3.7; N, 8.8 and Cu, 10.0 [calc. for $\text{C}_{32}\text{H}_{22}\text{CuN}_6\text{O}_6 \cdot 0.5\text{MeOH}$: C, 61.17; H, 3.79; N, 8.78 and Cu, 9.96]. ESI-MS m/z 656.79 [calc. for $[\text{ML}_2 + \text{Cl}]^-$ 656.08]. FTIR (cm^{-1} , KBr pellet): 3444 (broad); 1640; 1537; 1311; 1243; 1221; 559; 406.

$\text{Cu}(\text{L}^3)_2$ (6). A dark green solid was obtained. Yield: 162.3 mg (98%). Elem. an. (%) found C, 58.0; H, 3.8; N, 8.4; S, 9.6 [calc. for $\text{C}_{32}\text{H}_{22}\text{CuN}_4\text{O}_4\text{S}_2 \cdot 0.5\text{MeOH}$: C, 58.24; H, 3.61; N, 8.36; S, 9.57]. ESI-MS m/z 653.80 [calc. for $[\text{ML}_2 + \text{H}]^+$ 654.04]. FTIR (cm^{-1} , KBr pellet): 3445; 3356; 3253; 3057; 1636; 1624; 1600; 1559; 1509; 1449; 1361; 1316; 1228; 1172; 1148; 1065; 1044; 949; 873; 852; 834; 748; 707; 624; 470.

$\text{Zn}(\text{L}^1)_2$ (7). A yellow solid was obtained. Yield: 148 mg (79%). Elem. an. (%) found C, 61.8; H, 4.0; N, 13.3 and Zn, 10.0 [calc. for $\text{C}_{32}\text{H}_{24}\text{N}_6\text{O}_4\text{Zn}$: C, 61.79; H, 3.89; N, 13.51 and Zn, 10.51]. ESI-MS m/z 643.92 [calc. for $[\text{ML}_2 + \text{Na}]^+$ 643.11]. ^1H NMR (δ , ppm; DMSO- d_6) 6.36, 7.01, 7.26 (pyrrolyl ring); naphthalene: 7.26, 7.29, 7.45, 7.74, 7.80 and 8.46; 8.68 (HC=N, imine); OH: 13.32; and NH (pyrrole): 12.6. ^{13}C NMR (δ , ppm; DMSO- d_6) 110.52; 111.37 (pyr); 120.36; 120.46 (pyr); 123.27; 125.41 (pyr); 125.84; 126.72; 126.72 (pyr); 127.72; 128.90; 129.53; 135.8; 148.17 (imine); 156.03 (naph); 167.20 (COZn). FTIR (cm^{-1} , KBr pellet): 3380 (broad); 3187; 1576; 1546; 1231; 1223; 1150; 547; 428.

$\text{Zn}(\text{L}^2)_2$ (8). A yellow solid was obtained. Yield: 131.9 mg (71%). Elem. An. (%) found C, 61.9; H, 3.9; N, 8.9 [calc. for $\text{C}_{32}\text{H}_{22}\text{N}_4\text{O}_6\text{Zn}$: C, 61.60; H, 3.55; N, 8.98]. ESI (+) m/z 623.15 [calc. for $[\text{ML}_2 + \text{H}]^+$ 623.08]. ESI-MS m/z 621.14 [calc. for $[\text{ML}_2 - \text{H}]^-$ 621.08]. ^1H NMR (δ , ppm; MeOD- d_4) 6.58 (fur); 7.07 (fur); 7.25 (naph); 7.30 (naph) 7.46 (naph); 7.64 (imine); 7.69 (naph); 7.84 (naph); 8.43 (fur); 8.55 (naph). ^{13}C NMR (δ , ppm; MeOD- d_4) furanyl: 112.01; 114.33; 140.61; 148.97; naphthalene: 110; 118.84; 120.48; 123.15; 125.65; 128.14; 128.33; 130; 136.66; 154.87; imine: 145.55. FTIR (cm^{-1} , KBr pellet): 3416, 3210 (broad); 1638; 1520; 1310; 1243; 1223; 554; 409.

$\text{Zn}(\text{L}^3)_2$ (9). A bright yellow solid was obtained. Yield: 96.4 mg (49%). Elem. An. (%) found C, 61.0; H, 3.7; N, 8.8; S, 10.6 [calc. for $\text{C}_{32}\text{H}_{22}\text{N}_4\text{O}_4\text{S}_2\text{Zn} \cdot 1.5(\text{C}_{16}\text{H}_{12}\text{N}_2\text{O}_2\text{S})$: C, 61.12; H, 3.66; N, 8.91; S, 10.20]. ESI-MS m/z 655.10 [calc. for $[\text{ML}_2 + \text{H}]^+$ 655.04]; 653.20 [calc. for $[\text{ML}_2 - \text{H}]^-$ 653.04]. ^1H NMR (δ , ppm; DMSO- d_6) 7.16 (thioph); 7.29 (naph); 7.35 (thioph); 7.47 (naph); 7.54 (thioph); 7.79 (2H, naph); 7.89 (naph); 8.42 (naph); 8.65 (imine). ^{13}C NMR (δ , ppm; DMSO- d_6) 110.78; 121; 123.96 (thioph); 126; 126.88; 128.36 (thioph); 128.4; 128.88; 130.61; 131.7 (thioph); 136.34; 139.54 (thioph); 143.88 (imine); 154.70; 164.11 (COZn). FTIR (cm^{-1} , KBr pellet): 3440 (broad); 3167; 1578; 1554; 1240; 1219; 1150; 536; 411.

4.3 X-ray diffraction

A crystal of ligand precursor HL^2 was selected, covered with polyfluoroether oil, and mounted on a nylon loop. Crystallographic data were collected using graphite monochromated Mo-K α radiation ($\lambda = 0.71073 \text{ \AA}$) on a Bruker AXS-KAPPA APEX II diffractometer, at room temperature. Cell parameters were retrieved using Bruker SMART software and refined using Bruker SAINT on all observed reflections. Absorption correction was applied using SADABS.⁵² Structure solution and refinement were performed using direct methods with the program SIR2019,⁵³ included in the package of programs WINGX-

1 (calc. for $[L + H]^+$ 297.34); 295.15 (calc. for $[L - H]^-$ 295.34). ^1H NMR (δ , ppm; DMSO- d_6) 7.17 (thioph); 7.32 (naph); 7.36 (naph); 7.51 (thioph + naph); 7.71 (thioph); 7.76 (naph); 7.91 (naph); 8.4 (naph); 8.67 (imine); 11.25 (OH); 11.93 (NH). ^{13}C NMR (δ , ppm; DMSO- d_6) 110.76; 120.7; 124; 126.1; 127; 128.2; 128.4 (thioph); 128.9; 129.5 (thioph); 130.4; 131.6 (thioph); 136; 139 (thioph); 143.72 (imine); 154.19; 163.76 (carbonyl). FTIR (cm^{-1} , KBr pellet): 3440 (OH, stretching), 3246; 3058 (NH on Schiff base moiety); 1639 (carbonyl); 1621; 1600; 1558 (imine); 1227 (naphthol, OH).

4.2.2 Synthesis of complexes. The synthesis of the complexes followed the general procedure: 2 eq. of the corresponding ligand precursor were deprotonated in MeOH using 2 eq. of sodium acetate. Then 1 eq. of either $\text{CuCl}_2 \cdot 2\text{H}_2\text{O}$, $\text{VOCl}_2 \cdot 2\text{H}_2\text{O}$ or $\text{ZnCl}_2 \cdot 2\text{H}_2\text{O}$ was added and the mixture was left to stir at $\sim 40^\circ\text{C}$ for 2.5 h. For the oxidovanadium(IV) complexes, degassed MeOH and N_2 atmosphere were used throughout the synthetic procedure. The solid compounds formed in these reactions were collected by filtration, washed with cold MeOH and dried under vacuum.

$\text{VO}(\text{L}^1)_2$ (1). A brown solid was obtained. Yield: 87.5 mg (70%). Elem. an. (%) found C, 61.1; H, 4.0; N, 13.0 and V, 8.4 [calc. for $\text{C}_{32}\text{H}_{24}\text{N}_6\text{O}_5\text{V} \cdot 0.5\text{MeOH}$: C, 61.04; H, 4.10; N, 13.14 and V, 7.97]. ESI-MS m/z 654.82 [calc. for $[\text{ML}_2 + \text{MeOH} - \text{H}]^-$ 654.15]. FTIR (cm^{-1} , KBr pellet): 3383 (broad); 3231 (medium broad); 1642; 1612; 1578; 1543; 1241; 1216; 1147; 897; 554; 404.

$\text{VO}(\text{L}^2)_2$ (2). A brown solid was obtained. Yield: 129.6 mg (68.6%). Elem. an. (%) found C, 60.4; H, 3.5; N, 8.5 and V, 7.8 [calc. for $\text{C}_{32}\text{H}_{22}\text{N}_4\text{O}_5\text{V} \cdot 0.5\text{H}_2\text{O}$: C, 60.58; H, 3.65; N, 8.83 and V, 8.03]. ESI-MS m/z 644.28 [calc. for $[\text{ML}_2 + \text{H}_2\text{O} + \text{H}]^+$ 644.09]; 658.44 [calc. for $[\text{ML}_2 + \text{MeOH} + \text{H}]^+$ 658.09]. FTIR (cm^{-1} , KBr pellet): 3433 (broad); 1640; 1532; 1296; 1242; 1219; 906; 555; 401.

$\text{VO}(\text{L}^3)_2$ (3). A dark brown solid was obtained. Yield: 164.8 mg (99%). Elem. an. (%) found C, 52.9; H, 3.4; N, 7.6; S, 8.81 [calc. for $\text{C}_{32}\text{H}_{22}\text{N}_4\text{O}_5\text{S}_2\text{V} \cdot 4\text{H}_2\text{O}$: C, 52.67; H, 4.14; N, 7.68; S, 8.79]. ESI-MS m/z 688.96 [calc. for $[\text{ML}_2 + \text{MeOH} - \text{H}]^-$ 688.61]. FTIR (cm^{-1} , KBr pellet): 3445 (broad); 3253; 3057; 1642; 1621; 1600; 1559; 1511; 1449; 1361; 1319; 1228; 1174; 1151; 1068; 1044; 973; 949; 873; 855; 834; 748; 707; 627; 473.

$\text{Cu}(\text{L}^1)_2$ (4). A light brown solid was obtained. Yield: 105 mg (84.7%). Elem. an. (%) found C, 61.6; H, 4.0; N, 13.1 and Cu, 10.0 [calc. for $\text{C}_{32}\text{H}_{24}\text{CuN}_6\text{O}_4 \cdot 0.5\text{MeOH}$: C, 61.36; H, 4.12; N, 13.21 and Cu, 9.99]. ESI-MS m/z 618.27 [calc. for $[\text{ML}_2 - \text{H}]^-$ 618.12]; 654.39 [calc. for $[\text{ML}_2 + \text{Cl}]^-$ 654.12]. FTIR (cm^{-1} , KBr pellet): 3430 (broad); 3167; 1578; 1554; 1240; 1219; 1150; 556; 405.

$\text{Cu}(\text{L}^2)_2$ (5). A light green solid was obtained. Yield: 131.5 mg (84%). Elem. an. (%) found C, 61.4; H, 3.7; N, 8.8 and Cu, 10.0 [calc. for $\text{C}_{32}\text{H}_{22}\text{CuN}_4\text{O}_6 \cdot 0.5\text{MeOH}$: C, 61.17; H, 3.79; N, 8.78 and Cu, 9.96]. ESI-MS m/z 656.79 [calc. for $[\text{ML}_2 + \text{Cl}]^-$ 656.08]. FTIR (cm^{-1} , KBr pellet): 3444 (broad); 1640; 1537; 1311; 1243; 1221; 559; 406.

$\text{Cu}(\text{L}^3)_2$ (6). A dark green solid was obtained. Yield: 162.3 mg (98%). Elem. an. (%) found C, 58.0; H, 3.8; N, 8.4; S, 9.6 [calc. for $\text{C}_{32}\text{H}_{22}\text{CuN}_4\text{O}_4\text{S}_2 \cdot 0.5\text{MeOH}$: C, 58.24; H, 3.61; N, 8.36; S, 9.57]. ESI-MS m/z 653.80 [calc. for $[\text{ML}_2 + \text{H}]^+$ 654.04]. FTIR (cm^{-1} , KBr pellet): 3445; 3356; 3253; 3057; 1636; 1624; 1600; 1559; 1509; 1449; 1361; 1316; 1228; 1172; 1148; 1065; 1044; 949; 873; 852; 834; 748; 707; 624; 470.

$\text{Zn}(\text{L}^1)_2$ (7). A yellow solid was obtained. Yield: 148 mg (79%). Elem. an. (%) found C, 61.8; H, 4.0; N, 13.3 and Zn, 10.0 [calc. for $\text{C}_{32}\text{H}_{24}\text{N}_6\text{O}_4\text{Zn}$: C, 61.79; H, 3.89; N, 13.51 and Zn, 10.51]. ESI-MS m/z 643.92 [calc. for $[\text{ML}_2 + \text{Na}]^+$ 643.11]. ^1H NMR (δ , ppm; DMSO- d_6) 6.36, 7.01, 7.26 (pyrrolyl ring); naphthalene: 7.26, 7.29, 7.45, 7.74, 7.80 and 8.46; 8.68 (HC=N, imine); OH: 13.32; and NH (pyrrole): 12.6. ^{13}C NMR (δ , ppm; DMSO- d_6) 110.52; 111.37 (pyr); 120.36; 120.46 (pyr); 123.27; 125.41 (pyr); 125.84; 126.72; 126.72 (pyr); 127.72; 128.90; 129.53; 135.8; 148.17 (imine); 156.03 (naph); 167.20 (COZn). FTIR (cm^{-1} , KBr pellet): 3380 (broad); 3187; 1576; 1546; 1231; 1223; 1150; 547; 428.

$\text{Zn}(\text{L}^2)_2$ (8). A yellow solid was obtained. Yield: 131.9 mg (71%). Elem. An. (%) found C, 61.9; H, 3.9; N, 8.9 [calc. for $\text{C}_{32}\text{H}_{22}\text{N}_4\text{O}_6\text{Zn}$: C, 61.60; H, 3.55; N, 8.98]. ESI (+) m/z 623.15 [calc. for $[\text{ML}_2 + \text{H}]^+$ 623.08]. ESI-MS m/z 621.14 [calc. for $[\text{ML}_2 - \text{H}]^-$ 621.08]. ^1H NMR (δ , ppm; MeOD- d_4) 6.58 (fur); 7.07 (fur); 7.25 (naph); 7.30 (naph) 7.46 (naph); 7.64 (imine); 7.69 (naph); 7.84 (naph); 8.43 (fur); 8.55 (naph). ^{13}C NMR (δ , ppm; MeOD- d_4) furanyl: 112.01; 114.33; 140.61; 148.97; naphthalene: 110; 118.84; 120.48; 123.15; 125.65; 128.14; 128.33; 130; 136.66; 154.87; imine: 145.55. FTIR (cm^{-1} , KBr pellet): 3416, 3210 (broad); 1638; 1520; 1310; 1243; 1223; 554; 409.

$\text{Zn}(\text{L}^3)_2$ (9). A bright yellow solid was obtained. Yield: 96.4 mg (49%). Elem. An. (%) found C, 61.0; H, 3.7; N, 8.8; S, 10.6 [calc. for $\text{C}_{32}\text{H}_{22}\text{N}_4\text{O}_4\text{S}_2\text{Zn} \cdot 1.5(\text{C}_{16}\text{H}_{12}\text{N}_2\text{O}_2\text{S})$: C, 61.12; H, 3.66; N, 8.91; S, 10.20]. ESI-MS m/z 655.10 [calc. for $[\text{ML}_2 + \text{H}]^+$ 655.04]; 653.20 [calc. for $[\text{ML}_2 - \text{H}]^-$ 653.04]. ^1H NMR (δ , ppm; DMSO- d_6) 7.16 (thioph); 7.29 (naph); 7.35 (thioph); 7.47 (naph); 7.54 (thioph); 7.79 (2H, naph); 7.89 (naph); 8.42 (naph); 8.65 (imine). ^{13}C NMR (δ , ppm; DMSO- d_6) 110.78; 121; 123.96 (thioph); 126; 126.88; 128.36 (thioph); 128.4; 128.88; 130.61; 131.7 (thioph); 136.34; 139.54 (thioph); 143.88 (imine); 154.70; 164.11 (COZn). FTIR (cm^{-1} , KBr pellet): 3440 (broad); 3167; 1578; 1554; 1240; 1219; 1150; 536; 411.

4.3 X-ray diffraction

A crystal of ligand precursor HL^2 was selected, covered with polyfluoroether oil, and mounted on a nylon loop. Crystallographic data were collected using graphite monochromated Mo-K α radiation ($\lambda = 0.71073 \text{ \AA}$) on a Bruker AXS-KAPPA APEX II diffractometer, at room temperature. Cell parameters were retrieved using Bruker SMART software and refined using Bruker SAINT on all observed reflections. Absorption correction was applied using SADABS.⁵² Structure solution and refinement were performed using direct methods with the program SIR2019,⁵³ included in the package of programs WINGX-

1 (calc. for $[L + H]^+$ 297.34); 295.15 (calc. for $[L - H]^-$ 295.34). ^1H NMR (δ , ppm; DMSO- d_6) 7.17 (thioph); 7.32 (naph); 7.36 (naph); 7.51 (thioph + naph); 7.71 (thioph); 7.76 (naph); 7.91 (naph); 8.4 (naph); 8.67 (imine); 11.25 (OH); 11.93 (NH). ^{13}C NMR (δ , ppm; DMSO- d_6) 110.76; 120.7; 124; 126.1; 127; 128.2; 128.4 (thioph); 128.9; 129.5 (thioph); 130.4; 131.6 (thioph); 136; 139 (thioph); 143.72 (imine); 154.19; 163.76 (carbonyl). FTIR (cm^{-1} , KBr pellet): 3440 (OH, stretching), 3246; 3058 (NH on Schiff base moiety); 1639 (carbonyl); 1621; 1600; 1558 (imine); 1227 (naphthol, OH).

4.2.2 Synthesis of complexes. The synthesis of the complexes followed the general procedure: 2 eq. of the corresponding ligand precursor were deprotonated in MeOH using 2 eq. of sodium acetate. Then 1 eq. of either $\text{CuCl}_2 \cdot 2\text{H}_2\text{O}$, $\text{VOCl}_2 \cdot 2\text{H}_2\text{O}$ or $\text{ZnCl}_2 \cdot 2\text{H}_2\text{O}$ was added and the mixture was left to stir at $\sim 40^\circ\text{C}$ for 2.5 h. For the oxidovanadium(IV) complexes, degassed MeOH and N_2 atmosphere were used throughout the synthetic procedure. The solid compounds formed in these reactions were collected by filtration, washed with cold MeOH and dried under vacuum.

$\text{VO}(\text{L}^1)_2$ (1). A brown solid was obtained. Yield: 87.5 mg (70%). Elem. an. (%) found C, 61.1; H, 4.0; N, 13.0 and V, 8.4 [calc. for $\text{C}_{32}\text{H}_{24}\text{N}_6\text{O}_5\text{V} \cdot 0.5\text{MeOH}$: C, 61.04; H, 4.10; N, 13.14 and V, 7.97]. ESI-MS m/z 654.82 [calc. for $[\text{ML}_2 + \text{MeOH} - \text{H}]^-$ 654.15]. FTIR (cm^{-1} , KBr pellet): 3383 (broad); 3231 (medium broad); 1642; 1612; 1578; 1543; 1241; 1216; 1147; 897; 554; 404.

$\text{VO}(\text{L}^2)_2$ (2). A brown solid was obtained. Yield: 129.6 mg (68.6%). Elem. an. (%) found C, 60.4; H, 3.5; N, 8.5 and V, 7.8 [calc. for $\text{C}_{32}\text{H}_{22}\text{N}_4\text{O}_5\text{V} \cdot 0.5\text{H}_2\text{O}$: C, 60.58; H, 3.65; N, 8.83 and V, 8.03]. ESI-MS m/z 644.28 [calc. for $[\text{ML}_2 + \text{H}_2\text{O} + \text{H}]^+$ 644.09]; 658.44 [calc. for $[\text{ML}_2 + \text{MeOH} + \text{H}]^+$ 658.09]. FTIR (cm^{-1} , KBr pellet): 3433 (broad); 1640; 1532; 1296; 1242; 1219; 906; 555; 401.

$\text{VO}(\text{L}^3)_2$ (3). A dark brown solid was obtained. Yield: 164.8 mg (99%). Elem. an. (%) found C, 52.9; H, 3.4; N, 7.6; S, 8.81 [calc. for $\text{C}_{32}\text{H}_{22}\text{N}_4\text{O}_5\text{S}_2\text{V} \cdot 4\text{H}_2\text{O}$: C, 52.67; H, 4.14; N, 7.68; S, 8.79]. ESI-MS m/z 688.96 [calc. for $[\text{ML}_2 + \text{MeOH} - \text{H}]^-$ 688.61]. FTIR (cm^{-1} , KBr pellet): 3445 (broad); 3253; 3057; 1642; 1621; 1600; 1559; 1511; 1449; 1361; 1319; 1228; 1174; 1151; 1068; 1044; 973; 949; 873; 855; 834; 748; 707; 627; 473.

$\text{Cu}(\text{L}^1)_2$ (4). A light brown solid was obtained. Yield: 105 mg (84.7%). Elem. an. (%) found C, 61.6; H, 4.0; N, 13.1 and Cu, 10.0 [calc. for $\text{C}_{32}\text{H}_{24}\text{CuN}_6\text{O}_4 \cdot 0.5\text{MeOH}$: C, 61.36; H, 4.12; N, 13.21 and Cu, 9.99]. ESI-MS m/z 618.27 [calc. for $[\text{ML}_2 - \text{H}]^-$ 618.12]; 654.39 [calc. for $[\text{ML}_2 + \text{Cl}]^-$ 654.12]. FTIR (cm^{-1} , KBr pellet): 3430 (broad); 3167; 1578; 1554; 1240; 1219; 1150; 556; 405.

$\text{Cu}(\text{L}^2)_2$ (5). A light green solid was obtained. Yield: 131.5 mg (84%). Elem. an. (%) found C, 61.4; H, 3.7; N, 8.8 and Cu, 10.0 [calc. for $\text{C}_{32}\text{H}_{22}\text{CuN}_4\text{O}_6 \cdot 0.5\text{MeOH}$: C, 61.17; H, 3.79; N, 8.78 and Cu, 9.96]. ESI-MS m/z 656.79 [calc. for $[\text{ML}_2 + \text{Cl}]^-$ 656.08]. FTIR (cm^{-1} , KBr pellet): 3444 (broad); 1640; 1537; 1311; 1243; 1221; 559; 406.

$\text{Cu}(\text{L}^3)_2$ (6). A dark green solid was obtained. Yield: 162.3 mg (98%). Elem. an. (%) found C, 58.0; H, 3.8; N, 8.4; S, 9.6 [calc. for $\text{C}_{32}\text{H}_{22}\text{CuN}_4\text{O}_4\text{S}_2 \cdot 0.5\text{MeOH}$: C, 58.24; H, 3.61; N, 8.36; S, 9.57]. ESI-MS m/z 653.80 [calc. for $[\text{ML}_2 + \text{H}]^+$ 654.04]. FTIR (cm^{-1} , KBr pellet): 3445; 3356; 3253; 3057; 1636; 1624; 1600; 1559; 1509; 1449; 1361; 1316; 1228; 1172; 1148; 1065; 1044; 949; 873; 852; 834; 748; 707; 624; 470.

$\text{Zn}(\text{L}^1)_2$ (7). A yellow solid was obtained. Yield: 148 mg (79%). Elem. an. (%) found C, 61.8; H, 4.0; N, 13.3 and Zn, 10.0 [calc. for $\text{C}_{32}\text{H}_{24}\text{N}_6\text{O}_4\text{Zn}$: C, 61.79; H, 3.89; N, 13.51 and Zn, 10.51]. ESI-MS m/z 643.92 [calc. for $[\text{ML}_2 + \text{Na}]^+$ 643.11]. ^1H NMR (δ , ppm; DMSO- d_6) 6.36, 7.01, 7.26 (pyrrolyl ring); naphthalene: 7.26, 7.29, 7.45, 7.74, 7.80 and 8.46; 8.68 (HC=N, imine); OH: 13.32; and NH (pyrrole): 12.6. ^{13}C NMR (δ , ppm; DMSO- d_6) 110.52; 111.37 (pyr); 120.36; 120.46 (pyr); 123.27; 125.41 (pyr); 125.84; 126.72; 126.72 (pyr); 127.72; 128.90; 129.53; 135.8; 148.17 (imine); 156.03 (naph); 167.20 (COZn). FTIR (cm^{-1} , KBr pellet): 3380 (broad); 3187; 1576; 1546; 1231; 1223; 1150; 547; 428.

$\text{Zn}(\text{L}^2)_2$ (8). A yellow solid was obtained. Yield: 131.9 mg (71%). Elem. An. (%) found C, 61.9; H, 3.9; N, 8.9 [calc. for $\text{C}_{32}\text{H}_{22}\text{N}_4\text{O}_6\text{Zn}$: C, 61.60; H, 3.55; N, 8.98]. ESI (+) m/z 623.15 [calc. for $[\text{ML}_2 + \text{H}]^+$ 623.08]. ESI-MS m/z 621.14 [calc. for $[\text{ML}_2 - \text{H}]^-$ 621.08]. ^1H NMR (δ , ppm; MeOD- d_4) 6.58 (fur); 7.07 (fur); 7.25 (naph); 7.30 (naph) 7.46 (naph); 7.64 (imine); 7.69 (naph); 7.84 (naph); 8.43 (fur); 8.55 (naph). ^{13}C NMR (δ , ppm; MeOD- d_4) furanyl: 112.01; 114.33; 140.61; 148.97; naphthalene: 110; 118.84; 120.48; 123.15; 125.65; 128.14; 128.33; 130; 136.66; 154.87; imine: 145.55. FTIR (cm^{-1} , KBr pellet): 3416, 3210 (broad); 1638; 1520; 1310; 1243; 1223; 554; 409.

$\text{Zn}(\text{L}^3)_2$ (9). A bright yellow solid was obtained. Yield: 96.4 mg (49%). Elem. An. (%) found C, 61.0; H, 3.7; N, 8.8; S, 10.6 [calc. for $\text{C}_{32}\text{H}_{22}\text{N}_4\text{O}_4\text{S}_2\text{Zn} \cdot 1.5(\text{C}_{16}\text{H}_{12}\text{N}_2\text{O}_2\text{S})$: C, 61.12; H, 3.66; N, 8.91; S, 10.20]. ESI-MS m/z 655.10 [calc. for $[\text{ML}_2 + \text{H}]^+$ 655.04]; 653.20 [calc. for $[\text{ML}_2 - \text{H}]^-$ 653.04]. ^1H NMR (δ , ppm; DMSO- d_6) 7.16 (thioph); 7.29 (naph); 7.35 (thioph); 7.47 (naph); 7.54 (thioph); 7.79 (2H, naph); 7.89 (naph); 8.42 (naph); 8.65 (imine). ^{13}C NMR (δ , ppm; DMSO- d_6) 110.78; 121; 123.96 (thioph); 126; 126.88; 128.36 (thioph); 128.4; 128.88; 130.61; 131.7 (thioph); 136.34; 139.54 (thioph); 143.88 (imine); 154.70; 164.11 (COZn). FTIR (cm^{-1} , KBr pellet): 3440 (broad); 3167; 1578; 1554; 1240; 1219; 1150; 536; 411.

4.3 X-ray diffraction

A crystal of ligand precursor HL^2 was selected, covered with polyfluoroether oil, and mounted on a nylon loop. Crystallographic data were collected using graphite monochromated Mo-K α radiation ($\lambda = 0.71073 \text{ \AA}$) on a Bruker AXS-KAPPA APEX II diffractometer, at room temperature. Cell parameters were retrieved using Bruker SMART software and refined using Bruker SAINT on all observed reflections. Absorption correction was applied using SADABS.⁵² Structure solution and refinement were performed using direct methods with the program SIR2019,⁵³ included in the package of programs WINGX-

1 4.7.2 **Brine shrimp lethality bioassay.** In order to evaluate
the general toxicity of the different compounds, a test of
lethality to *Artemia salina* brine shrimp was performed as
described in ref. 66. Concentrations of 10 ppm of each com-
5 pound were tested. The number of dead larvae was recorded
after 24 hours and used to calculate the lethal concentration
(%), according to eqn (5).

$$\text{Lethal concentration (\%)} = \frac{(\text{Total}_{A. salina} - \text{Alive}_{A. salina})}{\text{Total}_{A. salina}} \times 100 \quad (5)$$

15 4.7.3 **In vitro antitumor activity of the compounds.** All
tested compounds were dissolved in dimethyl sulfoxide (DMSO;
Sigma-Aldrich). Human breast adenocarcinoma MCF7 and
non-small cell lung carcinoma H1299 were purchased from
the ATCC (Rockville, MD, USA); human colon adenocarcinoma
HCT116 p53+/+ and p53-/- cell lines were provided by B.
Vogelstein (The Johns Hopkins Kimmel Cancer Center, Balti-
20 more, MD, USA). Tumor cells were cultured in RPMI-1640 with
UltraGlutamine (Lonza, VWR), supplemented with (10%) fetal
bovine serum (FBS; Merck Millipore, VWR). Cell lines were
maintained in a humidified incubator at 37 °C with 5% CO₂.
Cells were routinely tested for mycoplasma infection using the
25 MycoAlert™ PLUS mycoplasma detection kit (Lonza, VWR).
Human cancer cells were seeded in 96-well plates at a density
of 7.5 × 10³ (H1299) and 5.0 × 10³ (MCF7 and HCT116) cells
per well, followed by analysis of the compounds' effect on cell
proliferation after 48 h treatment with serial dilutions (3.13–50
30 μM) of compounds, as described in ref. 67. The solvent (DMSO);
maximum concentration used 0.25%) was included as control.
The IC₅₀ (μM) of the compounds was determined. Data are
mean ± SEM of 4 independent experiments.

35 Conflicts of interest

Q6

40 Acknowledgements

This work was supported by Fundação para a Ciência e a Tecnologia
(FCT) (projects UID/QUI/00100/2019, UID/MULTI/04349/2013, UID/
BIO/04565/2013, RECI/QEQ-QIN/0189/2012, RECI/QEQ-MED/0330/
2012, UID/DTP/04567/2016, UID/04138/2019, SAICTPAC/0019/2015,
45 PTDC/QUI-QAN/32242/2017, PD/BD/128320/2017, SFRH/BD/135797/
2018 and SFRH/BPD/107834/2015) and Programa Operacional
Regional de Lisboa (LISBOA-01-0145-FEDER-007317). The Portu-
guese NMR and Mass Spectrometry IST-UL Centers are acknowl-
50 edged for access to the equipment

References

1 S. Thota, D. A. Rodrigues, P. D. M. Pinheiro, L. M. Lima,
55 C. A. M. Fraga and E. J. Barreiro, *Bioorg. Med. Chem. Lett.*,
2018, 28, 2797–2806.

2 Z. H. Xu, X. W. Zhang, W. Q. Zhang, Y. H. Gao and
Z. Z. Zeng, *Inorg. Chem. Commun.*, 2011, 14, 1569–1573.

3 A. A. R. Despaigne, F. B. Da Costa, O. E. Piro,
E. E. Castellano, S. R. W. Louro and H. Beraldo, *Polyhedron*,
2012, 38, 285–290. 5

4 K. Hruskova, E. Potuckova, T. Hergeselova, L. Liptakova,
P. Haskova, P. Mingas, P. Kovarikova, T. Simunek and
K. Vavrova, *Eur. J. Med. Chem.*, 2016, 120, 97–110.

5 D. R. Guay, *Drugs*, 2001, 61, 353–364.

6 M. Alagesan, N. S. P. Bhuvanesh and N. Dharmaraj, *Eur.*
J. Med. Chem., 2014, 78, 281–293. 10

7 M. Sutradhar, Rajeshwari, T. R. Barman, A. R. Fernandes,
F. Paradinha, C. Roma-Rodrigues, M. F. C. G. da Silva and
A. J. L. Pombeiro, *J. Inorg. Biochem.*, 2017, 175, 267–275. Q7

8 R. Grybos, J. Szklarzewicz, A. Jurowska and M. Hodorowicz,
J. Mol. Struct., 2018, 1171, 880–887. 15

9 K. M. Ibrahim, I. M. Gabr and R. R. Zaky, *J. Coord. Chem.*,
2009, 62, 1100–1111.

10 K. M. Ibrahim, I. M. Gabr, G. M. Abu El-Reash and
R. R. Zaky, *Monatsh. Chem.*, 2009, 140, 625–632. 20

11 R. R. Zaky, K. M. Ibrahim and I. M. Gabr, *Spectrochim. Acta*,
Part A, 2011, 81, 28–34.

12 R. R. Zaky, T. A. Yousef and K. M. Ibrahim, *Spectrochim.*
Acta, Part A, 2012, 97, 683–694.

13 D. Matoga, *Polyhedron*, 2013, 50, 576–581. 25

14 H. D. Yin and S. W. Chen, *Inorg. Chim. Acta*, 2006, 359,
3330–3338.

15 P. Paciorek, J. Szklarzewicz, A. Jasinska, B. Trzewik, W. Nitek
and M. Hodorowicz, *Polyhedron*, 2015, 87, 226–232.

16 P. Singh, D. P. Singh and V. P. Singh, *Polyhedron*, 2014, 81,
56–65. 30

17 J. C. Pessoa, S. Etcheverry and D. Gambino, *Coord. Chem.*
Rev., 2015, 301, 24–48.

18 S. Tardito and L. Marchio, *Curr. Med. Chem.*, 2009, 16,
1325–1348. 35

19 C. Marzano, M. Pellei, F. Tisato and C. Santini, *Anti-Cancer*
Agents Med. Chem., 2009, 9, 185–211.

20 J. Osredkar and N. Sustar, *J. Clin. Toxicol.*, 2011, S:3. Q8

21 D. Desbouis, I. P. Troitsky, M. J. Belousoff, L. Spiccia and
B. Graham, *Coord. Chem. Rev.*, 2012, 256, 897–937. 40

22 O. G. Tsay, S. T. Manjare, H. Kim, K. M. Lee, Y. S. Lee and
D. G. Churchill, *Inorg. Chem.*, 2013, 52, 10052–10061.

23 S. Rodriguez-Hemida, A. B. Lago, R. Carballo, O. Fabelo and
E. M. Vazquez-Lopez, *Chem. – Eur. J.*, 2015, 21, 6605–6616.

24 F. Borbone, U. Caruso, S. Concilio, S. Nabha, B. Panunzi,
S. Piotto, R. Shikler and A. Tuzi, *Eur. J. Inorg. Chem.*, 2016,
818–825. 45

25 Q. K. Wu, H. D. Yin and D. Q. Wang, *Acta Crystallogr., Sect.*
E: Struct. Rep. Online, 2011, 67, O277–U1933.

26 I. Correia, J. C. Pessoa, M. T. Duarte, R. T. Henriques,
M. F. M. Piedade, L. F. Veiros, T. Jakusch, T. Kiss,
A. Dornyei, M. M. C. A. Castro, C. F. G. C. Geraldés and
F. Aveçilla, *Chem. – Eur. J.*, 2004, 10, 2301–2317.

27 I. Correia, J. C. Pessoa, M. T. Duarte, M. F. M. da Piedade,
T. Jackush, T. Kiss, M. M. C. A. Castro, C. F. G. C. Geraldés
and F. Aveçilla, *Eur. J. Inorg. Chem.*, 2005, 732–744. 55

- 1 28 D. E. Hamilton, *Inorg. Chem.*, 1991, 30, 1670–1671.
- 29 R. G. Cavell, W. Byers, P. M. Watkins and E. D. Day, *Inorg. Chem.*, 1972, 11, 1591–1597.
- 30 M. Mathew, A. J. Carty and G. J. Palenik, *J. Am. Chem. Soc.*, 1970, 92, 3197–3198.
- 31 A. Rockenbauer and L. Korecz, *Appl. Magn. Reson.*, 1996, 10, 29–43.
- 32 U. Sakaguchi and A. W. Addison, *J. Chem. Soc., Dalton Trans.*, 1979, 569–608.
- 33 G. Tabbi, A. Giuffrida and R. P. Bonomo, *J. Inorg. Biochem.*, 2013, 128, 137–145.
- 34 N. D. Chasteen, *Biological Magnetic Resonance*, Plenum, New York, 1981.
- 35 T. S. Smith, R. LoBrutto and V. L. Pecoraro, *Coord. Chem. Rev.*, 2002, 228, 1–18.
- 36 J. C. Pessoa, S. M. Luz and R. D. Gillard, *J. Chem. Soc., Dalton Trans.*, 1997, 569–576.
- 37 S. Gorelsky, G. Micera and E. Garribba, *Chem. – Eur. J.*, 2010, 16, 8167–8180.
- 38 T. Yanai, D. P. Tew and N. C. Handy, *Chem. Phys. Lett.*, 2004, 393, 51–57.
- 39 B. X. Huang, H. Y. Kim and C. Dass, *J. Am. Soc. Mass Spectrom.*, 2004, 15, 1237–1247.
- 40 R. Rajan and P. Balaram, *Int. J. Pept. Protein Res.*, 1996, 48, 328–336.
- 41 F. Samari, B. Hemmateenejad, M. Shamsipur, M. Rashidi and H. Samouei, *Inorg. Chem.*, 2012, 51, 3454–3464.
- 42 N. Ribeiro, R. E. Di Paolo, A. M. Galvao, F. Marques, J. C. Pessoa and I. Correia, *Spectrochim. Acta, Part A*, 2018, 204, 317–327.
- 43 W. R. Lakowicz, *Principles of Fluorescence Spectroscopy*, Springer, 3rd edn, 2006.
- 44 M. van de Weert and L. Stella, *J. Mol. Struct.*, 2011, 998, 144–150.
- 45 B. Sekula, K. Zielinski and A. Bujacz, *Int. J. Biol. Macromol.*, 2013, 60, 316–324.
- 46 D. Buttar, N. Colclough, S. Gerhardt, P. A. MacFaul, S. D. Phillips, A. Plowright, P. Whittamore, K. Tam, K. Maskos, S. Steinbacher and H. Steuber, *Bioorg. Med. Chem.*, 2010, 18, 7486–7496.
- 47 F. Wang, H. D. Yin, J. C. Cui, Y. W. Zhang, H. L. Geng and M. Hong, *J. Organomet. Chem.*, 2014, 759, 83–91.
- 48 J. Dam, Z. Ismail, T. Kurebwa, N. Gangat, L. Harmse, H. M. Marques, A. Lemmerer, M. L. Bode and C. B. de Koning, *Eur. J. Med. Chem.*, 2017, 126, 353–368.
- 49 M. K. Koley, N. Duraipandy, M. S. Kiran, B. Varghese, P. T. Manoharan and A. P. Koley, *Inorg. Chim. Acta*, 2017, 466, 538–550.
- 50 I. Correia, P. Adao, S. Roy, M. Wahba, C. Matos, M. R. Maurya, F. Marques, F. R. Pavan, C. Q. F. Leite, F. Avecilla and J. C. Pessoa, *J. Inorg. Biochem.*, 2014, 141, 83–93.
- 51 I. Correia, S. Roy, C. P. Matos, S. Borovic, N. Butenko, I. Cavaco, F. Marques, J. Lorenzo, A. Rodriguez, V. Moreno and J. C. Pessoa, *J. Inorg. Biochem.*, 2015, 147, 134–146.
- 52 G. M. Sheldrick, *SADABS, Program for Empirical Absorption Correction*, University of Göttingen: Göttingen, Germany, 1996.
- 53 M. C. Burla, R. Caliandro, B. Carrozzini, G. L. Cascarano, C. Cuocci, C. Giacovazzo, M. Mallamo, A. Mazzone and G. Polidori, *J. Appl. Crystallogr.*, 2015, 48, 306–309.
- 54 L. J. Farrugia, *J. Appl. Crystallogr.*, 2012, 45, 849–854.
- 55 G. M. Sheldrick, *Acta Crystallogr., Sect. A: Found. Crystallogr.*, 2008, 64, 112–122.
- 56 G. M. Sheldrick, *SHELX97 - Programs for Crystal Structure Analysis (Release 97-2)*, Institut für Anorganische Chemie der Universität, Tammanstrasse 4, D-3400 Göttingen, Germany, 1998.
- 57 M. W. Schmidt, K. K. Baldrige, J. A. Boatz, S. T. Elbert, M. S. Gordon, J. H. Jensen, S. Koseki, N. Matsunaga, K. A. Nguyen, S. J. Su, T. L. Windus, M. Dupuis and J. A. Montgomery, *J. Comput. Chem.*, 1993, 14, 1347–1363.
- 58 J. Pina, D. Sarmento, M. Accoto, P. L. Gentili, L. Vaccaro, A. Galvao and J. S. S. de Melo, *J. Phys. Chem. B*, 2017, 121, 2308–2318.
- 59 N. J. Greenfield, *Nat. Protoc.*, 2006, 1, 2876–2890.
- 60 S. M. Kelly, T. J. Jess and N. C. Price, *Biochim. Biophys. Acta, Proteins Proteomics*, 2005, 1751, 119–139.
- 61 V. D. Suryawanshi, L. S. Walekar, A. H. Gore, P. V. Anbhule and G. B. Kolekar, *J. Pharm. Anal.*, 2016, 6, 56–63.
- 62 A. Coutinho and M. Prieto, *J. Chem. Educ.*, 1993, 70, 425–428.
- 63 J. T. Marques and R. F. M. de Almeida, *J. Chem. Educ.*, 2013, 90, 1522–1527.
- 64 G. Jones, P. Willett, R. C. Glen, A. R. Leach and R. Taylor, *J. Mol. Biol.*, 1997, 267, 727–748.
- 65 G. Sciortino, J. R. G. Pedregal, A. Lledos, E. Garribba and J. D. Marechal, *J. Comput. Chem.*, 2018, 39, 42–51.
- 66 E. Ntungwe, J. Marçalo, C. Garcia, C. Reis, C. Teodósio, C. Oliveira, C. Oliveira, A. Roberto and P. Rijo, *Biomed. Biopharm. Res.*, 2017, 14, 95–108.
- 67 L. Raimundo, M. Espadinha, J. Soares, J. B. Loureiro, M. G. Alves, M. M. M. Santos and L. Saraiva, *Br. J. Pharmacol.*, 2018, 175, 3947–3962.

50

50

55

55



Royleanone Derivatives From *Plectranthus* spp. as a Novel Class of P-Glycoprotein Inhibitors

Catarina Garcia^{1,2†}, Vera M. S. Isca^{1,3†}, Filipe Pereira¹, Carlos M. Monteiro³, Epole Ntungwe^{1,2}, Francisco Sousa¹, Jelena Dinic⁴, Sivi Holmstedt⁵, Amílcar Roberto¹, Ana Díaz-Lanza², Catarina P. Reis³, Milica Pesic⁴, Nuno R. Candeias^{5,6}, Ricardo J. Ferreira⁷, Noélia Duarte³, Carlos A. M. Afonso³ and Patrícia Rijo^{1,3*}

¹Center for Research in Biosciences & Health Technologies (CBIOS), Universidade Lusófona de Humanidades e Tecnologias, Lisboa, Portugal, ²Department of Biomedical Sciences, Faculty of Pharmacy, University of Alalá, Alalá de Henares, Spain, ³Instituto de Investigação do Medicamento (Med.U.Lisboa), Faculty of Pharmacy, Universidade de Lisboa, Lisboa, Portugal, ⁴Institute for Biological Research "Siniša Stanković" - National Institute of Republic of Serbia, University of Belgrade, Belgrade, Serbia, ⁵Faculty of Engineering and Natural Sciences, Tampere University, Tampere, Finland, ⁶LAQV-REQUIMTE, Department of Chemistry, University of Aveiro, Aveiro, Portugal, ⁷Science for Life Laboratory, Department of Cell and Molecular Biology, Uppsala University, Uppsala, Sweden

OPEN ACCESS

Edited by:

Jose Maria Prieto,
Liverpool John Moores University,
United Kingdom

Reviewed by:

Mariaelssandra Contino,
University of Bari Aldo Moro, Italy
Guillermo Raul Schinella,
National University of La Plata,
Argentina

*Correspondence:

Patrícia Rijo
patricia.rijo@ulusofona.pt

[†]These authors share first authorship.

Specialty section:

This article was submitted to
Ethnopharmacology,
a section of the journal
Frontiers in Pharmacology

Received: 30 April 2020

Accepted: 30 September 2020

Published: 17 November 2020

Citation:

Garcia C, Isca VMS, Pereira F, Monteiro CM, Ntungwe E, Sousa F, Dinic J, Holmstedt S, Roberto A, Diaz-Lanza A, Reis CP, Pesic M, Candeias NR, Ferreira RJ, Duarte N, Afonso CAM and Rijo P (2020) Royleanone Derivatives From *Plectranthus* spp. as a Novel Class of P-Glycoprotein Inhibitors. *Front. Pharmacol.* 11:557789. doi: 10.3389/fphar.2020.557789

Cancer is among the leading causes of death worldwide. One of the most challenging obstacles in cancer treatment is multidrug resistance (MDR). Overexpression of P-glycoprotein (P-gp) is associated with MDR. The growing incidence of cancer and the development of MDR drive the search for novel and more effective anticancer drugs to overcome the MDR problem. Royleanones are natural bioactive compounds frequently found in *Plectranthus* spp. The cytotoxic diterpene 6,7-dehydroroyleanone (**1**) is the main component of the *P. madagascariensis* (Pers.) Benth. essential oil, while 7 α -acetoxy-6 β -hydroxyroyleanone (**2**) can be isolated from acetonic extracts of *P. grandidentatus* Gürke. The reactivity of the natural royleanones **1** and **2** was explored to obtain a small library of new P-gp inhibitors. Four new derivatives (6,7-dehydro-12-O-*tert*-butyl-carbonate-royleanone (**20**), 6,7-dehydro-12-O-methylroyleanone (**21**), 6,7-dehydro-12-O-benzoylroyleanone (**22**), and 7 α -acetoxy-6 β -hydroxy-12-O-benzoylroyleanone (**23**) were obtained as pure with overall modest to excellent yields (21–97%). P-gp inhibition potential of the derivatives **20–23** was evaluated in human non-small cell lung carcinoma NCI-H460 and its MDR counterpart NCI-H460/R with the P-gp overexpression, through MTT assay. Previously prepared diterpene 7 α -acetoxy-6 β -benzoyloxy-12-O-(4-chloro)benzoylroyleanone (**4**), has also been tested. The P-gp inhibiting effects of compounds **1–4** were also assessed through a Rhodamine 123 accumulation assay. Derivatives **4** and **23** have significant P-gp inhibitory potential. Regarding stability and P-gp inhibition potential, results suggest that the formation of benzoyl esters is a more convenient approach for future derivatives with enhanced effect on the cell viability decrease. Compound **4** presented higher anti-P-gp potential than the natural diterpenes **1**, **2**, and **3**, with comparable inhibitory potential to Dexverapamil. Moreover, derivative **4** showed the ability to sensitize the resistant NCI-H460/R cells to doxorubicin.

Keywords: *Plectranthus*, Diterpenes, Royleanones, stability, *Artemia salina*, P-gp activity

INTRODUCTION

Cancer is among the leading causes of death worldwide with an estimated 18.1 million new cancer cases and 9.6 million cancer deaths in 2018 (Bray et al., 2018). One of the most challenging obstacles in cancer treatment is multidrug resistance (MDR). MDR is responsible for over 90% of deaths in cancer patients receiving traditional chemotherapeutics or novel targeted drugs. MDR can be caused by numerous mechanisms in cancer cells, such as activation of DNA repair mechanisms, elevated metabolism of xenobiotics, genetic factors, and increased activity of drug efflux pumps. (Bukowski et al., 2020). Nonetheless, the most common mechanism of MDR is the overexpression of drug efflux transporters of the ATP binding cassette (ABC) family. Three major proteins of the ABC family, namely P-glycoprotein (P-gp, also referred to as MDR1), MDR-associated protein 1 (MRP1), and breast cancer resistance protein (BCRP), were shown to play a critical role in MDR (Mohammad et al., 2018). These efflux pumps are present in the cell membrane of a variety of normal tissues and have a protecting role against xenobiotic substances and toxic compounds. Therefore, they can interfere with drug administration, by reducing the intracellular accumulation of many anticancer drugs to sub-therapeutic levels, thus decreasing or abolishing chemotherapy efficacy (Nanayakkara et al., 2018). P-gp is the best-studied drug efflux pump of the family of ABC transporters. Cancer cells upregulate P-gp expression as an adaptive response to evade chemotherapy mediated cell death. This process leads to resistance against the currently available anticancer drugs in many different types of cancers (Sharom, 2007; Nanayakkara et al., 2018; Robinson and Tiriveedhi, 2020). Consequently, the development of P-gp inhibitors is gaining much importance in numerous research works. Several P-gp inhibitors have been discovered by *in silico* and pre-clinical studies. Although P-gp inhibitors showed high efficacy *in vitro* and *in vivo* studies, very few have successfully passed all phases of the clinical trials and none of them have been approved by the U.S. Food and Drug Administration (FDA) for clinical use in cancer treatment (Nanayakkara et al., 2018; Robinson and Tiriveedhi,

2020). After three generations of P-gp inhibitors, a fourth generation comprised of nature-originated compounds has emerged (Dinić et al., 2020). Therefore, identification of natural compounds that can exert anticancer effects and at the same time revert the MDR contributes to the efforts of the cancer research community to combat this multifactorial disease.

The genus *Plectranthus* (Lamiaceae) is used in traditional medicine in southern Africa and it is known as a source of bioactive natural products (Lukhoba et al., 2006; Rice et al., 2011). The major classes of secondary metabolites present in these plants are diterpene quinones, coleanones, and royleanones, with pharmacological activities (Bernardes et al., 2018; Rijo et al., 2013), including antiproliferative properties (Burmistrova et al., 2013; Ladeiras et al., 2016). One of those diterpenes, 6,7-dehydroroyleanone (1) (Figure 1), which has been reported with antioxidant, antimicrobial, and cytotoxic activities (Gazim et al., 2014; García et al., 2018), is the main component of *P. madagascariensis* (Pers.) Benth essential oil (Kubínová et al., 2014). Other example is the 7 α -acetoxy-6 β -hydroxyroyleanone (2) (Figure 1), that can be isolated from extracts of *P. grandidentatus* Gürke and identified as an antimicrobial agent (Rijo et al., 2014a; Bernardes et al., 2018) with a strong inhibitory effect against five human cancer cell lines MCF-7 (breast adenocarcinoma), NCI-H460 (non-small cell lung cancer), SF-268 (CNScancer), TK-10 (renal cancer) and UACC-62 (melanoma) (Marques et al., 2002). Although the derivatization of aromatic abietane diterpenoids has been described (González, 2014), the two non-aromatic *p*-quinone abietanes, 1 and 2, are suitable for derivatization. The analysis of the royleanone one chemical structure pointed to the particular acidity of the 12-hydroxyl group, due to the presence of the *p*-quinone in ring C. Alongside with the presence of this group, compound 2 possesses another free hydroxyl group at C-6, suitable for coupling different moieties.

In a previous hemi-synthetic study, the derivatives 6,7-dihydroxyroyleanone (3) and 7 α -acetoxy-6 β -benzoyloxy-12-O-(4-chloro)benzoyloxyroyleanone (4) (Figure 1) were successfully prepared from the lead molecule 2 (Rijo, 2013). Compound 3 is a natural product isolated from *P. grandidentatus* Gürke, which can also be obtained by basic hydrolysis of compound 2 (Rijo, 2013). Furthermore, the patented

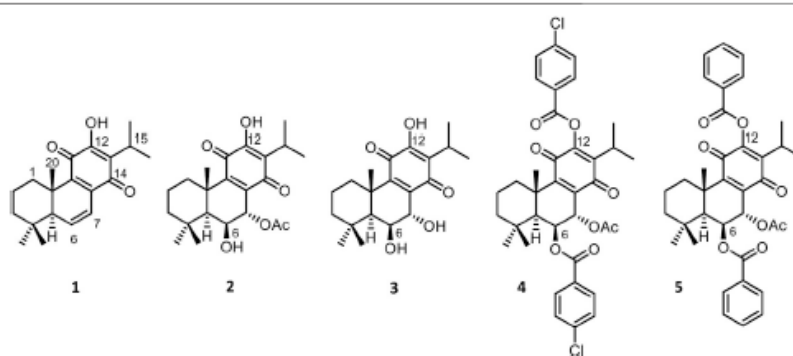
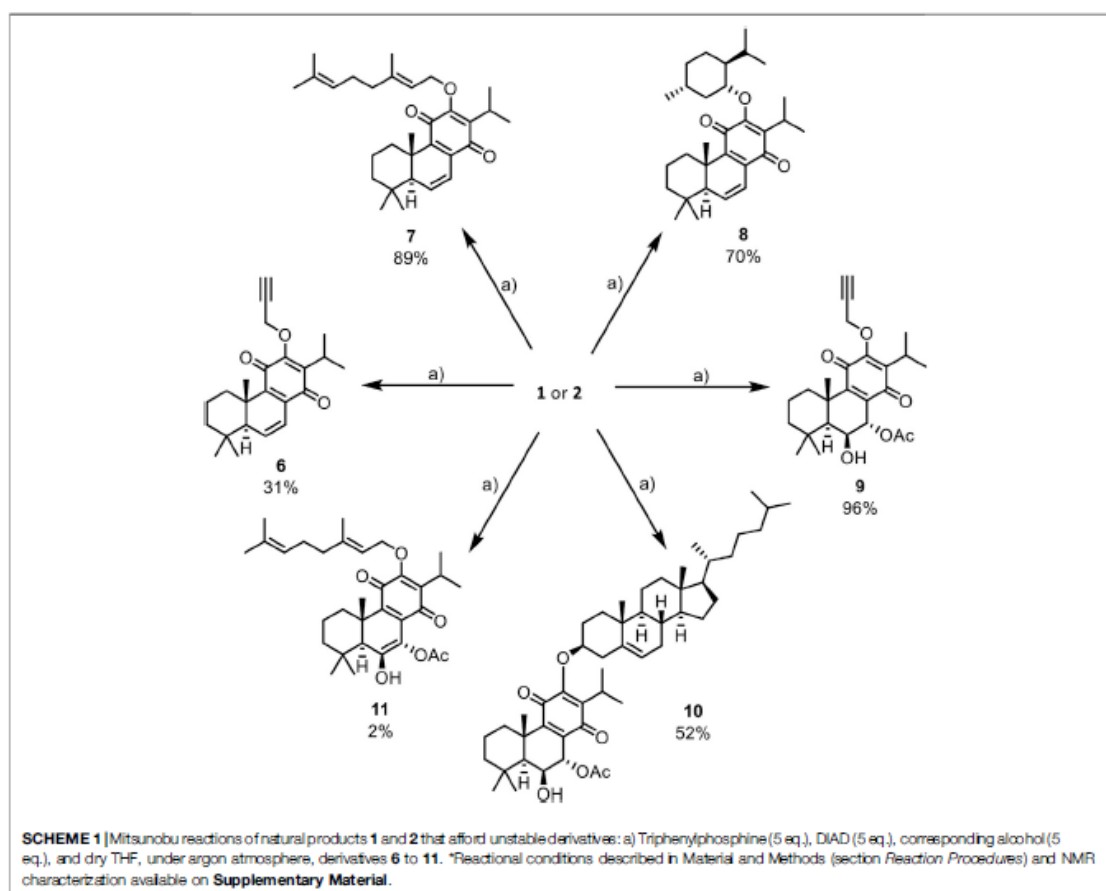


FIGURE 1 | Natural and semisynthetic royleanones: 6,7-dehydroroyleanone (1) and 7 α -acetoxy-6 β -hydroxyroyleanone (2), 6,7-dihydroxyroyleanone (3), 7 α -acetoxy-6 β -benzoyloxy-12-O-(4-chloro)benzoyloxyroyleanone (4) and 7 α -acetoxy-6 β -benzoyloxy-12-O-benzoyloxyroyleanone (5).



diterpene 7 α -acetoxy-6 β -benzoyloxy-12-*O*-benzoylroyleanone (**5**) (**Figure 1**) was also obtained by semi-synthesis from compound **2**. The derivate **5** has shown selective modulation on Protein kinase delta isoform (PKC- δ). A key study reports that **5** strongly inhibited the proliferation of colon cancer cells by inducing a PKC- δ -dependent mitochondrial apoptotic pathway involving caspase-3 activation (Bessa et al., 2018). Besides, another study reported an important Structure-Activity Relationship (SAR) for substituted royleanone abietanes, where an electron-donating group at positions 6 and/or 7 in the abietane skeleton is required for improving cytotoxic effect. Additionally, higher cytotoxic effects were observed for substituents with log *p* values between 2 and 5 (Matias et al., 2019). Herein in this study, we report some royleanone reactivity features, which will allow us to obtain insights on the SAR and identify hit cytotoxic molecules.

RESULTS AND DISCUSSION

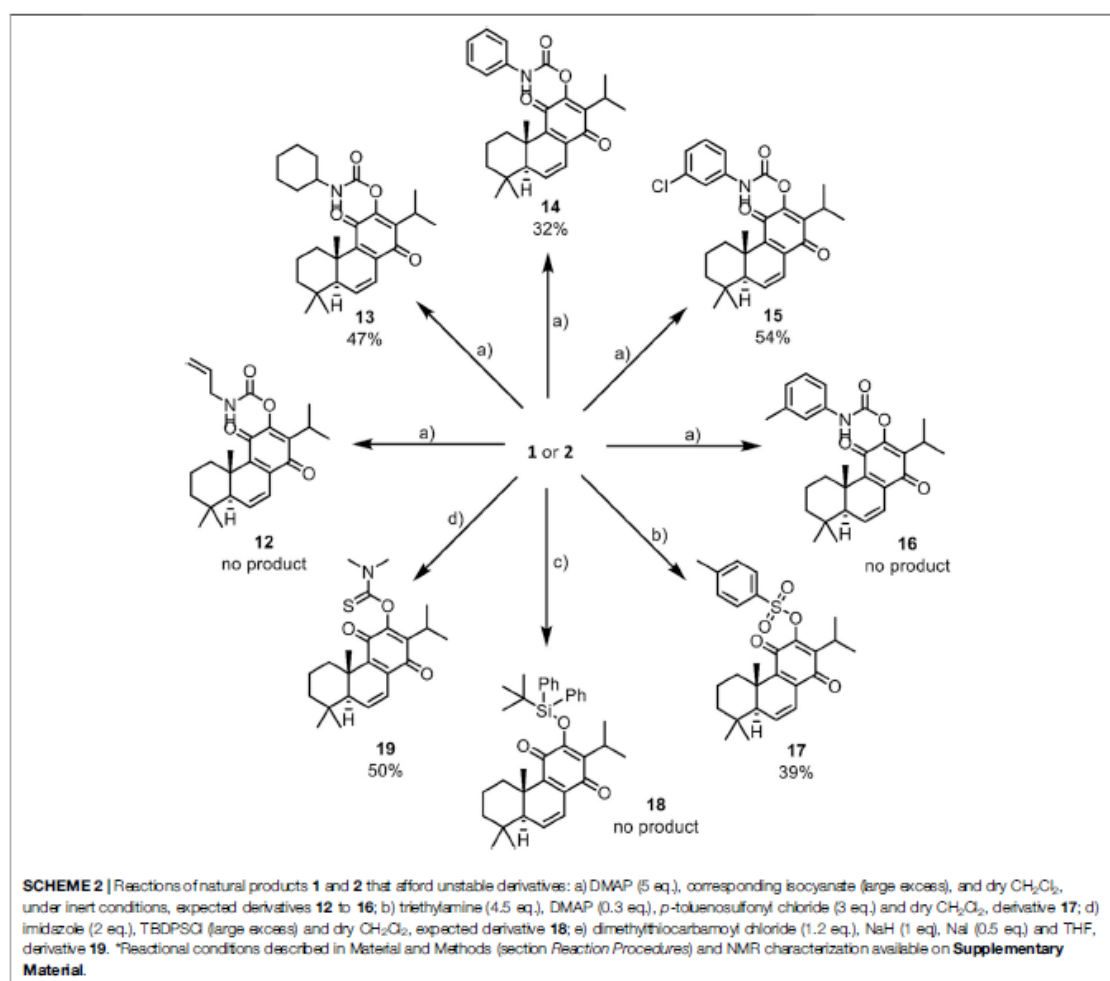
Semisynthesis and Stability of Royleanones

In this work, the reactivity of two royleanones was explored to prepare a small library of compounds of enhanced effect on the

cell viability decrease potential and anti-P-gp activity. Several hemisynthetic reactions were performed on natural compounds **1** and **2** (**Figure 1**). Compounds **1** and **2** were subjected to short time microwave-assisted Mitsunobu and benzoylation reactions. Additionally, molecule **1** was subjected to carbamoylation, tosylation, and introduction of TBDPS (*tert*-butyldiphenylsilyl) group. Royleanone **2** was also subjected to methylation reaction and introduction of Boc (*tert*-butyloxycarbonyl) group. The predicted structures and the isolated derivatives (**6–23**) are shown in **Schemes 1–3**.

Unfortunately, the obtained products have encountered stability issues: the derivatives **6** to **19** (**Scheme 1** and **2**) tend to degrade after isolation. On the other hand, the introduction of Boc group (**20**), methylation (**21**), and benzoylation (**22** and **23**) reactions (**Scheme 3**) were accomplished with success, affording pure products with overall good yields (97% for derivative **20**, 28% for methylated derivative **21** and 50% and 69% for benzoylated derivatives **22** and **23**, respectively).

The Mitsunobu products (**6** to **11**, **Scheme 1**) have displayed a high rate of decomposition, thus hampering their isolation as



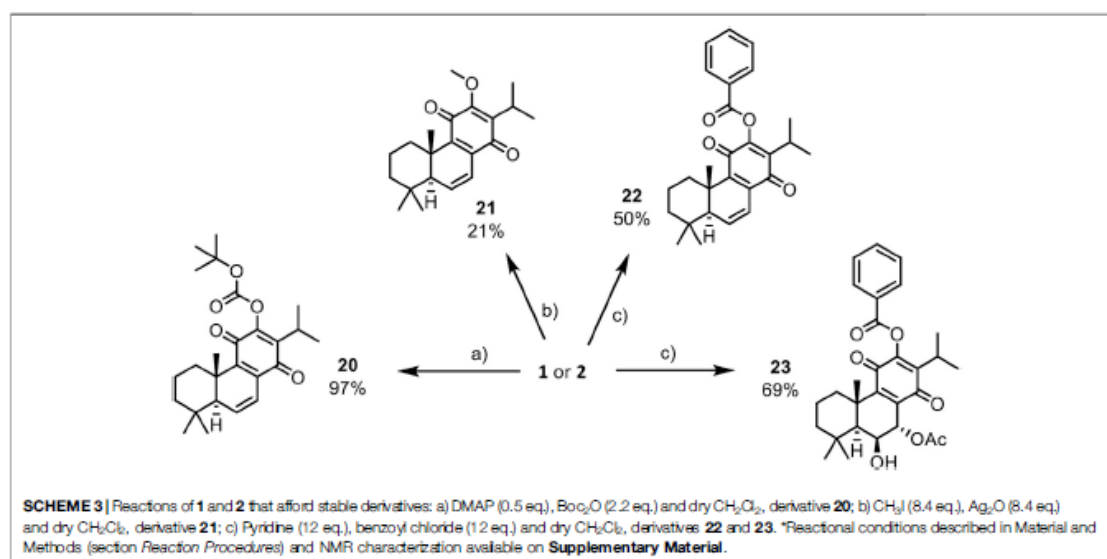
pure products. Several chromatographic techniques have been used, namely silica preparative TLC, silica and alumina columns as well as preparative HPLC. Despite the several purification techniques tested for the isolation of derivatives **6** to **11**, they invariably decomposed during such steps. This degradation was also observed in the carbamoylation reactions (derivatives **13** to **15**, **Scheme 2**), tosylation (**17**), and thiocarbonylation (**19**). Despite the presence of allyl (**12**) and *m*-tolyl (**16**) carbamates and silyl ether (**18**) in the TLC analysis of the reaction mixtures, the compounds decomposed before purification and no characterization could be done.

The mechanism of decomposition was deduced to be the same, regardless the *O*-substituents, and we used the derivative 6,7-dehydro-12-(prop-2'-yn-1'-yloxy)-royleanone (**6**, **Scheme 1**), as a substrate model in further studies. The hemisynthesis of derivative **6** was repeated several times, and the isolation of the compound of

interest was attempted through numerous methods. An alumina column was used for its isolation, as well as preparative TLC and semi-preparative HPLC. Nonetheless, regardless of the technique, the compound isolated was never obtained in its pure form.

In the analytical HPLC analysis of compound **6** three peaks stand out, one of which was identified as the parent compound **1** (23.31 min), using its characteristic UV spectrum as a fingerprint. This fact may indicate that compound **6** tends to decompose to a much more stable scaffold—the starting material (**1**).

In an attempt to better understand the lack of stability of the compounds, derivative **6** was subjected to LC-MS analysis. The ESI positive mass spectra indicated a mass of m/z 355 $[M + Na]^+$. Although it was not possible to identify the moiety or cleavage pattern responsible for the result, some decomposition mechanisms based on the presence of the mentioned fragment were considered (**Figure 2**).



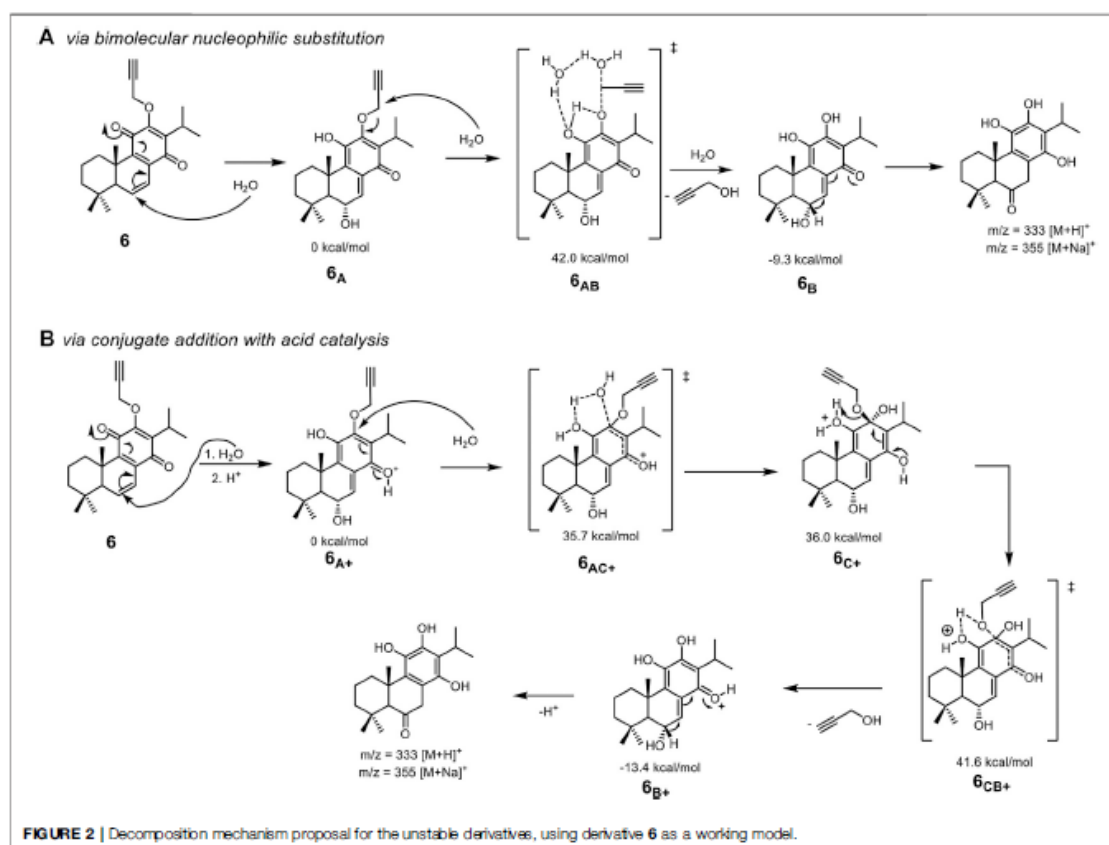
Decomposition Mechanism of Unstable Derivatives

The decomposition of derivative **6** was studied by Density Functional Theory (Parr and Yang, 1989) to elaborate a mechanism and facilitate the future preparation of more stable derivatives (Figure 2). Different mechanisms for decomposition have been suggested based on computational calculations. Nucleophilic substitution at a more reactive side chain seems the preferential route, while an acid-catalyzed conjugate addition should operate in the case of less electrophilic side chains. The decomposition is likely to start with a nucleophilic attack by water on position 6 to provide **6_A**, being followed by a bimolecular nucleophilic substitution by water on the propargylic position, through calculated **6_{AB}**, as shown in Figure 2A). This second step was determined to have an energy barrier (ΔG^\ddagger) of 42.0 kcal/mol and, upon the establishment of hydrogen bonds network with water molecules. Notwithstanding the high energy barrier, the process is energetically favorable with the intermediate **6_B** being 9.3 kcal/mol more stable than **6_A**. The 1,2-hydride migration in **6_B** delivers the aromatized molecule identified in HRMS.

The attack of water at position 12 of **6_A** in a conjugate addition fashion, was considered but determined highly unlikely due to an energy barrier of 55.6 kcal/mol. However, this energy barrier lowers significantly when in the presence of acid catalysis (Figure 2B). In that case, tetrahedral intermediate **6_C**, was identified in the computational calculations, with the overall energy barrier of the release of propargyl alcohol being 41.6 kcal/mol. This alternative mechanism, in which a proton source is required, is likely to be more relevant in decomposing derivatives that miss the electrophilic position prone for an $\text{S}_{\text{N}}2$ reaction. This being the case for most of the unstable products.

Effects of Royleanones in Multidrug Resistance Mechanisms of Cancer Cells

The P-gp inhibition potential of all stable derivatives obtained, derivatives **20** to **23**, was investigated. Moreover, derivative **4**, previously prepared (Rijo, 2013), was also assessed. Non-small cell lung carcinoma is particularly hard to treat due to its highly resistant and metastatic profile. Therefore, NCI-H460 and its corresponding MDR cell line NCI-H460/R with the overexpression of P-gp was a suitable model for testing the anticancer effect and P-gp inhibitory effect of our compounds. MRC-5 was selected as a normal cell line due to its bronchial epithelial origin. The effect of derivatives **20** to **23** was illustrated according to the fluorescence activity ratio (FAR) and sensitivity index (SI) (Table 1). Based on the FAR (values above 1.50 indicate P-gp inhibition) and SI (values above 20 account for P-gp inhibition), we could see that only derivatives **4** and **23** have the ability to inhibit P-gp activity, with FAR values of 1.71 and 2.10, respectively, and SI of 21.60 and 26.50, respectively. Additionally, derivative **23** has shown a comparable inhibitory potential to the well-known P-gp inhibitor, Dexverapamil (FAR 2.13 and SI 26.90) (Isca et al., 2020). A recent study used molecular docking and molecular dynamics to explore the interaction of derivatives **4** and **23** with P-gp and suggested that the presence of aromatic moieties increases the binding affinity of royleanone derivatives toward P-gp (Isca et al., 2020). On the other hand, derivative **22** is also a benzoylated derivative, nonetheless, it does not show the ability to inhibit P-gp activity. The difference between derivatives **4**, **23**, and **22** is that they are obtained from different natural products. Namely, derivative **4** and **23** are prepared from royleanone **2**, and derivative **22** is obtained from royleanone **1**. It means that derivatives **4** and **23** displayed a hydroxyl group in position 6



and an acetoxy group in position 7, while derivative **22**, displayed a double-bond (C=C) in these 6 and 7 positions. This suggests that the substituents in position 6 (-OH) and 7 (-OAc) can also contribute to P-gp interaction. Further studies should be conducted to assess this hypothesis.

Derivatives **4** and **23** showed to be promising candidates for P-gp inhibition, nonetheless, due to the small amount of compound **23** available, we choose the royleanone **4** for further studies. Accordingly, the effect of compound **4** was investigated in NCI-H460, NCI-H460/R cell lines, and normal embryonal bronchial epithelial cells MRC-5. Royleanone **4** showed high toxicity in all cell lines tested, with IC_{50} of $1.9 \pm 0.4 \mu\text{M}$ for NCI-H460, $2.2 \pm 0.4 \mu\text{M}$ for NCI-H460/R, and $2.0 \pm 0.3 \mu\text{M}$ for MRC-5 cell lines. In previous studies, García et al. (2018) and Matias et al. (2019) established the toxicity of the natural diterpenes **1**, **2**, and **3** in the same cell lines. Royleanone **2** is more efficient than **1** and **3**, with IC_{50} of $2.7 \mu\text{M}$ for NCI-H460, $3.1 \mu\text{M}$ for NCI-H460/R, and $8.6 \mu\text{M}$ for MRC-5 cell lines (García et al., 2018; Matias et al., 2019). According to these results, the derivatization of royleanone **2** into derivative **4** lead to a decrease in cell viability in all cell lines tested. However, compounds **1**, **2**, and **three** were selective toward cancer cells (García et al., 2018;

Matias et al., 2019), while derivative **4** was equally active against normal cells.

In general, P-gp inhibitors can block drug binding sites either competitively, non-competitively, or allosterically. Many inhibitors, namely, verapamil, cyclosporin A, *trans*-flupentixol, among others, are themselves transported by P-gp (Amin, 2013). On the contrary, royleanones **1–4** showed the same efficacy in sensitive and MDR cancer cells implying that they could not be P-gp substrates. Moreover, Isca et al. (2020) based on docking simulations also suggest that derivatives **4** and **23** act as non-competitive efflux inhibitors.

The P-gp inhibiting effects of compounds **1** to **4** were additionally assessed through a Rhodamine 123 (Rho123) accumulation assay (Figure 3). The obtained results indicate that derivative **4** has comparable inhibitory potential to Dexverapamil (Figure 3). Dexverapamil belongs to the second generation of P-gp inhibitors, known as a competitive inhibitor (Robey et al., 2018). In our experiments with Rho123, Dexverapamil competes with Rho123 for binding P-gp and thus increases the Rho123 accumulation. Recent publications imply that verapamil (first-generation inhibitor) can increase the ATPase activity of P-gp and thus by exhausting the ATP

TABLE 1 | P-gp inhibition by derivatives 4, 20, 21, 22, and 23 in the human NSCLC MDR cancer cell line.

| Treatments | MFI ^a | FAR ^b | SI ^c |
|--------------------|------------------|------------------|-----------------|
| NCI-H460 control | 134.10 | | |
| NCI-H460/R control | 16.96 | | 12.65 |
| DexVER | 36.07 | 2.13 | 26.90 |
| 4 ^d | 28.97 | 1.71 | 21.60 |
| 20 | 23.71 | 1.40 | 17.68 |
| 21 | 19.48 | 1.15 | 14.53 |
| 22 | 18.25 | 1.08 | 13.61 |
| 23 ^d | 35.54 | 2.10 | 26.50 |

^aThe measured mean fluorescence intensity (MFI) was used for the calculation of the fluorescence activity ratio (FAR).

^bVia the following equation: $FAR = MFI_{MDR\ sensitive} / MFI_{MDR\ control}$. FAR values above 1.50 indicate P-gp inhibition.

^cThe sensitivity index (SI) was calculated on the basis of the measured mean fluorescence intensity (MFI) expressed via the following equation: $SI = (MFI_{MDR\ sensitive} \times 100) / MFI_{MDR\ sensitive\ control}$. SI values above 20 account for P-gp inhibition.

^dResults published in Isca et al. (2020).

Sensitive cancer cell line and its MDR counterpart used in the study: non-small cell lung carcinoma-NSCLC (NCI-H460 and NCI-H460/R).

DexVER was applied at the same concentration (20 μ M) as tested derivatives.

suppress P-gp function (Lee et al., 2019). It is well known that some substrates of P-gp can exert an inhibitory effect on P-gp if they are applied in higher concentrations (Durmus et al., 2015). On the other side, there are substrates of P-gp such as doxorubicin which cannot inhibit P-gp. Quite opposite, doxorubicin induces the expression of P-gp (Wu et al., 2016). Accordingly, we also evaluated the ability of **4** to sensitize resistant NCI-H460/R cells to doxorubicin (Table 2). Results showed that derivative **4** was able to sensitize MDR cells to doxorubicin. All three concentrations of compound **4** used to reverse the doxorubicin resistance achieved similar efficacy.

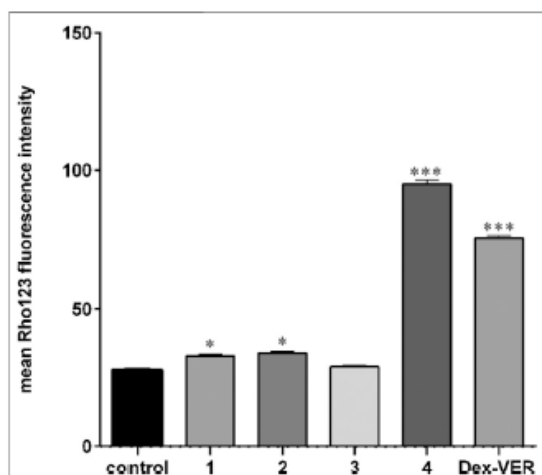


FIGURE 3 | Royleanone derivatives increase the Rhodamine 123 accumulation implying anti-P-gp activity. Experiments were performed in triplicates (n = 3). Significant difference compared to control: * p < 0.05, *** p < 0.001.

TABLE 2 | Derivative 4 sensitizes the NCI-H460/R cell line to doxorubicin.

| Combined treatments | IC ₅₀ for DOX (μ M) | Relative reversal factor |
|-----------------------|-------------------------------------|--------------------------|
| DOX | 2.774 \pm 0.025 | — |
| 4 (0.5 μ M) + DOX | 0.823 \pm 0.016 | 3.37 |
| 4 (1.0 μ M) + DOX | 0.594 \pm 0.017 | 4.67 |
| 4 (2.0 μ M) + DOX | 0.608 \pm 0.020 | 4.56 |

DOX concentrations used in the experiments: 0.1, 0.25, 0.5, 1 and 2.5 μ M.

Importantly, sub-IC₅₀ concentrations (0.5 and 1 μ M) can reverse doxorubicin resistance. Therefore, derivative **4** can be considered as a new P-gp inhibitor useful in combination with classic chemotherapeutics.

CONCLUSIONS

In this work, the reactivity of two natural royleanones was explored to obtain a small library of new P-gp modulators. Several hemisynthetic reactions were performed and successful results were obtained when performing methylation and benzylation, and introduction of Boc group, affording compounds **20** to **23** as pure with overall good yields.

P-gp inhibition potential of the stable derivatives (**20–23**) was evaluated. Previously prepared diterpene **4**, has also been tested. From the tested derivatives, compounds **4** and **23** have significant P-gp inhibitory potential.

Regarding stability and P-gp inhibition potential, results suggest that the formation of benzoyl esters is a more convenient approach for future derivatives with enhanced cytotoxicity. Furthermore, this study suggests that the moieties in positions 6 and 7 of royleanones are also important for interaction with the P-gp. Further studies are needed to disclose this hypothesis.

Additional studies with royleanone **4**, indicate an increase of anti-P-gp potential in comparison to the natural diterpenes **1**, **2**, and **3**, similar to Dexverapamil inhibitory potential. Moreover, derivative **4**, showed the ability to sensitize the resistant NCI-H460/R cells to doxorubicin. This diterpene could be considered as a novel P-gp inhibitor useful in combination with classic chemotherapeutics.

MATERIALS AND METHODS

Plant Material

The plant material, *P. madagascariensis* (Pers.) Benth. and *P. grandidentatus* Gürke were cultivated in Parque Botânico da Tapada da Ajuda (Instituto Superior Agrário, Lisbon, Portugal) from cuttings obtained from the Kirstenbosch National Botanical Garden (Cape Town, South Africa). Voucher specimens were deposited in Herbarium João de Carvalho e Vasconcellos (ISA). The plant name has been checked with <http://www.theplantlist.org> (The Plant List, Version 1.1, 2013). The extraction and isolation process of **1** and **2** were performed according to Garcia et al. (2018) and Bernardes et al. (2018), respectively.

Reaction Procedures

The Mitsunobu reactions were carried out with microwave irradiation, according to a previous report (Buonomo and Aldrich, 2015): **1** (10 mg, 0.032 mmol) or **2** (10 mg, 0.026 mmol), corresponding alcohol (5 eq.), triphenylphosphine (5 eq.) and DIAD (5 eq.) in 4.5 ml dry THF, were irradiated with microwaves at 300 W and 60 °C for 45 min under argon atmosphere. Conditions for Carbamoylation: A mixture of **1** (20 mg, 0.064 mmol), DMAP (5 eq.) and excess of the corresponding isocyanate, in 0.5 ml dry CH₂Cl₂, were stirred at room temperature under inert conditions until consumption of the starting material as judged from TLC. Tosylation Conditions: A mixture of **1** (15 mg, 0.048 mmol), triethylamine (4.5 eq.), DMAP (0.3 eq.) and *p*-toluenesulfonyl chloride (3 eq.), in 0.5 ml dry CH₂Cl₂ were stirred until consumption of the starting material as judged from TLC. Introduction of the TBDPS group: A mixture of **1** (15 mg, 0.048 mmol), imidazole (2 eq.) and excess of *tert*-butyldiphenylchlorosilane in 1 ml dry CH₂Cl₂ was stirred at room temperature. Thiocarbamoyl: **1** (15 mg, 0.048 mmol) was added to a suspension of sodium hydride (1 eq.) in 0.4 ml THF, followed by sodium iodide (0.5 eq.) and dimethylthiocarbamoyl chloride (1.2 eq.). The mixture was left stirring at room temperature until consumption of the starting material. Introduction of Boc group: A mixture of **1** (15 mg, 0.048 mmol), DMAP (0.5 eq.) and Boc₂O (2.2 eq.) in 0.5 ml of dry CH₂Cl₂ was left stirring at room temperature. Methylation: A mixture of **1** (15 mg, 0.048 mmol) (1 eq.), methyl iodide (8.4 eq.) and silver oxide (8.4 eq.), in 0.5 ml of dry CH₂Cl₂ was left stirring at room temperature. Benzoylation: A mixture of **1** (15 mg, 0.048 mmol) or **2** (10 mg, 0.026 mmol), pyridine (12 eq.) and benzoyl chloride (12 eq.), in 2 ml dry CH₂Cl₂ was left stirring at room temperature until complete consumption of the starting material as judged by TLC.

Semi-preparative HPLC-Diode Array Detector Analysis

The analytical method was carried out in an Agilent Technologies 1200 Infinity Series system with a diode array detector (DAD), equipped with a Zorbax® XDB-C18 (250 × 4.0 mm i.d., 5 μm) column, from Merck and ChemStation Software. The sample was injected in acetone, 10 mg/ml. Each injection was analyzed with a gradient elution mixture composed of solution A (methanol), solution B (acetonitrile), and solution C (0.3% trichloroacetic acid in water) was used as follows: 0 min, 15% A, 5% B, and 80% C; 20 min, 70% A, 30% B and 0% C; 25 min, 70% A, 30% B and 0% C; and 28 min, 15% A, 5% B and 80% C. The flow rate was set at 1 ml/min and 20 μL of the sample were injected.

Chemical Stability Evaluation by LC-MS

LC-MS/MS analysis was performed using a Zorbax Eclipse XBD-C18, 4.6 × 250 mm (5 μm) and the mobile phase consisted of 0.5% formic acid in Milli-Q water (eluent A) and acetonitrile + 0.5% formic acid (eluent B). A flow rate of 0.3 ml/min was used, with the following gradient program: 0–30 min from 70 to 5% A, 30–45 min at 5% A, 45–65 min 70% A.

Cells and Cell Culture

Non-small cell lung carcinoma cell line NCI-H460 was purchased from the American Type Culture Collection, Rockville, MD. NCI-H460/R cells were selected originally from NCI-H460 cells and cultured in a medium containing 100 nM doxorubicin (Pescic et al., 2006). Cell lines were subcultured at 72 h intervals using 0.25% trypsin/EDTA and seeded into a fresh medium at the following densities: 8,000 cells/cm² for NCI-H460 and 16,000 cells/cm² for NCI-H460/R.

MTT Test

MTT assay is based on the reduction of 3-(4, 5-dimethyl-2-thiazolyl)-2,5-diphenyl-2H-tetrazolium bromide into formazan dye by active mitochondria of living cells. Cells grown in 25 cm² tissue flasks were trypsinized, seeded into flatbottomed 96-well tissue culture plates (2,000 cells/well), and incubated overnight in 100 μL of appropriate medium. After 24 h, the cells were treated with compounds **1** to **4** (1–25 μM) and incubated for 72 h in complete medium. The combined effects of **4** simultaneously applied with doxorubicin were also studied. In simultaneous treatments, three concentrations of **4** (0.5, 1, and 2 μM) were combined with five concentrations of doxorubicin (0.1, 0.25, 0.5, 1, and 2.5 μM). After 72 h, 100 μL of MTT solution (1 mg/ml) was added to each well, and plates were incubated at 37°C for 4 h. Formazan product was dissolved in 200 μL dimethyl sulfoxide. The absorbance of the obtained dye was measured at 540 nm using an automatic microplate reader (LKB 5060–006 Micro Plate Reader, LKB, Vienna, Austria). Half maximal inhibitory concentration (IC₅₀ value) was defined as the concentration of the drug that inhibited cell growth by 50% and calculated by non-linear regression analysis using GraphPad Prism6 software.

Rhodamine 123 Flow Cytometry Assay

Rhodamine 123 accumulation was analyzed by flow cytometry utilizing the ability of Rhodamine 123 to emit fluorescence. The intensity of the fluorescence is proportional to Rhodamine 123 accumulation. Studies were carried out with Dexverapamil and compounds **1** to **4**. NCI-H460 and NCIH460/R cells were grown to 80% confluence in 75 cm² flasks, trypsinized, and resuspended in 10 ml centrifuge tubes in a Rhodamine 123-containing medium. The cells were treated with diterpenes and Dexverapamil (5 and 20 μM) and incubated at 37°C in 5% CO₂ for 30 min. At the end of the incubation period, the cells were pelleted by centrifugation, washed with PBS, and placed in cold PBS. The samples were kept on ice in dark until the analysis of the CyFlow Space Partec flow-cytometer (Sysmex Partec GmbH, Germany). The fluorescence of Rhodamine 123 was assessed on the FL1 channel. A minimum of 20,000 events was assayed for each sample and the obtained results were analyzed using Summit Dako Software.

Density Functional Theory

All calculations were performed using the Gaussian 16 software package (Frisch et al., 2016), without symmetry constraints. The PBE1PBE functional was employed in the geometry optimizations. That functional uses a hybrid generalized gradient approximation (GGA), including a 25% mixture of Hartree-Fock (Hehre et al., 1986)

exchange with DFT (Parr and Yang, 1989) exchange-correlation, given by Perdew, Burke, and Ernzerhof functional (PBE) (Perdew, 1986; Perdew et al., 1997). The optimized geometries were obtained with a standard 6-31G(d,p) (Ditchfield et al., 1971; Hehre et al., 1972; Hariharan and Pople, 1974; Gordon, 1980) basis set.

Transition state optimizations were performed with the Synchronous Transit-Guided Quasi-Newton Method (STQN) developed by Peng and Bernhard Schlegel (1993) and Peng et al. (1996). Frequency calculations were performed to confirm the nature of the stationary points, yielding one imaginary frequency for the transition states and none for the minima. Each transition state was further confirmed by following its vibrational mode downhill on both sides and obtaining the minima presented on the energy profile.

DATA AVAILABILITY STATEMENT

The raw data supporting the conclusions of this article will be made available by the authors, without undue reservation, to any qualified researcher.

REFERENCES

- Amin, M. L. (2013). P-glycoprotein inhibition for optimal drug delivery. *Drug Target Insights* 7, 27–34. doi:10.4137/DTLS12519.
- Bernardes, C. E. S., Garcia, C., Pereira, F., Mota, J., Pereira, P., Cebola, M. J., et al. (2018). Extraction optimization, structural and thermal characterization of the antimicrobial abietane 7 α -acetoxy-6 β -hydroxyroyleanone. *Mol. Pharm.* 5, 1412–1419. doi:10.1021/acs.molpharmaceut.7b00892.
- Bessa, C., Soares, J., Raimundo, L., Loureiro, J. B., Gomes, C., Reis, F., et al. (2018). Discovery of a small-molecule protein kinase C δ -selective activator with promising application in colon cancer therapy article. *Cell Death Dis.* 9. doi:10.1038/s41419-017-0154-9.
- Bray, F., Ferlay, J., Soerjomataram, I., Siegel, R. L., Torre, L. A., and Jemal, A. (2018). Global cancer statistics 2018: GLOBOCAN estimates of incidence and mortality worldwide for 36 cancers in 185 countries. *CA Cancer J. Clin.* 68, 394–424. doi:10.3322/caac.21492.
- Bukowski, K., Kciuk, M., and Kontek, R. (2020). Mechanisms of multidrug resistance in cancer chemotherapy. *Int. J. Mol. Sci.* 21, 3233. doi:10.3390/ijms21093233.
- Buonomo, J. A., and Aldrich, C. C. (2015). Mitsunobu reactions catalytic in phosphine and a fully catalytic system. *Angew. Chemie - Int. Ed.* 54, 13041–13044. doi:10.1002/anie.201506263.
- Burmistrova, O., Simões, M. F., Rijo, P., Quintana, J., Bermejo, J., and Estévez, F. (2013). Antiproliferative activity of abietane diterpenoids against human tumor cells. *J. Nat. Prod.* 76, 1413–1423. doi:10.1021/np400172k.
- Dinić, J., Efferth, T., García-Sosa, A. T., Grabovac, J., Padrón, J. M., Pajeva, L., et al. (2020). Repurposing old drugs to fight multidrug resistant cancers. *Drug Resist. Updates* 52, 100713. doi:10.1016/j.drug.2020.100713.
- Ditchfield, R., Hehre, W. J., and Pople, J. A. (1971). Self consistent molecular-orbital methods. IX. An extended Gaussian-type basis for molecular-orbital studies of organic molecules. *J. Chem. Phys.* 54, 724–728. doi:10.1063/1.1674902.
- Dumus, S., Hendriks, J. J., and Schinkel, A. H. (2015). Apical ABC transporters and cancer chemotherapeutic drug disposition. *Adv. Cancer Res.* 125, 1–41. doi:10.1016/b9ac.2014.10.001.
- Frisch, M. J., Trucks, G. W., Schlegel, H. B., Scuseria, G. E., Robb, M. A., Cheeseman, J. R., et al. (2016). *Gaussian 16, revision C.01*. Available at: <https://gaussian.com/gaussian16/>.
- García, C., Silva, C. O., Monteiro, C. M., Nicolai, M., Viana, A., Andrade, J. M., et al. (2018). Anticancer properties of the abietane diterpene 6,7-dehydroroyleanone

AUTHOR CONTRIBUTIONS

The manuscript was written through the contributions of all authors.

FUNDING

Support for this work was provided by FCT through UIDP/04567/2020, UIDB/04567/2020, and Ph.D. grant SFRH/BD/137671/2018. CSC-IT center for Science Ltd., Finland is acknowledged for the computational resources' allocation. The Academy of Finland is acknowledged for the financial support to N.R.C (Decisions No. 326487 and 326486).

SUPPLEMENTARY MATERIAL

The Supplementary Material for this article can be found online at: <https://www.frontiersin.org/articles/10.3389/fphar.2020.557789/full#supplementary-material>

- obtained by optimized extraction. *Future Med. Chem.* 1, 1177–1189. doi:10.4155/fmc-2017-0239.
- Gazim, Z. C., Rodrigues, F., Amorin, A. C. L., De Rezende, C. M., Sokovic, M., Tešević, V., et al. (2014). New natural diterpene-type abietane from tetradenia riparia essential oil with cytotoxic and antioxidant activities. *Molecules* 19, 514–524. doi:10.3390/molecules19010514.
- González, M. A. (2014). Synthetic derivatives of aromatic abietane diterpenoids and their biological activities. *Eur. J. Med. Chem.* 87, 834–842. doi:10.1016/j.ejmech.2014.10.023.
- Gordon, M. S. (1980). The isomers of silacyclopropane. *Chem. Phys. Lett.* 76, 163–168. doi:10.1016/0009-2614(80)80628-2.
- Hariharan, P. C., and Pople, J. A. (1974). Accuracy of AH n equilibrium geometries by single determinant molecular orbital theory. *Mol. Phys.* 27, 209–214. doi:10.1080/0026897400100171.
- Hehre, W. J., Ditchfield, R., and Pople, J. A. (1972). Self-consistent molecular orbital methods. XII. Further extensions of Gaussian-type basis sets for use in molecular orbital studies of organic molecules. *J. Chem. Phys.* 56, 2257–2261. doi:10.1063/1.1677527.
- Hehre, W. J., Radom, L., Schleyer, P. v. R., and Pople, J. (1986). *Ab initio molecular orbital theory*. New York: John Wiley & Sons.
- Isca, V. M. S., Ferreira, R. J., Garcia, C., Monteiro, C. M., Dinic, J., Holmstedt, S., et al. (2020). Molecular docking studies of royleanone diterpenoids from *Plectranthus* spp. as P-glycoprotein inhibitors. *ACS Med. Chem. Lett.* 11 (5), 839–845. doi:10.1021/acsmchemlett.9b00642.
- Kubínová, R., Pořízková, R., Navrátilová, A., Farsa, O., Hanáková, Z., Bačinská, A., et al. (2014). Antimicrobial and enzyme inhibitory activities of the constituents of *Plectranthus madagascariensis* (Pers.) Benth. *J. Enzyme Inhib. Med. Chem.* 29, 749–752. doi:10.3109/14756366.2013.848204.
- Ladeiras, D., Monteiro, C. M., Pereira, F., Reis, P., Afonso, C. A. M., and Rijo, P. (2016). Reactivity of diterpenoid quinones: royleanones. *Curr. Pharmaceut. Des.* 22, 1682–1714. doi:10.2174/1381612822666151211094521.
- Lee, T. D., Lee, O. W., Brimacombe, K. R., Chen, L., Guha, R., Lusvardi, S., et al. (2019). A high-throughput screen of a library of therapeutics identifies cytotoxic substrates of P-glycoprotein. *Mol. Pharmacol.* 119, 115964. doi:10.1124/mol.119.115964.
- Lukhoba, C. W., Simmonds, M. S. J., and Paton, A. J. (2006). *Plectranthus*: a review of ethnobotanical uses. *J. Ethnopharmacol.* 103, 1–24. doi:10.1016/j.jep.2005.09.011.
- Marques, C. G., Pedro, M., Simões, M. F., Nascimento, M. S., Pinto, M. M., and Rodríguez, B. (2002). Effect of abietane diterpenes from *Plectranthus grandidentatus* on the growth of human cancer cell lines. *Planta Med.* 68, 839–840. doi:10.1055/s-2002-34407.

- Matias, D., Nicolai, M., Saraiva, L., Pinheiro, R., Faustino, C., Diaz Lanza, A., et al. (2019). Cytotoxic activity of royleanone diterpenes from *Plectranthus madagasariensis* Benth. *ACS Omega* 4, 8094–8103. doi:10.1021/acsomega.9b00512
- Mohammad, I. S., He, W., and Yin, L. (2018). Understanding of human ATP binding cassette superfamily and novel multidrug resistance modulators to overcome MDR. *Biomed. Pharmacother.* 100, 335–348. doi:10.1016/j.biopha.2018.02.038
- Nanayakkara, A. K., Follit, C. A., Chen, G., Williams, N. S., Vogel, P. D., and Wise, J. G. (2018). Targeted inhibitors of P-glycoprotein increase chemotherapeutic-induced mortality of multidrug resistant tumor cells. *Sci. Rep.* 8, 967. doi:10.1038/s41598-018-19325-x
- Parr, R. G., and Yang, W. (1989). Density functional theory of atoms and molecules. New York: Oxford University Press. doi:10.1002/qua.560470107
- Peng, C., Ayala, P. Y., Schlegel, H. B., and Frisch, M. J. (1996). Using redundant internal coordinates to optimize equilibrium geometries and transition states. *J. Comput. Chem.* 17, 49–56. doi:10.1002/(SICI)1096-987X(19960115)17:1<49::AID-JCC5>3.0.CO;2-0
- Peng, C., and Bernhard Schlegel, H. (1993). Combining synchronous transit and quasi-Newton methods to find transition states. *Isr. J. Chem.* 33, 449–454. doi:10.1002/ijch.199300051
- Perdew, J. P., Burke, K., and Ernzerhof, M. (1997). Generalized gradient approximation made simple [Phys. Rev. Lett. 77, 3865 (1996)]. *Phys. Rev. Lett.* 78, 1396. doi:10.1103/PhysRevLett.78.1396
- Perdew, J. P. (1986). Density-functional approximation for the correlation energy of the inhomogeneous electron gas. *Phys. Rev. B* 33, 8822–8824. doi:10.1103/PhysRevB.33.8822
- Peskic, M., Markovic, J. Z., Jankovic, D., Kanazir, S., Markovic, I. D., Rakic, L., et al. (2006). Induced resistance in the human non small cell lung carcinoma (NCI-H460) cell line *in vitro* by anticancer drugs. *J. Chemother.* 18, 66–73. doi:10.1179/joc.2006.18.1.66
- XXX. The plant list. Version 1.1 (2013). Available at: <http://www.theplantlist.org/>. (Accessed May 15, 2019).
- Rice, L. J., Brits, G. J., Potgieter, C. J., and Van Staden, J. (2011). Plectranthus: a plant for the future? *South Afr. J. Bot.* 77, 947–959. doi:10.1016/j.sajb.2011.07.001
- Rijo, P., Duarte, A., Francisco, A. P., Semedo-Lemsaddek, T., and Simões, M. F. (2014a). *In vitro* antimicrobial activity of royleanone derivatives against gram-positive bacterial pathogens. *Phyther. Res.* 28, 76–81. doi:10.1002/ptr.4961
- Rijo, P., Faustino, C., and Simões, M. F. (2013). Antimicrobial natural products from Plectranthus plants. *Formatex Res. Cent.* 2, 922–931.
- Rijo, P., Matias, D., Fernandes, A. S., Simões, M. F., Nicolai, M., and Reis, C. P. (2014b). Antimicrobial plant extracts encapsulated into polymeric beads for potential application on the skin. *Polymers* 6, 479–490. doi:10.3390/polym6020479
- Rijo, P., Faustino, C., and Simões, M. F. (2014). "Antimicrobial natural products from Plectranthus plants; Formatex Research Center," in Microbial pathogens and strategies for combating them: science, technology and education, Editor A. Méndez-Vilas, 922–931, ISBN (13) Vol. 2: 978-84-942134-0-3.
- Robey, R. W., Pluchino, K. M., Hall, M. D., Fojo, A. T., Bates, S. E., and Gottesman, M. M. (2018). Revisiting the role of ABC transporters in multidrug-resistant cancer. *Nat. Rev. Canc.* 18, 452–464. doi:10.1038/s41568-018-0005-8
- Robinson, K., and Tiriveedhi, V. (2020). Perplexing role of P-glycoprotein in tumor microenvironment. *Front. Oncol.* 10, 265. doi:10.3389/fonc.2020.00265
- Sharom, F. J. (2007). ABC multidrug transporters: structure, function and role in chemoresistance. *Pharmacogenomics* 9, 105–127. doi:10.2217/14622416.9.1.105
- Wu, J., Lin, N., Li, F., Zhang, G., He, S., Zhu, Y., et al. (2016). Induction of P-glycoprotein expression and activity by aconitum alkaloids: implication for clinical drug–drug interactions. *Sci. Rep.* 6, 25343. doi:10.1038/srep25343

Conflict of Interest: The authors declare that the research was conducted in the absence of any commercial or financial relationships that could be construed as a potential conflict of interest.

Copyright © 2020 García, Isca, Pereira, Montáro, Ntungwe, Sousa, Dinic, Holmstedt, Roberto, Díaz-Lanza, Reis, Pesic, Candéias, Ferreira, Duarte, Afonso and Rijo. This is an open-access article distributed under the terms of the Creative Commons Attribution License (CC BY). The use, distribution or reproduction in other forums is permitted, provided the original author(s) and the copyright owner(s) are credited and that the original publication in this journal is cited, in accordance with accepted academic practice. No use, distribution or reproduction is permitted which does not comply with these terms.

